Renovation techniques for fatigue cracked orthotropic steel bridge decks

F.B.P. de Jong

Renovation techniques for fatigue cracked orthotropic steel bridge decks

Proefschrift

ter verkrijging van de graad van doctor
aan de Technische Universiteit Delft,
op gezag van de Rector Magnificus prof.dr.ir. J.T.Fokkema,
voorzitter van het College voor Promoties,
in het openbaar te verdedigen op dinsdag 9 januari 2007 om 15.00 uur

door

Foppe Bouk Peter DE JONG

civiel ingenieur
geboren te Groningen

Dit proefschrift is goedgekeurd door de promotor:

Prof.ir. F.S.K. Bijlaard

Samenstelling promotiecommissie:

Rector Magnificus	Voorzitter
Prof.ir. F.S.K.Bijlaard	Technische Universiteit Delft, promotor
Prof.dr.ir. P. van Bogaert	Universiteit Gent
Prof.dr.ir. A.A.A. Molenaar	Technische Universiteit Delft
Prof.Dr.-Ing G.Sedlacek	Rheinisch-Westfälische Technische Hochschule Aachen
Prof.ir. H.H.Snijder	Technische Universiteit Eindhoven
Prof.dr.ir. J.Wardenier	Technische Universiteit Delft
M.H.Kolstein	Technische Universiteit Delft

Published and distributed by:

F.B.P.de Jong
Email: peterdej@dds.nl

ISBN-10: 90-9021412-7
ISBN-13: 978-90-9021412-2

Cover illustration by Bouke de Jong

Printed in the Netherlands

Table of Contents

Summary

Renovation techniques for fatigue cracked orthotropic steel bridge decks

The study presented in this thesis is focused on renovation techniques for orthotropic steel bridge decks.

In the past many orthotropic steel bridges have been built, the vast majority of these bridges were built between 1960 and 1980. In the last decade several fatigue cracks have been detected in the deck structure of these bridges, nearly always in the heavy vehicle lane. The most frequently observed fatigue crack in the Netherlands is also the most severe crack. This crack is located in the deck plate at the crossing of crossbeam and trough girder. This crack was observed for the first time on the Van Brienenoord bascule bridge in 1997, at that time a 7 year old bridge. Analyses showed that the cracks were fatigue cracks, caused by the cyclic loading of the axles of heavy vehicles in the heavy vehicle lane. At this moment deck plate cracks have been observed in approximately 10 bridges in the Netherlands, both in movable bridges with a thin epoxy surfacing, as well as in fixed bridges, with a thick asphalt surfacing. The principal objective of the research program was to develop renovation techniques for these orthotropic bridge decks, and to get a better insight into the fatigue behaviour of the bridges.

The renovation techniques are part of a proposed maintenance philosophy for steel bridge decks. This probabilistic philosophy consists of three main parts: lifetime calculations, inspections and renovation techniques. The research was split up into parts all of which were necessary for the implementation of the philosophy in practical situations.

Research was done into traffic loads on bridges. The stress ranges in the bridges are related to the axle and vehicle loads. The number of stress cycles is related to the amount of traffic. With respect to the loads, footprints for several tyres have been measured. Footprint sizes differ with wheel load and inflation pressure. In addition axle load spectra are given based on measurements on the Moerdijk Bridge. With respect to the traffic volume properties the number of lorries, the average number of axles per lorry and the distribution of the lorries over the day has become clear.

The stress pattern in the deck plate at the crack location was researched and calculations and

tests with several footprints have been done. The conclusion is that for fatigue verifications of deck plate cracks at the crossbeam the stress calculation can be based on a clamped beam model.

A fatigue detail classification is necessary for lifetime calculations. Fatigue tests were done for the deck plate crack at the crossbeam location. Based on the fatigue tests detail classifications have been derived for several crack lengths. These classifications are relatively high, and exceed the classifications according to the design standards in the Eurocode.

An extensive research program with the Lintrack (Accelerated Pavement Testing) was performed, on a bridge deck test panel both with and without different surfacing layers. This simulated the situation on fixed respectively movable bridges. Insight into the behaviour and influence of surfacing on the steel bridge deck was the main purpose of this program. It turned out that the stress in the steel deck structure was very sensitive to the temperature of the asphalt surfacing. Besides that composite action was not observed for mastic asphalt. A comparison of theoretical and numerical analysis with both field measurements on bridges and tests in the Lintrack points towards a modelling with a flexible interface between steel deck plate and asphalt surfacing.

Before applying a renovation technique, cracks in the deck plate probably have to be repaired. For cracked deck plates submerged arc welding is a good repair method. The three advantages of submerged arc welding are the high speed of execution; the welding takes place only from the top of the deck plate, and the relatively limited welding shrinkage. Parameter settings for the welding process were established with research. The current (Amps) was the most important parameter in determining the depth of penetration. The maximum depth of penetration that can be achieved is approximately between 65% and 75% of the deck plate thickness. Fatigue tests showed that the detail classification of cracks repaired with submerged arc welding is only slightly lower as the detail classification for the uncracked situation with parent material.

For fixed bridges the replacement of the asphalt surfacing with a reinforced high performance concrete surfacing (RHPC) of approximately 50 mm is an effective renovation method. A relatively stiff epoxy interface between steel and concrete makes composite action between steel and RHPC possible. Calculations and tests in the laboratory showed that the stresses in deck plate and trough web were significantly reduced. Four fatigue tests were successfully applied on test panels, the applied loading sequence represented more than 50 years heavy vehicle traffic on the Moerdijk Bridge.

In a pilot project the RHPC surfacing was applied on a part of the Caland Bridge near

Rotterdam in 2003. Strain gauges were attached to the bottom side of the deck plate of this bridge before the renovation. Extensive stress spectra measurements were performed before and after the renovation for a good comparison. The results showed a large reduction in the stress ranges due the passing axles. Reduction factors for the stress range in the deck plate of 0.2 and for the stress range in the trough web of 0.4 are proposed. With this reduction the lifetime of the bridge deck is significantly extended.

For movable bridge decks three solutions that extend the lifetime of the orthotropic deck structure were researched; bonding a second steel deck plate at the old steel deck plate, filling the troughs in the wheel tracks with polyurethane and the application of an ultra high performance concrete layer on top of the steel deck plate.

A bonded steel plate gave a stress reduction factor of approximately 0.5 for the stress range in the deck plate. In a fatigue test however delamination of the adhesive layer between the two steel plates occurred. With an improved bonding layer, delamination can probably be avoided. This should be researched. Trough filling gives a stress reduction factor of approximately 0.12 up to 0.8 for the stress range in the deck plate. Besides that in two fatigue tests large deck plate cracks grew. These observations make this an unreliable renovation technique and because of that no further research is recommended. Thin RHPC gives a stress reduction factor of approximately 0.18 up to 0.28 for the stress range in the deck plate. This renovation has not yet been tested in fatigue. Therefore this method is thought to be a promising solution, but a lot more research is necessary.

The general conclusion is that the researched renovation techniques for movable bridge decks have not brought the significant extension of the lifetime required. With these renovation techniques new durability problems are introduced on the bridge. For two techniques: bonding steel plates and the reinforced high performance concrete layer additional research is recommended. With this conclusion in mind, it should be considered that building a new bridge, or bridge deck, is a better alternative than renovating an old bridge with fatigue cracks. The technical disadvantages of a renovation are obvious, and in that case the financial implications of building a new bridge can be accepted.

The proposed maintenance philosophy of orthotropic steel bridge decks, guarantees the safety of the structure with the required safety level, described with the reliability index β. The target reliability index for fatigue deck plate cracks should be at the level of serviceability limit state, $\beta = 1.8$. With this target reliability index an approach to bridges that is too conservative can be avoided.

An important tool in the maintenance philosophy is a lifetime calculation model with respect

to deck plate cracks. A reliable calculation model for fatigue damage has been presented. The calculation results are accurate, both for the movable bridges with a thin epoxy surfacing and for the fixed bridges with mastic asphalt surfacing. This means that an accurate modelling of the behaviour of asphalt surfacing with respect to the stresses in the steel deck construction is obtained. Based on this lifetime calculation system inspection programs can be made. This lifetime calculation is valid for existing bridge decks with fatigue damage but can also be used for the design of new bridge decks.

Several inspection techniques have been presented briefly. For guaranteeing safety up to the moment of a renovation of the bridge, visual and Crack PEC inspection are the appropriate techniques, and during a renovation technique TOFD is the appropriate inspection technique.

Peter de Jong

Samenvatting

Renovatietechnieken voor orthotrope stalen brugdekken met vermoeiingsscheuren

Het onderzoek in dit proefschrift heeft ten doel het ontwikkelen van renovatietechnieken voor stalen orthotrope brugdekken.

In het verleden zijn er veel orthotrope stalen bruggen gebouwd. Een groot deel van deze bruggen is gebouwd tussen 1960 en 1980. Het laatste decennium zijn er meerdere typen vermoeiingsscheuren gevonden in de dekken van deze bruggen, vrijwel altijd in de zwaarstbelaste rijstrook. De meest voorkomende scheur is tevens de ernstigste scheur. Deze scheur bevindt zich in de dekplaat ter plaatse van de kruising tussen dwarsdrager en trogligger. Deze dekplaatscheur is voor het eerst waargenomen in 1997 in het dek van de bascule van de Van Brienenoord brug, deze brug was destijd slechts 7 jaar oud. Analyses hebben uitgewezen dat de vermoeiingsscheuren veroorzaakt worden door de zich steeds herhalende aspassages van vrachtvoertuigen in de zwaarstbelaste rijstrook. Momenteel zijn in circa een tiental bruggen in het Nederlandse rijkswegennet dergelijke dekplaatscheuren gevonden, zowel in beweegbare bruggen met een dunne epoxy slijtlaag, alswel in vaste bruggen met een dikke asfaltslijtlaag. Het belangrijkste doel van het uitgevoerde onderzoek is het ontwikkelen van renovatiemethoden voor deze brugdekken, en het verkrijgen van een beter inzicht in het vermoeiingsgedrag van deze rijdekken.

De renovatiemethoden maken deel uit van een voorgestelde onderhoudsfilosofie voor brugdekken. Deze probabilistische aanpak bestaat uit een drietal belangrijke onderdelen: levensduurberekeningen, inspecties en renovatiemethoden. Het onderzoek is opgesplitst in een aantal deelonderzoeken die alle noodzakelijk zijn om de onderhoudsfilosofie in de praktijk te kunnen implementeren.

Er is onderzoek gedaan naar de verkeersbelastingen op bruggen. De grootte van de spanningswisselingen in het dek is gerelateerd aan de as- en voertuiggewichten. Het aantal spanningswisselingen is gerelateerd aan de hoeveelheid vrachtverkeer. Om de belastingen in kaart te brengen zijn wielprenten van verschillende bandentypen onderzocht. Het bleek dat de wielprenten afhankelijk zijn van de belasting en de bandenspanning. Daarnaast zijn aslastspectra gegeven, die gebaseerd zijn op metingen op de Moerdijkbrug. Ten aanzien van de verkeershoeveelheid zijn de aantallen vrachtwagens, het aantal assen per wagen en de

verdeling van het verkeer per etmaal onderzocht.

De spanningsverdeling in de dekplaat ter plaatse van de scheurlocatie is onderzocht. Berekeningen en testen met verschillende wielprentafmetingen zijn uitgevoerd. De conclusie is dat voor vermoeiingsberekeningen van dekplaatscheuren de spanning in het dek bepaald kan worden met een ingeklemd ligger model.

Een vermoeiingsclassificatie is noodzakelijk om levensduurberekeningen uit te kunnen voeren. Vermoeiingstesten zijn uitgevoerd voor de dekplaatscheur ter plaatse van de dwarsdrager. Op basis van deze testen zijn classificaties bepaald voor verschillende scheurlengtes. Deze classificaties zijn relatief hoog.

Een uitgebreid proevenprogramma is uitgevoerd met de Lintrack (een zwaar verkeer simulator) op een test brugdek zonder alswel met slijtlagen, wat de situatie op beweegbare bruggen respectievelijk vaste bruggen simuleert. Inzicht in het gedrag van slijtlagen en de invloed van de slijtlaag op het stalen rijdek was het belangrijkste doel van dit programma. Het is gebleken dat de spanningen in de stalen dekplaat zeer afhankelijk zijn van de temperatuur van de asfaltslijtlaag. Daarnaast is er geen constructieve samenwerking tussen staal en asfalt geconstateerd. Een vergelijking van een analytische benadering, met zowel metingen aan bestaande brugdekken en de resultaten van de testen in de Lintrack maakt duidelijk dat het gebruikelijke membraan tussen de stalen dekplaat en de asfalt slijtlaag zeer flexibel is, waardoor geen constructieve samenwerking tot stand komt.

Indien er scheuren in de dekplaat geconstateerd worden dienen deze in principe gerepareerd te worden voordat de renovatietechniek toegepast wordt. Dekplaatscheuren kunnen goed gerepareerd worden middels het onder poederdek lasproces. De voordelen van onder poederdek lassen zijn de hoge uitvoeringssnelheid doordat er alleen vanaf de bovenkant gewerkt wordt en tevens de relatief kleine laskrimp. Door middel van testen zijn de parameters voor het lasproces bepaald. De stroomsterkte is het meest van invloed op de inbranding. De maximale bereikbare inbranding is circa 65% tot 75% van de dekplaatdikte. Uitgevoerde vermoeiingstesten hebben aangetoond dat de vermoeiingsclassificatie van een onder poederdek gerepareerde dekplaat slechts weinig lager ligt dan voor een normale dekplaat met moedermateriaal.

Voor vaste bruggen is een laag gewapend hoge-sterkte beton van ca. 50 mm een uitstekende renovatiemethode. Deze betonlaag vervangt dan de asfaltslijtlaag. Een relatief stijve epoxylaag tussen de stalen dekplaat en het beton, verbindt de lagen aan elkaar en maakt constructieve samenwerking mogelijk. Berekeningen en testen in het laboratorium laten zien dat de spanningen sterk verminderd worden. Een viertal vermoeiingsproeven zijn uitgevoerd

op test panelen. De toegepaste belasting gedurende deze vermoeiingsproeven staat gelijk aan minimaal 50 jaar vrachtverkeer op de Moerdijkbrug.

In een pilot project is deze hoge-sterkte betonoverlaging in 2003 aangebracht op een deel van de Calandbrug nabij Rotterdam. Rekstroken zijn aangebracht op de onderzijde van de dekplaat alvorens het brugdek gerenoveerd werd. Uitgebreide rekspectrametingen zijn uitgevoerd zowel voor als na de renovatie voor een goede vergelijking. De resultaten laten een sterke reductie zien van de spanningswisseling ten gevolge van het passeren van een as. Een reductiefactor voor de spanningswisseling in de dekplaat van 0.2 en voor de spanningswisseling in het trogbeen van 0.4 is bepaald. Met deze reductie is de levensduur van het rijdek sterk verlengd.

Voor beweegbare bruggen zijn drie renovatietechnieken, die de levensduur van het stalen brugdek verlengen, onderzocht: het verlijmen van een extra staalplaat bovenop het bestaande dek, het vullen van de trog met een polyurethaan, en het aanbrengen van een laag zeer hoge-sterkte beton op de bestaande dekplaat.

Een verlijmde staalplaat levert een reductiefactor op van ongeveer 0.5 voor de spanning in de dekplaat. In een vermoeiingstest is echter delaminatie opgetreden in de lijmlaag tussen de twee staalplaten. Met een verbeterde lijmtechniek kan dit wellicht vermeden worden, maar dit dient onderzocht te worden. Het vullen van troggen geeft een spanningsreductiefactor tussen circa 0.12 en 0.8 voor de spanning in de dekplaat. Daarnaast zijn in een tweetal vermoeiingstesten lange dekplaatscheuren gegroeid. Dit alles maakt deze techniek tot een onbetrouwbare techniek, derhalve wordt vervolgonderzoek niet aanbevolen. Een dunne betonlaag geeft een spanningsreductiefactor van circa 0.18 to 0.28 voor de spanning in de dekplaat. Deze methode is echter nog niet op vermoeiing beproefd. Het lijkt een veelbelovende renovatietechniek, maar veel aanvullend onderzoek is nog nodig.

De algemene conclusie is dat de onderzochte renovatietechnieken voor beweegbare brugdekken nog niet de gewenste levensduurverlenging hebben gebracht. Daarenboven worden met deze methoden ook nieuwe duurzaamheidsproblemen gecreëerd. Voor twee technieken, staalplaat verlijmen en zeer hoge-sterkte beton, is aanvullend onderzoek nodig. Met deze conclusie moet overwogen worden of het vernieuwen van een beweegbare brug geen beter alternatief is dan een renovatie indien zich vermoeiingsscheuren voordoen. De nadelen van de renovatietechnieken zijn duidelijk en dat maakt dat de extra kosten gemoeid met het vervangen van een brugdek geaccepteerd kunnen worden.

De voorgestelde onderhoudsfilosofie voor orthotrope stalen brugdekken garandeert de veiligheid van de constructie met de benodigde veiligheid. De veiligheid wordt beschreven

met de betrouwbaarheidsindex β. De benodigde betrouwbaarheidsindex voor dekplaatscheuren in stalen rijdekken bevindt zich op het niveau van de bruikbaarheidsgrenstoestand, $\beta = 1.8$. Met deze waarde van de betrouwbaarheidsindex kan een te conservatieve aanpak vermeden worden.

Een belangrijk onderdeel in de onderhoudsfilosofie zijn de levensduurberekeningen voor dekplaatscheuren. Een betrouwbaar rekenmodel voor vermoeiing is opgesteld. De rekenresultaten stemmen in grote lijnen overeen met de waargenomen scheuren in diverse bruggen, zowel voor vaste bruggen met een gietasfaltslijtlaag als voor beweegbare bruggen met een dunne epoxyslijtlaag. Dit betekent dat er een geschikte modellering van het gedrag en invloed van de asfaltslijtlaag op de spanning in het stalen rijdek is ontwikkeld. De berekende levensduren kunnen als basis dienen voor inspectieprogramma's. Met het rekenmodel kunnen zowel bestaande brugdekken met vermoeiing beschouwd worden, maar ook nieuwe brugdekken ontworpen worden op dekplaatscheuren.

Diverse inspectie technieken zijn gepresenteerd. Voor het borgen van de veiligheid van een brugdek totdat een renovatietechniek wordt aangebracht zijn visuele inspecties tezamen met de Crack PEC techniek de aangewezen technieken. Voor het in kaart brengen van de scheuren tijdens een renovatie is TOFD de aangewezen techniek.

Peter de Jong

Acknowledgements

The research presented in this dissertation was carried out at the Design and Construction department of the Faculty of Civil Engineering and Geosciences at the Delft University of Technology. Two sections of the department of Design and Construction were involved in the project “Prolonging the lifespans of orthotropic steel bridges”. The section of Structural and Building Engineering was responsible for the development of renovation techniques for steel bridges with severe fatigue damage. The section of Road and Railway Engineering was responsible for research into the behaviour of surfacing materials. The later is a subject of a PhD study that has been conducted by my colleague Tarig Medani.

I would like to thank all those people who helped, encouraged and supported me in the different phases of this project, without their efforts it would certainly never have been completed. First, I would like to thank my colleagues from the Structural and Building Engineering section of Delft University of Technology: Henk Kolstein, who initiated this project, and Frans Bijlaard for their contribution and the discussions. I would like to thank also the personnel from the Stevin 2 Laboratory. From this place I express my appreciation to the Ministry of Transport, from which I got the opportunity to work on this dissertation. I would like to thank my colleagues Frank van Dooren, Han Leendertz and Henk van der Weijde for their contributions. It was a pleasure to integrate the practical point of view of the Ministry as bridge owner, with the scientific approach at the University.

Special thanks are due to the following companies and institutions that supported this project: Contec ApS, SBO B.V. Specialistische Bedekkingen en Onderhouds Technieken, Smits Neuchatel Infrastructuur B.V., Shell Nederland Verkoopmaatschappij B.V., Bolidt Kunststoftoepassingen B.V., Vereniging Centraal Bureau voor Constructiewerkplaatsen, Rijkswaterstaat Bouwdienst, the Research School Integral Design of Structures and the Technology Foundation STW. I wish to express my appreciation to the members of the users panel (“gebruikerscommissie”) for their comments and discussions during our meetings.

Finally I gratefully acknowledge the continuous support of Agnes. Without her encouragement it would not have been finished yet.

Peter de Jong
Delft, 3 October 2006

1. Introduction

1.1 Fatigue phenomena in orthotropic steel bridge decks

In the past many orthotropic steel bridges have been built in the Netherlands and in many other countries. The vast majority of these bridges were built between 1960 and 1980. Figure 1-1 shows a cross-section and part view of a typical orthotropic bridge deck structure.

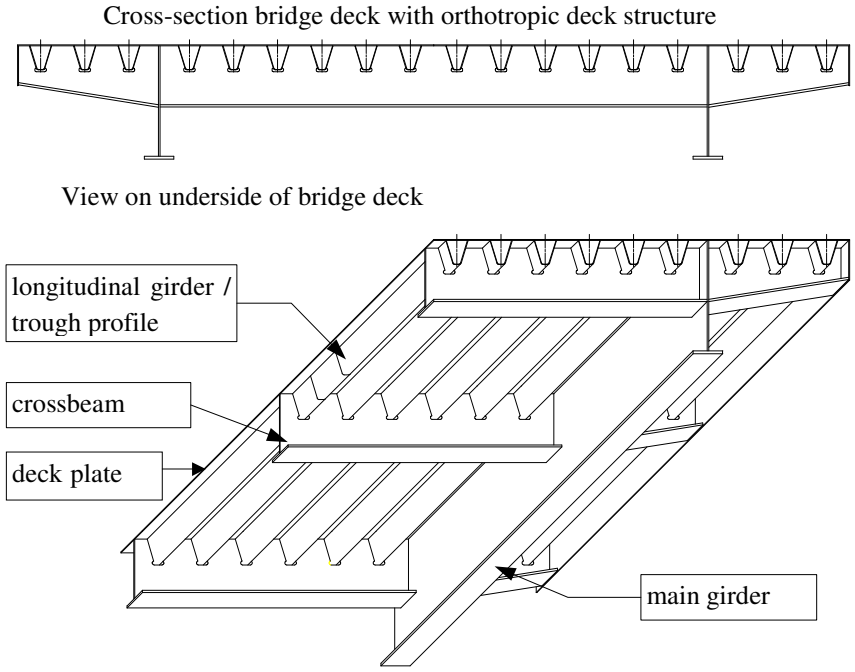

Figure 1-1: Orthotropic bridge deck structure

In the last decade several fatigue cracks have been detected in the deck structure of these bridges, nearly always in the heavy vehicle lane. In the Netherlands the most frequently observed fatigue crack is located in the deck plate at the intersection of the crossbeam and trough girder. Unfortunately this is also the most severe crack. The crack is shown in Figure 1-2. Also a deck plate crack in the field between the crossbeams is shown. This however is a crack type that has been observed only a few times.

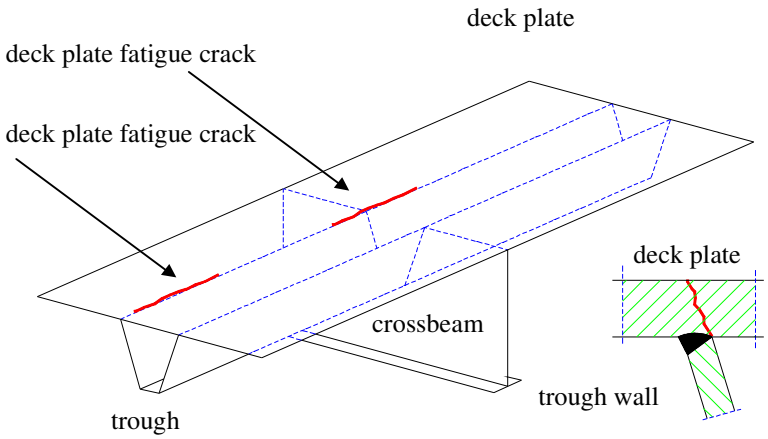

Figure 1-2: Deck plate cracks

The crack initiation is at the root of the longitudinal fillet weld between the trough web and the deck plate at the intersection of the crossbeam and the continuous closed trapezoidal stiffeners (troughs). After the initiation phase the crack growth is in the vertical direction from the underside to the top of the deck plate. After the crack has grown through the deck plate its growth is in the horizontal/longitudinal direction. When the crack lengthens it threatens the safety of the structure.

These deck plate cracks were first observed in 1997 in the Van Brienenoord bascule bridge in the harbour area of Rotterdam when the bridge was only 7 years old (Van der Weijde, 1998, 1999), (Kolstein, 1998). Analyses showed that the cracks were fatigue cracks, caused by cyclic loading from the wheels of heavy vehicles in the heavy vehicle lane.

As the orthotropic deck is a standard structure and traffic on other bridges in the Netherlands is comparable to that on the Van Brienenoord Bridge, clearly more cracks were to be expected. Currently deck plate cracks have been observed in approximately 10 bridges in the Netherlands and bridge owners have to expect many more bridges with fatigue cracks at deck plate level in the future.

The deck plate cracks are found both in the decks of fixed bridges with a thick asphaltic surfacing and in the decks of movable bridges that are usually surfaced with a thin epoxy layer. The presence of a thick asphaltic layer reduces the stress ranges, which leads to a somewhat longer lifespan.

The Van Brienenoord bascule bridge has been completely replaced, except for the hinges and

the counterweight part of the structure. This was an expensive solution. For many other bridges with this kind of fatigue damage it is also necessary to take measures to guarantee the safety of the structure. Renovation techniques that extend the fatigue lifetime are required for these bridge decks.

A research project was initiated at Delft University of Technology in 1999. The principal objectives of the research program were to develop renovation techniques for these orthotropic bridge decks and to get a better insight into the fatigue behaviour of the bridge decks. Additionally the research project should lead to a better insight into the response of the pavement surfacing material.

Two sections of the Faculty of Civil Engineering and Geosciences were involved in this research program. The Road and Railway Engineering section was responsible for research into the behaviour of surfacing and membrane materials, which are usually applied on orthotropic steel bridge decks. The section of Structural and Building Engineering was responsible for the research into the fatigue phenomena and the development of renovation techniques.

1.2 Aims of the research program

The main purpose of the research was to develop renovation techniques for orthotropic steel bridge decks with fatigue cracks in the deck plate at the connection of trough web and crossbeam. Renovation techniques are needed both for movable as well as for fixed bridges. As the spans of fixed bridges are much larger than the spans of movable bridges emphasis will be made on renovation techniques for fixed bridges. The purpose of the renovation techniques is to guarantee the safety of the bridge structure. Fatigue cracks possibly threaten the safety of the bridge deck structure and that should be avoided.

In addition to this the thesis should provide a model for bridge maintenance, with respect to fatigue, that gives a framework in which the renovation has a place. Bridge engineers have questions like:

- When can we expect fatigue cracks?
- How do we find possible fatigue cracks?
- When do we have to renovate the bridge?
- What is the lifetime of the bridge after a renovation?

This thesis has to provide a maintenance model that gives advice to bridge engineers in these questions. Figure 1-3 gives an idea of the maintenance model.

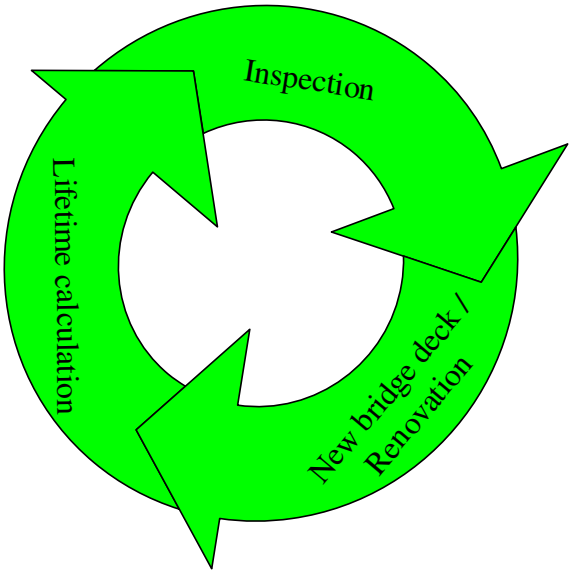

Figure 1-3: Maintenance model

With the general outlines of the research in mind it is possible to describe the aims in more detail.

The renewal of the Van Brienenoord bascule bridge was an expensive renovation, in which the whole bridge was renewed. This was in principle unnecessary as the fatigue problems only damage the deck structure in the heavy vehicle lane. Therefore the renovation techniques should also be cost-effective.

Reducing traffic disruption is also important. In a modern society traffic and transportation is of vital importance. The traffic disruption due to maintenance activities should be as little as possible. This means that the renovation techniques must provide permanent solutions, which significantly extend the fatigue life of the structure. It also means that the time needed for the implementation of a renovation technique should be as little as possible.

Given this strategy, the need for long term renovation techniques for orthotropic steel bridge decks with fatigue cracks is obvious.

Within the maintenance model it is essential that an accurate calculation of the fatigue lifetime of deck plates in bridges is available. The intention is that this calculation is valid both for movable bridges with a thin epoxy surfacing and for fixed bridges with a thicker asphalt surfacing.

Defining a maintenance model means also that the thesis should provide an insight to

inspection techniques for bridge decks. The properties of inspection techniques should be described.

1.3 The structure of the thesis; a brief description of each chapter

Figure 1-4 gives a diagrammatic overview of the thesis. In the outer circle the maintenance model, as presented in Figure 1-3, is visible. In this circle the maintenance loop with lifetime calculations, inspections and renovations becomes visible. Inside this outer circle information necessary for a successful implementation of the maintenance model is given.

The three chapters dealing with necessary information are described first. After that short introductions to the other chapters are given.

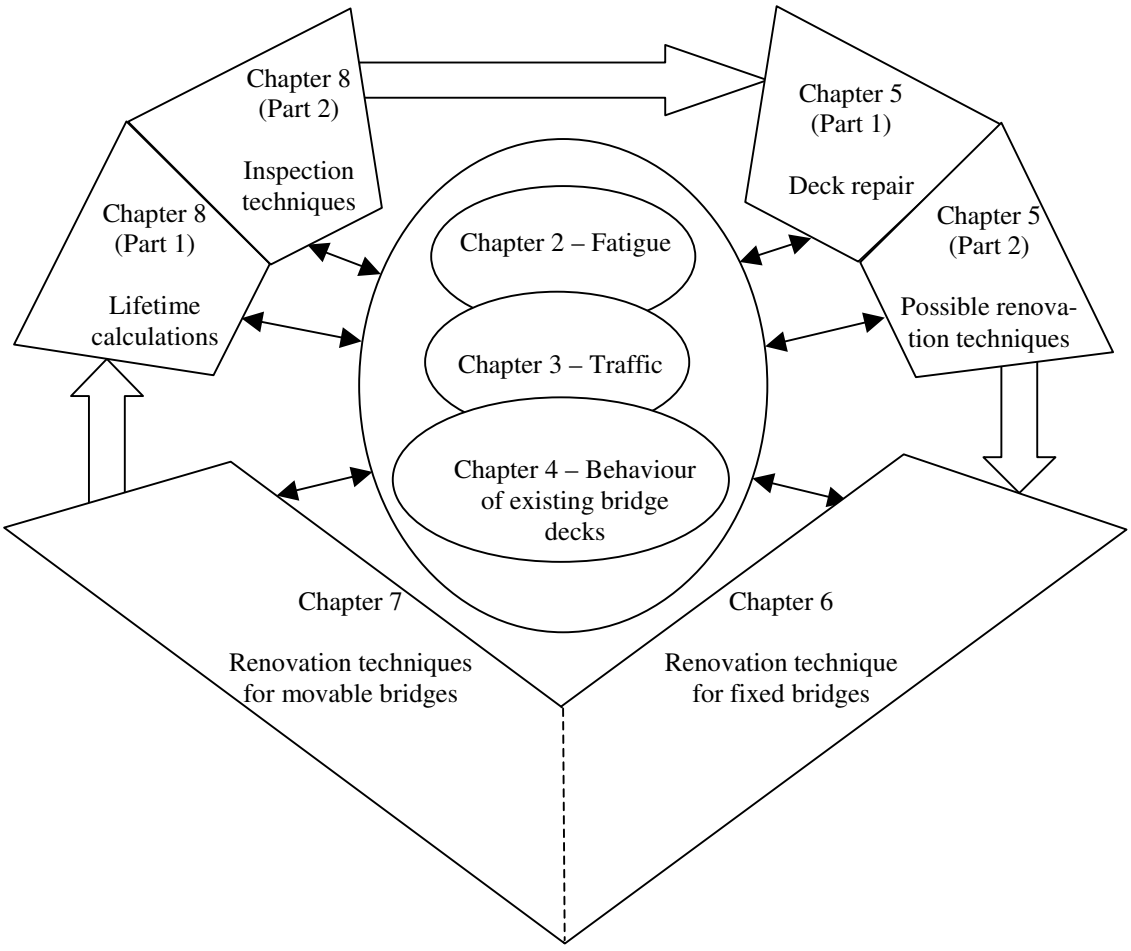

Figure 1-4: Scheme of the thesis

Chapter 2 is entitled ‘Orthotropic bridge decks; history and fatigue modes’ This chapter gives an introduction to the orthotropic steel bridge deck, descriptions of the development of this bridge deck structure in the 20th century and the components and their structural behaviour. An overview of fatigue phenomena in bridges is given. Several cracks are identified, nowadays the most severe cracks are at deck plate level. The heavy vehicles crossing the bridges cause the fatigue problems. The chapter ends with the conclusion that fatigue phenomena at deck plate level necessitates the development of renovation techniques for orthotropic bridge decks.

Chapter 3 is entitled ‘Traffic loads on bridges’. As heavy vehicles cause the fatigue problems it is obvious that information on the traffic loads is necessary. This chapter deals with the traffic loads on bridges. Aspects of bridge loads that are relevant to fatigue phenomena on deck plate level are discussed. Tyre types used on lorries, and footprint measurement tests with several tyres are described. As fatigue phenomena are related to the amplitude and the number of the stress cycles, knowledge about axle loading is relevant. Both axle load spectra derived from measurements in the past, as well as axle load spectra according to Eurocode 1 - Part 2 are discussed. For fatigue not only the loads but also the number of vehicles and axles is relevant. Parameters related to the number of the stress cycles in bridge decks are discussed.

Chapter 4 is entitled ‘Behaviour of existing orthotropic bridge decks’. This chapter describes the behaviour of orthotropic bridge decks with respect to cracks at deck plate level in detail. These are the cracks in the deck plate itself and cracks in the longitudinal weld between deck plate and trough web. First the local static behaviour of bridge decks is described. This is about the local stress distribution in the deck plate at the crossbeam location under wheel loading, the influence of the surfacing on the stresses in the deck plate and the ultimate load capacity of the deck plate with fatigue cracks in the deck plate under wheel loads. The second part of this chapter is about the fatigue behaviour of bridge decks at deck plate level; a literature survey and a description of fatigue tests for deck plate cracks that have been performed. The third part of chapter 4 describes a test program that has been performed in the Lintrack, a heavy vehicle simulator with running wheel load. Tests are performed on full-scale bridge deck panels, with different tyres, different loads, with and without surfacing layers, at different temperatures.

Chapter 5 is entitled ‘Deck repair and possible renovation techniques’. The first part of this chapter is about a research program into submerged arc welding (SAW) for deck plate cracks. Parameter settings for the welding process have been determined and additionally the fatigue behaviour of SAW welds is determined. This paragraph about SAW welding is located in this chapter for the simple reason that if there are cracks in the deck plate, the first step is repairing

the cracks. Subsequently a renovation technique can be applied to the whole bridge deck to enhance the lifetime of the bridge. In the second part of this chapter requirements are formulated for the development of the renovation techniques, and an overview of several ideas for renovation techniques is given. At the end of this part a few techniques have been selected for further research.

Chapter 6 is entitled 'Renovation method for fixed bridges – Reinforced High Performance Concrete'. In this chapter a solution that extends the lifetime of the orthotropic deck structure is described. In this solution the asphalt surfacing is removed and replaced by a layer of approximately the same thickness of reinforced high performance concrete (RHPC). The RHPC surfacing is reinforced with traditional bars and with steel fibres. Results of FE-models are discussed. Primary interest is the reduction of the stress in the steel deck plate due to the replacement of the asphalt surfacing by a RHPC surfacing. Material aspects and the interface layer between original steel deck plate and concrete surfacing are described. Several tests were done in the laboratory during the development stage of the RHPC surfacing layer; application tests, static tests and fatigue tests. After the test in the laboratory a pilot project on the Caland Bridge was carried out. On this heavily loaded bridge the RHPC surfacing was applied instead of the asphalt surfacing. Stress spectra measurements under normal traffic conditions were performed on this bridge before and after the renovation. These measurements are described.

Chapter 7 is entitled 'Renovation methods for movable bridges'. In this chapter three solutions for movable bridges that extend the lifetime of the orthotropic deck structure are described. These three methods, which reduce the stress ranges, are:

- Bonding a second steel deck plate to the old steel deck plate. The general idea of this method is that the deck plate becomes stiffer.
- Filling the troughs in the wheel tracks with polyurethane. The general idea of this method is that the deck plate becomes continuously supported.
- Application of an ultra high performance concrete layer to the top of the steel deck plate. The general idea of this method is that the deck plate becomes stiffer.

For all three methods tests and calculations are reported.

Chapter 8 is entitled 'Design and maintenance philosophy'. Previous chapters in this thesis are mainly focused on the behaviour of existing bridges and the development of renovation techniques. This chapter deals with other subjects, which are also necessary for a successful implementation of the maintenance philosophy. First a description of the proposed maintenance philosophy and its probabilistic background is given. Besides renovation techniques lifetime calculations and inspection techniques are also necessary. Systematic lifetime calculations of steel bridge decks are presented, including the influence of asphalt

surfacing. In addition this chapter describes in brief several inspections methods. Although the development of inspection techniques is outside the scope of the thesis, inspection techniques are of course also necessary for a successful implementation of the proposed strategy.

2. Orthotropic bridge decks; history and fatigue modes

2.1 Introduction

This chapter gives an introduction to the orthotropic steel bridge deck and describes its development in the 20th century. The components and the structural behaviour are described with an overview of fatigue phenomena in bridges. Several cracks are identified. Cracks at deck plate level are nowadays the most severe cracks. This chapter ends with the conclusion that fatigue phenomena at deck plate level necessitates the development of renovation techniques for orthotropic bridge decks.

2.2 Orthotropic steel bridge decks

2.2.1 Historical development

In the third decade of the 20th century, engineers in Germany and the USA were searching for an alternative to timber and concrete decks supported by stringers and crossbeams. They considered steel decks to be a promising alternative. The objectives were cost savings by a reduction of the steel mass and a reduction in weight, which affects the support structures such as piers, abutments etc. (Wolchuk, 1963), (Weitz, 1974), (Leendertz, 2003)

Battle deck

The first generation of steel bridge decks developed was the “Battle deck” concept. Figure 2-1 shows a typical cross-section of the battle deck construction. The deck consisted of a steel plate with a thickness of 10 to 20 mm, connected with welds to longitudinal I-beams at centre-to-centre distances of 250 to 850 mm. In these decks the crossbeam distances varied from 4.5 to 7.5 m. An asphaltic wearing course was used on the deck plate. The deck plate has two functions: 1. Supporting the traffic loads and distribution of the loads to the stiffeners. 2. Providing additional area to the top flange of the stiffeners (I-beam).

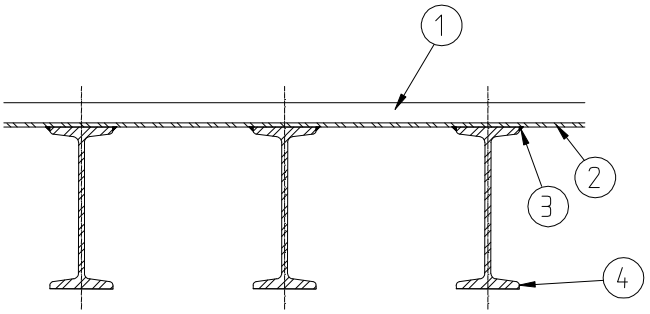

Figure 2-1: Cross-section of the battle deck. 1) wearing course, 2) deck plate, 3) longitudinal weld, 4) I-beam.

Beam grid deck

A further development was a deck structure with inverted T-beam stiffeners in the longitudinal and transverse directions, see Figure 2-2, with an asphaltic wearing course on the deck plate. The deck plate had three functions: 1. Supporting and distributing the traffic loads to the longitudinal and transverse stiffeners. 2. Providing a top flange for the longitudinal stiffeners. 3. Providing a flange for the transverse stiffeners. The system worked as an orthogonal anisotropic plate, abbreviated to orthotropic deck. Figure 2-2 shows a typical cross-section of the beam grid deck. There are only a few motorway bridges with battle deck or beam grid deck systems in the Netherlands.

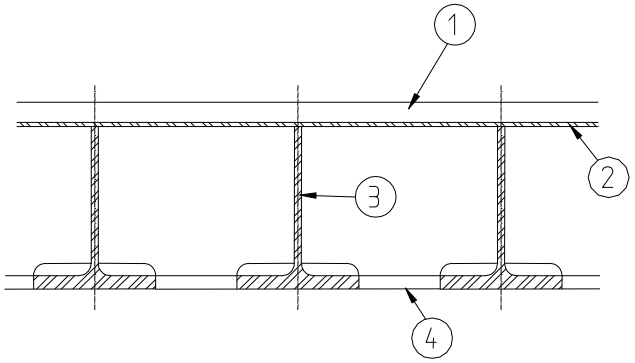

Figure 2-2: Cross-section of the beam grid deck: 1) wearing course, 2) deck plate, 3) T-sections in longitudinal direction, 4) T-sections in transverse direction

Open stiffeners

The search for a more economic use of materials and a reduction in labour needed for fabrication and assembly resulted, after the 2nd World War, in the orthotropic steel deck with open stiffeners and later on the orthotropic steel deck with closed stiffeners. The commonly used open stiffeners are strips, bulb profiles and angles. They are welded to the deck plate

with fillet welds in the longitudinal direction. Usually these stiffeners are continuous and pass through cut-outs in the crossbeams, often with cope holes. The cut-out is the part of the crossbeam web plate that has been removed to allow the stiffener to pass through. The minimum cut-out is the cross-section of the longitudinal stiffener. Sometimes the cut-out is larger than strictly necessary to allow the stiffener to pass through. This additional part of the cut-out is called a cope hole. Cope holes are used to ease fitting of the stiffener or to provide welding access. Open stiffeners are used for maximum spans of approximately 2 to 3 m. Figure 2-3 shows a cross-section of a deck with three types of open stiffeners

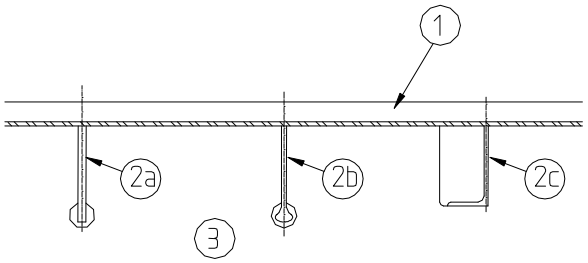

Figure 2-3: Cross-section of a deck with three types of open stiffeners: 1) wearing course, 2a) strip stiffener, 2b) bulb stiffener, 2c) angle stiffener, 3) crossbeam web

Closed stiffeners

The commonly used closed stiffeners can have a V-shaped, U-shaped or a trapezoidal cross-section, see Figure 2-4. Sometimes in the past the V-shaped stiffeners had an extension, so that the stiffener cross-section takes the form of a wineglass. This stiffener arrangement has been used often in Germany and is there known as the “Sektkelch” profile. The stiffeners are welded to the deck plate in the longitudinal direction.

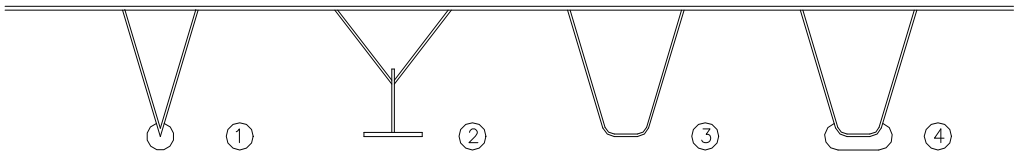

Figure 2-4: Different types of closed profiles

The closed stiffeners may be fitted between the crossbeams or may be continuous, passing through cut-outs in the crossbeam, or passing over supports at the crossbeam, the so-called floating deck structure. In many cases the cut-outs are enlarged with cope holes as a solution for fitting problems. Closed stiffeners are used for spans from approximately 3.0 up to 5.0 m. Figure 2-5 shows continuous trapezoidal stiffeners through three types of cut-out. Where closed stiffeners are used, the connections between stiffener and deck plate are only welded

from one side. The connection between an open stiffener and a deck plate is welded from both sides. Due to the large reduction in welding activities for closed stiffeners these types have been used in almost every orthotropic bridge deck built since approximately 1965.

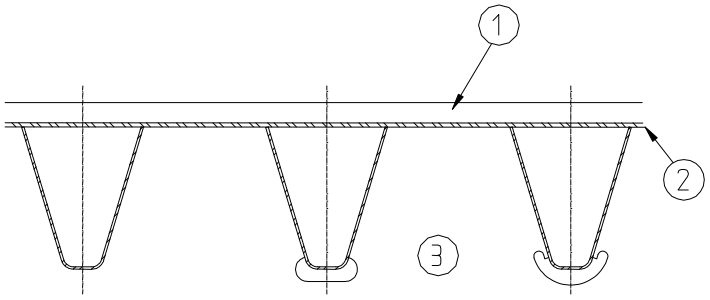

Figure 2-5: Cross-section of a deck with closed trapezoidal stiffeners through three types of cut-out. From left to right: a close fit, an oval cope hole and a "Haibach" cope hole (Haibach, 1983). 1) wearing course, 2) deck plate, 3) crossbeam web.

Steel bridge decks built in the Netherlands

In the past many orthotropic steel bridges have been built. Figure 2-6 gives an overview of the building history of steel bridge decks for motorway bridges in the Netherlands. The figure shows that the vast majority of these bridges, 70% up to 80%, were built between 1960 and 1980. Some carry traffic in both directions, others only carry traffic in one direction and thus two bridges are constructed: one for each traffic direction. Each bridge length is multiplied by the number of traffic directions on that bridge. This has led to the summarized lengths given in Figure 2-7. Note that the length of the bars for fixed bridges in this figure is divided by a factor 10. This length represents in general the total length of the heavy vehicle lanes. The orthotropic deck structure in the Netherlands is used for box-girder bridges, plate girder bridges, cable stayed bridges, tied arch bridges and truss bridges.

On the network of motorways in the Netherlands there are approximately 100 steel bridges, divided into movable and fixed types. There are many more steel bridges on the secondary road network. However fatigue is not a serious problem for the bridges on secondary roads, only the traffic flow of lorries on the motorways induces noticeable fatigue phenomena (De Jong, 2003, 2004-b, 2004-d). The deck plates of the majority of these bridges are stiffened with a trapezoidal trough profile. Most fixed bridge steel decks in the Netherlands are built with a deck plate thickness of 10 mm and almost every fixed bridge is surfaced with a mastic asphalt layer approximately 50 mm thick. Movable bridges are mainly built with a deck plate thickness of 12 mm. In the past, deck plate thicknesses were generally determined by the static capacity of the deck plate under maximum wheel loads and not by fatigue verification.

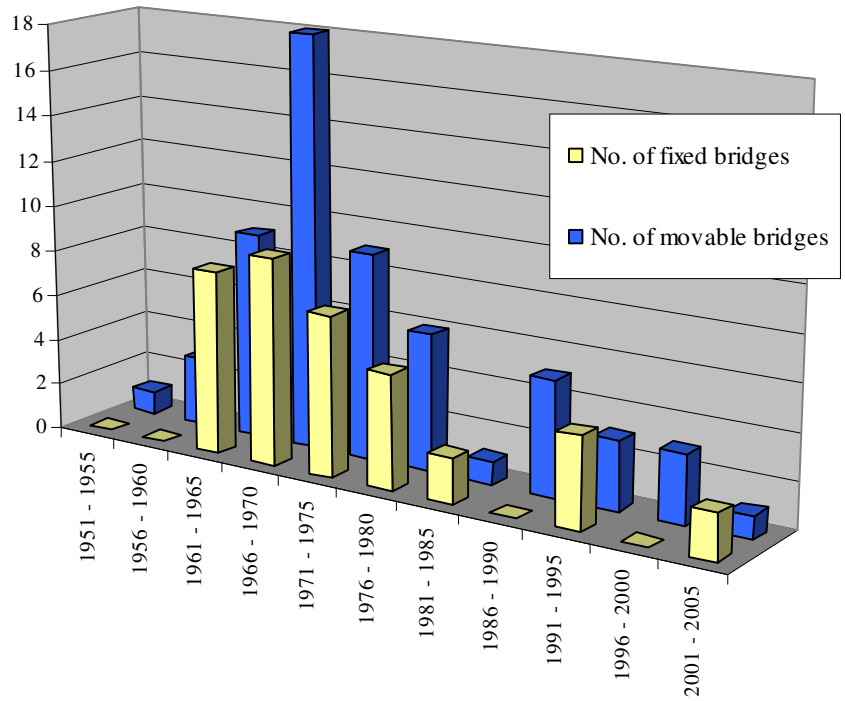

Figure 2-6: No. of fixed and movable bridges built in motorway bridges in the Netherlands

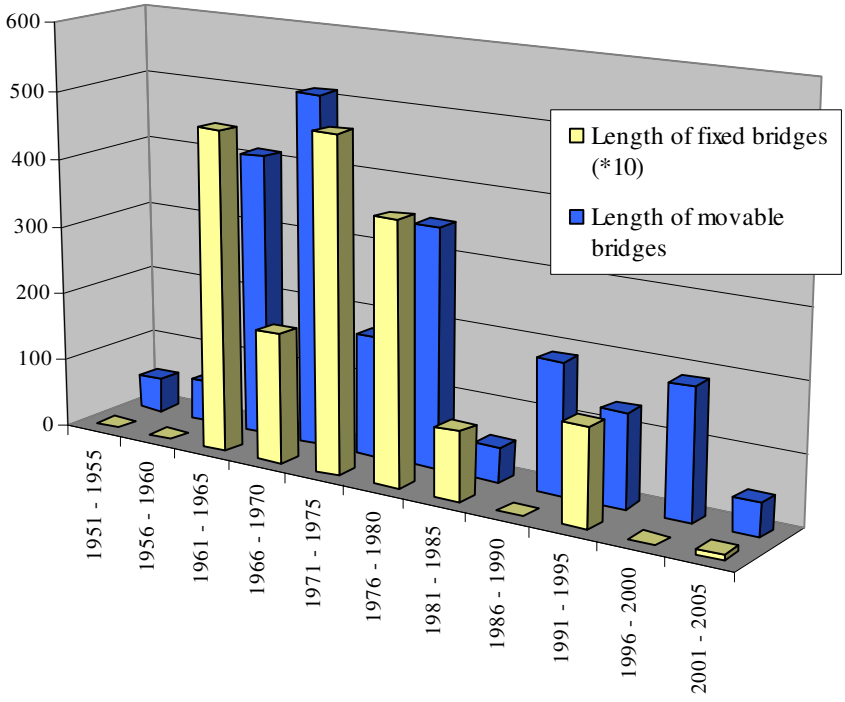

Figure 2-7: Summarized length of steel bridge decks in motorway bridges in the Netherlands

Orthotropic bridge decks in other countries

The majority of orthotropic decks for motorway bridges in Germany were also built between 1960 and 1980. Paschen has reported on fatigue and corrosion damage in German steel motorway bridges (Paschen, 1995). The report covers 27 bridges. From these bridges 8 are constructed with open stiffeners, 8 with the so-called "Sektkelch" profile and 11 with the closed trapezoidal profile. The total length of these bridges is about 20000 m but because each of the reported bridges carries traffic in two directions, the summarized length is about 40000 m. Steel bridge decks in Germany are mainly used for fixed bridges. Orthotropic decks in Germany normally have deck plate thicknesses of 12 or 14 mm and a surfacing layer of approximately 70 mm. A comparison between German and Dutch fixed bridges shows that German bridges have thicker plates and surfacing, and so are more robust. While Dutch engineers were highly motivated to continually reduce the weight of the bridge, German engineers were more focused on a strong and reliable bridge. This difference in engineering traditions explains the differences in chosen deck plate thicknesses.

In France the Normandy Bridge was constructed in the early nineties and the Millau viaduct is constructed a few years ago, opening for traffic in late 2004. The Millau viaduct crosses the river Tarn, has a total span length of 2460 m and is a multi cable-stayed bridge, with seven pylons. The bridge deck is a box girder with an orthotropic deck using trapezoidal stiffeners (Virlogeux, 2004-a, 2004-b).

The world's longest suspension bridge and one of the world's longest cable-stayed bridges are both in Japan. The Akashi Kaikyo suspension bridge (central span: 1991 m) and the Tatara cable-stayed bridge (central span: 890 m) were completed at the end of 20th century (Fujino, 2002-a). Both bridges have an orthotropic deck structure. (Honshu Shikoku Bridge Authority, 2005). Another major orthotropic bridge is the Trans-Tokyo Bay Highway Crossing, completed in 1997. This bridge is 11 km in total length and is a combined tunnel and multiple bridge route that includes a ten-span continuous steel box-girder bridge with a total length of 1630 m. (Fujino, 2002-b).

In Great Britain there are also many orthotropic decks in motorway bridges. Two well-known examples are the Severn crossing, a cable-stayed bridge and the Humber Bridge, a large suspension bridge.

2.2.2 Construction orthotropic bridge decks

The orthotropic bridge structure is used both for fixed and movable bridges. Figure 2-8 shows this structure, which has in general four main structural components:

- The deck plate

- The longitudinal stiffeners, generally closed trough profiles
- The crossbeams, also called floor beams
- The main girder

A surfacing layer is applied on top of the deck plate for both corrosion protection and skid resistance purposes.

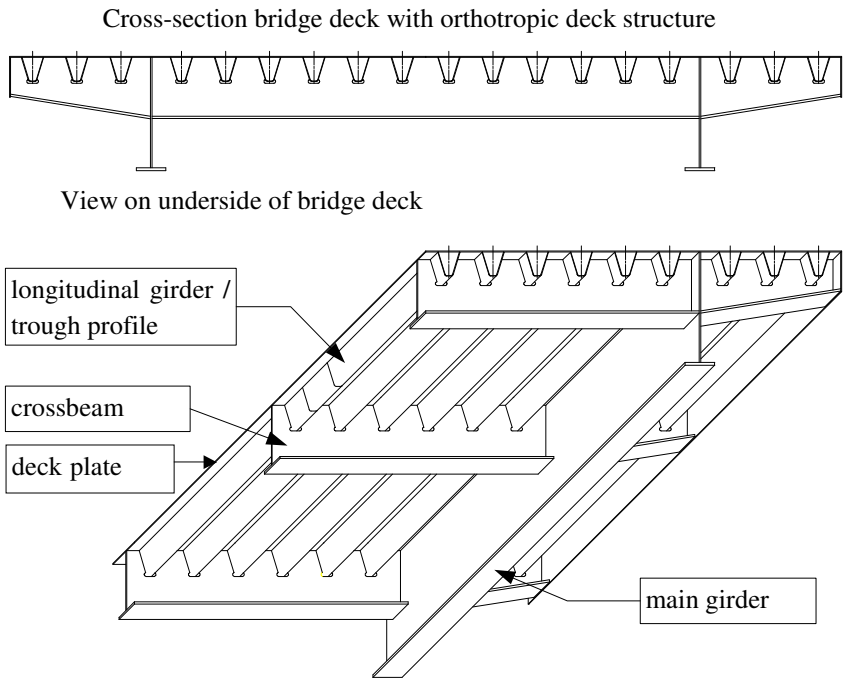

Figure 2-8: Orthotropic bridge deck structure, plate girder bridge

The orthotropic bridge deck is an integrated load carrying system (Wolchuk, 1963) and the deck plate is an essential part of the system.

The deck plate is the structural component, which directly supports the wheel loads and transmits these loads to the ribs, e.g. the webs of the longitudinal trough profiles. The webs of the troughs are spaced at 300 mm, for almost every bridge in the Netherlands and for many bridges in the rest of the world.

The deck plate forms the top flange of the longitudinal girder. This longitudinal girder is built up from the deck plate and the trough, which are welded together with longitudinal welds. The longitudinal girder transmits the wheel loads to the crossbeams.

The deck plate also forms the top flange of the crossbeams, which are generally spaced from 3

to 5 m apart. The crossbeams are the structural members that transmit the axle loads to the main girders.

The main girders are the components that transmit the vehicle loads to the bridge supporting structure. Figure 2-8 shows a relative simple plate girder bridge. It is also possible that the main girder system is a box girder, a cable stayed system, a tied arch, or a truss. In almost every main girder system the deck plate is an essential part of the load carrying system. For the plate girder bridge shown in Figure 2-8, the deck plate acts as the top flange of the main girder and it is possible that some troughs act as part of the top flange, depending on its effective width. For a self-anchored cable stayed bridge it is possible that the deck plate is in compression. For a tied arch bridge it is possible that the deck plate is part of the tension zone.

The deck plate system and the crossbeam system generate a transverse stress in the deck plate. The longitudinal girder and the main girder generate a longitudinal stress in the deck plate. For the design of an orthotropic bridge these four load-carrying systems should be analysed separately. For each system the stresses in the deck plate should be calculated. The calculated stresses should be combined conservatively for the check of the load carrying capacity.

2.3 Fatigue cracks in orthotropic bridge decks

2.3.1 Introduction

In the last decades several fatigue cracks have been detected in the deck structure of bridges. The cracks described in the following paragraphs are not the only ones that are possible in orthotropic bridges. Orthotropic bridges have been built in several ways, and there are many different details and typical connections. Therefore there are also many different types of cracks. The research presented in this thesis is directed towards cracks at the deck level of bridges with closed stiffeners and consequently crack types at other locations in the bridge structure are not extensively described. The cracks in the deck structure have been defined and divided into four categories:

1. Cracks in the deck plate
2. Cracks in the longitudinal weld between deck plate and trough web
3. Cracks in the trough splice joint
4. Cracks in the connection between trough profile and crossbeam

This thesis deals with cracks at deck plate level, which are those defined in category 1 and 2 above. These four crack types are briefly described, each description has four parts:

- An introduction, which explains the exact location of the crack in the deck structure.
- The mechanical background of the crack growth process.

- Visual observations for that specific crack type.
- A short list of bridges where that crack type has been observed .

2.3.2 Fatigue cracks in the deck plate

Introduction

The most frequently observed fatigue crack is located in the deck plate where the crossbeam crosses the trough girder. This crack is shown in Figure 2-9. The growth of this crack can be divided into three phases. Figure 2-10 shows these three crack phases. The crack initiation (phase 1) is at the root of the longitudinal fillet weld between the trough web and the deck plate at the intersection of the crossbeam and the continuous closed trapezoidal stiffeners. After initiation the crack growth is in a vertical direction from the underside to the top of the deck plate (phase 2). After the crack has grown through the deck plate it grows in the horizontal/longitudinal direction (phase 3). The crack has a semi-elliptical surface appearance. Various inspections and NDT tests (Schat, 1997-a, 1997-b, 1997-c) have shown that the length of the cracks on the underside of the deck plate is approximately four times the deck plate thickness longer than the crack length at the top surface.

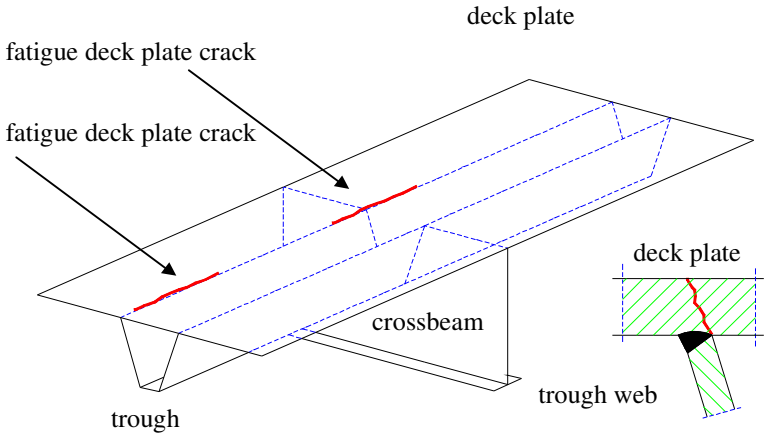

Figure 2-9: Deck plate cracks

Figure 2-9 also shows a deck plate crack at another location. This crack is roughly the same as the crack at the crossbeam location. The difference is that this crack appears in the area between the crossbeams, instead of the intersection of trough and crossbeam. Another difference is that this crack grows simultaneously in the vertical (phase 2) and horizontal directions (phase 3). The consequence is that long invisible cracks are likely to grow. This was observed on the Van Brienenoord Bridge in 1997 and on the movable part of the Caland Bridge in 2001. Deck plate cracks between the crossbeams have only been observed twice

whereas deck plate cracks at the location of the crossbeam web are often observed.

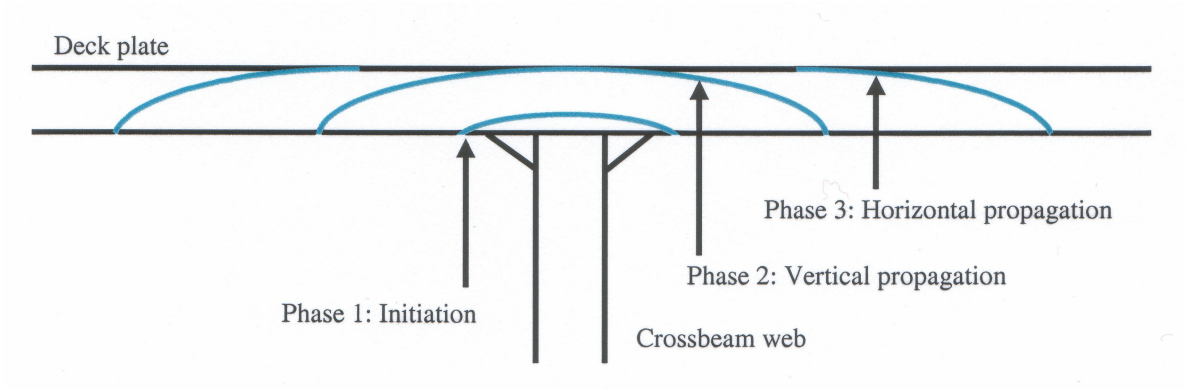

Figure 2-10: Crack growth phases deck plate crack at crossbeam

Mechanical background

The mechanical background of the deck plate crack at the crossbeam is as follows. The crossbeam web only supports the deck plate between the troughs. Between the webs of each trough (inside the trough) the crossbeam web does not support the deck plate, as the trough is continuous through the crossbeam. A local wheel load at the deck plate directly above a trough causes a deflection of the deck plate. The deck plate between two troughs and also the trough webs are welded to the crossbeam web. This causes a clamping moment at the deck plate with high stress concentration factors in the deck plate, when it is loaded with a heavy vehicle wheel. Due to this construction and clamping moments high local bending stresses will arise, thus causing fatigue cracks in the deck plate.

The mechanical background of the deck plate crack between the crossbeams differs significantly. The deck plate can be modelled as a multiple span girder over elastic supports. The supports are the webs of the trough profiles. The stress concentration effect or clamping moment do not arise for the crack between the crossbeams, therefore stress ranges in the deck plate are lower for this crack type. This crack type is thus a less severe fatigue problem than the deck plate crack at the crossbeam.

The deck plate cracks may be a threat to the safety of the deck structure. This threat arises only if cracks grow very large, e.g. when the cracks are through the thickness of the deck plate and have reached the critical length in longitudinal direction, see chapter 4. In the case of a crack with a critical length there is a risk of an indentation or a hole in the deck plate due to a heavy local wheel load. Because the deck plate is an integral part of the crossbeam, where it acts as the top flange, there is also a risk that the load bearing capacity of the crossbeam is insufficient for a heavy truck.

The deck plate cracks appear both in decks of fixed bridges with a thick asphaltic surfacing as well as in decks of movable bridges that are usually surfaced with a thin epoxy layer. The presence of a thick asphaltic layer however reduces the magnitude of the stress cycles hence resulting in a longer lifespan. Thin epoxy layers do not reduce the stress ranges in the deck plate and consequently have no effect on the lifespan of the deck structure.

Visual observations

Visual observation is one of the important methods of detecting fatigue cracks in the deck plate. Three major advantages of visual observations are the low cost, the speed of execution and that there is no need to remove surfacing layers. Due to the fact that the deck plate cracks initiate at the inside of the closed trough profile, at the root of the longitudinal weld, cracks are only visible in phase 3 of the growth process, when the cracks have grown through the deck plate and have a significant length on the top of the deck plate. This is the major disadvantage of visual observation. Detecting fatigue cracks in phases 1 and 2 is possible with non-destructive inspection technologies (NDT), see Chapter 8. In visual observations a distinction is made between cracks in movable bridge decks with a thin epoxy surfacing layer and cracks in bridge decks with a thick asphaltic surfacing layer.

Visual observations movable bridges

Figure 2-11 is a photograph of the visually observed cracks in the Van Brienenoord Bridge in summer 1997. Damage to the epoxy surfacing in the wheel tracks of the heavy vehicle lane is the first indication of deck plate cracks. The locations of the trough webs under the deck plate at a centre-to-centre distance of 300 mm are clearly visible. Figure 2-12 shows a detail of a visual observation. Also visible is the crack in the steel deck plate. Deformation of the steel deck plate at the crack location is the reason for this visibility. The length of the crack shown is approximately 50 cm.

Cracks become visible when they have a length of approximately 10 cm at the top surface of the deck plate see also paragraph 8.5.2. In this stage of the crack growth process the steel plate on both sides of the cracks is not deformed and the crack is more difficult to see, because it really is a hairline crack with small dimensions. The first visible indication of deck plate fatigue cracks are often brown lines on the epoxy surfacing at the location of the trough webs, indicating corrosion of the steel deck plate. If the epoxy wearing surface is not significantly damaged, but a brown discolouration from corrosion of the steel deck plate is visible, the epoxy surfacing can be removed locally with a chisel, to inspect the steel deck plate under the epoxy surfacing.

Figure 2-11: Visual observation of deck plate cracks in movable bridge

Figure 2-12: Detail visual observation of deck plate crack in movable bridge

Visual observations fixed bridges

Deck plate fatigue cracks in bridge decks with a thick asphaltic surfacing are more difficult to detect because visual observations of the asphalt layer are difficult to interpret. Factors, which govern the deterioration of the asphalt layer are its age, thickness and stiffness, the thickness of the steel deck plate, and the fatigue cracks in the steel deck plate. Therefore a lot of experience and skill is needed to determine the causes of a deteriorating asphalt structure. It is difficult to judge whether visually observed damage in the asphalt layer is due to fatigue deck plate cracks or to other causes.

Almost every fixed bridge in the Netherlands has a deck plate thickness of 10 mm, and the centre-to-centre distance between the trough webs is usually 300 mm. Furthermore almost every fixed bridge has a mastic asphalt surfacing layer approximately 50 mm thick. In cases where the construction differs from this standard arrangement, careful interpretation of visual observations is required. Reiterating, visual observations of the surfacing layer can only detect deck plate cracks that have already grown through the deck plate (phase 3).

Figure 2-13 shows a photograph of the asphaltic surfacing of the Caland Bridge on the A15 in the harbour area of Rotterdam. This photograph shows severe damage in the asphaltic surfacing. At some locations the asphalt is broken into pieces and at these locations fatigue crack growth through the deck plate is possible. On the other hand the total degradation of the asphalt layer points towards ageing of the asphalt structure. Because deck plate cracks had already been observed several times before on the Caland Bridge, the bridge owner wanted to be on the safe side. Therefore the asphalt layer was removed at the most damaged locations. A subsequent NDT inspection showed that no fatigue cracks had grown through the deck plate. The damage to this surfacing layer is mainly due to ‘normal ageing’ of the asphalt. After this NDT inspection a new asphalt layer was applied.

Figure 2-13 also shows some very long longitudinal cracks in the asphalt layer. The distance between these cracks is approximately 300 mm, which is the centre-to-centre distance between the trough webs. This mode of cracking of the asphalt surfacing is generally not an indication of fatigue cracks in the steel deck. The deck plate thickness of 10 mm is relatively small and wheel loads of heavy vehicles cause a deflection of the steel deck plate and the surfacing layer. This deflection produces a strain in the surfacing layer and the maximum strain occurs at the locations of the trough webs. In some circumstances this strain exceeds the ultimate strain of the asphaltic material and at that moment a crack in the asphalt layer is generated. These longitudinal cracks in the asphalt layer have been observed at several bridges, even on relative new bridges with a moderate traffic flow, and also in relative new surfacing layers.

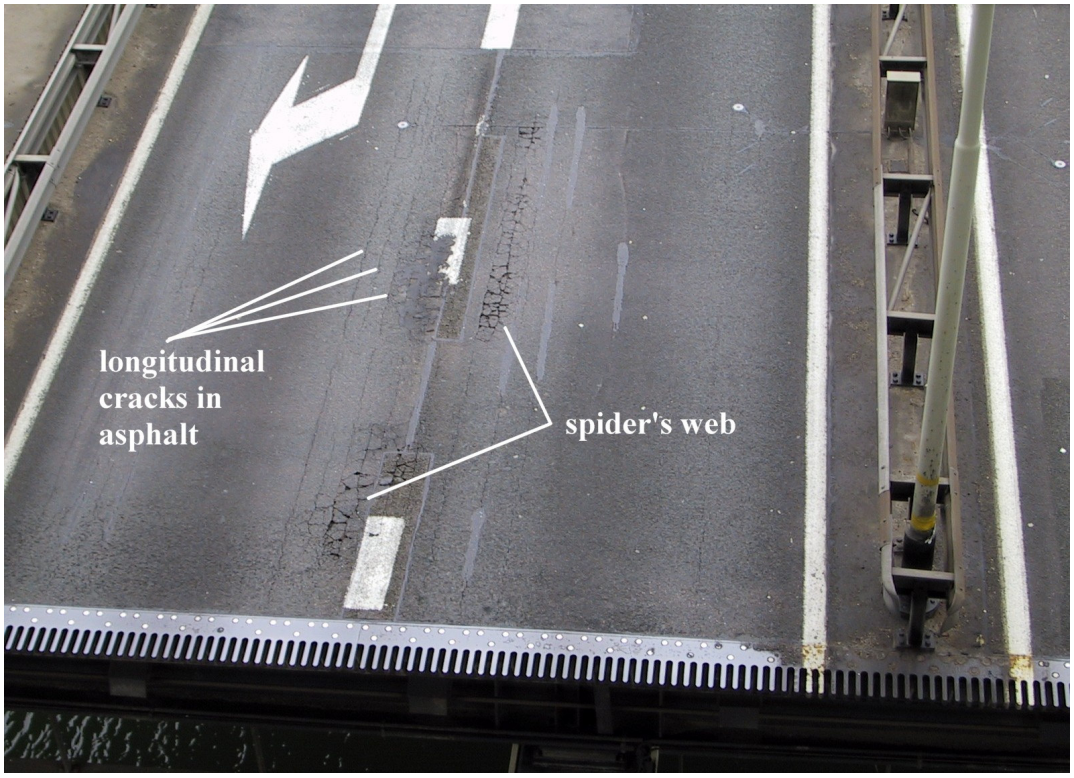

Figure 2-13: Visual observations possibly indicating deck plate cracks in fixed bridge

Figure 2-14 shows a kind of spider's web in the asphalt layer. This observation in combination with a relatively good condition of the rest of the asphalt layer may be an indication of a deck plate crack that has grown through the deck plate. These kinds of spider's webs have been observed several times on several bridges. Usually the asphalt layer is removed at those locations and a NDT inspection is carried out. Sometimes cracks that have grown through the deck plate have been found, but cracks that have initiated but not so far grown through the deck plate have also been found. In other cases no cracks were found.

On the Hagestein Bridge on the motorway A27 (Utrecht-Antwerp) a kind of spider's web was visible. After the removal of the asphalt structure and blasting the deck plate the crack shown in Figure 2-15 was visible. The length of this crack was 65 cm. A few repair techniques are available for this crack type. The simplest solution is a weld at the crack location. Another solution is to weld a plate on top of the deck plate and then apply a new asphalt layer. The disadvantage of both solutions is the poor fatigue behaviour. The advantage however is the speed of execution. Both solutions are therefore temporarily. These repair techniques and other techniques are described in (Boersma, 2003).

In normal situations the deck plate crack grows in the longitudinal direction along the trough

web–deck plate connection. Figure 2-15 shows a rather strange crack tip at the right side of the photo. It turned out that a stiffener splice joint is located on the underside of the deck plate at this position. Due to this joint a discontinuity occurs in the deck plate, which is responsible for the strange crack tip.

Figure 2-14: Visual observations possibly indicating deck plate crack

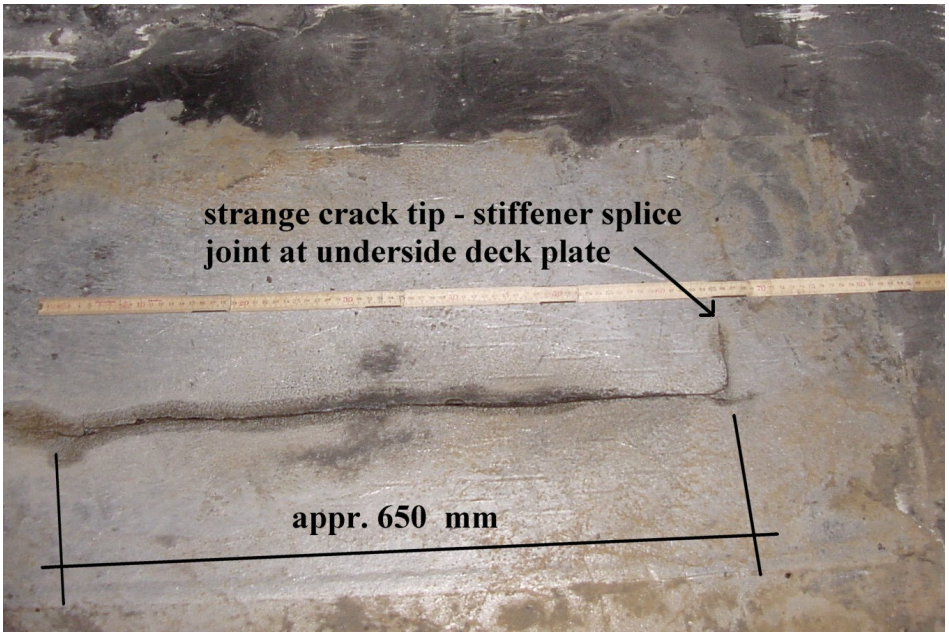

Figure 2-15: Deck plate crack after removal asphalt layer

Detected cracks

The first deck plate cracks in the Netherlands were discovered in 1997 in the Van Brienenoord bascule bridge. This bridge was the first where this kind of crack occurred. Since 1997 deck plate cracks have been detected by visual observations in several bridges. These bridges have been inspected very regularly since 1997. Table 2-1 summarizes the bridges in the Netherlands with fatigue cracks in the deck plate, which have already grown through the deck plate. On some bridges one single crack or a few cracks are detected while on other bridges many cracks have been detected. It is known from NDT inspections that on several other bridges phase 2 cracks are growing. Cracks in the deck plate in other countries have only been reported from Japan (Machida, 2004), (Yuge, 2004), (Miki, 2006).

Table 2-1: Detected deck plate cracks in the Netherlands

Bridge	Built	First visually observed fatigue crack	Years in service before first crack
Ketel Bridge, movable	1968	1998	30
Scharsterrijn, movable	1972	2002	30
Van Brienenoord, movable	1990	1997	7
Caland Bridge, movable part	1969	1998	29
Bridge Zijkanaal C, movable	1969	2003	34
Schinkel Bridges, movable	1970	2004	34
Caland Bridge, fixed part	1969	2002	33
Bridge Hagestein, fixed	1980	2002	22
Galecopper Bridge, fixed	1971	2002	31
Juliana Bridge, movable	1966	2001	35
Bridge Scharberg, fixed	1973	2003	30
Moerdijk Bridge, fixed	1976	2001	25
Tied arch Bridge Beek	1968	2004	36

The difference between the observations in the Netherlands and other countries raises the questions of whether this is a local problem and why deck plate cracks are not observed in other European countries. An understanding of the nature of fatigue phenomena reveals that fatigue is very sensitive to the amplitude of the stress ranges. A thicker deck plate and a thicker asphalt-surfacing layer lead to lower amplitudes of the stress ranges.

2.3.3 Fatigue cracks in the longitudinal weld between deck plate and trough web

Introduction

Figure 2-16 shows a fatigue crack in the longitudinal weld between the trough and the deck plate. The crack initiation is at the root of the longitudinal weld between the trough web and the deck plate. The initiation point can be at any location in the longitudinal direction, except at the intersection of the crossbeam and the continuous closed trapezoidal stiffeners. After the initiation phase the crack growth direction is through the weld towards the outer surface of the trough web. After the crack has grown through the weld it grows in horizontal/longitudinal direction along the weld. Provided that the crack length is limited, cracks in the longitudinal weld do not create a threat to safety and the integrity of the deck structure, because the deck plate is still functioning and possibilities exist for the redistribution of loads. It is possible that the crack will grow in a direction other than in the longitudinal weld between deck plate and trough wall, e.g. the crack may grow in the deck plate or in the trough wall. In the case of such irregular cracks there may be a threat to safety.

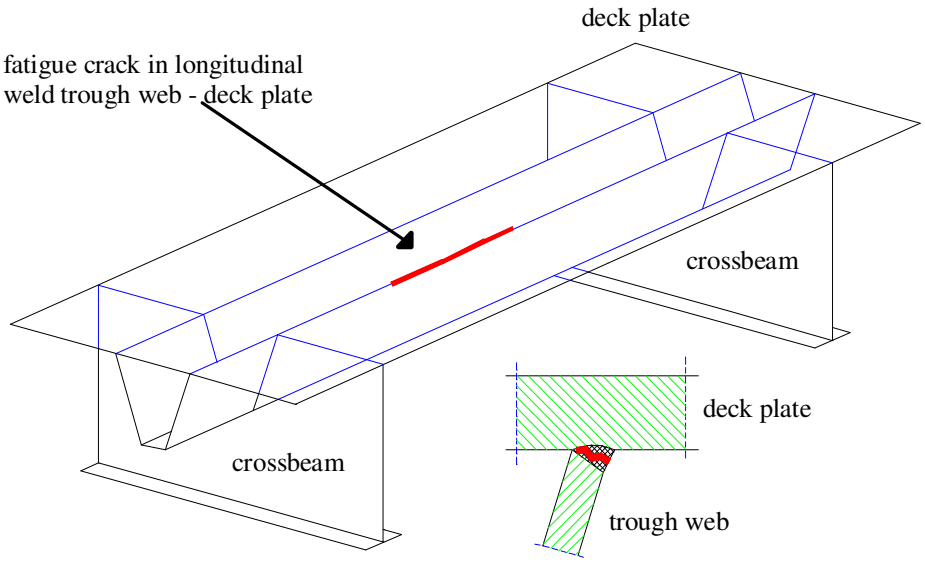

Figure 2-16: Cracks in the longitudinal weld trough-deck plate

Mechanical background

The mechanical background of this crack is as follows. The webs of the troughs support the deck plate. The deck plate is in fact a girder with multiple supports at distances of normally 300 mm. Local wheel loads cause a deflection of the deck plate between the trough webs at the location of the wheel load. The adjacent areas of the deck plate deflect in upwards

direction. Due to these deflections the trough webs are bent.

Due to the limited bending stiffness of the trough profiles, the trough webs are elastic and not rigid supports for the deck plate. The spring stiffness of the supports depends on the distance to the crossbeam. This elastic behaviour results in a maximum deflection at the location of the wheel load. Bending moments in deck plate and trough webs will arise due to these deformations. The bending moment in the trough web results in stresses in the longitudinal weld between deck plate and trough web. This stress in the trough web is the main cause of fatigue cracks in the longitudinal weld.

This crack type appears in the decks of both fixed and movable bridges but the thick asphaltic layer reduces the stress ranges in fixed bridges slightly, resulting in a longer lifespan for fixed bridges. The thin epoxy surfacing used on moveable bridges does not have this effect. The crack growth rate is strongly dependent on the quality of the longitudinal weld. From fatigue tests it is clear that the pre-weld gap between trough profile and the under side of the deck plate is one of the factors determining the fatigue behaviour of the weld (Kolstein, 1996). Another factor is the size of the weld. A full penetration weld shows a much better fatigue behaviour than a 3 mm fillet weld.

Visual observations

Visual observation is the most important method of detecting cracks in the longitudinal weld. The difference from the visual inspection of deck plate cracks is that the inspection must be carried out from the underside of the bridge deck structure. The advantages are low costs and the speed of execution. This type of crack originates from the inside of the trough thus it is only visible when it has grown through the weld and has reached a certain length. Due to the fact that this crack type only threatens the safety in case of very long cracks, inspections are less necessary. For easy visual detection of this type of crack it is very useful to paint the underside of the bridge deck white in the region where heavy vehicles wheel loads pass . Figure 2-17 shows a crack in the weld between deck plate and trough web.

Detected cracks

The existence of cracks in the longitudinal deck plate – trough web welds has been known of for approximately two decades. In the Netherlands the Moerdijk Bridge on the A16 motorway from Rotterdam to Antwerp is a well-known example of a bridge with this crack type. In 1999 the longitudinal welds at the locations of wheel loads were replaced with full penetration welds. In the Netherlands this crack type has already been observed in the Galecopper Bridges, the Kreekrak Bridges, Hagestein Bridge, Scharberg Bridge and several others. The crack type has also been detected in several bridges in other countries. For example,in Germany it has been observed in the Rheinbrücke A40 Duisburg-Leverkusen and the

Rheinbrücke A1 Leverkusen (Paschen, 1995), (Hemmert-Halswick, 2001) and in the UK in the Severn Bridge. (Gurney, 1992), (Paschen, 1995).

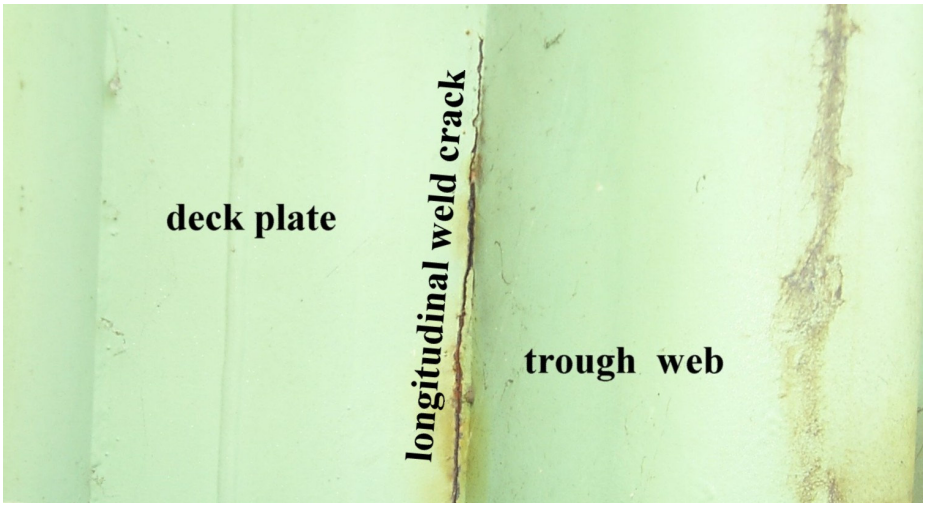

Figure 2-17: Visual observation crack in the longitudinal weld trough – deck plate

2.3.4 Fatigue cracks in the trough splice joint

Introduction

Figure 2-18 shows a fatigue crack in the trough splice joint. This splice joint is made in various ways but the most common detail for fixed bridges in the Netherlands is shown in the figure. The trough splice detail occurs under transverse deck welds and consists of a small length of trough fitted on site between the troughs already welded in the factory. Backing strips facilitate welding.

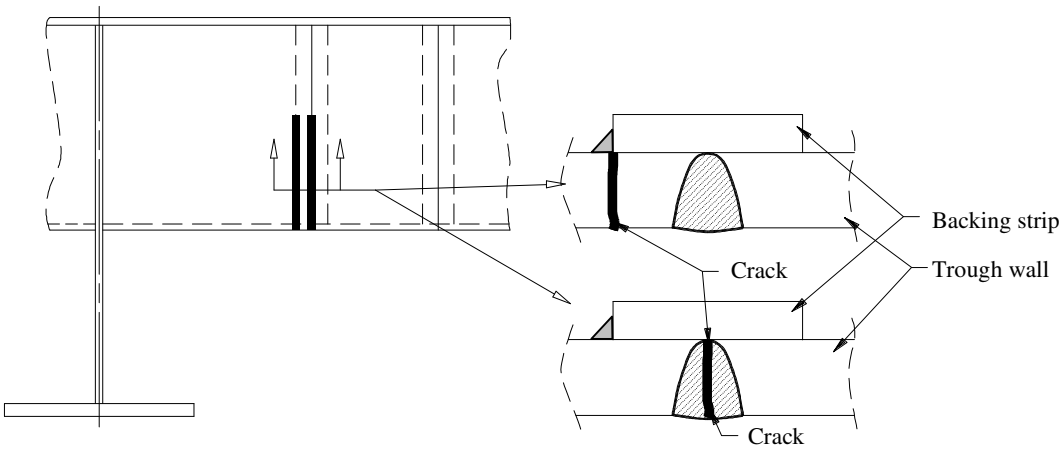

Figure 2-18: Crack in the stiffener splice joint

The crack usually initiates from the root of one of the welds at the bottom of the trough. In several bridges these cracks originating from the root of the full penetration weld have been observed. In some other bridges cracks have been observed in the parent material originating from the weld connecting the backing strip to the trough. Figure 2-18 shows the trough in elevation together with two cross-sections of the trough web. The cracks in the trough wall and in the weld connection are indicated. Cracks in the trough splice joint have been detected in several bridges in the past. Provided that crack dimensions are limited and because of the possibilities for redistributing the loads, this crack type does not threaten the safety. A considerable number of the observed cracks in the trough splice joint are due to poor weld quality.

Mechanical background

The mechanical background of this crack is as follows. Significant bending moments arise in the trough profile due to the passing vehicles and its axles resulting in considerable longitudinal bending stresses in the trough profile. The location of the splice joints in the trough profiles is normally chosen to be in the region with the lowest bending moment ranges. However there are still considerable stress ranges. These stresses in combination with the presence of a backing strip, lack of weld penetration and misalignment result in high stress concentrations. Fatigue cracks initiate at the locations of these stress concentrations. The crack growth rate is strongly dependent on the type and the quality of the weld between the two troughs (Kolstein, 1996, 2001), (Bruls, 1990).

Visual observation

Visual observation is the most important method of detecting cracks in the stiffener (trough) splice joint. The inspection must be carried out from the underside of the bridge deck structure. Figure 2-19 shows a crack in a stiffener splice joint. This crack has already grown relatively large. The crack is clearly visible, due to the movements of the crack and the trough under the traffic flow. At an earlier stage the crack is more difficult to see. For easy visual detection of this type of crack it is very useful to paint the underside of the bridge deck white in the region where heavy vehicles wheel loads pass

Detected cracks

Cracks in the stiffener splice joints have been observed on many bridges in the Netherlands. One of the first bridges where cracks in this joint were observed was the Muiden bridge in 1985. A fatigue crack in the stiffener splice joint occurs sometime during the lifetime of the bridge structure. This indicates that the crack growth is sensitive to the quality of the weld. In Germany this crack type has been observed in the Haseltalbrücke (Paschen, 1995).

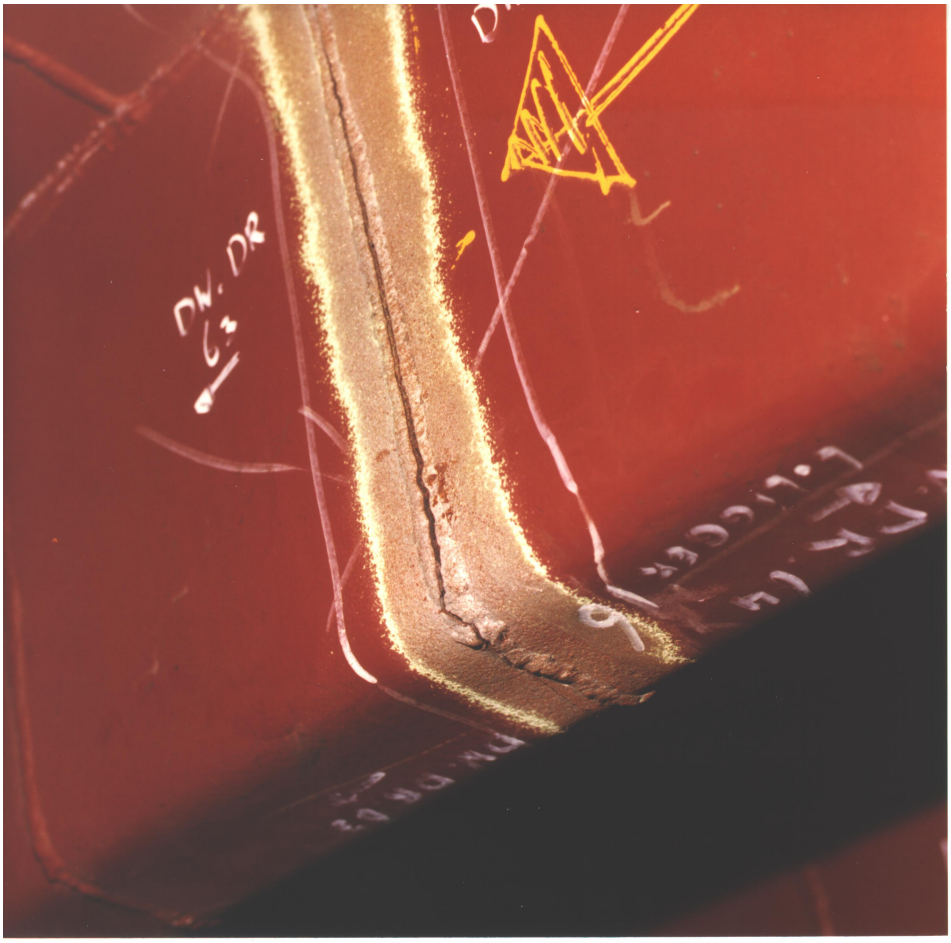

Figure 2-19: Visual observation crack in the stiffener (trough) splice joint

2.3.5 Fatigue cracks in the trough-crossbeam connection

Introduction

The connection between the trough stiffeners and the crossbeam is fabricated in several ways. The designer of a bridge deck decides whether troughs pass through the crossbeams or are fitted between them, and if they pass through, whether additional cope holes are used for ease of fitting or whether there is a close fit etc. Due to the number of options there are several types of trough-crossbeam web connections, and consequently several type of fatigue cracks in this connection. In Figure 2-20 to Figure 2-23 the different types are indicated. For an extensive description of the trough to crossbeam connections, see (Leendertz, 1995, 2003).

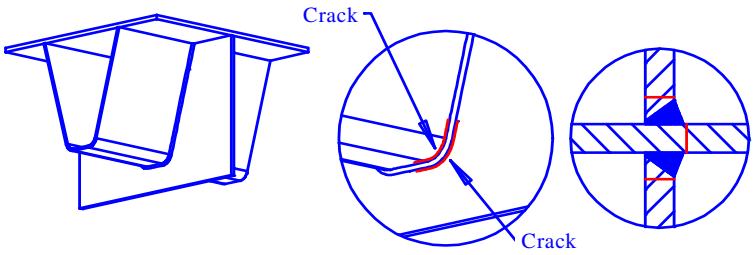

Figure 2-20: Fatigue cracks trough - crossbeam connection, trough fitted between crossbeam

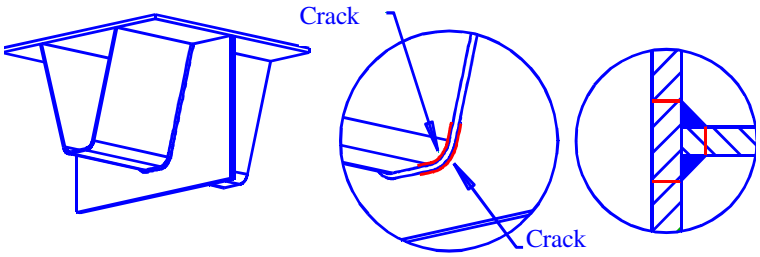

Figure 2-21: Fatigue cracks trough - crossbeam connection, continuous trough passing through the crossbeam

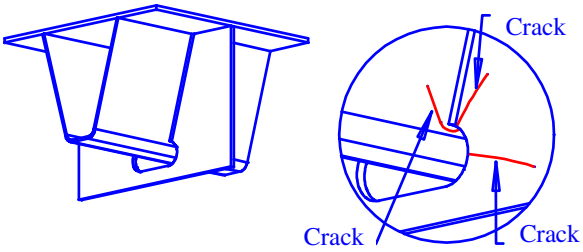

Figure 2-22: Fatigue cracks trough - crossbeam connection, continuous troughs with traditional cope holes

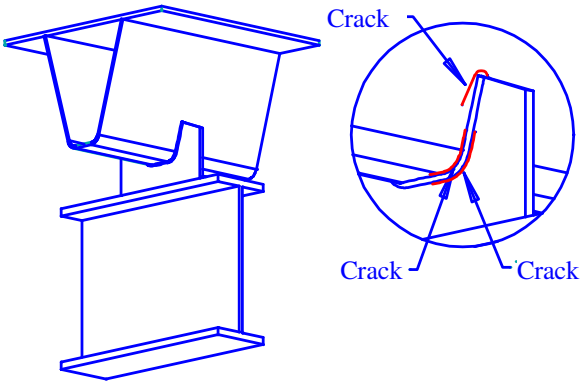

Figure 2-23: Fatigue cracks trough - crossbeam connection, floating deck structure

Mechanical background

In the earliest designs of decks with closed stiffeners, the trough was fitted between the crossbeam webs as shown in Figure 2-20 using a fillet weld. Depending on the resulting geometry of the weld, cracks were observed either at the trough side or the crossbeam side of the weld both in bridges and tests specimens. Analyses and research showed that the fillet welds had low fatigue strength and the increasing traffic flow caused large numbers of stress intervals in the bottom of the trough. The improved version of the detail has full penetration welds as shown in Figure 2-20, which increases the fatigue strength considerably. Specific attention must be paid to the rotation effect of the trough. When the crossbeam web is relatively rigid, this may become a source of fatigue cracks too.

Figure 2-21 shows an improved connection. Here a continuous trough passes through a close fit cut-out in the crossbeam and is welded all round. Although the details show a good behaviour with respect to fatigue generated by bending moments in the trough and the crossbeam "Vierendeel behaviour", the detail is not commonly used because of the small tolerances necessary on the trough and cut-out dimensions. When using the details in bridge structures and in fatigue test specimens, cracks developed as depicted in Figure 2-21 (Kolstein, 2001). Special attention must be paid to the rotation effect of the stiffener, which in case of a rigid crossbeam web may cause high stresses. Tests showed that V-shaped stiffeners were more susceptible to fatigue than trapezoidal stiffeners (Leendertz, 2003).

As a solution to the fitting problems the cut-out in the crossbeam web is enlarged with a cope hole. The traditional cope hole used to have an oval or trapezoidal shape, see Figure 2-22. Research by Haibach and Plasil (Haibach, 1983) resulted in a cope hole with a large radius under the trough and smaller radii near the connection to the trough, see Figure 2-5. In some bridges the original cope hole showed cracks at three locations. In bridges with the improved shaped cope holes no cracks have so far been found in bridges in the Netherlands. Analyses have shown that the improved cope holes result in lower stresses in the cope hole (Leendertz, 1995). Based on experience so far it could be concluded that the cope hole proposed by Haibach and Plasil is for many cases an improvement for the crossbeam web. Careful attention must be paid to the finish of the weld in order to avoid additional stress raisers.

The floating deck structure as shown in Figure 2-23 has been developed to reduce the problems associated with fitting and for easy fabrication and assembly. Until now no cracks have been observed in the depicted potential crack locations. Under traffic loads the deck moves in the transverse direction, which generates bending moments in the trough web and the deck plate. These bending moments cause stress intervals in the trough to deck connection that have to be added to the effects from the wheel loads. For this reason cracks in the longitudinal weld grow relatively fast in floating deck structures. For an extensive description

of the mechanical behaviour of the trough to crossbeam connections, see (Leendertz, 1995, 2003).

It can also be said that provided that the crack dimensions are limited the crack types defined in the trough to crossbeam connection do not threaten the safety, because of the possibilities for redistributing the loads. A considerable number of the observed cracks in the trough to crossbeam connections are due to poor weld quality.

Visual observations

Figure 2-24 shows a visually detected crack in a trough – crossbeam connection. The trough profile passes through the cut-out in the crossbeam web. The crack has already grown from the bottom side of the trough profile to the deck plate. For easy visual detection of this type of crack it is very useful to paint the underside of the bridge deck white in the region where heavy vehicles wheel loads pass

Figure 2-24: Visual observed fatigue crack trough – crossbeam connection

Detected cracks

In several bridges in the Netherlands various cracks in the connection between the trough profile and the crossbeam have been observed. During the lifetime of the bridge structure a fatigue crack sometimes occurs in the connection. If the quality of the welds is constant, the number of observed fatigue cracks should increase exponentially, due to the nature of the fatigue phenomena. This growth has not been observed, which indicates that the weld quality is not constant and that the crack growth is sensitive to the quality of the weld and the fit of

the parts comprising the connection.

Cracks in the trough-crossbeam connection have been observed in some bridges in Germany: Haseltalbrücke, Sinnbrücke Fulda-Würzberg, Rheinbrücke Leverkusen, Hochstrasse A Leverkusen and the Donaubrücke Sinzing. This crack type has also been observed in the Severn Bridge in the UK (Beales, 1979), (Paschen, 1995).

2.4 Conclusions: Need for long term renovation techniques

This chapter has described the development of the orthotropic bridge deck structure and the fatigue phenomena in bridges with these decks. Several types of fatigue cracks have been described in this chapter and it has been shown that many fatigue cracks have been observed. These cracks grow due to the amplitude and the number of the stress cycles in the bridge deck structure. The heavy vehicles and its axle loads induce these stress cycles.

In particular the cracks at deck plate level, which are cracks in the deck plate itself and cracks in the longitudinal weld between deck plate and trough web are discussed. Bridge owners must expect many bridges with fatigue cracks at deck plate level in the future. This thesis is directed towards these cracks at deck plate level.

The fatigue cracks potentially threaten the safety of the bridge structure. Therefore if a crack is observed repair is necessary to solve the local problem on a bridge structure.

In a modern knowledge based society traffic and transportation is of vital importance. One of the basics of such a society is a fully functioning network of motorways. A fully functioning network of motorways is characterised by minimizing the delay time and avoiding congestion. Road maintenance is one of the reasons for delay and traffic jams. Therefore time spent on maintenance should be short as possible while still achieving the required safety level. The strategy must be: maximizing availability, minimizing maintenance. Given this strategy the need for long term renovation techniques for orthotropic steel bridge decks with fatigue cracks is obvious (De Jong, 2002, 2004-c). These techniques should be applied to the bridge deck to reduce the amplitude of the stress cycles.

3. Traffic Loads on Bridges

3.1 Introduction

This chapter deals with traffic loads on bridges. Aspects of bridge loads that are relevant to fatigue phenomena at deck plate level are discussed. Paragraph 3.2 describes the different types of tyre that are fitted to lorries, and footprint measurement tests with several tyres are reported. Paragraph 3.3 describes lorry axle loads. As fatigue phenomena are related to the amplitude and number of the stress cycles, knowledge about axle loading is relevant. Both axle load spectra derived from measurements in the past and according to Eurocode 1 - Part 2 are discussed. Paragraph 3.4 describes the traffic volume properties: relevant parameters related to the number of the stress cycles in bridge decks are discussed. Paragraph 3.5 ends this chapter with some concluding remarks.

3.2 Tyres on heavy vehicles - Footprint measurements

3.2.1 Tyre types on heavy vehicles

In general three different wheel types can be distinguished on the axles of lorries on the motorways:

- Single (type A)
- Double (type B)
- Super single (type C)

Figure 3-1 gives the definition of these types of wheels according to the fatigue load models in Eurocode 1 - Part 2.

When two single wheels of (type A) are mounted together a double (type B) is created. For the purposes of this thesis each axle has two wheels even though axle B has four tyres. The double (type B) is also called dual. The super single (type C) is also called a wide base single. The single (type A) is mainly used for the front steering axle. The double (type B) is mainly used for the driven axles and sometimes for non-driven rear axles. The super single (type C) is mainly used for non-driven rear axles but nowadays sometimes for the front steering axle. The single (type A) and the double (type B) have been known for a long time. The super single (type C) is a relatively new. Since approximately the early nineties of the 20th century,

the super single (type C) has been mounted more often on non-driven rear axles instead of the double (type B). The super single (type C) is larger and more robust so that it can replace a double (type B) wheel assembly.

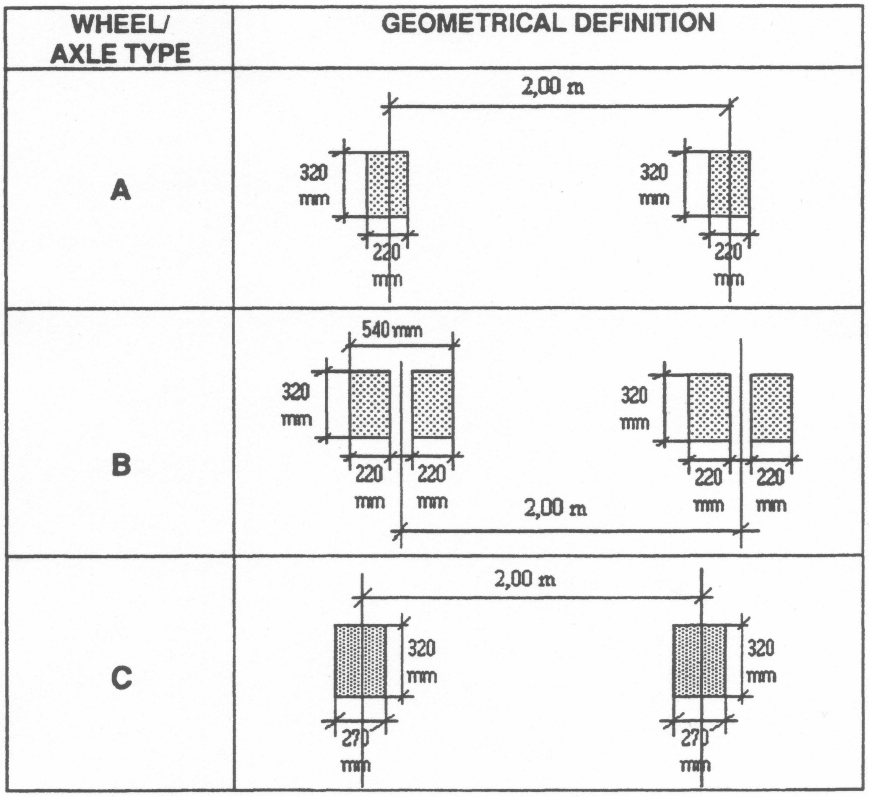

Figure 3-1: Wheel types Eurocode 1 – Part 2 (EN 1991-2, 2003)

Besides these three some manufacturers, like Michelin and Bridgestone, have developed a new type with a footprint width of approximately 450 mm. This tyre is intended to replace the double (type B) on the driven axle. Michelin has referred to this tyre as X one (495/45R22.5) (Michelin, 2004) and the Bridgestone tyre is called Greatec (495/45R22.5) (Bridgestone, 2004).

Knowledge of the contact area and the contact stresses at the interface between tyres and the road are relevant because the vehicle loads are transferred to the bridge deck structure through the tyres.

3.2.2 Contact stresses at the interface between tyre and pavement

Stress ranges in the steel bridge structure are generally raised to the third power for fatigue verifications, because the standard slope of fatigue curves for steel is m = 3. An accurate

prediction of the stresses is important in order to achieve accurate fatigue calculations and in order to predict the stresses accurately knowledge of the footprint pressures is necessary. Groenendijk has performed extensive research in the field of contact stresses between tyre and pavement (Groenendijk, 1998). Other authors have also addressed this topic (Pottinger, 1992), (Tielking, 1994), (De Beer, 1996).

Groenendijk measured the footprint pressure with the VRSPTA system: the Vehicle-Road Surface Pressure Transducer Array. The VRSPTA measures the stresses between relatively slow moving free-rolling tyres and the road surface. The VRSPTA measures vertical stresses, and longitudinal and lateral shear stresses. For this thesis only the vertical stresses are relevant because the shear stresses are very low for the steel structure. Groenendijk has performed tests for various combinations of wheel load, tyre inflation pressure and wheel speed for two wide base single tyres (type C).

With the VRSPTA system it is possible to measure stress patterns in the interface between tyre and pavement. Figure 3-2 gives an example of a measured 3D stress pattern for a 425/65 R22.5 tyre at 0.7 MPa inflation pressure, loaded with 100 kN, moving at 0.3 m/s. This figure is derived from (Groenendijk, 1998, p. 368).

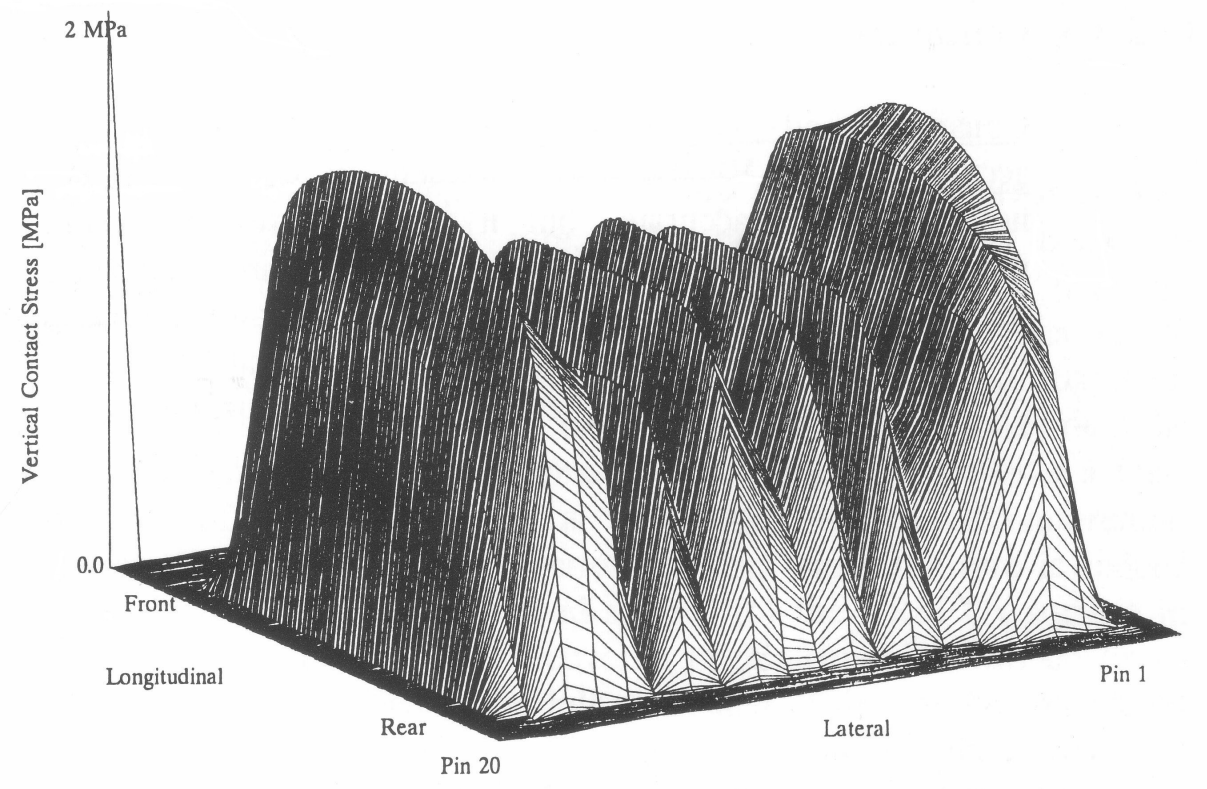

Figure 3-2: Example of measurement result VRSPTA

Groenendijk has formulated the following conclusions based on his research:

- The wheel load mainly governs the stresses at the tyre edges and the tyre pressure mainly governs the stresses around the centre of the tyre.
- The footprint length slightly varies over the tyre width.
- The tyre/pavement contact area can be modelled as a rectangle as wide as the tyre tread area, and with a length, which depends on load and inflation pressure. For the stress modelling, this area has to be divided into three zones in the transverse direction: two edge zones each 20% of the tyre width, and one middle zone covering the remaining 60%.
- The vertical contact stresses may be treated as uniformly distributed over each of the zones, but generally with different values for the middle and edge zones.

Groenendijk derived formulas for the footprint pressure:

$$\sigma_{z;ave;middle} = 422 - 1.20 \cdot F + 4.60 \cdot 10^{-3} \cdot F \cdot p + 0.322 \cdot p + 8.60 \cdot v$$

$$\sigma_{z;ave;edge} = 85.5 + 9.25 \cdot F + 0.290 \cdot p + 12.9 \cdot v$$

where:

F	Wheel load (kN)
p	Tyre inflation pressure (kPa)
v	Wheel speed (m/s)
$\sigma_{z;ave;middle}$	Average vertical contact stress over the middle 60% of the tyre width and the full tyre footprint length (kPa)
$\sigma_{z;ave;edge}$	Average vertical contact stress over the edges 2 x 20% of the tyre width and the full tyre footprint length (kPa)

From load, inflation pressure and velocity the vertical stresses can be calculated. After calculating the vertical stresses the footprint length can be calculated.

The formulas derived by Groenendijk are based on measurements for wide base tyres (type C). It may be assumed that these formulae are also valid for the single (type A) and the double (type B), because these tyre types differ only slightly from the super single (type C). It is not known if the formulas are valid for the newest tyre type with a width of approximately 450 mm.

3.2.3 Contact area measurements

As stated in the previous paragraph an accurate prediction of the stresses is important in order to achieve accurate fatigue calculations. Knowledge of the contact pressure and the size of the

footprint are essential to the accurate prediction of stresses in the bridge deck. Some tests were performed to investigate the dimensions of the tyre footprints at different loads and inflation pressure. In the tests reported in this paragraph a print of the contact area was made. The procedure was:

1. Paint the tyre.
2. Lower and load the tyre on a sheet of plain white paper.
3. Unload and lift the tyre from the paper.

The applied load was measured with a measuring unit under the white paper. Figure 3-3 gives an overview of the contact area measurements.

Figure 3-3: Contact area measurements

The tests were performed with the Lintrack apparatus, a heavy vehicle simulator, which was originally built for pavement testing. The Lintrack is described more in detail in Chapter 4 and (Groenendijk, 1998). The tyres, which were used for these tests, were also used in the test series in the Lintrack, which are reported in Chapter 4. These tests are also intended to check whether the formulas derived by Groenendijk are also valid for these tyre types. The tests were done for the four tyre types, but especially for the double (type B) and the super single (type C), because these are common tyre types on heavy vehicles with the highest loads, thus causing the major part of the fatigue in the steel construction. In total 21 footprints were created according to the test matrix in Table 3-1. The numbers in this table are the test numbers. For the single (type A) and the double (type B) 315/80R22.5 tyres were used, for the super single (type C) a 385/65R22.5 was used, and for the extra wide base (type D) the 495/45R22.5 was used.

Table 3-1: Matrix & numbers footprint measurements

Tyre	Inflation pressure (MPa)	25 kN	50 kN	80 kN	90 kN
Single (type A)	0.9	1	2		
Double (type B)	0.7	3	4	5	6
Double (type B)	0.9	7	8	9	10
Super single (type C)	0.9	11-13	14-15	16-17	18-19
Extra wide base (type D)	0.9			20	21

Photographs of the footprints, as well as measured width and length are given in Annex A. For almost every footprint, the area can be modelled as a square. Table 3-2 gives some clear results from the measurements. It is clearly visible that the footprint becomes significantly larger when the load increases. The header above each photograph is built up as follows: Test no. – Wheel type – Inflation pressure – Wheel load. The photos are not presented at exactly the same scale. Note that in this thesis axle B has two wheels although it has four tyres.

Table 3-2: Results footprint measurements double (type B) at 0.7 MPa inflation pressure

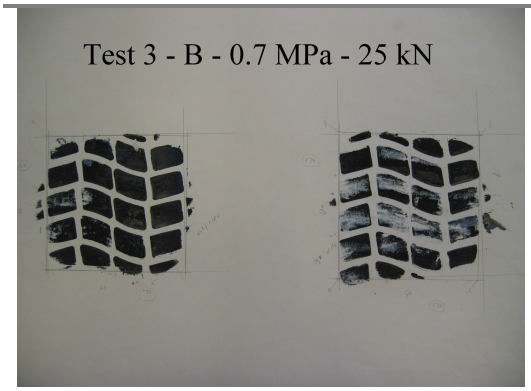

Left tyre: Width x Length = 172 x 163 mm
Right tyre: Width x Length = 170 x 174 mm

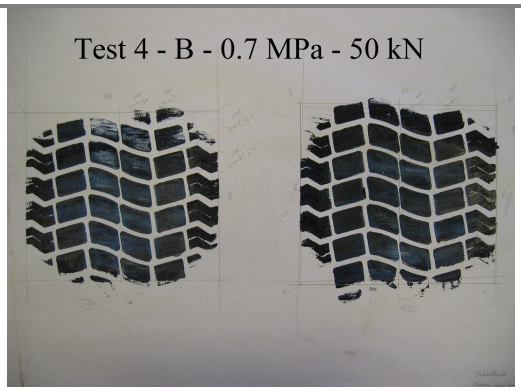

Left tyre: Width x Length = 251 x 215 mm
Right tyre: Width x Length = 250 x 228 mm

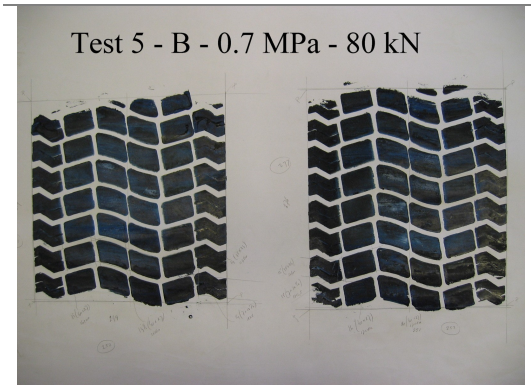

Left tyre: Width x Length = 252 x 261 mm
Right tyre: Width x Length = 253 x 277 mm

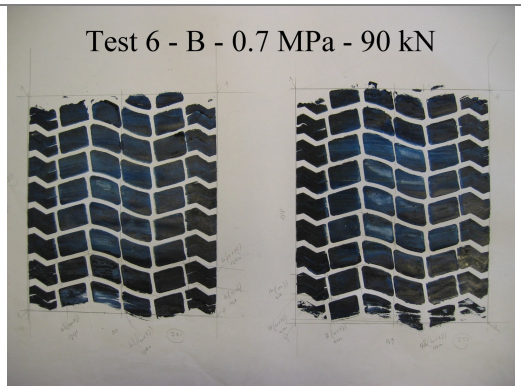

Left tyre: Width x Length = 251 x 285 mm
Right tyre: Width x Length = 253 x 304 mm

The contact area measurements were performed at 0 km/h. The formulas derived by Groenendijk are based on tests in the range from 1-10 km/h. It may be assumed that the formulas are also valid for stationary wheels. Within the range of 1-10 km/h the influence of the speed can be neglected. This speed range already encompasses an entire order of magnitude. It is assumed that is has not more influence over the range of actual traffic speeds (in the next order of magnitude: 10-100 km/h).

3.2.4 Conclusions

Some observations and conclusions can be drawn from measurements and calculations:

- When the load increases, the width of the double (type B) increases. At 25 kN total load, which is 12.5 kN per tyre, the width is approximately 65% of its maximum width. At approximately 50 kN total load, which is 25 kN per tyre, the width has reached its maximum of approximately 250 mm.
- For the double (type B) the measured footprint lengths are approximately 10-30% longer than the predicted values, see Annex A, and consequently the contact stresses, which will arise in practice are lower than those, which are calculated.
- For the super single (type C) the measured footprint lengths are approximately the same as the predicted values, see Annex A, and consequently the predicted contact stresses are approximately the same as those which will arise in practice.
- For loads of approximately 25 kN, both for the double (type B) and the super single (type C), the contact stress in the middle zone is significantly higher than in the edge zones. The load is then more concentrated in the centre zone. The more circular shapes of the footprints at this load level support this. This situation occurs with over-inflated/lightly loaded tyres.
- For loads of approximately 50 kN, for the double (type B) and the super single (type C), the contact stresses in the middle zone are about the same as those in the edge zones.
- For loads of approximately 80/90 kN, for the double (type B) and the super single (type C), the contact stress in the edge zones is significantly higher than in the middle zone. The footprints emphasize this, because the measured length at the edges is longer than in the middle zone. This situation occurs with under-inflated/overloaded tyres.
- The single (type A) behaves exactly the same as the double (type B).
- The footprint area of the extra wide base (type D) is concentrated towards the edge zones. This suggests that the contact stresses are also higher in the edge zones than in the middle zone.
- A comparison of the measured footprint sizes with the footprint sizes according to Eurocode 1 – Part 2 shows that the Eurocode gives footprint sizes related to very high loads.

  - The measured footprint for the single (type A) at 50 kN was approximately the same as the Eurocode dimensions.
  - The measured footprints for the double (type B) at 90 kN were slightly smaller than the Eurocode dimensions.
  - The measured footprint for the super single (type C) at 80 kN was approximately the same as the Eurocode dimensions.

  The maximum legal axle load for non-driven axles in the Netherlands is 100 kN and for driven axles 115 kN. Although some vehicles and axles are overloaded, the majority are legally loaded, see Figure 3-4, and consequently the footprint dimensions in the Eurocode are too large for the majority of tyres. Because stresses in e.g. the deck plate due to local wheel loads are sensitive to the footprint size, smaller footprints, dependent on the load level, should be considered, especially for fatigue verifications.
- A model, which takes these differences into account, takes the nominal width of the tyre as the footprint width and varies the length with the wheel load. The relatively small influence of the inflation pressure is neglected. Based on a linear regression analysis formulae for the footprint length (l_t) were derived:
  - For the single (type A): footprint length = 120 + 3.74 x F[in kN] (mm)
  - For the double (type B): footprint length = 120 + 1.87 x F[in kN] (mm)
  - For the super single (type C): footprint length = 117 + 2.54 x F[in kN] (mm)

3.3 Axle loads and properties

3.3.1 Introduction

The stress ranges at critical details induce fatigue phenomena. The amplitudes of the load cycles govern the stress ranges at these details. For some details, like the deck plate or the weld between deck plate and longitudinal stiffener, the axle loads are relevant. For other details, for instance in the main girder system, the vehicle loads are more relevant.

In the Netherlands extensive measurements have repeatedly been performed on the axle and vehicle loads on the motorways (Kolstein, 1979, 1983, 1990), (Henny, 1995), (Waarts, 1998), (Nieuwsma, 1999), (Vrouwenvelder, 2000-a, 2000-b). The measurements reported by Vrouwenvelder et.al. were performed by TNO on behalf of the Civil Engineering Division of the Ministry of Transport, Public Works and Water Management. Both vehicle and axle loads were measured.

These measurements and their analysis were performed for two reasons. One aim was to validate the static load models in Eurocode 1 – Part 2. Static load models are used for verification at the ultimate limit state. Do those static load models represent the traffic on

Dutch motorways? A second aim was to develop a detailed model for the actual fatigue loads on Dutch motorway bridges. This part concentrates on a description of the vehicle loads and a description of the axle loads. This thesis only describes the results of the measurements relevant to fatigue phenomena at deck plate level. Therefore only the results of the axle load measurements are described as the total vehicle loads are not relevant for the fatigue cracks at deck plate level.

Abnormal load vehicles, which are in general heavier than normal vehicles are also not described. However although the loads are significantly higher than those of normal lorries, the number of these vehicles is negligible and thus the influence on fatigue verifications is negligible.

The measurements were performed at four locations:

- Rheden, Motorway A34, Arnhem-Doesburg, measurements in 1978
- Eindhoven, Motorway A67, Knooppunt Leenderheide, measurements in 1994, 1996 and 1997
- Moerdijk, Motorway A16, Moerdijk Bridge, measurements in 1994, 1996 and 1998
- Arnhem, Motorway A12, IJsselbrug, measurements in 1994, 1996 and 1997

The measurements at Rheden were performed and described by Kolstein (Kolstein, 1979, 1983). Vrouwenvelder describes the measurements at the other three locations (Vrouwenvelder, 2000-a). These four locations were chosen, because at these locations heavily loaded traffic is expected. In total 10 measurements were performed. The measurement on the Moerdijk Bridge in 1998 comprised 81872 lorries. This is a recent measurement with by far the largest number of vehicles. The measurements took place in the heavy vehicle lane of the southbound carriageway. Heavy vehicles and other vehicle types in other lanes were not taken into account.

Nowadays weigh-in-motion systems (WIM) are state of the art techniques for measuring vehicle and axle loads. In the Netherlands there are some WIM stations in the motorways. These WIM stations measure the total vehicle load and the axle loads. The number of axles is measured, but the type of wheel (single, double, super single) is not determined. WIM stations measure the vehicle and axle load of each passing vehicle. Improvement in the accuracy is one of the major tasks at this moment.

For fatigue verifications the WIM results are less useful, because the measurements make no distinction between the different wheel types and the lack of accuracy means that they are less useful than the measurements results from the Moerdijk Bridge in 1998.

3.3.2 Axle load model

The axle load model is based on the measured axle loads at the Moerdijk Bridge in 1998 because it is the measurement with the largest number of axles. In addition to this it is the most recent measurement in which the super single (type C), which has been used widely since approximately 1990, is included. The axle load model described in this paragraph is given in (Vrouwenvelder, 2000-a). The distribution of the axle over the three different wheel types is about (Vrouwenvelder, 2000-b):

- 30 % - Single (type A)
- 40 % - Double (type B)
- 30 % - Super Single (type C)

In general the axle on which wheel type C is mounted nowadays, were mounted with doubles (type B) in the past, because the super single (type C) is a relatively new wheel type. Figure 3-4 gives the measured wheel load distribution at this bridge.

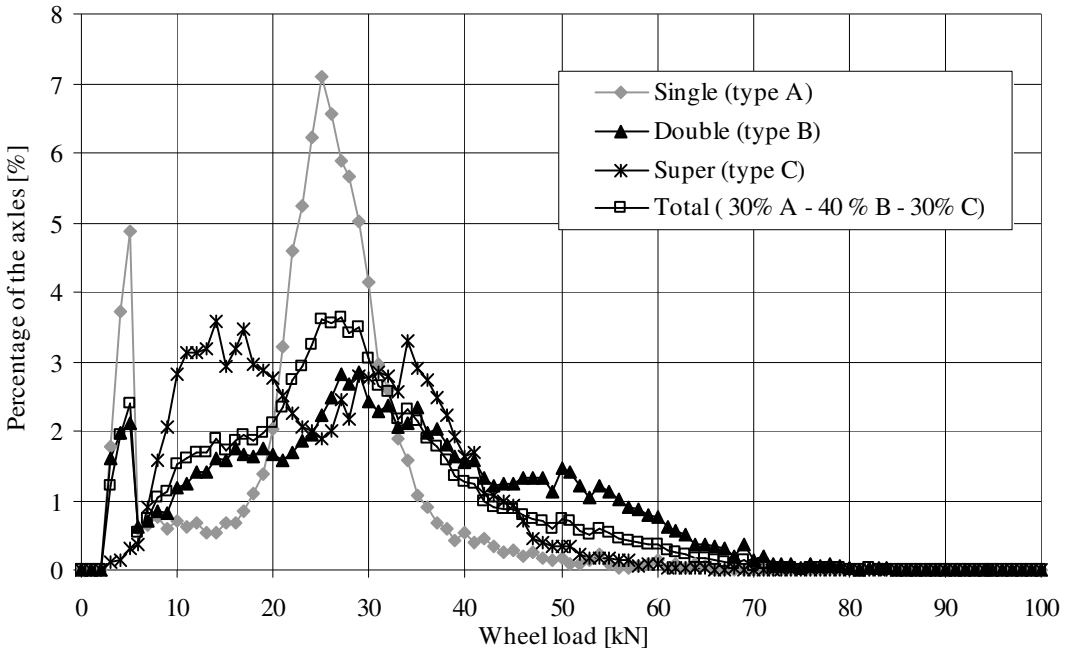

Figure 3-4: Measured wheel load distribution Moerdijk 1998 (Vrouwenvelder, 2000-b)

Based on the measurements a statistical model is chosen and the parameters are determined. The measured axle loads can be described with a lognormal function, given by:

$$f(x) = \frac{1}{\sqrt{2\pi}} \frac{1}{\sigma} \frac{1}{x} \exp\left(\frac{-(\ln(x) - \mu)^2}{2\sigma^2} \right)$$

Table 3-3 gives the determined parameters for the lognormal distribution of the axle loads.

Table 3-3: Parameters lognormal distribution axle loads

Parameters	Total	Single (A)	Double (B)	Super Single (C)
μ	3.25	3.22	3.40	3.22
σ	0.450	0.240	0.475	0.375

Annex B gives more figures. Both the distribution function and the cumulative distribution are presented for the different wheels. From the figures in Annex B it can be concluded that especially for the higher wheel loads the proposed lognormal distribution functions fit very well with the measured data. This is important with respect to fatigue verifications. As the stress ranges in fatigue verifications are in general raised to the third power, a proper load description of the higher loads is desirable. From the figures B-10, B-11 and B-12 in annex B it becomes clear that a significant gap exists between the Eurocode load model and the measured data on the Moerdijk Bridge.

3.3.3 Transversal distribution axles

The tracks of the axles are spread in the transverse direction. Due to this distribution the fatigue phenomena are less severe for cracks at deck plate level. Eurocode 1 - Part 2 models this transverse distribution in 5 blocks each 100 mm wide, with 7%, 18%, 50%, 18% and 7% of the traffic flow. Based on measurements a normal distribution with a standard deviation of 150 mm can be assumed for the transverse distribution (Blab, 1995, Vrouwenvelder, 2000-a). Figure 3-5 shows these transverse distributions.

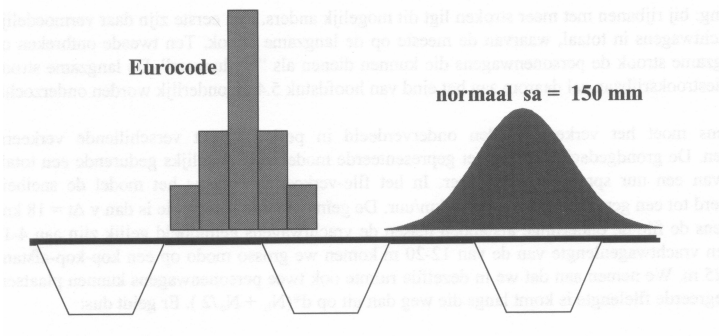

Figure 3-5: Transverse distribution axles

Figure 3-1 gives the axle configurations according to the Eurocode 1 – Part 2. In practice the distance between the outer edges for the different axle types is identical. This is in contrast to

the Eurocode where the distance between the centres of the tyres is taken identical for the different axle types. See Figure 3-6. The given transverse distribution is valid for the centre of the tyres on the outside. For the double (type B) the two tyres on the inside are not taken into account.

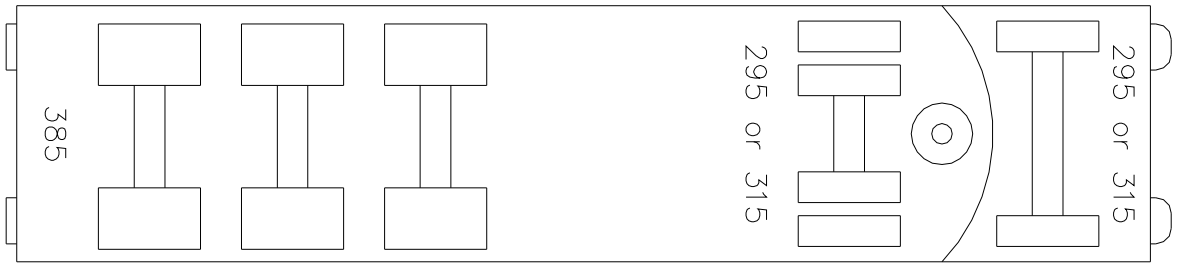

Figure 3-6: Distance between outer edges is identical for different axle types

For fatigue calculations of critical details, which are related to the location of the trough-deck plate connection, the location of the centre of the transverse distribution should be known precisely. The standard distance between the trough webs is 300 mm. The location of the centre should be known with an accuracy of approximately + or – 50 mm. Otherwise the influence of the transverse distribution is possibly either over- or under-estimated.

It is not really possible to determine this location with this accuracy. For bridges in the Netherlands no historic information is available to determine this location. Besides that it is known that the distance between the centre line of the transverse distribution and the edge of the traffic lane is not identical for each bridge. Therefore it is unknown where the centre of this transverse distribution is exactly located on the bridge deck in transverse direction. For this reason the centre line of the transverse distribution should be located at the most adverse position for design fatigue verifications.

3.4 Traffic volume properties

For fatigue verifications knowledge of the number of stress cycles is necessary. A few aspects are relevant:

- The number of lorries crossing bridges
- The number of axles per lorry
- The distribution of the traffic through the day
- The transverse distribution of the traffic flow

The first three aspects will be described in this paragraph, the transverse distribution has already been described in the previous paragraph.

3.4.1 The number of lorries crossing bridges

For the assessment of fatigue cracks at deck plate level the number of stress cycles is in general assumed to be the number of passing vehicle axles. On the Netherlands motorways a fine network of points is available for traffic intensity measurement (AVV, 2005). This network has been built up and is maintained by the Ministry of Transport, Public Works and Water Management. For these measurements the vehicles are divided in three categories:

- Category 1: up to 5.6 metres long
- Category 2: from 5.6 to 12.2 metres long
- Category 3: 12.2 metres and longer

For fatigue verifications only heavy vehicles should be taken into account in the calculations. It is difficult to decide whether category 2 should be taken into account in the fatigue verifications or not, it can be argued that it is better not to take this category into account:

- According to Eurocode 1 - Part 2 75% of the traffic can be thought of in category 3 for the category long distance, see Figure 3-9.
- Vehicle type counting has shown that approximately 75% - 80% of the counted heavy vehicles can be categorized as category 3. (Vrouwenvelder, 2000-a)
- The measured number of category 2 vehicles is approximately 60% of the total measured vehicles in categories 2 and 3.
- Due to the lower limit of category 2, a significant part of category 2 consists of longer passenger cars and small vans, which should be excluded from the fatigue verifications.

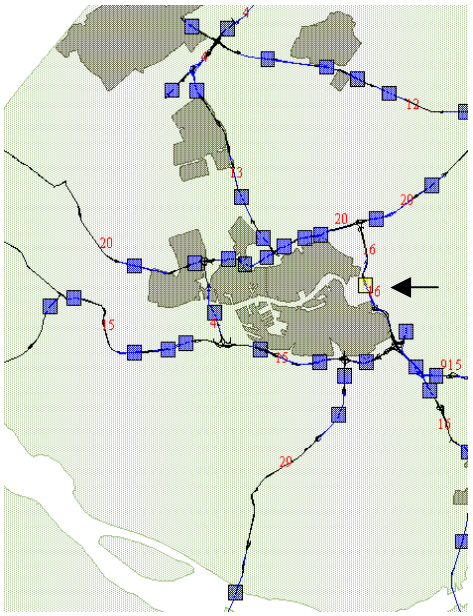

Figure 3-7: Measurement of traffic intensity; measure points near Rotterdam

Figure 3-7 gives an overview of the measurement points in the area around Rotterdam. The indicated point is the Van Brienenoord Bridge. The traffic intensity is measured at all these points. The network of measurement points was built up in the nineties. Exact measurements of the traffic flow are available for all bridges in the motorways from approximately 1995. For bridges built before then, no comprehensive measurements are available. However since approximately 1960 traffic measurements have taken place on the Dutch motorways. Based on these measurements average yearly traffic growth statistics are available and these can be used to extrapolate back to the year the bridges were built.

Figure 3-8 shows the measured data from the Van Brienenoord Bridge, for Monday to Friday intensities, for category 3. The total is the sum for both carriageways. On Saturday and Sunday approximately 10%-15% of the total Monday-Friday flow was recorded. The average yearly traffic volume growth on Dutch Bridges is about 2-4%. This percentage applies to both passenger cars and heavy vehicles, no significant difference in growth between those two categories is found although variations for individual bridges were found.

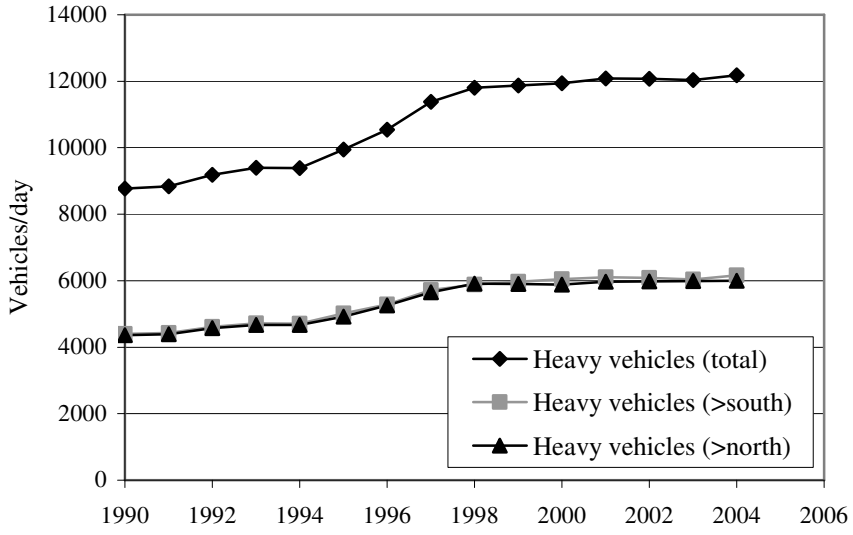

Figure 3-8: Measurement of traffic intensity Van Brienenoord Bridge (category 3)

The intensity of category 3 vehicles on the Moerdijk Bridge on the motorway A16, between Dordrecht and Breda, is probably the highest in the Netherlands. On this bridge nowadays approximately 8000 category 3 vehicles per direction are passing every workday. This means that approximately 2.5×10^6 category 3 vehicles per slow lane crossed the bridge in 2005. This is already more than the 2×10^6 lorries indicated for fatigue design in Eurocode – Part 2, table 4.5. For fatigue verifications the number of lorries and the yearly growth percentage to be taken into account should be chosen carefully.

With high intensities, such as those on the Van Brienenoord and Moerdijk Bridges, the right hand lane of motorways is predominantly used by heavy vehicles. The passenger cars segregate from the heavy vehicles and in practice the slow lane becomes a special truck lane. Sometimes this is a formal truck lane, prohibited for passenger cars, for example on the northward direction of the Van Brienenoord Bridge.

3.4.2 Average number of axles per lorry

The number of axles per lorry is recorded in the traffic measurements. Table 3-4 gives the average number of axles recorded. Usually the average number of axles per lorry varies between 4.0 and 4.5. The records indicate a slight increase in the average number of axles per lorry, which is for the main part due to the relative decrease of the vehicles with two axles, and the relative increase of the vehicles with 4 or 5 axles. (Kolstein, 1990), (Vrouwenvelder, 2000-a).

Table 3-4: Average number of axles per lorry

Measurement	Average number of axles
Rheden 1978	3.95
Arnhem 1994	3.95
Arnhem 1996	3.98
Arnhem 1997	4.04
Eindhoven 1994	4.42
Eindhoven 1996	4.38
Eindhoven 1997	4.38
Moerdijk 1994	4.21
Moerdijk 1996	4.25
Moerdijk 1998	4.28

In load model 4 Eurocode 1 - Part 2 gives a set of standard/equivalent lorries for fatigue verification. Figure 3-9 gives this set of lorries. The average number of axles per lorry, based on this model is 4.15. Because the steel bridges in the Netherlands with fatigue problems are all located on the motorways, the “long distance” column is the most appropriate model.

3.4.3 The distribution of the traffic over the day

The distribution of the traffic flow over the day is also measured (AVV, 2005). Figure 3-10 gives a graphical representation of the distribution of the heavy vehicles. It should be noted that the distribution of passenger cars over the day is different, due to the commuter traffic every morning and afternoon. This knowledge is necessary in relation to the modelling of the

influence of the asphalt surfacing on the stress ranges, because the behaviour of the asphalt surfacing is temperature and time dependent.

VEHICLE TYPE			TRAFFIC TYPE			
1	2	3	4	5	6	7
			Long distance	Medium distance	Local traffic	
LORRY	Axle spacing (m)	Equivalent axle loads (kN)	Lorry percentage	Lorry percentage	Lorry percentage	Wheel type
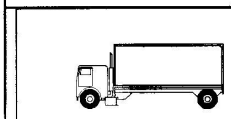	4,5	70 130	20,0	40,0	80,0	A B
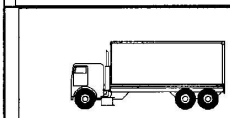	4,20 1,30	70 120 120	5,0	10,0	5,0	A B B
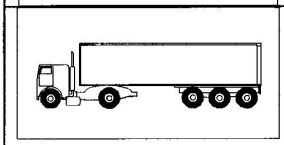	3,20 5,20 1,30 1,30	70 150 90 90 90	50,0	30,0	5,0	A B C C C
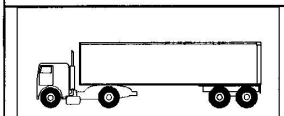	3,40 6,00 1,80	70 140 90 90	15,0	15,0	5,0	A B B B
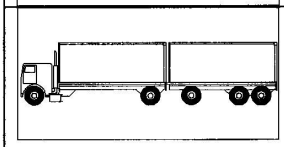	4,80 3,60 4,40 1,30	70 130 90 80 80	10,0	5,0	5,0	A B C C C

Figure 3-9: Standard/equivalent lorries EN 1991-2

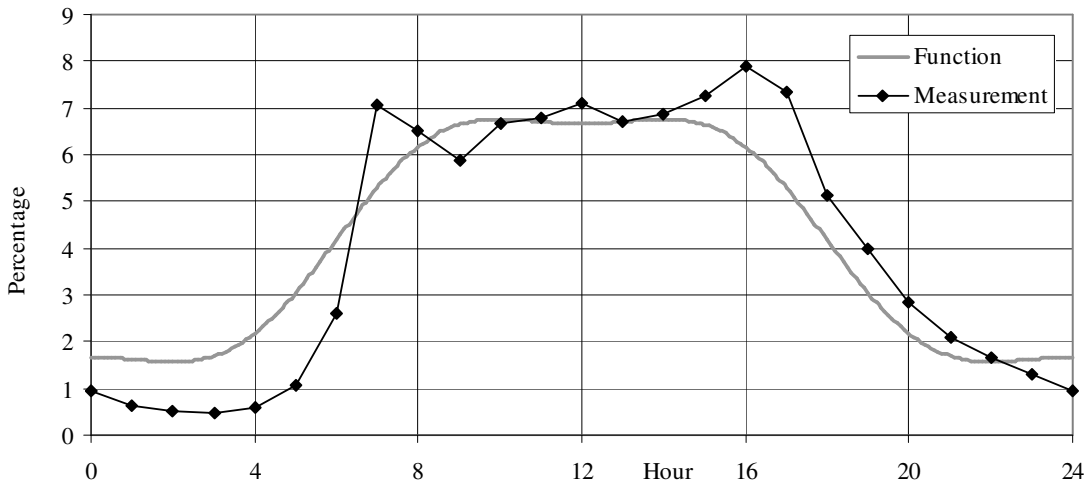

Figure 3-10: Lorries distribution in one day

The distribution of the traffic flow over 24 hours is based on several measurements on the Dutch motorways. A function is fitted to these results:

$$f_{day}(t) = \frac{1}{hrs_{day}} + 0.03 \cdot \sin\left(\frac{t \cdot 2\pi}{hrs_{day}} - \frac{\pi}{2}\right) - 0.005 \cdot \sin\left(\frac{t \cdot 6\pi}{hrs_{day}} - \frac{\pi}{2}\right)$$

In which hrs_{day} is the number of hours per day (24). Figure 3-10 also shows this function.

3.5 Concluding remarks

This chapter has discussed several aspects related to bridge loading that are relevant for fatigue phenomena at deck plate level. This paragraph summarizes the important points.

- Footprint sizes differ with wheel load and inflation pressure. The smaller the load, the smaller the footprint size. The influence of the footprint size on the stresses in, e.g. the deck plate, but also in other fatigue prone details, should be investigated. This is necessary because the stress ranges in these details are likely to vary with the footprint size, and thus the fatigue life.
- The axle load spectra are given based on measurements on the Moerdijk Bridge. There is a significant difference between the measured axle load spectra and that according to the Eurocode 1 – Part 2. Probably fatigue verifications with measured axle load spectra give more accurate results for fatigue at deck plate level. The measured axle load spectra should be used with partial safety factors.
- Relevant traffic volume properties are the number of lorries, the average number of axles per lorry and the distribution of the lorries over the day. With a fine meshed measurement network these traffic volume properties are available for almost every bridge on the network of motorways in the Netherlands. For the bridges with the highest flow of heavy vehicles the traffic flow now already exceeds the design values of the Eurocode 1 – Part 2.

4. Behaviour of existing orthotropic bridge decks

4.1 Introduction

This chapter describes the behaviour of orthotropic bridge decks with respect to cracks at deck plate level. These are the cracks in the deck plate itself and cracks in the longitudinal weld between deck plate and trough web.

Paragraph 4.2 describes the local static behaviour of bridge decks. Three topics are discussed: the local stress distribution in the deck plate under wheel loading, the influence of the surfacing on those stresses and a third part describes the ultimate load capacity of the deck plate with fatigue cracks under wheel loads.

Paragraph 4.3 describes the fatigue behaviour of bridge decks at deck plate level. The two parts of this paragraph are: a literature survey and a description of fatigue tests that were performed. This paragraph focuses both on the fatigue of deck plate cracks and on fatigue of the longitudinal weld between trough web and deck plate.

Paragraph 4.4 describes a test program that was performed in the Lintrack, a heavy vehicle simulator with running wheel load. Tests are performed on a full-scale bridge deck test panel, with different tyres, different loads, with and without surfacing layers and with different temperatures.

Paragraph 4.5 ends this chapter with some concluding remarks.

4.2 Static behaviour bridges

4.2.1 Introduction

This paragraph discusses the static behaviour of the bridge deck structure under wheel loading. The description is limited to the behaviour of the deck plate under wheel loading as this thesis is pointed towards fatigue cracking at deck plate level. The description has three

parts. Paragraph 4.2.2 discusses the stresses in the steel deck plate at the crossbeam location under wheel loading, Paragraph 4.2.3 discusses the stress reduction influence of the asphaltic surfacing applied on fixed bridges. Paragraph 4.2.4 attempts to define a critical deck plate crack length at the location of the crossbeam.

4.2.2 Stress distribution in the deck plate

This paragraph is about the stress in the steel deck plate at the crossbeam location under wheel loading.

4.2.2.1 Analytical analysis

Several researchers have addressed the topic of stresses in orthotropic bridge decks under wheel loading. Both analytical and numerical calculations as well as measurements were performed. Cullimore has reported on the stresses in the deck plate caused by wheel loads (Cullimore, 1981). Nunn and Cunninghame have reported also reported on this topic (Nunn, 1974). However these publications do not refer to the stress distribution in the deck plate under wheel loading at the location where the longitudinal trough stiffener passes through the crossbeam. The reason is as these publications are about bridge panels where the troughs are fitted between the crossbeams and are not continuous through them.

For fatigue verifications of the deck plate crack at the crossbeam location the basis of the determination of the stress ranges is a valid mechanical model for the stress calculation. Because the literature gives no results, a simplified analytical model was adopted to calculate the stress in the deck plate at the fatigue crack location. This analytical model is assumed to represent the situation in real bridge decks. Tests were performed to verify this assumption, see paragraph 4.2.2.2.

Figure 4-1 shows the mechanical model assumed for the stress calculation. The deck plate between the two legs of the trough is modelled as a simple clamped beam. The span of this beam is 300 mm, which is the distance between the trough legs. For the deck plate crack at the intersection of the crossbeam, deck plate and trough web, a clamped beam is considered to be a valid model because crossbeam, deck plate and trough web are welded together at that location.

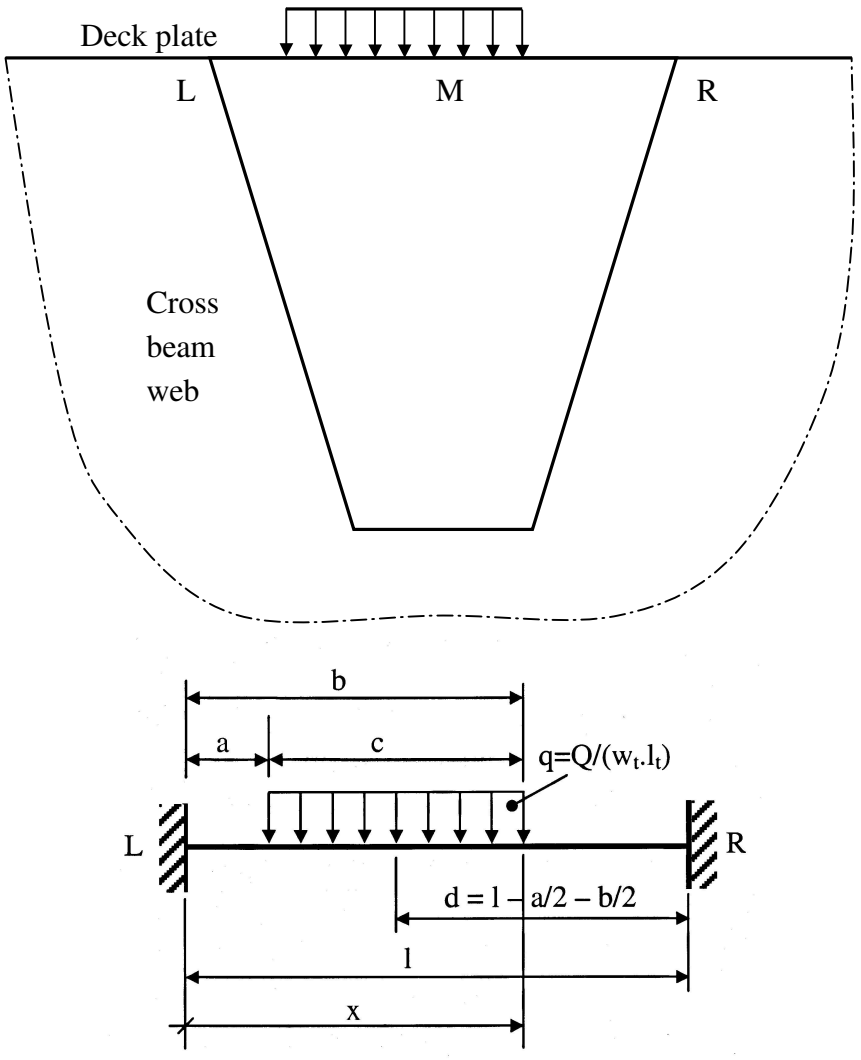

Figure 4-1: Mechanical model deck plate stress calculation

The moment at the crack location L, is given by:

$$M_L = \frac{qc}{24l}\left(24\frac{d^3}{l} - 6\frac{bc^2}{l} + 3\frac{c^3}{l} + 4c^2 - 24d^2\right)$$

$$q = \frac{Q}{w_t \cdot l_t}$$

with:

Q	the wheel load (N)
q	the uniformly distributed wheel load (N/mm)
w_t	the width of the tyre footprint (mm)
l_t	the length of the tyre footprint (mm)
l	the span of the deck plate between the trough webs, usually 300 mm.

With these formulae the moment at the crack location can be calculated for each x-coordinate. This model assumes no wearing course hence the dispersion of loads through the wearing course is not taken into account.

4.2.2.2 Measurements

Introduction

Within the framework of this thesis experimental studies were performed to determine stress patterns in the deck plate at the intersection of the crossbeam and continuous longitudinal girders (troughs). These measurements are extensively described in (De Jong, 2005-d). Strain gauges were applied to a test panel at many locations, all measuring in transverse direction. The experimental work was intended to verify the assumed mechanical model adopted to calculate the maximum stress at the crack location. Figure 4-2 is a drawing of the test panel and is referred to as test panel A.

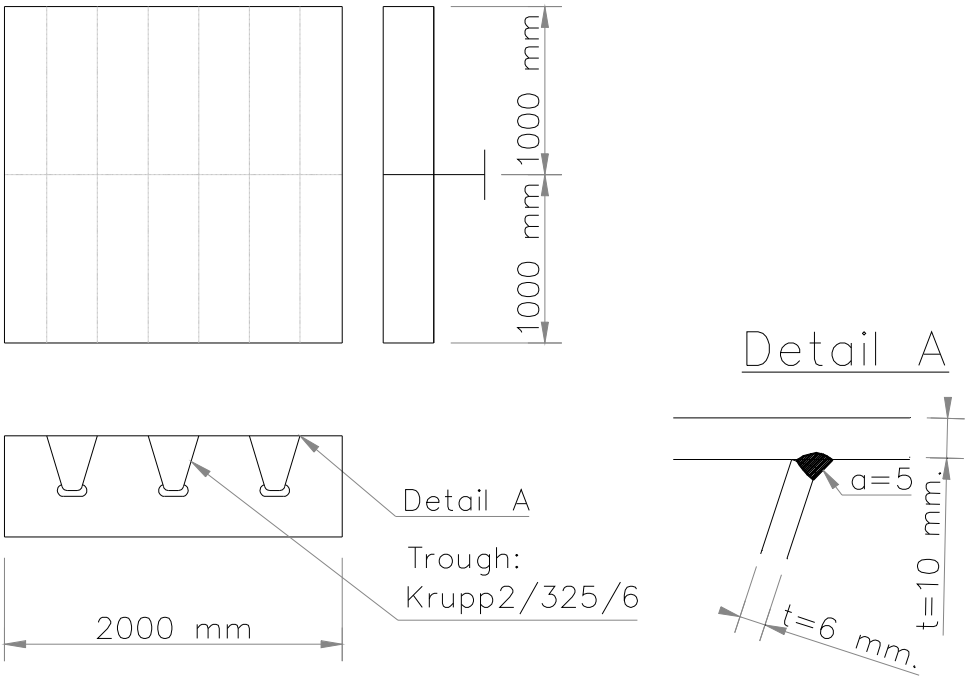

Figure 4-2: Test panel A used for stress distribution measurement

The test panel was 2m long and 2m wide. It consisted of a crossbeam, 3 troughs and a deck plate. The deck plate had a thickness of 10 mm as had the web of the crossbeam. The 3 troughs were standard Krupp-2/325/6 profiles and cope holes were provided where the troughs passed through the crossbeam The longitudinal weld between trough web and deck plate has a throat dimension, a, of 5 mm. Test panel A had no surfacing layer. After the tests to investigate the stress distribution this panel was subsequently used for fatigue tests, which are reported in paragraph 4.3.3.

Within this thesis several strain gauge measurements are reported. From the measured strains, stresses are calculated with the constitutive relation: $\sigma = E\varepsilon$. Because the stiffness modulus for steel is exactly 210.000 MPa, there is a direct relation between strain and stress. Therefore in this thesis stresses in steel parts calculated as a result of strain gauge measurements are considered measured stresses.

Strain gauges

At several locations on the deck plate strain gauges were mounted to measure the strains under different loadings. Annex C gives an overview of the arrangement of the applied strain gauges. All three troughs were fitted with gauges, especially the middle trough because the determination of the stress patterns is done for this trough. The strain gauges were all applied to the top of the steel deck plate. They measured the strain in transverse direction; perpendicular to the weld, because the stresses responsible for fatigue crack growth are in transverse direction. The longitudinal direction is the direction of the traffic flow and is the direction of the troughs. The strain gauges at the location of trough 2 (central) are mounted for measurement of static stress patterns and also for the subsequent fatigue test. The strain gauges on the 1st and the 3rd trough profiles were only mounted for the subsequent fatigue test.

Applied strain gauges trough 2

Trough 2 was provided with a large number of strain gauges in order to measure the stress patterns under different wheel loads accurately. Figure 4-3 shows these gauges. In this figure several lines are defined, from line A-A to line I-I, see Annex C for more information. At several locations groups of 5 strain gauges were mounted with intermediate distances of 2 mm. These groups were positioned at locations where maximum strains were expected, in order to determine the exact level and the exact location of the maximum strain. Because of the symmetry around the crossbeam web and around the longitudinal axis, only one of the four parts was provided with an extensive strain gauge pattern.

Applied strain gauges troughs 1 and 3

The applied configurations of strain gauges for the troughs 1 and 3 were identical and were

partly based on the configuration used in previous measurements (Kolstein, 1999, 2000). The configuration for troughs 1 and 3 was formed by 18 strain gauges (1.1 - 1.18 and 3.1 - 3.18), these gauges were mounted immediately above the web of the crossbeam and also immediately above the welds between the trough webs and the deck plate. Compared to the configuration that was applied at trough 2 the configuration used at troughs 1 and 3 was rather small. That was because of the precise measurement of the stress patterns would take place above trough 2. The results from the strain gauges at trough 1 and 3 were used to see if they gave the same results as the gauges in trough 2 and also to check whether cracks were growing during the subsequent fatigue test.

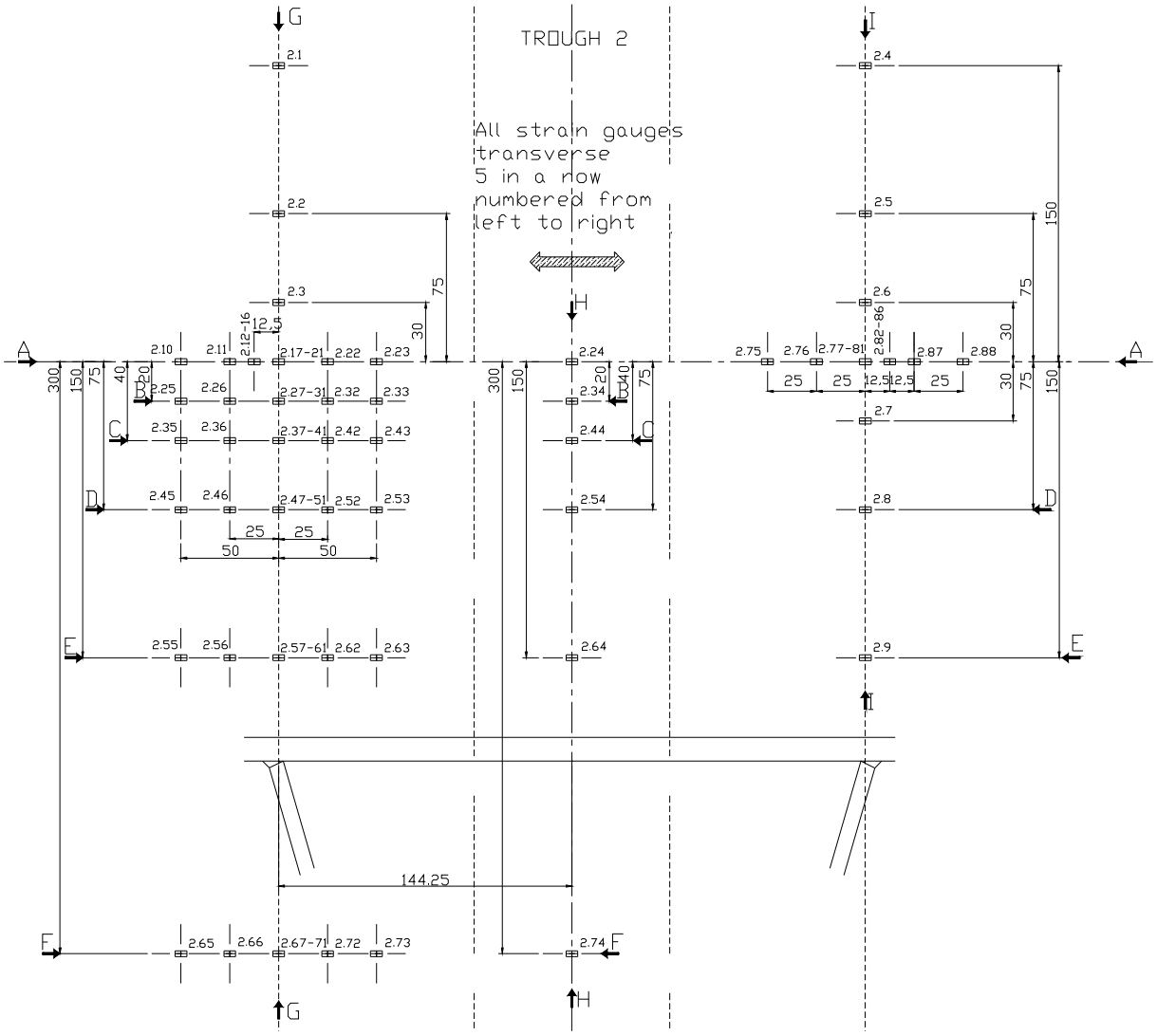

Figure 4-3: Strain gauges trough 2

Where the trough web crossed the crossbeam web three strain gauges in line were used. This allowed a gradient to be derived at this location, which was necessary for the fatigue detail classification of the fatigue cracks. Strain gauges were also applied to the deck plate on the longitudinal line of the weld between crossbeam and trough web. These gauges were necessary in order to measure the effect on the strains of fatigue cracks that were growing in longitudinal direction.

Testing program

The measurements of the static strain patterns were performed for 11 different footprints. The length and width of these footprints were based on the measured footprint areas described in chapter 3, earlier tests (Kolstein, 1999, 2000-a) and the formats given in Eurocode 1991-2. Based on the results of Kolstein (Kolstein, 2000-a) a rough estimation of the wheel load that would cause a maximum stress of 220 MPa in the deck plate had been derived. Therefore each footprint had a different load. Table 4-1 shows the width and length for each test and the applied load. The width is in the transverse direction of the trough; the length in the longitudinal direction.

Table 4-1: Static tests measurement stress patterns

Test No.	*Width* (mm)	*Length* (mm)	F_{max} (kN)
BA1_S1	220	180	31
BA1_S2	220	250	34
BA1_S3	220	320	38
BA1_S4	250	160	35
BA1_S5	250	220	39
BA1_S6	250	270	42
BA1_S7	250	320	45
BA1_S8	270	320	49
BA1_S9	280	180	40
BA1_S10	280	240	44
BA1_S11	430	170	59

The loading procedure was divided in 8 steps. Figure 4-4 gives this loading procedure. Loading and unloading was performed at 1 kN/sec, and the minimum load $F_{min} \approx 0.2$ kN. Figure 4-5 shows the load application set-up.

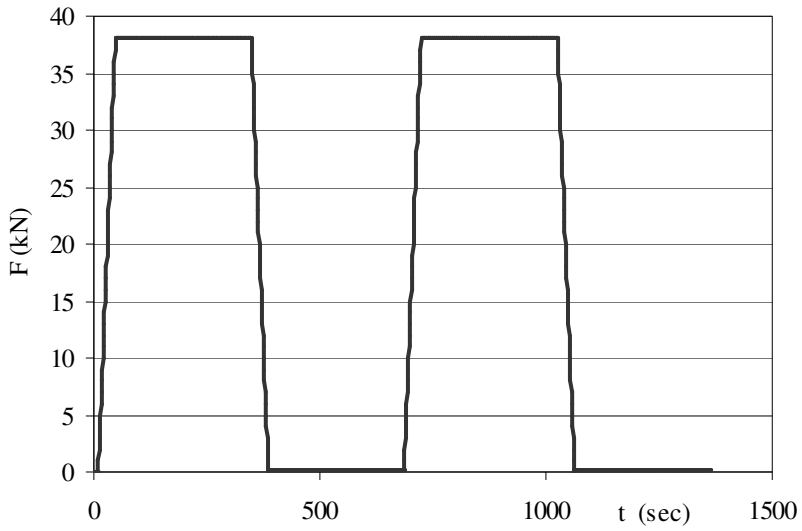

Figure 4-4: Loading procedure static tests panel A

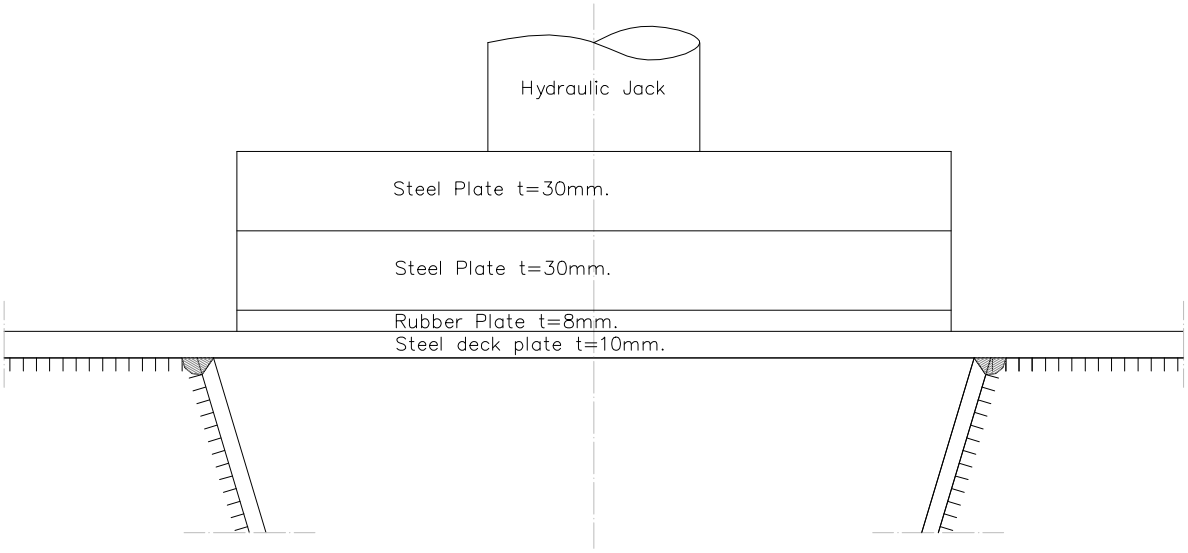

Figure 4-5: Load application static tests

Test and calculation results

The results of all the static measurements are in general 3 sets of figures.

1. The applied load as a function of time, *F(t)*
2. The measured strains in transverse direction (x) over defined lines at the bridge deck in x- and y-direction: $\varepsilon_x(x)$ and $\varepsilon_x(y)$
3. The measured strains in transverse direction (x) as a function of time for each strain gauge: $\varepsilon_x(t)$

The defined lines in transverse x-direction over the bridge deck are A-A, B-B, C-C, D-D, E-E

and F-F. The defined lines in longitudinal y-direction over the bridge deck are G-G, H-H and I-I. These lines are depicted in Figure 4-3. As all strain gauges were mounted in the transverse direction the strains reported are all in transverse direction. In Stevin Report 6.04.3 (De Jong, 2005-d) all these figures are depicted.

The analytical calculations are based on the formulas given in paragraph 4.2.2.1. To derive strains from the calculated moments, Hooke's law and measured plate thicknesses are used. The calculation of the section modulus was based on the measured thickness of the deck plate. Approximately 20 deck plate thickness measurements of test panel A were made with a caliper. The measured thickness varied from 10.35 mm to 10.50 mm and the average thickness was 10.45 mm.

The measured and calculated maximum strains are given in Table 4-2, for the locations Left, Right and Midspan. The locations Left and Right are those where the deck plate cracks grow, see Figure 4-1. The calculated values for L and R are the same due to symmetry. Test BA1-S11 was excluded from this table because the width of the tyre exceeds the distance of 300 mm between the trough webs, and thus the length of the clamped beam.

Table 4-2: Measured and calculated maximum strains at locations Left, Right and Midspan

Test No.	Measured Strain L ε_{xx} (x10^{-6})	Measured Strain R ε_{xx} (x10^{-6})	Measured Strain M ε_{xx} (x10^{-6})	Calculated Strain L&R ε_{xx} (x10^{-6})	Calculated strain M ε_{xx} (x10^{-6})
BA1_S1	1042	956	-516	1385	-753
BA1_S2	925	874	-487	1098	-596
BA1_S3	883	796	-472	955	-519
BA1_S4	1177	1064	-516	1648	-854
BA1_S5	1115	997	-514	1335	-692
BA1_S6	958	911	-484	1173	-608
BA1_S7	931	889	-488	1060	-549
BA1_S8	991	891	-481	1098	-556
BA1_S9	1168	1129	-548	1547	-778
BA1_S10	1095	1008	-530	1276	-642

Figure 4-6 gives the measured strain over the transverse line A-A, which is the line exactly at the crossbeam location, for test BA1-S8, with a footprint size of 270 mm by 320 mm. For an easy interpretation the deck plate and trough webs are sketched in this figure. The calculated maximum strain at the locations L (Left) and R (Right) for this footprint size is 1098x$10^{-6.}$ The locations are defined in Figure 4-1.

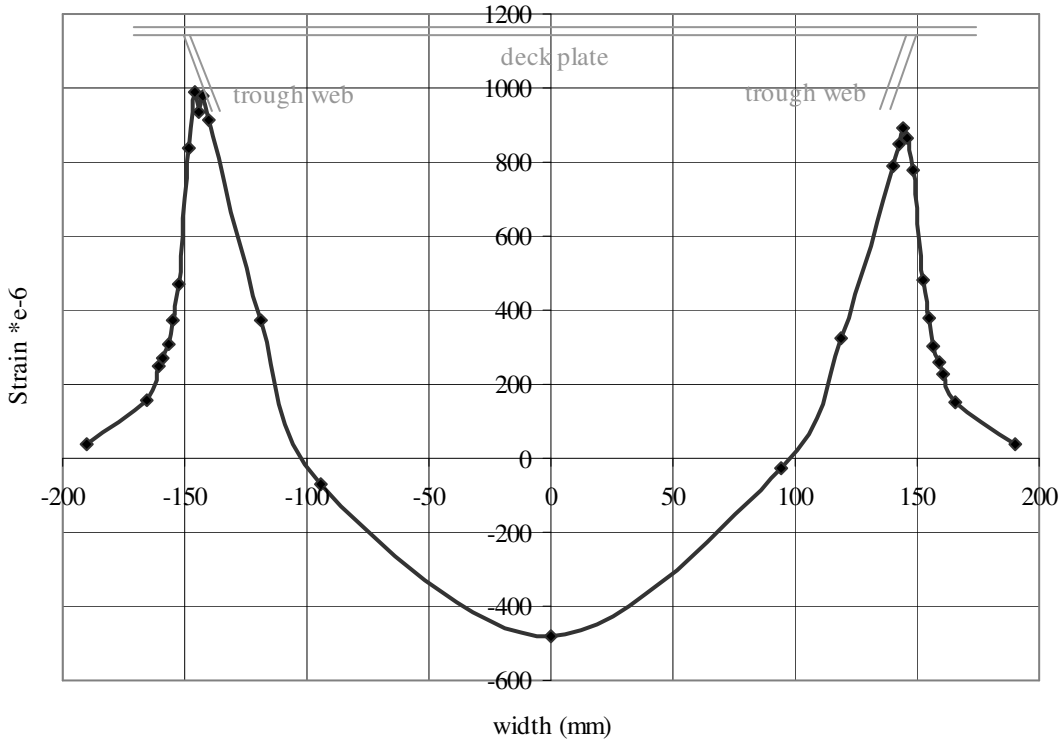

Figure 4-6: Measured strain over transverse line A-A test BA1_S8 (footprint 270 x 320 mm)

Dijkstra produced some FE-models to predict the stress at the crack location (Dijkstra, 1998). A wheel load of 100 kN with a footprint size of 300 wide by 320 mm long causes a stress at the crack location of 360 MPa (Dijkstra, 1998). However this footprint was not included in the tests. Test BA1_S8 gives the best comparison (270 mm wide, 320 mm long) and results in 208 MPa (left side) and 187 MPa (right side). The FE-model at 49 kN results in 176 MPa i.e. the FE-model results in a lower stress: 89% percent of the average measured stress. An explanation of the lower stress is found in the greater width of the FE-tyre. With the analytical formula it was calculated that with the same load and length of the footprint the calculated stress with a tyre of 300 mm wide is 91% percent of the stress of a tyre of 270 mm wide. Based on this comparison it can be concluded that the measured stresses are in line with the calculated stresses of Dijkstra.

Figure 4-7, Figure 4-8 and Figure 4-9 show the measured and calculated strain over the longitudinal lines G-G (Left), H-H (Midspan) and I-I (Right), for test BA1_S8, with a footprint size of 270 mm by 320. This footprint size was chosen as an example as it is the footprint size of the super single (type C). These graphical representations give the strain in transverse direction as a function of the location in longitudinal direction. For an easy interpretation the deck plate and trough webs are sketched in these figures.

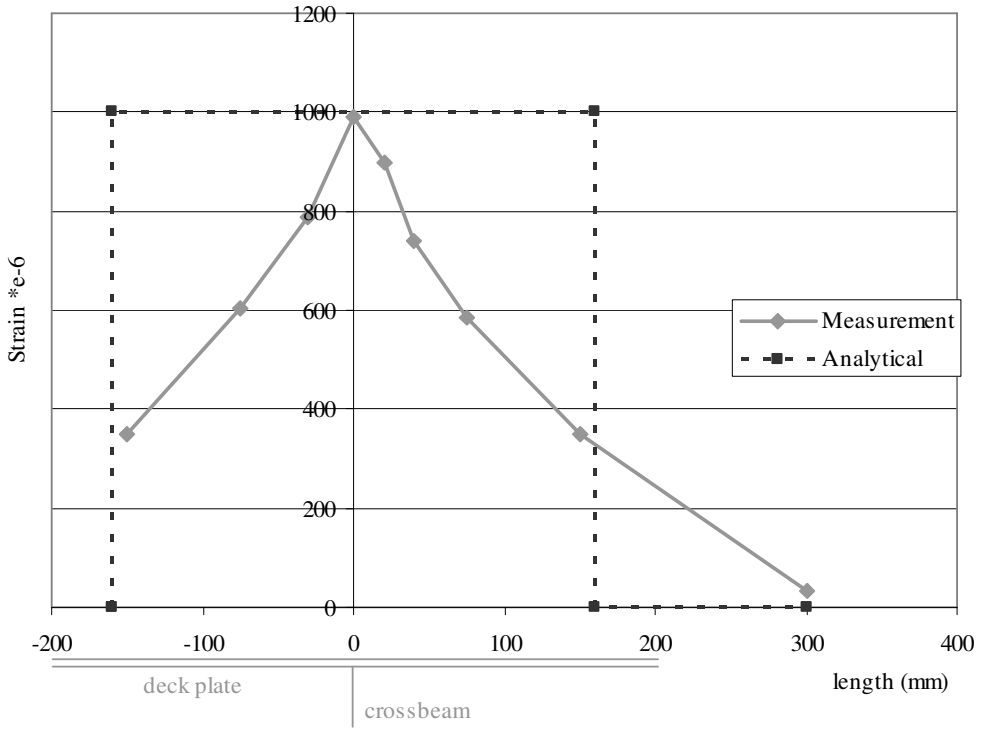

Figure 4-7: Strain over longitudinal line G-G (Left) test BA1_S8

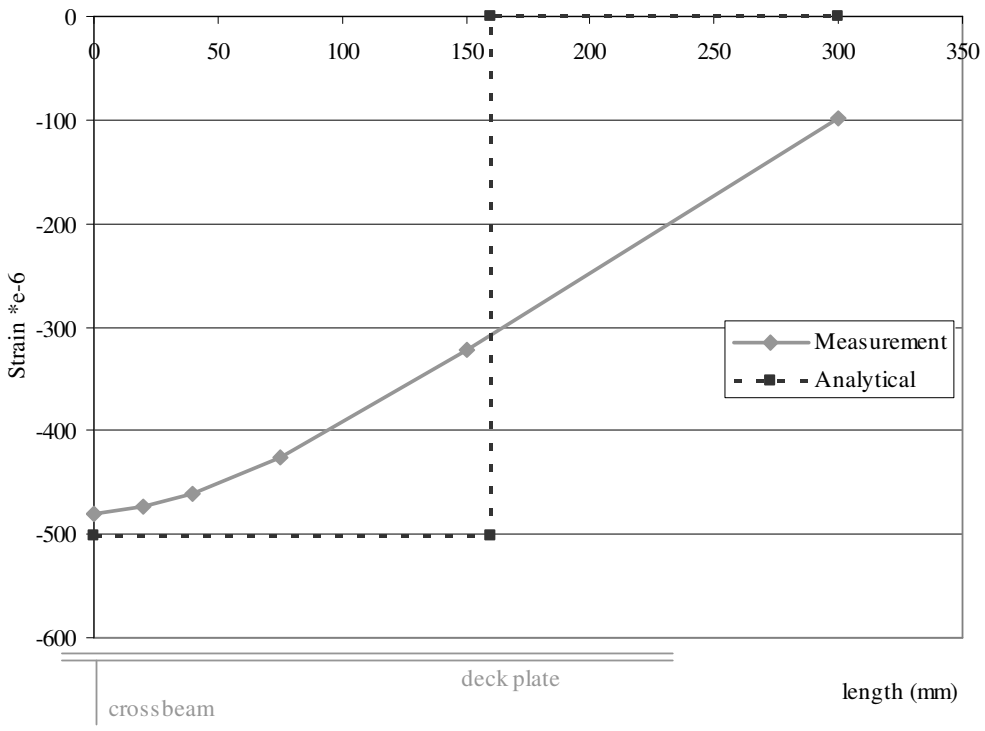

Figure 4-8: Strain over longitudinal line H-H (Midspan) test BA1_S8

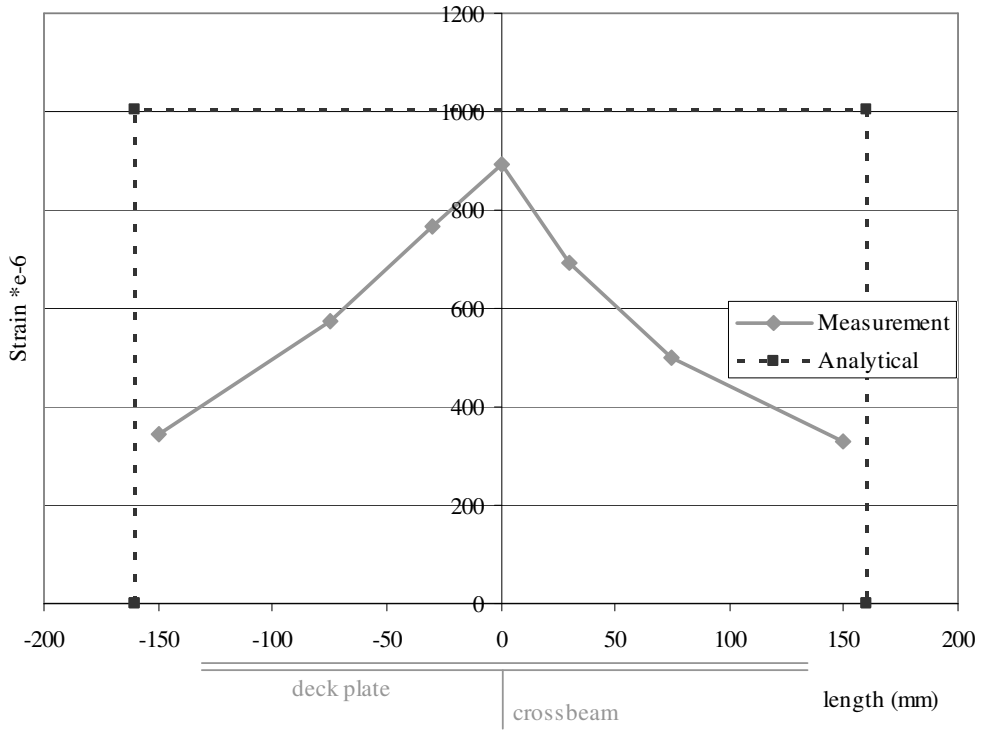

Figure 4-9: Strain over longitudinal line I-I (Right) test BA1-S8

The graphical representations along the lines G-G and I-I, show that the area under the line is significantly smaller for the tests than for the analytical model. This area is an indication of the size of the clamping moments. The moments were calculated for the three locations right, left and mid span on the assumption that the mechanical behaviour of the deck plate is according to the Bernoulli hypothesis. The formula used to derive the total moments at these three locations is:

$$M_{tot} = \sum_{i=y_b}^{y_e} \varepsilon_i \cdot E \cdot W_i$$

With:

M_{tot} total moment in a cross-section

y_b location along the longitudinal axis y where $\varepsilon_{xx} = 0$ at one side of the crossbeam (mm)

y_e location along the longitudinal axis y where $\varepsilon_{xx} = 0$ at the other side of the crossbeam (mm)

ε_i strain ε_{xx}

E stiffness modulus (210.000 MPa)

W_i section modulus per unit of length ($N/mm^2/mm$)

The total moments derived from the measurements and the total moments derived from the analytical calculations are given in Table 4-3. Figure 4-10 gives a representation of the calculated moments for test No. BA1_S8 with a footprint of 270 wide by 320 mm long.

Table 4-3: Measured and calculated maximum moments at locations Left, Right and Midspan

Test No.	Measured Moment L $M_{L;tot}$ (Nm)	Measured Moment R $M_{R;tot}$ (Nm)	Measured Moment M $M_{M;tot}$ (Nm)	Calculated Moment L&R $M_{L;tot}$ & $M_{R;tot}$ (Nm)	Calculated Moment M $M_{M;tot}$ (Nm)
BA1_S1	757	703	-631	953	-518
BA1_S2	772	740	-668	1049	-570
BA1_S3	837	784	-724	1168	-635
BA1_S4	810	743	-658	1008	-522
BA1_S5	849	778	-695	1123	-582
BA1_S6	842	816	-688	1210	-627
BA1_S7	896	875	-756	1296	-671
BA1_S8	937	867	-743	1342	-680
BA1_S9	857	809	-671	1064	-536
BA1_S10	883	823	-708	1170	-589

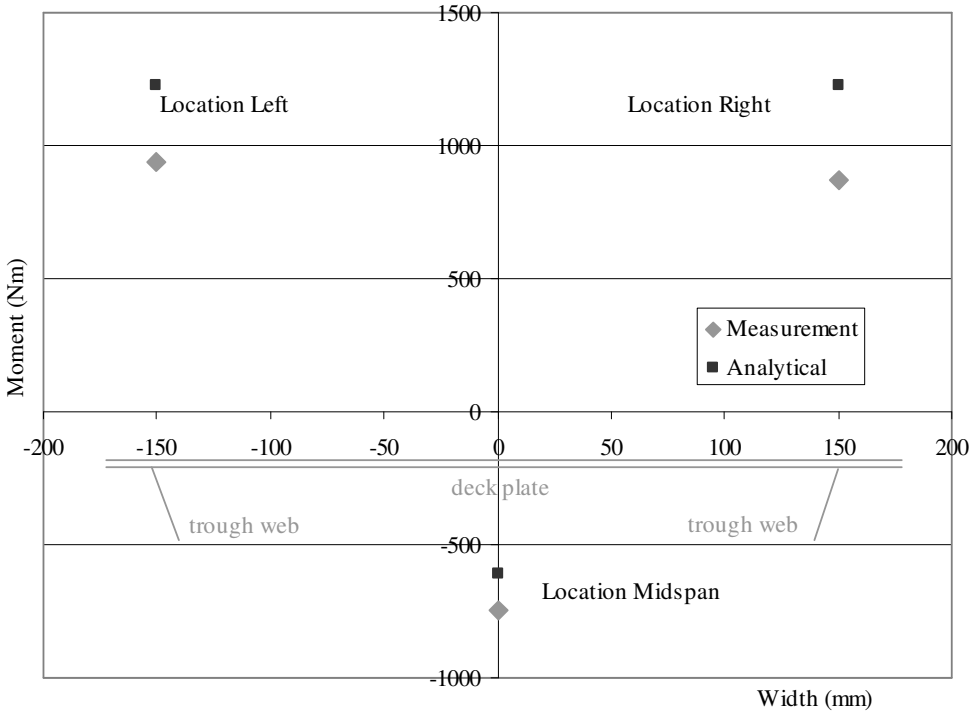

Figure 4-10: Calculated moments for test BA1_S8 (footprint 270 by 320 mm)

Discussion

A comparison between calculations and measurements was made. This comparison was made for all the footprints and not only for the 270 mm by 320 mm footprint. The four most important observations from this comparison are:

1. The analytical calculated stresses are significantly higher than the measured stresses. The average ratio analytical/measured stress for the Left and Right locations is 1.24. This ratio is 1.29 for the mid span location M. Figure 4-7, Figure 4-8 and Figure 4-9 suggest that there was more distribution of the loads in longitudinal direction than the analytical model allows for.
2. The analytical calculated moments for the Left and Right locations are significantly higher than the moments derived from the strain measurements. The average ratio analytical/measurement is 1.33 for the L and R (or Left and Right) locations.
3. The analytical calculated moment for the mid span location is significant smaller than the moment derived from the strain measurements. The average ratio analytical/measurement is 0.83 for the mid span location.
4. The analytical calculated difference between the maximum and the minimum moment is significantly higher than the difference derived from the strain measurements. The average ratio analytical/measurement is 1.11 for the difference between maximum and minimum moment.

For fatigue verifications it is important that accurate stress calculations are available. The analytical calculation model and the test results should give the same stresses and strains. There are two explanations for the differences between measurement and calculation for the Left and Right crack locations.

Explanation 1: wheel load distribution in the rubber – deck plate interface

Based on the four above-mentioned observations, it is supposed that the loads at the rubber-steel deck plate interface are not uniformly distributed, but that due to the deflection of the steel deck plate the load was distributed more to the edges of the footprint. If this is true, it is an explanation for the measured difference between maximum and minimum moment being smaller than that predicted by the analytical calculation.

Some FE-models of the test set-up were made to determine the vertical contact stress in the interface between the deck plate and the rubber plate (De Jong, 2005-d). The supposition that the load transfer is concentrated towards the edges of the foot plate is correct. If this load distribution is adopted in the analytical calculation the average ratio between the calculated and the measured maximum stress at the Left and Right locations is reduced to a factor 1.10 instead of 1.24 under a uniformly distributed wheel load.

Real wheel loads on bridges can however be treated as uniformly distributed loads, assuming that the inflation pressure is appropriate. The non uniform distribution of the load in the test was due to the test equipment in that the rubber layer chosen was too thin.

Explanation 2: Shorter span of the clamped beam

Figure 4-6 shows that the maximum strains are not located exactly at the trough web distance of 300 mm, but at strain gauges 5.75 mm inside the trough. Thus in the calculations the assumed span of the clamped beam could be reduced, which has the effect of reducing the difference between the calculated and measured values.

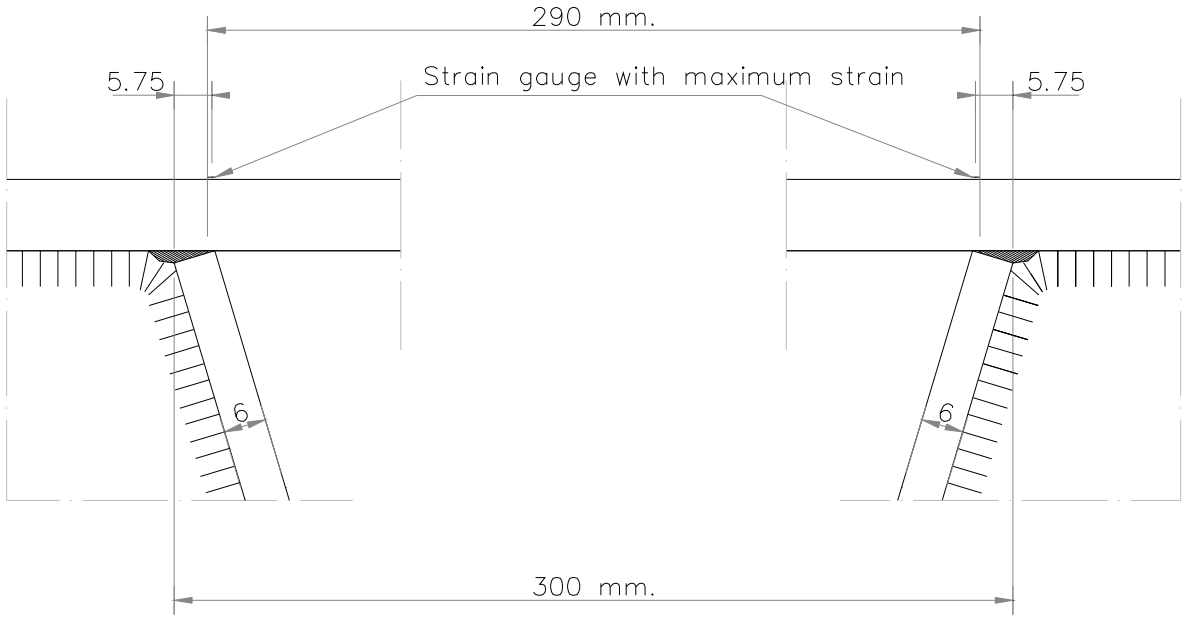

Figure 4-11: Span of the deck plate for clamped beam model

The span between the roots of the two longitudinal welds was approximately 292 mm and between the two strain gauges with the maximum strain was 300 – 2 x 5.75 = 288.5 mm. Thus the span of the clamped beam can be taken as 290 mm instead of 300 mm. The analytical calculated moments at the Left and Right location reduce by a factor of approximately 1.07 (De Jong, 2005-d).

Despite these explanations the clamped beam model is probably not valid. The fact that the measured moments are significantly lower than the analytical calculated moments for all three locations suggests that the beam was not fully clamped and rotation occurred. Because we are interested in the stress in the location of the crossbeam and the rotation occurred in the region outside the crossbeam web, rotation is not taken into account in the further analytical calculation.

Concluding remarks

- Analytical calculations and measurements of the strain in the deck plate under different footprint sizes were performed. The calculated and the measured strain for the deck plate fatigue crack locations Left and Right compare very well with each other, provided that:
  - in the analytical calculation of the tests results, a non-uniformly distributed load is adopted.
  - in the analytical calculation the real span of the clamped beam is taken as 290 mm of, instead of the nominal span of 300 mm.
- For fatigue verifications of deck plate crack this means that the stress calculations can be based on a clamped beam model, with the formula given in paragraph 4.2.2.1. For this calculation the wheel load can be modelled as a uniformly distributed load and the span of the clamped beam can be taken as 290 mm.
- The deck plate thickness of the test specimen was 10 mm. For thicker deck plates it can be assumed that the above mentioned conclusions are also valid, provided that the beam is a slender element.

4.2.3 Influence surfacing on stress distribution

4.2.3.1 Introduction

Steel bridge decks have a surfacing layer applied to the top surface of the deck. On movable bridges it is a thin epoxy layer approximately 8 mm thick. Fixed bridges usually have thick surfacing. Thin epoxy surfacing does not have a significant effect on the stresses in the steel structure but thick surfacing on steel bridge decks does.

Almost every fixed bridge in the Netherlands is built with a steel deck plate 10 mm thick and a mastic asphalt surfacing layer approximately 50 mm thick. An intermediate membrane, generally of bituminous material 2 or 3 mm thick, is applied, between the steel and the asphalt, see Figure 4-12. This membrane provides corrosion protection for the steel deck plate and a bond between the steel and the asphalt. Several authors have discussed the influence of the surfacing on the stresses in the steel deck construction. However there is a lack of fundamental understanding of the mechanisms. Surfacing has the effect of reducing traffic-induced stresses in the deck structure. This is thought to be partly due to the composite action with the deck plate in bending, and partly due to the load dispersal through the thickness of the asphalt layer (Medani, 2001-a).

The influence of the surfacing on the stress distribution is generally expressed as a stress reduction factor (SRF) for the stress in the steel structure, either in the trough web or in the deck plate. This is a simple approach for verifications of the steel structure. The factor (SRF) is defined as the quotient of the stress with surfacing and the stress without surfacing.

Figure 4-12: Asphalt surfacing on a steel plate with an intermediate membrane layer

4.2.3.2 Load dispersal through the surfacing

In current design practice surfacing is treated as a layer, which disperses load. This is described in Eurocode 1 – Part 2. The dispersal through the surfacing should be taken at a spread-to-depth ratio of 1 horizontally to 1 vertically down to the level of the middle plane of the steel deck plate. The concentrated wheel load should be taken as uniformly distributed on the whole contact area. This means that the Eurocode does not prescribe the distribution in the middle plane of the structural deck plate. However in practice this distribution is also taken as uniformly distributed. Figure 4-13 shows this load dispersal.

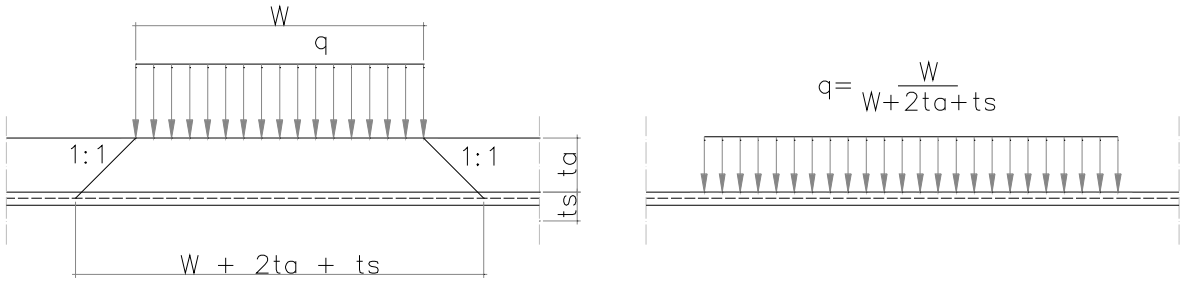

Figure 4-13: Load dispersal according to Eurocode 1 – Part 2

Some FE-models were made to verify this load dispersion (De Jong, 2001), one of these is shown in Figure 4-14. It is a 2D-model with plane stress elements, with a unit thickness of 1 mm. The height of the FE-model was 50 mm, the width approximately 500 mm. All nodes at the bottom line were restrained in x-, y- and z-direction. The wheel load was applied as a uniformly distributed line load on top of the surfacing. The line load was 0.4972 N/mm,

which was derived from a wheel of 35 kN, 220 mm wide and 320 mm long. The stiffness of the asphalt of the depicted model was 15000 MPa. The stiffness was varied, once at 1000 MPa, and once at 210000 MPa, which is the stiffness of steel.

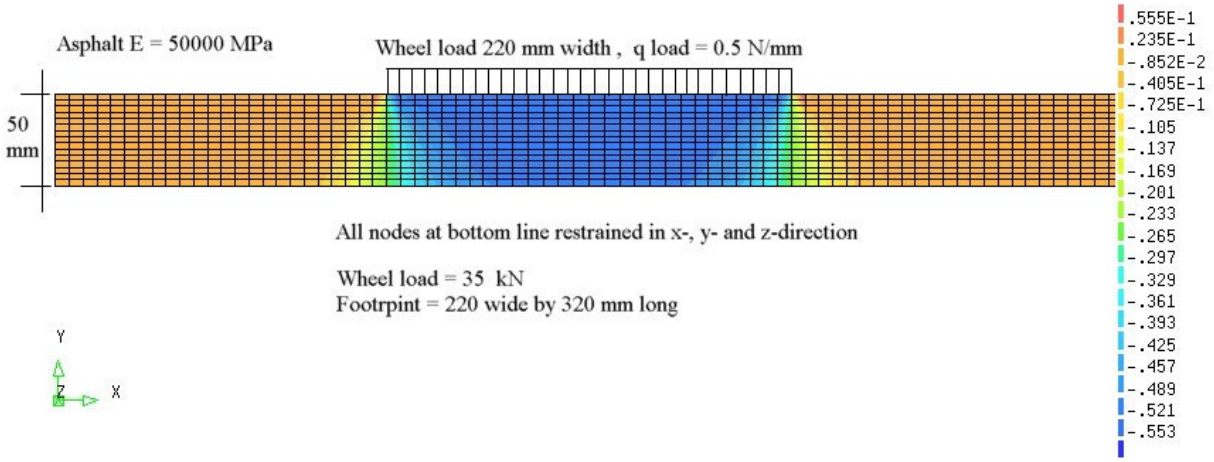

Figure 4-14: 2D FE-model load dispersion

Figure 4-15 shows the result of the calculation. The vertical contact stress in the bottom line of the asphalt layer is given. From this figure it is clear that the load is not uniformly distributed in the steel-asphalt interface, a trapezoidal model is more in accordance with reality.

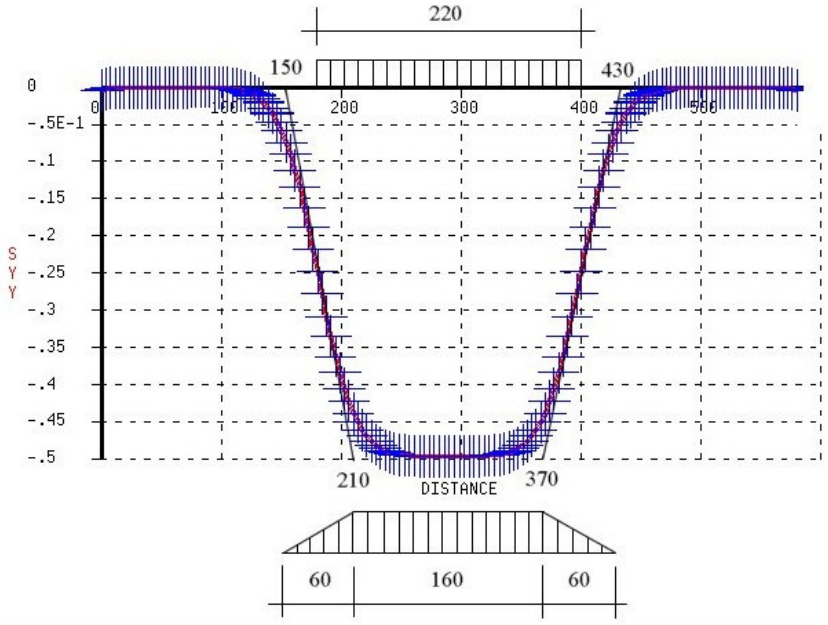

Figure 4-15: Stress in vertical direction at bottom line

Spread-to-depth ratio in Figure 4-15 is approximately 50-60, more or less the usual 1 to 1 ratio. Moreover the dispersal does not start from the edges of the wheel load. Approximately half of the dispersal is outside the tyre width and half is inside. The results of the models with other stiffness are the same as for 15000 MPa. Other parameters, which were varied in the FE calculations, were the Poison ratio (0,1 – 0.3 – 0.4999) and the constraints at the bottom line (x, y-, z- direction restrained, but also only in vertical y-direction restrained). Neither variation had any effect on the dispersal behaviour.

Based on this result three load models are available:
1. Uniformly distributed at the top surface of the asphalt in the contact area of the wheel load
2. Uniformly distributed in the middle plane of the steel deck plate, taking full account of load dispersal
3. Non-uniformly distributed trapezoidal shape of the contact pressure on the deck plate

These load models are depicted in Figure 4-16.

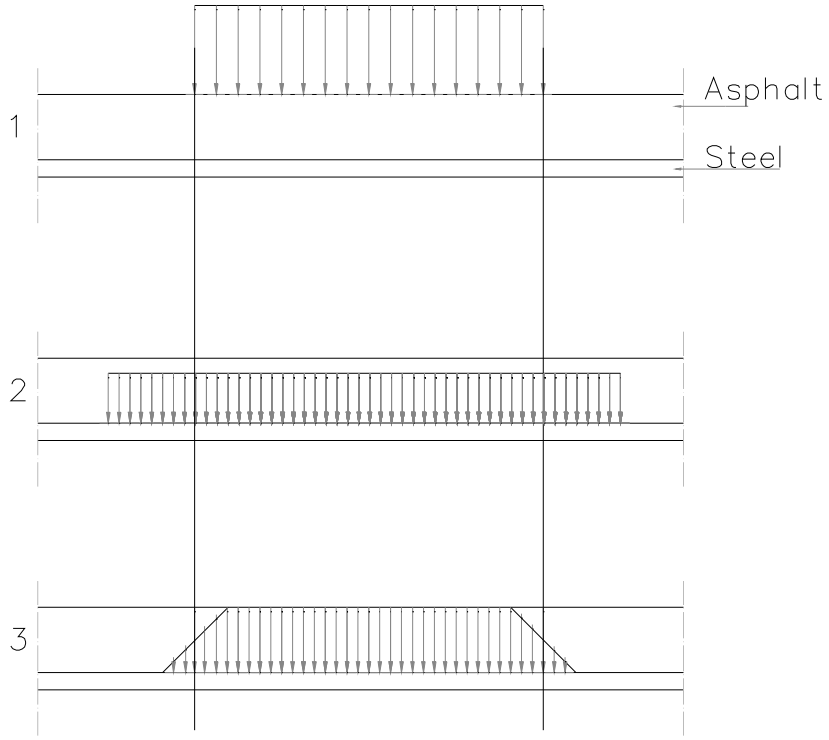

Figure 4-16: Models of load dispersal through surfacing

FE models were made of the deck plate at the intersection of the longitudinal girder and the crossbeam (De Jong, 2001). The three different load models are placed on top of the deck plate. Figure 4-17 gives the FE-model. The model is a 2D-model with plane stress elements,

with a unit thickness of 1 mm. It simulates the clamped beam model at the crossbeam location. The deck plate and two connecting parts of the crossbeam have been modeled. The outer sides of these crossbeam parts are restrained in x- and y-direction. The load is symmetrically placed on top of the deck plate.

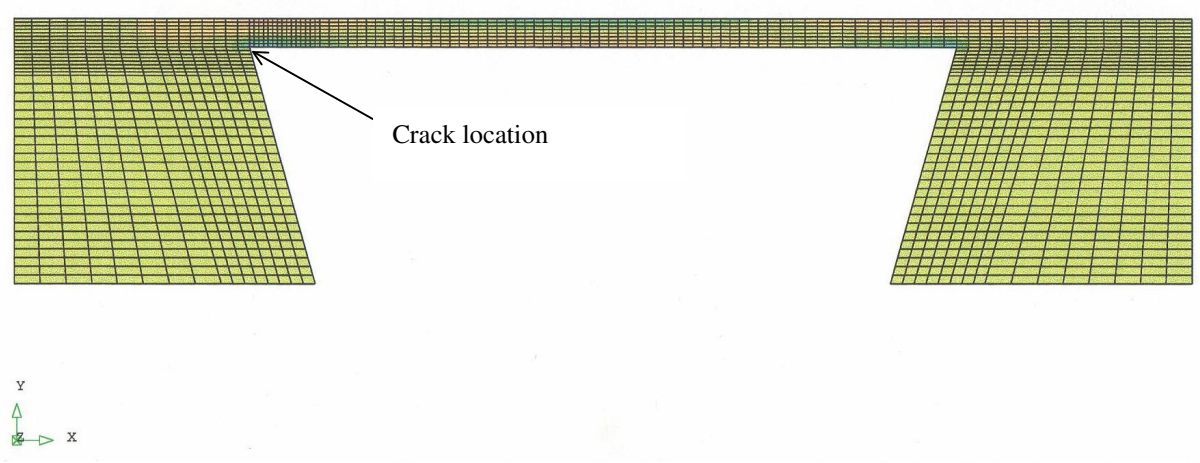

Figure 4-17: FE-model deck plate for stress calculation

The calculated stress at the location of the deck plate crack is given in Table 4-4.

Table 4-4: Stresses at crack location with different models of load dispersal

Load model, see Figure 4-16	Calculated stress FE-model MPa
1	-139.7
2	-99.8
3	-133.6

Stress reduction solely due to the effect of the load dispersal is negligible. This means that the stress reduction that occurs in practice is for the most part thought to be the effect of the surfacing acting as a beam to some extent in composite action with the steel deck plate.

Probably the simplified model of load dispersal given in the Eurocode covers both the load dispersal in reality, and the surfacing layer acting as a beam. At high temperatures the stiffness of the mastic asphalt layer is known to be very low, and thus in summer its contribution as a beam is small. In this case the load dispersal model in the Eurocode overestimates the stress reducing effects of the surfacing. The dispersal model in the Eurocode is useless for accurate fatigue verifications of deck plate cracks. The stress in the deck plate depends on the stiffness of the surfacing material. This stiffness is not taken into account in the Eurocode model.

4.2.3.3 Composite action

A simple mechanical model of a steel deck with asphalt surfacing is a linear elastic beam model. Both the steel deck plate and the asphalt surfacing are treated as beams. Both beams acting together carry the wheel load. One of the major design topics is the composite action between the steel plate and the surfacing layer. The stiffness of the intermediate membrane is one of the determining parameters for the composite action. With a membrane with very low stiffness composite action is negligible due to the shear displacements in the membrane. With a very high stiffness the shear displacements are negligible and almost a full composite action is possible, see Figure 4-18.

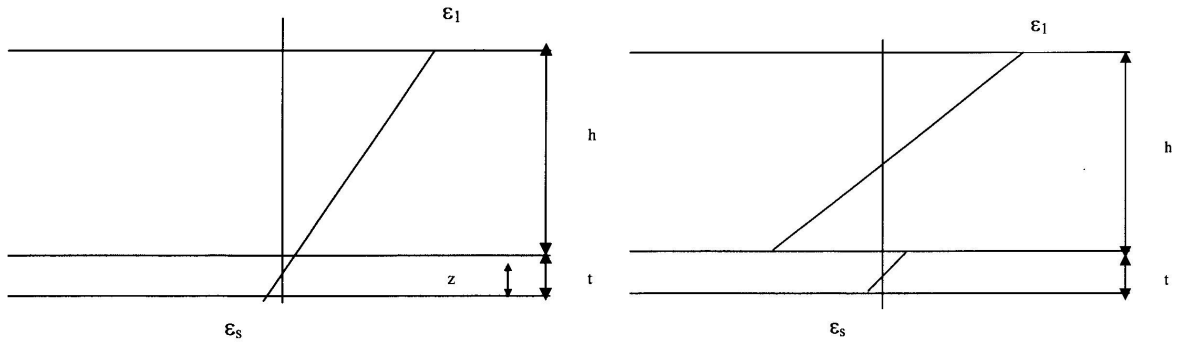

Figure 4-18: 100% composite action (left) and 0% composite action (right) (Medani, 2001-a)

Figure 4-19 shows the results of a theoretical analysis of the strain reduction due to composite action, which was performed by Kolstein (Kolstein, 1997, 1999-b, 2004-c).

The following parameters were varied in the analysis of Kolstein: the steel plate thickness (10-16 mm), the wearing course thickness (5-80 mm), the dynamic bending stiffness moduli of the wearing course (1000-30000 MPa) and the behaviour of the interlayer between the wearing course and the steel plate (flexible or stiff, see Figure 4-18). The model used consists of a beam (width 1 mm), which is loaded by a constant bending moment, which results in 70 MPa for a 12 mm steel plate without a wearing course layer. The calculated strains at the underside of the steel plate and the top of the wearing course are shown in Figure 4-19.

Figure 4-19 shows that the strain reduction in the 12 mm steel plate, with an asphalt surfacing of 50 mm with a stiffness of 16.000 MPa and a flexible interface, is approximately 85%-90%. For a stiffness of 2000 MPa, the reduction is still approximately 40%. Epoxy surfacings on movable bridges are 7 or 8 mm thick. For these surfacings a perfect bonding between steel and epoxy may be assumed, and thus a stiff interface. From the right part of Figure 4-19 it is clear that a small strain reduction is possible.

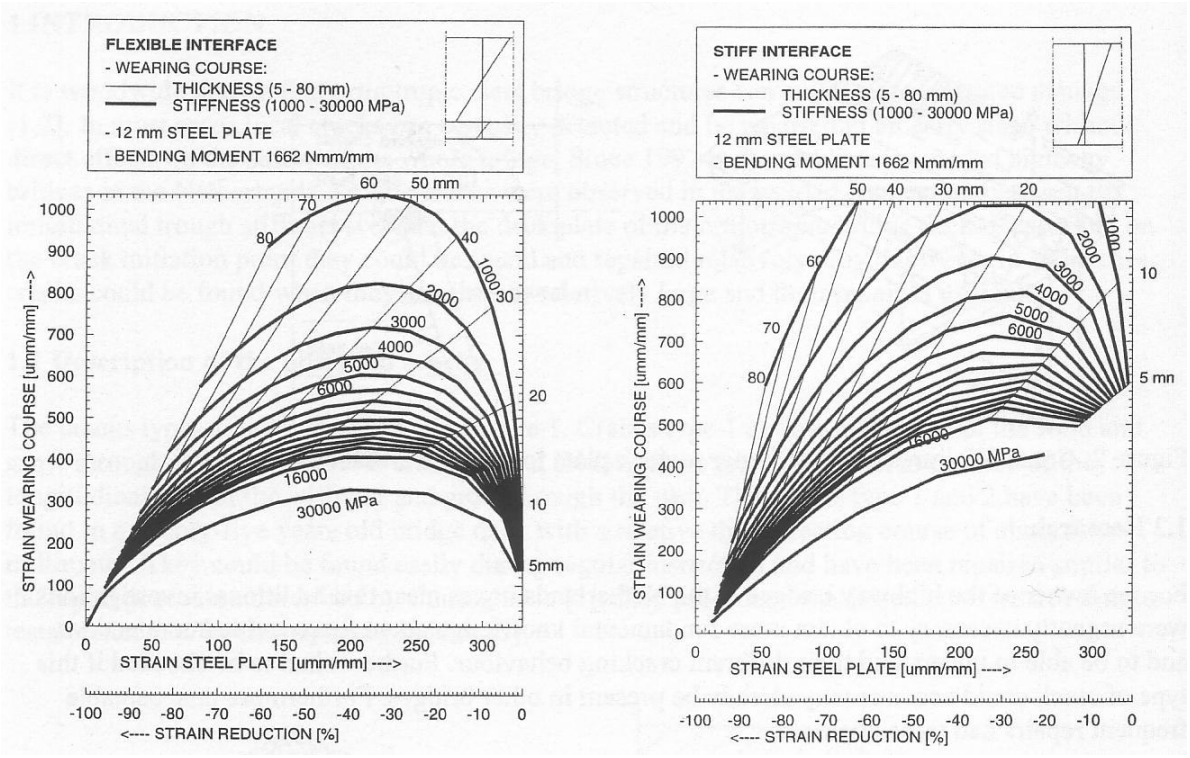

Figure 4-19: Theoretical analysis of the composite action on steel decks by Kolstein

4.2.3.4 Surfacing design methods

Medani and Huurman have performed an extensive literature survey in the field of asphalt surfacings on orthotropic steel bridge decks (Medani, 2001-a, 2006), (Huurman, 2003, 2004). Their conclusion is that no universally accepted method for the design of surfacings is available. Some theories are available, to estimate the stresses/strains in the different layers. But these theories are all based on one or both of the following assumptions:

- Linear strain gradient in the asphalt and the steel
- The gradient of strain through the depth of the asphalt and the steel are equal

In these theories the steel plate and the surfacing layer are treated as beams. However, an extensive experimental program conducted by Hameau et al (1981) has indicated that both assumptions might not be true, according to Medani (2001).

Medani concludes that there is a significant lack of knowledge in the field of design methods for asphalt surfacing on bridge decks. Factors that contribute to this lack of knowledge are:

- The adhesion and composite action between the steel deck and the asphalt surfacing is unknown.
- Very high strain levels. The strain levels measured at the top of the surfacing of an orthotropic deck are quite high (in the order of 1400 μm/m) compared with estimated strain levels of 120-150 μm/m in normal pavements. It is doubtful whether, under such

circumstances, the material will still behave linearly.
- Practice has shown that the existing linear models for estimation of strains in the asphalt have limited success in predicting the behaviour of the surfacing.
- The nature of loading in bridges is cyclic. This means that even if the stress level in the asphalt is less than the apparent strength of the material, the repetition of loading can lead to failure. Furthermore, the flexibility of the structure (vibration of the bridges) can enhance the distress process.
- The vibration of the bridges and the geometry of the structure can also lead to a non-linear response of surfacing materials.
- In linear models distinction between the response of the material in tension and compression is not possible. This implies that linear models can not predict the mode of damage correctly.

Medani concludes that a non-linear material model, which can describe the rather complicated response of the asphaltic surfacings on orthotropic steel decks, is needed (Medani, 2001-b, 2006). He concludes that the Asphalt Concrete Response (ACRe) material model can describe successfully the different aspects of asphaltic materials behaviour e.g. elasticity, visco-plasticity and cracking. The ACRe model was developed and experimentally validated at TU Delft. (Erkens, 2002). The most important finding is that there is a need for a new design procedure for surfacing on orthotropic steel decks. Such a procedure should be based on a proper understanding of the behaviour of the different materials involved, as well as the influence of the geometry of the structure. Fortunately, there are tools, which can be used to achieve these objectives. These tools comprise accurate non-linear material models and tailor-made finite element based programs (CAPA-3D, Computer Aided Pavement Analysis). Furthermore Medani is convinced that such tools will lead to more sophisticated procedures that can be used efficiently both at the design and the construction phase (quality control).

4.2.3.5 Site measurements of stress reduction due to asphalt

Several measurements on existing bridges have been performed in the past in order to derive stress reduction factors and the influence of the temperature on the stress reduction. In the Netherlands a few measurements were performed in the last decade. Kolstein reports these measurements (Kolstein, 1997, 2004-c). The measurements were performed on two bridges for several temperatures:
- Caland Bridge 1998 (2-7°C, 10-20°C and 20-33°C)
- Moerdijk Bridge 1994 & 1995 (5°C, 15°C and 35°C)

For both bridges the measurements were repeated at different times of the year to clarify the influence of the asphalt temperature. The Caland Bridge has a fixed part with a 10 mm steel deck plate and 50 mm thick mastic asphalt, and a movable part with a 12 mm steel deck plate and a thin epoxy surfacing 8 mm thick. The Moerdijk Bridge has three different deck plate

thicknesses: 10, 12 and 14 mm and is surfaced with a mastic asphalt surfacing approximately 60 mm thick.

Site measurements on the Caland Bridge

Strain gauges were applied to several locations on the underside of the bridge deck structure. The gauges were only mounted on the trough web. Identical sets of gauges were mounted on the fixed bridge 10 mm deck plate and on the lift bridge 12 mm deck plate. Figure 4-20 gives a schematic overview of the position of the strain gauges. The strain gauges were applied to the troughs in the wheel tracks of the heavy vehicle lane. The stress variations were measured and the stress ranges calculated with a rain flow analysis. The results are given as frequency curves in Figure 4-21. These curves give the cumulative number of stress cycles with a stress range larger than a given stress range.

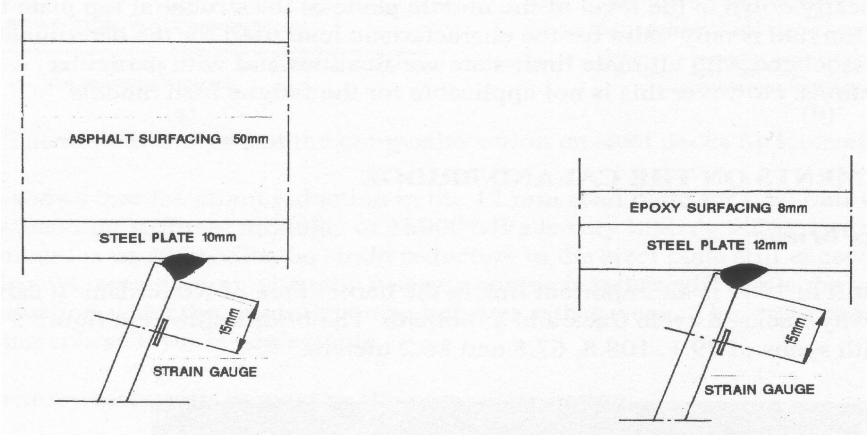

Figure 4-20: Strain gauge positions - site measurements-Caland Bridge

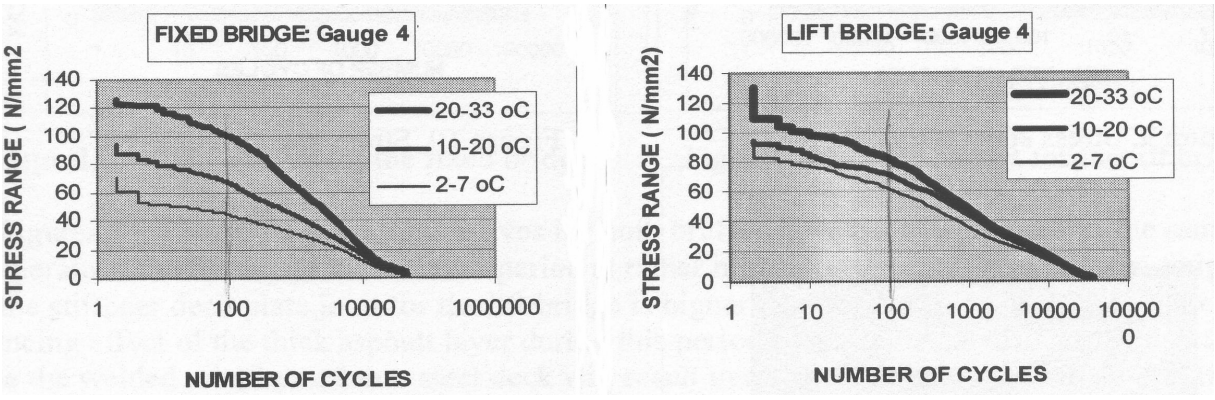

Figure 4-21: Measured stress spectra - Caland Bridge

Site measurements on the Moerdijk Bridge

Strain gauges were applied at several locations on the underside of the bridge deck structure. The gauges were mounted on the trough web, the underside of the deck plate and the

underside of the longitudinal girder. Identical sets of gauges were mounted on the bridge sections with 10, 12 and 14 mm deck plate thickness. Figure 4-22 gives a schematic overview of the applied strain gauges. The strain gauges were applied in the area of the wheel tracks of the heavy vehicle lane. They measured in transverse direction at trough web and deck plate.

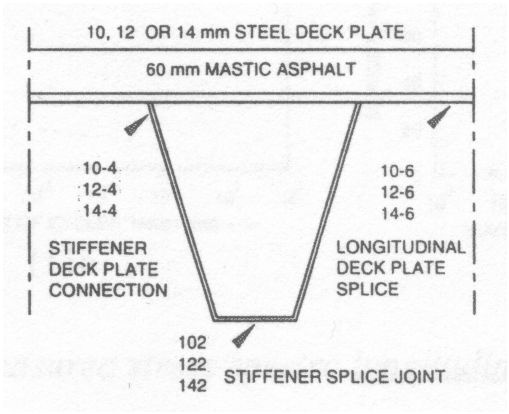

Figure 4-22: Strain gauges site measurements - Moerdijk Bridge

The stress variations were measured and the stress ranges calculated with a “rain flow” analysis. The results are given as frequency curves in Figure 4-23 for the trough web and in Figure 4-24 for the deck plate.

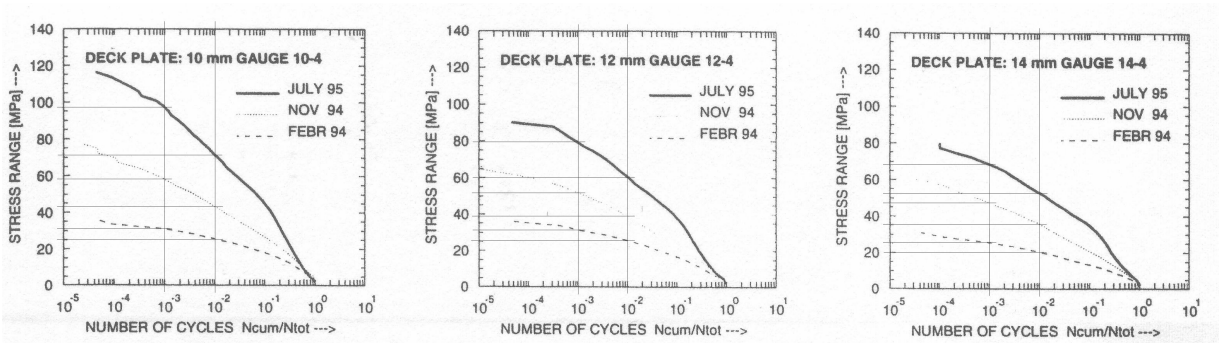

Figure 4-23: Measured stress spectra Moerdijk Bridge trough-deck plate connection

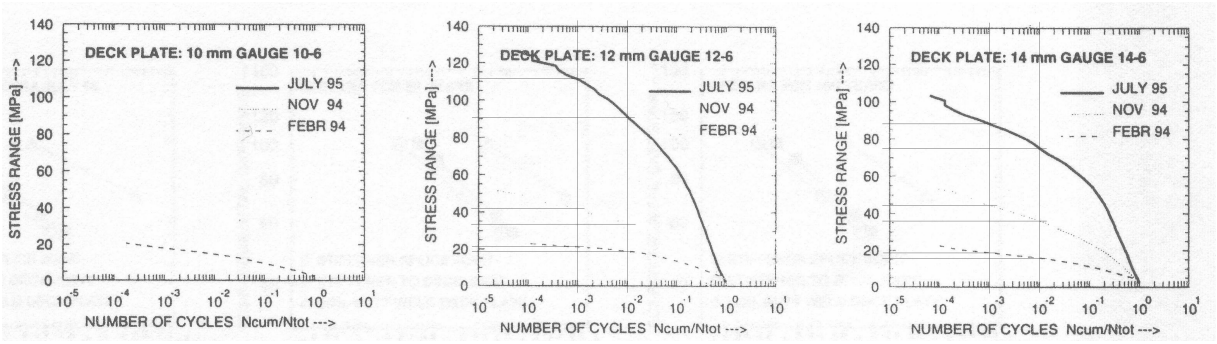

Figure 4-24: Measured stress spectra Moerdijk Bridge deck plate

Concluding remarks - site measurements

The measured stresses on the Caland Bridge were:

- $\Delta\sigma$ at N = 100 at 20-33 °C = 100 MPa for the fixed bridge
- $\Delta\sigma$ at N = 100 at 20-33 °C = 80 MPa for the lift bridge
- $\Delta\sigma$ at N = 100 at 10-20 °C = 68 MPa for the fixed bridge
- $\Delta\sigma$ at N = 100 at 10-20 °C = 74 MPa for the lift bridge
- $\Delta\sigma$ at N = 100 at 2-7 °C = 44 MPa for the fixed bridge
- $\Delta\sigma$ at N = 100 at 2-7 °C = 62 MPa for the lift bridge

From the measurements stress reduction factors were derived as follows:

In order to compare the measured stress ranges of the fixed and the lift bridge the lift bridge values should be multiplied with a factor 1.44, which is the quotient of the section modulus for deck plate thickness 12 mm and 10 mm. For this comparison it is assumed that the measured stress spectra on the lift bridge at the highest temperature represent the situation with no surfacing at best. The derived stress reduction factors are as follows for the trough web at the location of the longitudinal weld:

- Stress reduction factor at 20-33 °C = 100/(1.44x80) = 0.87
- Stress reduction factor at 10-20 °C = 68/(1.44x80) = 0.59
- Stress reduction factor at 2-7 °C = 44/(1.44x80) = 0.38

It was not possible to derive stress reduction factors from the measurements at the Moerdijk Bridge, because there is no comparison with a bridge deck without surfacing. However it is possible to get an impression, by making a comparison between the measurements in the different periods. The comparison is made for the stress ranges $\Delta\sigma$ at $N_{cum}/N_{tot} = 10^{-2}$ and $N_{cum}/N_{tot} = 10^{-3}$, and for the three deck plate thicknesses. The stress reduction factors are not significantly dependent on the deck plate thickness.

Assuming that the stress reduction factor for the highest temperature (35 °C) in Figure 4-23 is the same as the factor derived from the Caland Bridge for the trough web, an indication of the stress reduction factor for the trough web at the location of the longitudinal weld is:

- Stress reduction factor at 35 °C = 0.8 – 0.9
- Stress reduction factor at 15 °C = 0.5 – 0.6
- Stress reduction factor at 5 °C = 0.3 – 0.4

Assuming a stress reduction factor of 0.9 for the highest temperature (35 °C) an indication of the stress reduction factor for the deck plate is:

- Stress reduction factor at 35 °C = 0.8 – 0.9
- Stress reduction factor at 15 °C = 0.35 – 0.45
- Stress reduction factor at 5 °C = 0.15 – 0.25

At this point both the results of the theoretical analysis performed by Kolstein as shown in Figure 4-19 and indications of the stress reduction factors due to surfacing derived from the site measurements are available. It should be noted that a comparison of the theoretical and the experimental results points towards a theoretical analysis with a flexible interface for fixed bridges with a fairly thick surfacing. For movable bridges with a thin epoxy surfacing a theoretical analysis with a stiff interface is more in accordance with the measurements as shown in Figure 4-21.

4.2.3.6 Concluding remarks

This paragraph has discussed the stress reduction due to surfacing. Common design practice calculates with load dispersion with a spread-to-depth ratio of 1-to-1. For ultimate load capacity verifications this is probably a practical model, but for fatigue verifications this model is useless. The stress reduction is for the most part thought to be the effect of the surfacing acting as a beam, with some composite action with the steel deck plate. The composite action between the steel deck plate and the surfacing depends to a large extent on the stiffness of the membrane between steel and asphalt. A simplified theoretical analysis, according to Bernoulli's hypothesis has shown that significant stress reductions are achievable. However this hypothesis is not correct for asphalt surfacing on steel bridges. Medani has shown that a design method is necessary, which takes into account the non-linear behaviour of the asphalt material and the membrane. This design method is especially needed for the design of the surfacing.

In addition to the indistinct modelling of the stress reduction, site measurements were performed on the Caland and Moerdijk bridges. The measurements were performed with thick asphaltic and with epoxy surfacings. From these measurements indications for stress reduction factors were derived. A comparison of the theoretical analysis and the measurements points towards a model with a flexible interface for fixed bridges.

4.2.4 Ultimate load capacity deck plate with fatigue cracks

In this paragraph a test is reported that gives insight into the ultimate load capacity of a cracked bridge deck plate. The tests were performed on test panel B that had been used earlier for fatigue tests to derive a detail classification for the deck plate crack at the crossbeam. These fatigue tests as well as test panel B are described in paragraph 4.3.3. Cracks grew in this bridge deck panel due to the fatigue test. In this test panel one location was chosen where a wheel load was placed to test the ultimate load capacity of the deck plate. It is necessary to know which crack length in the deck plate, threatens the safety, see Figure 2-9. The longer the crack, the lower the ultimate static capacity of the deck plate. If the capacity is too low, an indentation in the deck plate due to a passing axle is possible. Such an indentation possibly

threatens the safety thus it is appropriate to get an idea of the ultimate capacity of the deck plate for several crack lengths.

4.2.4.1 First test

A static test was been performed on one location of test panel B. At the end of the fatigue test the cracks in test panel B were up to approximately 100 mm. Longer cracks were needed for the ultimate capacity test. Cracks were made in the deck plate with a machine, which is visible in Figure 4-25. The lengths of these cracks were 300 mm at one side and 100 mm at the other.

The test load application was displacement controlled, with a velocity of 0.1 mm/sec. The load was applied to a 30 mm thick steel plate and between this steel plate and the deck plate of the test panel was a 60 mm thick rubber layer. The used footprint is 270 wide by 320 mm long. The result of this test is presented in Figure 4-26. The deflection is the deflection of the piston above the 30 mm steel plate. The arrows 1, 2, 3 and 4 give the sequence of the test.

Figure 4-27 shows the rubber layer compressed at the maximum load of 439 kN, and a photograph of the deformation after unloading. The maximum load of the testing device was 439 kN. Regarding the rather strange shape at the top of the deflection-load curve, the software assumes that loads above 400 kN will not be applied in that particular testing machine. The load that was actually applied on the bridge deck was slightly above 400 kN, a maximum of 439 kN, according to the testing machine display. The software has recorded a load of 400 kN in the test file, although it was higher in reality. For loads up to 400 kN, the curve is correct, for loads above 400 kN an indication is given by grey dots.

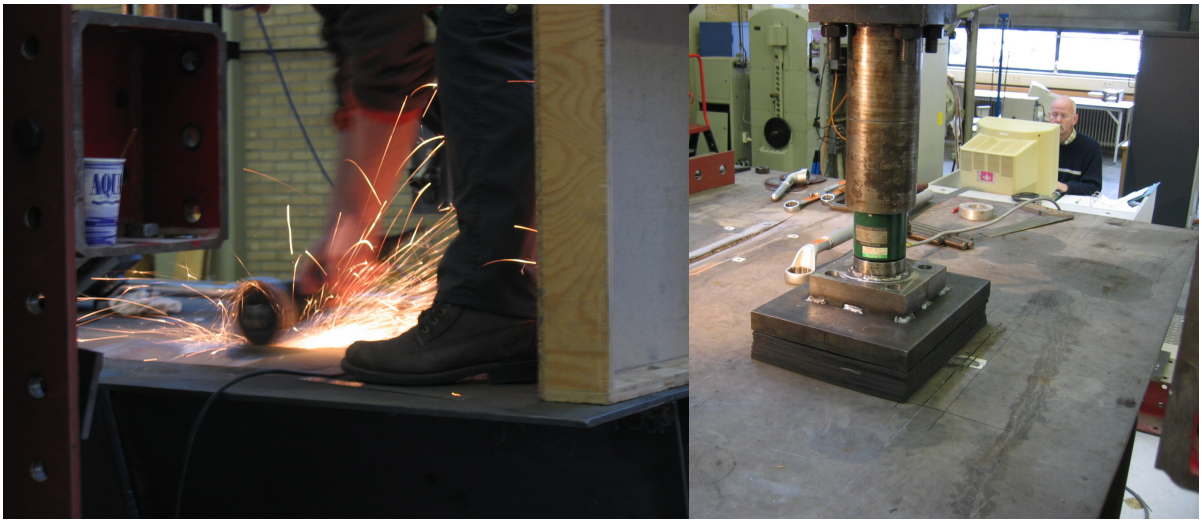

Figure 4-25: Making cracks (left), load application (right)

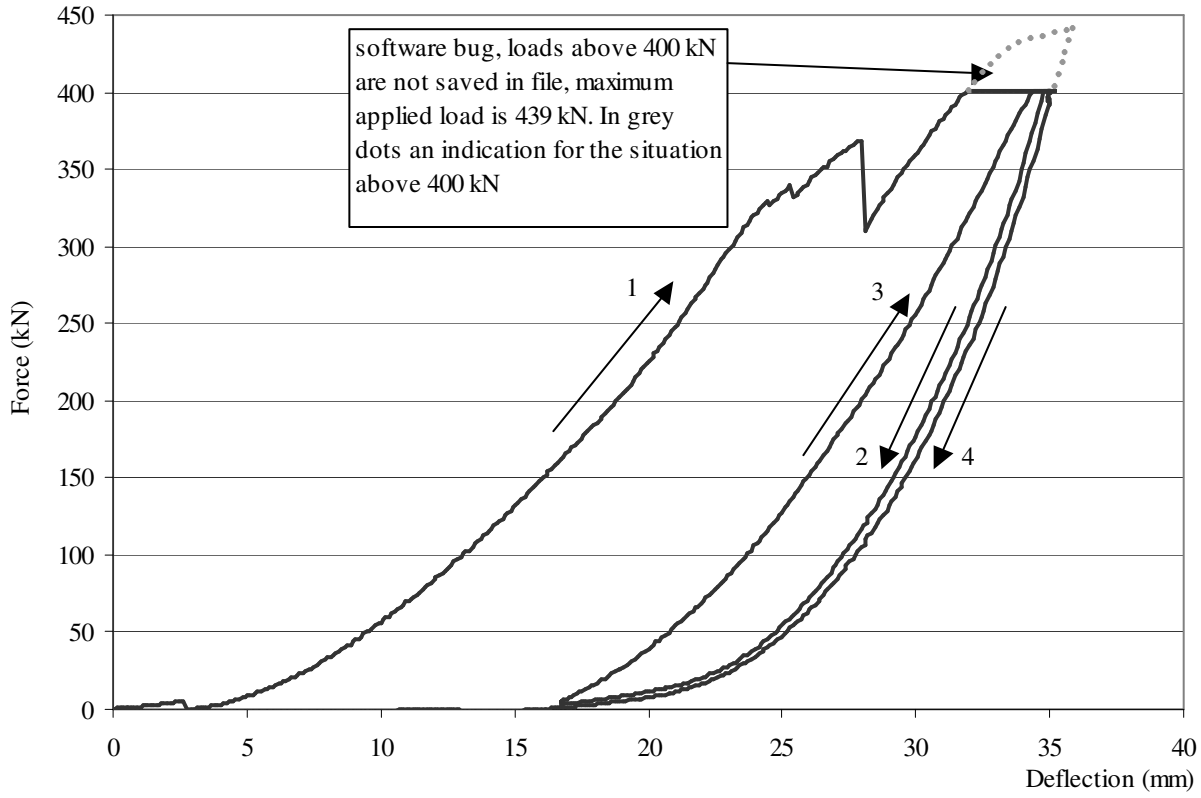

Figure 4-26: Ultimate load test deck plate crack

Figure 4-27: Compression at maximum load (left), deformation after unloading (right)

A few comments on this first test result:

- Two load cycles were applied: loading – unloading – loading - unloading
- Due to the compression of the rubber layer the deflection-force relation is non-linear.
- During the first loading a little cracking in the steel deck occurred. This is shown by a

sudden decrease in the load of approximately 50 kN at a deflection of 27 mm. At that moment some cracking noise was audible.

- A total deflection of the cylinder of approximately 35 mm was observed. Roughly 50% is due the rubber compression, roughly 50% is due to the (plastic) deformation of the deck plate.

The first conclusion is that a load of 439 kN in a bridge deck with two cracks (100 and 300 mm), has only created a relatively small deformation of the deck plate. With real wheel loads on bridge decks up to approximately 100 kN, the conclusion must be that these cracks lengths do not really threaten safety.

4.2.4.2 Other tests

The question after the first test was: what crack length then is threatening the safety? To research this, the cracks were made longer, step by step, as depicted in the left side of Figure 4-25. The crack lengths and the test results are given in Table 4-5.

Table 4-5: Results ultimate load capacity tests deck plate

Test No	Crack length left side (mm)	Crack length right side (mm)	Maximum applied load (kN)
1 (st02)	300	100	439
2 (st03)	400	100	439
3 (st04)	500	100	439
4 (st05)	500	200	439
5 (st07)	500	300	439
6 (st08)	500	400	439
7 (st10)	500	500	439
8 (st11)	600	600	439
9 (st12)	700	700	439
10 (st13)	800	800	439

For all tests it can again be said that the plastic deformation of the deck plate is limited. During the tests of course the deformation becomes somewhat larger, but after the 10^{th} test with two cracks at both sides of 800 mm, the maximum deformation was not more than approximately 50 mm. Once again in these tests also, the maximum applied load was not limited due to failure of the structure, but to the 439 kN maximum load of the testing device.

4.2.4.3 Conclusion

There are some obvious reasons to be careful with the results of this test:

- The test was only done at one location
- The load dispersal through the rubber layer was not exactly the same as a wheel load on a bridge deck

The reported test only gives a rough estimation of the ultimate limit state load. More tests and a numerical modelling can probably give more insight into the ultimate load capacity of a deck plate with fatigue cracks. But for the moment one crack of at least 500 mm is thought not to be a threat to the safety of the structure. Although the tests have been performed with longer cracks, 500 mm is chosen to be on the safe side.

This is enough information. It is not necessary to do more tests in a testing device with a higher load capacity. This becomes obvious, if the maximum applied load in the test described in this paragraph is compared to:

- Measured wheel loads, see Figure 3-4
- Fatigue load model 4 from Eurocode 1-3, see Figure 3-9
- Maximum allowed axle loads on motorway of 115 kN
- Maximum design axle load of 300 kN of a tandem system according to Eurocode 1-3

4.2.5 Concluding remarks

With respect to the local stress distribution due to wheel loads the following conclusion can be drawn:

- The stress at the location of the deck plate crack can be calculated with a clamped beam model. The wheel load can be modelled as a uniformly distributed load and the span of the clamped beam can be taken as 290 mm, instead of the nominal 300 mm.

With respect to the influence of asphalt on the stress in the steel structure:

- Common design practice calculates load dispersion with a spread-to-depth ratio of 1-to-1. For ultimate load capacity verifications this is probably a practical model, but for fatigue verifications this model is useless. The stress reduction is for the most part thought to be due to the effect of the surfacing acting as a beam, with a certain amount of composite action with the steel deck plate.
- The composite action between the steel deck plate and the surfacing depends to a large extent on the stiffness of the membrane between steel and asphalt. A simplified theoretical analysis, according to Bernoulli's hypothesis has shown that significant stress reductions are achievable. However this hypothesis is not correct for asphalt surfacing on steel bridges. Medani has shown that a design method, which takes into account the non-linear

behaviour of the asphalt material and the membrane is necessary. This design method is especially needed for the design of the surfacing.
- Besides the indistinct modelling of the stress reduction, site measurements were performed on the Caland and Moerdijk bridges. The measurements were performed with thick asphaltic as well as with epoxy surfacings. From these measurements indications for stress reduction factors were derived. A comparison of the theoretical analysis with the measurements points towards a model with a flexible interface for fixed bridges.

With respect to the ultimate load capacity of the deck plate with fatigue cracks:
- The reported test only gives a rough estimation of the ultimate limit state.
- More tests and numerical modelling can probably give more insight into the ultimate load capacity of a deck plate with fatigue cracks.
- For the moment one crack of at least 500 mm is thought not to be a threat to the safety of the structure.
- Deformation under the ultimate load was limited. The structures gives a warning before excessive deformation occurs.

4.3 Fatigue behaviour bridges

4.3.1 Introduction

Several researchers have contributed to the knowledge of fatigue behaviour of orthotropic steel bridge decks. The detail classifications established in Eurocode 3 (EN 1993-1-9:2005) are based on research performed in the past. Paragraph 4.3.2 gives an overview of the work that was done in this field in the last few decades. This leads to the conclusion that, especially for deck plate cracks, there is a lack of knowledge. Paragraph 4.3.3 describes fatigue tests to derive more detailed information about the fatigue behaviour of deck plate cracks.

4.3.2 Literature review

4.3.2.1 S-N detail classification of the longitudinal trough web – deck plate weld

Kolstein has reported on the fatigue strength of different fatigue prone details in orthotropic bridge decks (Kolstein, 1996). This publication gives an overview of research that was performed in the previous decade at several universities and research institutes. The research reported by Kolstein was partly funded by the former European Coal and Steel Community. The research programmes studied the fatigue behaviour of several details in orthotropic bridge decks:
- Longitudinal weld between trough web and deck plate, see Figure 2-16 and Figure 2-17

- The connection between longitudinal trough profile and the crossbeam, see Figure 2-20 to Figure 2-24
- The stiffener (trough) splice joint, see Figure 2-18 and Figure 2-19

Only the research into the fatigue behaviour of the longitudinal weld between trough web and deck plate is described in this thesis.

Detail classification longitudinal weld trough web-deck plate

Studies of the fatigue behaviour of the longitudinal weld between trough web and deck plate were carried out by Janss (Janss, 1988), Bignonnet (Bignonnet, 1990), Bruls (Bruls, 1990) and Gurney (Gurney, 1987, 1992). Janss and Gurney researched the fatigue behaviour of manual weld connections. Bignonnet and Bruls researched the influence of the automatic welding procedure and the influence of the gap between the deck plate and the trough web before welding. Before the production of the fatigue test specimens the welding parameters of the automatic welding procedure were optimised. It was shown that full penetration welds with a lack of penetration less than 1 mm can be achieved (Kolstein, 1996). Figure 4-28 shows the test set up used, which was the same for all these fatigue tests.

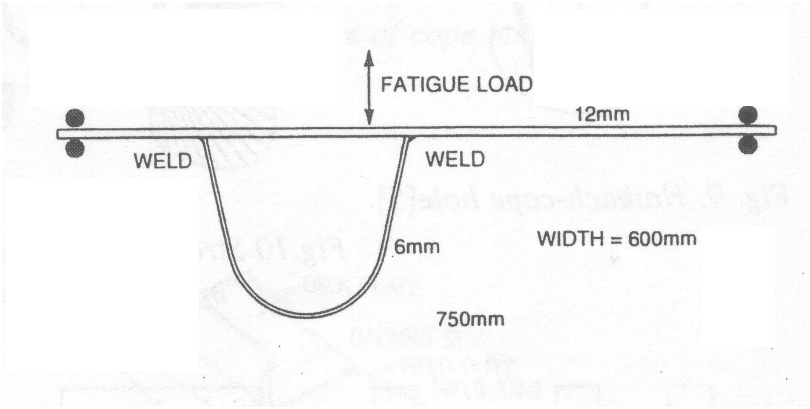

Figure 4-28: Fatigue test set up longitudinal weld deck plate - trough web

Two conclusions can be drawn from the reported tests, see Figure 4-29:

- From the test it became clear that there was no significant difference between the fatigue behaviour of specimens with a 2 mm gap between the trough web and the deck plate and those with no gap.
- The fatigue strength of the connection made with automatic submerged arc welding is significantly greater than one made by manual arc welding, due the greater penetration and the larger throat of the weld.

Both conclusions are logical. The stress range in the trough web is responsible for fatigue cracks in the longitudinal weld. A full penetration weld instead of a fillet weld reduces the eccentricity significantly, and thus reduces the stress in the longitudinal weld. Increasing the size of the throat also reduces the stress in the longitudinal weld.

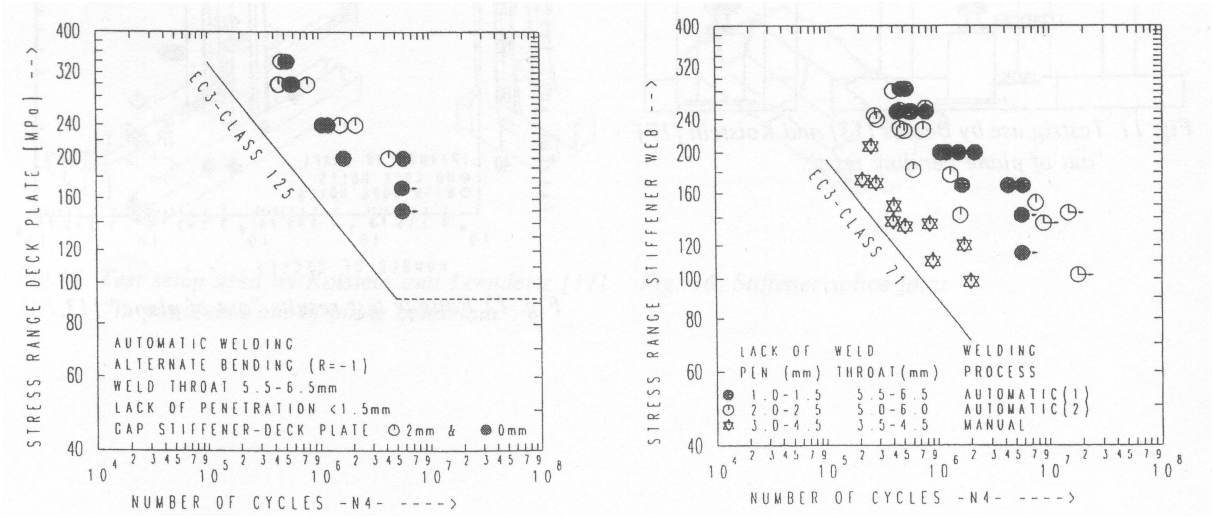

Figure 4-29: Test results fatigue tests longitudinal weld (Kolstein, 1996)

Table 4-6 gives derived fatigue detail classifications, which were based on the four mentioned research projects. The detail classifications are given for the research data and for design situations. The detail classification for the measured data is based on the measured stress range from a gauge adjacent to the weld toe i.e. the crack location. The detail classifications for design situations are higher, because these classifications are based on the nominal stress in the trough web at the weld toe. A stress gradient in the trough web was measured with the strain gauges, and thus an extrapolated nominal stress could be calculated. This made it possible to derive these design classifications.

Table 4-6: Fatigue detail classification weld trough web – deck plate (Kolstein, 1996)

Description	No of tests	Research data	Design recommendations
Fillet welded joint, lack of penetration > 4mm	84	56	63
Partial penetration welded joint, lack of penetration 2 mm	16	50	56
Full penetration welded joint, throat thickness 6 mm, manual weld	26	80	90
Full penetration welded joint, throat thickness 6 mm, automatic weld	13	90	100

Eurocode 3 - Part 1.9, however gives less details and the values of the detail classifications are significantly lower. A partial penetration weld with a ≥ t has a detail classification of 71

MPa, and a fillet weld or partial penetration weld with a < t has a detail classification of 50 MPa, where a is the throat thickness of the weld and t the thickness of the trough web.

4.3.2.2 S-N detail classification of the deck plate crack at the crossbeam location

In 1997 deck plate cracks were found in the Van Brienenoord bascule bridge, see paragraph 2.3.2. At that time, this crack type was almost unknown and knowledge about its fatigue behaviour was not available. In order to develop a fatigue detail classification of this joint Kolstein performed some full scale laboratory tests on two orthotropic bridge deck panels (Kolstein, 2000-a). The deck plate thickness of these panels was 12 mm. For the fatigue tests a footprint of 270 mm wide by 320 long was used, representing a super single. In all tests the wheel load was located above the crossbeam and the longitudinal girder connection. The load range of the tests was 80.1 kN (test No. 16, trough 4), and 80.0 kN (test No 17, trough 6). In total three results that are valuable for the derivation of a fatigue detail classification were obtained. Table 4-7 gives the number of test specimen cycles at the time when a crack was first detected by visual inspection and the number of cycles and length of crack at the last visual inspection at the end of the fatigue test. The detail classifications derived by Kolstein are given in Table 4-8, both for the length at the first observation of the crack as well as for a crack length on top of the deck plate of 50 mm.

Table 4-7: Cycles at visual observations of cracks at topside deck plate (Kolstein, 2000-a)

	First Visual Crack		End fatigue test	
Test No.	*N*	Length (mm)	*N*	Length (mm)
16, trough 4, web G	1362500	43	3264809	129
16, trough 4, web H	1362500	16	3264809	148
17, trough 6, web K	1072190	7	5412392	121

Table 4-8: Fatigue detail classifications (Kolstein, 2000-a)

	NEN	EC	NEN	EC
Crack length	f.v.c.	f.v.c.	50 mm	50 mm
S-N value design	101	172	101	171

4.3.2.3 Crack growth models & fracture mechanics

The available fatigue standards do not cover the crack in the deck plate at the intersection of the longitudinal trough girder and the crossbeam. As such a classification was necessary in order to make a new design for the bascule part of the Van Brienenoord Bridge in 1997/1998 a detail classification was derived using a fracture mechanics crack growth analysis (Dijkstra, 1998). This crack growth analysis was based on a flat plate (the deck plate) with a semi-

elliptical surface crack at the weld root (weld between deck plate and the trough wall). The effect of the stress concentration due to the crossbeam web was taken into account by reducing the applied stress as the crack width increases. The stress reduction rate was taken in accordance with the calculated stress distribution from the FEM analysis. An average crack growth rate curve (*da/dN-ΔK* curve) was used. For the analysis the applied hot spot bending stress range was taken at a level of 100 MPa.

The lifetime from an initial crack to a through crack was calculated at 7.55 million cycles. This corresponds with an average classification ($\Delta\sigma_k$) of 91 MPa at 10 million cycles, which is N_c according to the Dutch fatigue code NEN 2063 (NEN 2063, 1988). In Eurocode format this means a classification of 156 MPa. The design values of the detail classification are 67 MPa according to the Dutch NEN 2063 standard and 115 MPa to the Eurocode standard. The classification corresponds to a crack with a depth just equalling the thickness of the deck plate and a length of 0 mm at the top of the deck plate. Dijkstra has described this crack growth model more extensively (Dijkstra, 2002). A crack growth curve for the deck plate crack at the intersection of trough and crossbeam from his report is shown in Figure 4-30.

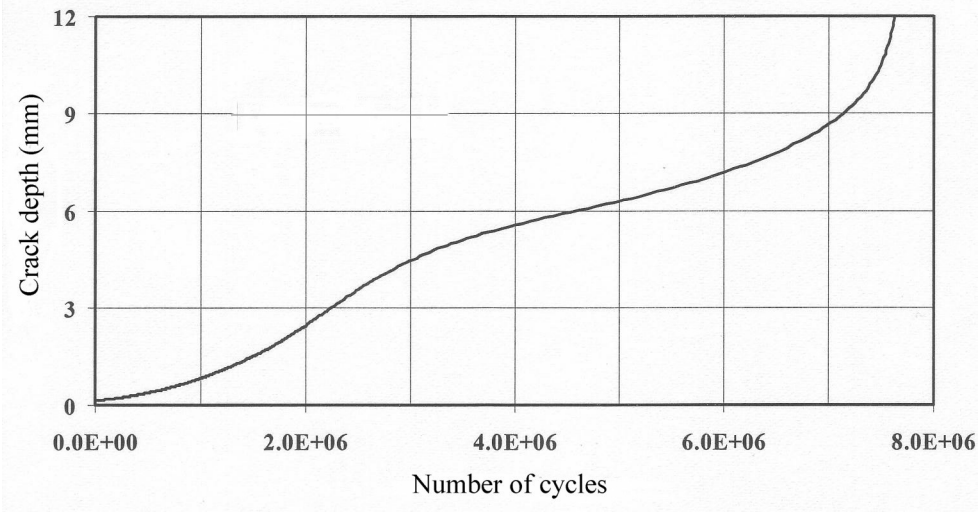

Figure 4-30: Crack growth curve - deck plate crack (Dijkstra, 2002)

4.3.3 Fatigue tests - deck plate fatigue cracks

4.3.3.1 Description of tests

Introduction

Within the framework of this thesis full-scale laboratory experiments were performed in order to determine the fatigue behaviour of the deck plate at the intersection of the crossbeam and

the longitudinal trough girder. That in brief is the objective of the research described in this paragraph. Although full-scale experiments were performed by Kolstein (Kolstein, 2000-a), more test data is necessary in order to derive an accurate detail classification for the deck plate crack at the crossbeam location.

Strain gauges were applied to the test panels at many locations. The results of these studies are presented in this paragraph. From the experimental work S-N detail curves were derived for different crack sizes.

Test panels

For the fatigue tests two bridge deck panels were used: test panel A and test panel B. Test panel A was also used for the earlier performed static measurements, described in 4.2.2.2. and is shown in Figure 4-2.

Test panel B was 4 m long and 2m wide. The panel was built with two crossbeams, 3 troughs and a deck plate. The deck plate was 10 mm as were webs of the crossbeams. The 3 troughs were standard Krupp-2/325/6 profiles. Cope holes were provided at the connection of the troughs to the crossbeams to give a better fit of the two parts. The longitudinal weld between trough web and deck plate had a 5 mm throat dimension. Figure 4-31 shows test panel B.

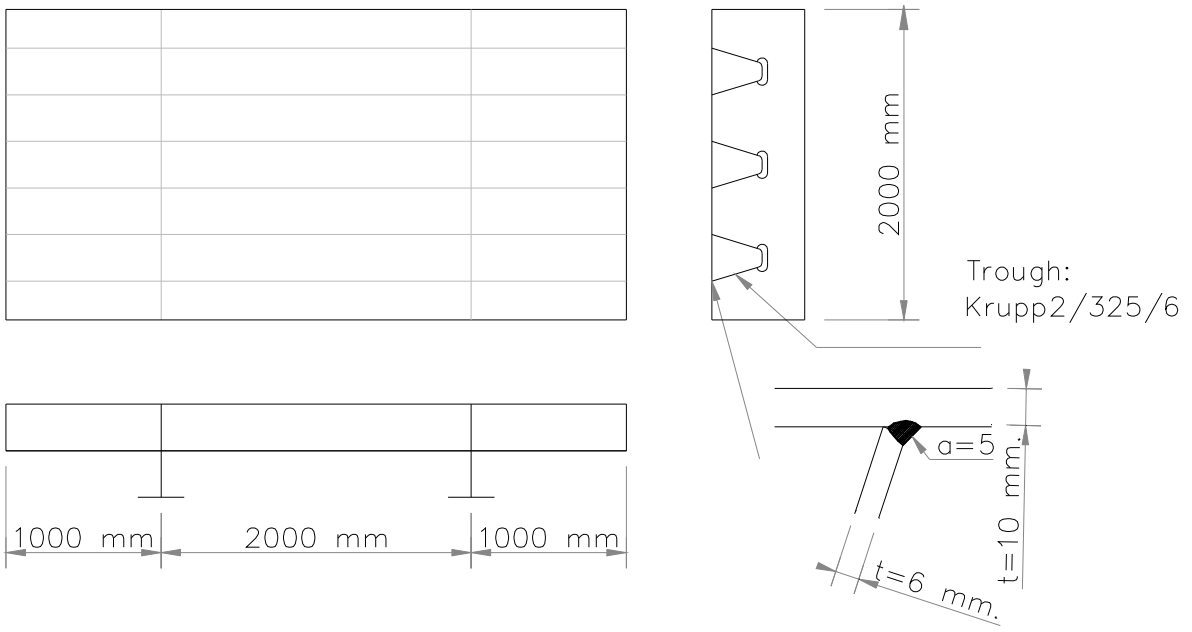

Figure 4-31: Test panel B

Strain gauges

At several locations on the steel deck plate strain gauges were mounted to measure the strains under different loadings. Paragraph 4.2.2.2 describes the exact location of all strain gauges for

panel A. Extensive strain measurements have taken place on test panel A and for that reason a limited number were applied to test panel B. Each intersection of trough web, crossbeam web and deck plate was provided with three strain gauges. These gauges were all mounted on the top of the deck plate. In total 6 strain gauges for each trough-crossbeam connection were mounted as shown in Figure 4-32.

Test set up

For the fatigue tests the test panels were placed in the test rig. The test set up was assembled in the Stevin laboratory and the maximum vertical load was 400 kN. For more information on the test set up, see (De Jong, 2005-e).

The fatigue tests were performed in several phases. Test panel A was the first panel subjected to the fatigue test followed by panel B. For panel A troughs 1 and 3 were subjected to the fatigue test simultaneously. Trough 2 was tested individually.

For panel B all the troughs were tested individually. The method of application of the load was the same as for the static tests on panel A, see Figure 4-5. The load was applied on a load area of 270 mm by 320 mm. (width x length), representing the super single tyre from Eurocode 1991-2, see chapter 3. The applied loads were measured during the test, and are given in Table 4-9.

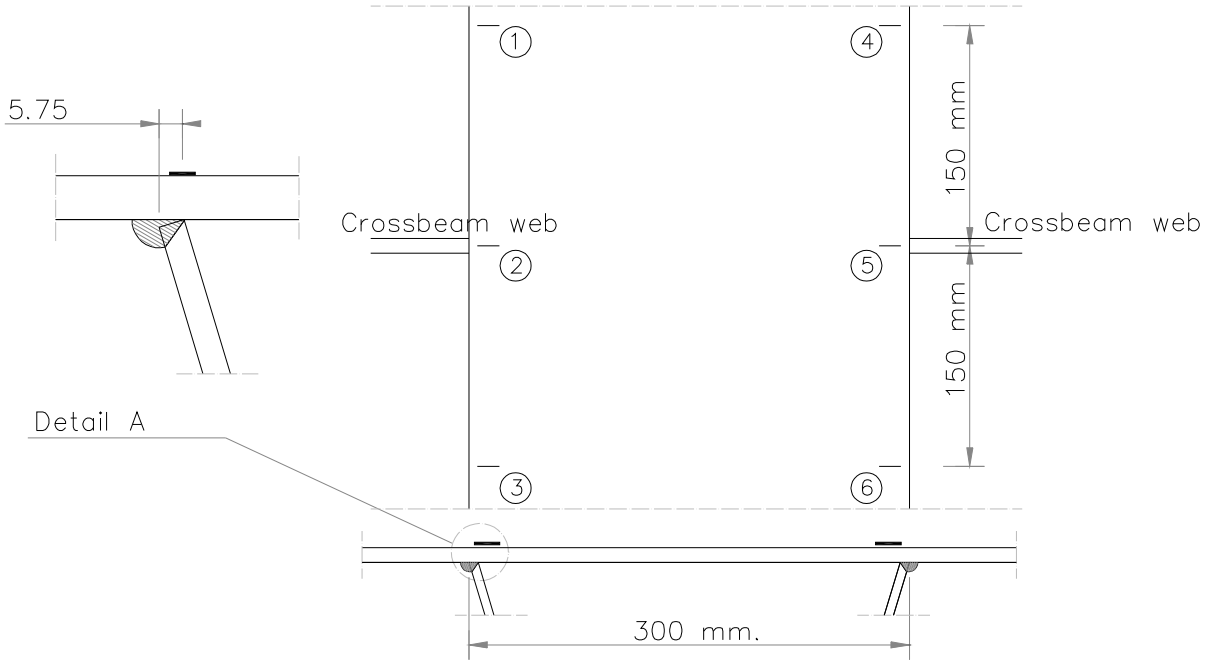

Figure 4-32: Strain gauges at a trough-crossbeam connection test panel B

Table 4-9: Applied loads - fatigue tests

Test no.	Description	F_{min} (kN)	F_{max} (kN)	Range (kN)	R-ratio
C & B	Panel A trough 1	5	68.78	63.78	0.073
E & F	Panel A trough 2	5	69.30	64.30	0.072
A & D	Panel A trough 3	5	69.01	64.01	0.072
br202	Panel B crossbeam 1 trough 1	5	80.27	75.27	0.062
br203	Panel B crossbeam 1 trough 2	5	80.15	75.15	0.062
br204	Panel B crossbeam 1 trough 3	5	79.97	74.97	0.063
br-08	Panel B crossbeam 2 trough 1	5	93.76	88.76	0.053
br-09	Panel B crossbeam 2 trough 2	5	77.18	72.18	0.065
br-10	Panel B crossbeam 2 trough 3	5	77.19	72.19	0.065

4.3.3.2 Test results

During the fatigue test the strains were measured continuously. A complete overview of the measured strain ranges is given in Stevin Report 6.04.4 (De Jong, 2005-e). The cracks in test panel A are identified with A, B, C, D, E and F. A was the first visually observed crack, F was the last. The locations of these cracks in test panel A are shown in Figure 4-33.

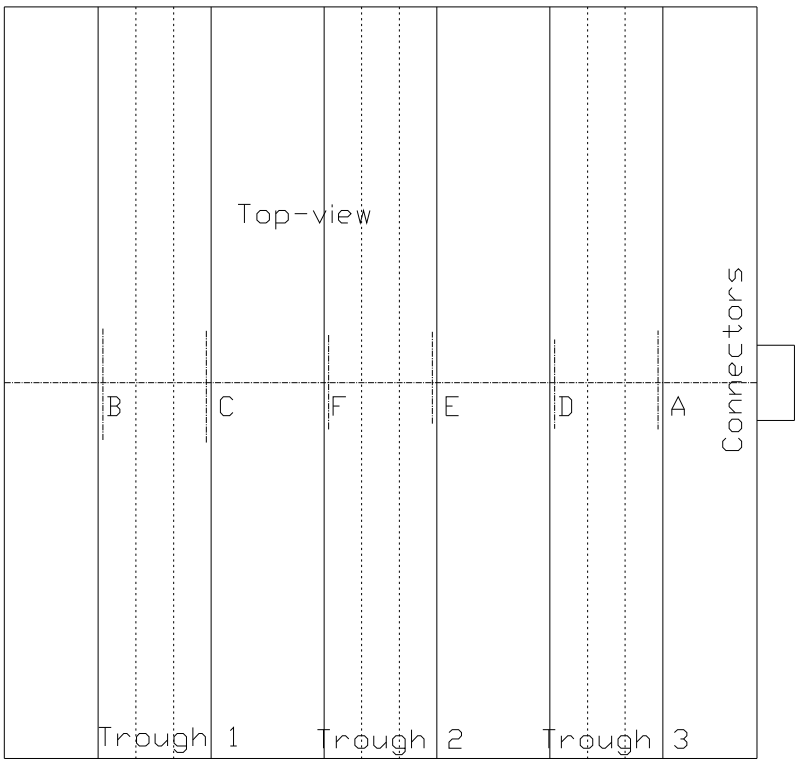

Figure 4-33: Cracks in test panel A

The cracks in test panel B are identified with br202, br203 and br204 for the first crossbeam and br-08, br-09 and br-10 for the second crossbeam. Each of these six indications has a left and a right variant, indicated with “a” or “b”.

During the fatigue tests the bridge deck structure was visually inspected on a regular basis. For test panel A, the first visual crack at the top surface of the deck plate was observed after the number of stress cycles shown in Table 4-10. The lengths of the cracks are from 22 to 36 mm and the average length of the first visually observed crack was 28 mm. After this first visual observation of a fatigue crack the test was continued in order to obtain longer cracks. During this continuation the crack length was monitored. Table 4-10 also gives the number of cycles and the length of the cracks at the end of the fatigue test of test panel A.

Table 4-10: Cycles at the first and last visual observations of top surface deck plate cracks in panel A

	First Visual Crack		End fatigue test	
Test No.	*N*	Length (mm)	*N*	Length (mm)
trough 3 A	1310910	36	3055450	165
trough 1 B	1141172	34	3055450	208
trough 1 C	1561051	26	3055450	201
trough 3 D	1650740	23	3055450	136
trough 2 E	1140605	22	3205000	150
trough 2 F	1472200	23	3205000	155

The crack growth is given in Figure 4-34. On the horizontal axis the cycles after the first visual crack are given. On the vertical axis the crack length on top of the deck plate is given, see Figure 4-38. Table 4-11 and Figure 4-35 give the same information for test panel B. It should be noted from the tables that the number of cycles before the first visual observation is clearly dependent on the applied loads. For both test panel A and test panel B a function that describes the average crack growth rate was derived from a linear regression analysis. These functions are given in the figures. It is obvious from the comparison between the crack growth rate in test panel A and panel B that there is a strong correlation between the applied load range and the crack growth rate.

The load ranges for test panel A were all approximately 64 kN. The load ranges for test panel B vary from 72 to 89 kN. In the function for test panel B the results of br-08 were excluded, which makes that the load ranges for the included tests vary between 72 and 75 kN.

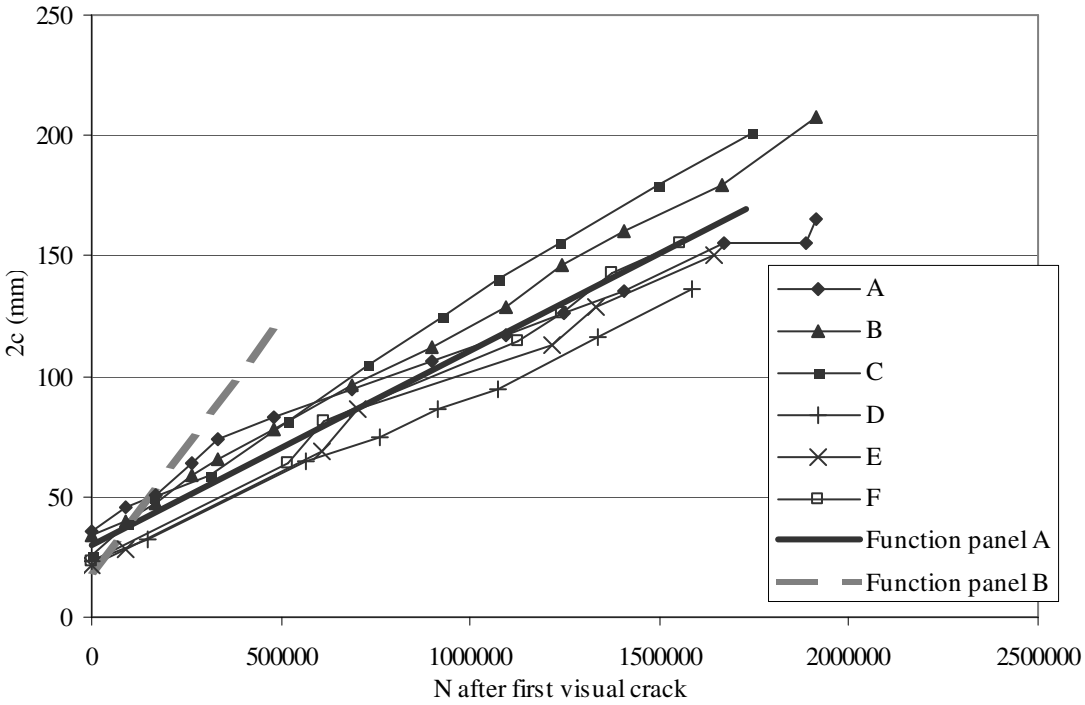

Figure 4-34: Crack growth test panel A after first visual crack observation

Table 4-11: Cycles at the first and last visual observations of top surface deck plate cracks in panel B

	First Visual Crack		End fatigue test	
Test No.	*N*	Length (mm)	*N*	Length (mm)
br202 A	875431	5	1036042	40
br202 B	479221	10	1036042	120
br203 A	679663	12	1119456	92
br203 B	1119456	73	1119456	73
br204 A	477622	10	779815	85
br204 B	477622	10	779815	74
br-08 A	166209	25	280345	50
br-08 B	280345	15	280345	15
br-09 A	539944	30	901153	90
br-09 B	869925	8	901153	15
br-10 A	667255	10	1010108	75
br-10 B	771073	40	1010108	95

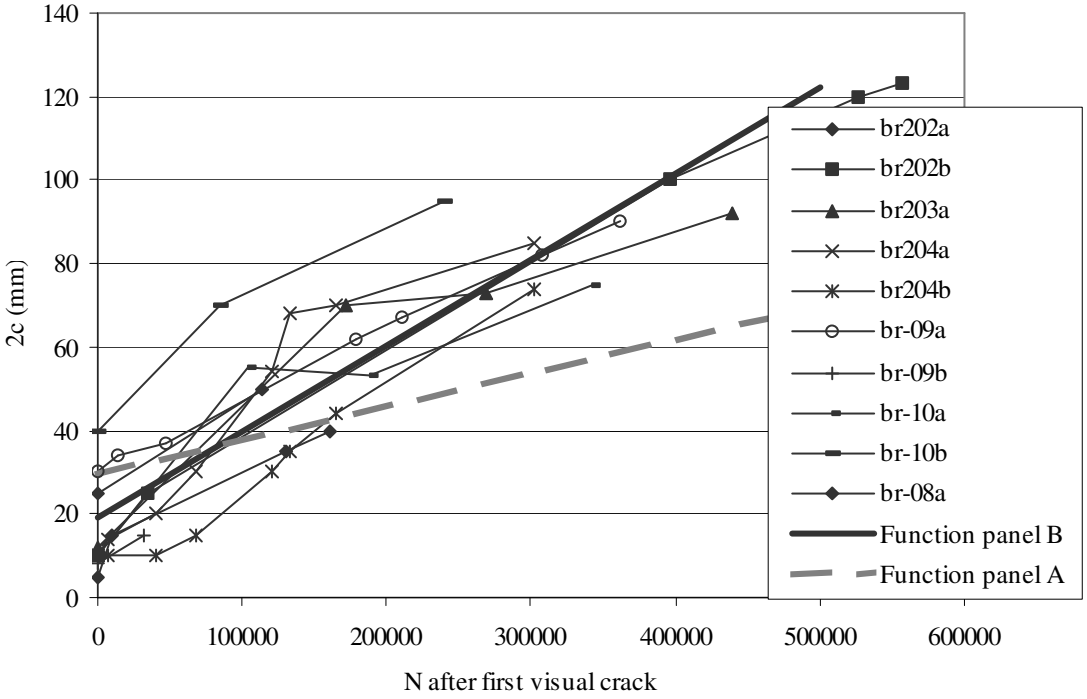

Figure 4-35: Crack growth test panel B after first visual crack observation

The crack dimensions reported in the tables were measured during the fatigue test. A small amount of petroleum was smeared on the deck plate. After a few moments the crack tip was "breathing". At this moment the exact location of the tip was visible and the crack could be measured with great accuracy.

From Figure 4-34 and Figure 4-35 it is clear that after the crack was observed the crack growth rate in the longitudinal direction at the top surface of the deck plate was constant for a crack length up to 200 mm.

Dye Penetrant inspection

After the fatigue test the cracks of test panel A were made visible by a dye penetrant inspection technique. Photographs of the 6 cracks in test panel A are shown in Figure 4-36 and 4-37. From this inspection two points became obvious:

- The visible length in the dye penetrant inspection was a little bit, approximately 10-30 mm, smaller than the previously measured length during the fatigue test.
- The cracks are not a straight line above the weld between trough web and deck plate, they show a curvature towards the inner side of the trough. Cracks detected in bridges however are nearly always a straight line above the weld between trough and deck plate.

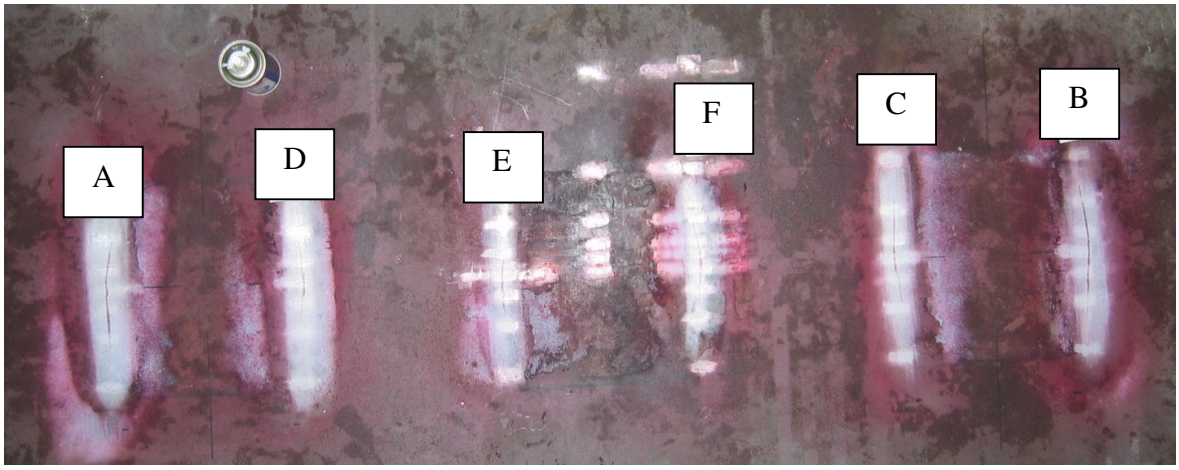

Figure 4-36: Overview detected cracks in test panel A after dye penetrant inspection

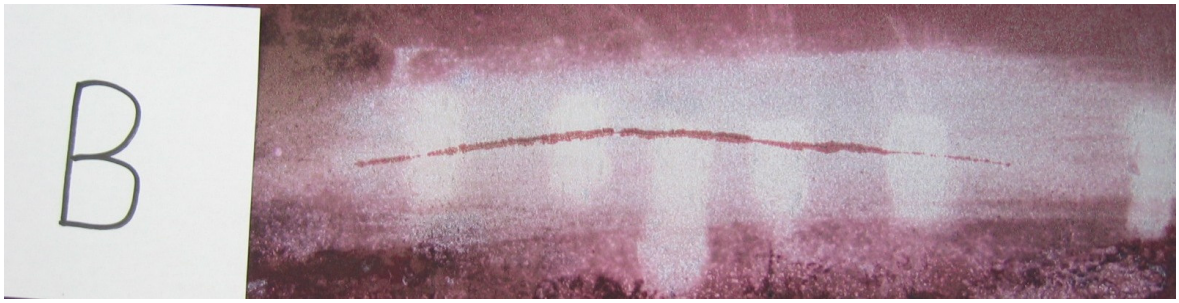

Figure 4-37: Fatigue crack B in test panel A after dye penetrant inspection

This difference between the test panel and real bridges is due to the test set up. In reality the stress is at a maximum when the tyre load passes the location of the crack tip. At that moment the stress is perpendicular to the longitudinal weld and consequently the crack normally propagates in the longitudinal direction. In the test panel the load area was fixed and the tyre load was placed symmetrically at the intersection of the crossbeam web and longitudinal trough profile. Due to this fixed position the principal stress in the deck plate becomes slightly rotated towards the crossbeam web and consequently the crack tip curves, as is visible in Figure 4-36 and 4-37.

Crack growth function

For test panel A and test panel B a function that describes the average crack growth rate was derived from a linear regression analysis. These functions are given in the figures. A strong correlation between the applied load range and the crack growth rate is obvious from the comparison between the crack growth rate in test panels A and B. For test panel A $d2c/dN = 8.1\text{x}10^{-5}$, for test panel B $d2c/dN = 2.6\text{x}^{-4}$.

According to usual definitions in fracture mechanics the crack depth is defined as "*a*" (mm) and the total crack length as "*2c*" (mm), however in this case the dimension *2c* is defined at the top surface of the crack, because the observations took place from the top surface of the bridge deck. Figure 4-38 defines the crack sizes.

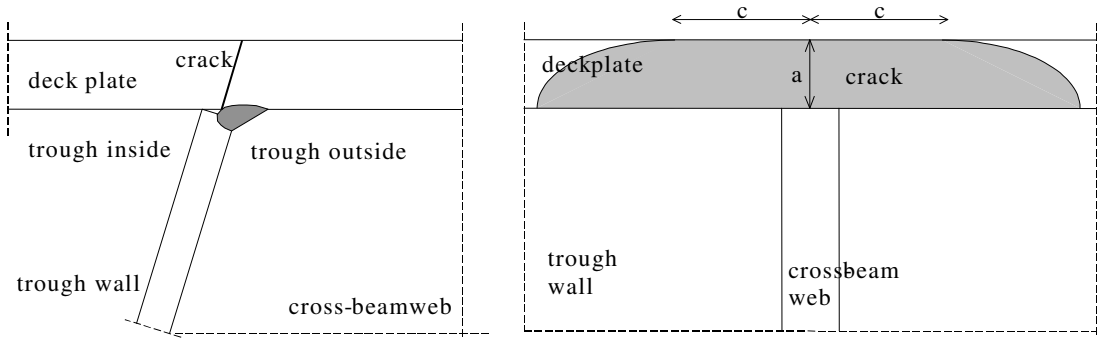

Figure 4-38: Definition crack sizes

All the data is presented on a log-log scale, and a linear regression analysis is executed. Figure 4-39 shows the result of the analysis. This is done to obtain a formula for *d2c/dN* as a function of $\Delta\sigma$, where $\Delta\sigma$ is the stress range in the transverse direction at the crack location. This is the maximum in line A-A, see Figure 4-3 and Figure 4-6. This formula is:

$$\log\frac{d2c}{dN} = \log C_0 - m_0 \cdot \log\Delta\sigma$$

with:
m_0 = 2.95
$\log C_0$ = -11.13

The value of this analysis for practical calculations is limited, because no verification can take place based on data from bridges with fatigue cracks. Although cracks are observed on a lot of bridges, there are no reliable observations of crack growth data.

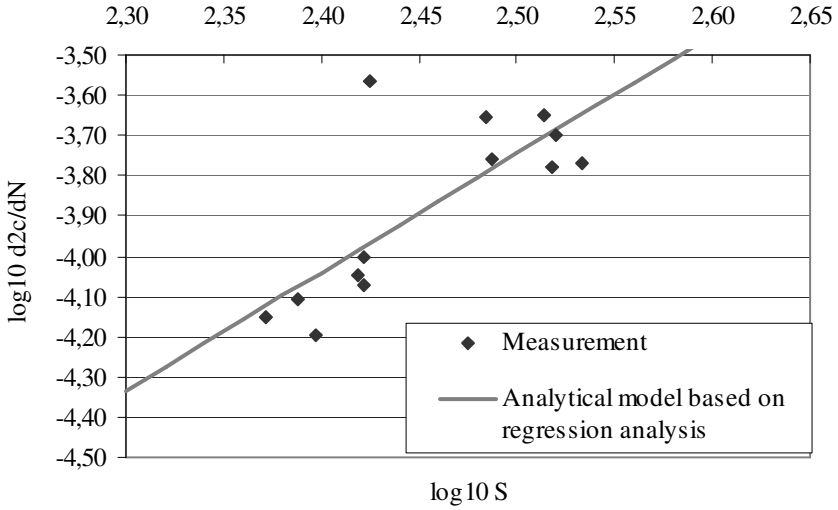

Figure 4-39: Crack growth function - deck plate crack

4.3.3.3 Detail classification deck plate crack

Calculation procedure

The test data was used to derive fatigue detail classifications. This paragraph describes the statistical procedure, which was used to calculate the values of the classifications. The purpose of the analysis was to derive characteristic values. For fatigue design these characteristic values should be divided by a factor γ_m. The characteristic values are calculated for 95% survival probability on a two-sided confidence level of 75% of the mean. These values are the same as the values on which the detail classifications in the Eurocode are based.

The calculation procedure is given in an IIW document (Hobbacher, 2003):

1. Calculation of $\log_{10}$ for stress range $\Delta\sigma$ ($\log S$) and for the number of cycles N ($\log N$).
2. Performing linear regression analysis for $\log S$ - $\log N$. $\log S$ is the independent variable because the number of cycles is considered as a function of the stress range. Derive the values for m and $\log C$ for the formula: $\log N = \log C - m \cdot \log S$
3. Calculation of $\log S^*$ at $\log C$ for all test results, using the slope m obtained from the regression analysis. Calculation with formula: $\log S^* = \log S - \dfrac{\log C - \log N}{m}$
4. Calculation of standard deviation for $\log S^*$. The average, $\log S^*_{mean}$, is 0.
5. Calculation of the characteristic values $\log S^*_{char}$, with formula $\log S^*_{char} = \log S^*_{mean} - k \cdot Stdv$. The value of k is a function of the required survival probability, the required confidence level and the size of the data set. k = 2.73 for 10 data points, 2.46 for 15 data points and 2.32 for 20 data points. Linear interpolation is used to

derive the *k*-values for other sizes of the data set. (Hobbacher, 2003)

6. Calculation of log $S_{char;c}$ and $S_{mean;c}$ at log N_c, using the slope m obtained from the regression analysis.

with:

Log S	Log_{10} of the stress range $\Delta\sigma$
Log S^*	Log_{10} of the stress range $\Delta\sigma$ at log C
Log S^*_{mean}	Mean of Log S^* at log C
Log S^*_{char}	Characteristic value of log S^* at log C
Log $S_{mean;c}$	Mean value of log S at log N_c
Log $S_{char;c}$	Characteristic value of log S at log N_c
Log N	$\log_{10}$ of the number of cycles N
Log C	Constant, intersection with horizontal axis (Log N)
N_c	Number of cycles at classification, 2 million cycles for Eurocode format, 10 million cycles for the NEN 2063 format (Dutch fatigue code)

Definition of failure point

To derive a fatigue detail classification it is essential to decide which crack length is considered as failure of the deck plate. A fatigue crack in the deck plate can be considered as an ultimate limit state or as a serviceability limit state. Eurocode 0, EN 1990:2002, defines these states. Ultimate limits are defined as states associated with collapse or with other similar forms of structural failure. They generally correspond to the maximum load-carrying resistance of a structure or structural member. Serviceability states are states that correspond to conditions beyond which specified service requirements for a structure or structural member are no longer met.

It is obvious that cracks in the deck plate do not threaten the structural integrity when they are short. The structural integrity is threatened if the cracks have grown through the deck plate and have reached a significant length at the top surface of the deck plate. Paragraph 4.2.4 describes some tests to derive this critical length. From the tests it is not exactly clear what this length is. For the moment a critical length of 500 mm at the top surface of the deck plate has been assumed. At this crack length plastic deformation of the deck plate is possible in the event of a heavy axle load. As the deck plate also acts as the top flange of the crossbeam in many orthotropic bridge deck structures the capacity of the crossbeam also decreases as the crack grows to a length of approximately 500 mm.

As fatigue design calculations are intended to guarantee that no structural failure occurs during the service life of a structure, a crack length of approximately 500 mm could be defined as crack length at which the fatigue detail classification is chosen for the ultimate

limit state, see paragraph 4.2.4. However the tests were concluded when the crack's length at the top surface was approximately 100 to 150 mm. Based on the performed tests detail classifications for four crack sizes have been defined:

1. Crack length top surface of deck plate = 0 mm
2. First visual crack (indicated with f.v.c.)
3. Crack length top surface of deck plate = 50 mm
4. Crack length top surface of deck plate = 100 mm

If the crack size associated with failure is defined at 0 mm or at the first visual crack, the definition is in accordance with usual practice for the derivation of fatigue detail classifications. The disadvantage of the definition at the first visual cracks is that the length of the cracks varies. The advantage of the definitions associated with cracks of 50 or 100 is the longer calculated fatigue life. Deriving the detail classification at all four definitions enables the designer to calculate crack growth rates. The inspection methods to detect these cracks are discussed in chapter 8.

Calculation of the number of cycles at 0, 50 and 100 mm

A direct relation between $\Delta\sigma$ and N is only available for the crack length associated with the first visual crack. For all the cracks the average crack growth rate, indicated with *d2c/dN*, is calculated by a linear regression analysis. With this crack growth, the number of cycles for crack lengths 0, 50 and 100 mm were calculated. The observed crack length, which is closest to crack lengths of 0, 50 and 100 mm, was used for these calculations.

Types of analysis

Four different analyses were performed to derive detail classifications.

1. Separate determinations of slope *m* for each crack length part based on all test results
2. Separate determinations of slope *m* for each crack length part based on reduced test results
3. Unified determination of slope *m* for all crack lengths based on all test results
4. Unified determination of slope *m* for all crack lengths based on reduced test results

In total 18 cracks were created in the fatigue test. For all four failure definitions a dataset of maximum 18 points ($\Delta\sigma$,N) was available. For the separate determinations of m, the linear regression analysis was performed on each dataset of 18 points individually. Those four slopes m differ from each other, which had strange effects on the detail classification, see Figure 4-40 and Figure 4-41. For this reason an analysis was added. In this second analysis the slope is determined on the basis of 4x18 = 72 data points. This leads to a more satisfactory slope m.

Another decision was the size of the datasets. Some data is not excluded from the fatigue

analysis. For instance crack br202a, see Table 4-11, with a length of 40 mm, is not grown to a length of 50 mm and 100 mm. Then it is questionable if the results can de extrapolated to these lengths. For this reason detail classifications are based on the complete set of 18 data points, and also on reduced data sets. Statistical evaluation of the data sets for the four cracks sizes has led to the results described in Stevin Report 6.04.4 (De Jong, 2005-e).

The 4th analysis with determination of one slope *m* of the fatigue curve, based on the reduced set of data, is the basis of the derived fatigue detail classifications. This analysis is discussed in this thesis. For fatigue calculations of orthotropic steel bridge decks the calculated detail classifications based on one slope *m* and a reduced data set are recommended.

The fatigue detail classifications were calculated both for the format of the Eurocode 3 (EN 1993-1-9:2005) and the NEN 2063 (NEN 2063:1988) format, the Dutch fatigue standard. In Eurocode 3 the detail classification is taken at $2x10^6$ cycles and in the NEN 2063 the detail classification is taken at $1x10^7$ cycles. Log *N* for the Eurocode format is 6.30 and log *N* for the NEN format is 7.00.

Results fatigue detail analysis

For analysis 1 and 2 with different slopes *m* for the different crack sizes, the calculation procedure gives strange results. Figure 4-40 shows the results of analysis 1 based on different slopes *m* and the total set of 18 data points. With an increasing crack length, from 0 to 100 mm, the derived slope of the regression line decreases from approximately 2.5 to 3.5. In Figure 4-40 the derived regression lines for different crack size definitions cross each other. Due to these different slopes the detail classification decreases with increasing crack size, as shown in Figure 4-41, for the classification according to the NEN format. Decrease of the fatigue strength with increasing crack growth is impossible. Therefore the analysis should be based on one determined slope *m* for the curves of all crack size definitions. This slope *m* is based on the test data, which is thought to be more accurate than the standard slope $m = 3$ from fatigue codes.

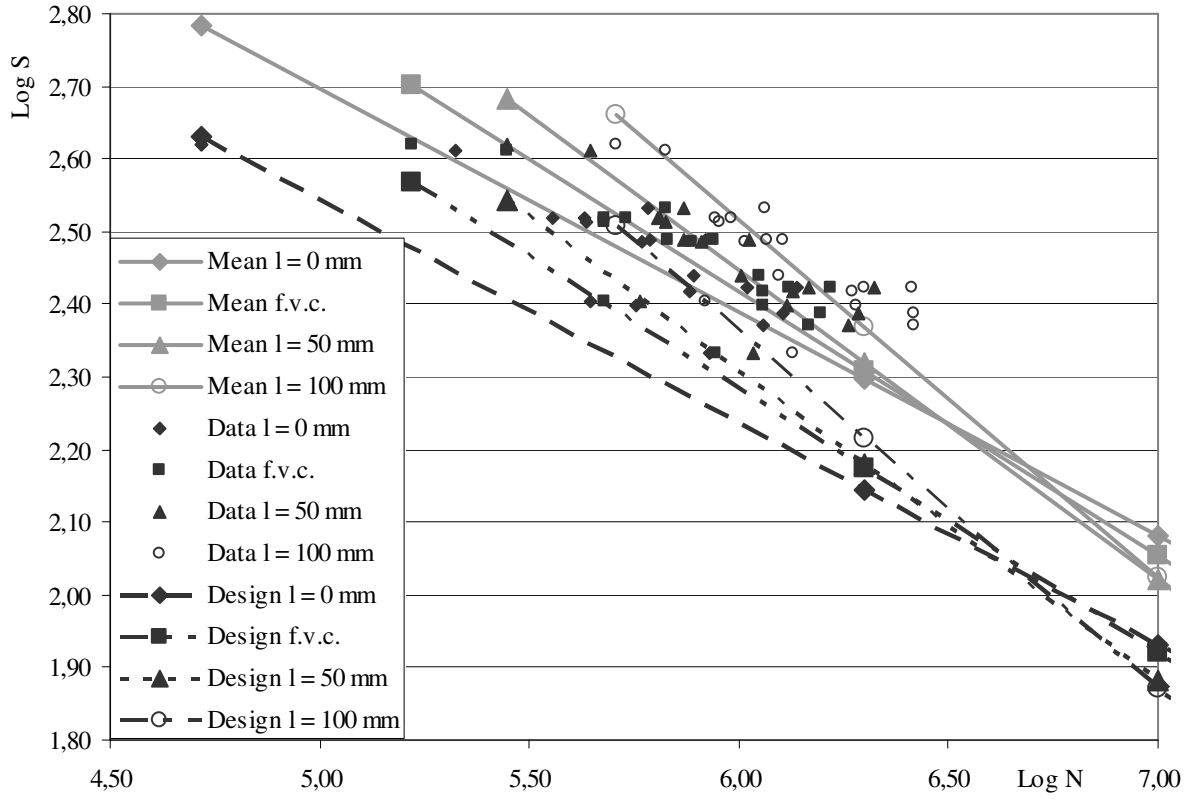

Figure 4-40: Fatigue S-N curves - deck plate cracks – analysis type 1

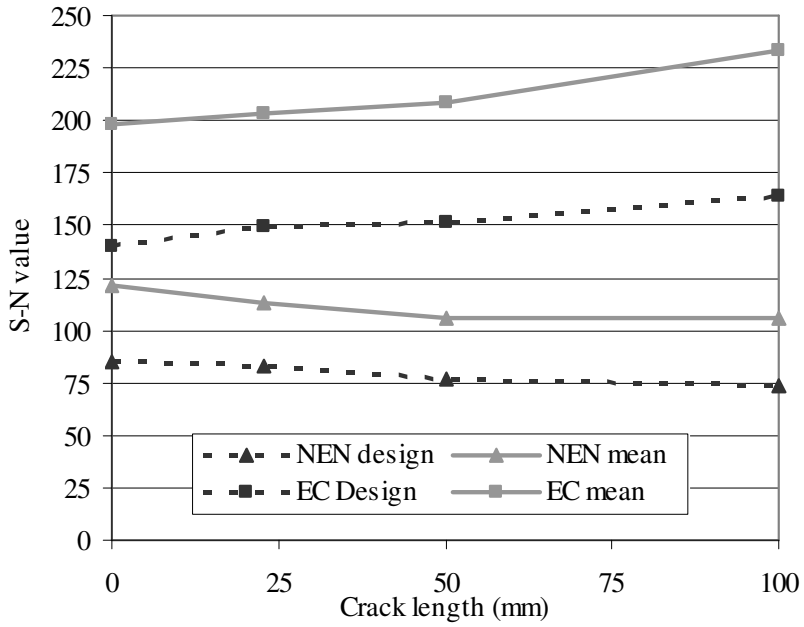

Figure 4-41: Detail classifications - deck plate cracks – analysis type 1

The linearly measured/interpolated numbers of cycles and the measured stresses were used to calculate log *N* and log *S*. *N*, *S*, log *N* and log *S* are given for the four crack size definitions in Stevin Report 6.04.4 (De Jong, 2005-e). Based on this data the regression analysis was performed and the results are given in Table 4-12. Based on this calculated slope *m* of the detail curves the detail classifications were calculated. The determined classifications are given in Table 4-13. The test results and the lines based on the regression analysis both for mean and design values are given in Figure 4-42. These are given for the four different defined crack sizes. Figure 4-43 gives the detail classification as function of the crack size. In the tables and figures f.v.c. stands for first visual crack.

Table 4-12 – Results of regression analysis (one slope *m* & reduced test data)

Crack length	0 mm	f.v.c.	50 mm	100 mm
Log *C*	12.93	13.02	13.09	13.24
m	2.89	2.89	2.89	2.89

Table 4-13 - Fatigue detail classifications (one slope *m* & reduced test data)

	NEN	EC	NEN	EC	NEN	EC	NEN	EC
Crack length	0 mm	0 mm	f.v.c.	f.v.c.	50 mm	50 mm	100 mm	100 mm
No of tests	15	15	17	17	15	15	14	14
S-N value design	84	147	92	161	99	173	111	194
S-N value mean	113	197	121	211	128	223	144	251

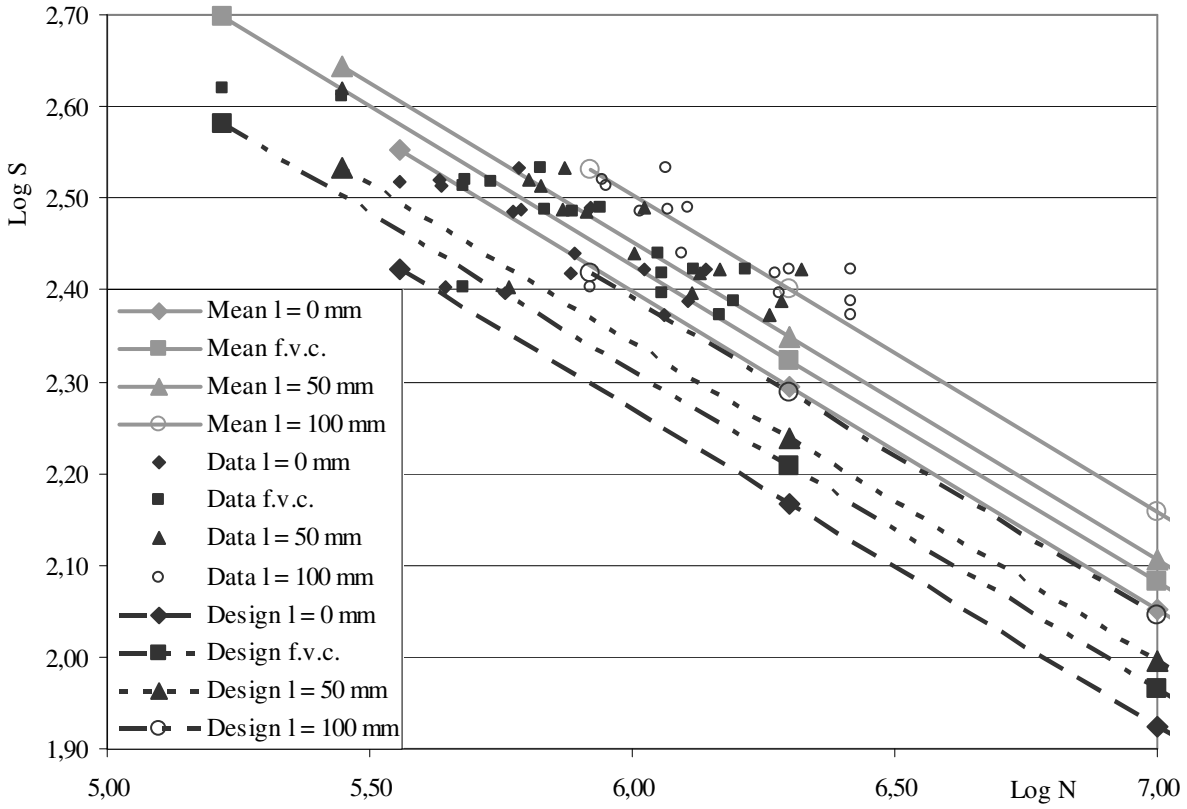

Figure 4-42: Fatigue S-N curves - deck plate cracks – analysis type 4

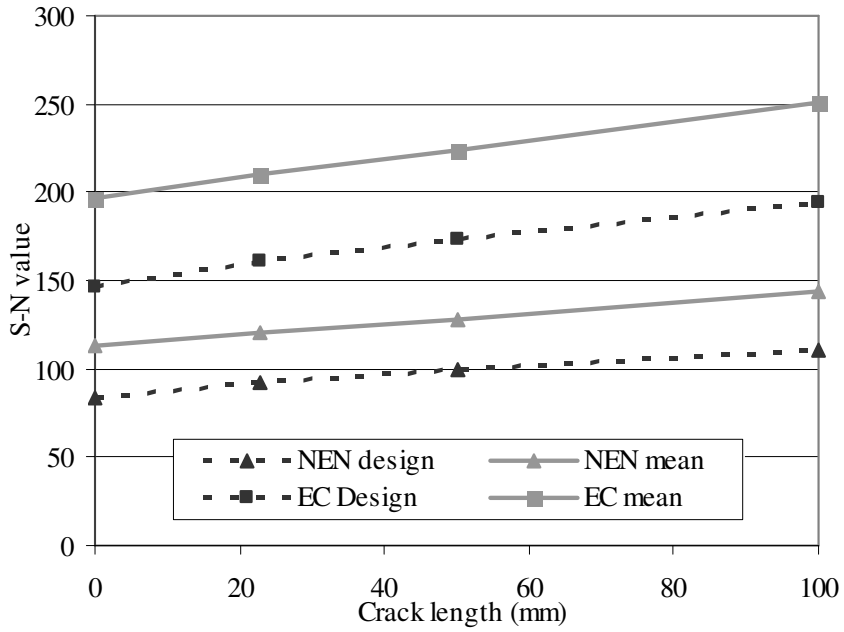

Figure 4-43: Detail classifications - deck plate cracks – analysis type 4

The results of the tests performed by Kolstein (Kolstein, 2000-a) are in accordance with the results from the test panel A and B. This is shown in Figure 4-44.

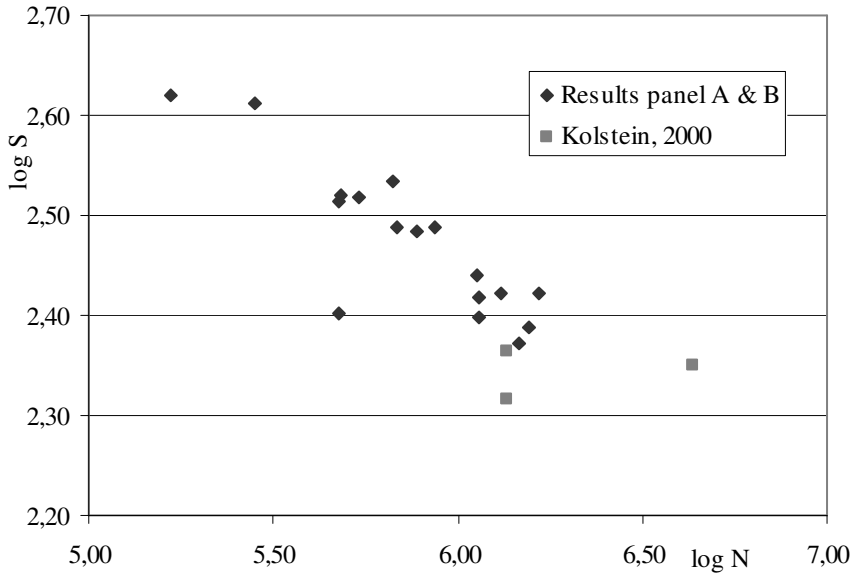

Figure 4-44: Test results - first visual crack

4.3.4 Conclusion

This paragraph has presented several results for the detail classification of a crack in the deck plate at the crossbeam location. Results from literature, both tests and crack growth models were described. In addition a fatigue testing program was performed. Detail classifications were derived for deck plate cracks, see Table 4-13. Use of the detail classifications from this table is proposed for fatigue calculations.

4.4 Lintrack test program: experimental and numerical

4.4.1 Introduction

This paragraph describes the tests that were performed with the Lintrack, a heavy vehicle simulator, on a real bridge deck panel. Paragraph 4.4.2 describes the Lintrack testing facility and paragraph 4.4.3 describes the extensive testing program that was executed in it. Paragraph 4.4.4 describes the analysis procedure for the raw data obtained. Paragraph 4.4.5 gives the test results. Paragraph 4.4.6 describes the numerical analysis that was performed and paragraph 4.4.7 ends this part about the Lintrack experiment with some concluding remarks.

4.4.2 Lintrack Testing facility

The experiments were conducted in the Lintrack (LINear TRACKing apparatus), a heavy vehicle simulator originally built for accelerated testing of surfacing. The Lintrack is very useful because it gives the possibility of simulating real lorry traffic on bridge decks. This paragraph describes the Lintrack. The description is based on the more extensive description that can be found in (Groenendijk, 1998). The Road and Railroad Research Laboratory of Delft University of Technology and the Road and Hydraulic Engineering Division of the Ministry of Transport, Public Works and Water Management jointly own the Lintrack, which was designed, constructed and tested between 1987 and 1991.

Lintrack consists of a 20m long dual steel gantry, along which a loading carriage can move back and forth. Figure 4-45 shows a side view. Basically it is an apparatus with a moving wheel load. The load can be varied between 15 and 100 kN and the velocity can be varied between 0 and 20 km/h.

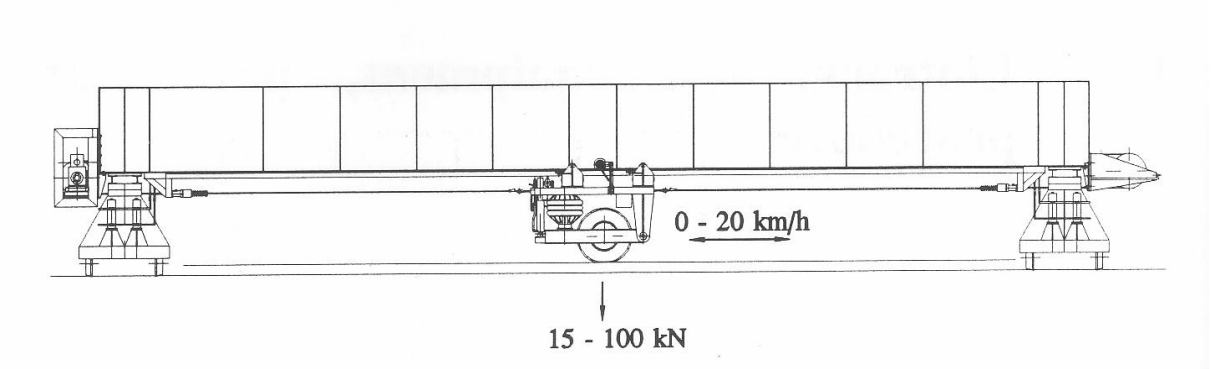

Figure 4-45: Side view of Lintrack

Figure 4-46 is a photograph of the loading carriage of the Lintrack. Different tyres can be mounted on this carriage. For the tests described in this thesis the single (type A), the double (type B), the super single (type C) and the extra wide base (type D) were used. Pneumatic bellows between the upper and lower parts of the loading carriage apply the wheel load. Compressed air is supplied from a cylinder mounted on the loading carriage, see Figure 4-46. Pneumatic load application prevents leakage of hydraulic oil onto test surfacings.

The movement of the loading carriage is effected with two steel cables and an electric motor. The total running length of the loading carriage is about 12 m and the maximum speed is around 20 km/h although lower speeds are also possible. To reach this speed, acceleration and deceleration take approximately 4 m, so a 4 m measuring length remains where the carriage has a constant speed.

Figure 4-46: Loading carriage of the Lintrack

Besides the movement in longitudinal direction over a distance of 12 m, it is possible to move the Lintrack in the lateral direction. A bogie, running on rails, supports either end of the steel gantry. These 55 m long rails run perpendicular to the gantry across the whole test area. This is very useful for creating influence surfaces or a transverse distribution of the wheel loads when testing surfacing.

To shelter the test sections from climatic influences such as rain and sunshine during testing, the entire installation is covered with a enclosure (23 m long, 6m wide, 5 m high), which moves with the installation. The Lintrack facility is also equipped with a heating system in order to control the temperature of material being tested, which is appropriate because temperature dependency is characteristic of the behaviour of bituminous surfacing materials.

Attached to the mobile enclosure is a separate control cabin, also movable on the rails, which houses most of the control and measurement systems. Figure 4-47 shows the Lintrack with the enclosure, the test area, the rails for lateral movement and the control cabin on the rails on the right hand side. The loading carriage has an on-board battery to power the electronics and an infrared (IR) communication system is used to transmit data to and from the loading

carriage. The wheel load is derived from a pressure gauge in the pneumatic bellows that apply the wheel load. Readout is in 0.1 kN steps, and accuracy is about ± 0.5 kN. This gauge measures the pressure 12 times in the middle section of 4 m. Due to the roughness of the asphalt surfacing, it is possible that the wheel load varies somewhat and therefore these frequent measurements are appropriate.

Figure 4-47: Lintrack with test area

The longitudinal Y-position of the wheel (in the wheel rolling direction) is determined by an incremental rotation encoder mounted on the cable drive wheel. Accumulation of errors is prevented by a reset to zero when a magnetic proximity switch is triggered by a part of the carriage in its rearmost position. Readout is in mm, accuracy is within ± 1% of the readout value. The transverse X-position is determined in a comparable way with a similar accuracy.

4.4.3 Description of test

This paragraph gives a description of the test specimen, the instrumentation and the testing program. The testing program was performed with and without surfacing. The sequence was:

1. Apply strain gauges to steel deck
2. Testing program on the deck without surfacing
3. Applying surfacing and strain gauges on membrane and top of surfacing
4. Testing program on the deck with surfacing

In the following three sub-paragraphs the test specimen, the instrumentation and the testing program are described. Each paragraph describes the situation first without and then with surfacing.

4.4.3.1 Test specimen

Figure 4-48 shows a detailed drawing of the bridge deck test panel. The test panel was similar to the majority of orthotropic steel bridge decks used in the Netherlands at least with respect to the deck plate behaviour, as it was built with a deck plate 10 mm thick and Krupp 2/325/6 profile troughs. The deck plate thickness of 10 mm was chosen because almost every fixed bridge in the Netherlands has this deck plate thickness. The distance between the transverse crossbeams was 2 m, whereas in practice 4 m is a normal spacing. This distance was reduced in the test specimens to create more intersections between crossbeam and trough profile. This reduced spacing is thought to have no effect on the behaviour at the crossbeam locations, as the influence length of wheel loads is even less.

The crossbeams were continuously supported and although this and the spacing differ from normal practice, it was only expected to affect the trough-crossbeam behaviour; no effect on deck plate behaviour was expected. For ease of fabrication cope holes were used in the trough-crossbeam connection. The longitudinal weld between trough web and deck plate had a throat dimension of about 6mm and a maximum lack of penetration of 1 mm.

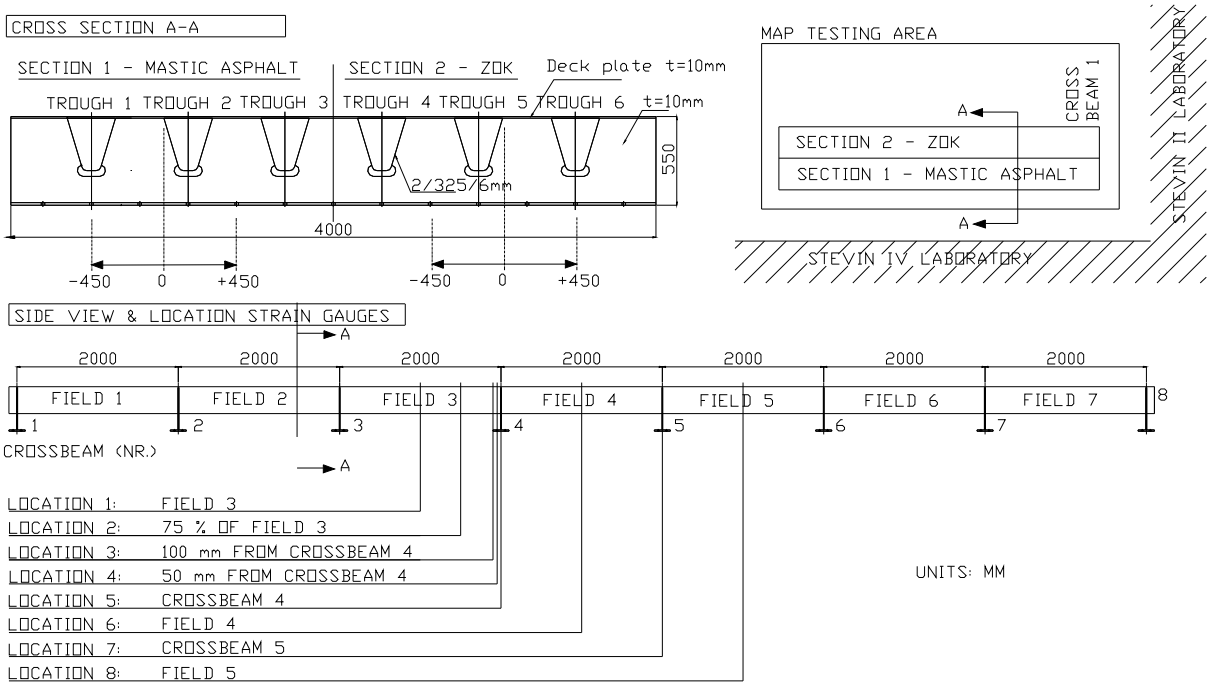

Figure 4-48: Test panel Lintrack & locations of strain gauges

The test panel was tested without and with surfacing. After completion of the experimental program on the test panel without surfacing, two types of surfacing were applied. Application of the surfacing during the experiments enabled the simulation of both movable bridge decks with a thin epoxy surfacing, and fixed bridges with thick surfacing. Two types of thick surfacing were applied:

- A layer of 50 mm mastic asphalt. This type of surfacing is used on the majority of the fixed steel bridges in the Netherlands.
- A layer of 50 mm ZOK. ZOK is an acronym for Zeer Open Kunststof. It is an open graded surfacing and the binder between the stones is polymer based, instead of bitumen.

Application of the surfacing

The following four steps were taken in applying the thick surfacing:

- The steel deck plate was shot blasted to Sa 2.5, in order to ensure a good bond between the intermediate membrane and the steel deck plate, see Figure 4-49. Immediately after shot blasting, primers were applied to the steel deck plate appropriate to the two types of surfacing. Figure 4-50 shows these different coloured primers, black on section 1 (mastic asphalt) and red on section 2 (ZOK).

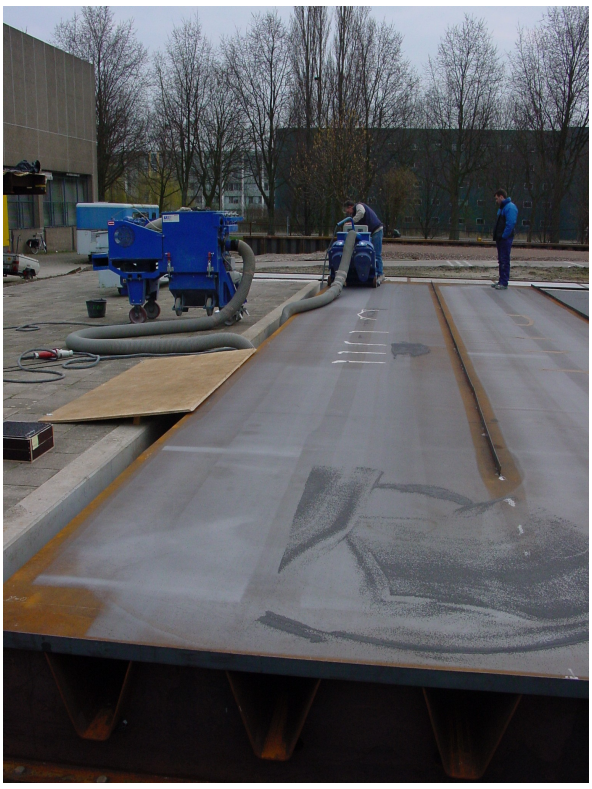

Figure 4-49: Shot blasting deck plate before application surfacing

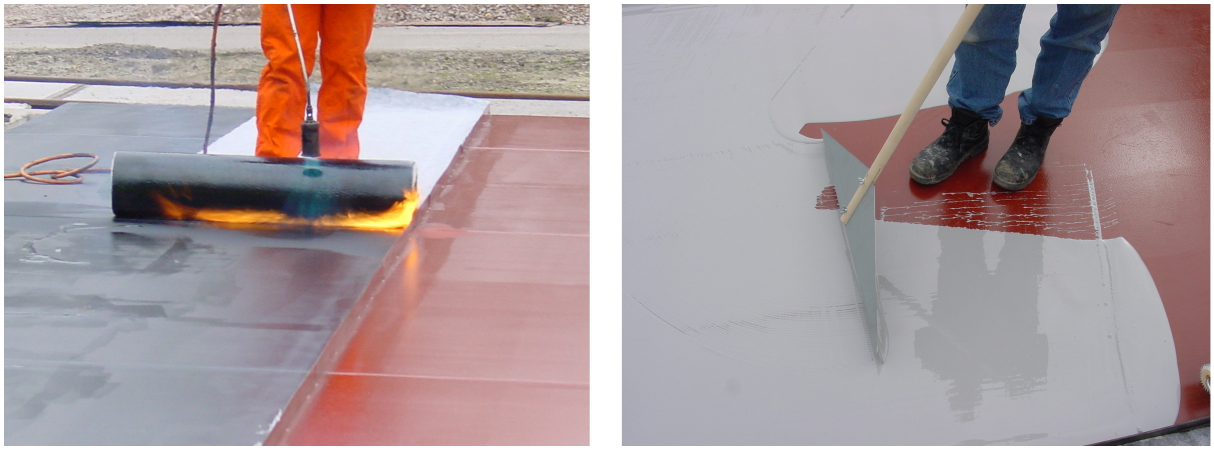

Figure 4-50: Primers and application of membranes for mastic asphalt (left) and ZOK (right)

- A bituminous membrane was applied to the bridge deck section that was to be surfaced with mastic asphalt and a polyurethane membrane to the bridge deck section that was to be surfaced with ZOK, see Figure 4-50. The membrane for the ZOK part was sprinkled with granular material to provide shear resistance at the interface between the membrane and ZOK.
- Strain gauges were applied on top of the membrane layer, both for section 1 (mastic asphalt) and section 2 (ZOK). First the strain gauges were attached on the membrane and then they were protected, with bitumen or polyurethane. Figure 4-51 shows this for section 2 (ZOK). For section 1 with mastic asphalt, strain gauges and protection were similar.

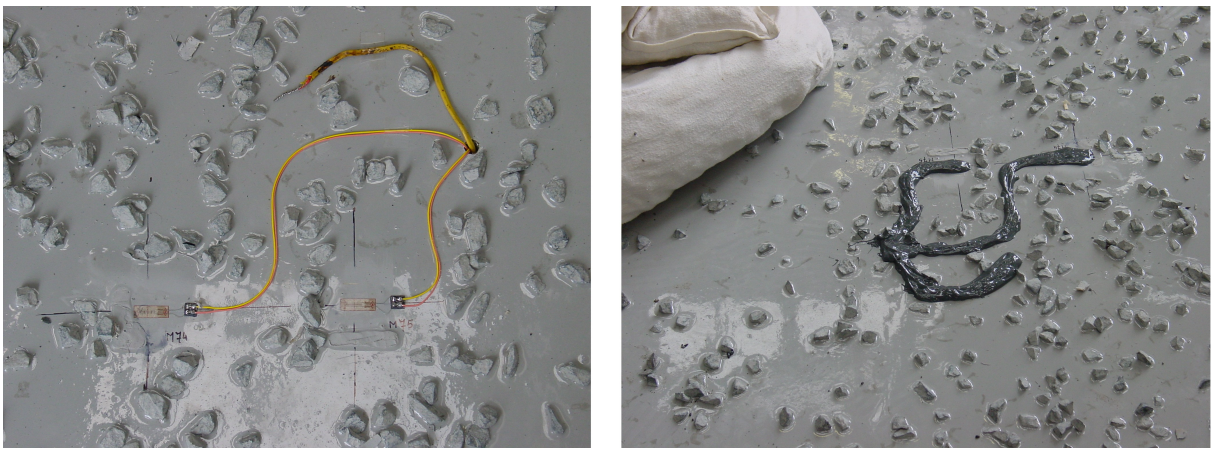

Figure 4-51: Strain gauges on ZOK membrane (left) with protection (right)

- The 50 mm thick surfacing was applied to the membrane layers, mastic asphalt in section 1 and ZOK in section 2. For a detailed description of these materials and their properties,

see (Medani, 2006). Figure 4-52 shows the application of the ZOK surfacing on the test panel.

Figure 4-52: Application ZOK surfacing of 50 mm

4.4.3.2 Instrumentation and measurements

This paragraph is about the location of the strain gauges. The strain gauges were installed at several cross-sections on the bridge deck test panel. The location and the type of the strain gauges are explained. In the longitudinal direction the test panel was divided into two sections, each 2m x 14m. The troughs 1, 2 and 3 formed section 1, the troughs 4, 5 and 6 formed section 2. In particular the middle troughs of each section, troughs 2 and 5, were equipped with strain gauges. Figure 4-48 shows the sections, troughs, and locations of the strain gauges.

The strain gauges were applied on three different parts of the structure:

- Strain gauges on the steel parts of the structure; the ‘steel’ gauges
- Strain gauges on the top surface of the membrane layer; the ‘membrane’ gauges
- Strain gauges on the top surface of the surfacing layer; the ‘surface’ gauges

The ‘steel’ and ‘membrane’ gauges are type FLA10 and the ‘surface’ gauges are type PL60. Because the surfacing is a granular material longer gauges are necessary.

At first only the ‘steel’ gauges were applied to the bridge panel and subsequently the experiments on the bridge panel without surfacing layers took place. After completion of this part of the testing program, the two surfacing layers were applied. The strain gauges on top of

the membrane layer and on top of the surfacing layer were applied during and after application of the surfacing.

The strain gauges were primarily mounted in the transverse direction with only a few, those which were applied on the bottom surface of the troughs, in the longitudinal direction. To increase the accuracy and the interpretation of the measurements, strain gauge configurations in several cross-sections are more or less similar to each other. The ‘surfacing’ gauges were especially duplicated in this way, because less accuracy was expected from this type of gauge. At locations where ‘surfacing’ gauges were duplicated the ‘steel’ gauges were also duplicated.

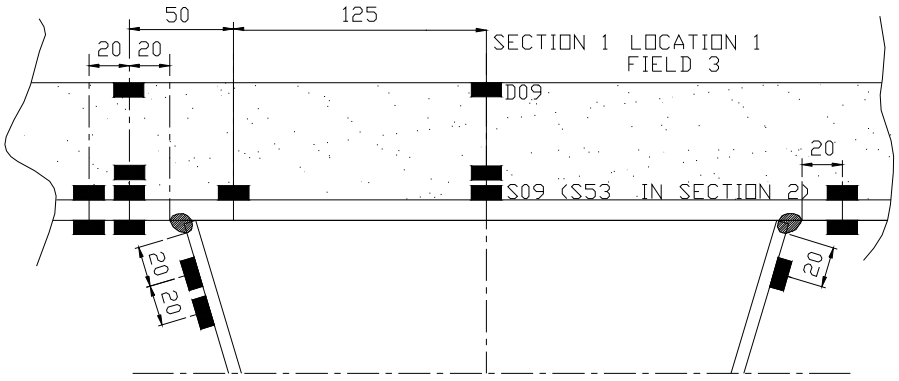

Figure 4-53: Strain gauges, Section 1 field 3

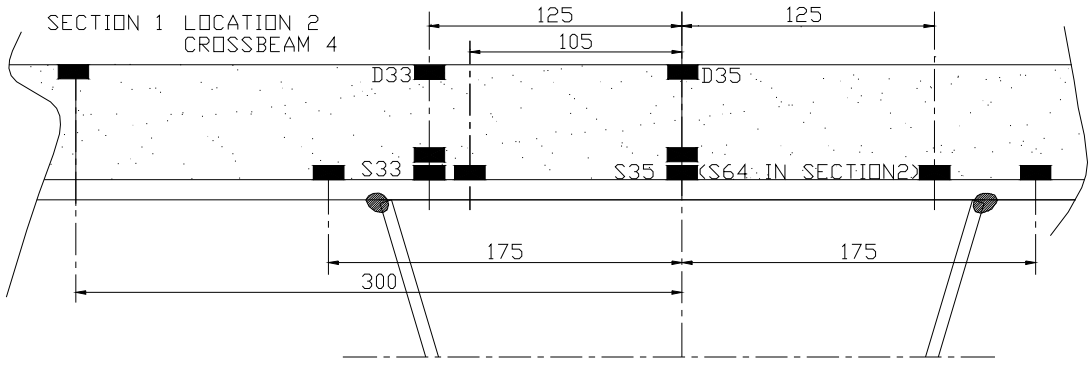

Figure 4-54: Strain gauges, Section 1 crossbeam 4

Figure 4-53 and Figure 4-54 show as example two sets of strain gauges. In both sections similar sets of gauges were attached to several crossbeams and fields between the crossbeams at the 8 locations pointed out in Figure 4-48. Because the longitudinal axis of the test panel is a line of symmetry the strain gauges in section 2 were mirrored with the gauges in section 1. Annex D contains the exact location of all strain gauges.

The surfacing applied in section 1 was mastic asphalt. During the application procedure the maximum temperature of the mastic asphalt is approximately 200 ºC. This temperature could possibly have had a negative effect on the membrane gauges, although in small tests which were performed before application of the surfacing on the bridge deck panel the applied strain gauges in the membrane layer still functioned well after application of mastic asphalt. But to be absolutely safe the strain gauges in the membrane layer were duplicated so that if for any reason a strain gauge failed the duplicate could be used as a fall back.

Strain gauges were mounted both in the field between two crossbeams, and at the crossbeam location. In general strain gauges were mounted at the following locations:

- The bottom and web of the trough
- The top and bottom surface of the deck plate.
- The top of the surfacing layer. (It is impossible to mount strain gauges on the underside of the surfacing layer.)
- The top surface of the intermediate membrane layer.

At certain locations two gauges were mounted in line in order to allow extrapolation of the strain to the toe of the weld.

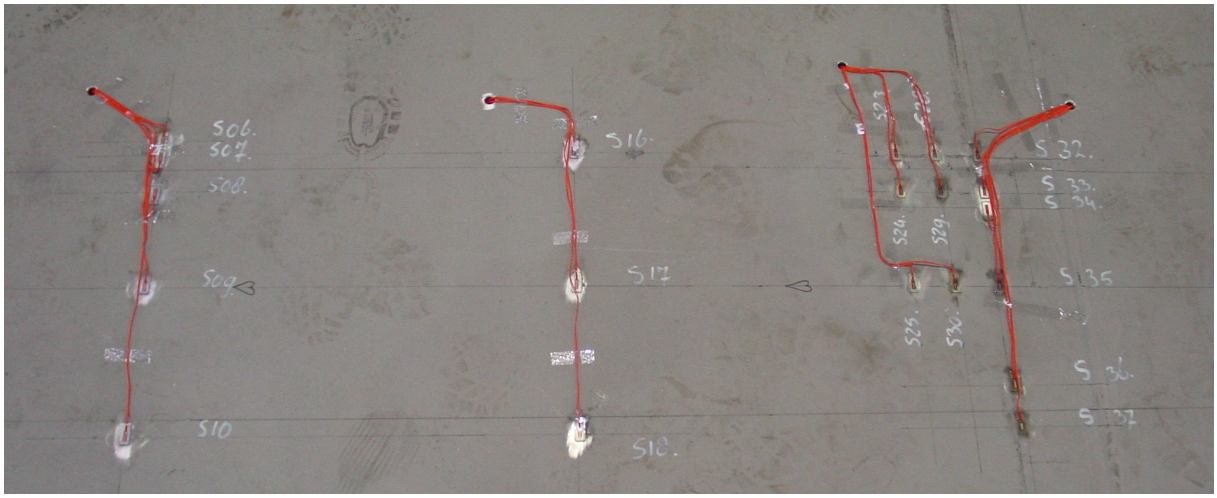

Figure 4-55: Strain gauges on top of the steel deck plate, section 1, locations 1 to 5

Figure 4-55 shows some strain gauges that were applied on top of the steel deck plate, in section 1, locations 1 to 5. At the cross-sections 3, 4 and 5, see Figure 4-48, strain gauges were applied 10 cm from the crossbeam (cross-section 3), at 5 cm from the crossbeam (cross-section 4) and at the location of the crossbeam (cross-section 5). The crossbeam web acts as a discontinuity in the assembly. Due to the fact that the crossbeam web, trough and deck plate are welded together, the crossbeam is in fact a boundary constraint to the deck plate, which prevents rotation of the deck plate at the intersection of crossbeam web, trough wall and the

deck plate. To model this discontinuity strain gauges were mounted at 5 and 10 cm distances from the crossbeam. The strain gauges in cross-section 3 and 4 were only mounted in section 1 and were only used in the test series without surfacing layers. After ending this test series these strain gauges were removed and the surfacing layers applied.

After application of the strain gauges, the gauges and the connecting cables were protected with a synthetic material, as shown in Figure 4-56.

Figure 4-56: Protection of strain gauges on top of steel deck plate, section 1, locations 1 to 5

Before application of the strain gauges on top of the surfacing, the top of the surfacing layer had to be ground locally in order to ensure a flat surface on which the strain gauges could be applied. After grinding the strain gauges were applied, see Figure 4-57 and also protected, see Figure 4-58.

After protecting the strain gauges the connecting cables were also protected. The connecting cables for strain gauges on top of the steel deck plate and on the membranes were passed through a hole, as shown in Figure 4-55. The connecting cables for the strain gauges on top of the surfacing were routed on top of the surfacing to the side of the test plate, as shown in Figure 4-59.

In addition to the strain gauges six thermocouples were mounted in the interface between the membrane and surfacing, three in section 1 (mastic asphalt) and three in section 2 (ZOK). These thermocouples were necessary for controlling the temperature of the surfacing. Besides two strain gauges that are applied on top of the membrane one thermocouple is visible in Figure 4-51.

Figure 4-57: Strain gauges on top of mastic asphalt surfacing (duplicated gauges)

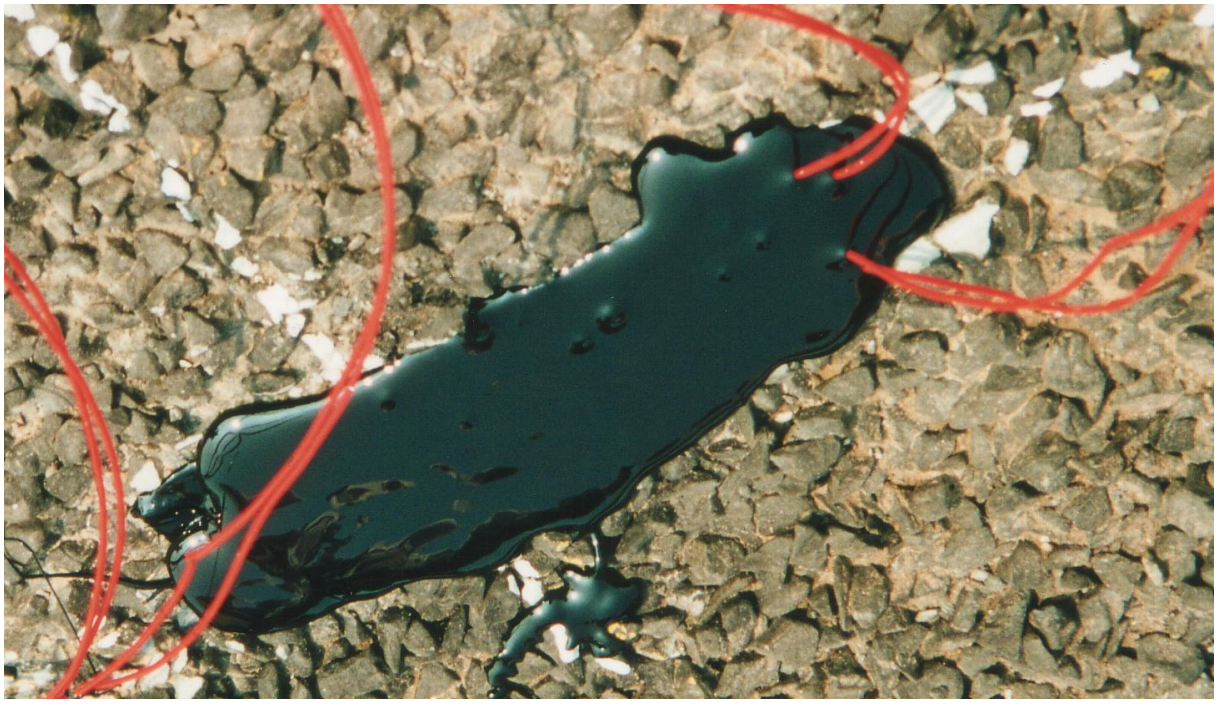

Figure 4-58: Protection of strain gauges on top of mastic asphalt surfacing

Figure 4-59: Connecting cables with protection on top of the surfacing

4.4.3.3 Test program

This paragraph briefly describes the testing program that was executed in the Lintrack. Stevin Report 6.03.6 (De Jong, 2005-a) gives a complete description of the tests. The essence of all the tests is strain measurement, in this way deriving influence lines and surfaces for the strain gauges. The experiments were basically a series of identical tests, in which a few parameters were varied. These parameters were the wheel load, the wheel type, the velocity of the wheel, the presence and temperature of the surfacing. Table 4-14 summarizes the parameters involved.

In addition the surfacing type was varied, although it is not mentioned in the table, because of the two different surfacings in section 1 and section 2. The influence lines and surfaces were obtained for all reasonable combinations of the parameters. The test program was performed before and again after the application of the surfacings. The testing program was executed both in section 1 (Mastic asphalt) and in section 2 (ZOK).

Table 4-14: Parameters - Lintrack experiments

Wheel load	Wheel type	Velocity	Surfacing
25 kN	Single (Type A)	0 km/h	No surfacing
50 kN	Double (Type B)	2 km/h	Surfacing 0 °C
	Super Single (Type C)	20 km/h	Surfacing 15 °C
	Extra Wide Base (Type D)		Surfacing 30 °C

This test program was performed in the following sequence:

- December 2000 to March 2001 - tests without surfacing
- December 2001- tests with surfacing at 0 ºC
- March 2002 to April 2002 - tests with surfacing at 15 ºC
- June 2002 - tests with surfacing at 30 ºC

The surfacings, including the strain gauges on the membrane and on top of the surfacing, were applied between April 2001 – June 2001.

In order to derive an influence line, the loading carriage of the Lintrack moves forward and backwards once. In essence influence surfaces are a set of influence lines. The influence surfaces have a width of 900 mm and the distance between two influence lines is 50 mm.

The tests on the bridge deck with surfacing were roughly the same as the tests without surfacing: some validation tests (0 km/h), static tests (2 km/h) and dynamic tests (20 km/h). However there were a few differences with respect to the static tests. These tests were very time consuming, therefore the following decisions were made:

- The static tests with surfacing at 2 km/h were only carried out at 50 kN, whereas the static tests without surfacing were also done at 25 kN.
- Because wheel types A and C are more or less the same, type C is simply somewhat wider, the static test with wheel type A with surfacing were reduced compared to the static tests without surfacing.

Wheel load and wheel type

The wheel loads were chosen on basis of wheel load measurements on Dutch motorways (Vrouwenvelder, 2000-a), see Figure 3-4. The two loads chosen cover the part of the axle loads which, to a large extent, produces the fatigue damage.

Three of the four wheel types were the usual wheel types as described in Eurocode 1- Part 2. The footprints of the tyres used were measured and the measured width and length are smaller than in the Eurocode, see Chapter 3. By using a heavy vehicle simulator this effect is taken into account.

Velocity

The tests were conducted with three different velocities: 0, approximately 2 and approximately 20 km/h. Tests at 0 km/h were called validation tests. Tests at 2 km/h were called static and tests at 20 km/h were called dynamic. The terms static and dynamic might possibly give rise to confusion. Within the framework of the description of the experiments in the Lintrack, the meaning of static and dynamic is as follows. In static tests strains were measured excluding dynamic effects in the surfacing layers. The wheel moves with a low velocity of approximately 2 km/h, and it is assumed that this low velocity does not introduce dynamic effects. This assumption was validated with some strain measurements with a wheel velocity 0 km/h with the wheel positioned on the bridge deck location with defined characteristics. In the so-called dynamic tests strains were measured including possible dynamic effects in the surfacing layers. In the dynamic tests the wheel moves at the maximum velocity of the Lintrack apparatus, approximately 20 km/h. The difference between the static tests and the dynamic tests was the velocity of the moving wheel.

Surfacing and temperatures

The experiments on the bridge deck panel after application of the surfacing took place three times at three different surfacing temperatures. These three temperatures were approximately 0, 15 and 30 °C. These temperatures are ‘low’, ‘normal’ and ‘high’ if temperatures in normal conditions are considered. Although asphalt temperatures can be far higher than 30 °C, this temperature was chosen as the maximum temperature, because the tests were primarily intended to measure the strain reductions in the steel structure. Besides this consideration another reason to choose these three temperatures is that at 0 °C, asphalt is thought to react elastically with a relatively high stiffness, at 15 °C asphalt will react elastically with a low stiffness or visco-elastic and at 30 °C the asphalt will react visco-elastically or plastically (Medani, 2006). Besides that the stiffness of mastic asphalt at 30 °C is that high that a very low stiffness modulus, below 1000 MPa is expected, see Figure 8-6. In that case temperatures above 30 °C will not cause a big difference of the expected stress in the steel deck plate.

In both the static and dynamic tests the measuring frequency is 250 Hz. In this way measurement data is obtained every 22 mm at the maximum speed of 20 km/h. This distance between the data points is acceptable because with this distance the measured maximum strains of influence lines are very accurate.

4.4.4 Analysis procedure

Many experiments were performed in the Lintrack and the results were stored in so-called buffer files, which contain the raw data. In general three types of experiments were

performed. Each experiment resulted in one buffer file.

- 'Validation' experiments (128 experiments)
- 'Static' experiments (676 experiments)
- 'Dynamic' experiments (64 experiments)

There are in total 868 buffer files, which together have a size of 2.6 GB on the hard disk. Because of the size of the files the data processing to analyse and interpret the experiments should be intelligent and computerized. This paragraph describes the procedures of data processing in Phase 1 and, analysing and interpretation in Phase 2

4.4.4.1 Phase 1: data processing

The results of the measurements in the buffer files were processed in order to get numerical and graphical representations of the data. Analysis and interpretation in the second phase are based on these representations. Three discrete steps were performed to produce the representations

Repair and filtering of buffer files

In the first step the original files were repaired and then after this action they were filtered. Repair and filtering of the buffer files was performed with Linrep.exe, which is software specially written for the analysis of the Lintrack experiments. Repair was necessary for two reasons:

- Sometimes while executing a single experiment something would go wrong, which necessitated repetition of the experiment. The original buffer file then contains two measurements. The file repair removes the first incorrect results and retains only the results of the second measurement in the buffer file.
- The Lintrack apparatus measures the wheel load while the wheel runs over the test section. The instrumentation to measure the load is located on the moving part of the Lintrack and the measured load is sent to the measuring computer using an infrared connection. This connection is a critical feature and sometimes the connection fails so that only the predefined weight of the moving part of the Lintrack is written in the buffer file. Linrep.exe has an option to insert a user-defined wheel load, to correct this.

While analyzing some measurements it became clear that the measurement contained not only the strain signal due the moving wheel load but also an additional high frequent signal. It was necessary to remove this signal by filtering it from the measured signal and a filter option is implemented in linrep.exe. The parameters of the filter are:

- filter frequency (options:10, 25, 50, 100 and 150 Hz)
- filter order (options: 2nd, 4th, 6th, 8th, 10th order)

The measured strains from different buffer files were analysed. From these analyses it became

clear that only the buffer files of the static experiments contained this noise on the signal. The signal in the dynamic buffer files was correct. The noise in the static files was removed from the signal. At first the best combination of filter frequency and filter order was determined from several combinations. A 4^{th} order, 50 Hz filter turned out to be the best filter. All the static files were filtered in this way.

Creating ASCII data files

In the second step with a specially written computer program lex2.exe ASCII data files were produced from the repaired and filtered buffer files. The ASCII data files contain the data that can easily be read by Matlab. Lex2.exe creates ASCII-files, with one or more 2 dimensional sheets with measured strains from the buffer files. A sheet is in fact a numerical representation of an influence surface. A file header is created with information about the experiment and the data in the ASCII-file. The choice of strain gauges to incorporate in an ASCII-file is free. For each ASCII file the user can define one or more strain gauges. This gives the user the ability to cluster strain gauges in an ASCII file. The strain gauges were divided in 11 groups. These groups are given in Table 4-15. Each group includes all the strain gauges mounted in a particular cross-section of the bridge deck panel. Figure 4-60 shows the location of the strain gauge groups at the bridge deck panel and the area for which the results from the buffer files were evaluated.

Table 4-15: Strain gauge groups

No	Description & Location		Steel	Membrane	Surfacing
1	Section 1	Location 1	S01 - S12	M07 M09	D07 D09
2	Section 1	Location 3, 4 & 5	S21 - S37	M33 M35	D80 D33 D35
3	Section 1	Location 6	S38 - S43	M40 M41 M42	D40 D41 D42
4	Section 1	Location 7	S44 S45	M44 M45	D44 D45 D81
5	Section 1	Location 8	S46 - S48	M47 M48	D47 D48
6	Section 2	Location 1	S49 - S60	M53 M55	D53 D55
7	Section 2	Location 5	S61 - S67	M64 M66	D64 D66 D82
8	Section 2	Location 6	S68 - S73	M70 M71 M72	D70 D71 D72
9	Section 2	Location 7	S74 S75	M74 M75	D74 D75 D83
10	Section 2	Location 8	S76 - S78	M76 M78	D76 D78
11	Section 1	Location 2	S13 - S20		

The user has to define the buffer files from which the data is picked up. The use of wildcards is permitted. The choice of the area in which the results from the buffer files are evaluated is free, because the influence length of a wheel is rather short for strain gauges at deck plate level. The choice of the size of the mesh in x and y-direction is free. For example: the static

experiments were carried out at 2 km/h with a sample rate of 250 Hz. This means that the buffer file contains a measured strain for each 2.222 mm. To reduce the size of the ASCII file a size of 10 mm in y direction can be chosen. An ASCII file includes only one temperature, one, wheel type, one wheel load and one velocity. For a comparison for example of wheel types A and C, at least two ASCII files are necessary. It is possible to create these ASCII file in one session. The program creates a unique name for an ASCII file. The file name contains the encoded properties of the experiment. The name of the ASCII file shows the experiment recorded in the file.

Example: The ASCII file H09S2C5002 is a three-dimensional array of 8 sheets (1 sheet with information and 7 sheets with measurement data), which contains the results (the underlined characters explain the ASCII file name) of an experiment at 30 °C (High temperature), with 7 sheets for 7 strain gauges: of strain gauge group 09 (S74, S75, M74, M75, D74, D75, D83), for section 2 (S2), for wheel type C, for wheel load 50 kN, for velocity 02 km/h.

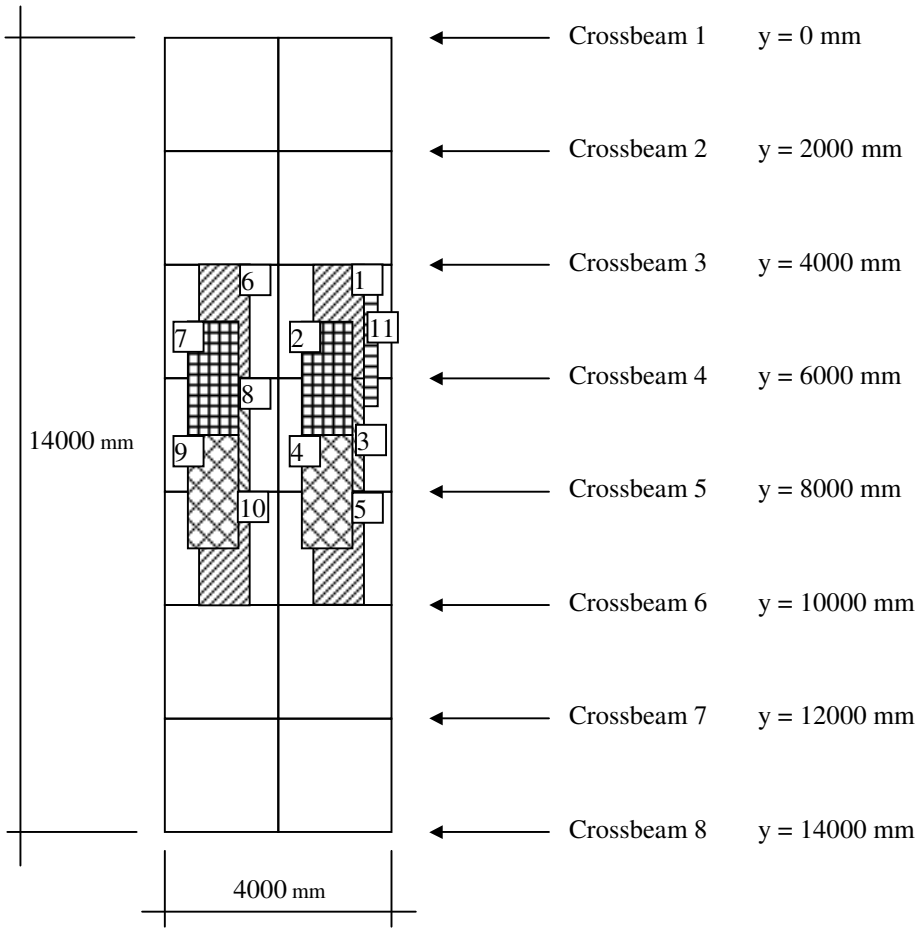

Figure 4-60: Location of strain gauge groups & area influence surfaces

Figure 4-61 shows the structure of this ASCII file. An entire sheet in this ASCII files represents an influence surface. Influence lines, both in longitudinal and transverse directions can be obtained easily from the sheets.

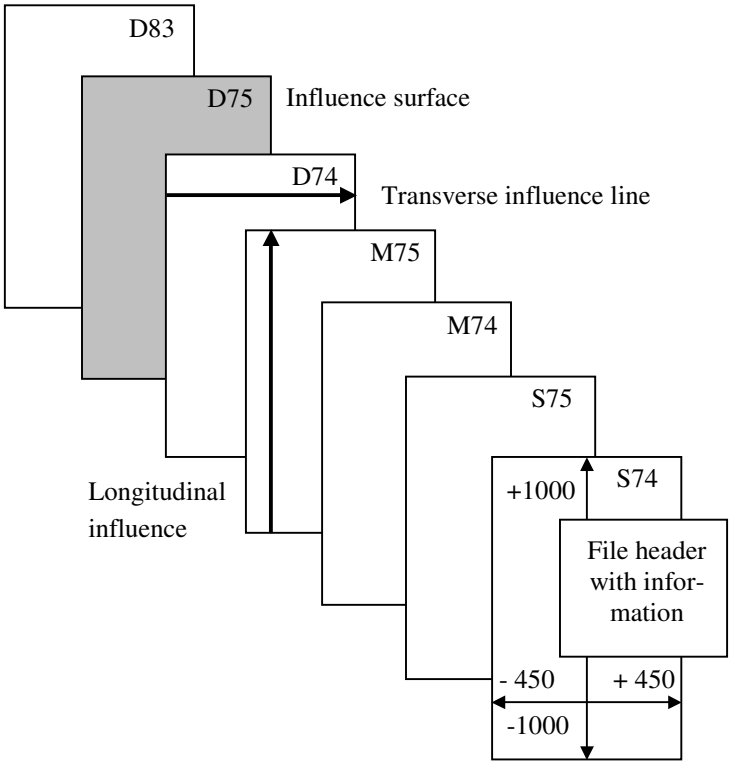

Figure 4-61: Structure ASCII data files

The chosen size of the mesh is the same for all ASCII files:

- 10 mm in longitudinal direction (y-direction) for the static experiments
- 25 mm in longitudinal direction (y-direction) for the dynamic experiments
- 25 mm in transverse direction both for static and dynamic experiments

The dimensions of the area for which the results in the buffer files were evaluated and written in the ASCII files are:

- -450 to 450 mm in transverse direction. This is the entire width in the experiments.
- -1000 to +1000 mm in longitudinal direction compared to the location of the strain gauge group in longitudinal direction. From preliminary analysis it became clear that the influence length of a moving wheel load is rather short, approximately 1000 - 1500 mm. Therefore the area is limited to –1000 to +1000 mm in longitudinal direction.

During the experiments it became clear that it is very difficult to perform them with exactly the planned wheel load. The tolerance on the wheel load is approximately + or – 5 kN. This is

a significant tolerance and is due to the roughness of the test sections. For the further analyses the strains were linearly normalized to 25 or 50 kN, assuming that linear normalization is correct.

In the second step of the data processing in total 572 ASCII data files were created, according to Table 4-16.

Table 4-16: Number of ASCII data files

Surfacing	No. of groups	No. of wheel types	No. of loads	No. of velocities	No. of ASCII files
G (no)	11	4	2	2	176
L (≈0 °C)	11	4	1 (only 50 kN)	1 (only 2 km/h)	44
L (≈0 °C)	11	4	2 (25 and 50 kN)	1 (only 20 km/h)	88
M (≈15 °C)	11	4	1 (only 50 kN)	1 (only 2 km/h)	44
M (≈15 °C)	11	4	2 (25 and 50 kN)	1 (only 20 km/h)	88
H (≈30 °C)	11	4	1 (only 50 kN)	1 (only 2 km/h)	44
H (≈30 °C)	11	4	2 (25 and 50 kN)	1 (only 20 km/h)	88
				Total	572

Creating graphical presentations

In the third step the ASCII data files are processed to graphical representations of the measured data. For this step several Matlab scripts were written. (De Jong, 2005-b). The ASCII files can easily be red with programs like Microsoft Excel, Microsoft Word, notepad or Text Pad. Due to their structure the generated ASCII files are very suitable for data processing and creating graphical representations with Matlab. The formal format and structure of the ASCII files enables computerized mass production of the graphical representations. This gives an enormous time saving.

4.4.4.2 Phase 2: Analysis & Interpretation

Phase 2 comprises the analysis and interpretation of the numerical and graphical representations of the results. The aim of the analysis and interpretation is to draw conclusions about:

- The influence of wheel type, wheel load, temperature and the velocity of the wheel on the stress pattern and stress level in the bridge deck structure.
- The differences between a bridge without surfacing, a bridge deck with asphaltic surfacing and a bridge deck with a ZOK surfacing.
- The composite action between the steel deck plate and the surfacing layer.

- The reliability of the measurements. Special attention will be paid to the strain measurements of the membrane layer and the surfacing layers because these types of strain measurements are relative new.

4.4.5 Test results

4.4.5.1 Behaviour of strain gauges

Before the test results are shown, the behaviour of the strain gauges is discussed in this paragraph. As described in paragraph 4.4.3.3 the experiments in the Lintrack were performed from December 2000 to June 2002.

The vast majority of the strain gauges attached to the steel parts were still functioning correctly in June 2002, only a few were damaged during the experiments. The majority of the strain gauges attached to the membrane layer, both for the mastic asphalt and the ZOK layer were damaged during and sometimes before the experiments. In particular nearly all the strain gauges on the membrane of the ZOK surfacing were damaged at an early stage in the testing including the duplicated strain gauges.

This can also be said for the strain gauges applied to the top of the surfacing, both for the mastic asphalt and the ZOK layer. These gauges were also damaged during and sometimes before the start of the experiments. The strain gauges on the top of the ZOK were nearly all damaged at an early stage in the testing again including the duplicated gauges. Damaged strain gauges on the top of the surfacing were replaced before the test series at the high temperature in June 2002. A significant part of these replaced strain gauges failed again during execution of the test in June 2002.

From the influence surface it is clear if a strain gauge was damaged or not and if the results are reliable. An example of a damaged strain gauge is given in Figure 4-62. Although the wheel load is visible in this figure, the scatter in the transverse direction is nearly of the same magnitude as the measurement results, which makes the measured strain unreliable. In addition a strain influence surface like this is often quickly followed by a complete failure of the strain gauge.

The failure of a lot of the strain gauges at the membrane and top of the surfacing is thought to be the effect of the loading with a moving wheel load, which damages the gauges and is also thought to be deterioration due to the weather conditions. The strain gauges at the top of the surfacing and the membrane were subjected, for a long time to rain, sunshine, frost-thaw cycles etc.

Due to the malfunctioning of the strain gauges on top of the membrane and on top of the surfacing it will be difficult to derive conclusions especially with respect to the composite action between steel deck plate and surfacing.

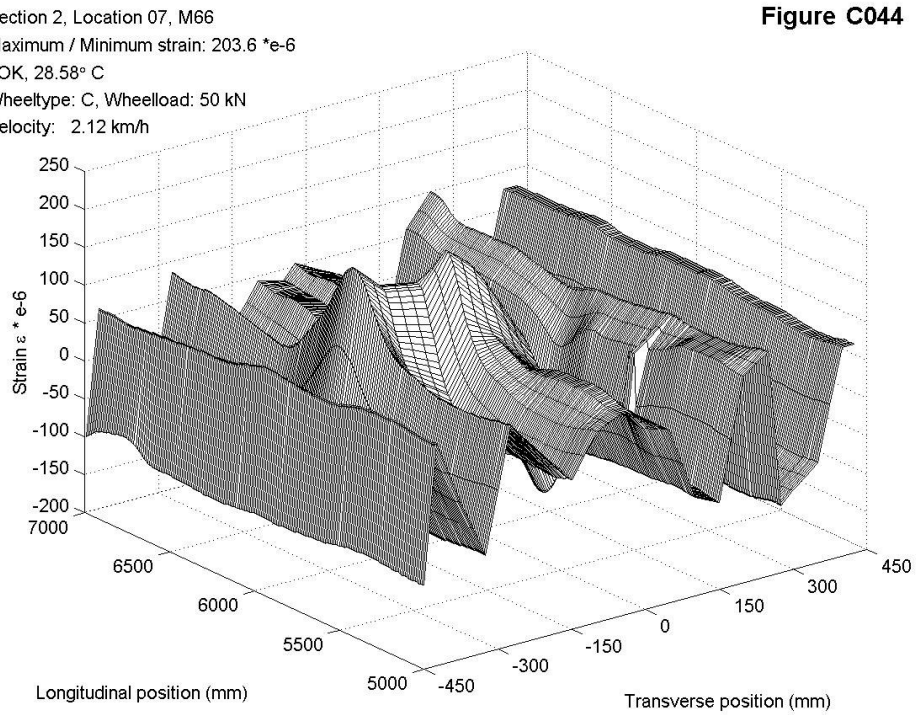

Figure 4-62: Example of an influence surface from a damaged strain gauge.

4.4.5.2 Results validation measurements at 0 km/h

The objective of the validation measurements with a velocity of 0 km/h was to validate the assumption that a velocity of approximately 2 km/h has no dynamic effects on the strains in bridge deck and surfacing. Therefore characteristic locations on the bridge were defined in the test program. It was essential that the wheel load position was exactly at these characteristic locations on the bridge. The procedure of the validation measurements was:

- Move the loading carriage with lifted wheel to the characteristic position
- Lower and load the wheel
- Unload and lift up the wheel
- Move back to start position

During execution of the control measurements it transpired that is was impossible to locate the wheel load with the required accuracy at the characteristic location in longitudinal direction. Two specific problems were discovered:

- It was difficult to locate the lifted wheel load exactly at the characteristic location
- During application of the wheel load, the loading carriage with the wheel rolled backwards or forward in longitudinal direction. This is thought to be the effect of the roughness of the surface and the low friction of the loading carriage of the Lintrack in longitudinal direction.

The accuracy of the achieved longitudinal position was approximately + 15 and – 15 cm from the required position. Due to this lack of precision in longitudinal positioning, the measured strains varied significantly. Analysis of the validation measurements showed that this variation was approximately 30%. This percentage is derived on basis of repeated validation measurements on the same characteristic location. The reliability of the measurements is therefore limited. Analysis also revealed that the measured strain in the validation measurements were about the same as the measured strains at the static 2 km/h experiments. The measured strain in the validation experiment was sometimes smaller and sometimes larger than the comparable strain in the static measurement. Analysis showed that the variations of repeated and comparable static (2 km/h) experiments were significantly smaller than the observed variations of the validation experiments.

For this reason it was concluded that the results of the static (2km/h) experiments are about the same as the results of the validation (0km/h) experiments. No influence from the velocity of 2 km/h was observed. The assumption that the experiments with a velocity of 2 km/h can be classified as experiments at 0 km/h is therefore correct.

4.4.5.3 Results measurements at 2 km/h and 20 km/h

Influence surfaces were created with Matlab for several strain gauges. These influence surfaces are presented in (De Jong, 2005-b). In this paragraph some results for strain gauges near the location of the fatigue crack in the deck plate at the intersection trough-crossbeam are presented. Strain gauges indicated with an S were attached to the steel deck plate, with an M were attached to the intermediate membrane layer and with a D were attached to the top of the asphalt or ZOK layer.

The longitudinal position is measured from crossbeam 1, see Figure 4-48. The transverse position varies between –450 and 450 mm. For section 1 (mastic asphalt), 0 mm is the left web of trough 2, for section 2 (ZOK), 0 mm is the right web of trough 5, see Figure 4-48. Figure 4-63 to Figure 4-76 show a number of influence surfaces. Information is in the upper left corner of each influence surface.

The figures represent the measured strains. For the strain gauges attached to the steel parts the stress can be calculated easily by multiplying it with the stiffness modulus of 210000 MPa. For stresses in membrane and surfacing it is rather difficult to derive the stresses due to the

temperature dependency of the material properties, and the uncertainty with respect to the stiffness of the material.

The figure caption is built up with 8 fields separated with a minus sign:

- The section number: S1 (Mastic Asphalt) or S2 (ZOK)
- The location on the bridge, see Figure 4-48, for example: crossb.4
- The strain gauge number, for example: S33, see Figure 4-53
- The surfacing type with three options, no surfacing, MA for mastic asphalt in section 1 and ZOK for section 2. If the surfacing is mastic asphalt or ZOK, also the temperature is given
- The wheel type: A (single), B (double), C (super single) or D (extra wide base),
- The wheel load
- The velocity
- The measured maximum or minimum strain

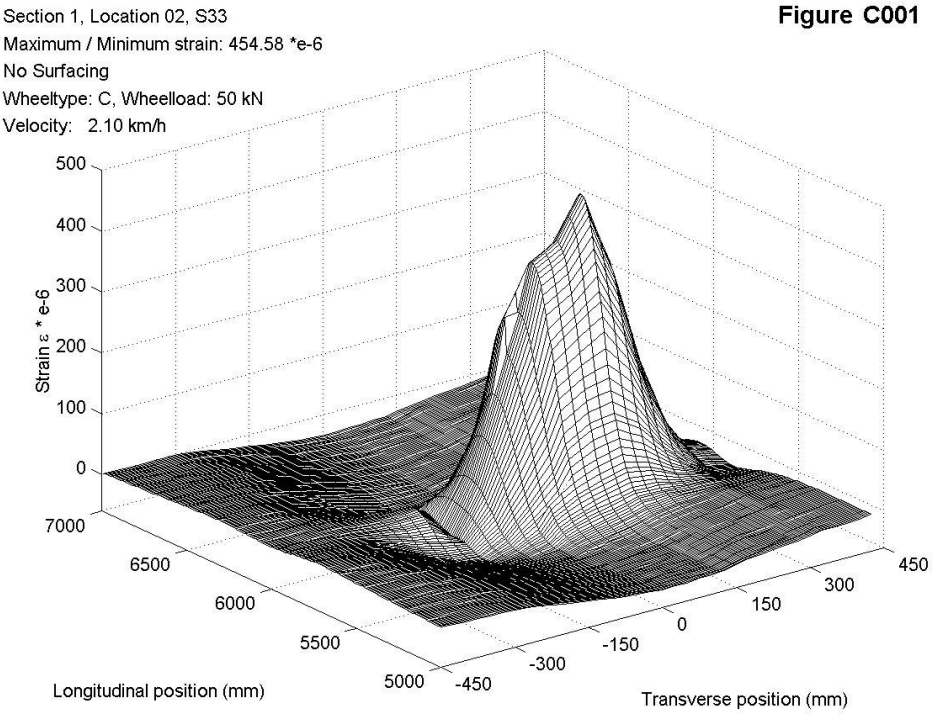

Figure 4-63: S1-crossb.4-S33-no surfacing-wheel C 50 kN-2.1 km/h-max.strain 454.58xe-6

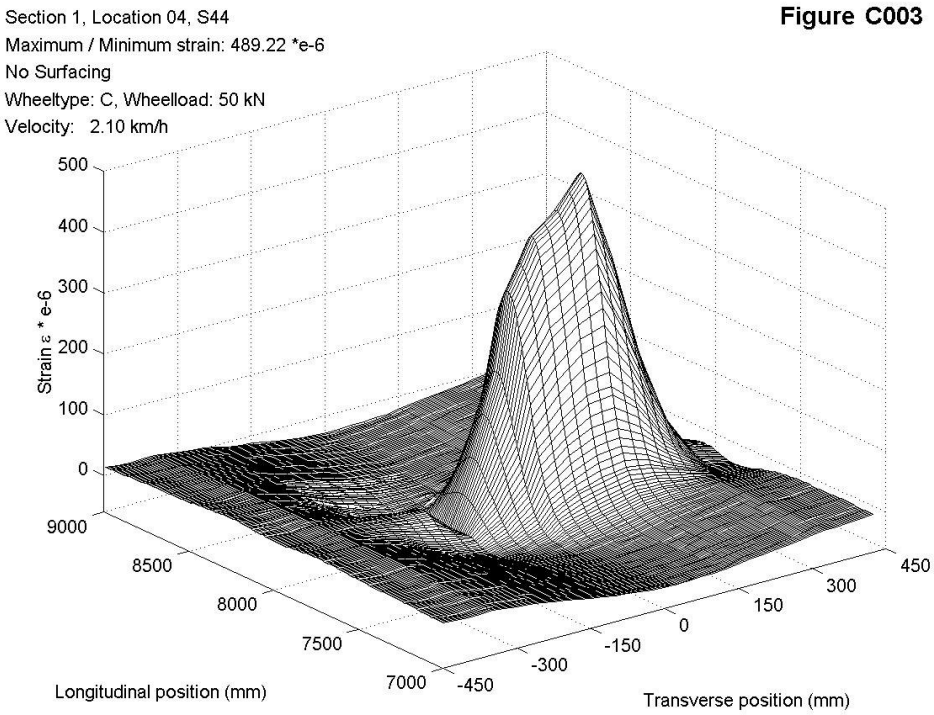

Figure 4-64: S1-crossb.5-S44-no surfacing-wheel C 50 kN-2.1 km/h-max.strain 489.22xe-6

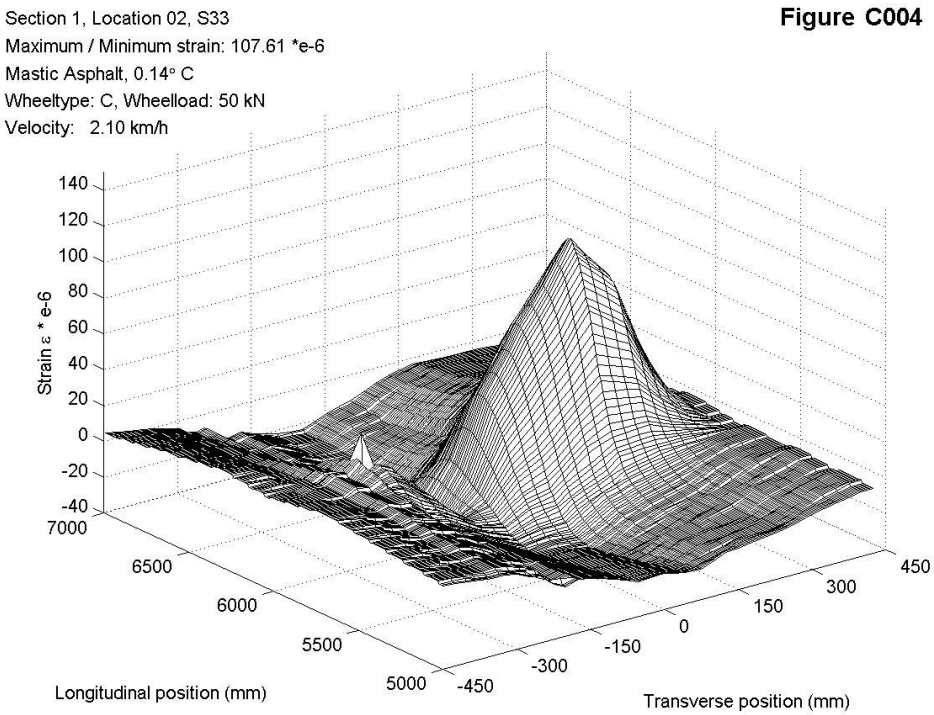

Figure 4-65: S1-crossb.4-S33-MA 0.14°C-wheel-C 50 kN-2.1 km/h-max.strain 107.61xe-6

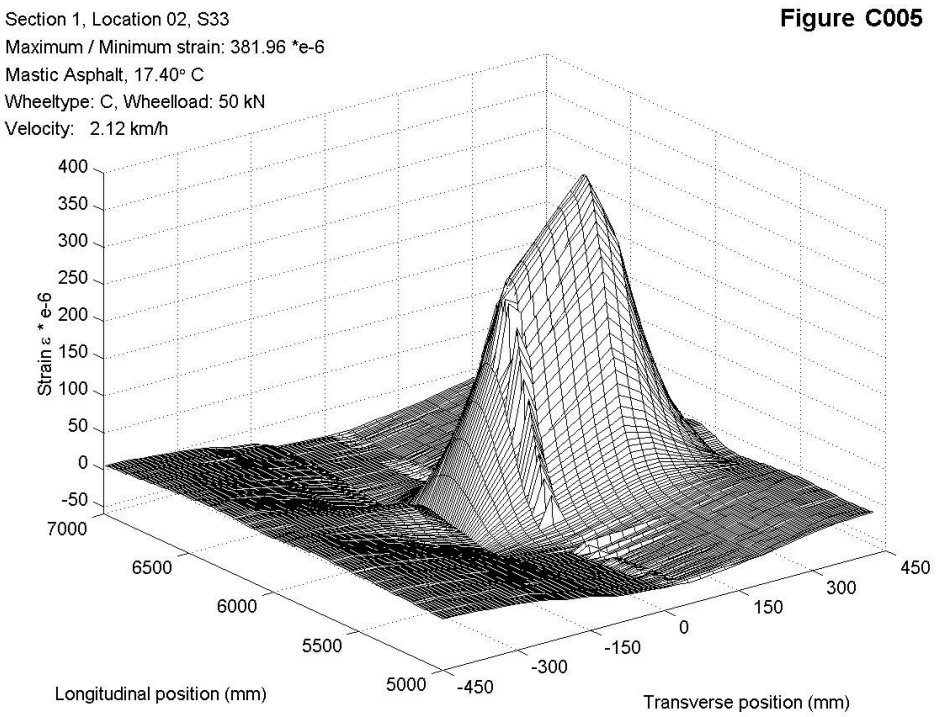

Figure 4-66: S1-crossb.4-S33-MA 17.40°C-wheel-C 50 kN-2.1 km/h-max.strain 381.96xe-6

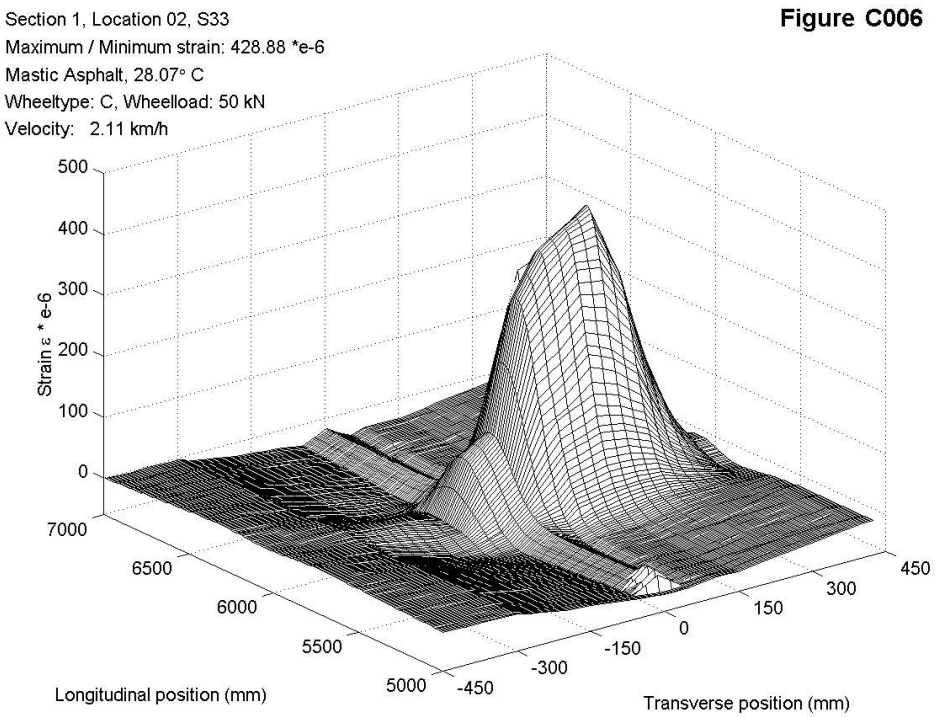

Figure 4-67: S1-crossb.4-S33-MA 28.07°C-wheel C-50 kN-2.11 km/h-max.strain 428.88xe-6

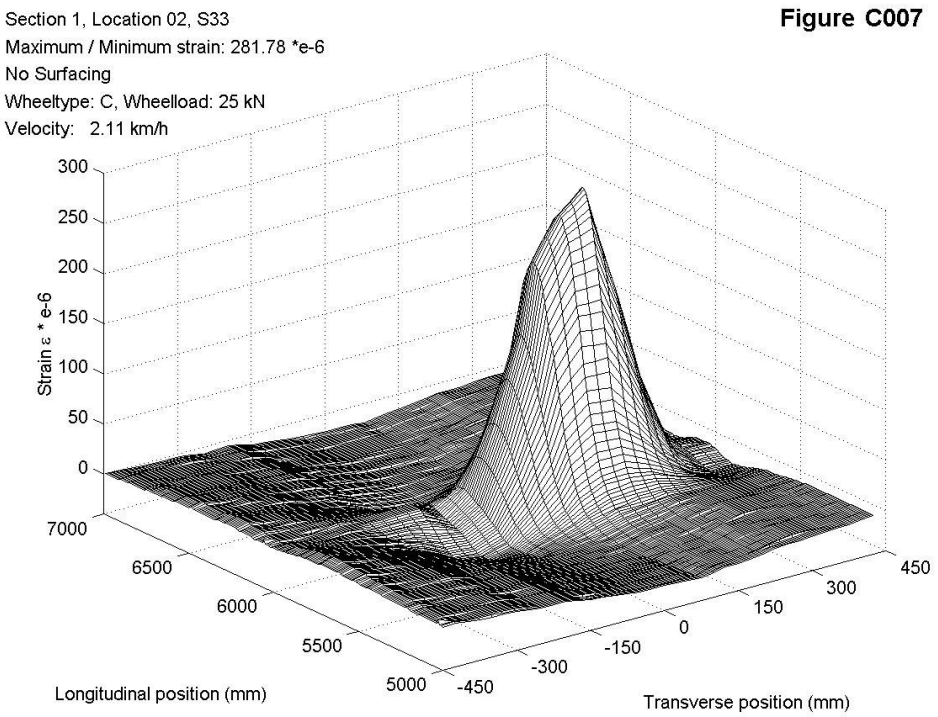

Figure 4-68: S1-crossb.4-S33-no surfacing-wheel C-25 kN-2.1 km/h-max.strain 281.78xe-6

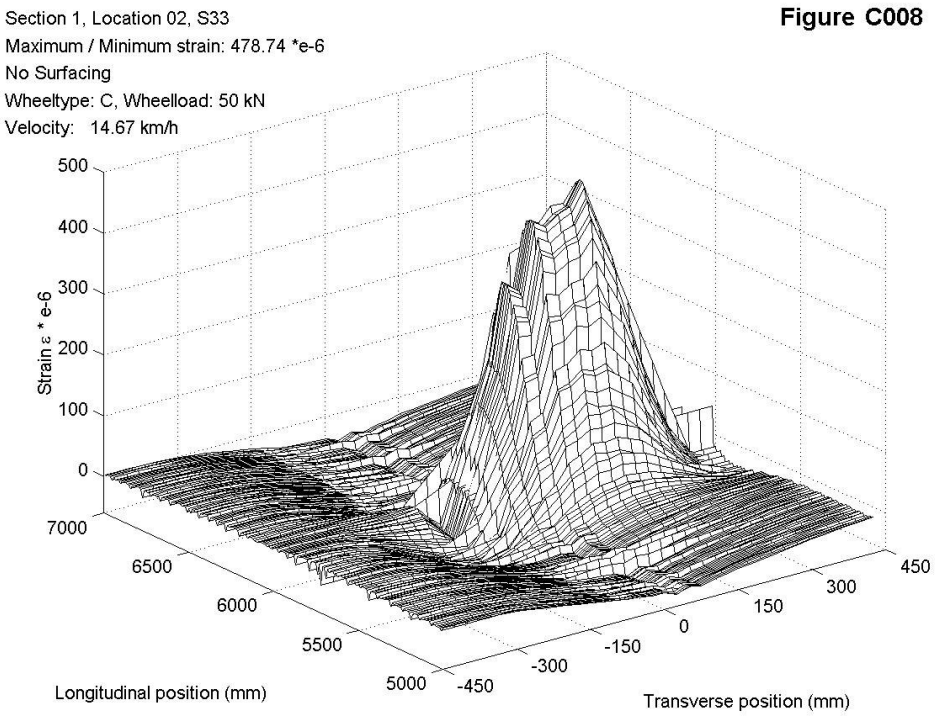

Figure 4-69: S1-crossb.4-S33-no surfacing-wheel C-50 kN-14.67 km/h-max.strain 478.74xe-6

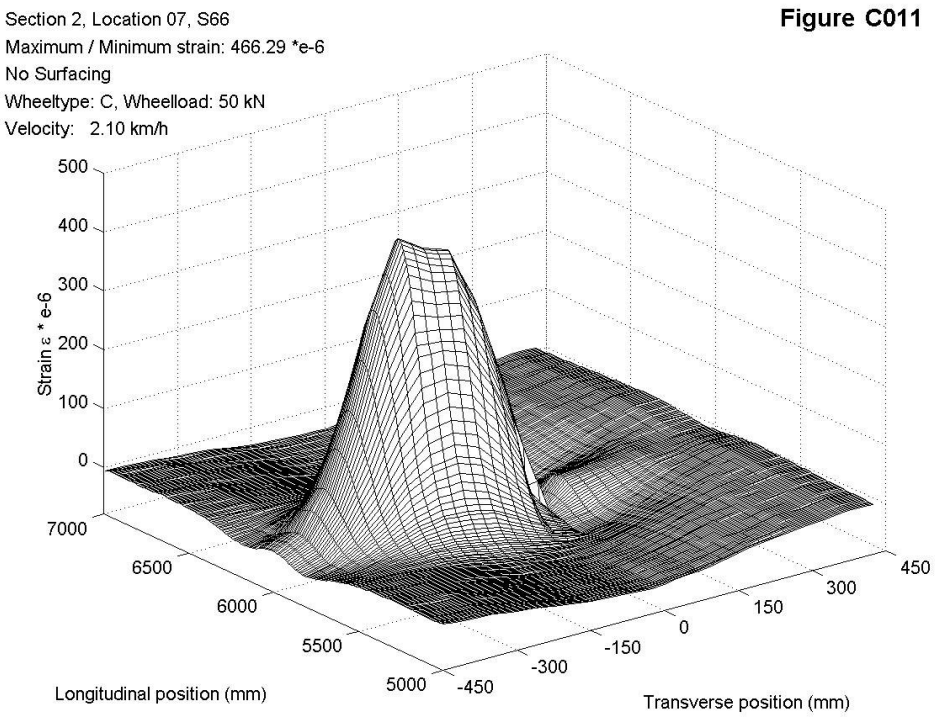

Figure 4-70: S2-crossb.4-S66-no surfacing-wheel C-50 kN-2.10 km/h-max.strain 466.29xe-6

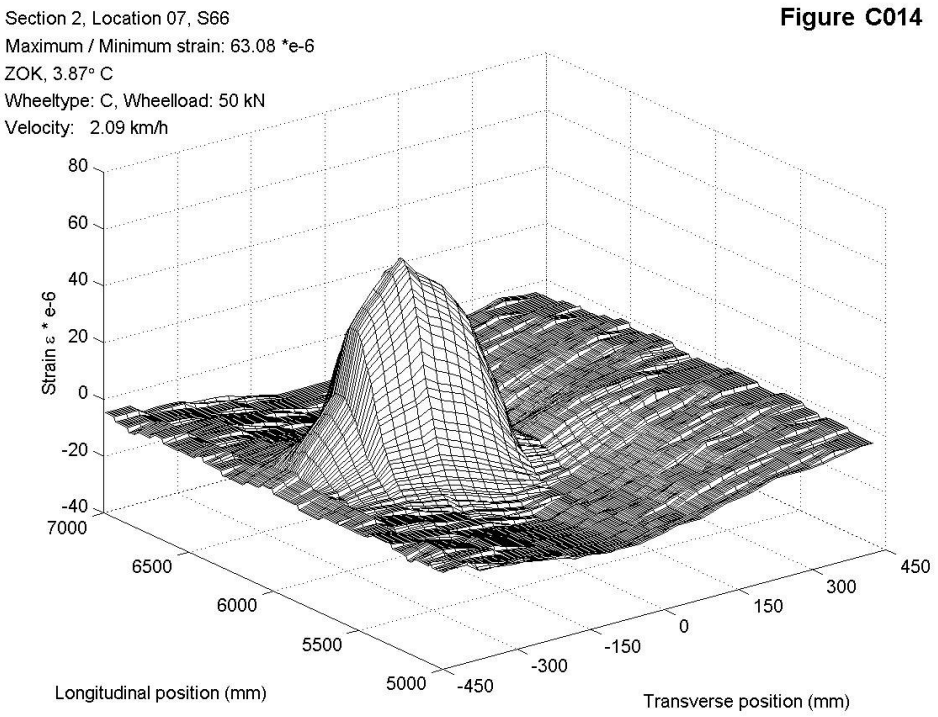

Figure 4-71: S2-crossb.4-S66-ZOK 3.87ºC-wheel C-50 kN-2.09 km/h-max.strain 63.08xe-6

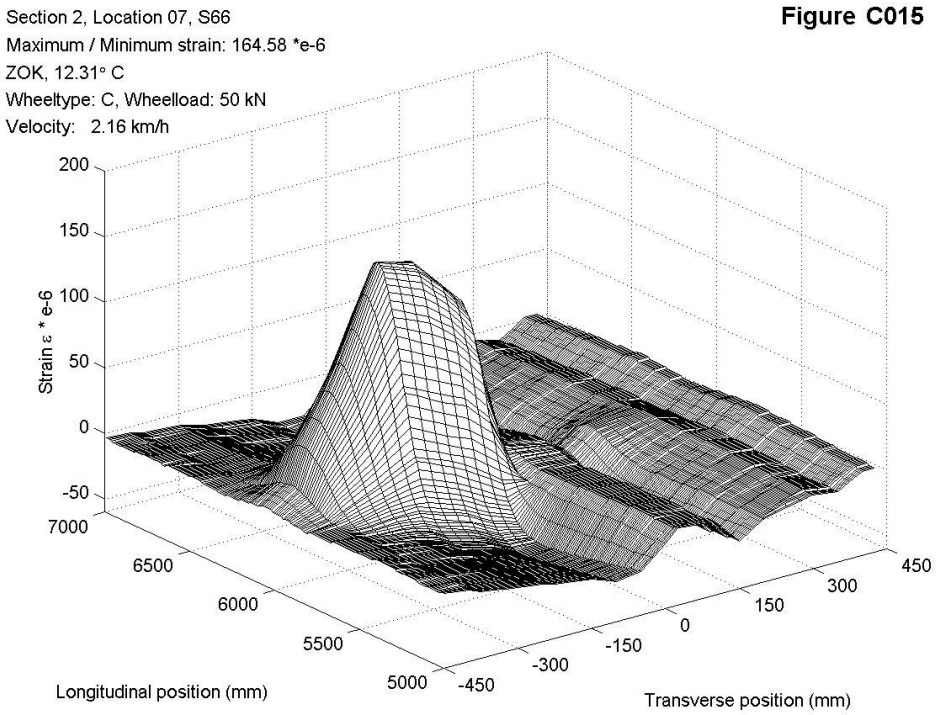

Figure 4-72: S2-crossb.4-S66-ZOK 12.31ºC-wheel C-50 kN-2.09 km/h-max.strain 164.6xe-6

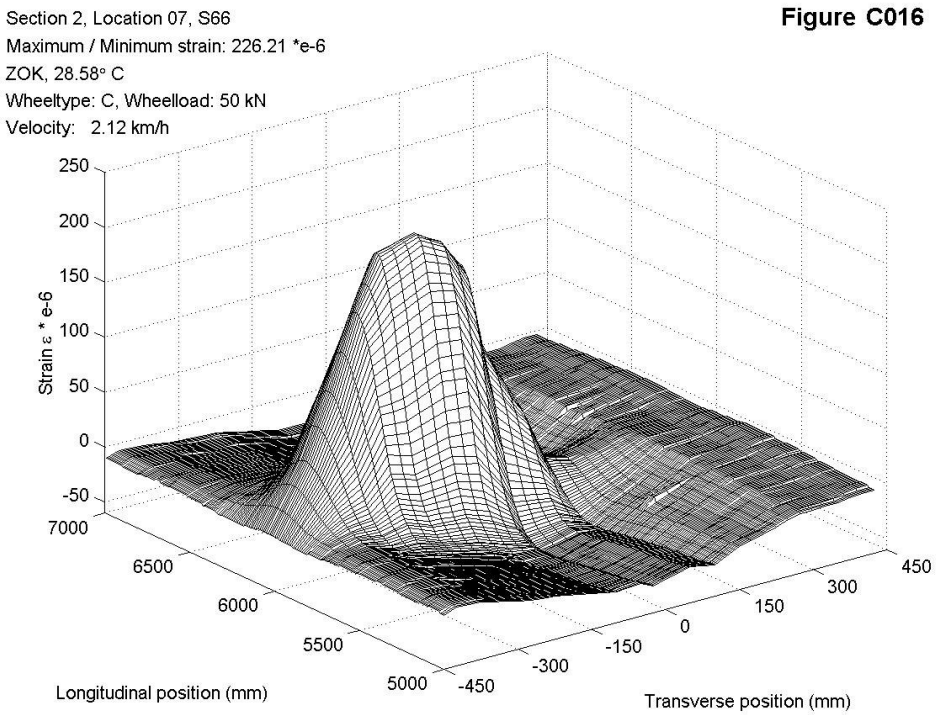

Figure 4-73: S2-crossb.4-S66-ZOK 28.58ºC-wheel C-50 kN-2.12 km/h-max.strain 226.2xe-6

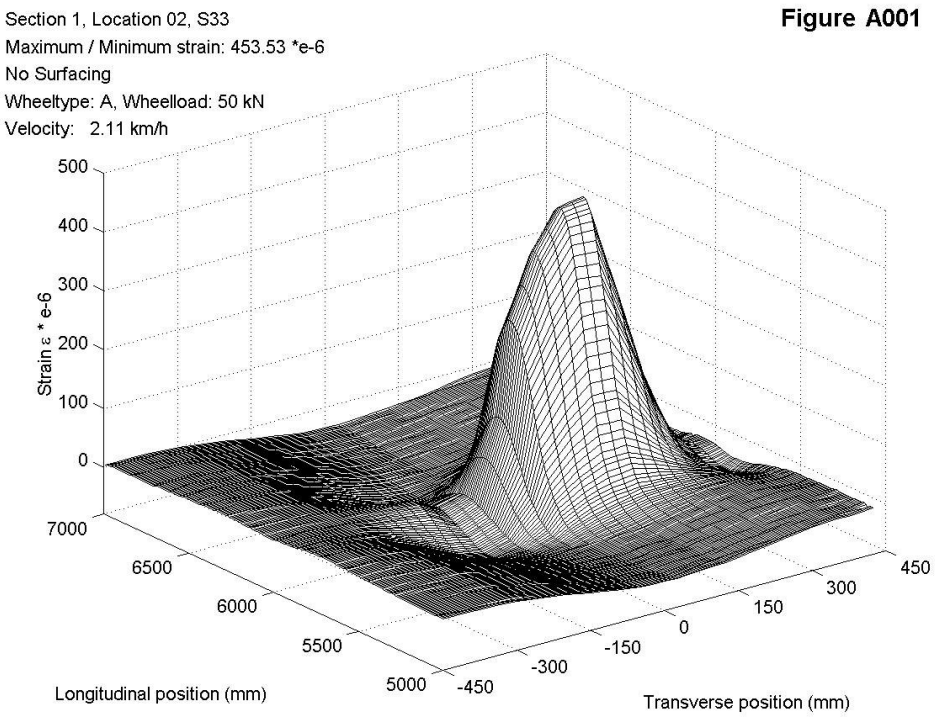

Figure 4-74: S1-crossb.4-S33-no surfacing-wheel A-50 kN-2.11 km/h-max.strain 453.53xe-6

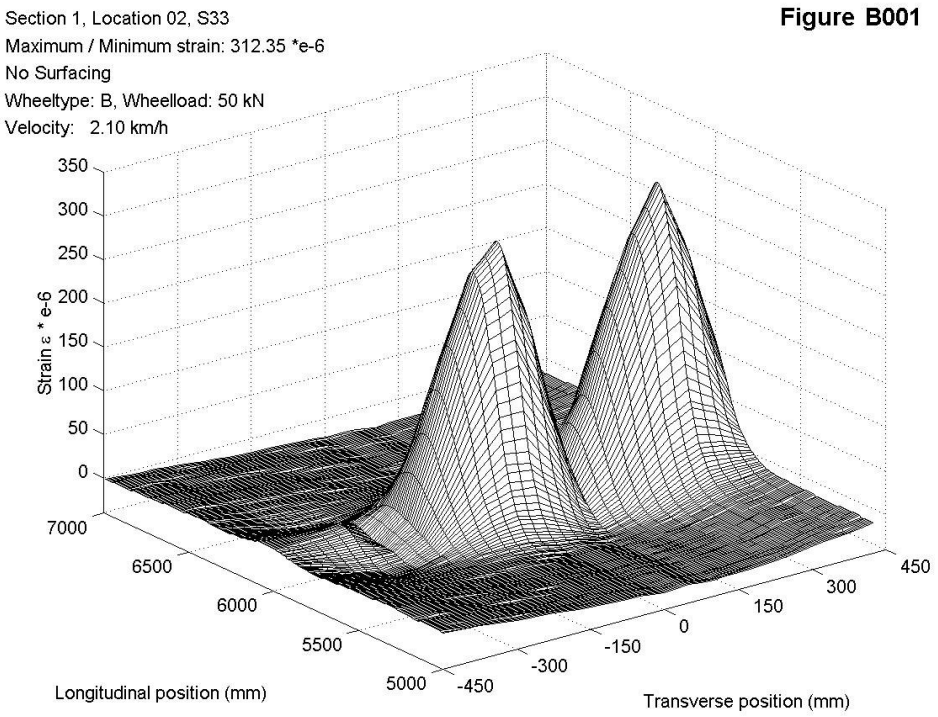

Figure 4-75: S1-crossb.4-S33-no surfacing-wheel B-50 kN-2.1 km/h-max.strain 312.35xe-6

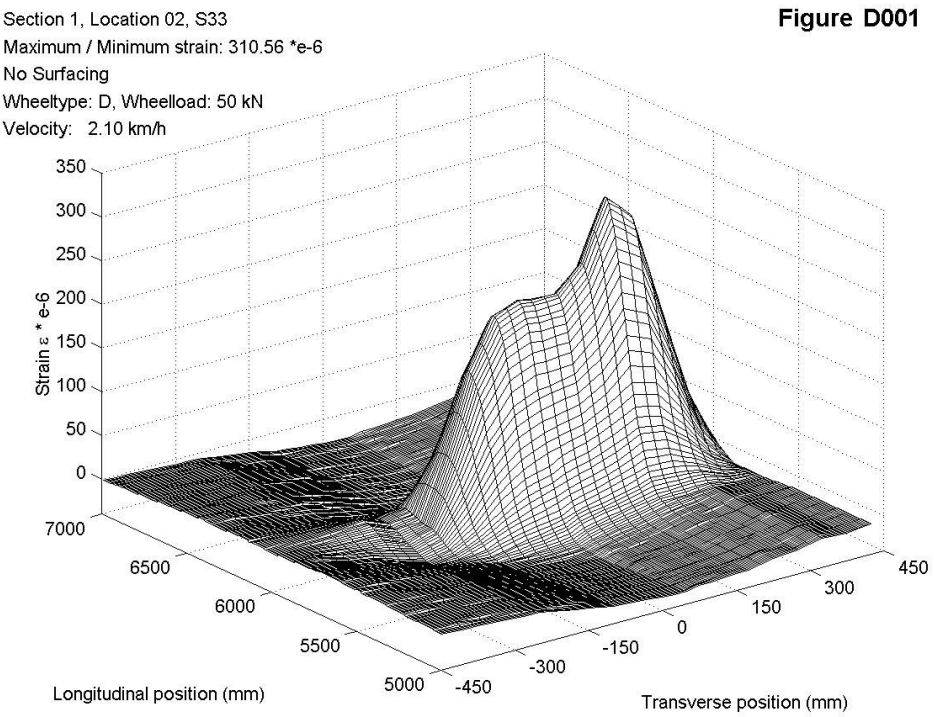

Figure 4-76: S1-crossb.4-S33-no surfacing-wheel D-50 kN-2.1 km/h-max.strain 310.56xe-6

The tables E-1, E-2 and E-3 in Annex E summarize more maximum or minimum strains for strain gauges near the deck plate crack at the intersection of the longitudinal trough girder and crossbeam, for strain gauges applied to the steel, the membrane and the surfacing layer respectively. Some results for strain gauges mid span between the trough webs are also included. For the location of the strain gauges, see Annex D.

Table E-4 in Annex E summarizes some results for strain gauges near the longitudinal weld trough-deck plate. Some of the strain gauges at the membrane layer and the top of the surfacing layer were damaged during the tests. Failure of these gauges is obvious from the influence surfaces. Disturbed strain gauges are indicated with X.

4.4.5.4 Composite action between steel and surfacing

One of the goals of the experiments in the Lintrack was to obtain more insight into the composite action between the steel deck plate and the surfacing layer. Therefore it was necessary to obtain a complete view of the strains from all the gauges on steel, membrane and surfacing in cross-sections of the test panel with a characteristic location of the wheel load.

The chosen characteristic positions of the wheel load were, for both section 1 and section 2:

- In the transverse direction centered above the trough (+150 mm for section 1, and -150

mm for section 2, see Figure 4-48)
- In the longitudinal direction, the wheel loads were placed midspan in field 3, at crossbeam 4, midspan in field 4, at crossbeam 5, midspan in field 5, see Figure 4-48.

The strains in these cross-sections are derived for the super single (type C) at 50 kN at 2 km/h, because with the super single (type C), more tests were performed than with the single (type A), and because the measured strains of the super single (type C) are easier to interpret with respect to composite action than the measured strains for the double (type B) and the extra wide base (type D), because the footprint of the super single does not exceed the width of the trough.

Table 4-17 gives the cross-sections for which the strains are tabulated. The tabulated strains are given in Annex E in the tables E-5 to E-14. If strain gauges were damaged, this is indicated with in X in the tables.

Table 4-17: Cross-sections with strain distribution for composite action

Longitudinal position	Transverse position	Temperatures	Table
Section 1, field 3	+ 150 mm	0 ºC, 15 ºC, 30 ºC	E-5
Section 1, crossbeam 4	+ 150 mm	0 ºC, 15 ºC, 30 ºC	E-6
Section 1, field 4	+ 150 mm	0 ºC, 15 ºC, 30 ºC	E-7
Section 1, crossbeam 5	+ 150 mm	0 ºC, 15 ºC, 30 ºC	E-8
Section 1, field 5	+ 150 mm	0 ºC, 15 ºC, 30 ºC	E-9
Section 2, field 3	-150 mm	0 ºC, 15 ºC, 30 ºC	E-10
Section 2, crossbeam 4	-150 mm	0 ºC, 15 ºC, 30 ºC	E-11
Section 2, field 4	-150 mm	0 ºC, 15 ºC, 30 ºC	E-12
Section 2, crossbeam 5	-150 mm	0 ºC, 15 ºC, 30 ºC	E-13
Section 2, field 5	-150 mm	0 ºC, 15 ºC, 30 ºC	E-14

As examples the results of two cross-sections are given. For section 1 with mastic asphalt in field 3 at 0 ºC and again for section 1 at crossbeam 4 also at 0 ºC, see Figure 4-77 and Figure 4-78.

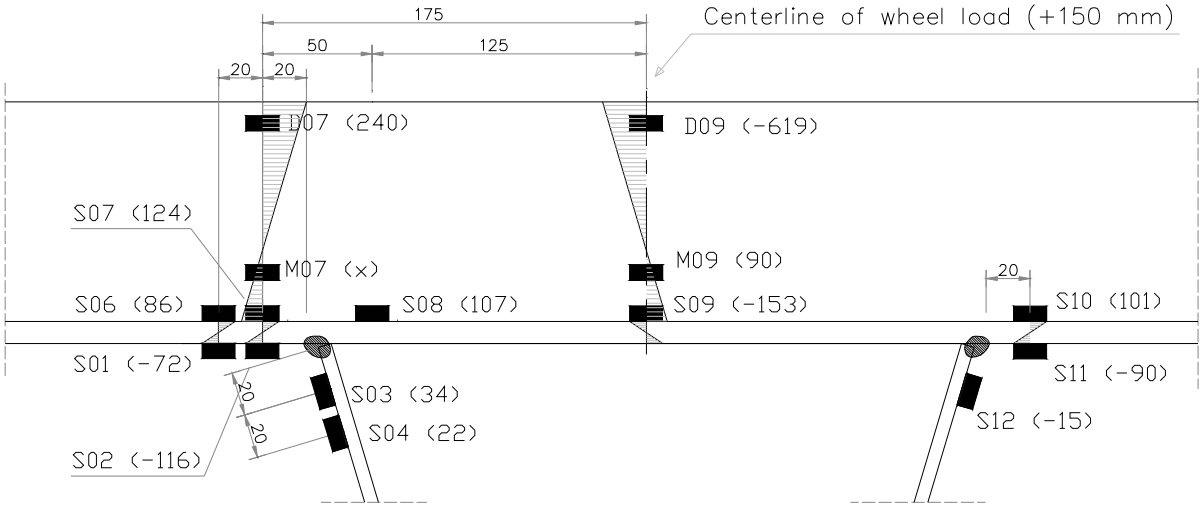

Figure 4-77: Strain in cross-section in field 3 with mastic asphalt, 0 ºC, wheel C at 50 kN

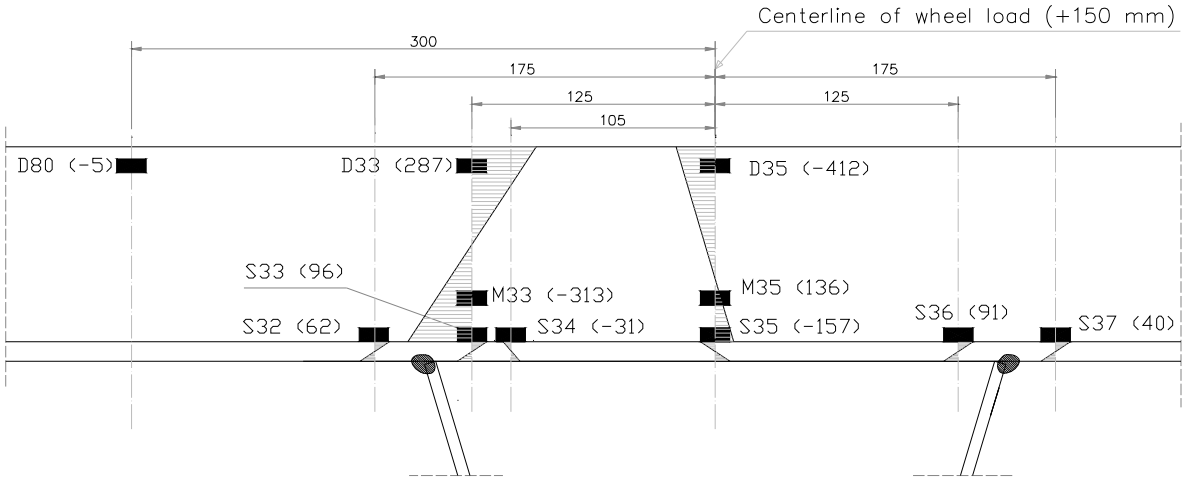

Figure 4-78: Strain in cross-section at crossbeam 4 with mastic asphalt, 0 ºC, wheel C, 50 kN

The following observations relate section 1 with mastic asphalt:

- Strains at the top surface and at the underside of the deck plate are about the same, but with opposite signs.
- Strains at the top surface of the deck plate and strains at the top surface of the membrane have an opposite sign. This means that shear slip in the interface is apparent.
- Strains at the top surface of the membrane, which is thought to be the underside of the surfacing and at the top surface of the surfacing have opposite signs.

Based on these observations the conclusion is that no composite action was observed for mastic asphalt. The behaviour of the mastic asphalt surfacing on the test panel tended towards the stress distribution depicted in the right side sketch of Figure 4-18.

The following observations relate section 2 with ZOK:

- Strains at the top surface and at the underside side of the deck plate are about the same, but with opposite signs. This suggests that there is no composite action, see the right side sketch of Figure 4-18
- Strains at the top of the membrane layer seem to be approximately the same as strain on the top surface of the steel deck plate. This suggests that there is no shear slip in the intermediate membrane, thus indicating full composite action, according to the left sketch of Figure 4-18
- There were only a few observations, due to the number of failed strain gauges on the membrane and the surfacing in section 2 with the ZOK surfacing.

Based on the limited observations and the contradictory indications of the measured strains, no conclusions can be drawn with respect to the composite action of the test panel and the ZOK surfacing.

4.4.5.5 Evaluation of measured strains

An analysis of the results of the strain measurements in the Lintrack shows a few things and the conclusions are formulated in this paragraph. The influence surface numbers (e.g. C001) on which these conclusions are based are given against each conclusion. See the tables E-1, E-2, E-3 and E-4 in Annex E for the measured strains. The conclusions are generally based on the strain given in these tables but some are also based on results that are not listed here. These results are indicated between brackets. See (De Jong, 2005-b) for these results and the influence surfaces.

With respect to the reduction of the stresses due to the two surfacing types at three different temperatures the following stress reduction factors for the strains in the steel construction are derived in conclusion 1 to 6. The reduction is in comparison with a bridge deck without surfacing. Table 4-18 summarizes the stress reduction factors. The stress reduction factors are defined as the quotient between the stress with surfacing divided by the stress without surfacing.

1. The stress reduction factor for mastic asphalt at approximately 0 °C for the steel deck plate is approximately 0.2-0.3 and for the trough web approximately 0.5.
    a. C001 C004
    b. A001 A004
    c. B001 B004
    d. D001 D004
    e. C019 C021
    f. C172 C176
2. The stress reduction factor mastic asphalt at approximately 15 °C for both the steel deck

plate and the trough web is approximately 0.7-0.8.
   a. C001 C005 (A001 A005 B001 B005 D001 D005)
   b. C019 C022 (A019 A022 B019 B022 D019 D022)
   c. C172 C177 (A172 A177 B172 B177 D172 D177)
3. The stress reduction factor for mastic asphalt at approximately 30 °C for both the steel deck plate and the trough web is 0.9-1.0.
   a. C001 C006 (A001 A006 B001 B006 D001 D006)
   b. C019 C023 (A019 A023 B019 B023 D019 D023)
   c. C172 C178 (A172 A178 B172 B178 D172 D178)
4. The stress reduction factor for ZOK at approximately 0 °C for the steel deck plate is approximately 0.1-0.2 and for the trough web approximately 0.3-0.5.
   a. C011 C014 (A011 A014 B011 B014 D011 D014)
   b. C028 C030 (A028 A030 B028 B030 D028 D030)
   c. C181 C183 (A181 A183 B181 B183 D181 D183)
5. The stress reduction factor for ZOK at approximately 15 °C for the steel deck plate is approximately 0.3-0.4 and for the trough web approximately 0.5-0.6.
   a. C011 C015 (A011 A015 B011 B015 D011 D015)
   b. C028 C031 (A028 A031 B028 B031 D028 D031)
   c. C181 C184 (A181 A184 B181 B184 D181 D184)
6. The stress reduction factor for ZOK at approximately 30 °C for the steel deck plate is approximately 0.5 and for the trough web approximately 0.6-0.7.
   a. C011 C016 (A011 A016 B011 B016 D011 D016)
   b. C028 C032 (A028 A032 B028 B032 D028 D032)
   c. C181 C185 (A181 A185 B181 B185 D181 D185)
7. The differences between duplicated strain gauges are small, smaller than 15%.
   a. C001 C002 C003 C011
   b. C019 C028
   c. C172 C173 C181 C182
8. The strains due to wheel A are approximately the same as the strains due to wheel C. Strains under wheels B and D are smaller than under wheel C. This is mainly the effect of the width of the footprint. The larger the footprint the smaller the strain at the same load level.
   a. C001 A001 B001 D001
   b. C004 A004 B004 D004
   c. C007 A007 B007 D007
   d. C172 A172 B172 D172
9. Half the load does not mean half the strains Due to a smaller footprint from a smaller load, the load is more concentrated, causing higher strains.
   a. C001 C007

b. A001 A007
c. B001 B007
d. D001 D007
e. C172 C179
f. C181 C186

10. A velocity up to 20 km/h does not significantly influence the strains
    a. C001 C008
    b. C172 C180
    c. C181 C187
11. Both surfacing materials are sensitive to temperature differences, but mastic asphalt is more temperature sensitive then ZOK.
12. The strains in the steel deck plate are approximately the same with no surfacing as with mastic asphalt surfacing at approximately 30 °C. This indicates also that the usual modelling based on a spread-to-depth ratio is less valid for surfacings.

Table 4-18: Stress reduction factors for strain and stress in steel structure

	Deck plate	Trough web
No surfacing	1.0	1.0
Mastic asphalt approximately 0 °C	0.2-0.3	0.5
Mastic asphalt approximately 15 °C	0.7-0.8	0.7-0.8
Mastic asphalt approximately 30 °C	0.9-1.0	0.9-1.0
ZOK approximately 0 °C	0.1-0.2	0.3-0.5
ZOK approximately 15 °C	0.3-0.4	0.5-0.6
ZOK approximately 30 °C	0.5	0.6-0.7

4.4.6 Numerical analysis Lintrack tests

The accompanying FE-models were made in order to calculate the stresses in the bridge deck. Models were made for the calculation of stresses in the steel parts and to investigate the behaviour of the surfacing layer. These sophisticated FE-models were made by Huurman and Medani (Medani, 2006), (Huurman, 2003, 2004). Medani motivated that a new pavement design method is necessary for surfacings on orthotropic steel bridge decks, see paragraph 4.2.2.4 (Medani, 2006). He concluded that the ACRe material model can describe the behaviour of a pavement appropriate. Medani performed many tests to determine the parameters of mastic asphalt for the ACRe model. This material model is incorporated in the CAPA 3D FE-package. This paragraph describes their work. Two structural FEM's of the bridge deck were developed within the (Computer Aided Surfacing Analysis) CAPA FE-

package. The models are given in Figure 4-79. One model may be used to compute stress and strain when the load is placed over a crossbeam, while the other model is valid when that load is placed between two crossbeams.

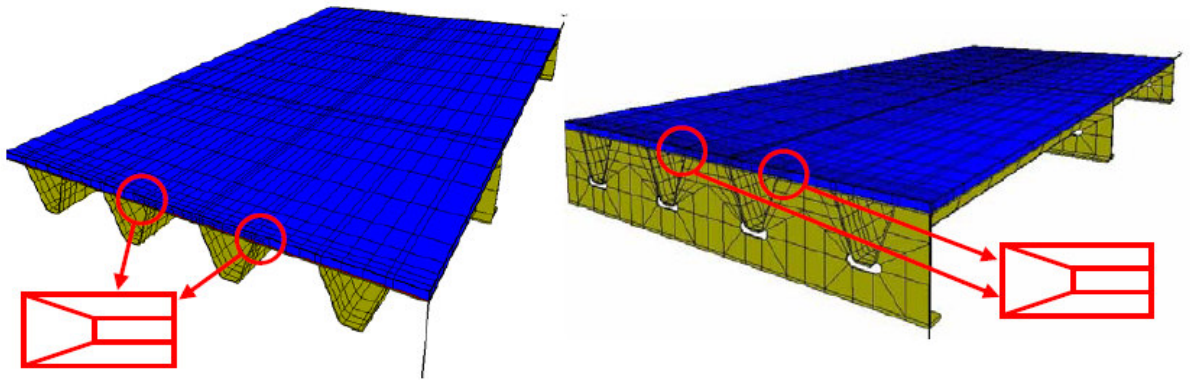

Figure 4-79: CAPA FE-models for loads between crossbeams (left) and on crossbeams (right)

The measurements showed that the maximum strain in the steel deck plate often occurs in strain gauge S09. This gauge was located at the upper surface of the deck plate between two crossbeams. The gauge was situated over the centreline of a longitudinal stiffener. It was decided arbitrarily that the model should be validated on the measured data obtained with gauge S09.

Figure 4-80 gives an example of the modelled response of the unsurfaced bridge deck. The observed differences between measurement and FE-calculations are within a range of -6.6% to 6.9%. As the scatter in measured data is of the same order of magnitude as the differences between the calculated and the measured strains, it proves the very high accuracy of the finite element model.

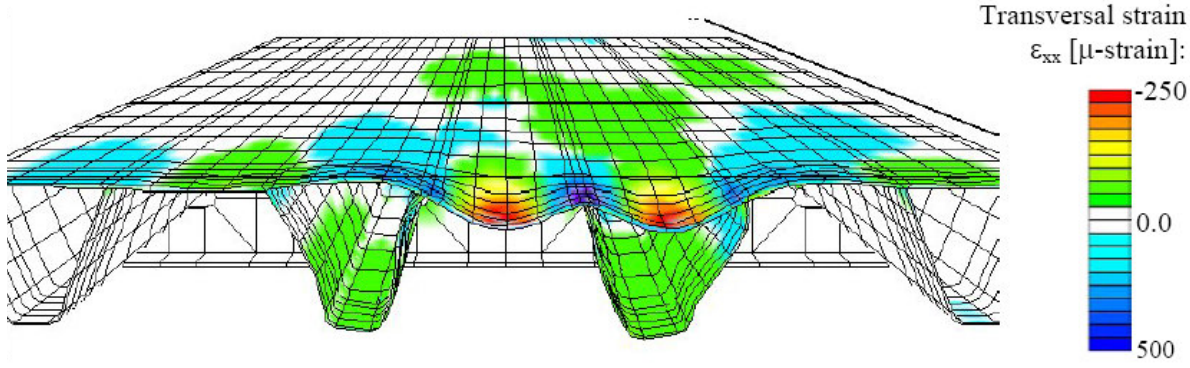

Figure 4-80: Indication of lateral strain ε_{xx} in the deformed bridge deck without surfacing (150x) under a 50 kN double wheel (type B)

When the bridge is surfaced the situation becomes much more complex. Now the results of the calculation will also depend on the mechanical behaviour of the surfacing material and the membrane interface bonding the surfacing to the steel deck plate. The membrane interface material and the mastic asphalt will show a complex mechanical response, which is dependent on frequency (strain rate) and temperature. The response will show elastic, viscous and plastic components, as is the case for any bitumen bound material. An example of the deformed mesh with an indication of strain is given in Figure 4-81.

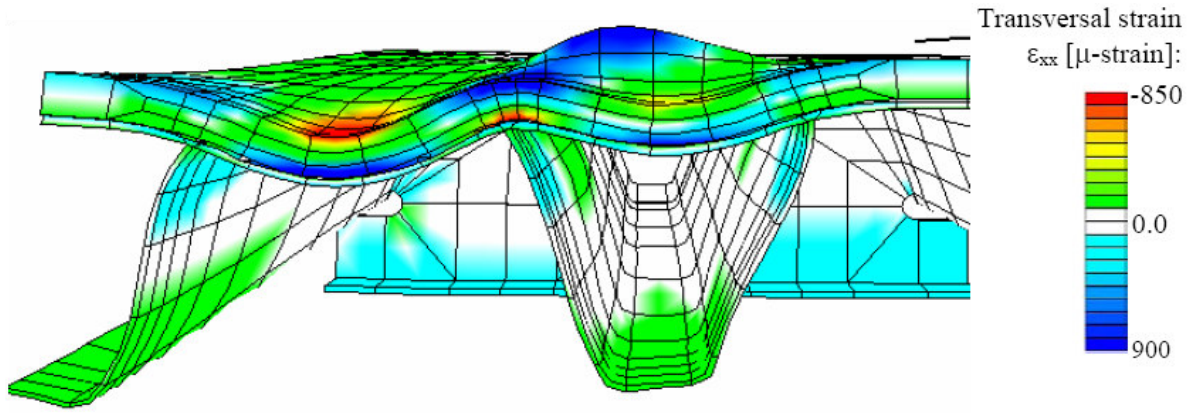

Figure 4-81: Deformed bridge deck (250x) with transverse strain ε_{xx} under a 14.5 tons dual wheel axle (50 mm 5000 MPa surfacing on 1 N/mm^2 membrane interface).

Figure 4-82 shows the development of lateral strain over the height of the surfacing as calculated with the model. In this figure ε_{xx} is given under a 14.5 tons double wheel type in the field between the crossbeams. In this model a 50 mm surfacing with stiffness of 3000 MPa and a cross beam spacing of 3000 mm is used. Figure 4-82 clearly indicates that the strain gradient in the surfacing is not linear. Furthermore it also indicates that the strain gradient in the surfacing is not necessarily equal to the gradient in the steel.

Measurements on the bridge surfaced with mastic asphalt at 0 ºC for the super single (type C) were back-calculated. In total 10 calculations were made. Back-calculating the measured strain in the steel deck plate proved to be troublesome. There is no combination of surfacing stiffness and membrane interface stiffness that will lead to a proper back-calculated strain in the steel and in the surfacing. The best estimate of the strain in the steel deck in combination with an accurate surfacing strain is obtained when a stiff surfacing is placed over an extremely soft membrane interface (Huurman, 2004).

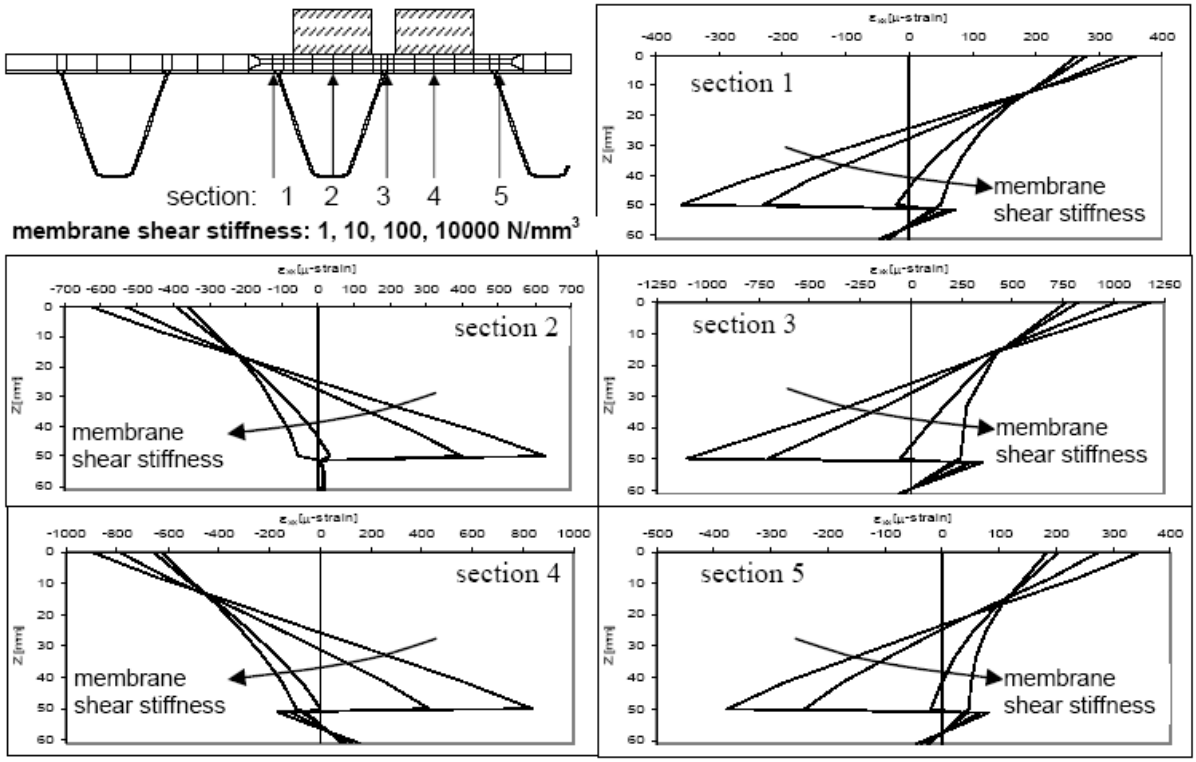

Figure 4-82: Calculated lateral strain over the height of the surfacing

4.4.7 Concluding remarks Lintrack test program

An extensive research program, both experimental and numerical was performed. The behaviour and influence of surfacing on the steel bridge deck was the main issue. This research was described. This paragraph highlights the main conclusions:

With respect to the instrumentation:

- The vast majority of the strain gauges attached to the membrane and the top of both surfacings were damaged during and sometimes before execution of the experiments. Therefore it is difficult to derive conclusions with respect to the composite action between steel deck plate and surfacing.

With respect to composite action:

- Composite action was not observed for mastic asphalt. The behaviour of the mastic asphalt surfacing on the test panel tends towards the stress distribution depicted in the right side sketch of Figure 4-18.
- No conclusions can be drawn for the ZOK surfacing due to the limited observations and contradictory indications of the measured strains on the ZOK surfacing.

- The best estimate with the FE-models of the strains in the steel deck and surfacing is obtained when a stiff surfacing is placed over an extremely soft membrane interface. In this modelling there is only a little composite action

With respect to the influence of wheel type, wheel load and velocity on the stress in the steel bridge deck:

- The single (type A) and the super single (type C) induced approximately the same strains in the bridge deck. Strains under the double (type B) and the extra wide base (type D) were smaller compared wheel A and C.
- Half the load does not mean half the strains Due to a smaller footprint from a smaller load, the load is more concentrated, causing higher strains.
- Differences in velocity from 0 km/h up to 20 km/h did not significantly influence the strains.

With respect to stress reduction due to the surfacing

- Significant stress reductions were achieved with surfacings on top of the steel deck plate. However there was little reduction for mastic asphalt at 30 °C. Table 4-18 summarizes the measured stress reduction factors.

4.5 Concluding remarks

This paragraph summarizes the main conclusions of this chapter. With respect to the calculation of local stresses at the crack location in the deck plate due to wheel loading these conclusions can be drawn:

- For fatigue verifications of deck plate cracks at the crossbeam location the stress calculations can be based on a clamped beam model.
- For this calculation the wheel load can be modelled as a uniformly distributed load and the span of the clamped beam can be taken as 290 mm.

With respect to the fatigue behaviour of deck plates:

- Based on fatigue tests detail classifications were derived for several cracks lengths.
- These classifications are proposed for fatigue calculations.

With respect to the ultimate load capacity of the deck plate with fatigue cracks:

- Cracks up to 50 cm long do not threaten the traffic safety

With respect to the effects of asphalt surfacing:

- The stress reduction in the steel due to surfacing is for the major part the effect of the

surfacing acting as a beam, to a certain extent in composite action with the steel deck plate.

- A comparison of theoretical and numerical analysis with both field measurements on bridges and tests in the Lintrack points towards a model with a flexible interface for fixed bridges.

5. Deck repair and possible renovation techniques

5.1 Introduction

This chapter deals with several subjects that are combined because they are all preliminary before the application of a renovation method.

Paragraph 5.2 is about a research program into submerged arc welding (SAW) for deck plate cracks. Parameter settings for the welding process and the fatigue behaviour of SAW deck plate welds were determined. This paragraph about SAW welding is also included in this chapter for the simple reason that if there are cracks in the deck plate the first step is to repair these cracks. Subsequently a renovation technique can be applied to the whole bridge deck to enhance the lifetime of the bridge.

Paragraph 5.3 describes the requirements that are formulated for the development of the renovation techniques. Paragraph 5.4 gives an overview of several ideas for renovation techniques. At the end of this paragraph a few techniques have been selected for further research and the reasons why other solutions are thought not to be the best solutions are explained. The requirements and the several ideas are described as preliminary because they are raised at the beginning of the development of the renovation techniques.

Paragraph 5.5 end this chapter with some concluding remarks.

5.2 Fatigue crack repair before application of renovation methods

Before applying a renovation technique normally cracks in the deck plate have to be repaired, although in some cases this may not be not necessary. Two requirements have to be fulfilled if a crack is to remain:

- Cracks are so small that it becomes clear from a fatigue analysis that the required lifetime will be achieved without repairing them.
- The static ultimate load capacity of the deck plate is sufficient even when cracked.

The normal assumption is however that the cracks have to be repaired. Therefore repair

techniques are required in order to recreate a deck plate without fatigue cracks. There are several options for these repairs:

- Replace part of the deck plate approximately 450 mm wide and with a length dependent on the crack length.
- 'Classical' manual metal arc welding
- Submerged arc welding (De Jong, 2004-f)

With the submerged arc welding technique (SAW) the creation of the weld is automated. There are three advantages of submerged arc welding; the process is fast; the welding takes place only from the top of the deck plate, and the weld shrinkage is relatively small. A disadvantage is that due to the automated procedure only straight cracks can be repaired with this technique. Because experience with the submerged arc welding technique on fatigue cracked deck plates was limited a research program was set up to develop this technique and establish the best repair parameters.

Figure 5-1: Submerged arc welding

Figure 5-1 shows a photograph of the welding machine (left) and a detail photograph (right). This technique is describes by The Welding Institute (TWI) (TWI, 2006) as follows, see Figure 5-2. "SAW involves the formation of an arc between a continuously-fed bare wire electrode and the workpiece. The process uses a flux to generate protective gases and slag, and to add alloying elements to the weld pool. A shielding gas is not required. Prior to welding, a thin layer of flux powder is placed on the workpiece surface. The arc moves along the joint line and as it does so, excess flux is recycled via a hopper. Remaining fused slag layers can be easily removed after welding. As the arc is completely covered by the flux layer, heat loss is extremely low. This produces a thermal efficiency as high as 60% (compared with 25% for manual metal arc). There is no visible arc light, welding is spatter-free and there is no need for fume extraction. SAW is usually operated as a fully-mechanised or automatic

process, but it can be semi-automatic. Welding parameters: current (Amps), arc voltage and travel speed all affect bead shape, depth of penetration and chemical composition of the deposited weld metal. Because the operator cannot see the weld pool, greater reliance must be placed on parameter settings. SAW is normally operated with a single wire on either AC or DC current. Common variants are: twin wire, triple wire, single wire with hot wire addition, metal powder addition. All contribute to improved productivity through a marked increase in weld metal deposition rates and/or travel speeds."

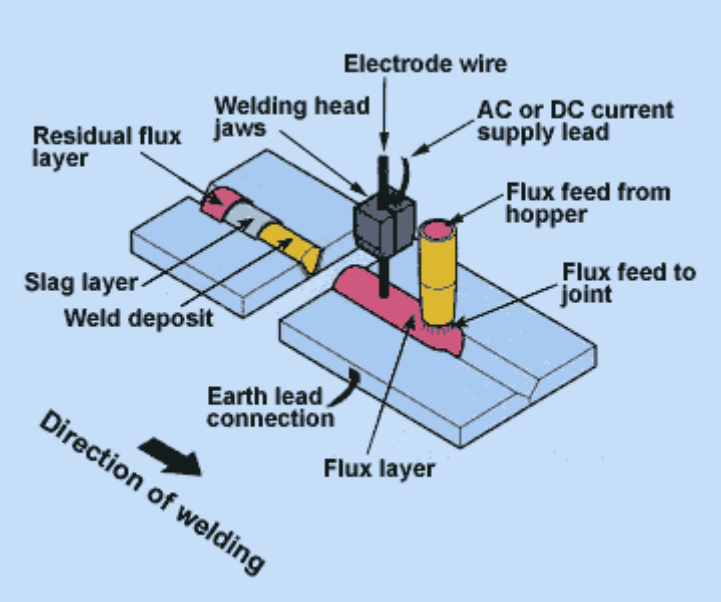

Figure 5-2: Submerged arc welding scheme (TWI, 2006)

The research program was focused on two topics:

- Determination of the parameter settings, see paragraph 5.2.1
- Determination of the fatigue behaviour of SAW repaired deck plates, see paragraph 5.2.2

5.2.1 Tests submerged arc welding

5.2.1.1 Test program

Determination of the parameters settings is important. The first part of the research program focused on this aspect. The parameters that lead to the maximum possible depth of penetration were researched. The background of maximizing the depth of penetration is that the fatigue behaviour is better with greater penetration. On the other hand parameters settings that cause too much heat input leading to the weld burning through the deck plate should be avoided.

The main questions are:

- What is the relationship between current and depth of penetration?
- What is the relationship between voltage and depth of penetration?
- What is the effect of the travel speed?
- What is the effect of the crack angle α, see Figure 5-3?
- In which situations is the weld burned through the deck plate?
- What is the effect of variations in the deck plate thickness: 10, 12 or 14 mm?

Test plates have been welded with these test specifications:

- 10 plates with thickness 10, 12 or 14 mm
- Current between 500 and 950 Amps
- Dimensions of the plates according to Figure 5-3
- With two velocities: 450 mm/min and 600 mm/min
- All specimen were made from plate material S355J2G3
- The crack angle (α) is chosen as 70°, see Figure 2-9

These parameters were based on the limited experience that was available. A few preliminary test were performed with plates of 10 mm and a current of approximately 650 Amps. The achieved depth of penetration was about 70% of the plate thickness. Some test parameters were changed during the test. After completion of all the SAW welds in the 10 test specimen, 10 locations were chosen from which macros were taken to determine the depth of penetration.

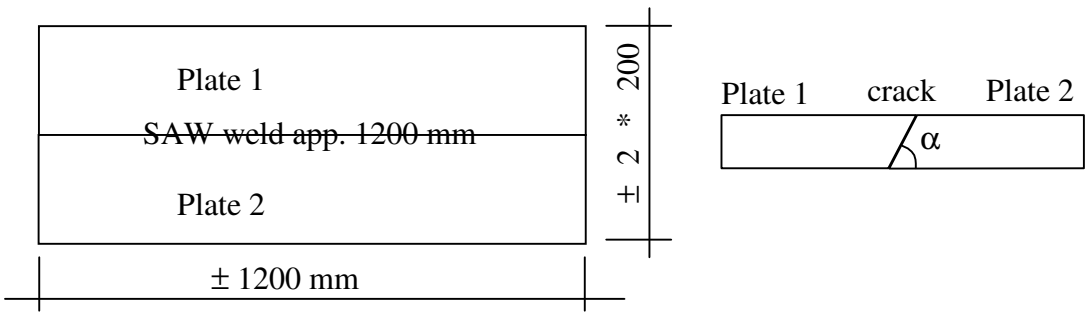

Figure 5-3: Set up test specimen and plate dimensions SAW tests

The tests were conducted on Monday 9 February 2004 at the firm Takke Breukelen. The welding machine was fed with a single wire, type L 61, with a diameter of 4 mm. FX860 was used as flux powder. These choices were based on the experience of the firm with submerged arc welding. The tests were performed in the sequence: 4, 5, 8, 9, 6, 1, 2, 3, 7, 10

The weld shrinkage was measured at 4 positions on each specimen, see Figure 5-4.

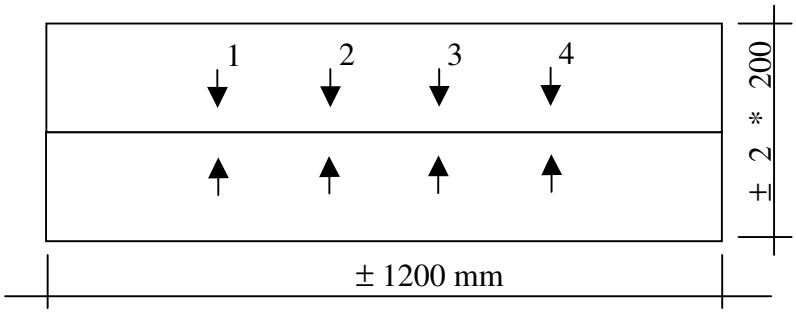

Figure 5-4: Location shrinkage measurements

5.2.1.2 Test results

An extensive description of the procedure and test results is given in Annex H. During the test series modifications were made to the current, see Annex H. Some modifications will be discussed in this paragraph. Figure 5-5 gives for example a photograph of a macro from test specimen 2. The plate thickness was 10 mm, the velocity 600 mm/min, the current 650 Amps and the voltage 25 Volt. The achieved depth of penetration was 7.5 mm.

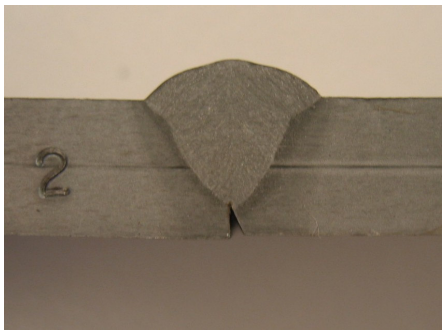

Figure 5-5: Macro from submerged arc welded specimen

Excentricity

Due to the fact that the fatigue crack grows at an angle (α) of approximately 70° and not exactly in vertical direction, the location of the wire in the transverse direction is thought to influence the depth of penetration. To simulate this, the wire is positioned at a different location in the transverse direction on test specimen 6. Figure 5-6 shows this displacement of 4 mm.

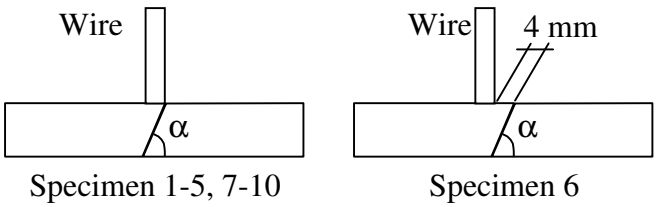

Figure 5-6: Location wire in transverse direction

Backing strip simulating trough web

Another modification made during the tests was the simulation of the trough web. In reality in bridges the crack, which originates at the root of the weld above the trough web and then grows through the deck plate, see Figure 2-9. It can be assumed that the presence of the trough web under the crack prevents the weld prematurely burning through the deck plate. To simulate the trough web a backing strip was added to test specimens 3 and 10, see Figure 5-7.

Figure 5-7: Backing strip to simulate trough web

Burn through

Figure 5-8 shows an example of a burn through. In several tests the weld burnt through the deck plate. From photos of burn through it becomes clear that a burn through occurs over a short length. For a few centimeters the weld sags through the deck plate. At the moment the burn through is complete, there is in fact a gap of approximately 5 mm between both sides of the crack. This gap is filled with flux powder. The liquid weld metal disappears through the underside of the steel. It is clear that this situation should be avoided on bridges. If it occurs, the only way to solve the problem is to completely replace a part of the deck plate. In Figure 5-8 the weld travel direction is from left to right. The weld started in the upper left corner and immediately burnt through the deck plate.

Figure 5-8: Burn through due to excess weld energy

Weld shrinkage

Table 5-1 gives the measured shrinkage at the four measurement points per specimen. The numbering 1,2,3,4 is in the direction of the weld production and given on the photographs in Annex H. An asterisk (*) after the value indicates that burn through has occurred at that specific location. Grey shading indicates that a small gap was observed between the two parts of the deck plate before SAW process.

Table 5-1: Welding shrinkage (mm)

Specimen	Point 1	Point 2	Point 3	Point 4
1	0.35	0.60 *	0.35	0.50
2	0.65	0.35	0.40 *	0.30
3	0.65 *	0.70	0.50	0.60
4	1.35	0.10	0.30	0.40
5	0.25 *	0.80 *	0.35 *	1.70
6	0.35 *	0.39 *	0.45 *	0.55
7	1.20	0.85	1.20	0.80 *
8	0.80	0.45	0.55	0.60
9	0.50 *	0.35 *	0.20 *	0.45 *
10	1.00	0.85	0.65	0.45

It is surprising to see that there is no correlation between shrinkage and the welding parameters, the presence of a gap, or burn through. From the limited experience with submerged arc-welding on bridges it is known that the measured shrinkage is approximately 0.2 – 0.4 mm. From the test reported in this paragraph an average shrinkage about 0.5 mm was found. It can be assumed that differences between test set up and real bridges situations are responsible for the relatively large shrinkage in the tests.

Depth of penetration

The most relevant results from the tests are the measured depths of penetration. These are given in Annex H.11. The depth of penetration for 8 specimens is between 65% and 75% of the plate thickness and for 2 specimen 54% and 86%.

The depth of penetration for specimen 6 with an eccentric wire was 86%. As this was the only test specimen made with an eccentric wire, a few more test specimen were made to research the influence of the eccentricity. Two plates with a thickness of 10 mm were SAW welded with 4 mm eccentricity. The dimensions of these two specimens, 11 and 12 were the same as the previous 10 specimens. From these two plates 6 macros were taken. From these tests it became clear that the enormous depth of penetration for specimen 6 was exceptional.

Conclusion

- Firstly eccentricity of the wire seemed to be important to achieve depth of penetration. To investigate this, additional tests with eccentric wire positioning were performed. The depth of penetration of these specimens varies between 60% and 80% which means that the eccentricity is 4 mm is not an important parameter.
- A gap between the two plates of a specimen has led sometimes to a burn through at relatively low current, specimen 9
- The current is the most important parameter in determining the depth of penetration.
- The eccentricity does not influence the current that leads to burn through.
- The voltage influences the depth of penetration only slightly. With lower voltages the shape of the weld is more pronounced and the top of the weld is relatively high measured from the top of the original deck plate. This is not a problem because the shape can be changed with a machine, see Figure 4-25.
- The maximum currents achieved at specimen without a backing strip or eccentricity were:
    - I = 650 Amps for t = 10 mm (specimen 2)
    - I = 730 Amps for t = 12 mm (specimen 5)
    - I = 840 Amps for t = 14 mm (specimen 9)
- Application of a backing strip has the following consequences:
    - For plates with a thickness of 10 mm the maximum achieved current is the same as for the situation without backing strip, the depth of penetration decreases approximately 1 mm, the weld becomes somewhat wider.
    - For plates with a thickness of 14 mm the maximum achieved current increases, the depth of penetration does not change compared to the situation without backing strip, the weld becomes somewhat wider.
    - A higher current is necessary to achieve the same depth of penetration if a backing strip simulating a trough web is present. The risk of a burn through decreases in the presence of a backing strip or trough web.
- The maximum depth of penetration that can be achieved without a burn through is approximately between 65% and 75% of the deck plate thickness
- The general conclusion is that submerged arc welding for deck plate crack repair is an option provided that the:
    - Gap between the two plate halves at the crack is small
    - There is no height difference between the two plate halves at the crack location

5.2.2 Fatigue tests submerged arc welded deck plate

5.2.2.1 Fatigue test set up

There is a good possibility of repairing deck plates with fatigue cracks with the submerged arc welding process and a depth of penetration of approximately 65% to 75% can be achieved. For fatigue calculations for a bridge deck repaired in this way it is necessary to know the fatigue behaviour of the deck plate after the submerged arc welding process. The fatigue tests have been reported by Vogelzang and Kolstein (Vogelzang, 2003), (Kolstein, 2006-b)

Therefore in total 12 test specimen were taken from the tests described in the previous paragraph.

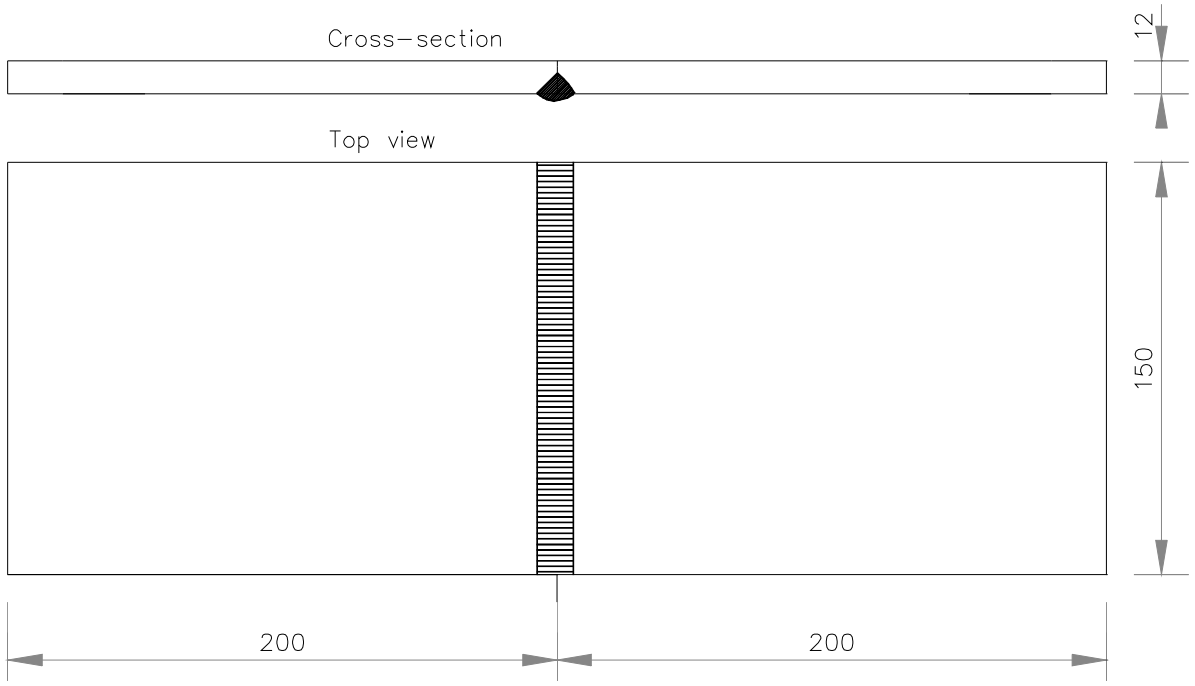

Figure 5-9: Dimensions - Test specimen fatigue test SAW sawn from welded deck plate

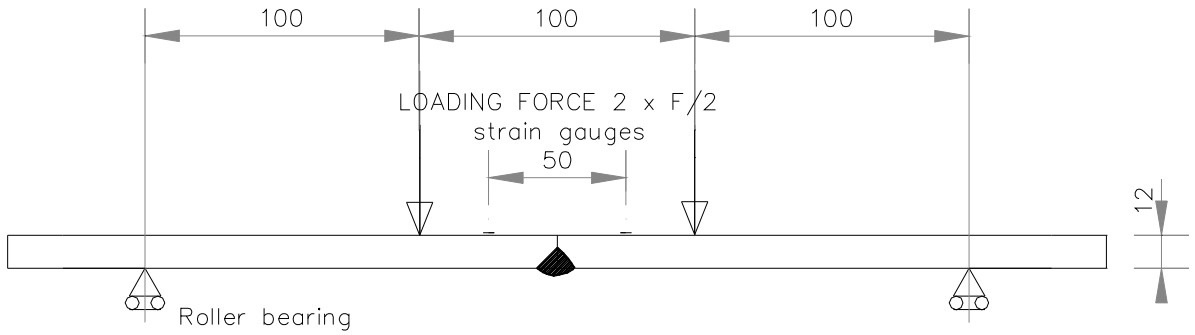

Figure 5-10: Test set up fatigue test SAW welded deck plate

Two strain gauges were located on the steel plate. The plates were subjected to four-point bending tests. The test specimens were positioned upside down in the test machine in order to generate compression at the side of the remaining part of the crack and tension at the side of the SAW weld. This simulates the situation in real bridges where from theoretical linear elastic analysis compression at the root of welded is thought to occur. Due to the welding shrinkage in reality tensile stresses can occur. Figure 5-11 shows the four-point bending test set up. The load cycle was different for each specimen in order to enable the derivation of a fatigue detail classification. The applied load cycles were between 5.37 kN and 17 kN. From the results of the fatigue test a fatigue detail classification can be calculated. The calculation procedure is described in paragraph 4.3.3.3.

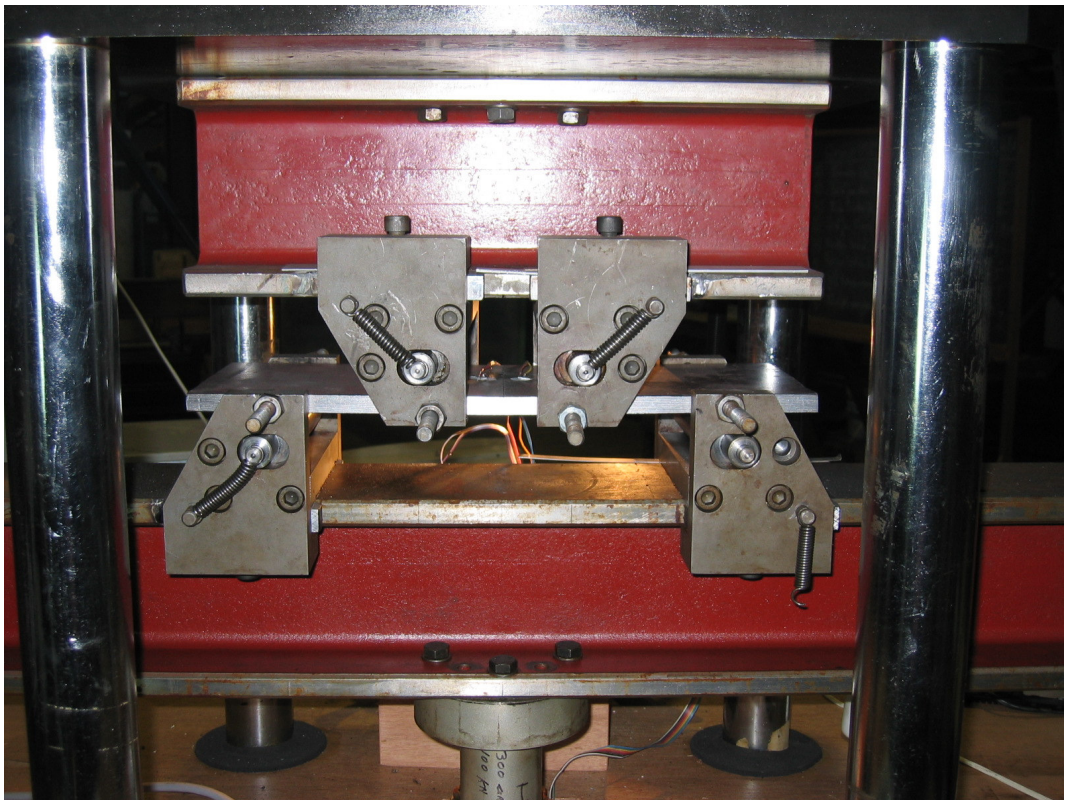

Figure 5-11: Four-point bending test set up - SAW welded deck plate

Test results and detail classification

The results of the fatigue tests are given in Figure 5-12. The data points represent the failure of the test specimen. Failure is defined as the moment that the test specimens collapse under the test load due to static overloading of the remaining net area of the cross-section. Based on this an S-N fatigue detail classification is calculated, according to the procedure described in paragraph 4.3.3.3. In the regression analysis of the curve on log-log scale a slope of m = 3.75 is calculated. The average classification ($\Delta\sigma k$) is 96 MPa at 10 million cycles, which is N_c

according to the Dutch fatigue code NEN 2063. In Eurocode format this means a classification of 147 MPa at 2 million cycles. The design values of the detail classification are 70 MPa according to the Dutch NEN 2063 standard and 108 MPa to the Eurocode standard.

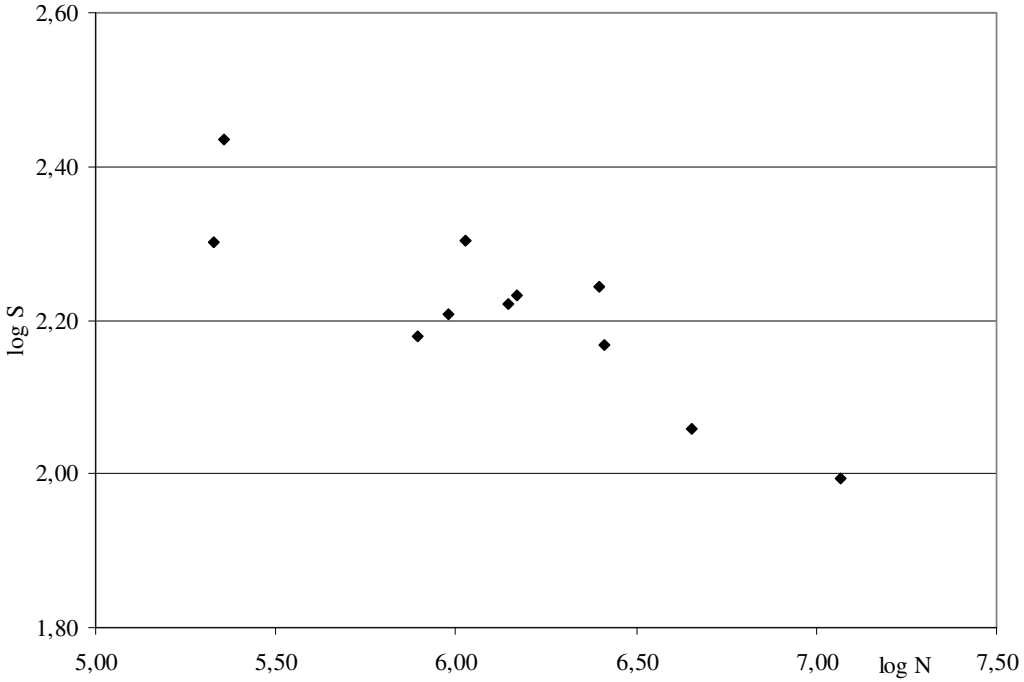

Figure 5-12: Results fatigue tests SAW weld deck plate

It is important to compare these classifications with the detail classifications for deck plate cracks. These detail classifications are described in paragraph 4.3.2.3 and 4.3.3. In Figure 4-30 a fatigue crack growth curve is given for a crack growing through the deck plate. There are two differences between the test specimen and the crack growth curve:

- There is an initial defect of approximately 5 mm in the SAW welded plates in contrast to the crack growth analysis in which there is no initial defect.
- The definition of failure is different. For the crack growth analysis failure is defined as the crack that has just grown through the deck plate and has a length of 0 mm at the top surface of the plate. For the fatigue tests on the SAW welded plates it is collapse under the test load.

Differences in detail classification due to both effects are eliminated in the following way:

The depth of penetration in the test specimen was approximately 7 mm with a test plate thickness of 12 mm, this became clear from inspection of both halves of the test specimen

after collapse, see Figure 5-13. A penetration of 7 mm means that there was an initial defect of a = 5 mm in the plate. From the crack growth curve, given in Figure 4-30 a detail classification can be calculated for the crack growth between a = 5 mm and a = 12 mm. For this crack growth approximately 4.2×10^6 cycles are necessary at 100 MPa using a slope m = 3. This corresponds with an average detail classification of 75 MPa at 10 million cycles, which is N_c according to the Dutch fatigue code NEN 2063. For a crack growth from a = 0 mm to a = 12 m the detail classification is 91 MPa. The difference due to depth of penetration can be modelled with a factor 1.21, which is 91 divided by 75.

Figure 5-13 shows the cross-section of one of the test specimen after collapse. The test specimens have a width of 150 mm. The SAW weld is at the bottom and the depth of penetration is approximately 7 mm. The remaining initial defect, which is visible in the upper part of the steel plate is about 5 mm. The fatigue crack is clearly visible. The elliptical form of the fatigue crack is also clear and at the outer edges the static collapse at the end of the fatigue test is visible. The fatigue crack has not grown through the deck plate, but there is approximately 1 mm remaining thickness of the plate. For an easy interpretation it is thought that this is equal to a crack grown through the deck plate. In that case the length of the crack at the top side of the deck plate (it is the bottom side in the figure) is about 75 mm. Other photographs of collapsed SAW welds show the same length.

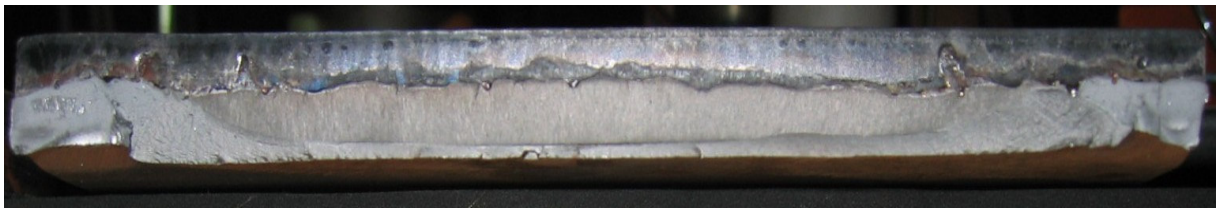

Figure 5-13: SAW welded plate after collapse under test load

In paragraph 4.3.3.3 detail classifications were derived for crack lengths of 50 and 100 mm at the top surface of the deck plate. For a crack length of 50 mm the mean value is 128 MPa, for a crack length of 100 mm this value is 144 MPa. If the average of these values is taken for a classification for a crack length of 75 mm, the detail classification is 136 MPa, all according to the NEN 2063 format. From the same test the detail classification for a crack length of 0 mm on top of the deck plate is 113 MPa. This means that a factor 113 divided by 136 = 0.83 can be assumed for the difference in failure definition.

If the average value for the detail classification derived from the regression analysis is corrected with these two factors, a notional detail classification of 97 MPa (96 MPa x 1.21 x 0.83) is derived. This is described as a notional detail classification because it is a

classification assuming that the depth of penetration of the SAW weld equals the plate thickness. This value however can be compared to the detail classification of 113 MPa, see table 4-12.

This makes clear that fatigue calculations of deck plates repaired with the SAW welding procedure should be performed with a slightly lower classification, 97 MPa instead of 113 MPa. In addition to this the starting point of the fatigue calculation can be an initial crack, which equals the lack of penetration. Calculate with an initial crack is only possible with the depicted crack growth curve in Figure 4-30.

5.3 Requirements of renovation techniques

This paragraph describes the requirements formulated for the development of the renovation techniques. Before describing the various requirements something should be said about the general philosophy.

The general philosophy is that specific quantitative requirements are different for each bridge, e.g. the renovation should give a fatigue free bridge deck for 25 years. Requirements differ for each bridge, because the bridges differ from each other, the traffic on the bridges is different, and because the wishes of bridge owners are not the same on different bridges. Thus specific quantitative requirements are bridge specific. This means that the requirements for this thesis are formulated in a qualitative and descriptive way. If for instance a renovation technique results in a bridge deck that is free from fatigue cracks for 20 years, it might be a good solution for one bridge, but unacceptable for another.

In general it can be said that the most economically favourable solution should be chosen. To determine which the most economically favourable solution is, all aspects have to be considered. Some relevant aspects are: lifetime enhancement, durability, mechanical and technical properties, safety, time needed for execution, traffic disruption, financial efforts. The bridge owner should set the criteria for the specific bridge and rate them in order of importance. In this decision process the bridge owner has the option to decide on a new bridge or bridge deck instead of renovating the existing deck with fatigue cracks.

In addition to this the research and development of the renovation techniques shows the properties of intended solutions during this process. The process of getting to renovation methods is more or less a trial and error process. This means that setting the quantitative criteria before the research phase is too rigid, qualitative and descriptive requirements are preferable.

The requirements of the renovations techniques are divided into several categories: general requirements, lifetime enhancement and durability, mechanical and technical properties, safety, execution and traffic disruption.

General requirements

- One of the main requirements is that the existing bridge deck remains undisturbed as much as possible.
- In general bridges and renovation methods must satisfy the requirements of the design rules for steel structures and orthotropic steel bridges (NEN 6700-series, NEN 6788 and the Eurocode 3).

Lifetime enhancement and durability

- The effect of the renovation on lifetime enhancement is one the main purposes of the renovation techniques. Increasing the total stiffness of the deck plate structure is one of the main criteria. The stiffness should be increased as much as possible.

Mechanical and technical properties

- For movable bridges decks, the addition of extra weight is limited by the capacity of the hinges. Extra weight on the bridge must be matched by extra weight at the counter weight and it must be possible to carry this extra weight

Safety

- Skid resistant surfacing is required.
- The longitudinal alignment must be smooth. Height differences of up to 10 mm are considered acceptable for this thesis. It is assumed that a practical solution to deal with this height difference can be developed.
- Height differences up to 10 mm in the longitudinal direction between carriageway lanes are acceptable, provided that a smooth transition is possible. It is assumed that a smooth transition is possible.

Execution and traffic disruption

- The time needed to apply a renovation technique should be as short as possible.
- One of the main purposes of repairing bridge decks is to guarantee a minimum of inconvenience to traffic in the period after the renovation. Therefore repair methods should guarantee a new long period of time without significant maintenance.

5.4 Overview of renovation techniques

5.4.1 Introduction

The main purpose of this paragraph is to set out a few repair methods for orthotropic steel bridges, which are suffering from fatigue cracks in the steel deck structure. Table 5-2 helps in getting an overview of the possible repair methods. This table is used as the basis for generating several renovation methods.

Table 5-2: Table of repair techniques

Parameter	A	B	C	D	E
Old Surfacing	50 mm traditional mastic asphalt	7 mm epoxy surfacing			
Existing fatigue cracks	Not repair the cracks	Repair the cracks			
Material	Steel	(High strength) concrete	Wood	Aluminium	Fibre reinforced plastic
Form	Board / planks	Extruded profiles	Poured layer	Plate material	Sandwich Panels
Connection	Welding	Bolting	Bonding	Vulcanization of rubber	
Connection Technology	0 % composite action	100 % composite action	Vertical connection at distances of 300 mm	Vertical support of the deck plate	

In the first column several parameters are given, the other columns give possible options for that parameter. An outline will be given of the parameters in the table. Table 5-2 is the basis of several repair methods. In principle the maximum number of possible repair methods can be obtained by combining each record from a parameter with each record of other parameters. In this way it is possible to generate many different repair methods. Many of the methods thus generated are not sensible, because a combination originating from the table is nonsense, e.g. poured layers from steel and extruded profiles from wood or concrete. Only the sensible generated repair methods are shown in this paragraph.

5.4.2 Parameters of renovation techniques

5.4.2.1 Old surfacing

Generally two types of surfacing have been applied to orthotropic steel bridges in the past. This originates from the fact that there are mainly two types of bridges, fixed and movable.

The fixed bridges are in general provided with a mastic asphalt layer 50 mm thick. Movable bridges have a surfacing of approximately 7 mm of epoxy resin, impregnated with granules to provide skid resistance. Although it is not a real design parameter, the type of the original surface is a part of the table because of the consequences it might have for the repair methods.

5.4.2.2 Existing fatigue cracks

Before implementing a repair method on a particular bridge deck the severity of the fatigue phenomena should be determined by both surveying techniques and by carrying out lifetime calculations. The resulting fatigue damage is used as the basis for the decision to repair the bridge. In principle there are two ways to treat the current fatigue cracks. The first is to renovate the bridge deck, without repairing the fatigue cracks. The other way is to repair the fatigue cracks before applying a renovation method to the bridge deck. A lifetime calculation of the renovated bridge deck should be made as a part of the design process. One of the parameters that influences the lifetime of a renovated bridge deck is the presence of old cracks. There are two options: to repair the cracks or to not repair the cracks. In both cases fatigue calculations should be made of crack growth. In general when the original fatigue cracks are repaired before applying a renovation method on the bridge deck, the original steel deck provides a bigger part in the required lifetime. In consideration of this the renovation method could probably be smaller. In general the decision on how to treat the existing fatigue cracks will influence the extent of the renovation methods, rather than influence the basics of the renovation method.

5.4.2.3 Material

There are many materials, which can fulfill a function in a repair method. Each material has its own advantages and disadvantages. The different materials, which can be used within a repair method for steel bridges, are steel, high performance concrete, timber, aluminium, fiber reinforced plastics. Rubber is not included in this group because it is not able to fulfill a structural function in a repair method, because of its very low stiffness.

5.4.2.4 Form

The repair methods can be made in several forms. For example: extruded profiles, planks or boards, poured layers like the traditional mastic asphalt layer. Sandwich panels are also a possibility, in principle these panels can be built from the materials, which are mentioned in the previous paragraph, another possibility is to use prefabricated sandwich panels for example.

5.4.2.5 Connection

All kinds of possible connections can be used. The possibilities vary from the conventional connections to innovative connections, which have not been used before in bridge design. The

conventional techniques in bridge design are welding and bolting. Other possible methods are bonding and using rubber vulcanization.

5.4.2.6 Structural technology

This looks a strange parameter. It is divided into four possibilities. These four possibilities each perform in a different way. The basics of the structural system of the repair methods vary within this parameter. The first possibility is to design a connection where no composite action is generated between the old existing structure and the new added materials. This implies in general that the interface layer between old and new structure doesn't have shear stiffness. Another possibility is a full composite action, in this case shear stiffness is necessary and the shear strength of the interface layer must equal the maximum shear stresses caused by the loading. The mechanical properties of a full composite action are more favourable. Because of the increase of the section modulus and the stiffness, less material is needed. The third possibility originates from the dimension of the steel bridge deck and the current fatigue phenomena. Bending stresses in the deck plate mainly cause the fatigue. Thus removing the bending stresses from the deck plate would probably decrease the fatigue and be a possible solution. The trough webs at a standard distance of 300 mm each support the deck plate. A repair method, which only has a structural vertical connection between the old material and the new material at the locations of the trough webs, reduces the bending stresses in the deck plate to a large extent. The fourth possibility is to add a layer under the existing deck plate that acts as a support in vertical direction, thus reducing the bending stresses in the deck plate.

5.4.3 Renovation method 1: high performance concrete

Figure 5-14 shows this renovation, which has the following characteristics:

Old surfacing	50 mm traditional mastic asphalt
Existing fatigue cracks	(Not) repair the cracks
Material	High performance concrete
Form	Poured layer
Connection	Bonding
Structural Technology	Composite action

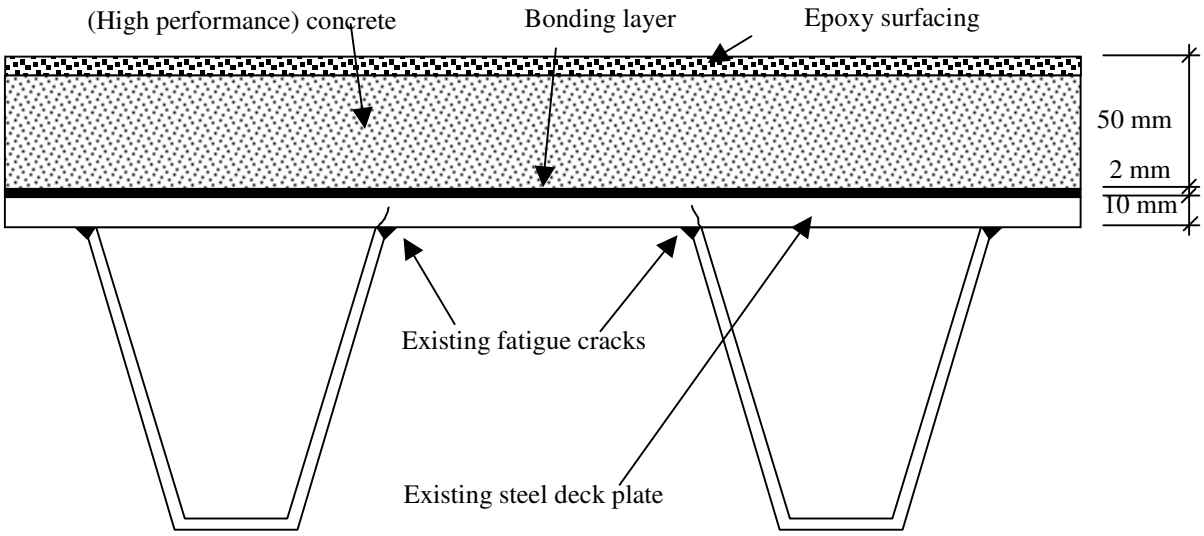

Figure 5-14: High performance concrete

In this figure the vertical scale of the deck plate and renovation method differs from the vertical scale of the troughs. This is the same for all other renovation methods later on in this chapter. This renovation method is applicable at the crossbeams and also in the field between the crossbeams. Therefore this renovation method is convenient for the most severe cracks in the heavy vehicle lane, at the crossbeam and in the field. The mastic asphalt layer should be removed, including the interface layer between steel plate and the asphalt. If cracks are found a decision must be taken either to repair them or let them remain. The next important step is to produce a bonding layer between the steel and the high performance concrete. The purpose of the bonding layer is to provide shear strength and stiffness in the interface layer between steel and concrete if composite action is required. This layer should provide sufficient shear capacity in both interface layers. The next step is to apply the concrete layer; this layer should have a thickness of approximately 50 mm. The reinforcement of this layer has to be determined. The last step in the procedure is to cover the concrete with an epoxy surfacing to provide the required roughness for skid resistance. Shot blasting the concrete is also probably sufficient.

Advantages

- Tolerances and dimensions are not critical
- Significant increase in the stiffness: large stress reduction
- It is thought to be a durable solution

Disadvantage

- Concrete cracking

- Lack of experience with bonding layers

5.4.4 Renovation method 2: bonded timber planks

Figure 5-15 shows this renovation method, which has the following characteristics:

Old surfacing	50 mm traditional mastic asphalt
Existing fatigue cracks	(Not) repair the cracks
Material	Timber
Form	Board / planks
Connection	Bonding
Structural Technology	Composite action

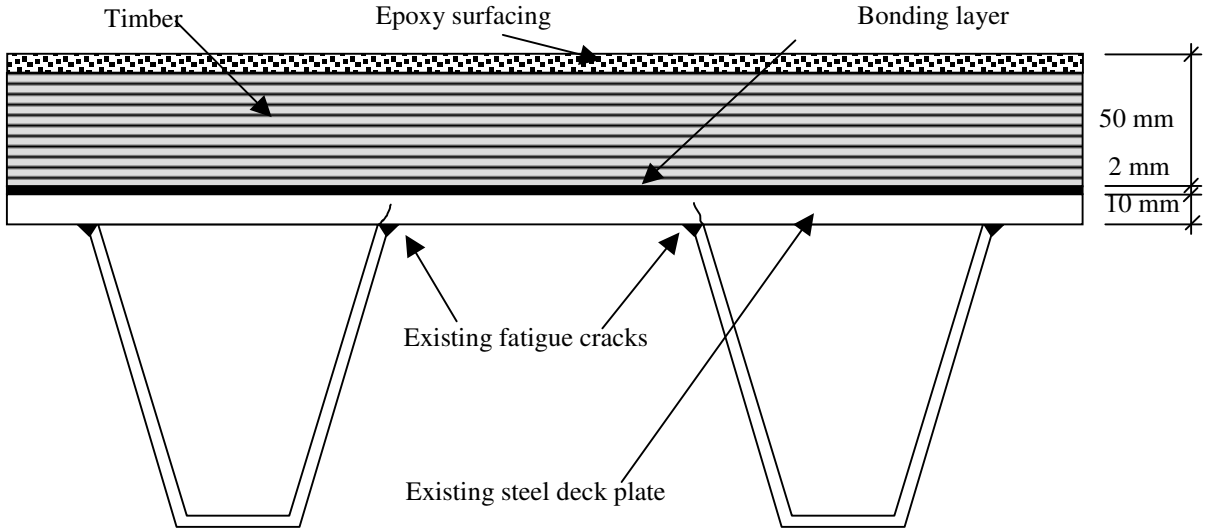

Figure 5-15: Bonded timber planks

This renovation method is applicable at the crossbeams and also in the field between the crossbeams. Therefore this renovation method is convenient for the most severe cracks in the heavy vehicle lane, at the crossbeam and in the field. It is also possible to apply this renovation method only at the crossbeam. If this method is only applied at the crossbeam only a few planks have to be bonded to the steel deck. The mastic asphalt layer should be removed, including the interface layer between steel plate and the asphalt. If cracks are found a decision must be taken either to repair them or let them remain. The next important step is to produce a bonding layer between the steel and the wooden planks. The next step is to apply the timber planks, which should have a thickness of approximately 50 mm. The last step in the procedure is to apply an epoxy surfacing on top of the planks.

Advantage

- Applicable to local spots, for instance only at the crossbeam.

Disadvantages

- Many discontinuities between planks and asphalt
- Material properties and durability of timber
- Lack of experience with bonding layers
- Critical installation procedure as the pot life of the adhesive is limited

5.4.5 Renovation method 3: bolted timber planks

Figure 5-16 shows this renovation method, which has the following characteristics:

Old surfacing	50 mm traditional mastic asphalt
Existing fatigue cracks	(Not) repair the cracks
Material	Timber
Form	Board / planks
Connection	Bolting
Structural Technology	No composite action

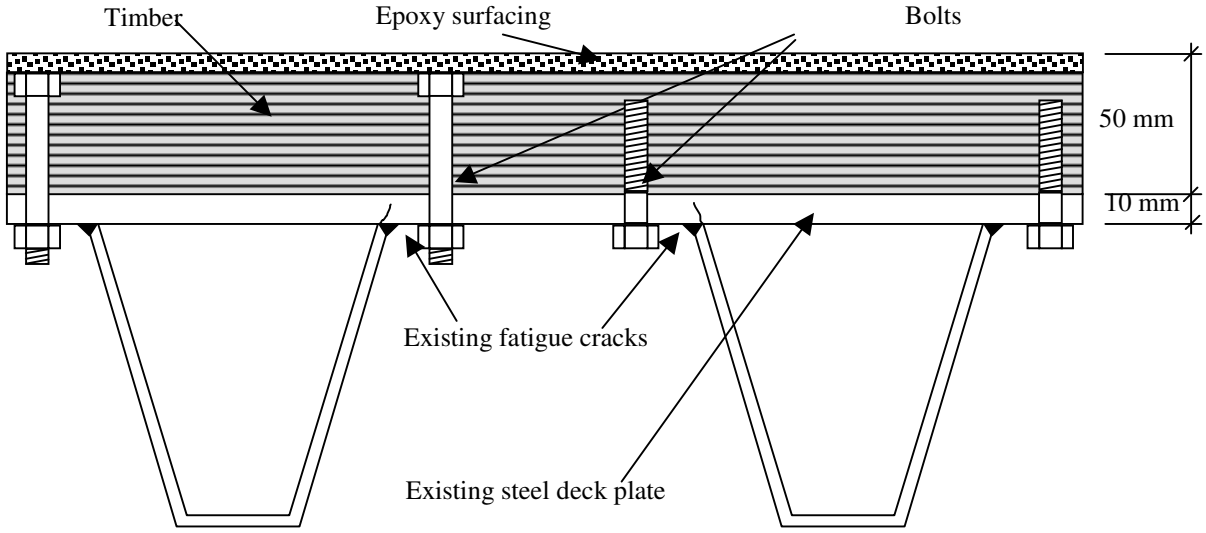

Figure 5-16: Bolted timber planks

This is in fact the same renovation method as described in the previous paragraph, except that the connection method is changed. Instead of bonding the wooden planks, they are bolted and consequently composite action cannot be expected from this type of connection. This

renovation method is applicable at the crossbeams and also in the field between the crossbeams. It is also possible to apply this renovation method only at the crossbeams. If this method is only applied at the crossbeam only a few planks are bolted to the steel deck. The mastic asphalt layer should be removed, including the interface layer between steel plate and the asphalt. If cracks are found a decision must be taken either to repair them or let them remain.

The next step is to apply the timber planks, with a thickness of approximately 50 mm. The planks should be connected with bolts. The design of this bolting connection is not exactly known. A few options have been shown in Figure 5-16. The properties of this connection should be determined. The last step is the application of an epoxy surfacing.

Advantages
- Applicable to local spots, for instance only at the crossbeam

Disadvantages
- Many discontinuities between planks and asphalt
- Material properties of wood
- Fatigue behaviour of the bolted connection
- Bolts combined with timber require a lot of maintenance
- No composite action, small stress reduction expected
- Corrosion protection of the steel deck

5.4.6 Renovation method 4: bolted aluminium planks

Figure 5-17 shows this renovation method, which has the following characteristics:

Old surfacing	50 mm traditional mastic asphalt
Existing fatigue cracks	(Not) repair the cracks
Material	Aluminium
Form	Board / planks
Connection	Bolting
Structural Technology	Vertical connection at distances of 300 mm

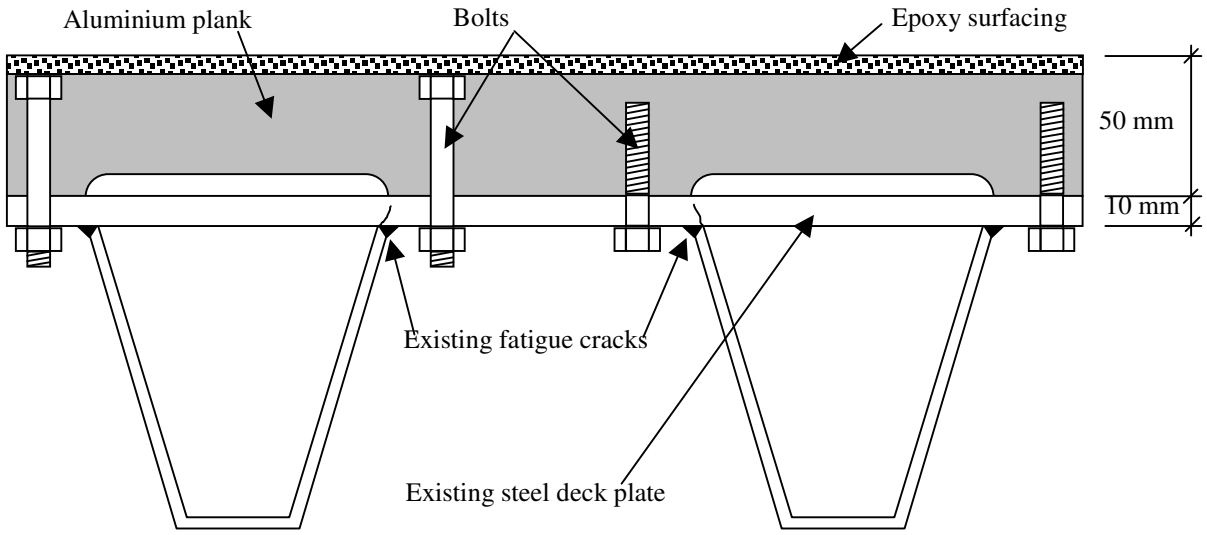

Figure 5-17: Bolted aluminium planks

This renovation method is applicable at the crossbeams and also in the field between the crossbeams. Therefore this renovation method is convenient for the most severe cracks in the heavy vehicle lane, at the crossbeam and in the field. It is also possible to apply this repair method only at the crossbeam.

The aluminium planks should have a thickness of approximately 50 mm. The aluminium planks do not have a uniform thickness. Aluminium is a material with can be extruded and extruded planks are therefore appropriate for use with vertical connections at distances of 300 mm each. The aluminium planks should be thicker where a vertical connection between the old steel structure and the new aluminium planks are required. The planks should be thinner where these vertical connections are not required.

Advantages
- Applicable at local spots, for instance only at the crossbeam
- Possibilities with extruded profiles
- Stress reduction in old steel structure

Disadvantages
- Difference in thermal expansion coefficient
- Difference in electric potential causing corrosion
- Fatigue behaviour and durability of bolted connection
- Corrosion protection of the steel deck

5.4.7 Renovation method 5: bonded aliminium planks

Figure 5-18 shows this renovation method, which has the following characteristics:

Old surfacing	50 mm traditional mastic asphalt
Existing fatigue cracks	(Not) repair the cracks
Material	Aluminium
Form	Board / planks
Connection	Bonding
Structural Technology	Vertical connection at distances of 300 mm

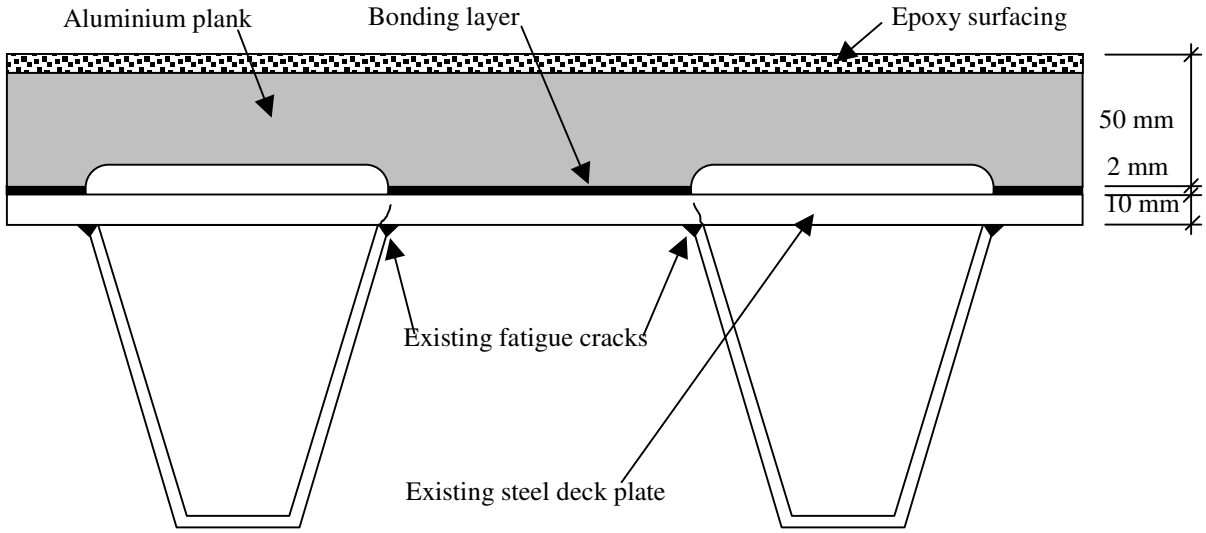

Figure 5-18: Bonded aluminium planks

This is in fact the same repair method as described in the previous paragraph, only the connection changed.

Advantages

- Applicable at local spots for instance only at the crossbeam
- Possibilities with extruded profiles
- Stress reduction in old steel structure

Disadvantages

- Difference in thermal expansion coefficient
- Difference in electric potential causing corrosion

- Lack of experience with bonded connections
- Critical installation procedure as the pot life of the adhesive is limited

5.4.8 Renovation method 6: formed steel plate, bolted connection

Figure 5-19 shows this renovation method, which has the following characteristics:

Old surfacing	50 mm traditional mastic asphalt
Existing fatigue cracks	(Not) repair the cracks
Material	Steel
Form	Formed plate material
Connection	Bolting
Structural Technology	Vertical connection at distances of 300 mm

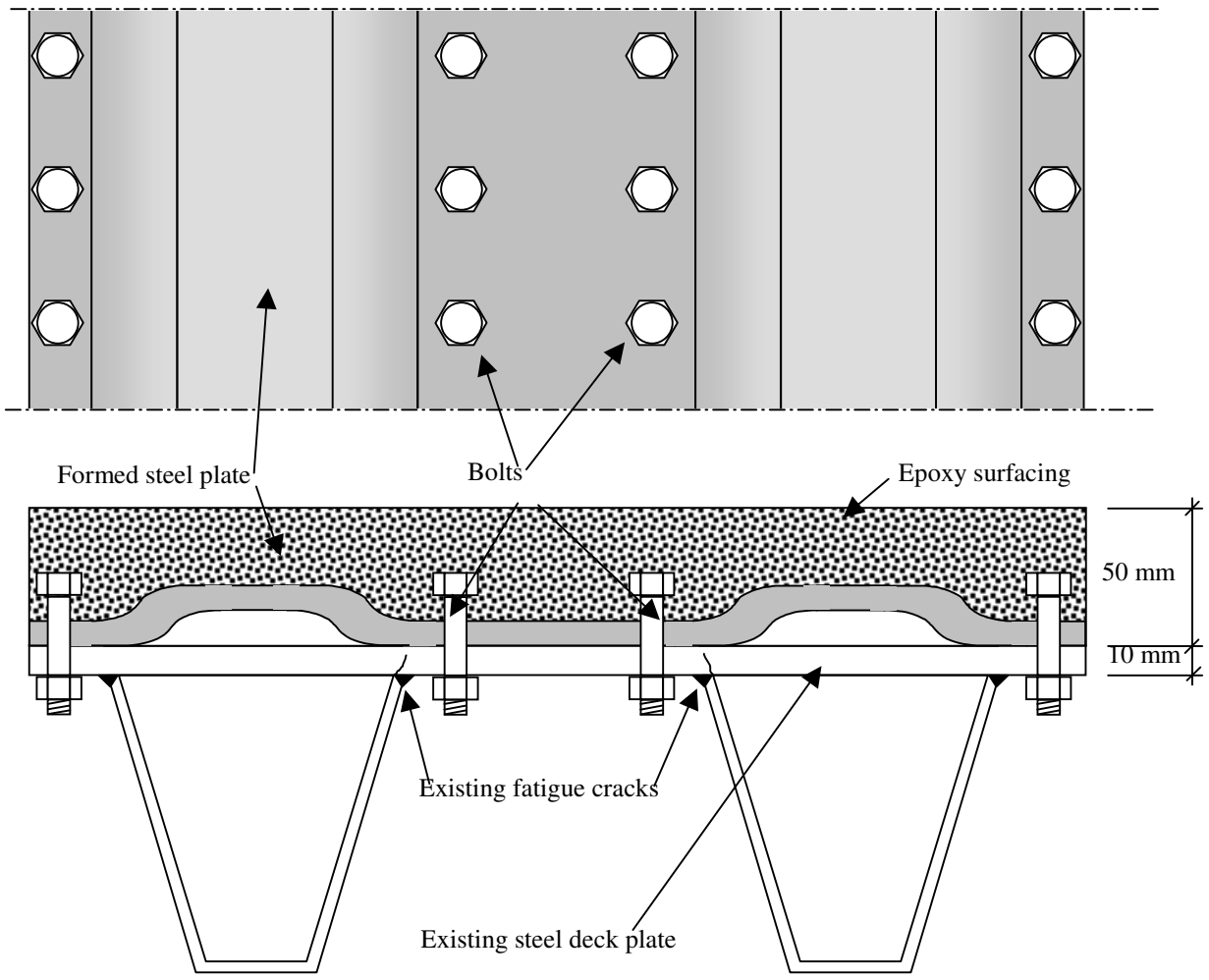

Figure 5-19: Formed steel plate, bolted connection

This renovation method is applicable at the crossbeams and also in the field between the crossbeams. Therefore this renovation method is convenient for the most severe cracks in the heavy vehicle lane, at the crossbeam and in the field. The renovation method consists of a formed steel plate. The steel plate is formed in such a way that there is no vertical connection between old and new steel structure above the troughs. Vertical connections are only located between the troughs. The first steps are as in the foregoing methods. The next step is to apply the formed steel plate. The thickness, height and form of this steel plate should be determined. The steel plate should be connected to the old steel structure by bolting. The length of the formed steel plate has also to be determined. An epoxy surfacing is necessary for skid resistance but also for protection of the bolts. It also levels the differences in height of the formed steel plate.

Advantages
- Applicable at local spots, for instance only at the crossbeam
- Stress reduction in old steel structure

Disadvantage
- Fatigue behaviour of bolted connection
- Corrosion protection of intermediate layer is difficult.
- Difficult to cope with tolerances
- Corrosion protection of the steel deck

5.4.9 Renovation method 7: formed steel plate, bonded connection

Figure 5-20 shows this renovation method, which has the following characteristics:

Old surfacing	50 mm traditional mastic asphalt
Existing fatigue cracks	(Not) repair the cracks
Material	Steel
Form	Formed plate material
Connection	Bonding
Structural Technology	Vertical connection at distances of 300 mm

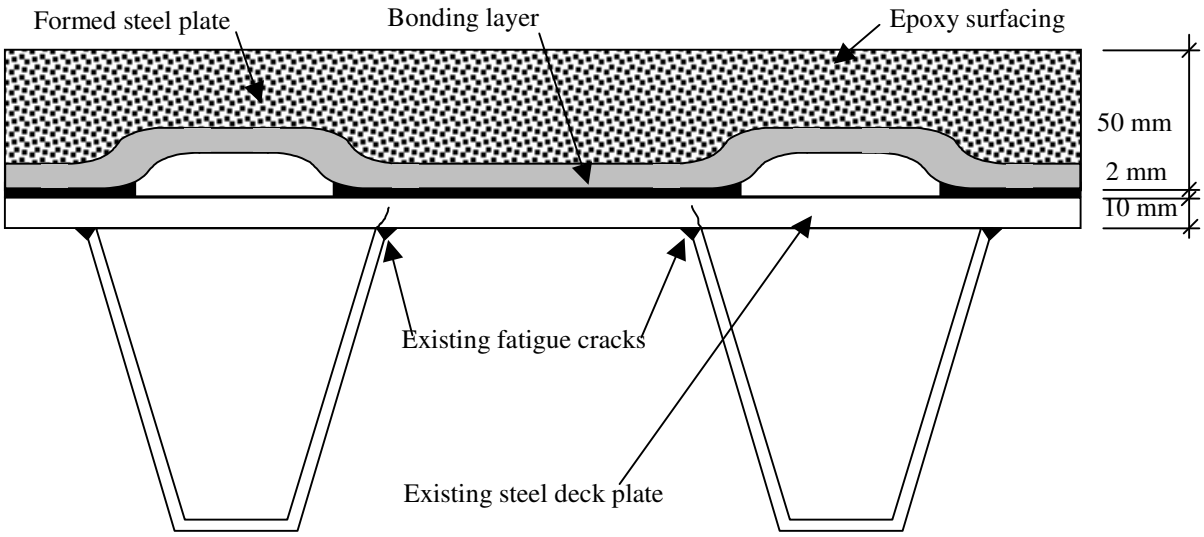

Figure 5-20: Formed steel plate, bonded connection

This is in fact the same renovation method as described in the previous paragraph, only the connection changes. Instead of bolting the formed steel plates are bonded in this repair method.

Advantages
- Applicable at local spots, for instance only at the crossbeam
- Stress reduction in old steel structure

Disadvantage
- Lack of experience with bonded connections
- Discontinuous bonding layer
- Difficult to cope with tolerances
- Critical installation procedure as the pot life of the adhesive is limited

5.4.10 Renovation method 8: bonded aluminium extruded profiles

Figure 5-21 shows this renovation method, which has the following characteristics:

Old surfacing	50 mm traditional mastic asphalt
Existing fatigue cracks	(Not) repair the cracks
Material	Aluminium
Form	Extruded profile
Connection	Bonding
Structural Technology	100 % composite action

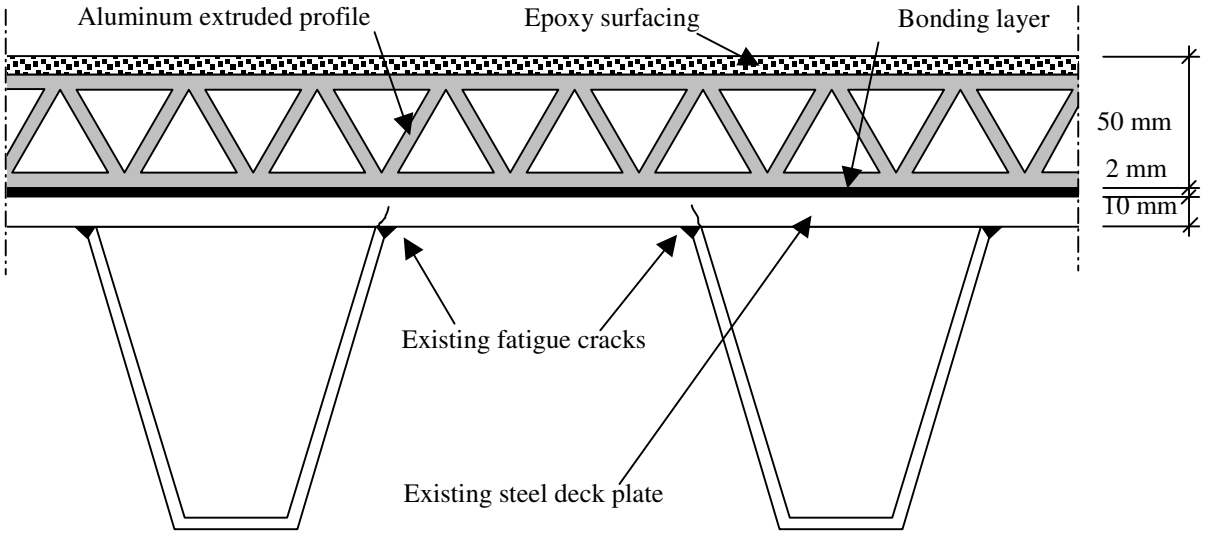

Figure 5-21: Bonded aluminium extruded profiles

This renovation method is applicable at the crossbeams and also in the field between the crossbeams. Therefore this renovation method is convenient for the most severe cracks in the heavy vehicle lane, at the crossbeam and in the field. The aluminium profiles should have a height of approximately 50 mm. The aluminium profiles can be connected in two different ways. In the first way the longitudinal direction of the profile is the longitudinal direction of the troughs and bridge, this is depicted in Figure 5-21. In the other way the longitudinal direction of the extruded profiles is the transverse direction of the troughs and bridge.

Advantages

- Possibilities with extruded profiles
- Stress reduction in old steel structure

Disadvantages

- Difference in thermal expansion coefficient
- Difference in electric potential causing corrosion
- Lack of experience with bonded connection
- Critical installation procedure as the pot life of the adhesive is limited
- Prefabricated panels may not be compatible with the uneven surface of an existing steel bridge deck

5.4.11 Renovation method 9: steel plate connected with rubber vulcanization

Figure 5-22 shows this renovation method, which has the following characteristics:

Old surfacing	50 mm traditional mastic asphalt
Existing fatigue cracks	(Not) repair the cracks
Material	Steel
Form	Plate
Connection	Rubber vulcanization
Structural Technology	0 % composite action

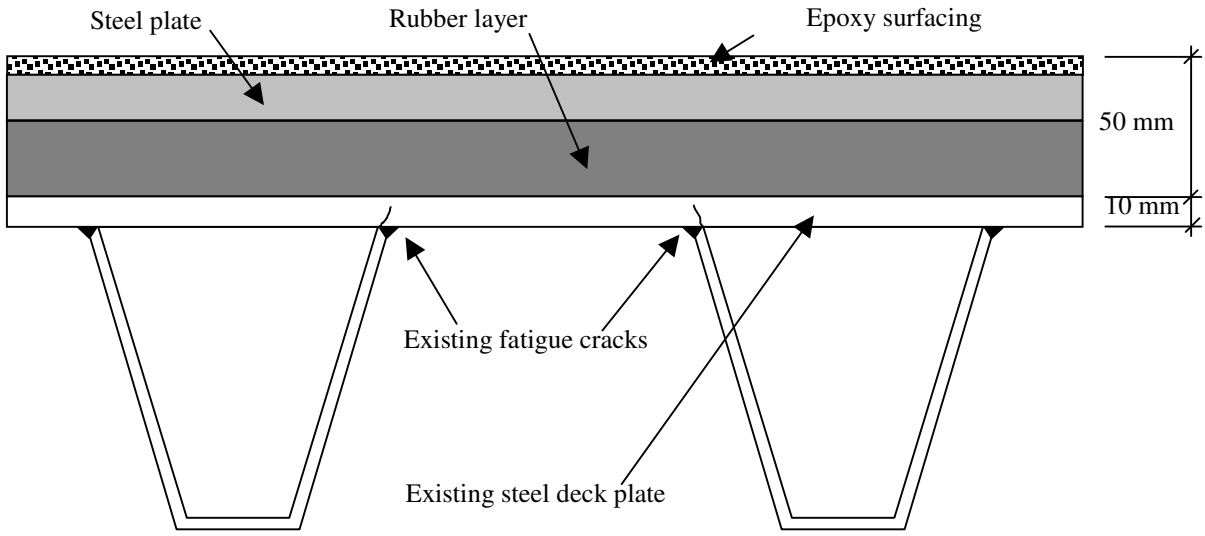

Figure 5-22: Steel plate connected with rubber vulcanization

This is in fact the renovation method from the M.Sc thesis of Overduin (Overduin, 1999). He performed analytical and laboratory research on this type of renovation method. Due to the very low stiffness of the rubber matrix no composite action between the two steel plates is expected. This renovation method is applicable at the crossbeams and in the field between the crossbeams. If applied it should be applied on both, it is not an appropriate method for a particular detail. Therefore this repair method is convenient for the most severe cracks in the heavy vehicle lane, at the crossbeam and in the field.

The mastic asphalt layer should be removed, including the interface layer between steel plate and the asphalt. If cracks are found a decision must be taken either to repair them or let them remain. The new steel deck plate should be added and then the next step is to vulcanize a rubber layer between the old steel deck plate and the new steel plate. The purpose of this rubber layer is to connect both steel plates. The last step in the procedure is to cover the new

steel plate with an epoxy surfacing to provide the required surface roughness

Advantages

- Tolerances and dimensions are not critical

Disadvantages

- No composite action at all
- Stress reduction limited
- Difficult installation process as the polyurethane is applied after the new steel plate

5.4.12 Renovation method 10: steel plate connected with polyurethane layer

Figure 5-23 shows this renovation method, which has the following characteristics:

Old surfacing	50 mm traditional mastic asphalt
Existing fatigue cracks	(Not) repair the cracks
Material	Steel
Form	Plate
Connection	Polyurethane or comparable elastomer
Structural Technology	100 % composite action

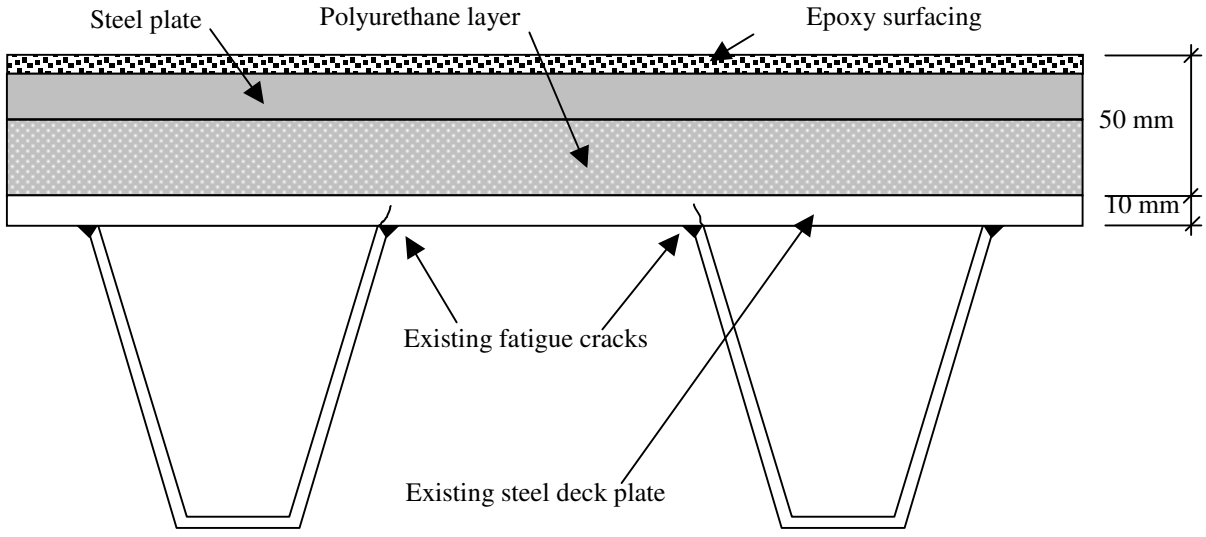

Figure 5-23: Steel plate connected with polyurethane layer

This is in fact the same method as described in the previous paragraph, except that in this method polyurethane is used instead of rubber in the interface layer between the two steel plates. Due to the higher stiffness of the polyurethane foam layer it might be possible to achieve composite action between the two steel plates. A comparable method, known as the

SPS technique, was incorporated in a research program at the BASt (Friedrich, 2005).

Advantages
- Tolerances and dimensions are less critical

Disadvantages
- Fatigue and durability of polyurethane
- Difficult installation process as the polyurethane has to be applied after the new steel plate is in place

5.4.13 Renovation method 11: prefabricated bonded sandwich panel

Figure 5-24 shows this renovation method, which has the following characteristics:

Old surfacing	50 mm traditional mastic asphalt
Existing fatigue cracks	(Not) repair the cracks
Material	Steel & polyurethane
Form	Sandwich Panel
Connection	Bonding
Structural Technology	100 % composite action

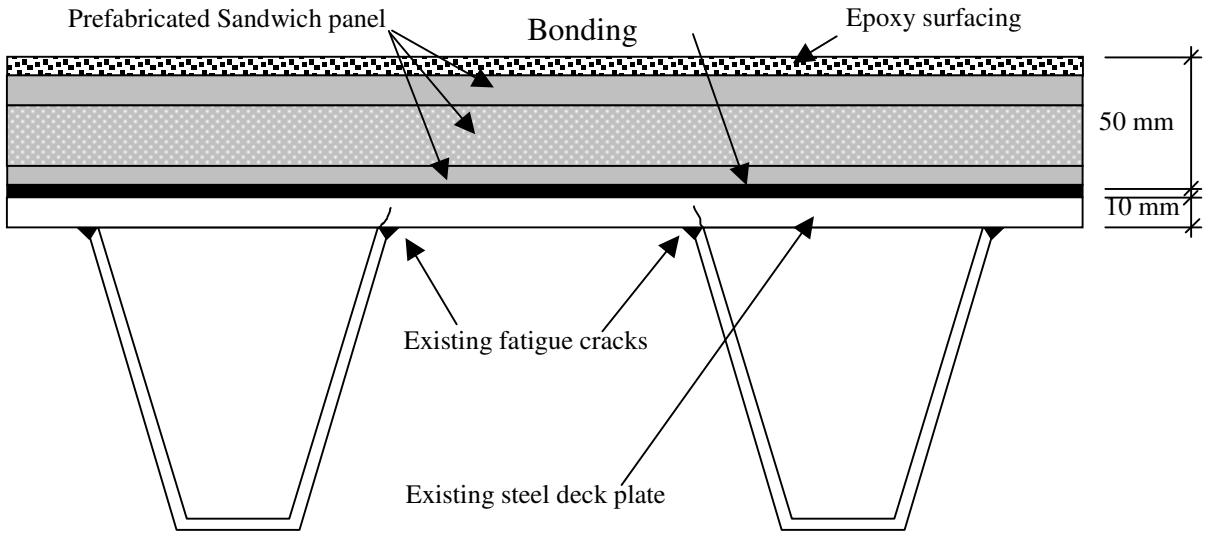

Figure 5-24: Prefabricated bonded sandwich panel

This renovation method consists of a prefabricated sandwich panel. This panel has to be bonded to the old steel structure. The sandwich panel has three layers: an upper and lower

steel plate separated by a polyurethane layer. The mastic asphalt layer should be removed. The next important step is to apply a bonding layer between the steel deck plate and the sandwich panel and directly after that apply the sandwich panel on the bonding layer.

Advantages
- Prefabrication of the sandwich panel

Disadvantages
- Fatigue and durability of polyurethane
- Lack of experience with bonding layer
- Critical installation procedure as the pot life of the adhesive is limited
- Prefabricated panels may not be compatible with the uneven surface of an existing steel bridge deck

5.4.14 Renovation method 12: second steel plate bonded to existing deck

Figure 5-25 shows this renovation method, which has the following characteristics:

Old surfacing	7 mm epoxy surfacing
Existing fatigue cracks	(Not) repair the cracks
Material	Steel
Form	Plate material
Connection	Bonding
Structural Technology	100 % composite action

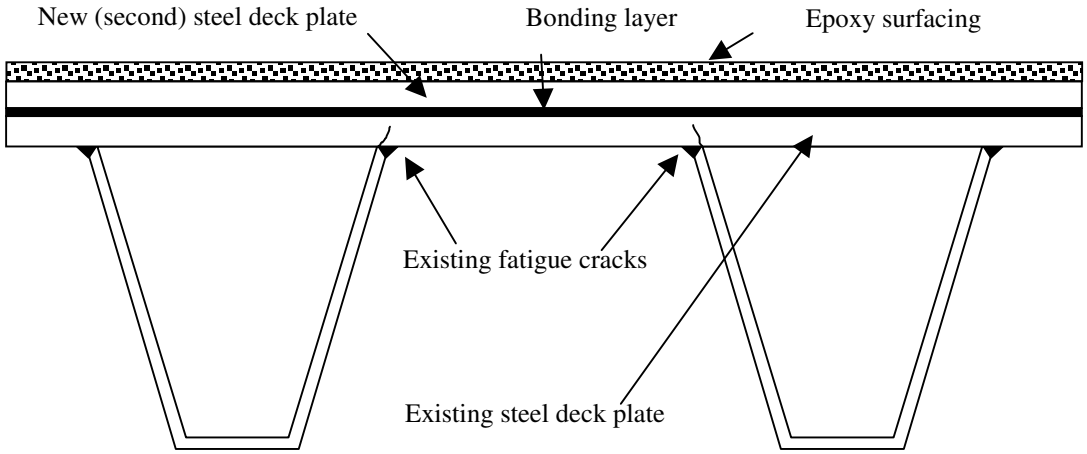

Figure 5-25: Second steel plate bonded to existing deck

This renovation method is intended for bridge decks, which are only covered with a thin epoxy surfacing, thus it is an appropriate method for movable bridges, which mainly are surfaced with a thin epoxy surfacing. The epoxy-surfacing layer should be removed. If cracks are found a decision must be taken either to repair them or let them remain. The next important step is to produce a bonding layer between the two steel plates. The purpose of the bonding layer is providing shear strength and stiffness in the interface layer between the two steel plates which is required if composite action is needed. This layer should provide sufficient shear strength in both interface layers. The thickness of this new steel deck plate should be designed to suit the requirements. The new steel plate should be applied to the bonding layer. The last step in the procedure is to apply an epoxy surfacing to the new steel plate for skid resistance.

Advantages
- Only small additional height
- Tolerances and dimensions are not critical

Disadvantages
- Lack of experience with bonded layers
- Critical installation procedure as the pot life of the adhesive is limited

5.4.15 Renovation method 13: trough filling

Figure 5-26 shows this renovation method, which has the following characteristics
(Old) surfacing: 7 mm epoxy surfacing or 50 mm mastic asphalt
Existing fatigue cracks: (Not) repair the cracks

Material:	Plastic
Form:	Poured
Connection:	Bonding
Structural Technology:	Vertical support of deck plate

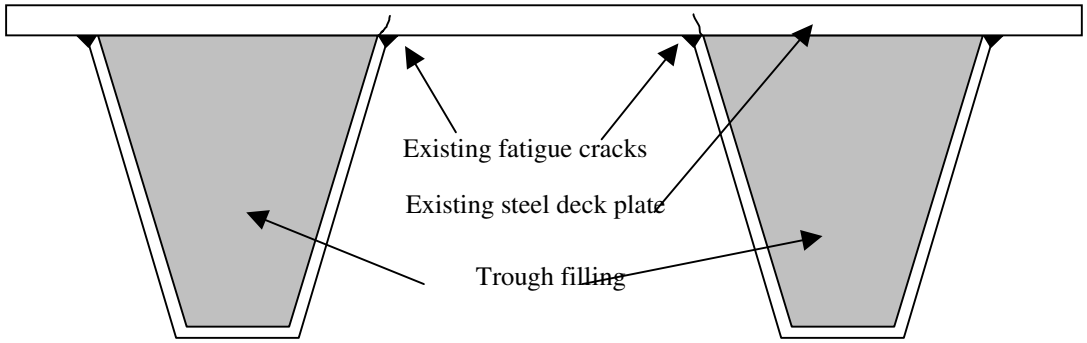

Figure 5-26: Trough filling

This renovation method is intended for movable bridges, but it is also possible to apply it to fixed bridges. For the application of the trough filling it is not necessary to remove the old surfacing, but for the detection and repair of fatigue cracks in the deck plate the surfacing has to be removed. The trough filling is thought to act as a spring support for the deck plate. This requires a filling material, for instance polyurethane, which has enough stiffness. In addition to this the filling material should be fully in contact with the underside of the deck plate.

Advantages
- Renovation takes place from beneath the deck
- Less traffic disruption

Disadvantages
- Deck plate between the troughs is not renovated
- Contact between underside of deck plate and filling material is difficult to achieve

5.4.16 Selected renovation techniques for further investigation

In the previous paragraphs 13 possible renovation techniques have been briefly described. From this 13 a limited number of techniques have been selected for further research. The selected methods are:
- Renovation method 1: High performance concrete on fixed bridges

- Renovation method 12: Bonding a second steel deck plate
- Renovation method 13: Trough filling

The choice is made on basis of engineering judgement. Renovation techniques with bolted connections were not selected for further research because it was thought that bolted connections would not give a satisfactory durability. Renovation techniques with prefabricated panels were not selected for further research mainly because of the problems that were foreseen with respect to the tolerances. In addition to this a few renovation methods were not selected due to the fact that severe problems with the corrosion protection of the steel bridge deck were to be expected. Also the fact that already bridges with severe deck plate cracks were observed in the first phase of the research project urged to develop as soon as possible renovation techniques.

Renovation method 9, an additional steel plate on an intermediate thick rubber layer, is suitable for further research, however there two reasons, why this is not researched more into detail here. First the method with high performance concrete is thought to be more effective and easier to apply than method 9, which method is already partly researched by Overduin (Overduin, 1999). Secondly a comparable method, known as the SPS technique, was incorporated in a research program at the BASt (Friedrich, 2005).

In general can be said that renovation method 1 is the method from which the most effective stress reduction was expected, and thus the biggest extension of the lifetime of the deck plate structure. The same holds for renovation method 12 when applied to movable bridge decks. Renovation method 13 is thought to be the technique that can be applied with little or no disturbance to the traffic flow on the bridge.

The further research, which has been performed on these renovation methods is reported in chapter 6 for fixed bridges and chapter 7 for movable bridges.

5.5 Concluding remarks

At the end of this chapter some concluding remarks can be made:

With respect to the requirements of renovation techniques, the two major requirements are:
- The existing bridge deck remains undisturbed as much as possible.
- Effective lifetime enhancement. Increasing the total stiffness of the deck plate structure is one of the main criteria and the stiffness should be increased as much as possible.

With respect to the developed SAW-welding process for crack repair:

- Submerged arc welding is a good repair method for detected cracks. The advantages of SAW-welding are that the speed of execution is high, the welding takes place only from the top of the deck plate, and weld shrinkage is relatively limited.
- Parameter settings for the welding process were determined by research. The current is the most important parameter affecting the depth of penetration.
- The maximum depth of penetration that can be achieved without a burn through is approximately between 65% and 75% of the deck plate thickness

With respect to the fatigue behaviour of cracks repaired with SAW welding:

- The detail classification of a deck plate with a SAW repaired crack is only slightly lower than the detail classification for the uncracked situation with parent material, 97 MPa instead of 113 MPa according to the Eurocode format

With respect to possible renovation techniques:

- Several ideas of possible renovation techniques have been briefly described and from these a limited number were selected for further research. These were the alternatives:
    - High performance concrete on fixed bridges
    - Bonding a second steel deck plate
    - Trough filling
- Renovation techniques with bolted connections were not selected because it was thought that bolted connections would not give a satisfactory durability.
- Renovation techniques with prefabricated panels were not selected mainly because of the problems that were foreseen with respect to tolerances.
- In addition to these a few renovation methods were not selected due to the fact that severe problems with the corrosion protection of the steel bridge deck were anticipated.

6. Renovation method for fixed bridges – Reinforced High Performance Concrete

6.1 Introduction

In this chapter a solution that extends the lifetime of the orthotropic deck structure is described. In this solution the asphalt surfacing is removed and replaced by a layer of approximately the same thickness of reinforced high performance concrete (RHPC). The RHPC surfacing is reinforced with traditional bars and with steel fibres. This renovation method is suitable for fixed bridges.

Paragraph 6.2 gives an introductory description of this method and the application phases are described in brief.

Paragraph 6.3 reports the results from FE-models. Primary interest is the reduction of the stress in the steel deck plate due to the replacement of the asphalt surfacing by a RHPC surfacing.

Paragraph 6.4 discusses the material, chemical and durability aspects of the high performance concrete surfacing. The bonding interface layer between original steel deck plate and concrete surfacing is described in this paragraph and the results of several tests, which were carried out, are reported.

Paragraph 6.5 gives a summary of the application tests that were performed in the development stage. These tests were performed to get an idea of aspects, which are related to the application and execution on a larger scale.

Paragraph 6.6 describes static tests that were performed on bridge deck test panels with a RHPC surfacing. The results of two test panels are described: one with and one without fatigue cracks in the deck plate.

Paragraph 6.7 reports the fatigue tests. These tests were performed on the same panels as the static tests, after the static tests. This paragraph also reports some static tests that were

performed during the fatigue test.

Paragraph 6.8 is about a pilot project on the Caland Bridge. A RHPC surfacing was applied instead of the asphalt on this heavily loaded bridge. Stress spectra measurements were performed on this bridge before and after the renovation. These measurements are described.

Paragraph 6.9 provides a summarized overview of all the calculated and measured stresses and strains reported in this chapter.

Paragraph 6.10 ends this chapter with some concluding remarks.

6.2 Introductory description RHPC surfacing

A description of the developed system is given in this paragraph. It will become clear why this solution is chosen. To prevent fatigue in the deck plate stress ranges in it have to be reduced and to reduce the stress ranges the stiffness of the deck plate structure must be increased.

Fixed bridges in the Netherlands usually have a wearing course of approximately 50 mm mastic asphalt, with a relative low stiffness compared to the stiffness of RHPC. It is possible to replace this asphalt with a wearing course with a higher stiffness. RHPC is a material with this higher stiffness and a wearing course of RHPC with roughly the same thickness as the mastic asphalt surfacing is a solution to reduce the stress ranges. If an intermediate layer with sufficient shear properties between steel and concrete is possible, composite action between steel and concrete can be achieved. In that case the total stiffness of the composite deck plate structure might be increased significantly, probably up to a factor 10.

Increasing the total stiffness of the deck plate structure is one of the main requirements of the renovation techniques, see chapter 5. Then the stress ranges in the steel deck plate are greatly reduced and consequently the fatigue life is far better.

Both prefabricated concrete panels, and cast in situ concrete are possible solutions for the fatigue problems. Prefabricated concrete panels would have to be bonded to the steel deck plate. A disadvantage of prefabricated panels is that it is very difficult to cope with discontinuities in the steel deck, and also that there are gaps in the concrete layer. These two disadvantages led to the decision to develop a system with cast in situ concrete. Figure 6-1 shows this surfacing system. The steel deck structure, the bonding layer between steel and concrete, the mesh reinforcement and the concrete are depicted in this figure.

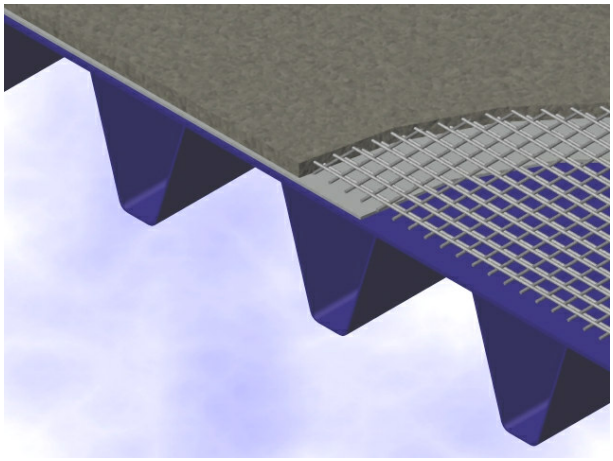

Figure 6-1: RHPC surfacing system

Applying an RHPC surfacing to an existing bridge deck with a mastic asphalt surfacing is divided into several phases. The details of these phases are the result of several tests that will be explained later in this chapter. The phases are:

1. Removal of the existing mastic asphalt surfacing
2. Visual and ultrasonic inspection of the deck plate structure to detect all the fatigue cracks in the deck plate, for example a TOFD (Time of Flight Diffraction)-inspection, see chapter 8 for inspection techniques.
3. Repair of detected cracks if they are bigger than the repair criterion, for example by submerged arc welding of the deck plate crack, see chapter 5 for this repair technique of cracks.
4. Shot blasting the surface of the steel deck plate to Sa 2.5 to achieve the necessary surface characteristics for bonding between an epoxy interface layer and the steel deck plate.
5. Application of a thin two-component epoxy based surfacing sprinkled with calcinated bauxite aggregate (3-6 mm)
6. Removal of any unbonded bauxite granules, after the intermediate epoxy layer has cured because unbonded granules form weak points in the bond between concrete and epoxy.
7. Placing reinforcement in 3 layers ∅8 mm spaced at 50 mm. The direction of the reinforcement bars in the bottom layer is transverse, in the middle layer it is longitudinal and in the top layer it is transverse. A vertical spacer is located between the epoxy layer and the reinforcement. Often a reinforcement bar ∅8 mm spaced at 500 mm is used as a vertical spacer.
8. Casting the HPC concrete strength class C110, reinforced with steel fibres and acrylic fibres.
9. Compacting, power floating and curing the material in order to create a very dense

surface.
10. Shot blasting or applying an epoxy surfacing in order to create a skid resistant surface for the traffic

When these steps are complete the bridge deck is ready for traffic again. The development of the RHPC wearing course started following the fatigue problems with the Van Brienenoord Bridge in 1997. In 2003 a part of the Caland Bridge in the harbour area of Rotterdam was resurfaced with RHPC instead of mastic asphalt. In 2005 and 2006 two other bridges in the Netherlands were renovated. Both the Moerdijk Bridge on the A16 motorway and the Lek Bridge near Hagestein on the A27 motorway were resurfaced with RHPC. On these bridges the concrete was shot blasted for skid resistance. After surfacing it became clear that on both bridges the skid resistance was not sufficient and especially on the Moerdijk Bridge the longitudinal alignment was not correct; a bumpy roadway was created, thus causing discomfort for road users. A solution is to apply an epoxy surfacing on the concrete. With such an epoxy surfacing is already many experience on movable bridges. These aspects are outside the scope of this thesis, because they are related to the execution of the resurfacing. Besides that these aspects do not have negative effects on the stress reduction in the steel structure, and thus no negative effect on the fatigue life of the bridge deck (Kolstein, 2006-a).

6.3 Numerical research and results

6.3.1 Research program

Pover has performed extensive Finite Element calculations (Pover, 2002, 2004) at the Civil Engineering Division of Rijkswaterstaat. Different models both with shell elements and solid elements were made. The general purpose of the FE-models was to quantify the stress range reduction in the deck plate at the fatigue prone locations due to the renovation method. This paragraph reports the results of these extensive FE-models with particular attention to the FE-models with solid elements.

The models with shell elements were made in order to determine the relevant properties for the FE-models with solid elements. The parameters that were varied in the FE-models were the deck plate thickness, the dimension of the crossbeams, and the dimension of the troughs. From the results of the FE-models with shell elements, as expected, it became clear that the local wheel loading on the deck plate dominates. The results of the FE-models with shell elements are not reported further in this thesis.

The main reason for the emphasis on the FE-models with solid elements is that the stress reduction cannot be adequately determined with shell elements. Modelling a structure with

shell elements is an option for one made of slender elements. A bridge deck with a layer of 50 mm RHPC on top of the steel deck plate is no longer a slender element and the location of the neutral axis in such a multilayer structure is difficult to determine.

Stresses in the deck plate at the fatigue prone locations are due both to the local deck plate bending and to the crossbeam behaviour. In the majority of orthotropic bridge deck structures the deck plate acts as top flange of the crossbeam, in which case the stresses due to crossbeam behaviour might be relevant.

Three types of FE-models with solid elements were made by Pover:

- FE-models only representing local deck plate behaviour at the crossbeam location, described in paragraph 6.3.1.1
- FE-models representing both local deck plate behaviour and crossbeam behaviour at the crossbeam location, described in paragraph 6.3.1.2
- FE-models representing local deck plate behaviour between two crossbeams, described in paragraph 6.3.1.3

The FE-models are not presented in the order in which they were made. The first FE-models made were those that represented both local deck plate behaviour and crossbeam behaviour at the crossbeam location. After that the models presented in paragraph 6.3.1.1 were made and finally those representing local deck plate behaviour between two crossbeams were made.

The FE-models were made for the calculation of the stress reduction in fixed and movable bridges. The results for fixed bridges are given in this chapter. The results for movable bridges are given in chapter 7. However sometimes a few results for movable bridges are given in this chapter.

6.3.1.1 FE-models - only local deck plate behaviour at crossbeam

Introduction

FE-models were made to calculate the reduction of the stress in the deck plate at the crossbeam location, see Figure 2-9 for the crack at this location. The model described in this paragraph solely represents the deck plate behaviour at the crossbeam location.

In real bridges the deck plate usually also acts as the top flange of the crossbeam. In the model described this mechanism is prevented by a continuous vertical support of the crossbeam. This model is also used for a comparison with a static test of a bridge deck panel with a RHPC surfacing. This test is described in paragraph 6.6.1.

Several different FE-models were made with solid elements for this crack location:

1. A standard model, only the orthotropic deck structure, with a deck plate thickness 12 mm and without any surfacing or renovation method (STD12)
2. A variant on the standard model with a deck plate thickness of 10 mm (STD10)
3. A variant on the standard model with a mastic asphalt surfacing of 50 mm on the deck plate (ASF)
4. A variant on the standard model with a RHPC surfacing of 50 mm on the deck plate (BET_50_12)
5. A variant on the standard model with a RHPC surfacing of 50 mm on the deck plate and a deck plate thickness of 10 mm (BET_50_10)
6. A variant on the standard model with a RHPC surfacing of 80 mm on the deck plate and a deck plate thickness of 10 mm (BET_80_10)
7. A variant on the standard model with an RHPC surfacing of 50 mm on the deck plate and in addition troughs filled with polyurethane foam, assuming adhesion between filling and the steel (CSB). Filling troughs with polyurethane foam is a renovation method that was developed for movable bridge decks. See chapter 7 for more information.
8. A variant on the standard model with an RHPC surfacing of 50 mm on the deck plate and in addition troughs filled with polyurethane foam, without any bonding between filling and the steel (CSB_without_a).

More FE-models with polyurethane foam are reported in more detail in chapter 7, as that chapter describes renovation methods for movable bridges.

At this point a comment on the words ‘standard’ and ‘reference’ should be made. The standard model comprises only bare steel. For the calculation of the stress reduction due to a renovation technique a comparison is made between two FE-models, representing the situation before and after application of the renovation method. For movable bridge decks this means that the standard model is also the reference model. For fixed bridges the reference model is mainly the FE-model with an asphalt surfacing.

The FE-model is comprised of one crossbeam, one full and one half trough, which are standard Krupp 2/325/6 profiles. The model is 2000 mm long either side of the crossbeam, i.e. the total length of the model is 4000 mm. The crossbeam web is 10 mm thick, the bottom flange is 16 mm thick and 200 mm wide. The troughs are continuous through the crossbeams. Figure 6-2 depicts the variant on the standard reference FE-model with the RHPC surfacing (no. 4 BET_50_12).

The FE-model is built up with several predefined geometries for the welds, the deck plate, the crossbeam web and bottom flange, the trough profile, the bonding layer and the concrete

layer. These geometries were defined in such a way that they fit together to form the assembled model.

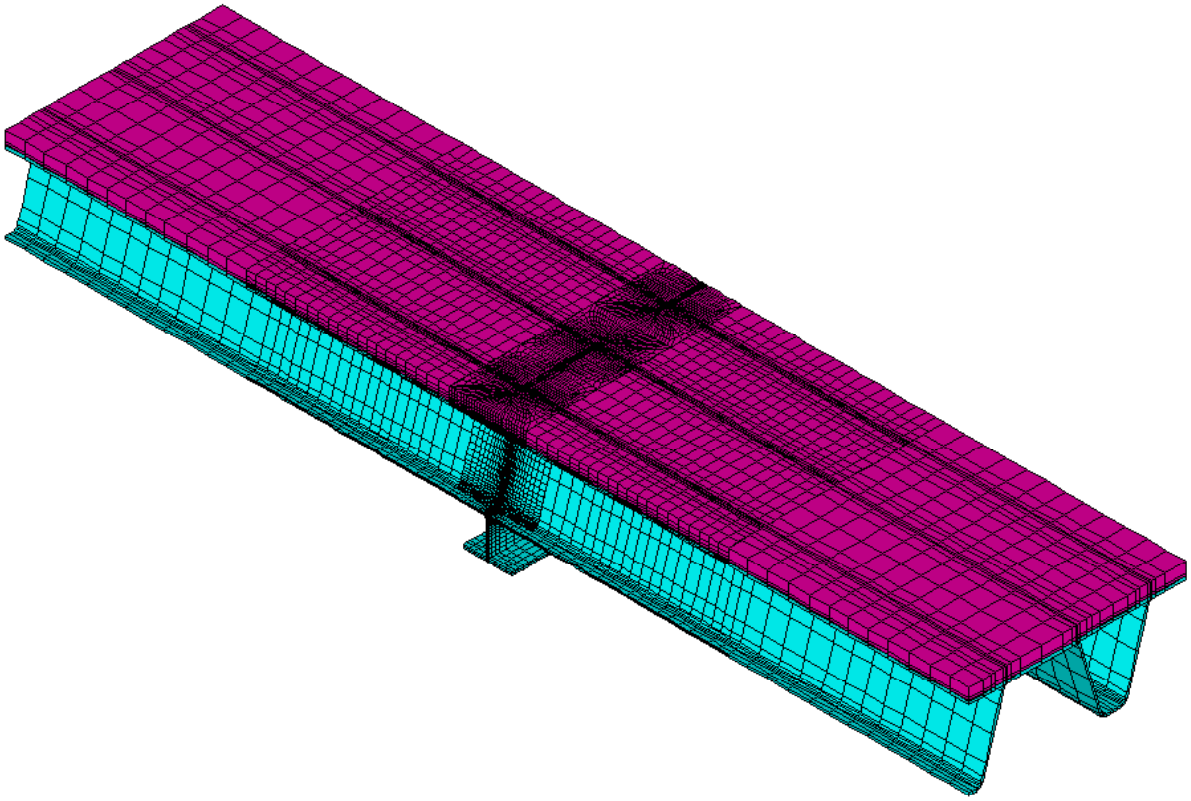

Figure 6-2: FE-model with RHPC surfacing layer

Material properties

- Material properties of steel are standard: Young's modulus E = 210000 MPa, Poisson ratio ν = 0.3, density ρ = 7820 kg/m^3, thermal coefficient α = 12x10^{-6}.
- Material properties for the welds are the same as for steel, except the E-modulus, which is taken at 90% of the E-modulus of steel.
- Material properties of the RHPC surfacing are: Young's modulus E = 50000 MPa (Braam, 2002-a; Buitelaar, 2004-b), see paragraph 6.4.2, Poisson ratio ν = 0.3, density ρ = 2400 kg/m^3, thermal expansion coefficient α = 12x10^{-6}. The concrete is modelled as a homogeneous layer. The reinforcement bars and cracks in the tension zones of the concrete are not modelled . Therefore the FE-model gives only a rough estimation of the effects of the RHPC layer on the bridge deck and gives no relevant results for the concrete layer.
- Material properties of the bonding layer between steel and RHPC surfacing are from the product data sheet of Sikadur 30 (Sika, 2006): Young's modulus E = 12800 MPa, Poisson

ratio ν = 0.3, density ρ = 1650 kg/m^3, thermal coefficient α = 90x10^{-6}. Research has shown that Sikadur 30 is a good epoxy bonding layer for RHPC on steel (Poulis, 2000-a). Therefore in the FE-models the properties of Sikadur 30 were used.

- The material properties of mastic asphalt are Young's modulus E = 5000 MPa, Poisson ratio ν = 0.3, density ρ = 2300 kg/m^3. The temperature dependency of the asphalt material is not taken into account. The chosen E-modulus represents a temperature of approximately 20 °C of the asphalt material on bridges, see Figure 8-6

Weld modelling longitudinal weld trough profile – deck plate

The modelling of the welds is also debatable. What is the best modelling for the weld geometry? The choice is between full penetration welds or with partial penetration. Modelling with partial penetration is a more realistic representation of the weld geometry in bridges. On the other hand, modelling partial penetration in FE-models is difficult, as it is not known if it will result in real stresses. Finally the choice was made to model full penetration welds. The disadvantage is that the modelling is better than the reality. On the other hand the FE calculations are intended to quantify the stress reduction and thus the weld modelling is applied both to the reference models without surfacing or with asphalt as well as in the models with the renovation methods. It is also a fact that the weld geometry is not a dominating parameter for the stress at the crack location for the common deck plate crack. Because the bending stress range in the deck plate due to local wheel loads only depends on the load, the thickness of the deck plate and the span of the deck plate the weld geometry only influences the theoretical span of the deck plate between the two trough webs. In the case of full penetration welds the theoretical span is slightly smaller compared to partial penetration welds. Figure 6-3 shows the FE-modelling of the full penetration weld between trough web and deck plate.

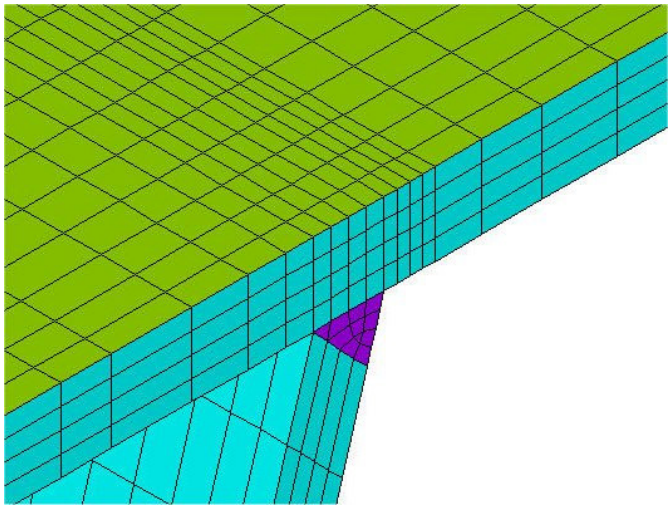

Figure 6-3: Full penetration weld between trough web and deck plate

From research published after the FE-models were made it has become clear that both the lack of penetration and the cross-section of the weld have a limited effect on the calculated stress at the root of the weld (De Corte, 2005, § 9.13). Based on this research it can be concluded that the chosen modelling with full penetration weld is appropriate for the calculation of the stresses and the stress reductions.

Boundary constraints

Figure 6-4 shows the boundary constraints of the FE-model. The bottom flange of the crossbeam is restrained for translations in y-direction. The deck plate at one end of the model is restrained for translations in z-direction. An axis of symmetry is located at the cross-section of deck plate and trough. There are no other boundary constraints in the model.

Loading

The centre of the wheel print is located on the intersection of crossbeam web and longitudinal axis of symmetry. The wheel footprint used in the FE-models is 320 mm long, 110 mm wide, and has a load of 58.5 kN. Because of the symmetry constraint this represents in fact wheel type A, the so-called single, from Eurocode 1 – Part 2, see paragraph 3.2, with a wheel load of 117 kN. This load was chosen because this is the maximum applied load on a test panel , see paragraph 6.6.1

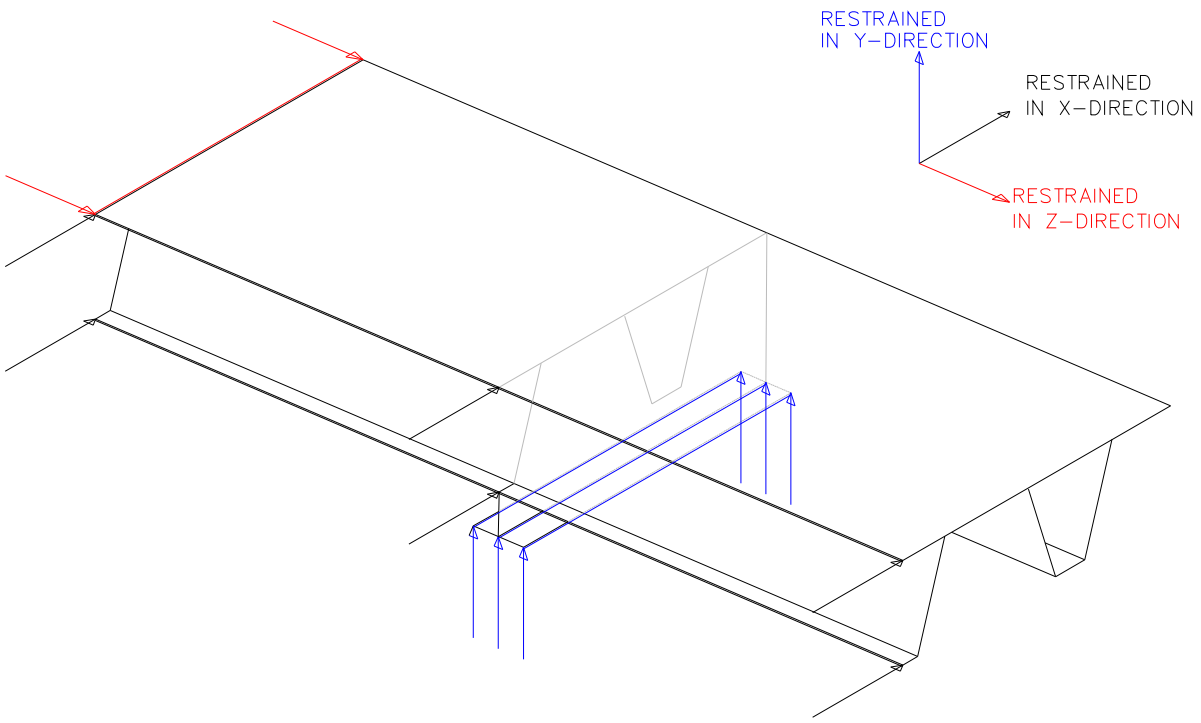

Figure 6-4: Boundary constraints FE-model

The reduction factors

The stress reduction due to the renovation method is based on a comparison of the peak stresses at the crack location due to a wheel load on the bridge deck. The peak stresses are at the same location in all models.

Figure 6-5 shows the calculated stress at the bottom of the deck plate in transverse x-direction both for the standard model with 12 mm deck plate and for the model with 50 mm RHPC surfacing. The troughs are also drawn in this figure to facilitate the interpretation of the results. Load cases 1 to 4 are the self-weight of the structure and are not reported in this thesis.

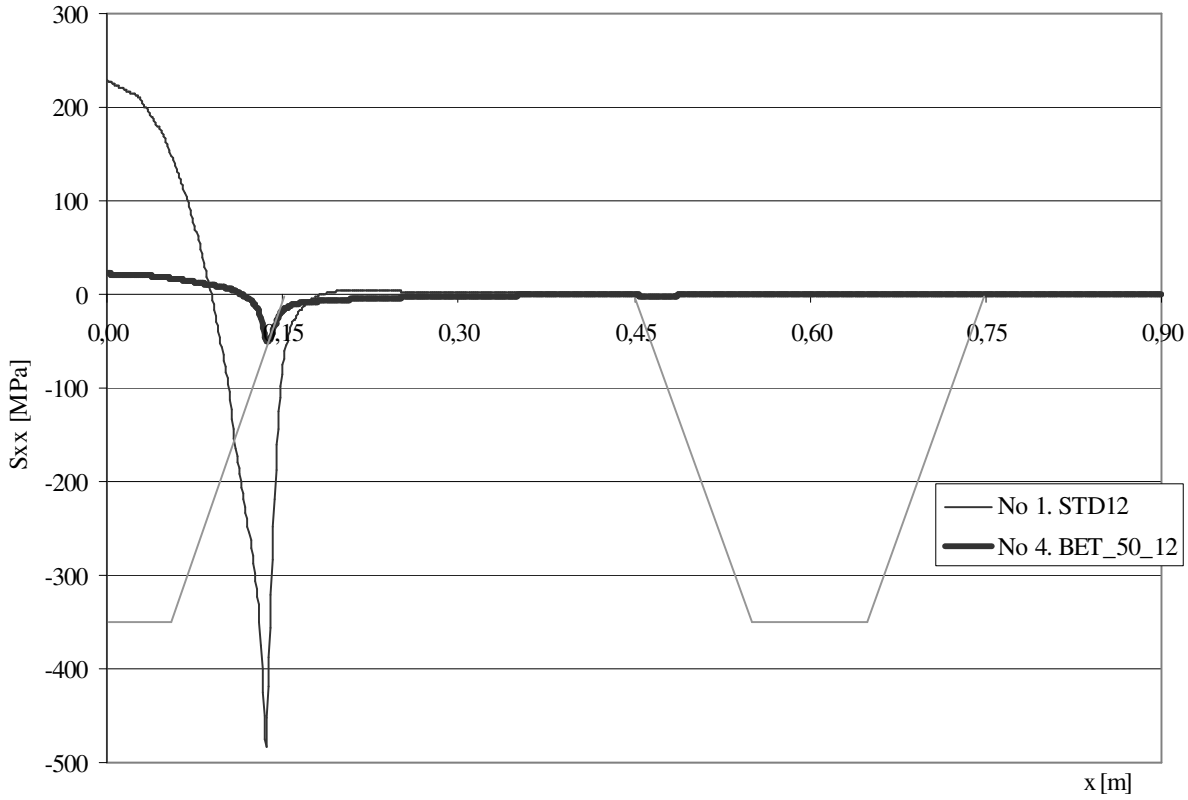

Figure 6-5: Stress at underside deck plate in x-direction, load case 5

The stress reduction factor is defined as the ratio of the calculated stress in the renovated panel divided by the stress in the unrenovated panel. The stress reduction factors on top and bottom of the deck plate are different of course, because the neutral axis of the structure moves. The main interest is the stress reduction factor at the bottom of the steel deck plate.

Table 6-1 gives the calculated stresses at the underside of the deck plate in the transverse x-

direction for the different load models at the crack location. This table also gives some relevant stress reduction factors. As fixed bridges are surfaced with a mastic asphalt layer reference is taken from the results from FE-model 3 (ASF_50_12). For movable bridges reference will be taken from the results from FE-model 1 (STD12), see chapter 7. The model reference is indicated within brackets.

Table 6-1: Stress σ_{xx} underside deck plate (MPa)

Model description	Stress σ_{xx} (MPa)	Stress reduction factor
1. Standard model, only deck plate 12 mm (STD12)	-483	
2. Deck plate 10 mm (STD10)	-643	
3. 50 mm mastic asphalt (ASF_50_12)	-250	
4. 50 mm RHPC (BET_50_12)	-49.7	0.20 (3)
5. 50 mm RHPC and 10 mm deck plate (BET_50_10)	-55.0	0.22 (3)
6. 80 mm RHPC and 10 mm deck plate (BET_80_10)	-32.2	0.13 (3)
7. 50 mm RHPC and trough filling (CSB)	-50.4	0.20 (3)
8. 50 mm RHPC and trough filling (CSB_without_a)	-53.4	0.21 (3)

At the midspan location, between the trough webs, this is at x = 0 m, the stresses are 228 MPa for model no. 1 (STD12) and 22 MPa for model no. 4 (BET_50_12). Note that the stress reduction factors for 5 and 6, with a 10 mm steel deck plate, are related to the model with a 12 mm deck plate, by lack of a 10 mm reference model with asphalt. This leads to a conservative overestimation of the stress reduction factor, because the calculated stress in a model with asphalt on a 10 mm deck plate would have been higher.

Conclusions

It became clear from the FE-models that a significant stress reduction factor is possible. The stress reduction factor due to the application of a RHPC surfacing can be approximately 0.20. This reduction is only for the local bending behaviour. Crossbeam behaviour is not included in this reduction factor.

Filling troughs, in addition to the application of the RHPC surfacing layer is shown to be unnecessary as it does not give any extra stress reduction. The trough filling is supposed to act as continuous spring support for the deck plate but due to the stiffness of the RHPC layer the deck plate hardly deflects under wheel loading and thus the trough filling is not loaded and thus gives no additional contribution to the stress reduction.

6.3.1.2 FE-models - local deck plate behaviour and crossbeam behaviour

Introduction

FE-models were made to calculate the reduction of the stress in the deck plate at the crossbeam location, see Figure 2-9 for the crack at this location. In the results described in this paragraph both local deck plate behaviour and crossbeam behaviour is incorporated. A few different FE-models were made with solid elements for this crack location:

1. A standard model, only the orthotropic deck structure with a deck plate thickness of 12 mm and without any surfacing or renovation method (STD)
2. A variant on the standard model with a RHPC surfacing of 50 mm on the deck plate (BET)
3. A variant on the standard with troughs filled with polyurethane foam (SCH)
4. A variant on the standard model with a second steel plate bonded onto the deck plate (STL)

The models with polyurethane foam and the second steel deck plate are reported in chapter 7, as this chapter describes renovation methods for movable bridges. These FE-models are intended to give a rough estimation of the situation in real bridges. A model with mastic asphalt was not made in this set of FE-models. Therefore the standard model serves as reference model.

The models are similar to the previous models, but have a few differences: The FE-models consist of four troughs, which are standard Krupp 2/325/6 profiles, and a deck plate of 12 mm. The crossbeam web is 10 mm thick and 800 mm high and the bottom flange is 16 mm thick and 200 mm wide. Figure 6-6 depicts the standard FE-model (no. 1 – STD). Figure 6-7 shows the FE-model with the RHPC surfacing (no. 2 – BET)

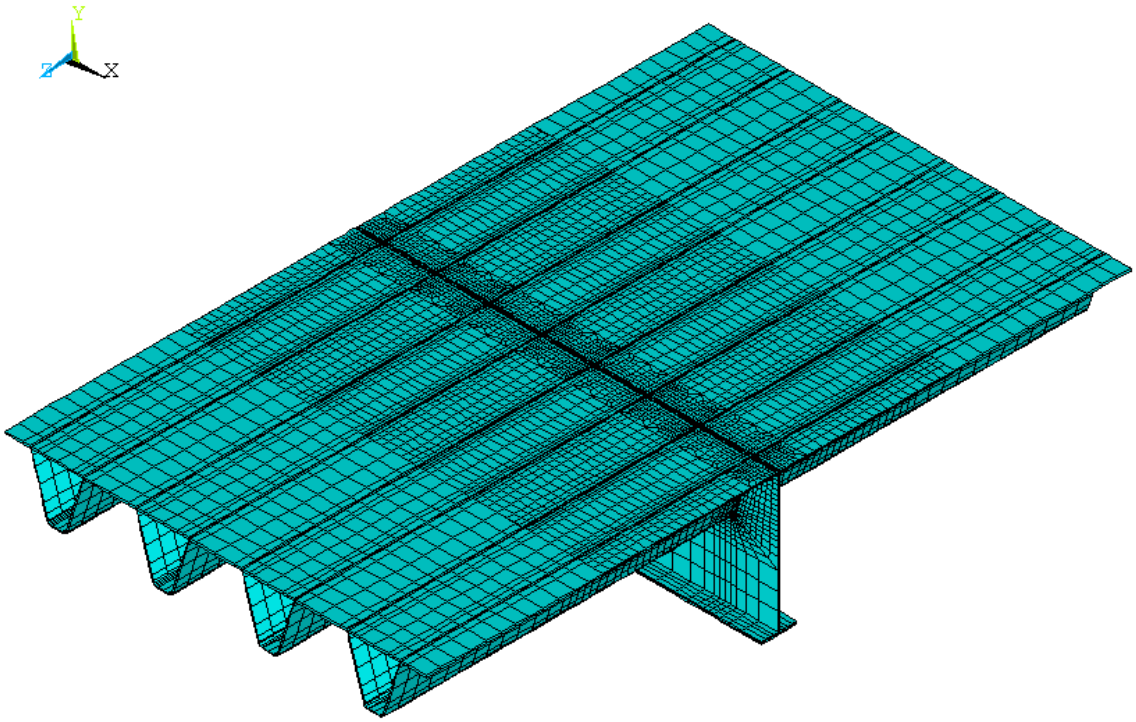

Figure 6-6: Standard FE-model (no. 1 – STD)

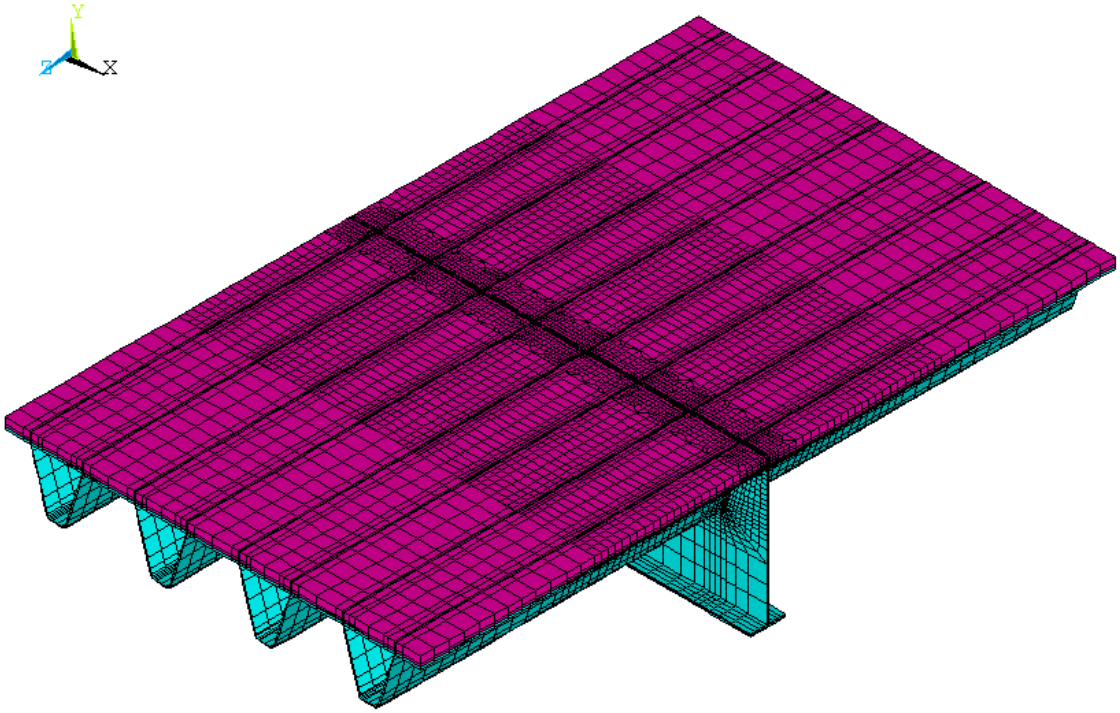

Figure 6-7: FE-model with RHPC surfacing (no. 2 – BET)

Material properties

The material properties are the same as those described in paragraph 6.3.1.1 above.

Boundary constraints

Figure 6-8 gives the boundary constraints of the FE-model.

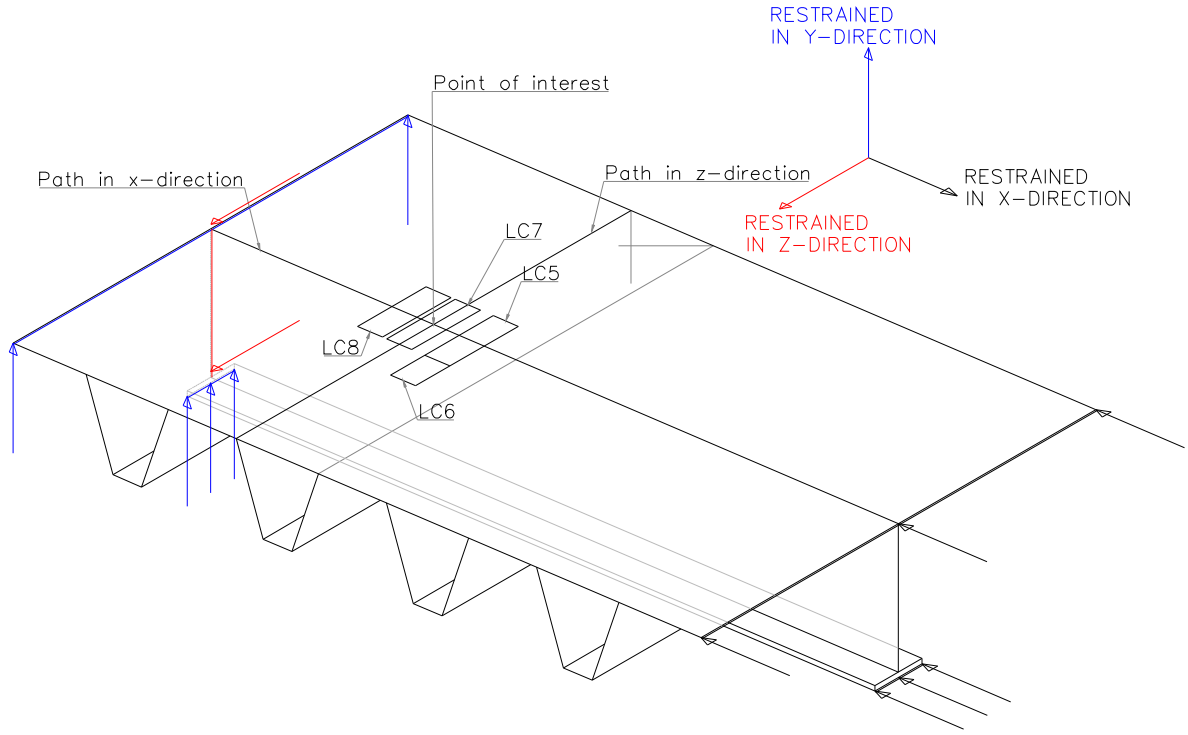

Figure 6-8: Boundary constraints FE-models and locations of wheel print on FE-model

The FE-model consists of one field. The main girder of the bridge is thought of as at the left side. The nodes at this side in deck plate, crossbeam web and crossbeam bottom flange are restrained for translations in y- direction. The nodes at this side in the crossbeam web are restrained in z-direction. At the other side an axis of symmetry is assumed, therefore the nodes at this axis of symmetry are restrained in x-direction. There are no other boundary constraints on the model.

The modelled part is only a part of a total bridge structure. Figure 6-9 gives a cross-section of a bridge deck. For this FE-model Pover has assumed that the crossbeams are clamped at the main girders (Pover, 2002). In real bridges it is doubtful of this is a good model. The mechanical model is shown in Figure 6-10 under the given symmetrical loading. Based on symmetry considerations only a quarter of the crossbeam structure had to be modelled, with the constraints as given in Figure 6-8.

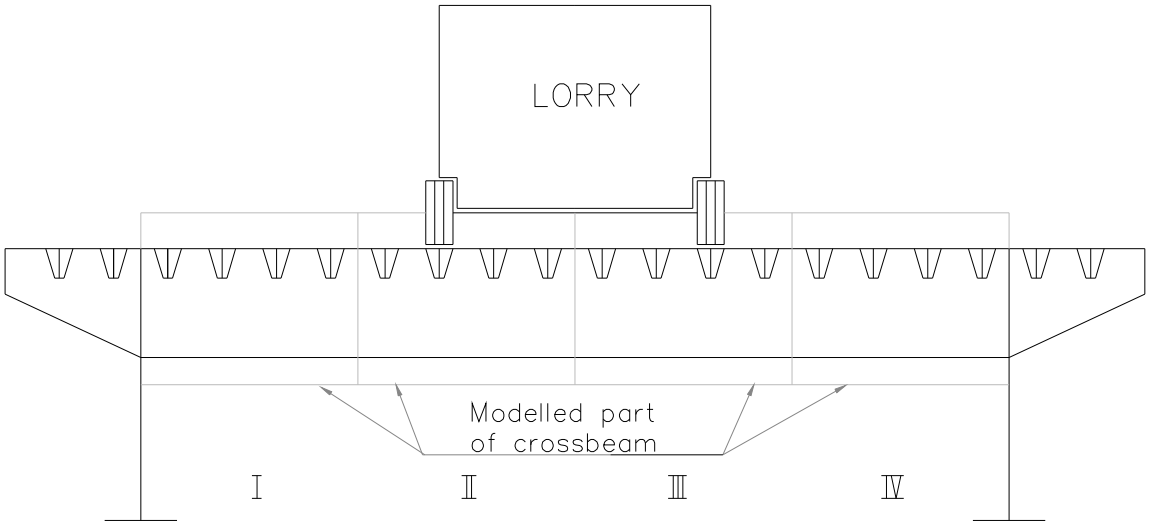

Figure 6-9: Modelled part of a crossbeam structure

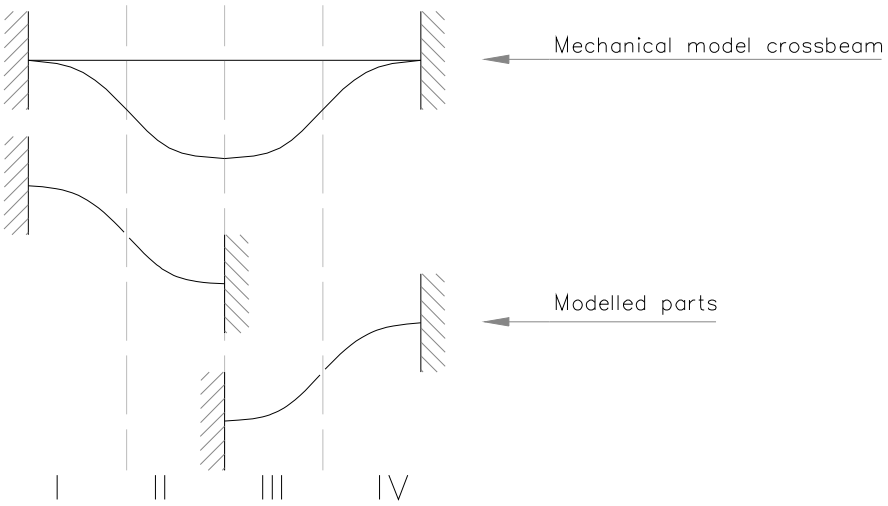

Figure 6-10: Mechanical model of a crossbeam section

Stresses in the deck plate at the fatigue prone location are due both to the local deck plate bending and to the crossbeam behaviour. This FE-model, with these boundary constraints, is considered to give an approximate estimation of the situation in real bridges. However from the results no distinction can be made with respect to the type of behaviour. As it is expected that the RHPC surfacing reduces the stress due to local deck plate bending more than the stress due to crossbeam behaviour, the model presented in this paragraph is in addition to the FE-model presented in paragraph 6.3.1.1, which only represents the local bending behaviour of the deck plate. Comparison of the FE-models with and without RHPC shows an overall reduction of the stress due to the RHPC surfacing.

Loading

The wheel footprint used in the FE-models is 320 mm long, 220 mm wide, and has a load of 35 kN. This is in fact wheel type A, the so-called single, from Eurocode 1 – Part 2, see paragraph 3.2. The standard axle load of 70 kN for the steering axle with wheel A is divided by two. The centre of the wheel print is placed in four positions the locations of which are given in Figure 6-8.

These four positions are:
1. Above the center of the second trough exactly above the crossbeam (Load case 5)
2. Above the center of the second trough besides the crossbeam (Load case 6)
3. Above the web of the second trough, located at the side of the main girder, exactly above the crossbeam (Load case 7)
4. Between the first and the second troughs exactly above the crossbeam (Load case 8)

Load cases 1 to 4 are self-weight of the structure and not reported in this thesis.

The stresses due to the wheel load are visualized along two lines on the bridge deck. Figure 6-8 shows these two lines.
1. In transverse direction (x-direction) of the model, along the top edge of the crossbeam, and at the top surface, the middle plane and the underside of the deck plate
2. In longitudinal direction (z-direction) of the model, along the top edge of the trough web of the second trough located at the side of the main girder,

The stress reduction factor

Figure 6-11 shows the calculated stress for load case 5 at the bottom of the deck plate in transverse x-direction along the transverse line 1, see Figure 6-8 for this line. Both the stress in the standard model without surfacing (no.1 –STD), as well as in the model with RHPC (no. 2 – BET) are given in this figure. The location of the wheel load is clearly visible in this graph.

The peak stresses at the left and right hand sides of the trough differ from each other. This is due to the crossbeam behaviour and the uneven deformation of the structure. However for the standard model the stresses at the left and right hand sides have the same order of magnitude, which means that the local wheel load is the governing parameter.

The peak stresses at left and right hand sides of the trough differ significantly from each other (left: -26.5 MPa, right: -2.5 MPa) for the model with concrete (no. 2). This difference shows that the stress due to local wheel loading is no longer the governing parameter. Stress due to crossbeam behaviour and the uneven deformation of the structure play a role in the total stress.

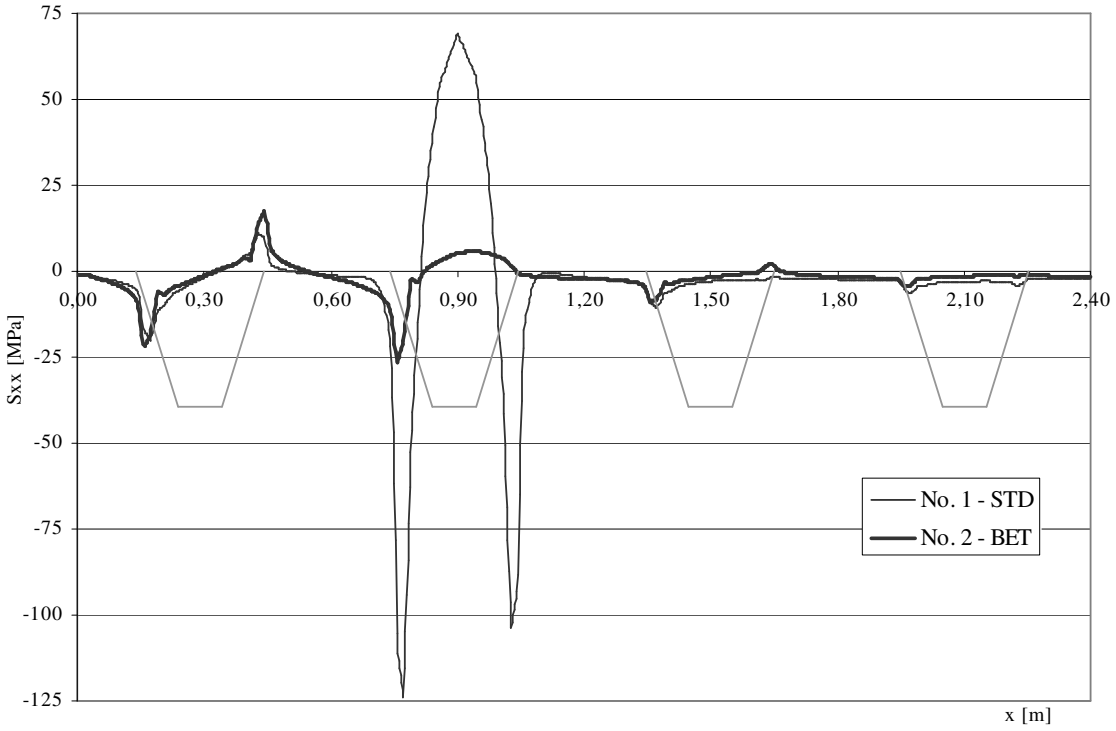

Figure 6-11: Stress - underside of deck plate in x-direction, load case 5

Load case 8 is thought to represent only the crossbeam behaviour, because the wheel load is located exactly between two troughs and thus directly transferred to the crossbeam web. In that case there would be theoretically no peak stress due to the local deck plate behaviour at the crack location (intersection crossbeam, deck plate, trough web). However from research it is known that the deflection of an orthotropic deck structure under loading leads to peak stresses at the intersection of deck plate and trough web, also if there is no local wheel load (Dijkstra, 1998). This peak stress is due to the imposed deformation of the deck plate structure, which differs from the theoretical deflection. In addition, why the stress is –12 MPa with RHPC surfacing and –4 MPa without any surfacing when load case 8 is thought to represent only the crossbeam behaviour cannot be explained, see Table 6-2. Due to this anomaly, it is impossible to derive separate stress reduction factors for the different mechanical mechanisms (local deck plate behaviour and crossbeam behaviour).

The stress reduction factors from load case 5 (the wheel footprint symmetrically located above a trough) are thought to represent both the local deck plate behaviour as well as the crossbeam behaviour. The stresses are determined at the root of the weld. The stress reduction factors on top and underside of the deck plate are different of course, because the neutral axis of the structure moves. The main interest is the stress reduction factor at the underside of the steel deck plate. Table 6-2 gives the calculated stresses in the transverse x-direction for the

different FE-models and load cases at the crack location along line 1, at the root of the longitudinal weld.

Table 6-2: Stress σ_{xx} - underside of deck plate along line 1 (MPa)

Stress σ_{xx} underside of deck plate in x-direction (MPa)	LC 5	LC 6	LC 7	LC 8
Standard model (no. 1 – STD)	-124	-86	-45	-4
RHPC (no. 2 – BET)	-26.5	-24	-18	-12
Stress reduction factor	0.21	0.28	0.40	

Shear stresses

The shear stress σ_{yx} was calculated for the FE-model with a RHPC surfacing at two interfaces:

- Top surface of the epoxy bonding layer at the interface with the RHPC surfacing

Underside of the epoxy bonding layer at the interface with the steel deck plate

Table 6-3 shows the shear stresses at these two interfaces. Load case 5 comprises both local deck plate behaviour and crossbeam behaviour. Load case 8 comprises mainly crossbeam behaviour because of the location of the footprint,, which is on the teeth of the crossbeam between the troughs, see Figure 6-8. Roughly half of the shear stress is due to local deck plate behaviour and roughly half is due to crossbeam behaviour.

Because of the calculated small shear stresses compared to the shear capacity of the interface, see paragraph 6.4.2, the shear stresses have not been reported by Pover for the models in paragraph 6.3.1.1 (only deck plate behaviour) and paragraph 6.3.1.3 (deck plate behaviour between crossbeams).

Table 6-3: Shear stresses at top and underside of the epoxy layer with RHPC (MPa)

Shear stress σ_{yx} (MPa)	LC 5	LC 6	LC 7	LC 8
Top side epoxy layer at interface with RHPC	2.02	1.72	1.39	1.12
Underside of epoxy layer at interface with Steel	2.13	1.69	1.40	1.09

Conclusion

From the FE-models is appears that a reduction factor of 0.2 to 0.4 might be possible, depending on the location of the local wheel load. The peak stress of load case 8 is due to the crossbeam behaviour and the uneven deformation of the crossbeam. The value of the reduction factor is not related to the effect of the RHPC surfacing. Therefore this value is not given in Table 6-2.

It should be noted that the reduction factor is based on a comparison of a model with the RHPC surfacing and a model with no surfacing. However the RHPC surfacing is intended to replace an asphalt surfacing and an asphalt surfacing leads also to a reduction of the stress. The calculated reduction factors probably give an overestimation of the reduction in reality, see paragraph 6.9 for more comments.

This FE-model gives only a rough estimation of the stress reduction due to the RHPC surfacing. The following remarks can be made:

- The stress in the deck plate due to crossbeam behaviour, and the peak stresses due to the uneven deformation of the crossbeam are not calculated separately
- The boundary constraints applied to the crossbeam are doubtful; do these constraints lead to a model that represents a real bridge structure?
- The crossbeam behaviour depends on its dimensions, its span and the loading on it. These parameters have not been varied in the FE-calculations, as in reality all bridges are different from each other.

Therefore it is not clear that the FE-model used is a good representation of the crossbeam behaviour and it is debatable whether the implicit ratios between the stressed parts in the FE-model are similar to those in real bridge structures. Therefore the calculated reduction percentages should be interpreted carefully. Paragraph 6.8 describes the application of the RHPC surfacing on the Caland Bridge and the strain gauge measurements on that bridge. The results of the FE-models and measurements will be compared in paragraph 6.9.

6.3.1.3 FE-models - local deck plate behaviour between crossbeams

Introduction

Based on the FE-models described in the previous paragraphs other FE-models were made, also built up with solid elements. The reduction in stress at the underside of the deck plate between two crossbeams was calculated with these FE-models. The stress was calculated at the location where the deck plate fatigue crack occurs, see Figure 2-9, and also at the location where the maximum stress is generated under local wheel loading. The stress in the trough web was also calculated with these FE-models because this stress is responsible for crack growth in the longitudinal weld between deck plate and trough web, see Figure 2-16.

Several different FE-models were made with solid elements for these crack locations:

1. A standard model, only the orthotropic deck structure without any surfacing or renovation method (STD)
2. A variant of the standard model with a RHPC surfacing on the deck plate (BET)
3. A variant of the standard model with a mastic asphalt surfacing on the deck plate (ASF)

4. A variant of the standard model with the troughs filled with polyurethane foam (SCH)
5. A variant of the standard model with a second steel plate bonded on the deck plate (STL)
6. A variant of the standard model both with troughs filled with polyurethane foam and a second steel plate bonded on the deck plate (CSS/CSE)

The models with polyurethane foam and the second steel deck plate are reported in chapter 7, which describes renovation methods for movable bridges.

The FE-models were built up with one crossbeam, three troughs, which are standard Krupp 2/325/6 profiles and a deck plate thickness 12 mm. The model is 2000 mm long either side of the crossbeam, the total length of the model is 4000 mm. The crossbeam web is 10 mm thick and 450 mm high, the bottom flange is 16 mm thick and 200 mm wide. The width of the model is 1.8 m.

Figure 6-12 shows one half of the standard model without any surfacing or renovation method. Figure 6-13 shows the FE-model variation with a RHPC surfacing on top of the deck plate. In comparison with the FE-models intended for calculation of the stresses at the crossbeam location the mesh is refined at one edge of the model.

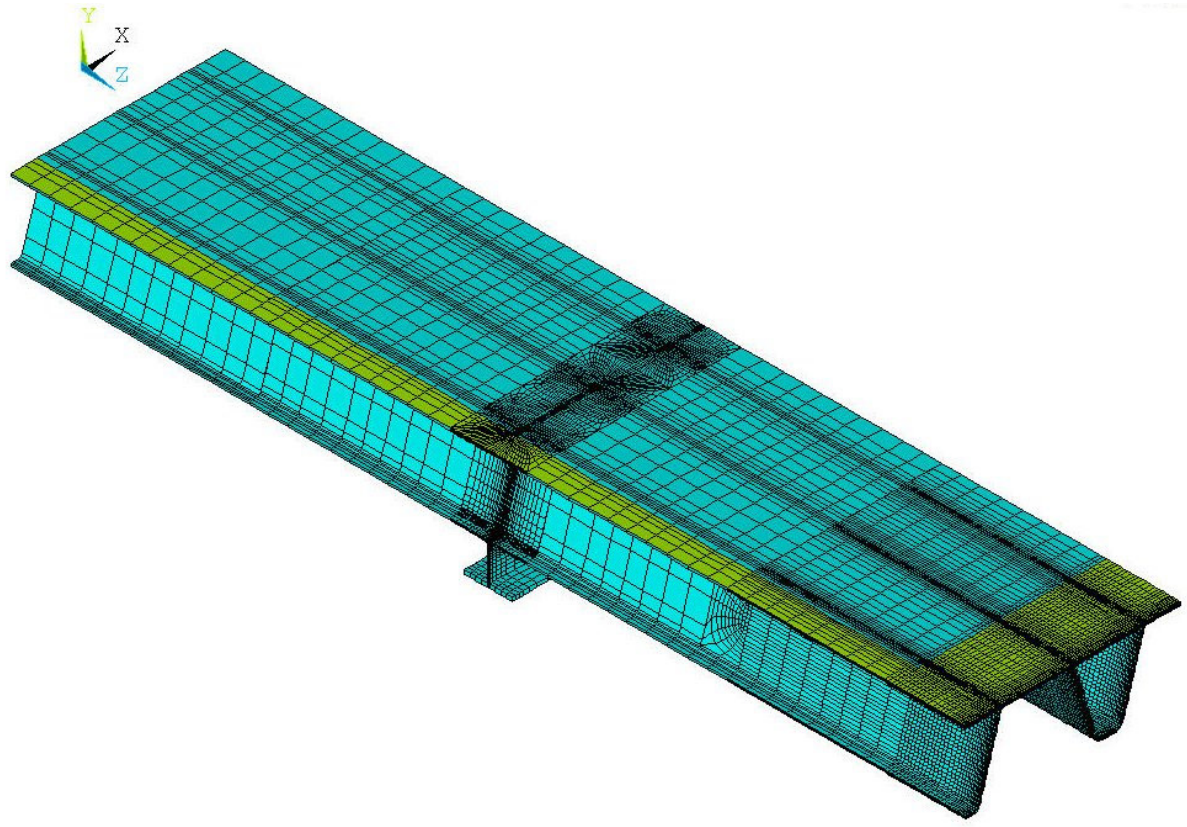

Figure 6-12: Half of the standard FE-model

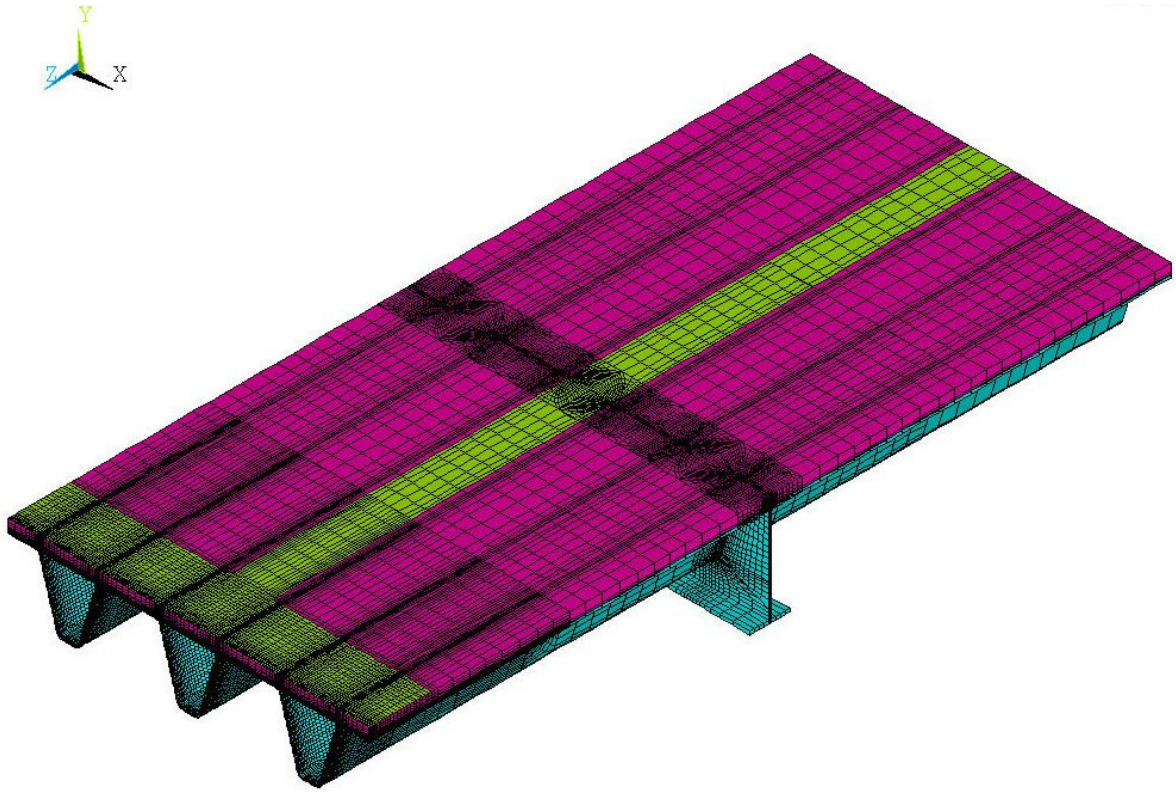

Figure 6-13: FE-model with RHPC surfacing

Material properties

The material properties are the same as those described in paragraph 6.3.1.1 above.

Boundary constraints

The FE-model consists of two half fields, in total one field. The long sides of the model are not supported. At the short sides of the model at the ends of troughs and deck plate a symmetry constraint is applied. The crossbeam is continuously supported.

Loading

The wheel footprint used in the FE-models is 320 mm long, 220 mm wide, and has a load of 35 kN. This is in fact wheel type A, the so-called single, from Eurocode 1 – Part 2, see paragraph 3.2. The centre of the wheel print is located at three positions:

1. Above the center of the second trough (Load case 5)
2. Above the left web of the second trough (Load case 6)
3. Between the first and the second troughs (Load case 7)

Figure 6-14 shows these three positions. Load cases 1 to 4 are the self-weight of the structure and are not reported in this thesis.

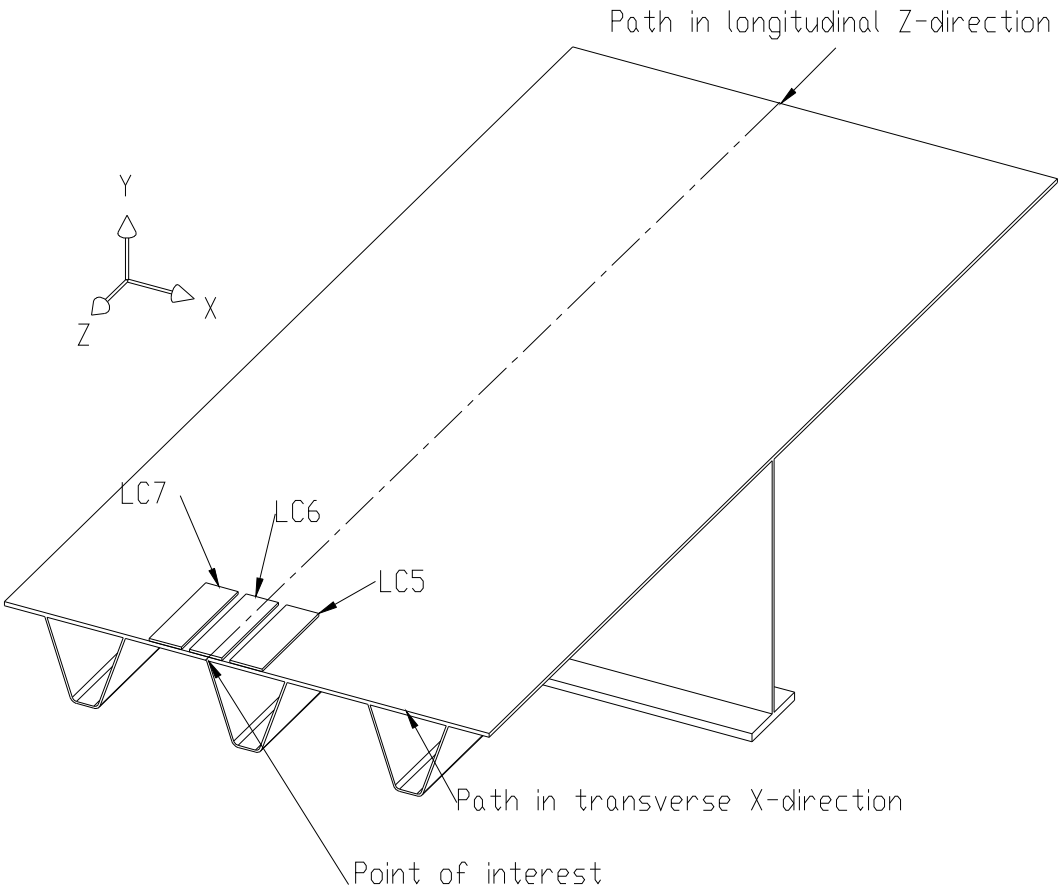

Figure 6-14: Locations wheel footprints on the FE-model

The stresses due to the wheel load are visualized along two lines on the bridge deck. Figure 6-14 shows these two lines.

1. Along the underside of the deck plate in transverse direction (x-direction) at the edge of the model.
2. Along the top surface of the left web of the middle trough in longitudinal direction (z-direction) of the model.

Stress reduction factors for stress in the deck plate

Figure 6-15 shows the calculated stresses at the underside of the deck plate under load case 5. The crack locations, i.e. the locations of the trough webs, are situated at approximately 0.75 m and 1.05 m. The interpretation of the calculated stresses at these connections, trough web – deck plate, leads to some problems. The calculated stresses fluctuate a lot at this location, which makes it difficult to quantify the stress reduction factor. In addition to this another aspect also makes it difficult to derive the stress reduction factor at the crack location. The bridge deck with the concrete surfacing shows a slight tensile stress at bottom of the adjacent

fields. This indicates that the wheel load is distributed over a wider part of the bridge deck structure. This leads to an extra reduction of the bending stress in the deck plate at the connection with the trough web. It is debatable whether the FE-model represents this distribution over a wider part of the bridge deck correctly.

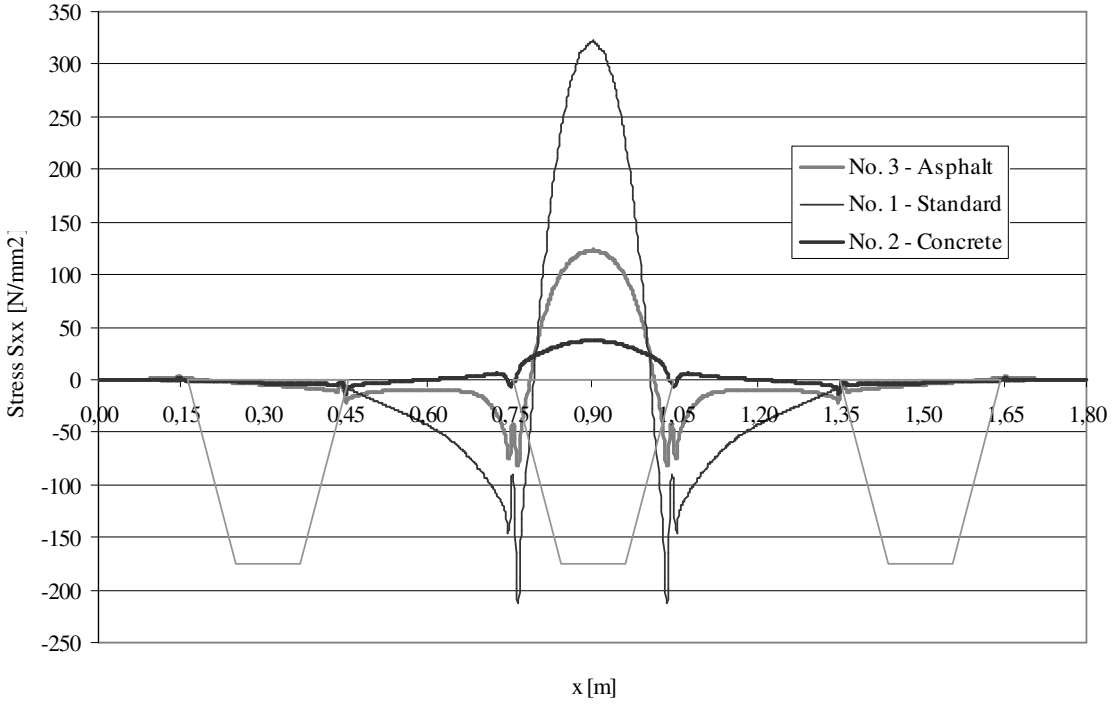

Figure 6-15: Stress bottom surface deck plate, path in x-direction, Loadcase 5

A comparison of the stresses at x = 0.9 m, this is midspan of the deck plate between two trough webs, can lead to a more realistic approach to the stress reduction. Therefore both the stresses at the crack location (x = 0.75 m), as well as at the midspan location of the deck plate (x = 0.9 m) are tabulated in Table 6-4. The reduction factor in this table is derived from a comparison between the RHPC-surfacing and the asphalt surfacing. From this table it also becomes clear that especially for load case 6 at the crack location, the stress changes from compressive to tensile. The maximum stresses for load cases 6 and 7 are not exactly midspan. Only for load case 5 is the maximum stress at midspan because of the location of the footprint centered above the trough. For load case 6 and 7 the maximum stress is taken, instead of the stress midspan between the trough webs.

It should be noted that it is a conservative approach to the stress reduction factor to calculate it at the location where the maximum stresses occur rather than at the crack location. The tensile stress at the underside of the deck plate due to the distribution over a wider part of the

deck structure leads to:

- A probable overestimation of the stress reduction at the crack location (the stress reduction factor becomes too small)
- An underestimation of the stress reduction at the location of the maximum stress (at x = 0.9 m for load case 5), (the stress reduction factor becomes too large)

Table 6-4: Stress (σ_{xx}) underside deck plate along line 1 (MPa)

Stress (MPa)	LC5	LC5	LC6	LC6	LC7	LC7
Location	crack	midspan	crack	maximum	crack	maximum
Standard model	-212	323	-120	120	-345	321
Asphalt	-82	123	-61	72	-158	113
RHPC	-1.2	37	6.3	28	-23	31
Reduction factor	0.01	0.30		0.39		0.27

Stress reduction factor for stress in the trough web

The stresses in the trough web are responsible for the growth of fatigue cracks in the longitudinal weld between trough web and deck plate. The application of a RHPC surfacing also reduces these stresses. Table 6-5 gives the calculated principal stresses in the trough web at the connection with the longitudinal weld. Local stress concentration effects are of course taken out of this principal stress.

Table 6-5: Principal stress in trough web at longitudinal weld (MPa)

Principal stress trough web (MPa)	LC5	LC5
	Outside trough web	Inside trough web
Standard model	135.7	-162.9
Asphalt	44.3	-71.9
RHPC	-2	-20.4
Reduction factor (RHPC/Asp)	x	0.28

From this table a difference between the stress at the outside and the inside of the trough becomes clear. Figure 6-16 shows these locations. This can be explained because the trough web is not only loaded in bending by the wheel load, but also loaded in compression. The stress reduction factor is again the ratio between stress with asphalt and with RHPC surfacing. This ratio is calculated for the stress at the inside of the trough web as the fatigue crack in the longitudinal weld initiates from the inside of the trough web.

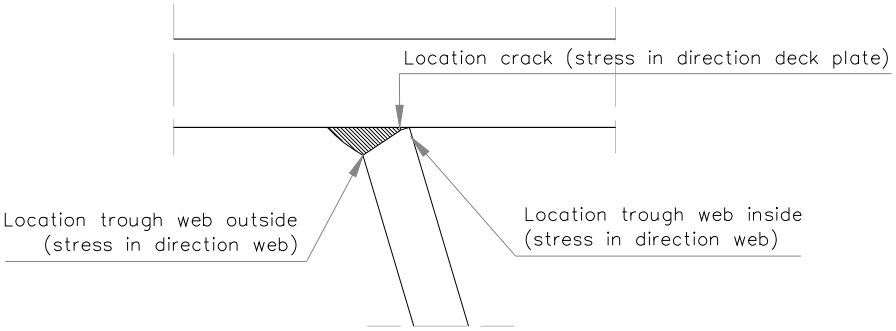

Figure 6-16: Locations crack, outside trough web and inside trough web

Conclusion

From the FE-models representing the local deck plate behaviour between the crossbeams it is difficult to draw conclusions. Table 6-4 shows that a stress reduction factor of 0.3 to 0.4 is possible, for the stress in the deck plate, depending on the location of the local wheel load.

It should be noted that the reduction factor is based on a comparison of a model with the RHPC surfacing and a model with asphalt surfacing. This explains why the calculated reduction factors are somewhat higher than those calculated in paragraph 6.3.1.2. Another explanation is that the chosen location of the stress comparison (at maximum stresses) causes a conservative approach to the stress reduction factors.

For the stress in the trough web a reduction factor of approximately 0.3 was derived with the FE-calculations.

6.4 Material, chemical and durability aspects of RHPC

6.4.1 Interface layer between steel and concrete & execution notions

An interface layer between steel and concrete is necessary. The functions of this interface layer are: corrosion protection for the steel deck plate, providing shear strength and stiffness, and providing tensile strength to the interface between steel and concrete. Shear strength and stiffness are necessary to enable composite action between steel and concrete, which is favourable in order to maximize the stress reduction in the steel deck plate. Although a stiff interface layer is needed, this layer should not be brittle. Besides this the ease of application and robustness of the result are important.

There are a few options for the intermediate layers (Nagtegaal, 2003):

1. Shear connectors welded onto the steel deck plate, a traditional method for steel-concrete

composite structures
2. Gauze welded onto the steel deck plate
3. A bonding layer of a few mm between steel and concrete

Casting the concrete directly onto a shot blasted steel deck plate with a primer, but without intermediate layer is not an option, because research has shown that this bonding method gives no tensile and shear strength in the steel-concrete interface (Poulis, 2000-a)

The first two options are time-consuming at the time of application and have the disadvantage of causing local stress concentrations. Various options for the bonding layer in combination with the application method of the concrete surfacing were researched by the Adhesion Institute of Delft University of Technology. With respect to the application method a choice can be made between prefabricated concrete panels or cast in situ concrete.

Adhesion tests on small test specimens were performed to optimize the bonding layer between concrete and steel. Three types of this interface were tested. (Poulis, 2000-a):
1. Prefabricated panels glued in-situ on the steel deck using a two-component epoxy paste adhesive
2. Casting the mortar on a wet two-component epoxy paste adhesive
3. Casting the mortar on a hardened two-component epoxy paste adhesive sprinkled with granite or bauxite using both reinforced and non-reinforced samples.

Tests (Poulis, 2000-a) and a literature survey on the bonding of concrete on a steel deck plate (Borger, 2000) indicate that options 1 and 2 are promising solutions. However for reasons of execution they were rejected. With prefabricated concrete panels it is difficult to cope with the discontinuities in the alignment of the steel bridge deck and casting the mortar on a wet adhesive only gives a good result, if the mortar is applied shortly after applying the adhesive. From the point of view of execution this is also difficult to control. Several types of epoxy were tested. It turned out that for option 3 Sika 30 is the epoxy with the most favourable properties. (Poulis, 2000-a)

The following few steps are the preferred method of bonding the concrete layer to the steel deck plate:
1. Shot blast the steel deck plate to Sa 2.5
2. Apply a primer
3. Apply a two-component epoxy adhesive layer of approximately 2-3 mm thick
4. Immediately sprinkle it with bauxite granules 3-6 mm, approximately 10-12 kg/m^2
5. After the epoxy layer has hardened remove unbonded bauxite granules

The intermediate layer built up in this way provides:

- Corrosion protection for the steel deck
- Shear and tensile strength in the interface steel-epoxy due to adhesion
- Shear and tensile strength in the interface epoxy-bauxite-concrete, due to the fact that the rough bauxite surface is embedded in the concrete.

The bonding layer is built up with an epoxy because there is a lot of experience with epoxy on movable bridge decks and because epoxy has a good resistance to water, which is necessary as the concrete is cast in-situ.

6.4.2 Concrete Properties

Concrete surfacing for bridge deck is based on that developed for industrial floors as described by Buitelaar (Buitelaar, 2004-b). One of the first large applications of the RHPC overlay was as topping for damaged pavements and industrial floors (Buitelaar, 1999, 2002).

The properties of the RHPC make it possible to use it as a topping or wearing course on a cracked and / or polluted sub base or even on an inadequate sub base made from different materials like asphalt concrete, concrete, wood, ceramics or steel. The concrete surfacing contains one or more layers of welded mesh reinforcement (bar diameter 6 – 20 mm and bar spacing 15 – 50 mm). The concrete mixture contains both steel fibres and acrylic fibres and is based on a special composite of pre-blended materials. Good properties of the concrete layer are possible due to the combination of the mortar, the welded mesh reinforcement and the steel fibres. High reinforcement percentages are possible without compacting problems. Due to the amount of conventional reinforcement bars and the steel fibres, a high bending tensile strength, and an optimal distribution of micro cracks are possible.

Besides this high performance concrete mixes also have high durability, impermeability and wear resistance. Based on the successful application as industrial floors, and the properties of this RHPC overlay it was expected that this system would be a good solution to the fatigue problems on steel bridge decks when applied as surfacing layer on the deck plate. The tests described in this chapter shown that this expectation was correct.

For the tests described in this chapter the mortar consists of:

25 kg	Contec binder N (with Portland cement 52.5, micro silica, polypropylene fibres, super plasticizer, additive to drive out air bubbles, additive to reduce the surface stress)
40 kg	sand (0.1 – 1.5 mm)
62.5 kg	granite (max. 4 mm)

4 kg steel fibres (diameter 0.4 mm, length 12.5 mm $f_{t;c}$ = 1200 MPa)
8.8 kg water
The mixing procedure was: mix granite and sand, add the binder, mix without water, add water, mix, add steel fibres, mix.

Braam performed many material tests on this mixture. The tests results were extensively described (Braam, 2002-a-b-c-d-e-f-g, 2003-a-b-c), (Buitelaar, 2004-b). The main results are described below.

Compressive strength & stiffness modulus
The compressive strength of the HPC with steel fibres was measured on 100 mm cubes and 100x100x400 mm prisms. The 28-day compressive strength was 117 MPa for the cubes and 84 MPa for the prisms. The 28-day E-modulus is 47.2 GPa, determined on the prisms. The development of the compressive strength is comparable to that of other mixtures of the same order of strength. (Braam, 2002-a), (Buitelaar, 2004-b)

Bending tensile strength
The bending tensile strength of the HPC with steel fibres, but without reinforcement, was measured with three-point bending tests on beams with a height of 50, 100 and 150 mm, a width of 150 mm and a span of 500 mm. The bending tensile strength was 9.8 MPa, 11.9 MPa and 9.6 MPa for, respectively, h = 50 mm, 100 mm and 150 mm. These results indicate that, in this range of element depth, the bending tensile strength is not size-dependent (Braam, 2002-f), (Buitelaar, 2004-b).

Time-dependent shrinkage behaviour of hardening concrete
The early-age deformation of the mixture was investigated using an autogenous deformation testing machine (ADTM). Both reinforced and non-reinforced specimens were cast in a temperature-controlled steel mould. The temperature of the hardening specimen was kept constant at 20 ºC. The specimens were covered such that there was no water or air exchange with the environment. The relatively large amount of reinforcing steel reduces the deformations by about 40%. Preventing evaporation of water from the mixture turned out to be essential for reducing the shrinkage. It is thought that the relatively high percentage of coarse aggregates, and power floating also have a reducing effect on the deformation (Braam, 2002-c), (Buitelaar, 2004-b).

Time-dependent shrinkage behaviour of hardened concrete
Six prisms (dimensions 100x100x400 mm with no steel bar reinforcement) were stripped from the mould after one day and sealed to prevent drying. Then, shrinkage measurements started. Because of the sealing, only autogenous shrinkage occurred. The specimens were

stored at 20 ºC and 50% relative humidity for 28 days. Then, the sealing was removed from three of the prisms; the other three prisms were kept sealed. The three unsealed specimens now also started to develop drying shrinkage. Measurements continued for a further 63 days. After 61 days, the deformation of the sealed prisms remained almost unchanged. The unsealed specimens (i.e. the prisms also subjected to drying shrinkage) demonstrated a considerable increase in deformation even after 97 days (Braam, 2002-e), (Buitelaar, 2004-b).

Tensile strength interface concrete – steel deck plate

The adhesion was measured on 77 mm diameter steel discs treated with an epoxy layer and a HPC layer. Two types of aggregates were sprinkled on the epoxy: Norwegian granite and bauxite. The specimens were tested displacement controlled in pure tension. Average bonding strength was 2.96 MPa (s.d. 0.29 MPa) for the specimens with granite and 4.81 MPa (s.d. 0.45 MPa) for the specimens with bauxite (Braam, 2002-b), (Buitelaar, 2004-b).

Shear strength interface concrete – steel deck plate

The shear strength in the interface concrete – steel deck plate were measured by three-point bending tests of steel deck plates with a bauxite sprinkled epoxy layer and a HPC overlay of 50 mm. The average shear strength was 11.2 MPa with the Norwegian granite and 12.5 MPa with the bauxite (Braam, 2002-b), (Buitelaar, 2004-b). Figure 6-17 shows this three-point bending test.

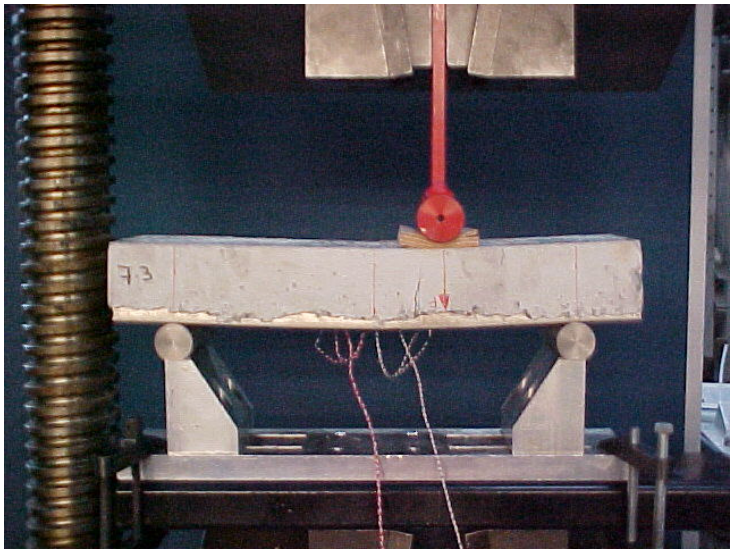

Figure 6-17 – Three-point bending test to determine the shear strength

Frost/thaw resistance in combination with de-icing chemicals

One side face of cubes, age 28 days, was exposed to a 3% (m/m) NaCl-solution and subsequently subjected to 12 hour cycles during which the temperature of a water bath varied

from –20 ºC to +20 ºC (RILEM, 1996). After 14 cycles a weight loss of 0.9-8.4 g/m^2 was found (average 3.6 g/m^2). The loss is small when compared with ordinary Portland cement mixtures, for which a loss of several kg per m^2 is found (Braam, 2003-b), (Buitelaar, 2004-b).

Chloride ion penetration

Cubes were placed in a NaCl solution (165 g/l). After core-drilling, slices were sawn and tested according to a standardized procedure (Nordtest, 1995). After 1, 6 and 12 months of exposure, chemical analyses demonstrated that when the amount of naturally available chloride was taken in account no chloride penetration could be detected (Braam, 2003-c), (Buitelaar, 2004-b).

6.5 Application tests reinforced high performance concrete

Before application of the RHPC surfacing to a bridge deck in a highway the appropriateness of the system for this application should be proved hence the laboratory tests and calculations described in the previous paragraphs. Besides the calculations and laboratory research there are also aspects related to the application and execution on a larger scale to be considered. To investigate these aspects two large application tests on a total area of 80 m^2 were performed.

6.5.1 Test set up

Two test areas were made on parts removed from the old Van Brienenoord bascule bridge. The bascule bridge was renewed in 1998 after detection of cracks in 1997, and the old bascule part was kept for research projects (Van der Weijde, 1998, 1999).

6.5.1.1 Application test 1

The first test area was prepared in October 2000. The area of the test surface was 60 m^2 (6 x 10 m) divided into two sections, each 30 m^2. Section one was treated with the epoxy layer sprinkled with bauxite, as described in the previous paragraph. On the other section, the concrete was cast on the steel deck plate without an intermediate layer. On this section there was not enough adhesion between the steel and concrete, as already stated in the previous paragraph.

The steel deck plate was shot blasted to Sa 2.5, and followed in section 1 by the application of an epoxy primer. Then the two-component epoxy layer sprinkled with calcinated bauxite 3-6 mm was applied. After the intermediate epoxy bonding layer had hardened the unbonded bauxite granules were removed, because unbonded granules are weak points in the connection between concrete and epoxy.

A galvanized edge-profile 50 x 50 mm was laid on the deck plate at the border of the test area. This edge-profile also functioned as a guide for the vibrating screed. A reinforcement bar ∅ 8 mm spaced at 500 mm is used as a vertical spacer. This spacer was laid out in the longitudinal direction of the bridge deck, i.e. the direction of the troughs. Subsequently the reinforcement in 3 layers ∅ 8 mm spaced at 50 mm was laid out. The direction of the bottom layer of reinforcement bars was transverse, the direction of the middle layer longitudinal and the direction of the top layer transverse.

The welded mesh reinforcement had not been produced automatically, but by hand. Due to this the distance between the single reinforcement bars was not always exactly 50 mm. At the overlap between reinforcement meshes this led to some problems with the placement of the meshes. Figure 6-18 shows this problem. This photograph was taken at the section where no intermediate epoxy bonding layer was applied. The overlap in the bottom and the top layer of the reinforcement were at the same location. This should be avoided in order to prevent problems with compacting the concrete.

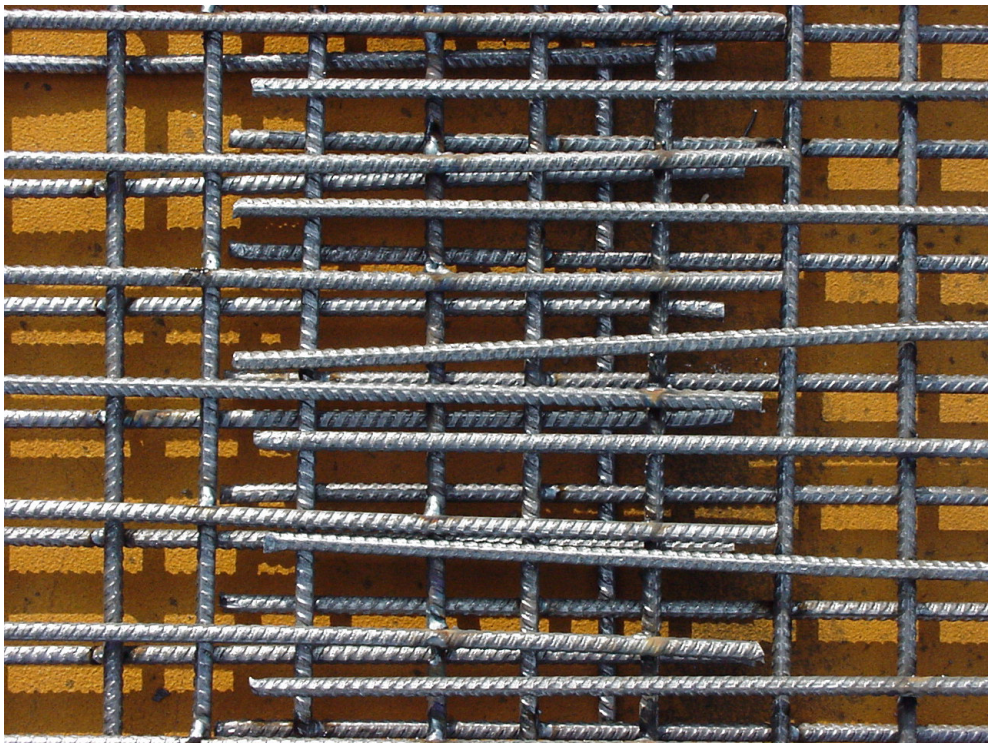

Figure 6-18: Bad quality of overlap mesh reinforcement at section without epoxy layer

Figure 6-19: Compacting with vibrating screed on test area 1

Figure 6-20: Power floating surface on test area 1

After control of the reinforcement the high performance concrete was cast. The concrete had strength class C110 and was reinforced with steel fibres and acrylic fibres. For the application tests the mortar was the same as the mortar used for the laboratory tests. Only the amount of steel fibres differs slightly. After the concrete was cast it was compacted with a double electrically driven vibrating screed, see Figure 6-19. The last step in the application test was power floating. This was done in order to create a very dense surface and to reduce shrinkage, see Figure 6-20. When the power floating was finished the test area was covered with plastic foil, to prevent evaporation of water.

After a few weeks cracks in the concrete overlay became visible. A number of drill cores were taken from the concrete overlay. This showed that the compaction of the mortar was not optimal. The wet concrete had not completely flowed into the interface between concrete and the epoxy layer. Air inclusions in the interface were detected and later research showed that some of the hammers of the vibrating screed were defective. This must have resulted in a lack of vibration energy.

6.5.1.2 Application test 2

The second test area was prepared in July 2001. Figure 6-21 shows application test area 2.

Figure 6-21: Application test area 2

The area of the second test surface was 12 m^2. The first test had shown problems in achieving a good compaction of the concrete overlay. The second test was intended to research the possibility of achieving good compaction and adhesion between concrete and bauxite layer if more vibration energy was applied. The difference from the first test was the compacting equipment. A double pneumatic high frequency vibrating screed was used in the second application test.

A number of drill cores were taken from the concrete overlay and visual inspection of these showed that good compaction had been achieved. The reinforcement bars were fully embedded in the concrete and no air inclusions were detected in the bauxite-concrete interface. Also on the second test area a small part of the interface has not been provided with the bauxite sprinkled epoxy layer, to check again if good adhesion between RHPC and the steel deck plate can be achieved without it. From the drill cores it was evident that the epoxy layer is necessary.

6.5.2 Concluding remarks

A few conclusions can be drawn from the applications tests.

- It is important that sufficient vibration energy is applied to the wet concrete in order to achieve a good compaction and avoid air inclusions. There are no quantitative measurements of the applied energy.
- The dimensions of the reinforcement mesh should be produced exactly at the nominal value. This will avoid problems with the placing of the reinforcement and with the compaction at overlap locations.
- It is not possible to predict the time needed for application of a RHPC surfacing on a real bridge on basis of these application tests.

6.6 Static tests at bridge panels with RHPC

Besides the FE-models and the tests on small specimen tests were performed on full-scale bridge deck test panels with a RHPC surfacing. Two test panels were used. The so-called TNO panel, as this panel is subjected to tests at the laboratory of TNO and test panel A with RHPC, subjected to tests at the university. Both panels are subjected to static tests as well as to fatigue tests. The fatigue tests are described in paragraph 6.7.

6.6.1 Static tests at TNO panel with RHPC

Figure 6-22 gives the test panel that was used for the tests at TNO. The static and fatigue tests are extensively reported by Van Straalen (Van Straalen, 2002-a). This test panel was cut from

application test panel 2, see paragraph 6.5.1.2. All the tests on the TNO panel were performed on the part treated with the bauxite sprinkled epoxy layer.

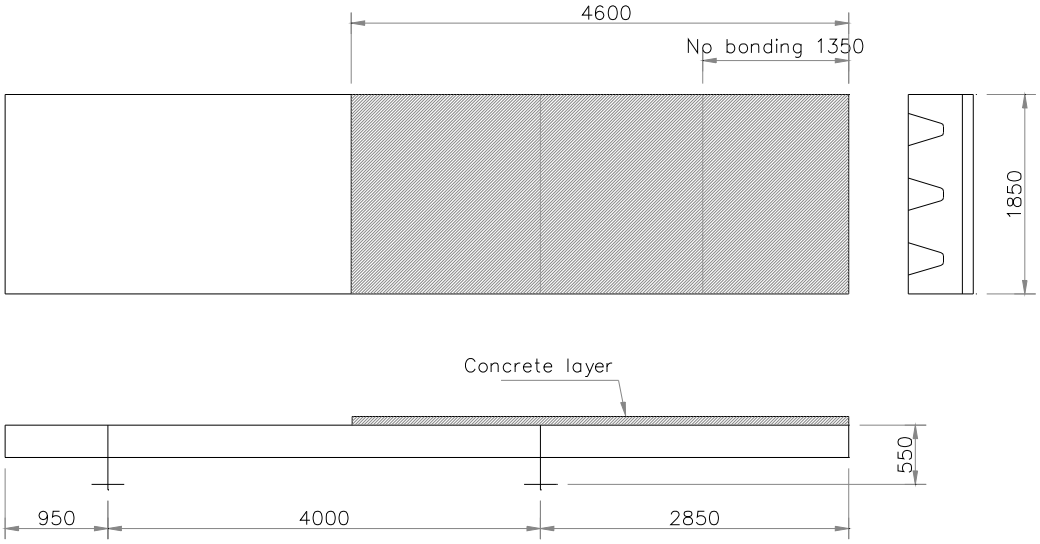

Figure 6-22: TNO panel for static and fatigue tests with RHPC surfacing

The wheel load was placed on an area of 270 mm wide and 320 mm long, which is the super single tyre (type C), see paragraph 3.2.1. This load was placed exactly symmetrically above the crossing of the middle trough and the crossbeam. Figure 6-23 shows this load set up.

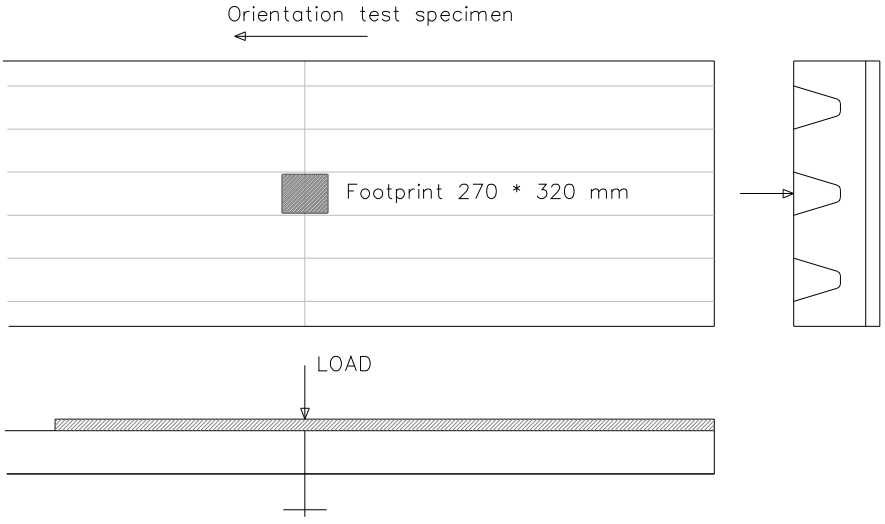

Figure 6-23: Location wheel load on TNO panel

The footprint differs from the footprint on the FE-models, see paragraph 6.3.1.1, as on the FE-models the footprint of the single tyre (type A, 220 mm wide) is used. From research with the

Lintrack it became clear that the footprints of the single and the super single result in approximately the same stresses, see paragraph 4.4.5.5. The same holds true for the static tests with different footprints at test panel A before application of the RHPC surfacing. See paragraph 4.2.2.2 for a comparison of the single (test BA1_S3) and the super single (test BA1_S8). Therefore it is possible to compare the results of the FE-models in paragraph 6.3.1.1 with the measurements in this paragraph.

6.6.1.1 Strain gauges at test panel

Strain gauges were applied on the bridge deck test panel. Figure 6-24 shows a cross-section of the strain gauges, Figure 6-25 shows a top view of the strain gauges on the underside of the deck and trough web and Figure 6-26 shows a top view of the strain gauges at the top of the concrete surfacing. Be aware that these figures are not on scale. The majority of the strain gauges measure in the transverse direction and only a few in the longitudinal direction.

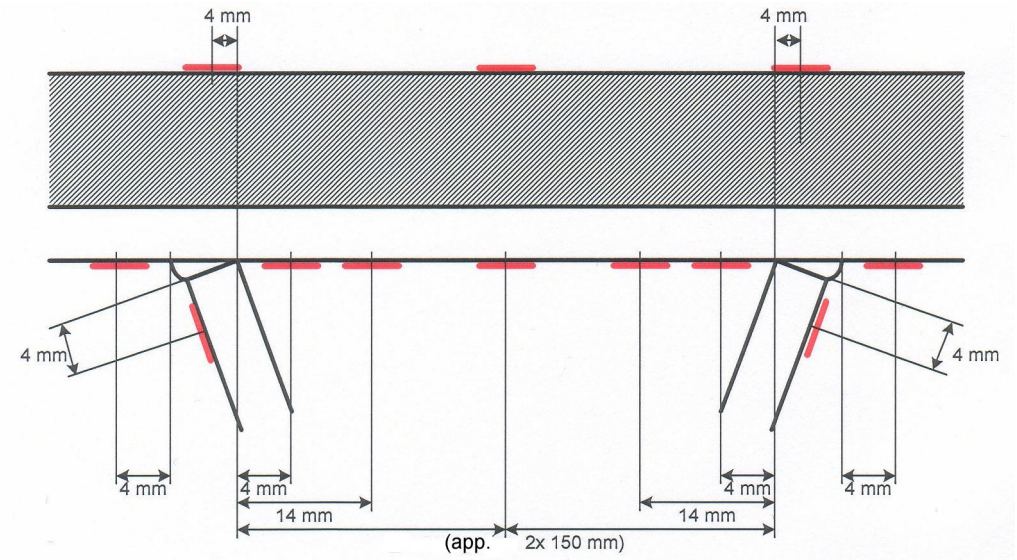

Figure 6-24: Cross-section strain gauges (not on scale)

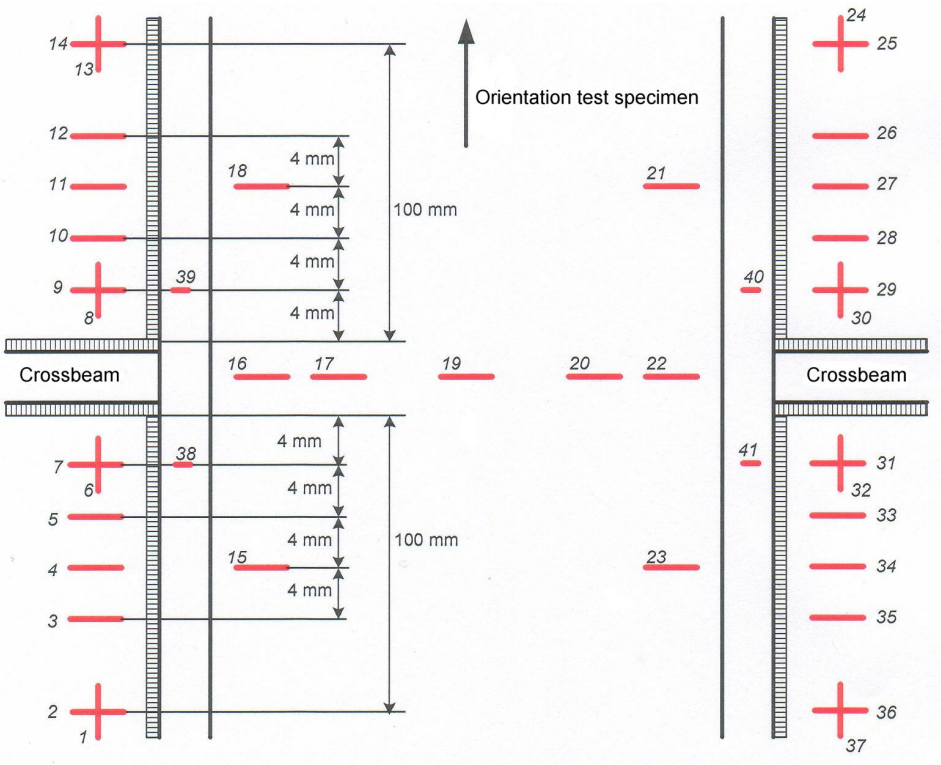

Figure 6-25: Top view of strain gauges at underside deck plate & trough web (not on scale)

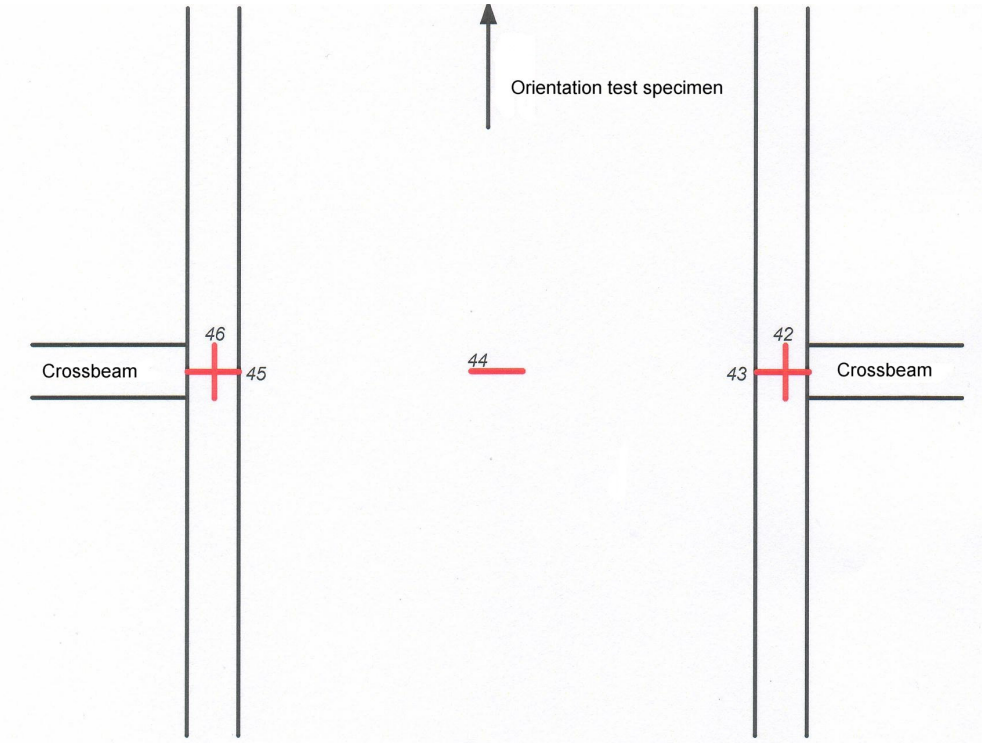

Figure 6-26: Top view of strain gauges at top side of concrete surfacing (not on scale)

The most relevant strain gauges for the determination of the stress reduction at the fatigue prone location are those that are attached at the underside of the deck plate, within the trough web and in line with the crossbeam. These strain gauges are numbered 16, 17, 19, 20 and 22.

6.6.1.2 Loading procedure

A load of 117 kN was applied 11 times. Subsequently 5 equal load cycles were applied. In one load cycle the load was in 5 equal steps set from 12 kN to the maximum load of 117 kN (12 – 33 – 54 – 75 – 96 – 117 – 96 – 75 – 54 – 33 – 12 kN). The results of these 5 load cycles are given in Figure 6-27, for the strain gauges 16, 17, 19, 20 and 22.

Figure 6-27 shows that only the strains for gauge 19 were exactly the same for all 5 load cycles. For the other strain gauges the measured strains for the five load cycles differed somewhat from each other. Analysis of the data however has shown that the measured strain range (from 12 to 117 kN) was nearly equal for all 5 load cycles. Table 6-6 gives the measured strain range ($\Delta\varepsilon$) at the load difference (ΔF) of 105 kN.

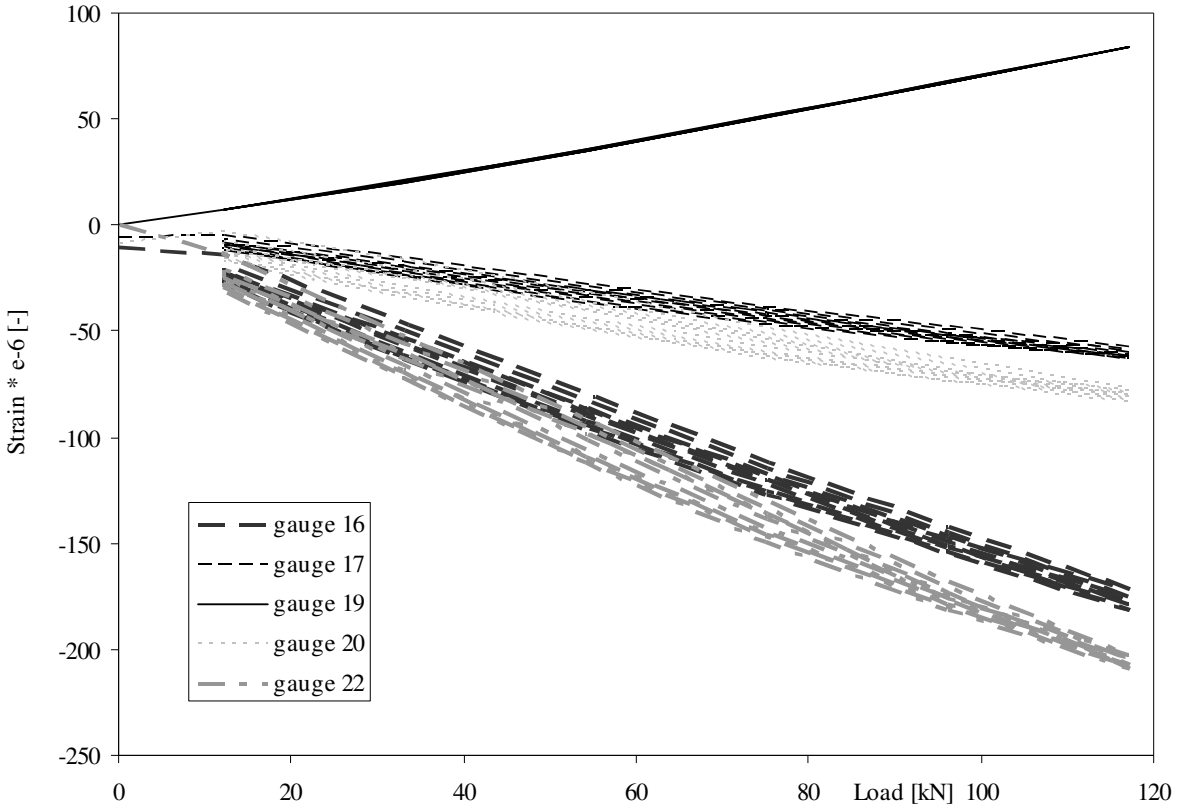

Figure 6-27: Results static loading procedure

Table 6-6: Measured strain range ($\Delta\varepsilon x10^{-6}$) at ΔF 105 kN (12-117 kN)

Cycle\gauge	16	17	19	20	22
1	-158	-53	77	-74	-189
2	-156	-52	77	-71	-184
3	-155	-52	77	-69	-183
4	-156	-53	77	-69	-183
5	-156	-52	77	-70	-182
Average	-156.2	-52.4	77	-70.6	184.2

6.6.1.3 Evaluation of measurements

A few comments on the results of the measurements:

- The difference between gauges 16 and 17 is relatively large, as well as the difference between the gauges 20 and 22. Considering the distance of 10 mm between 16 and 17 and between 20 and 22, it can be concluded that there is a high strain gradient. This is in accordance with the FE-models in presented paragraph 6.3.1 and in accordance with the measured strain gradient, see paragraph 4.2.2.2.
- The strain gradient between the gauges 16 and 17 is $10.38x10^{-6}$/mm. The strain gradient between the gauges 20 and 22 is $11.36x10^{-6}$/mm.
- Linear extrapolation of the strains to the crack locations leads to a strain of $-197x10^{-6}$ at the side of gauges 16 and 17 and to a strain of $-230x10^{-6}$ at the side of the gauges 20 and 22.
- Linear interpolation of the strains to the location at 12.5 mm from the reference line in Figure 6-24 leads to strains of $–68x10^{-6}$ at the side of gauges 16 and 17 and to $-88x10^{-6}$ at the side of the gauges 20 and 22. The position at 12.5 mm is the location of the strain gauges on test panel A with RHPC.
- It is also obvious that the strains at the side of gauges 16 and 17 are significantly lower than those at the side of strain gauges 20 and 22.
- There are two possible explanations for this difference. It can be assumed that the strain gauges at the side of gauges 20 and 22 are located somewhat more towards the crack location. Only a small deviation from the theoretical position can result in significant differences in the measured strains. Another possibility that explains the difference is that the wheel load was not placed exactly above the middle of the trough.

6.6.2 Static tests at test panel A with RHPC

6.6.2.1 Introduction

This paragraph describes static tests that were performed on test panel A after application of a RHPC surfacing. Before application of the RHPC surfacing 6 fatigue cracks were made in

the deck plate. This test panel is described in paragraph 4.2.2. The fatigue tests that were performed on this test panel are described in paragraph 4.3.3.

These cracks were not repaired before application of the RHPC surfacing. The results of the static and fatigue tests that were performed should give an answer to the question of whether it is possible to apply a RHPC surfacing directly on a bridge deck with fatigue cracks that have already grown through the deck plate. If this is possible, the repair of detected fatigue cracks can probably be abandoned, up to the length of fatigue cracks in the test. This saves time and money at the application.

The purpose of the static and fatigue tests was to determine the static and fatigue behaviour of the RHPC surfaced bridge deck with unrepaired fatigue cracks in the deck plate and compare it to the behaviour of an RHPC surfaced bridge deck without cracks.

6.6.2.2 Test panel A with RHPC surfacing

Static tests were performed on test panel A with a RHPC surfacing. Before application of the RHPC surfacing test panel A was used before for static and fatigue tests. The result of the fatigue test on the unsurfaced test panel A is a bridge deck test panel with 6 deck plate cracks with a length of 136 up to 208 mm, see Table 4-10, on the top surface of the deck plate. See Figure 4-33, Figure 4-36 and Figure 4-37 for photographs of these cracks.

These six cracks were all grown through the thickness of the steel deck plate. These cracks were not repaired before application of the RHPC surfacing. The main difference between the two test panels is that RHPC surfacing was applied to a deck without cracks (TNO panel), and to a deck with fatigue cracks (Test panel A with RHPC).

This means that on test panel A, only the application steps 4 to 9 as described in paragraph 6.2, were performed namely shot blasting the surface of the steel deck plate to Sa 2.5, applying an epoxy layer with bauxite aggregate (3-6 mm), removing the unbonded bauxite granules, applying reinforcement in 3 layers ∅8 mm spaced at 50 mm and, casting the concrete HPC strength class C110, reinforced with steel fibres and acrylic fibres and compacting, power floating and curing the surface in order to create a very dense surface. After curing a plastic foil was applied for 6 weeks to prevent evaporation of water.

Figure 6-28, Figure 6-29 and Figure 6-30 show the application process of the RHPC surfacing on test panel A.

Figure 6-28: Epoxy layer sprinkled with bauxite aggregate on test panel A

Figure 6-29: Mesh reinforcement & casting RHPC on test panel A

Figure 6-30: Test panel A with RHPC surfacing directly after power floating

6.6.2.3 Strain gauges

Many strain gauges had been attached to the top of the steel deck plate for the static and fatigue tests on the unsurfaced bridge deck. See Figure 4-3 and Annex C for these strain gauges. They were all removed before the application of the RHPC surfacing, because they and their connecting cables might disrupt the composite action between the steel and RHPC and it was necessary to allow shot blasting of the deck plate. This meant that the strain gauges could not be attached to the top surface of the steel deck plate but were attached to the underside instead. Strain gauges were attached to the top of the RHPC surfacing. To allow accessibility parts of the troughs were cut out, see Figure 6-31. The pieces that were cut out were welded back after the application of the strain gauges and before testing. Figure 6-32 depicts the strain gauges that were applied at the underside of the deck plate at trough 2. The strain gauges are all mounted in the transverse direction perpendicular to the weld.

Figure 6-31: Accessibility underside deck plate to attach strain gauges

Strain gauges on the underside of the steel deck plate were applied near the trough web on both sides of the trough and midspan between the two trough webs. At each of the four crack tips a pair of gauges was mounted. The location of these gauges is derived from the crack tip location. Figure 6-33 gives these locations. The location of the strain gauges at the crack tip is chosen from the results of the first fatigue test that was performed on panel A without surfacing. If the fatigue crack grows in longitudinal direction, during the fatigue test with RHPC surfacing, the strain ranges during the fatigue test will change.

From research it is known that the crack length at the bottom of the deck plate is approximately 2 to 4 times the deck plate thickness longer than the length on top, see paragraph 2.3.2. Therefore it was assumed that the fatigue cracks at the underside at both crack tips were 15 mm longer than the measured length on the top side of the deck plate, which is given in table Table 4-9. In general one strain gauge was placed at the crack tip location and the other strain gauge was placed 20 mm away from this assumed location. After the first fatigue test on test panel A, see paragraph 4.3.3, ultrasonic inspection of the underside fatigue cracks was performed (Bakker, 2003). Based on the results of this inspection and the ultrasonically determined crack lengths the location of some gauges was changed a little. Differences of up to 10 mm from the assumed location of the crack tip occur.

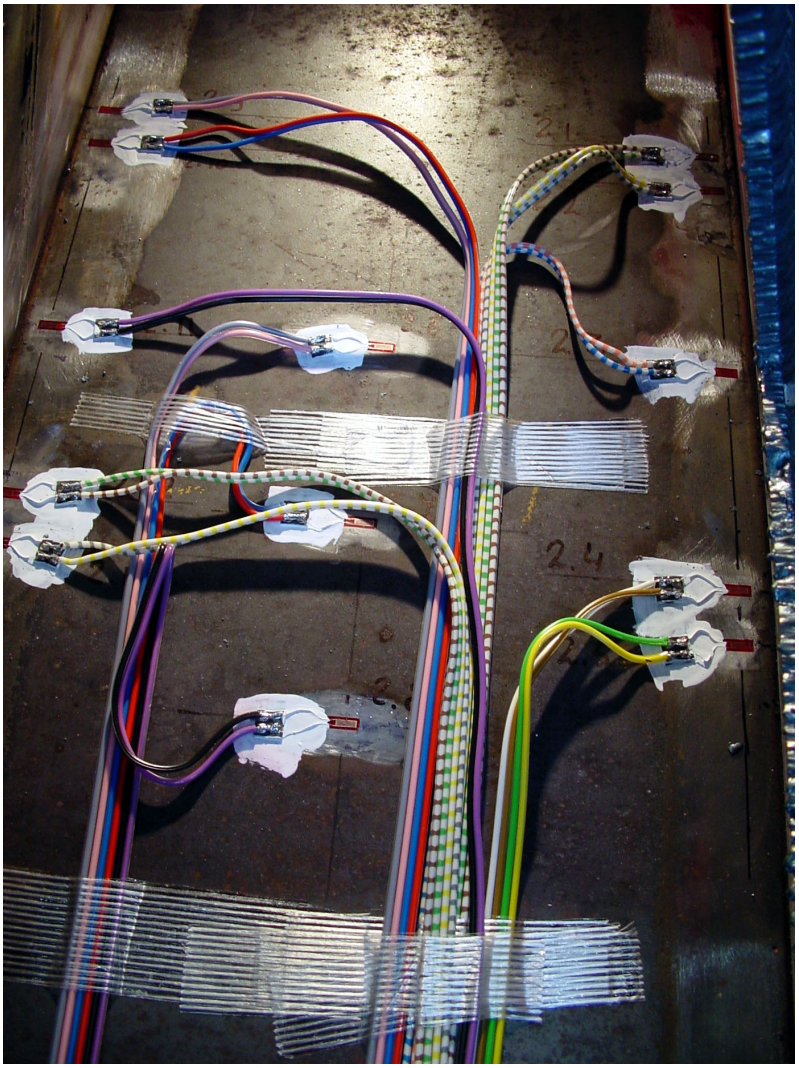

Figure 6-32: Strain gauges at underside deck plate of trough 2

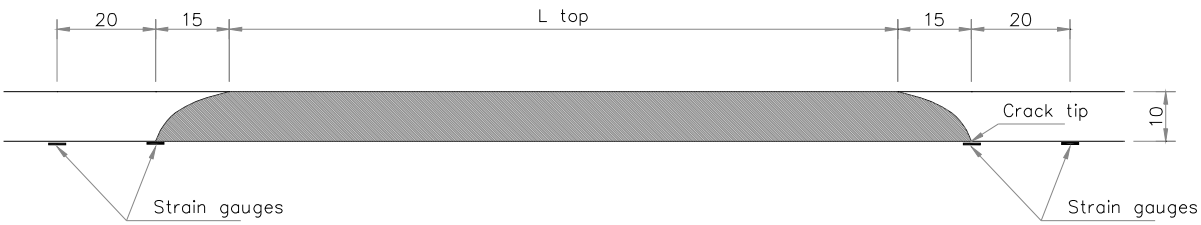

Figure 6-33: Location of strain gauges near crack tip

Figure 6-34 gives a schematic overview of the strain gauges that were applied to the steel deck plate. Figure 6-35 gives a schematic overview of the strain gauges that were applied at the top of the concrete surfacing. Annex F gives the strain gauges for trough 1 and 3.

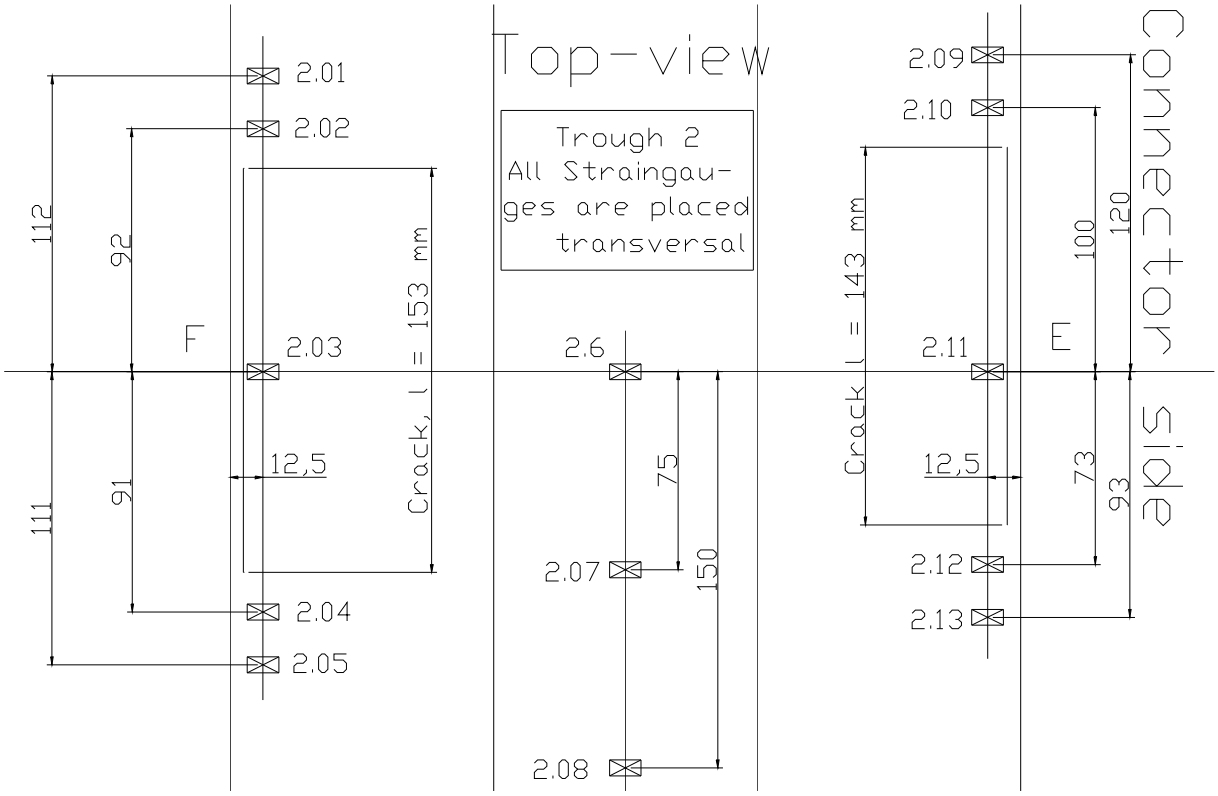

Figure 6-34: Top view of strain gauges at underside deck plate at trough 2

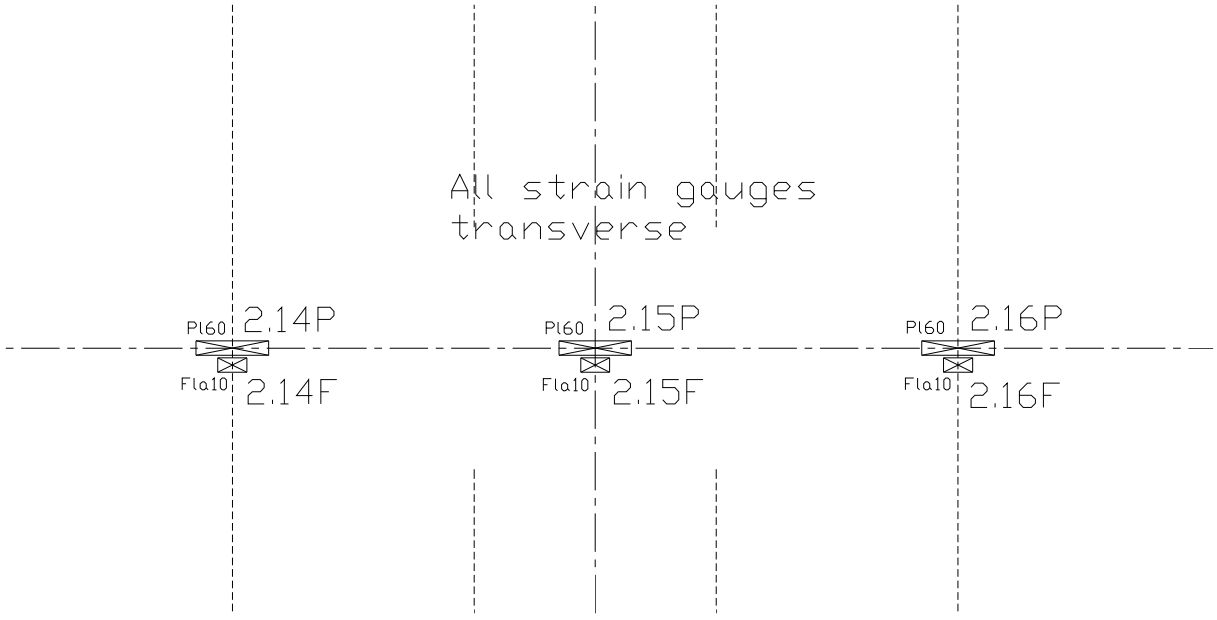

Figure 6-35: Top view of strain gauges at top side RHPC surfacing at trough 2

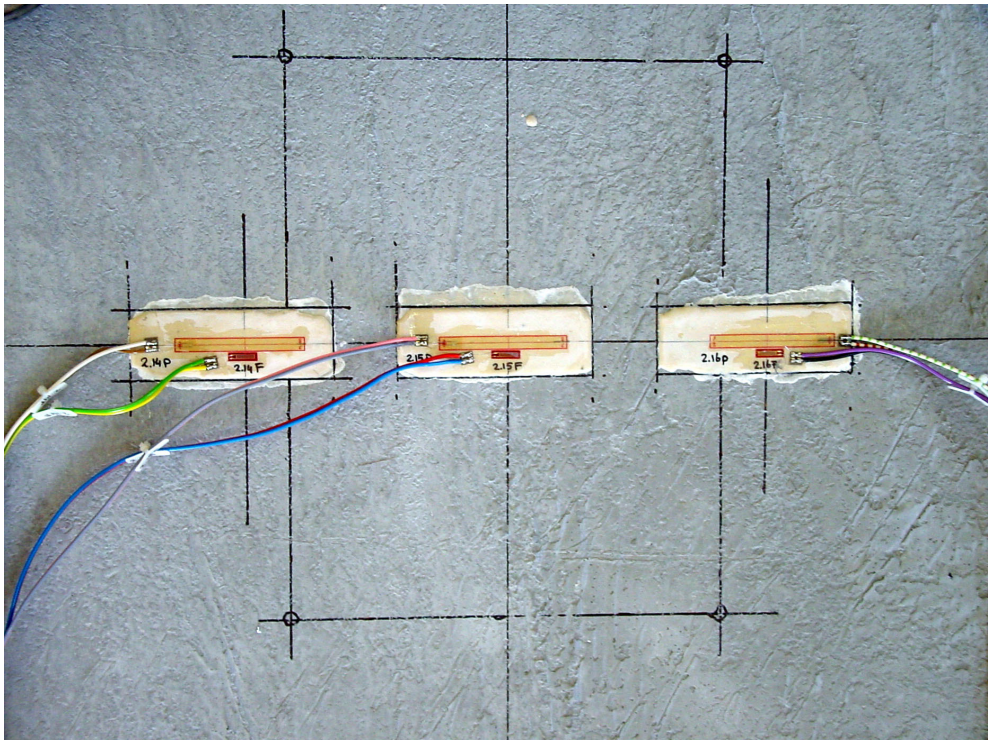

Figure 6-36: Strain gauges at top side RHPC surfacing of trough 2

Figure 6-36 shows the strain gauges on the top of the RHPC surfacing. The gauges were applied above both trough webs and midspan between the trough webs. At each location the strain gauges were duplicated, one was a long gauge of approximately 60 mm (PL-60), and one a short gauge of approximately 10 mm (FLA-10). These two types were applied to assure the reliability of the measurement.

6.6.2.4 Testing program

The load application was exactly the same as in figure 4-5. The footprint used for the static test was 270 mm wide and 320 mm long. This is the footprint of the super single, tyre type C. The rectangle in Figure 6-36 is the location of this footprint.

Three loading procedures were applied to each of the three troughs:

1. 5 times loading and unloading with $F_{min} \approx 0.2$ kN and $F_{max} = 49$ kN (0 – 49 – 0 – 49 – 0 – 49 – 0 – 49 – 0 – 49 – 0 kN). F_{max}, and the footprint for this first loading procedure were chosen at the same level as the static test BA1_S8, reported in paragraph 4.2.2.2. With a very large reduction expected, this load, was expected only to generate small stresses in the test panel.
2. 11 times loading and unloading with $F_{min} \approx 0.2$ kN and F_{max} from 50 kN up to 150 kN. For each cycle F_{max} was raised by 10 kN. (0 – 50 – 0 – 60 – 0 – 70 – 0 – 80 – 0 – 90 – 0 – 100

– 0 – 110 – 0 – 120 – 0 – 130 – 0 – 140 – 0 – 150 – 0 kN). The idea was that the test load slowly increased.

3. 5 times loading and unloading with $F_{min} \approx 0.2$ kN and $F_{max} = 150$ kN (0 – 150 – 0 – 150 – 0 – 150 – 0 – 150 – 0 – 150 – 0 kN)

For all three procedures loading and unloading was performed at 1 kN/sec. Between loading and unloading the load was held for 5 minutes at F_{max}. Between unloading and loading the load was held for 5 minutes at F_{min} which was slightly above 0 kN to prevent separation of the contact surface.

6.6.2.5 Test results

The test results are presented for the static tests at trough 2 and results for troughs 1 and 3 that differ significant from trough 2 are discussed. A total test report can be found in (De Jong, 2006-a).

Figure 6-37 shows the applied load on trough 2 according to loading procedure 1. This applied load was measured with a load cell.

Figure 6-38 shows the results from the strain gauges on the steel during loading procedure 1 at trough 2.

Figure 6-39 shows the results from the strain gauges attached at the RHPC surfacing during loading procedure 1 at trough 2.

Figure 6-40 shows the results from the strain gauges at the steel during loading procedure 2 at trough 2. Figure 6-41 shows the results from the strain gauges attached at the RHPC surfacing during loading procedure 2 at trough 2.

Figure 6-42 shows the results from the strain gauges at the steel during loading procedure 3 at trough 2. Figure 6-43 shows the results from the strain gauges attached at the RHPC surfacing during loading procedure 3 at trough 2.

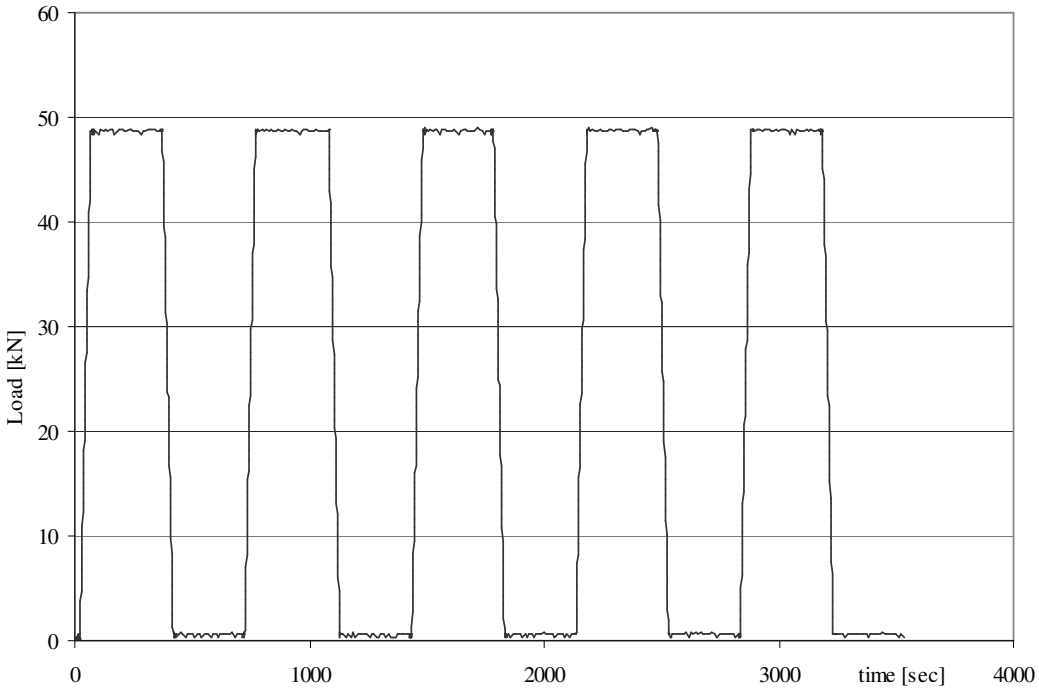

Figure 6-37: Loading procedure 1 at trough 2 ($F_{min} \approx 0.2$ kN and $F_{max} = 49$ kN)

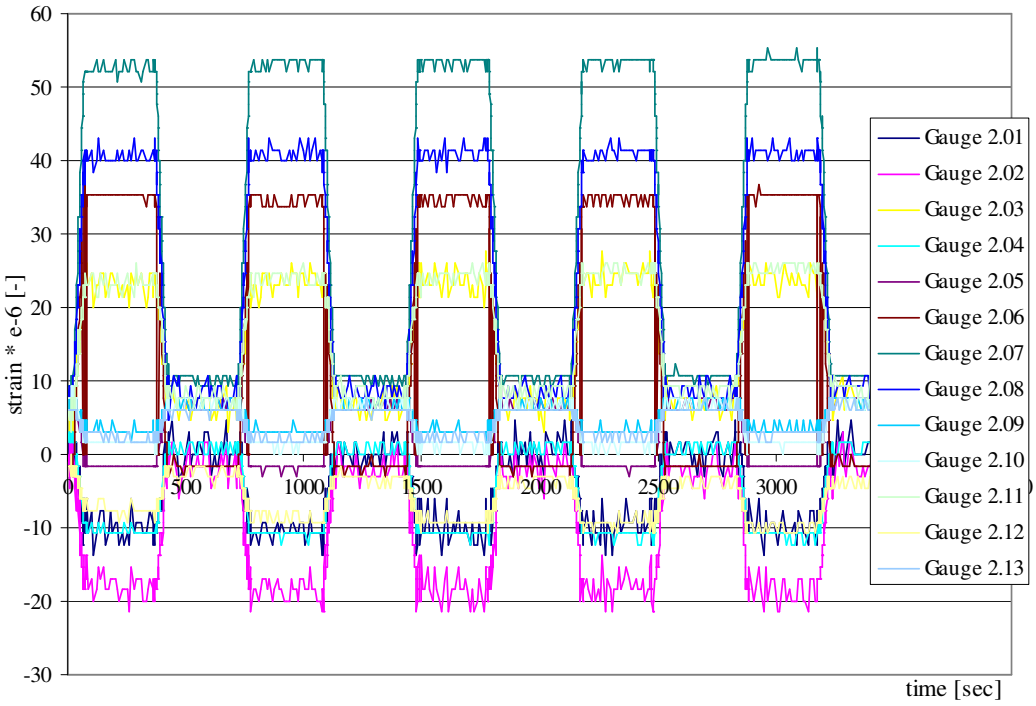

Figure 6-38: Results strain gauges on steel for loading procedure 1 at trough 2

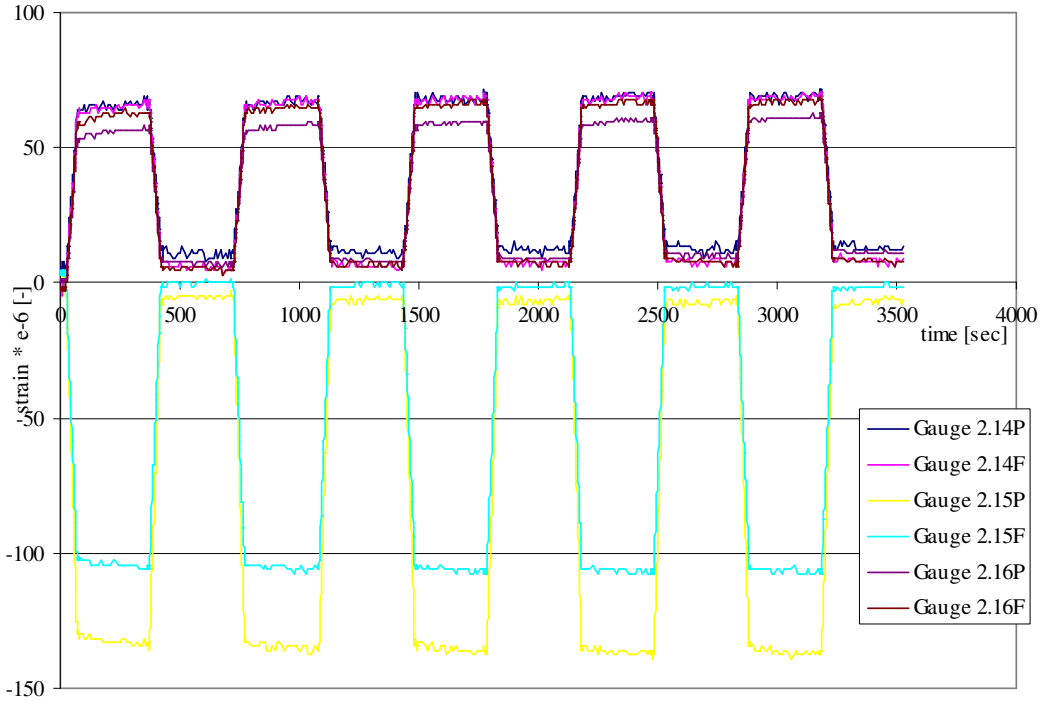

Figure 6-39: Results strain gauges on RHPC surfacing for loading procedure 1 at trough 2

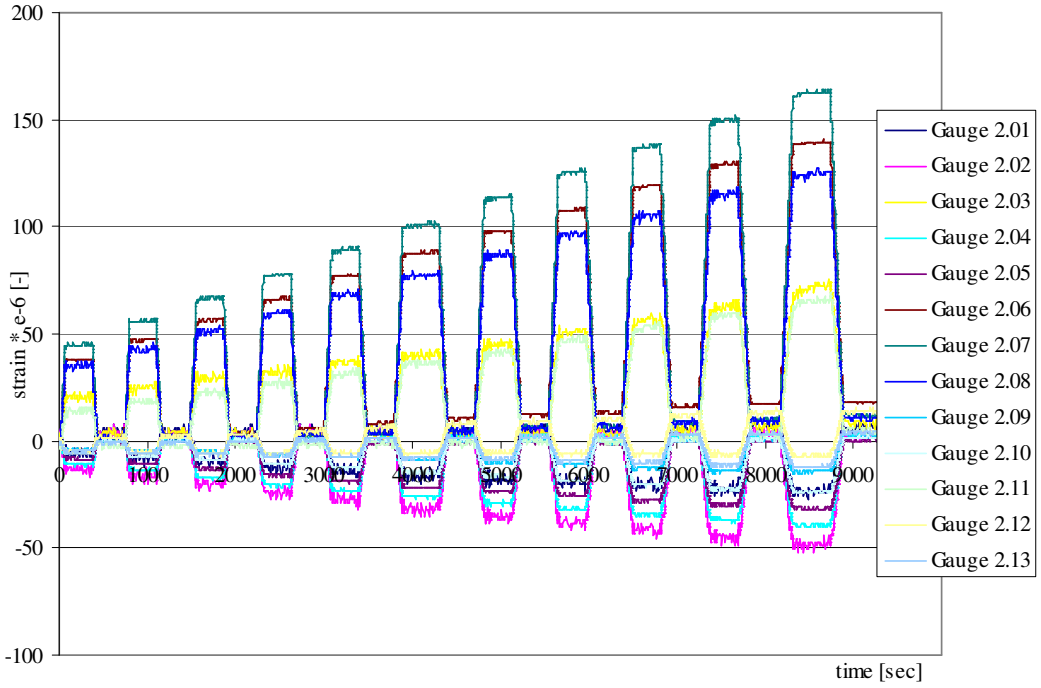

Figure 6-40: Results strain gauges on steel for loading procedure 2 at trough 2

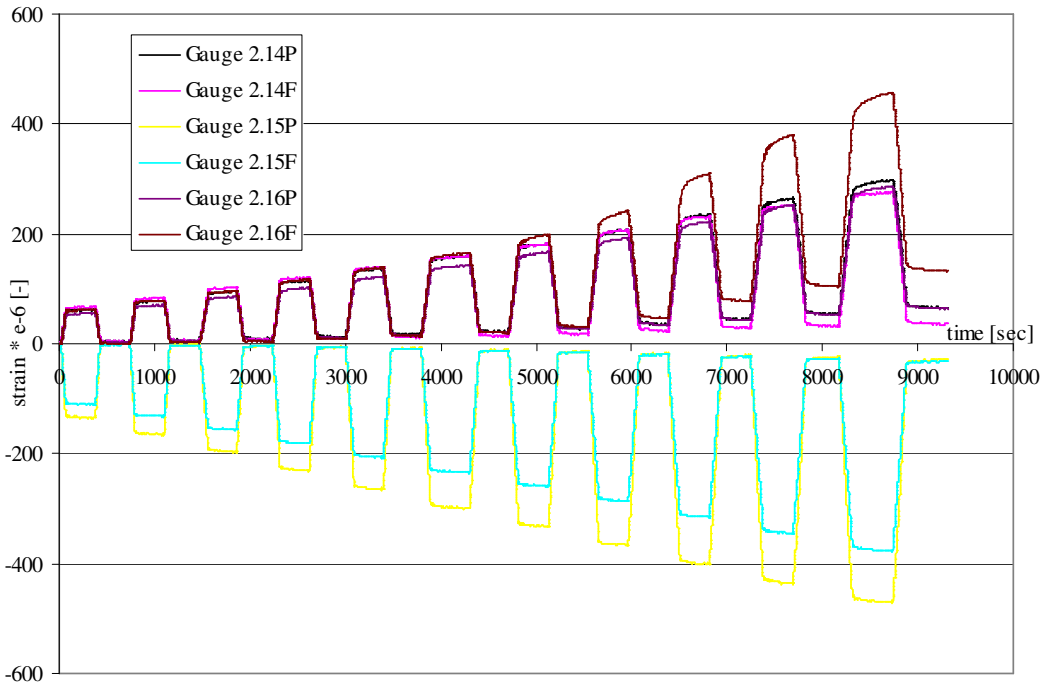

Figure 6-41: Results strain gauges on RHPC surfacing for loading procedure 2 at trough 2

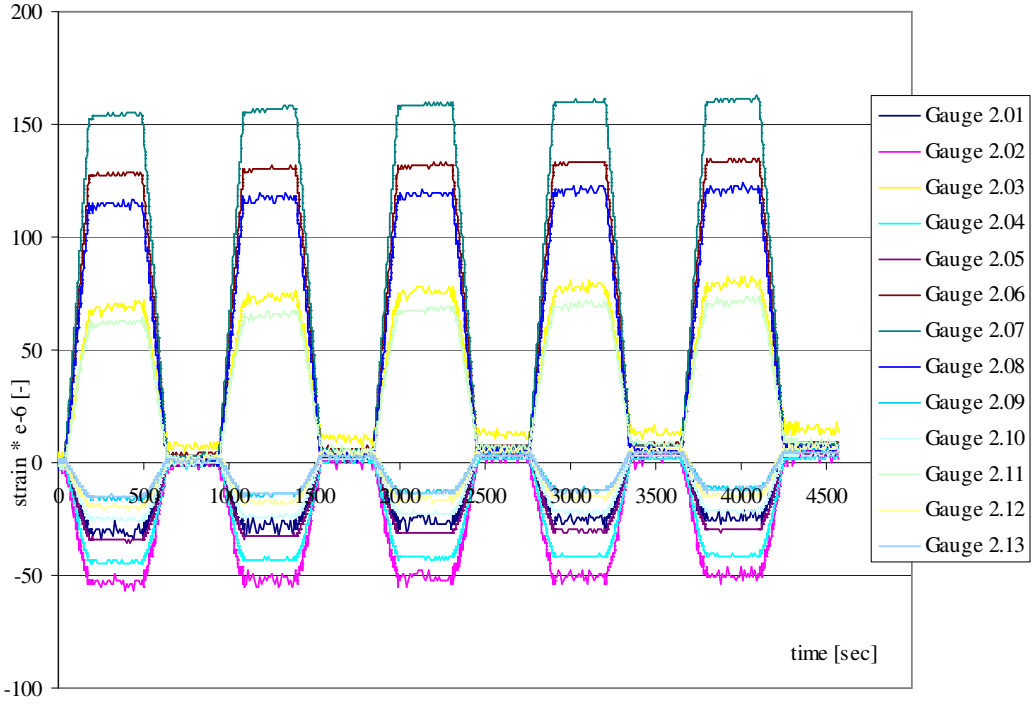

Figure 6-42: Results strain gauges on steel for loading procedure 3 at trough 2

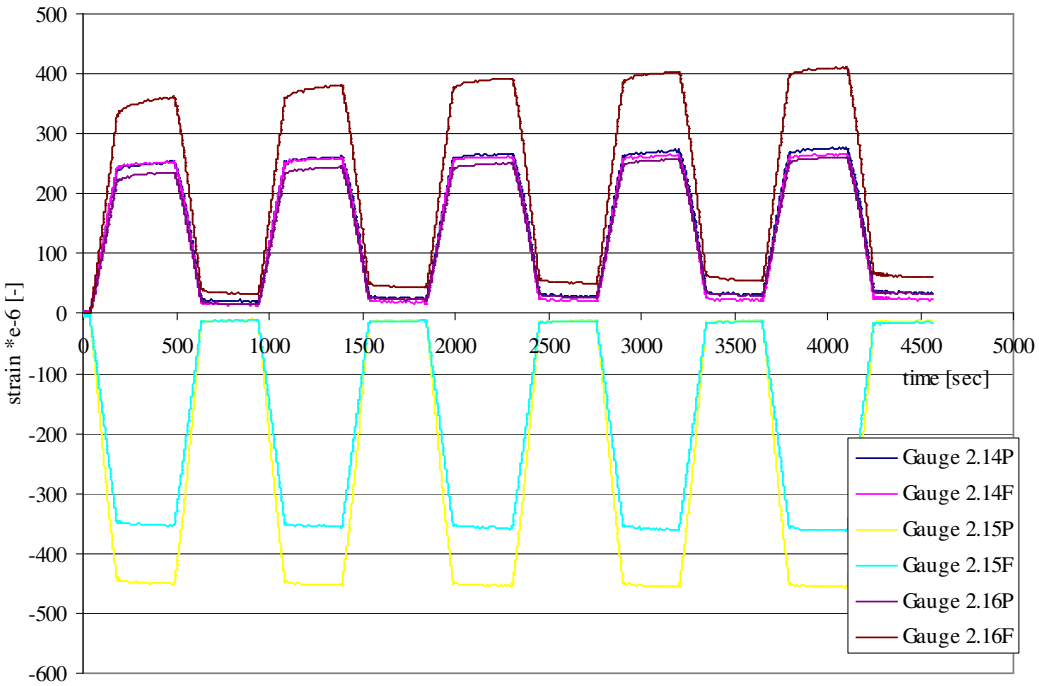

Figure 6-43: Results strain gauges on RHPC surfacing for loading procedure 3 at trough 2

6.6.2.6 Discussion and conclusion

With respect to the measured strains in the gauges on the steel:

- In general the values of the strains at the bottom of the steel are very low with these high wheel loads.
- Strains at the four cracks tips at the underside of the steel deck plate are very low. The strains vary between 0 and approximately -50×10^{-6} (≈ -10 MPa) during loading procedure 3 up to 150 kN, see Figure 6-42.
- Strain gauges 2.03 and 2.11 have measured tensile strains. Normally in a bridge deck without cracks at this location compressive strains are expected. This is probably due to the unrepaired fatigue deck plate crack in the test panel. However the strain gauge results near the cracks tips are all compressive.
- The strain gauges 2.06, 2.07 and 2.08 measured the biggest tensile strain, as it was expected.
- In the results for trough 2 the measured strain in gauges 2.06 is smaller as that in gauge 2.07. It is possible that due to the cracks in the steel deck plate the deck plate at the crossbeam, where gauge 2.06 is mounted, was relatively lightly loaded and the deck plate nearer the crack tips, where 2.07 is mounted, carried more load.

With respect to the measured strains in the gauges at the RHPC surfacing:

- Values of the strain at the RHPC surfacing were significantly higher than the strain at the steel.
- The gauges that were at the RHPC surfacing, PL-60 (60mm) and FLA-10 (10mm) gave different signals. These differences are significant, up to 30%, but they are not due to the type of strain gauges because sometimes a PL-60 gauge measured a bigger range than the FLA-10 gauge and sometimes a FLA-10 gauge measured a bigger range than the PL-60 gauge.
- During loading procedure 2 (F_{max} stepped from 50 kN up to 150 kN) something was happening with the strain gauges at the RHPC surfacing. When F_{max} was reached the strains were still growing. This phenomenon was most clearly visible during loading procedure 2, but also seen loading procedure 3. Note that at the start of loading procedure 3 strains are set to 0, but that at F_{min} during loading procedure 3 significant strains were measured, see Figure 6-43. The measured strains during loading procedure 1 do not show this phenomenon.
- It might therefore be assumed that during loading procedure 2 some kind of cracking or microcracking occurs in the RHPC surfacing, which influences the measured strains in the surfacing.
- This phenomenon is not observed in the strain gauges at the bottom of the steel deck plate.

The measured strains on test panel A with unrepaired fatigue cracks are comparable to the strains in the TNO panel without any cracks in the deck plate, see paragraph 6.9. It can be concluded that with respect to the static strains it is not necessary to repair the fatigue cracks in the deck plate. Repair is not necessary to avoid crack growth. It should be verified that the deck plate acting as top flange of the crossbeam, has sufficient capacity, with unrepaired cracks, if not the cracks have to be repaired.

A comparison of the measured strains at the bridge deck with the RHPC surfacing and the measured strains in exactly the same test panel before application of the RHPC surfacing can be made. Based on this comparison a conclusion can be drawn on the effectiveness of the RHPC surfacing layer.

The tests before application of the RHPC surfacing were reported in paragraph 4.2.2.2. Test BA1_S8 has the same loading and footprint as loading procedure 1 in this paragraph although strain gauges are not located in exactly the same locations. However two strain gauges can be compared. Strain gauge 2.06 is attached to underside of the steel deck plate where strain gauge 2.24, see Figure 4-3, from the previous test is attached to the top of the steel deck plate. Because in the previous test the deck plate was unsurfaced it can be assumed that the strains on top and bottom at this location are the same, although with opposite signs. The results of strain gauges 1.06 and 3.06 are also taken into account in the comparison, because they are attached on identical locations at troughs 1 and 3. The stress reduction factors are also given in this comparison. The stress reduction factor is taken as the stress with RHPC surfacing divided by the stress without any surfacing.

The measured strains at this location on the test panel without RHPC surfacing are:

- -481×10^{-6} (see Table 4-2 BA1_S8, gauge 2.24)

And on the test panel with RHPC surfacing are:

- 55×10^{-6} (gauge 1.06), stress reduction factor = 0.11
- 38×10^{-6} (gauge 2.06), stress reduction factor = 0.08
- 55×10^{-6} (gauge 3.06), stress reduction factor = 0.11

6.7 Fatigue tests at bridge panels with RHPC

6.7.1 Fatigue test at TNO panel with RHPC

After the static test, reported in paragraph 6.6.1, a fatigue test was performed. This test was performed in the laboratory of TNO. The test was reported by Van Straalen (Van Straalen, 2002-a, 2002-b). The wheel load (270 x 320 mm, width x length) was again centered above

the trough at the location of the crossbeam, see Figure 6-23. Figure 6-44 gives a photo of the fatigue test. In total 8.4×10^6 load cycles were applied in 4 steps, according to Table 6-7.

Figure 6-44: Full-scale fatigue test at test panel with RHPC surfacing.

Table 6-7: Loading fatigue test TNO panel with RHPC

Step	Nr of cycles	F_{min} (kN)	F_{max} (kN)	ΔF (kN)
1	4.2×10^6	12	117	105
2	1.4×10^6	15	152	137
3	1.4×10^6	19	187	168
4	1.4×10^6	23	233	210

Calculations (De Jong, 2006-b) have shown that this load set-up equals:

- 70 years of fatigue according to fatigue load model 4 from Eurocode 1991-Part 2
- 52 years of heavy vehicle traffic on the Moerdijk Bridge, with respect to fatigue of the steel deck plate. The Moerdijk Bridge is the most heavily loaded bridge deck in the Netherlands.

After the fatigue test an ultrasonic inspection from the underside of the deck plate was performed without detecting any crack in the steel deck plate. The conclusion is that the

replacement of the asphalt surfacing by a RHPC surfacing is a promising solution with respect to the fatigue life of orthotropic steel bridge decks.

During the fatigue test the static loading procedure as described in paragraph 6.6.1.2 was repeated 188 times. Figure 6-45 depicts the measured strain ranges for these static loading procedures.

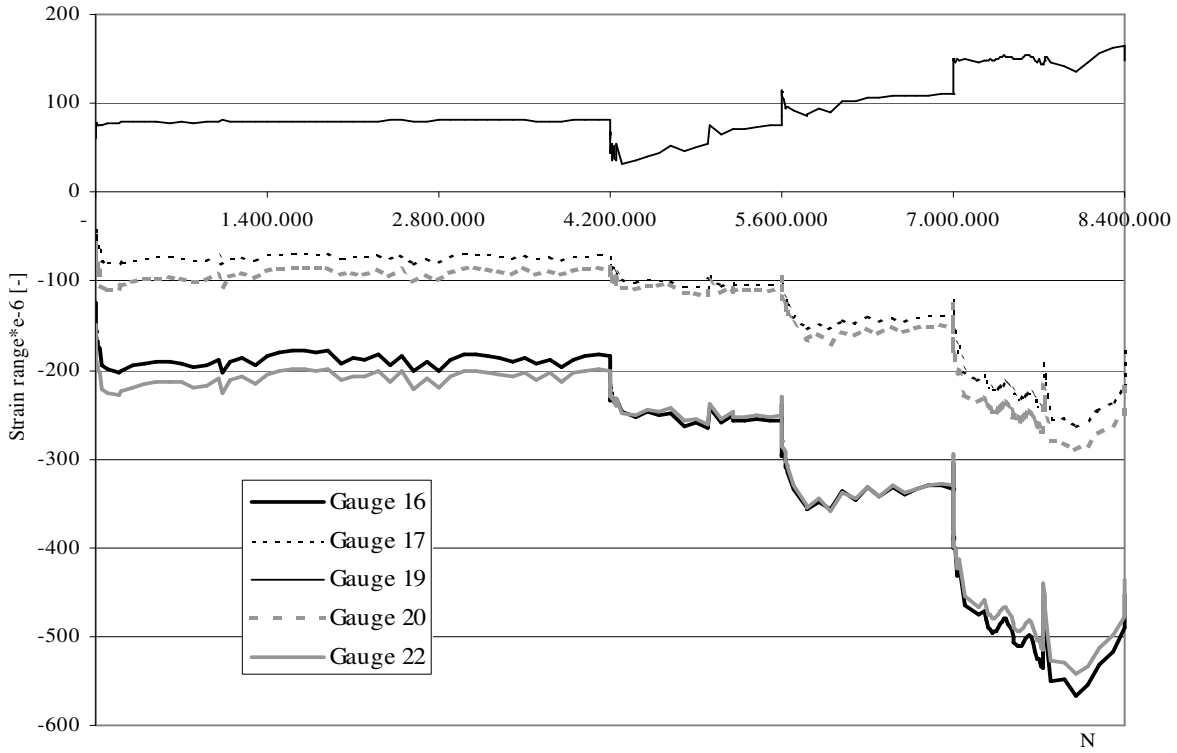

Figure 6-45: Results - some strain ranges on steel during fatigue test on TNO panel

Some remarks on this figure:

- The four phases in the fatigue test are clearly visible
- The strain ranges of the 4 gauges located towards the crack location (16,17, 20 and 22) increase when the load is increased in the subsequent test steps. Figure 6-24, Figure 6-25 and Figure 6-26 show the strain gauges.
- However the strain range for gauge 19 decreases significantly at 4.2×10^6 cycles at the beginning of step 2
- At the end of the last phase at 8.4×10^6 cycles the strain range for gauge 19 is approximately 2 times the range during the first test phase (up to 4.2×10^6 cycles), in line with the increase in the load from 105 kN to 210 kN
- From the start of phase 2 (4.2×10^6 cycles) to the end of phase 4 (8.4×10^6 cycles) the

strain range for gauge 19 increases by approximately a factor 3, from $50x10^{-6}$ up to $160x10^{-6}$. The load range however only increases by a factor 1.54 from 137 kN up to 210 kN.

- There was a period of several months between the end of the first phase and the start of the second phase at $4.2x10^6$ cycles. This could have had an effect on the measured ranges.

6.7.2 Fatigue tests on test panel A with RHPC

6.7.2.1 Introduction

Subsequent to the static test reported in paragraph 6.6.2 test panel A with RHPC surfacing was subjected to fatigue tests. The test panel and strain gauges have already been described. All three troughs were subjected to a fatigue test. During the fatigue test on each trough a few static measurements were performed with loading procedure 3 as described in paragraph 6.6.2.4.

6.7.2.2 Testing program

Approximately 10^7 load cycles were applied on each trough. On trough 1 in total $10.36x10^6$, on trough 2 in total $9.45x10^6$ and on trough 3 in total $8.65x10^6$ cycles were applied, as shown in Table 6-8. Calculations (De Jong, 2006-b) have shown that this load set-up equals:

- 163, 157 and 165 years of fatigue for trough 1, 2 and 3 respectively, according to fatigue load model 4 from Eurocode 1991 - Part 2
- 118, 113 and 119 years, for trough 1, 2 and 3 respectively, of heavy vehicle traffic on the Moerdijk Bridge, with respect to fatigue of the steel deck plate. The Moerdijk Bridge is the most heavy loaded bridge deck in the Netherlands.

Table 6-8: Loading fatigue test panel A with RHPC.

Trough	Step	No of cycles	F_{min} (kN)	F_{max} (kN)	ΔF (kN)
1	1	$6.45x10^6$	10	160	150
1	2	$3.9x10^6$	10	235	225
2	1	$5.47x10^6$	10	160	150
2	2	$3.98x10^6$	10	235	225
3	1	$2.5x10^6$	10	160	150
3	2	$5.15x10^6$	10	235	225

During the fatigue test static test procedure 3 (5 times loading and unloading with $F_{min} \approx 0.2$ kN and $F_{max} = 150$ kN (0 – 150 – 0 – 150 – 0 – 150 – 0 – 150 – 0 – 150 – 0 kN) was applied a few times on each trough. Table 6-9 summarizes these static tests during the fatigue test.

Table 6-9: Static loading procedure during fatigue test at test panel A with RPHC

Trough	No.	After no. of cycles
1	1	0
1	2	$2.34x10^6$
1	3	$6.46x10^6$
1	4	$1.036x10^7$
2	1	$4.2x10^5$
2	2	$2.02x10^6$
2	3	$4.14x10^6$
2	4	$9.45x10^6$
3	1	0
3	2	$2.34x10^6$
3	3	$2.53x10^6$
3	4	$4.57x10^6$
3	5	$8.65x10^6$

Trough 2 was the first trough tested. This trough was tested separately at a frequency of 2.7 Hz. To accelerate the fatigue tests troughs 1 and 3 were initially tested at the same time. Figure 6-46 shows the initial test configuration for these troughs. However the hydraulic equipment could not handle this and the maximum frequency was only 1.0 Hz. Therefore after $2.5x10^6$ stress cycles the test configuration was changed and trough 1 and 3 were tested separately, trough 1 first followed by trough 3, both with a testing frequency of about 2.7 Hz.

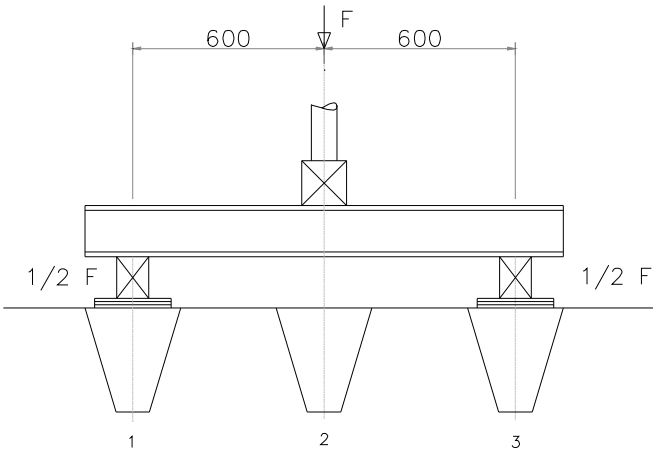

Figure 6-46: Initial fatigue test set-up for troughs 1 and 3 up to $2.5x10^6$ cycles

6.7.2.3 Test results

The results of the fatigue tests at panel A with RHPC surfacing are depicted in 6 figures. For all three troughs the strain ranges of the strain gauges on the steel and on the concrete surfacing are depicted. Figure 6-47 (steel) and Figure 6-48 (RHPC) give the measured strain ranges at trough 1, Figure 6-49 (steel) and Figure 6-50 (RHPC) for trough 2 and Figure 6-51 (steel) and Figure 6-52 (RHPC) for trough 3.

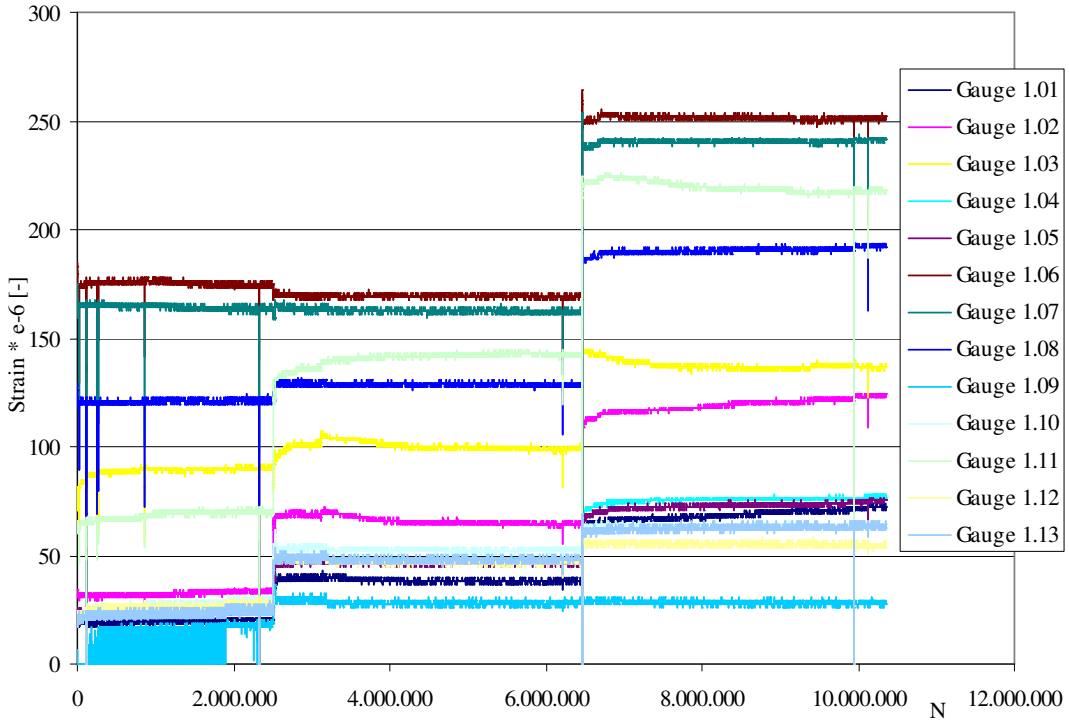

Figure 6-47: Results - strain ranges on steel at trough 1 during fatigue test

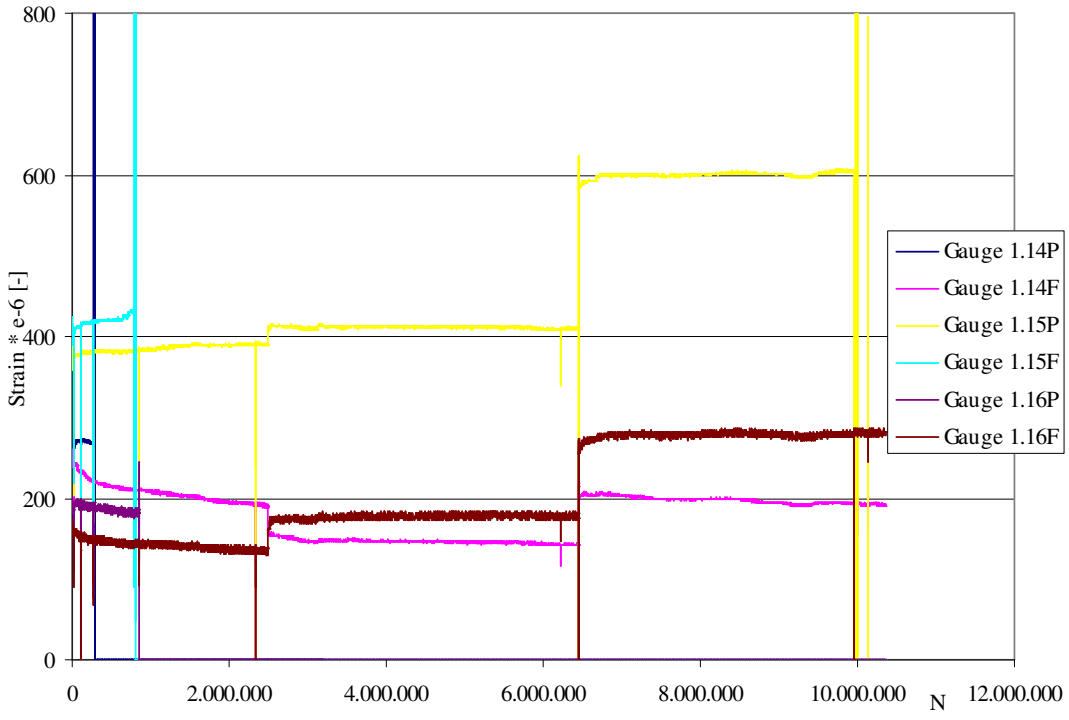

Figure 6-48: Results - strain ranges on RHPC at trough 1 during fatigue test

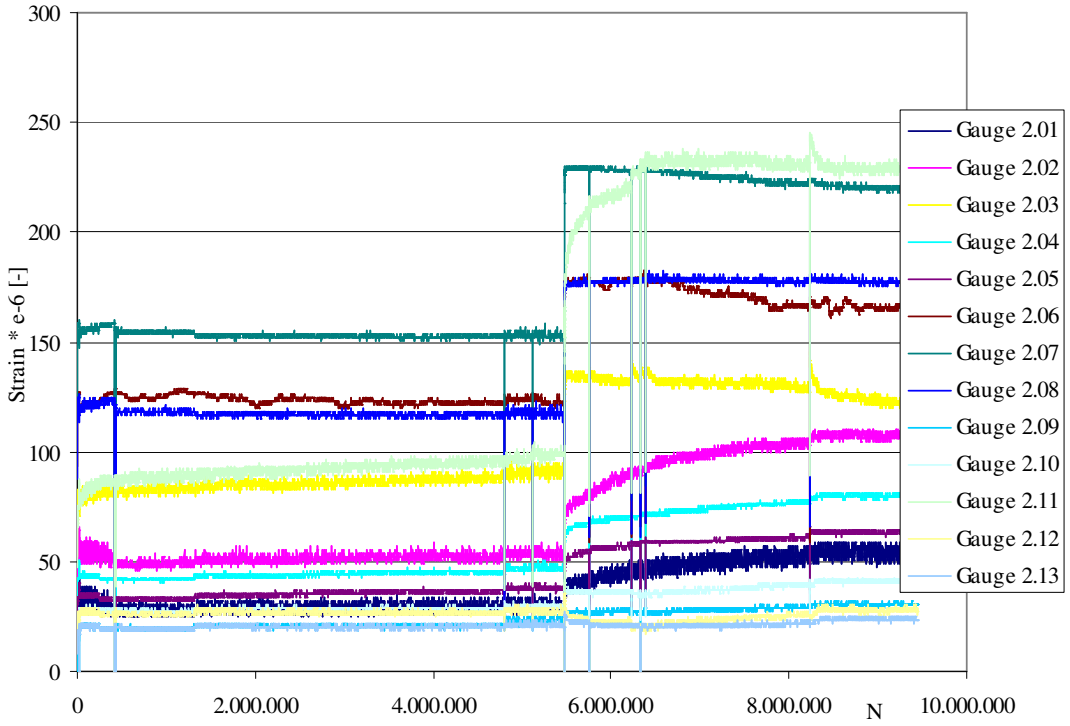

Figure 6-49: Results - strain ranges on steel at trough 2 during fatigue test

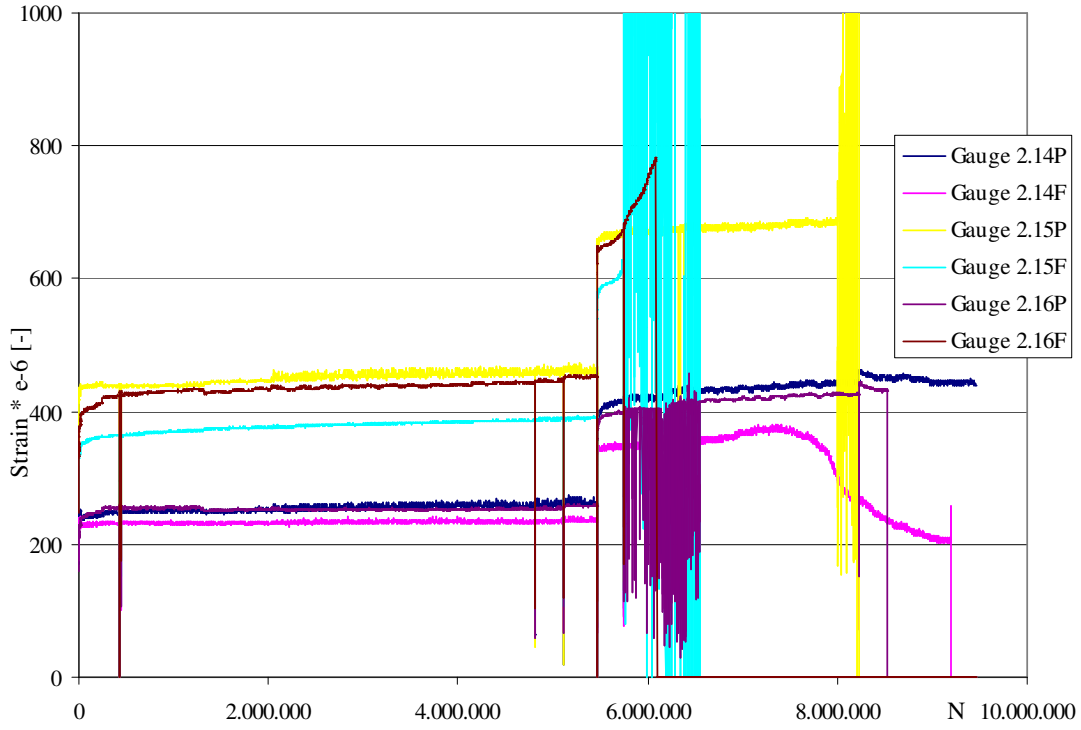

Figure 6-50: Results - strain ranges on RHPC at trough 2 during fatigue test

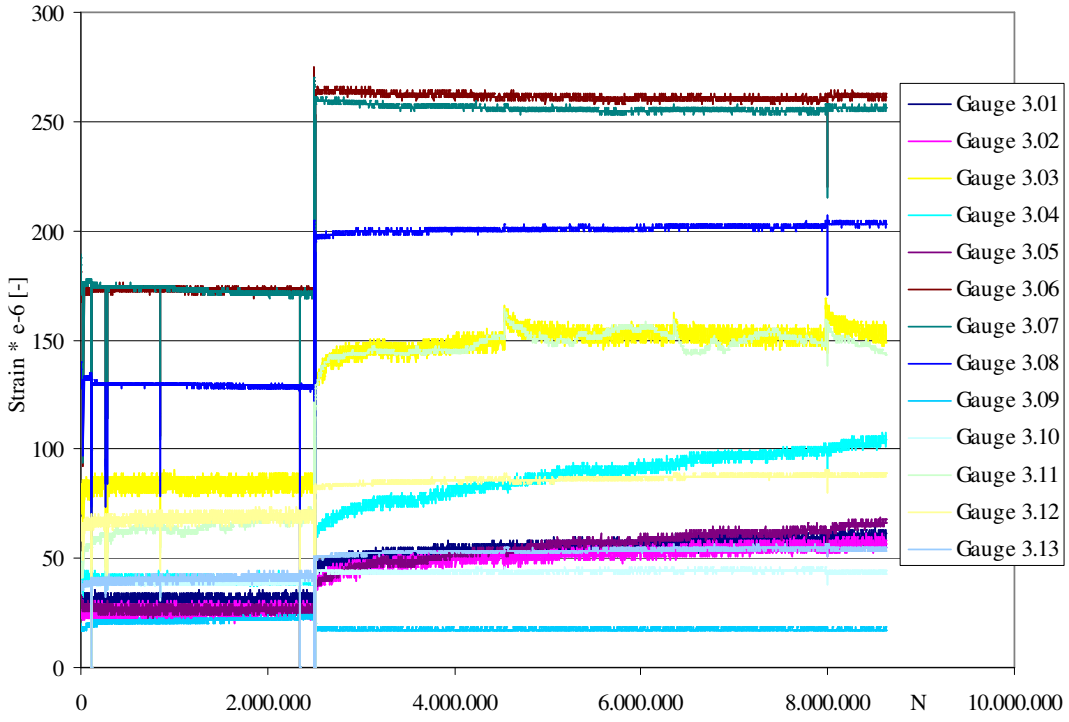

Figure 6-51: Results - strain ranges on steel at trough 3 during fatigue test

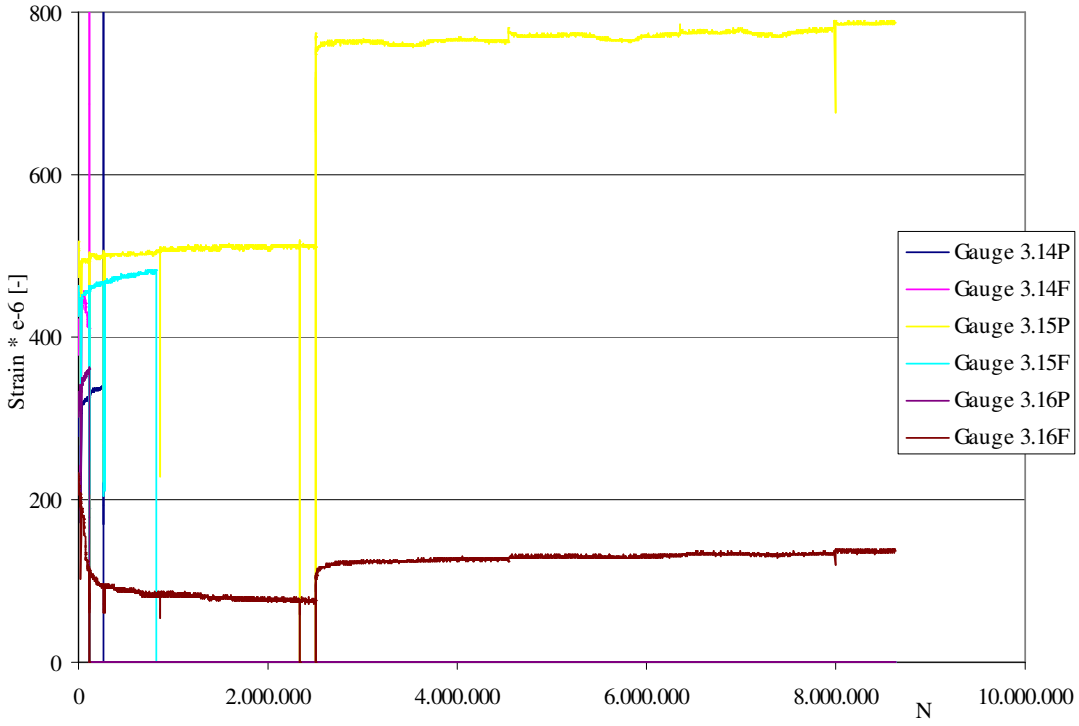

Figure 6-52: Results - strain ranges on RHPC at trough 3 during fatigue test

Figure 6-53 shows the results of the strain gauges attached to the steel during loading procedure 3 at trough 2 at the end of the fatigue test, after 9.45×10^6 cycles. Figure 6-42 shows the results of the same test at the same trough, but performed before the fatigue test. From a comparison it becomes obvious that the strain ranges have changed during the fatigue test.

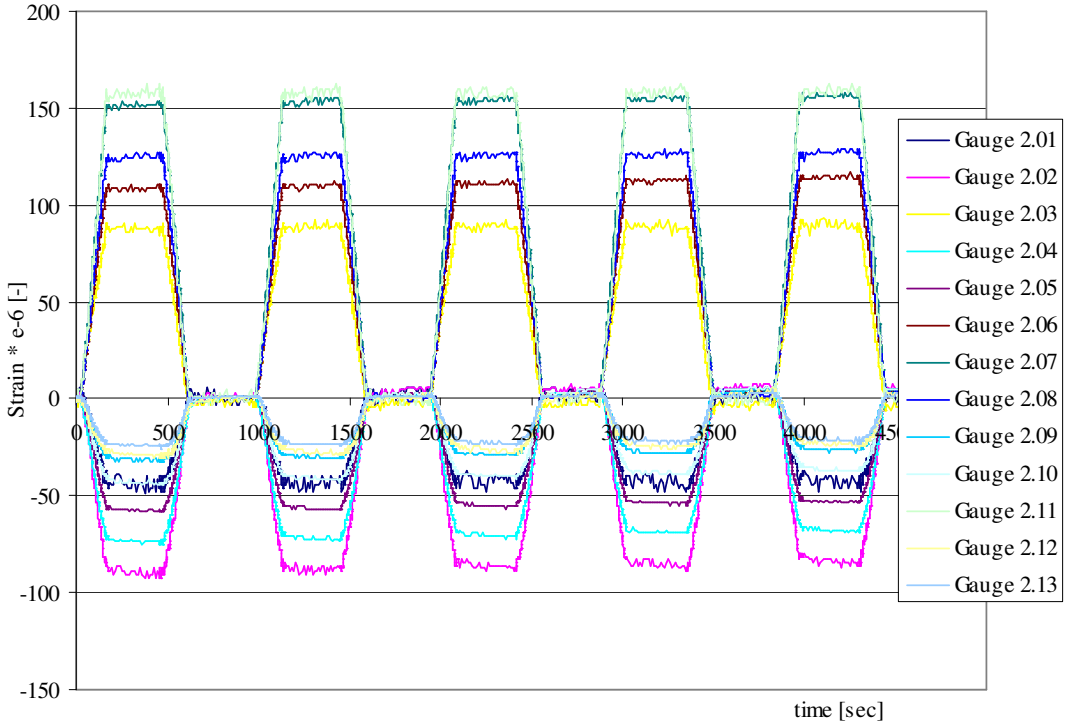

Figure 6-53: Results-strain gauges on steel at static loading procedure 3 at trough 2 after 9.45×10^6 cycles of fatigue test

In order to get a more detailed overview of the changes in measured strains Table 6-10, Table 6-11 and Table 6-12 were made. In these tables the strain ranges are tabulated for all strain gauges for each trough, for three test situations:

1. The static test performed before the fatigue test with loading procedure 3 (F_{max} = 150 kN)
2. The static test performed after the end of the fatigue test with loading procedure 3.
3. The measured strain ranges at the end of the fatigue test. The applied load cycle at the end of the fatigue tests was 225 kN for all troughs. For an easy comparison with the results of both static tests, the strain ranges were linearly calculated back to a load of 150 kN.

The last two columns of Table 6-10, Table 6-11 and Table 6-12 give two ratios:

- Static strain after the end of the fatigue test (2) / Static strain before the fatigue test (1). This ratio gives an idea of the changes in strain due to the effects of the fatigue test

- Strain range at end fatigue test (3) / Static strain after the end of the fatigue test (2). This ratio gives an idea of the effect of the loading frequency, or other effects related to time.

Table 6-10: Strains (ε x 10^6) - trough 1 at 150 kN

Description	Static begin $N = 0$	Static end $N = 10.36x10^6$	Fatigue $N = 10.36x10^6$	Static end (2) /Static begin (1)	Fatigue (3) / Static end (2)
Gauge 1.01	-3	-57	49	18.50	0.86
Gauge 1.02	-6	-97	82	15.75	0.85
Gauge 1.03	74	106	91	1.44	0.86
Gauge 1.04	6	-60	52	-9.75	0.87
Gauge 1.05	2	-58	50	-38.00	0.86
Gauge 1.06	192	174	168	0.90	0.97
Gauge 1.07	181	170	162	0.94	0.95
Gauge 1.08	137	135	128	0.99	0.95
Gauge 1.09	-8	-26	18	3.40	0.71
Gauge 1.10	-23	-52	43	2.27	0.82
Gauge 1.11	71	154	145	2.17	0.95
Gauge 1.12	-23	-48	36	2.07	0.75
Gauge 1.13	-20	-52	42	2.62	0.80

Table 6-11: Strains (ε x 10^6) - trough 2 at 150 kN

Description	Static begin $N = 0$	Static end $N = 9.45x10^6$	Fatigue $N = 9.45x10^6$	Static end (2) / Static begin (1)	Fatigue (3) / Static end (2)
Gauge 2.01	-31	-40	35	1.30	0.87
Gauge 2.02	-54	-89	73	1.66	0.82
Gauge 2.03	66	89	80	1.35	0.90
Gauge 2.04	-45	-74	53	1.66	0.72
Gauge 2.05	-34	-58	43	1.73	0.74
Gauge 2.06	127	109	110	0.86	1.00
Gauge 2.07	152	152	146	1.00	0.96
Gauge 2.08	114	126	118	1.11	0.93
Gauge 2.09	-15	-31	20	2.00	0.67
Gauge 2.10	-25	-43	27	1.75	0.62
Gauge 2.11	61	163	153	2.65	0.94
Gauge 2.12	-20	-29	19	1.46	0.67
Gauge 2.13	-15	-23	15	1.50	0.67

Table 6-12: Strains (ε x 10^6) - trough 3 at 150 kN

Description	Static begin $N = 0$	Static end $N = 8.65\text{x}10^6$	Fatigue $N = 8.65\text{x}10^6$	Static end (2) / Static begin (1)	Fatigue (3) / Static end (2)
Gauge 3.01	-35	-52	41	1.48	0.78
Gauge 3.02	-34	-46	37	1.36	0.80
Gauge 3.03	74	109	102	1.48	0.94
Gauge 3.04	-55	-94	70	1.69	0.74
Gauge 3.05	-37	-66	44	1.79	0.67
Gauge 3.06	183	186	175	1.02	0.94
Gauge 3.07	190	184	171	0.97	0.93
Gauge 3.08	141	144	136	1.02	0.94
Gauge 3.09	5	-17	11	-3.67	0.67
Gauge 3.10	-17	-43	30	2.55	0.69
Gauge 3.11	29	104	95	3.58	0.91
Gauge 3.12	-26	-81	59	3.12	0.73
Gauge 3.13	-11	-51	36	4.71	0.71

6.7.2.4 Discussion and conclusion

With respect to the measured strain ranges in the gauges on the steel:

- The ranges of the measured stresses for all troughs were measured during the whole test. The strain gauges were not damaged by the test. For test 1 and 3 the measured strain ranges are mostly constant, for trough 2 some changes are visible.
- For trough 1 the measured stress ranges change significantly at $2.5\text{x}10^6$ cycles. Due to the fact that the test set up was changed and where the footprint was placed again strain ranges changed. Some ranges decrease and some increase due to the change.
- The point where the load range increased from 150 kN to 225 kN is clearly visible for trough 1. The strain ranges nearly all increase also with a factor 1.5
- For trough 3 the change of the test configuration to separate tests for troughs 1 and 3 and the increase of the load range from 150 kN to 225 kN coincide at $2.5\text{x}10^6$ cycles. For trough 3 this means that some strain ranges increase with a factor less than 1.5 and some increase with a factor larger than 1.5
- The strains for the 8 gauges mounted at the crack tips are in general increased due to the fatigue test. This is evident from the ratio between 'Static strain after the end of the fatigue test (2)' and 'Static strain before the fatigue test (1)'. This observation does not lead to the conclusion that cracks are growing, because the strain ranges of the gauges 1.03, 1.11, 2.03, 2.11, 3.03 and 3.11 all increase comparable.
- The strain range at the end of the fatigue test (3) is smaller than the strain range at the last

static test (2). This is evident from the ratio 'Strain range at end fatigue test (3)' / 'Static strain after the end of the fatigue test (2)' Especially for the 8 gauges mounted at the crack tips this is a significant difference and tends to lead to the conclusion that the effect of the RHPC surfacing is greater if the loading frequency is higher. A greater effect suggests that the stiffness of the RHPC surfacing is dependent on the loading frequency. The loading frequency for the fatigue test is 2.7 Hz (T = 0.37 sec) and for the static tests approximately $1x10^{-3}$ Hz. ($T \approx$ 900-1000 sec). The tests to derive the stiffness modulus of the RHPC surfacing layer did not test this parameter, see paragraph 6.4.2. From literature it is known that the loading frequency is one of the parameters that can influence the stiffness of concrete mixtures

- During the first 500.000 cycles of the fatigue test the measured strain ranges change significantly. After 500.000 cycles the ranges are constant for a longer time. It is thought that these changes in the first phase of the fatigue test are a start phenomenon and that the changes of the ranges between 500.000 cycles and the end of the fatigue test show the real effect of the fatigue test. During the first 500.000 cycles it might be possible that cracks developed in the concrete.

With respect to the measured strain ranges in the gauges at the RHPC surfacing:

- Values of RHPC strain ranges are significantly higher than those attached of the steel.
- During the fatigue test both the small FLA-10 and the long PL-60 gauges on the concrete failed. Both gauges midspan (no. 15) above the trough as well as gauges above the trough webs (nos. 14 and 16) failed.
- From the gauges that did not fail (1.14F, 1.16F, 2.14P, 3.15P, 3.16F) it is clear that the strain ranges hardly changed during the fatigue test.

With respect to the fatigue behaviour:

- The measured strain ranges on test panel A with unrepaired fatigue cracks are about the same as those on the TNO panel without any cracks in the deck plate, see paragraph 6.9. During the fatigue test no crack growth was observed in either test panel and it might be concluded that it is not necessary to repair the fatigue cracks in the deck plate.

6.8 Field measurements - pilot project Caland Bridge

6.8.1 Description project

After the successful full-scale fatigue test on the TNO panel the next step in the development of the RHPC surfacing was application in a real motorway bridge (De Jong, 2004-e). The selected bridge for the first application was the Caland Bridge in the harbour area in

Rotterdam. This bridge is one of the bridges with severe fatigue problems in the deck plate. Besides this replacement of the asphalt surfacing was desirable, see Figure 2-13. The Caland Bridge is a combined railway-roadway bridge. The roadway part has an orthotropic deck structure. The bridge has two fixed spans and a movable part, see Figure 6-54.

Figure 6-54: Caland Bridge in the harbour area of Rotterdam

The fixed parts of this bridge have a deck plate thickness of 10 mm with a mastic asphalt layer of approximately 50 mm thickness and the trough webs are spaced as usual at 300 mm. The spans of the fixed parts are 180 m and 86 m. The movable part of this bridge has a deck plate thickness of 12 mm with a thin epoxy surfacing approximately 7 mm thick. The span of the movable part is 69 m. One direction of the shortest fixed span (86 m) was renovated with a RHPC surfacing. This direction has two traffic lanes. The area of the RHPC surfacing is approximately 650 m^2, 86 m long x 7.6 m wide.

This renovation was done from 29 April 2003 to 4 May 2003. The phases of this renovation project are described in paragraph 6.2. First the mastic asphalt surfacing was removed. After the removal of the asphalt an enclosure was erected over the whole working area to ensure that rain did not cause delay or impair the quality of the concrete surfacing. Subsequently the ultrasonic TOFD inspection was performed, see chapter 8 for this inspection technique. This is a very accurate technique, which can detect small cracks with a height of approximately 2

or 3 mm. The cracks, which were found were identified on the top of the steel deck plate. Some of these cracks had to be repaired and were repaired with the submerged arc welding procedure, see chapter 5. After the repair the new weld was magnetically tested. After the repairs the steel deck plate was shot blasted to Sa 2.5 and immediately the two-component epoxy was applied and sprinkled with bauxite. After the epoxy bonding layer had hardened the unbonded bauxite granules were removed and the mesh reinforcement was placed. Then the concrete was cast on the bridge deck and compacted with a vibrating screed. The thickness of the concrete layer is 60 mm. T-profiles 60 mm high at the edges of the concrete layer supported the vibration screed. The surface was made denser with power floating in order to prevent for shrinkage cracks in the concrete and the concrete was shot blasted for skid resistance. The enclosure was removed and the bridge was opened for traffic. The concrete layer was kept wet for one week after opening for traffic. This was also to minimize the shrinkage. Figure 6-55 to Figure 6-70 show the renovation of the Caland Bridge.

Figure 6-55: Caland Bridge

Figure 6-56: Removing asphalt

Figure 6-57: Removing asphalt

Figure 6-58: Placing covering

Figure 6-59: Ultrasonic TOFD inspection

Figure 6-60: Detected fatigue crack

Figure 6-61: Submerged arc welding

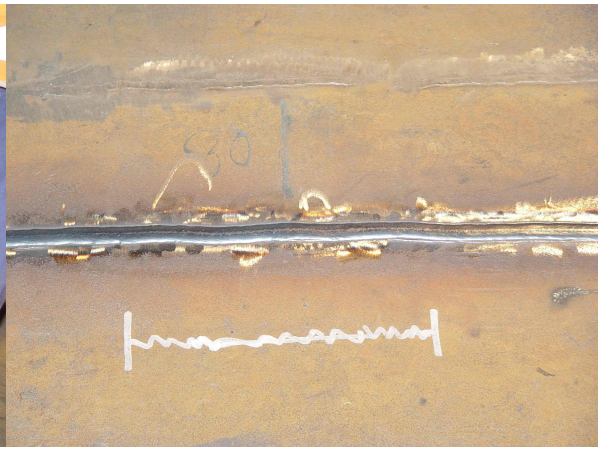

Figure 6-62: Repaired fatigue crack

Figure 6-63: Magnetic testing

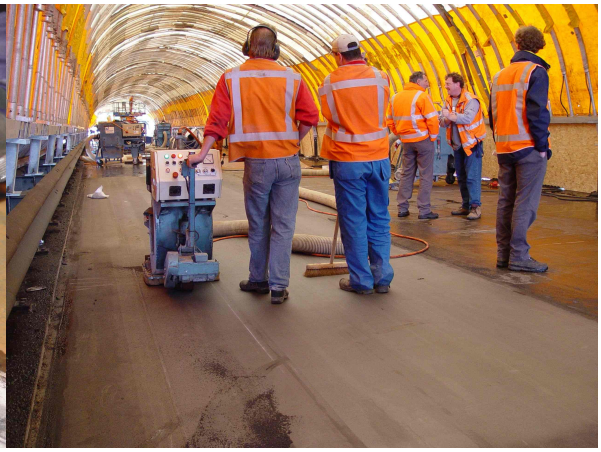

Figure 6-64: Shot blasting deck plate

Figure 6-65: Epoxy layer

Figure 6-66: Reinforcement

Figure 6-67: Reinforcement

Figure 6-68: Casting concrete

Figure 6-69: Power floating

Figure 6-70: Finished RHPC surfacing

6.8.2 Set-up strain gauge measurements

6.8.2.1 Test objective

Due to the replacement of the asphalt surfacing by a RHPC surfacing the stress ranges in the steel deck plate are reduced. In addition to the calculations with FE-models and the measurements on full-scale laboratory test panels, stress spectra measurements were performed on the Caland Bridge. These measurements are extensively described in (Kolstein, 2003). The stress spectra were measured under the conventional mastic asphalt surfacing and under the RHPC surfacing. Evaluation of the measurements gives a stress reduction factor due to the applied RHPC surfacing. It is the main objective of the measurements to derive this reduction factor.

6.8.2.2 Instrumentation

In September 2002 strain gauges were applied on the underside of the bridge deck structure in the right wheel track of the heavy vehicle lane. The span of the fixed span is 86 m and the strain gauges were applied at approximately 74 to 76 m in the traffic direction. This is approximately 10 m before lorries leave the bridge. The distance between strain gauges and the expansion joint is approximately 10 m. At this location dynamic amplification is limited. Therefore it is unnecessary to take a dynamic amplification factor into account.

Figure 6-71 shows a general view of the measured cross-sections. Pairs of strain gauges were attached at 9 locations. These strain gauges were positioned 15 mm from the weld toe and they were all positioned perpendicular to the longitudinal weld between trough web and deck plate. This means that the gauges all measured the transverse strain, see Figure 6-72.

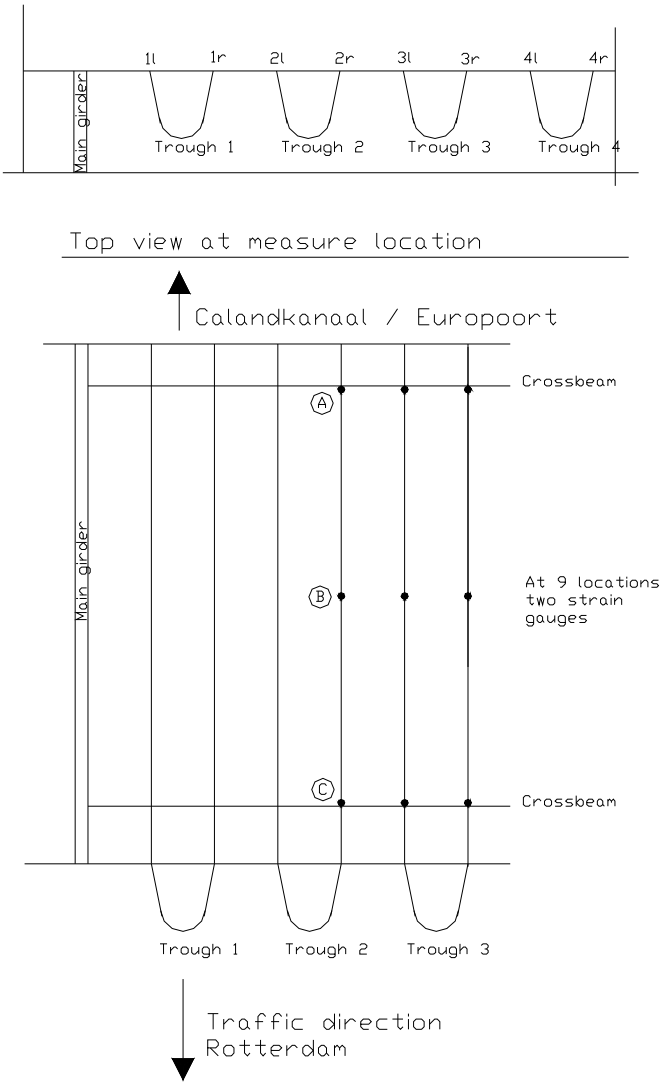

Figure 6-71: General view of the measured cross-sections A, B and C.

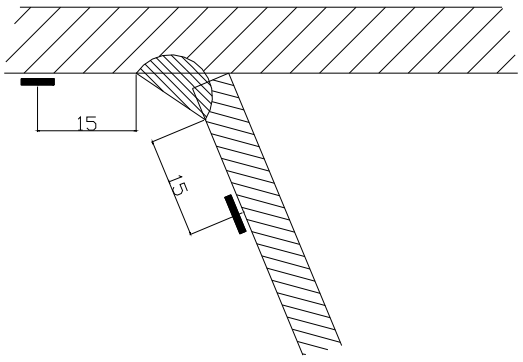

Figure 6-72: Gauge positions near the weld at cross-section A, B and C

As shown in Figure 6-73 the strain gauges near the crossbeam were located 20 mm from the crossbeam web. The numbering of the strain gauges is shown in Figure 6-74, Figure 6-75 and Figure 6-76. The location of the strain gauges was chosen so that the stress reduction both for deck plate cracks and for cracks in the longitudinal weld between deck plate and trough web was measured. Besides the strain gauges two temperature sensors were applied. One was connected to the underside of the steel deck plate and one was suspended in the free air.

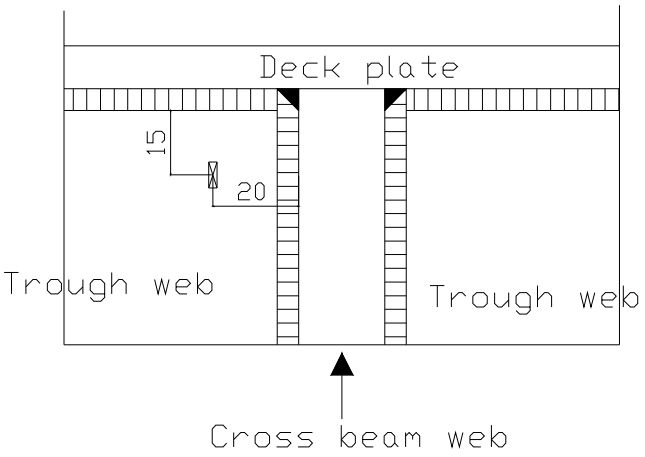

Figure 6-73: Gauge positions near the crossbeams at cross-section A and C

The main interest was the reduction of the stress range in the deck plate at the location of the crossbeam. The most interesting position for strain gauges was the underside of the deck plate at the crossbeam location within the trough at the root side of the longitudinal weld. To attach strain gauges at this location accessibility had to be created by cutting out a part of the trough, see paragraph 6.6.2.2 and Figure 6-31. Cutting out such a part of the trough reduces the static capacity of the longitudinal girder significantly, and necessitated the closing of this lane for traffic. However inconvenience to traffic was not allowed by the bridge owner and thus it was impossible to attach the strain gauges to underside of the deck plate at the inner side of the trough profile at the location of the crossbeam.

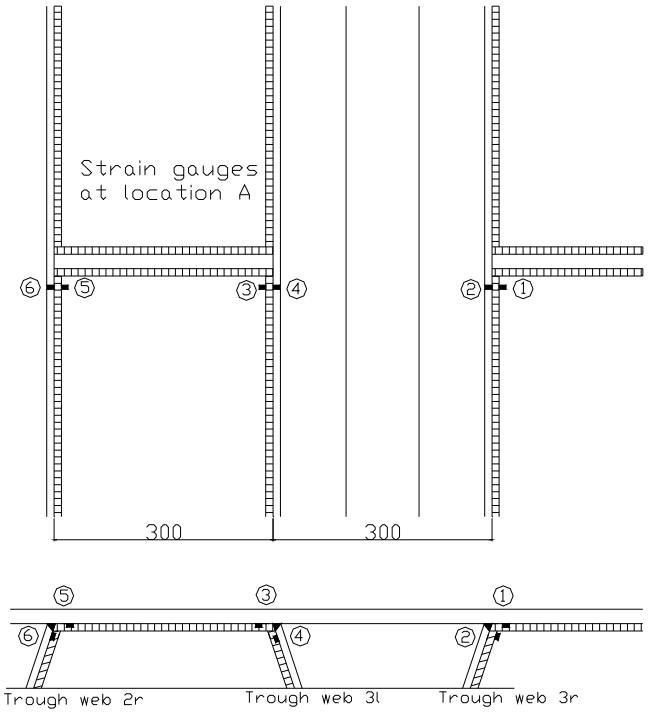

Figure 6-74: Numbering of the strain gauges at cross-section A

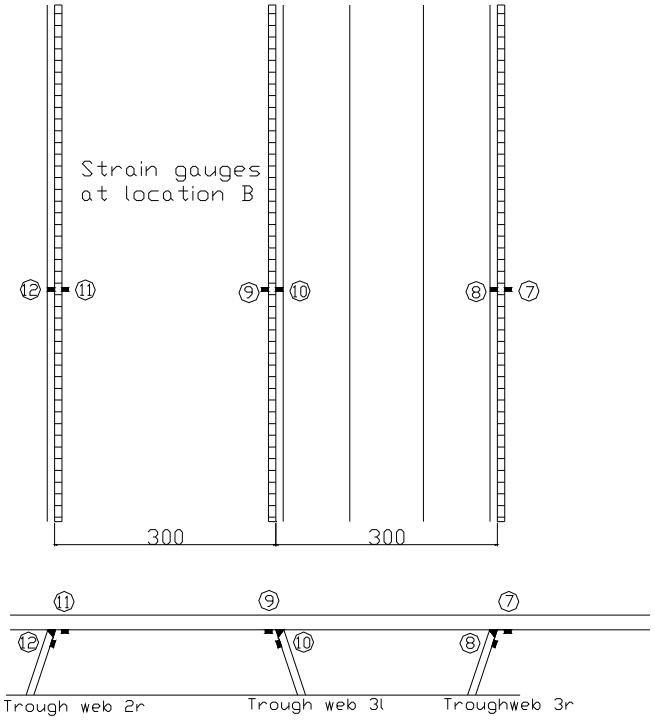

Figure 6-75: Numbering of the strain gauges at cross-section B

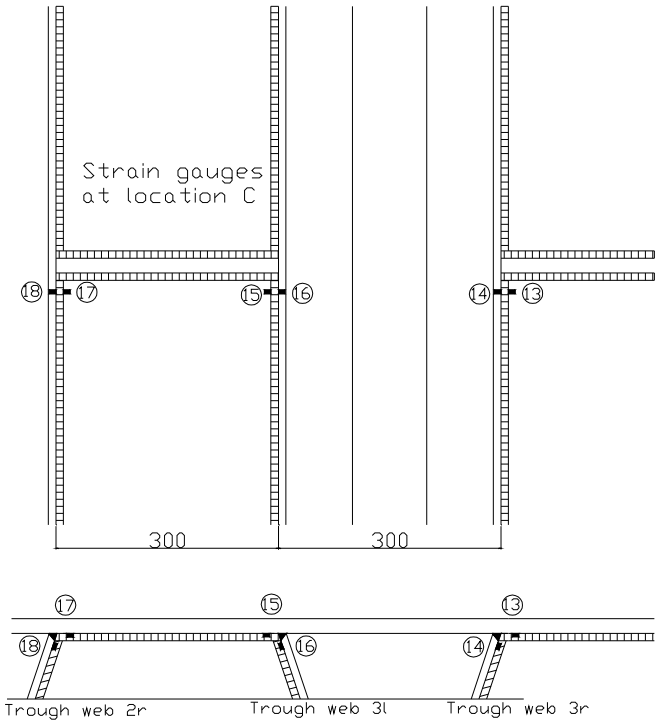

Figure 6-76: Numbering of the strain gauges at cross-section C

The induced stress ranges at the strain gauge locations were measured under normal traffic conditions on the Caland Bridge. Measurements were carried out over two periods:

- Week 10-17 2003: Steel deck plate with the mastic asphalt surfacing, before application RHPC surfacing
- Week 19-31 2003: Steel deck plate with the RHPC surfacing

The Caland Bridge was renovated in week 18.

Each axle of a heavy vehicle that passes the bridge generates a strain signal. Only the maximum strain is saved. Only the measurements for the weeks 14-17 and 19-23 were analysed .

6.8.3 Results of strain gauge measurements

The results of the strain gauge measurements are given in frequency curves. These curves give the cumulative number of stress cycles with a stress range larger than a given stress range. The results for the strain gauges at cross-section B are given in Figure 6-77, Figure 6-78 and Figure 6-79 for the strain gauges 7, 9 and 11 respectively at the underside of the deck plate and in Figure 6-80, Figure 6-81 and Figure 6-82 for the strain gauges 8, 10 and 12 respectively at the trough web.

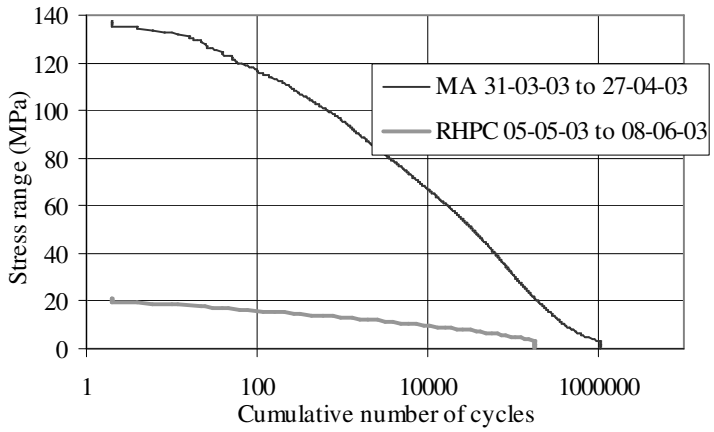

Figure 6-77: Frequency curve for strain gauge 7 – deck plate

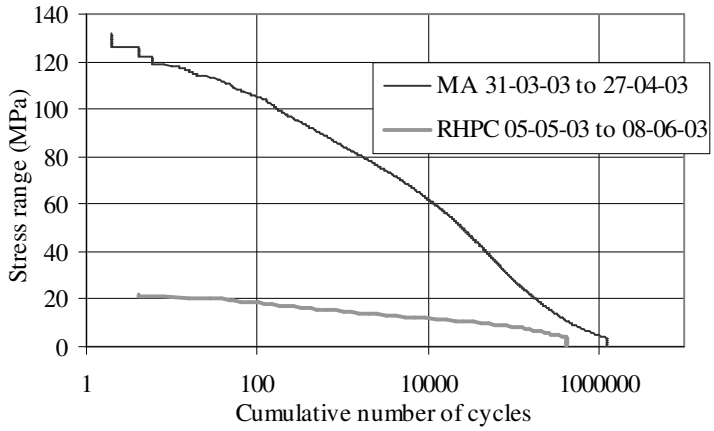

Figure 6-78: Frequency curve for strain gauge 9 – deck plate

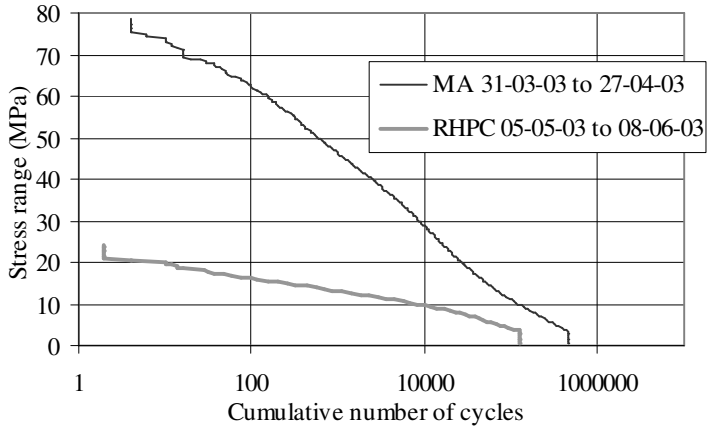

Figure 6-79: Frequency curve for strain gauge 11 – deck plate

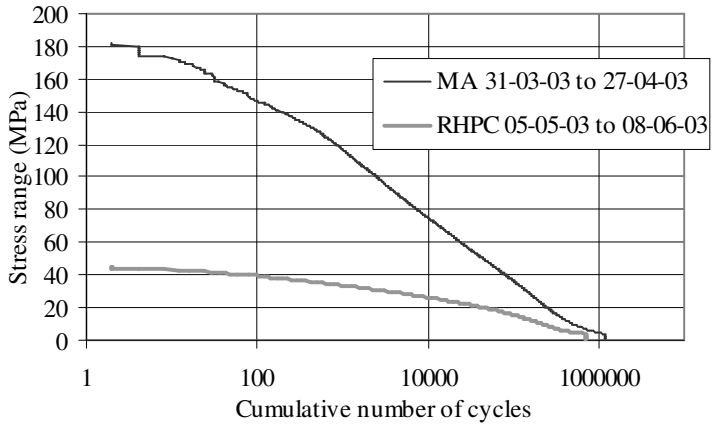

Figure 6-80: Frequency curve for strain gauge 8 – trough web

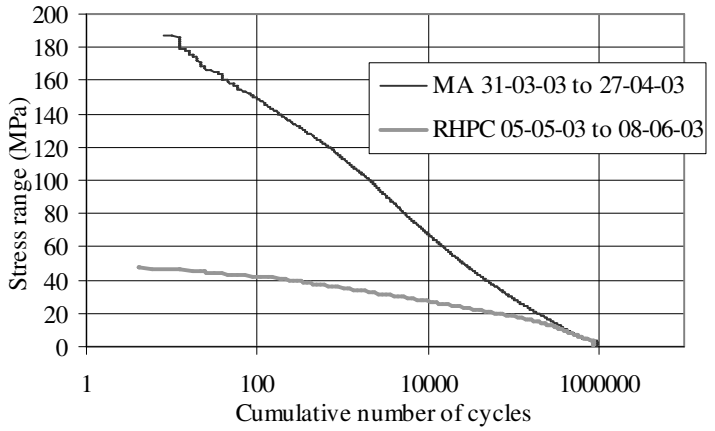

Figure 6-81: Frequency curve for strain gauge 10 – trough web

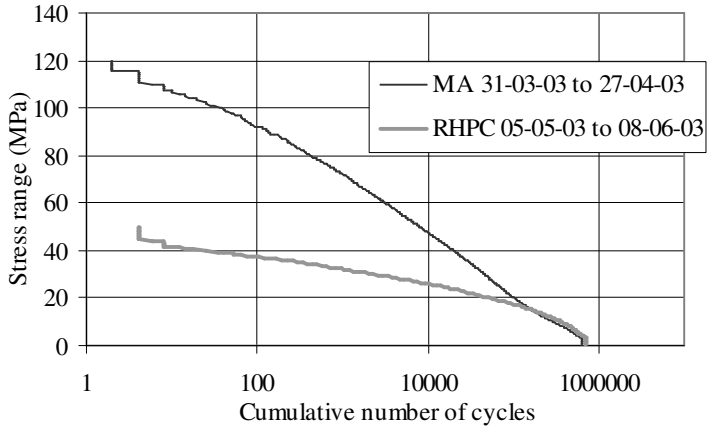

Figure 6-82: Frequency curve for strain gauge 12 – trough web

The main interest is the reduction in the stress range in the deck plate at the location of the crossbeam. As it was impossible to attach the strain gauges to underside of the deck plate at the inner side of the trough profile at the location of the crossbeam, a measurement at the most interesting location was impossible. Therefore the results of the measurements are given for the strain gauges at location B. The results at this location mid span between two crossbeams are not influenced by discontinuities in the structure. These discontinuities, which are due to the crossbeam web, are responsible for extra stiffness. This causes a stress reduction due to the RHPC, which is not representative of the stress reduction in the deck plate. These discontinuities influence the results of the strain gauges at locations A and C.

Variance in curves asphalt and RHPC

Figure 6-83 gives the frequency curves for strain gauge 7 in week 16, when the bridge deck was surfaced with mastic asphalt. Figure 6-84 gives the frequency curves for the same gauge, no 7, in week 23 in 2003, when the bridge deck was resurfaced with RHPC. Temperature regimes are about the same for the weeks 16 and 23 (Kolstein, 2003). It is obvious that the frequency curves for the period when the bridge is surfaced with mastic asphalt show more variance than the curves for the period when the bridge deck has been resurfaced with RHPC. In general the frequency curves for all 18 strain gauges under asphalt vary more from each other than the frequency curves for all the strain gauges under the RHPC surfacing.

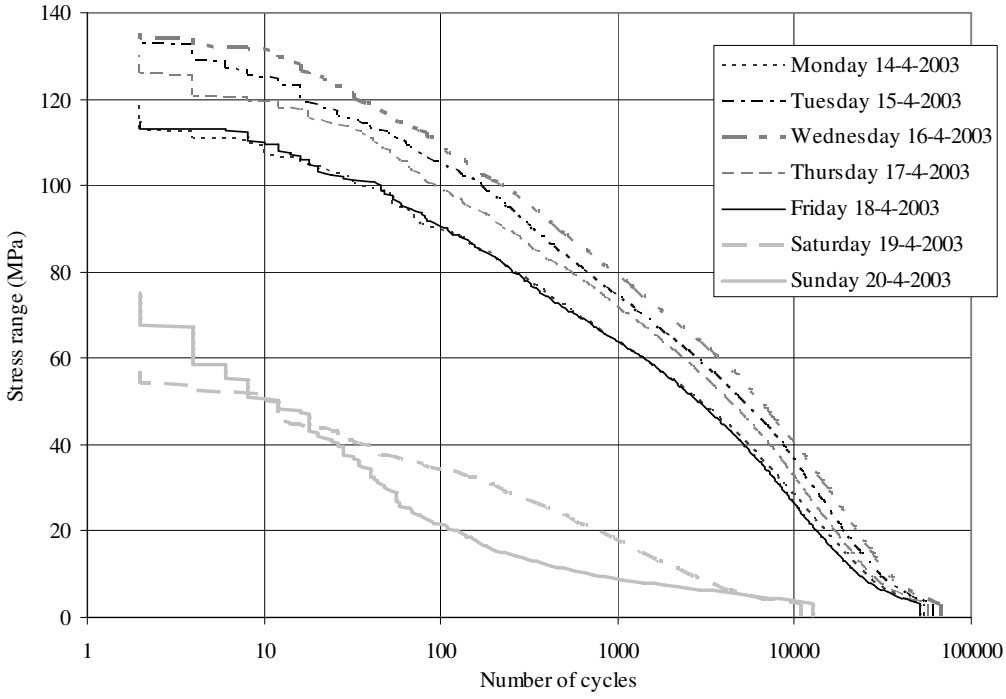

Figure 6-83: Frequency curves for strain gauge 7, mastic asphalt, week 16

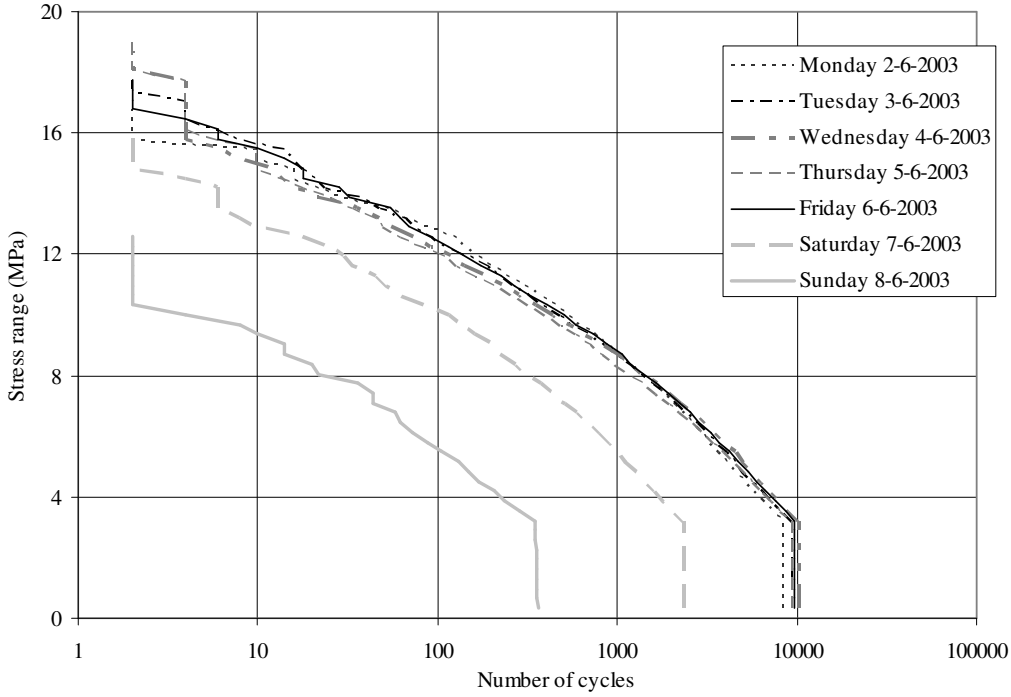

Figure 6-84: Frequency curves for strain gauge 7, RHPC, week 23

The explanation for this difference is as follows. It is known that the number and magnitude of the loads are roughly the same on Monday to Friday. Measurements have shown that the daily traffic density Monday to Friday is approximately the same and that traffic density on Saturday and Sunday is much lower (AVV, 2005). Research has also shown that the axle load spectra Monday to Friday are identical (Vrouwenvelder, 2000-a). This implies that differences between the frequency curves for Monday to Friday must be due to differences in the structural response of the bridge deck structure. For mastic asphalt significant differences between the frequency curves for Monday to Friday are visible. For the RHPC surfacing there are only slightly differences visible for the frequency curves for Monday to Friday. The assumed reason is that it is because the stiffness of asphalt is much more sensitive to temperature effects than the concrete overlay.

Stress reduction factor

A large reduction of the stresses is visible from the figures and only at the tails of the curves, is a smaller or even no reduction is visible. This is due to the effect that a passing vehicle not only generates local stresses in deck plate and trough web, but also more global stresses. As the reduction of the local stresses due to RHPC is the main concern the tails of the frequency curves are neglected in the analysis. To derive an indication of the stress reduction factor due the RHPC surfacing the cumulative numbers of cycles for RHPC are multiplied with a factor

0.8, because the curves in the Figure 6-77 to Figure 6-82 comprise data for 4 weeks of mastic asphalt and 5 weeks of RHPC. Then the stress range from the frequency curve is determined for the cumulative numbers of 100, 1000, 10000 and 100000 cycles. For mastic asphalt these values are given in Table 6-13, for RHPC they are given in Table 6-14. The stress reduction factor is defined as the stress for RHPC divided by the stress for mastic asphalt at the same number of cumulative cycles. These factors are given in Table 6-15.

Table 6-13: Mastic asphalt stress ranges (MPa)

Cycles	Gauge 7	Gauge 8	Gauge 9	Gauge 10	Gauge 11	Gauge 12
100	116	146	105	149	62	92
1000	95	117	85	113	46	72
10000	67	75	62	68	29	47
100000	31	36	28	29	11	20

Table 6-14: RHPC stress ranges (MPa)

Cycles	Gauge 7	Gauge 8	Gauge 9	Gauge 10	Gauge 11	Gauge 12
100	15	39	18	42	15	36
1000	13	33	15	34	13	31
10000	9	25	11	26	9	25
100000	4	14	7	17	0	16

Table 6-15: Stress reduction factors

Cycles	Gauge 7	Gauge 8	Gauge 9	Gauge 10	Gauge 11	Gauge 12
100	0.13	0.26	0.17	0.28	0.25	0.40
1000	0.14	0.28	0.17	0.30	0.27	0.43
10000	0.14	0.34	0.18	0.39	0.31	0.53
100000	0.13	0.38	0.26	0.59	0.00	0.79

From the figures and the tables becomes clear that a significant stress reduction is achieved by using a RHPC surfacing. For the strain gauges 11 and 12 a smaller reduction is achieved. This is due to the fact that these gauges are placed a little outside the wheel track, which means that the global behaviour becomes more visible. The higher stress reduction factors for a cumulative number of 100000 cycles are also due to this phenomenon. Based on these measured stress spectra, average reduction factors of 0.2 for the stress in the deck and 0.4 for the stress in the trough web are derived.

A simple approach to the lifetime enhancement due to this stress reduction factor uses the regular slope m = 3 of the fatigue detail curves. The lifetime enhancement factor in this simple approach is $1/(0.2^3)$ = 125 for fatigue cracks in the deck plate and $1/(0.4^3)$ = 16 for fatigue cracks in the longitudinal weld between trough web and deck plate. This is a conservative approach because a significant part of the stress ranges is in the region of the slope m = 5 or even below the fatigue limit.

6.9 Comparison calculations with tests

This paragraph provides a comparison of the results of the FE-models, the tests and the spectra measurements. For more background details of this comparison, see Annex G

Three aspects are compared:

- The stresses due to local deck plate behaviour in the steel deck plate of a deck of 12 mm with a 50 mm RHPC overlay at the crossbeam location
- The derived stress reduction factors
- The difference between the location at the crossbeam and the location between the crossbeams

The following results are tabulated for the comparison:

1. FE-models - only local deck plate behaviour at crossbeam, described in paragraph 6.3.1.1
2. FE-models - local deck plate behaviour and crossbeam behaviour, described in paragraph 6.3.1.2
3. FE-models - local deck plate behaviour between crossbeams, described in paragraph 6.3.1.3
4. Static tests at TNO panel with RHPC, described in paragraph 6.6.1
5. Static tests at test panel A with RHPC, described in paragraph 6.6.2
6. Fatigue test at TNO panel with RHPC, described in paragraph 6.7.1
7. Fatigue tests on test panel A with RHPC, described in paragraph 6.7.2
8. Static tests during fatigue test on test panel A with RHPC, described in paragraph 6.7.2
9. Field measurements - pilot project Caland Bridge, described in paragraph 6.8

For an easy comparison:

- For all results the stresses were calculated from the measured strains
- Stresses were calculated back to a load of 100 kN
- Stresses were determined at:
  - 0 mm from the root of the crack location
  - 12.5 mm from the root of the weld, which is the location where the strain gauges at

test panel A were mounted
  - 150 mm from the root of the weld, midspan between two trough webs
- The stresses at these locations were determined by linear interpolation or extrapolation if there was no result available at the specific location.

From research with the Lintrack it became clear that the footprints of the single tyre (type A) and the super single tyre (type C) result in approximately the same stresses. Therefore it is possible to compare the results of the FE-models based on the single with the results of the tests mainly based on the super single.

6.9.1 Local deck plate behaviour of 12 mm steel with 50 mm RHPC

Figure 6-85 shows the results of the calculations and the tests. In this figure the results for a bridge deck with a deck plate of 12 mm and 50 mm RHPC are only given, for the FE-model and the tests that represent local deck plate behaviour. Results from 2, 3 and 9 are therefore not incorporated in this figure.

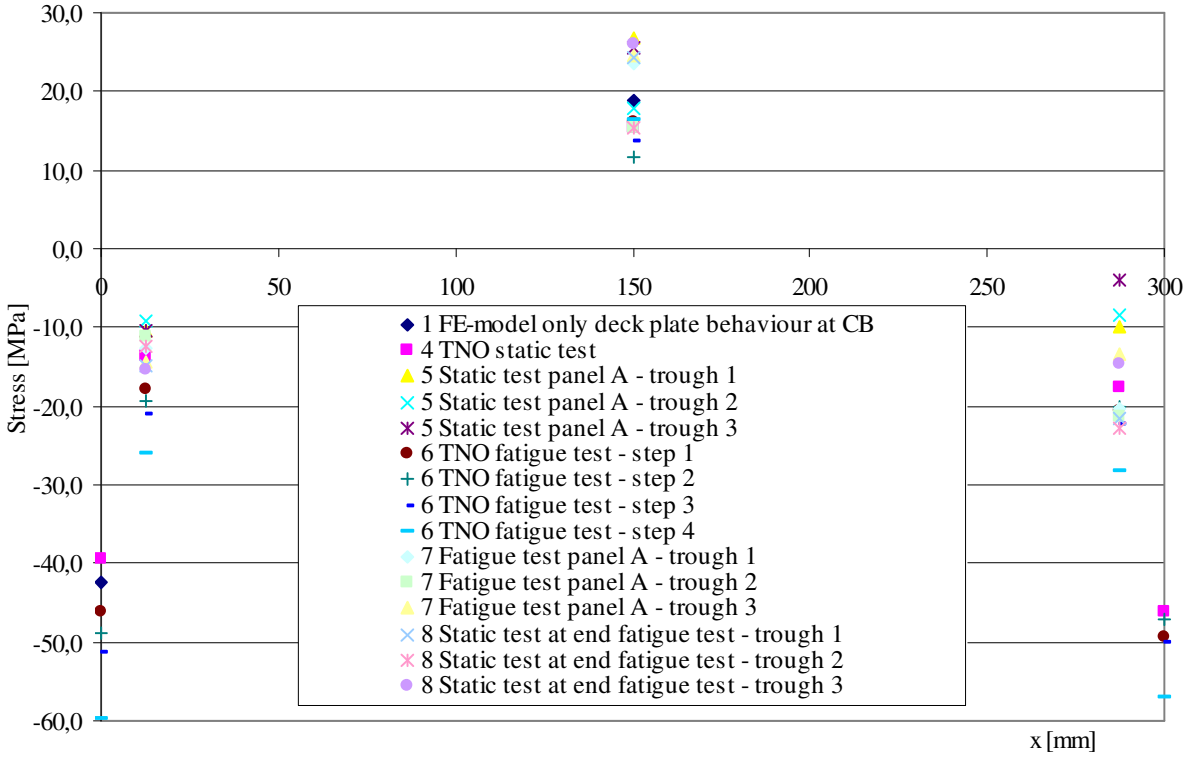

Figure 6-85: Comparison - stresses at bottom steel deck with RHPC (unit load of 100 kN)

From the results becomes clear that:

- The stresses from the different models and measurements for the crack location (both at 0 mm and at 300 mm) are about the same.
- The stresses at 12.5 mm from the crack location (12.5 mm and 287.5 mm in the figure) differ more from each other.
- The stresses at 150 mm midspan between the two crack locations differ more from each other, but are in the region 10 to 25 MPa.
- In general the results from the FE-models, the static tests at the TNO panel, the static tests at the test panel A, the fatigue test at the TNO panel and from the fatigue test at panel A are of the same order of magnitude.

6.9.2 The derived stress reduction factors

This paragraph is about the reduction factor due to the replacement of the asphalt surfacing with a RHPC surfacing. The reduction factor in this paragraph is defined again as the stress with an asphalt surfacing divided by the stress with a RHPC surfacing, at the crack location.

The following stress reduction factors (BET/ASF) were calculated with the FE-model that only represents local deck plate behaviour at the crossbeam location:

- 0.20 Situation with 50 mm surfacing layer and 12 mm steel deck plate
- 0.22 Situation with 50 mm surfacing layer and 10 mm steel deck plate
- 0.13 Situation with 80 mm surfacing layer and 10 mm steel deck plate

The following stress reduction factors (BET/ASF) were calculated with the FE-model that represents local deck plate behaviour between two crossbeams. All situations with a 50 mm surfacing layer and 12 mm steel deck plate:

- 0.30 For load case 5 with the wheel load above middle trough
- 0.39 For load case 6 with the wheel load above left web of middle trough
- 0.27 For load case 7 with the wheel load above left trough

The following average stress reduction factors (BET/ASF) were measured on the Caland Bridge.

- 0.14 For deck plate gauge 7
- 0.17 For deck plate gauge 9
- 0.28 For deck plate gauge 11
- 0.29 For trough web gauge 8
- 0.32 For trough web gauge 10
- 0.45 For trough web gauge 12

The averages are calculated with the values at 100, 1000 and 10000 cycles. The value at 100000 cycles is excluded because of its location in the tail of the measurement; see Figure 6-77 to Figure 6-82. It should be noted that the deck plate thickness of the Caland Bridge is 10 mm and that the applied RHPC surfacing has a thickness of 60 mm. It also should be noted that the strain gauges 7 to 12 were applied in the field between the crossbeams and not on the crossbeam location.

This specific thickness configuration on the Caland Bridge is not calculated with the FE-model that represents the behaviour between two crossbeams. The measured reduction factors however are far better than the calculated factors (0.30, 0.39 and 0.27 for the three different load cases). It is thought that the gap between FE-model and measurement would be smaller if the 10 mm steel and 60 mm RHPC configuration had been used in the FE-models, instead of the 12 mm steel and 50 mm RHPC configuration that was used.

Other explanations for the difference between FE-model and spectra measurements are:
- The stress reduction factors from the FE-models are calculated at the location where the maximum stress is located. Paragraph 6.3.1.3 explains that these stress reduction factors are conservative.
- Another explanation is that in the application of the RHPC surfacing on the Caland Bridge a layer thicker than 60 mm was applied, which causes additional stress reduction.

6.9.3 Difference between the location at the crossbeam and between the crossbeam

The following stresses are calculated for the crack location at the crossbeam (both for a footprint of 220 x 320 mm and load case 5 above the trough)
- -42.5 MPa for the FE-model that only represents local deck plate behaviour
- -75.7 MPa for the FE-model that represents both local deck plate behaviour as well as crossbeam behaviour. But of course crossbeam behaviour depends on the bridge structure.

This could lead to the conclusion that –33.2 MPa is due to crossbeam behaviour. In paragraph 6.3.1.2 however is already argued that the FE-model is only a rough estimation of the structure behaviour.

6.10 Conclusions

With respect to the general aspects of this renovation method:
1. The replacement of the asphalt surfacing with a reinforced high performance concrete surfacing (RHPC) is a good solution for the fatigue problems on steel bridge decks. It

significantly reduces the stresses in deck plate and trough web and hence it considerably extends the lifetime.
2. An epoxy interface layer between steel and concrete provides sufficient shear strength and capacity. This makes composite action between steel and RHPC possible.
3. Filling troughs in addition to the application of the RHPC surfacing layer is unnecessary, it does not give extra stress reduction.

With respect to the application process:
4. It is important that sufficient vibration energy is applied to the concrete in order to achieve a good compaction and avoid air inclusions.
5. The mesh dimensions of the reinforcement should be produced exactly at the nominal value in order to avoid problems with the placing of the mesh reinforcement and problems with the compaction at mesh overlap locations.

With respect to the reduction of the stresses:
6. If the asphalt surfacing is replaced by a RHPC surfacing the stresses are reduced significantly.
7. No clear reduction factor becomes apparent from the different FE-models and measurements, the factor varies between approximately 0.15 and 0.30.
8. The calculated and measured reduction factors for the deck plate vary between 0.08 and approximately 0.4, for deck plate cracks.
9. The measured reduction factors are in general smaller than the reduction factors calculated with the FE-models.
10. Especially for the FE-model representing local deck plate behaviour and crossbeam behaviour at the crossbeam location, and for the FE-model representing local deck plate behaviour between the crossbeams it is obvious that the applied boundary constraints lead to conservative calculated reduction factors. Therefore it is reasonable to rely more on the measured stress reduction factors.
11. From the FE-models it is not possible to derive separate stress reduction factors for the stress due to crossbeam behaviour.
12. The measurements on the Caland Bridge show no distinct crossbeam behaviour.
13. Therefore the measured reduction factors at the Caland Bridge in the field between the crossbeams, and the results of the models and test that only comprise local deck plate behaviour are appropriate for the crossbeam location.
14. A stress reduction factor for the stress in the deck plate of 0.2 and a stress reduction factor of 0.4 for the stress in the trough web are proposed.
15. The measured strains on test panel A with unrepaired fatigue cracks are about the same as the strains in the TNO panel without any cracks in the deck plate. It might be concluded that with respect to the static strains it is not necessary to repair fatigue cracks in the deck

plate, up to a crack length of approximately 100-150 mm.

With respect to the fatigue behaviour

16. Fatigue tests were successfully applied on the TNO panel and on test panel A. The applied loading sequence represents heavy traffic for more than 50 years for each test.
17. The measured strain ranges are mostly constant or show only some minor changes, during the whole test.
18. No fatigue crack growth was observed during the fatigue tests.
19. The measured strain ranges on test panel A with unrepaired fatigue cracks are about the same as the strains in the TNO panel without any cracks in the deck plate. During the fatigue test no crack growth was observed in either test panel. It might be concluded that it is not necessary to repair fatigue cracks in the deck plate, up to a crack length of 100-150 mm.
20. A simple conservative approach to the lifetime enhancement uses the regular slope $m = 3$ of the fatigue detail curves. The lifetime enhancement factor in this simple approach is $1/(0.2^3) = 125$ for fatigue cracks in the deck plate and $1/(0.4^3) = 16$ for fatigue cracks in the longitudinal weld between trough web and deck plate.
21. Due to the large reduction in the stresses in deck plate and trough web, a significant part of the stress ranges is in the region of the slope $m = 5$ or even below the fatigue limit. These stress ranges give only a small contribution to the fatigue damage.

7. Renovation methods for movable bridges

7.1 Introduction

In this chapter three solutions that extend the lifetime of the orthotropic deck structure of movable bridges are described.

Paragraph 7.2 describes the first method: bonding a second steel deck plate to the old steel deck plate. The general idea of this method is that the deck plate becomes stiffer, which reduces the stress ranges that induce fatigue. After an introduction, the adhesive layer and application methods are described. Subsequently the results of FE-models are elaborated. Primary interest is in the reduction of the stress ranges in the steel deck plate due to the renovation method. Then descriptions of the static and fatigue testing programs follow. Static as well as fatigue tests were performed both on small test specimen and full-scale bridge test samples. Ultrasonic tests before and after the fatigue tests are also described. Paragraph 7.2 ends with some concluding remarks.

Paragraph 7.3 describes the second method: filling the troughs in the wheel tracks with polyurethane. The general idea of this method is that the deck plate becomes continuously supported, which reduces the stress ranges that induce fatigue. After an introduction, the filling material and the application method are described. Subsequently the results of FE-models are elaborated. Primary interest is the reduction of the stress ranges in the steel deck plate due to the renovation method. After that the static testing program and fatigue testing programs are described. Static as well as fatigue tests were performed both on small test specimen and full-scale bridge test samples. Paragraph 7.3 ends with some concluding remarks.

Paragraph 7.4 describes the third method: the application of a reinforced ultra high performance concrete layer on top of the steel deck plate. The general idea of this method is that the deck plate becomes stiffer, and this reduces the stress ranges that induce fatigue. Various reinforcement concepts are elaborated. Subsequently two types of test are described: pull out tests and static bending tests. After that the fatigue characteristics of this renovation method are described. Finally a few alternatives that are appropriate for movable bridge decks are presented. Paragraph 7.4 ends with some concluding remarks and recommendations.

Paragraph 7.5 ends this chapter with some concluding remarks and gives a summary of the main results of this chapter.

7.2 Bonding a second steel deck plate at the old steel deck plate

7.2.1 Introduction

To prevent fatigue in the deck plate, stress ranges in the deck plate have to be reduced. To reduce the stress ranges in the deck plate the stiffness of the deck plate structure must be increased. Movable bridges with a steel orthotropic deck structure usually only have an epoxy surfacing of approximately 7 or 8 mm. A solution for fatigue deck plate cracks in movable bridge decks is a thicker deck plate. Achieving a thicker deck plate for existing bridges is possible by bonding an additional steel deck plate to the original deck plate. The effectiveness of this renovation method depends on the composite action between the old and the new steel deck plate. Bonding as a connection technology between the two steel plates is an optimal choice to achieve composite action. The applied adhesive layer should have sufficient shear properties to generate composite action. Figure 7-1 shows this renovation technique. The old steel deck structure, the adhesive layer, the new steel deck plate and a new epoxy surfacing are visible in this figure.

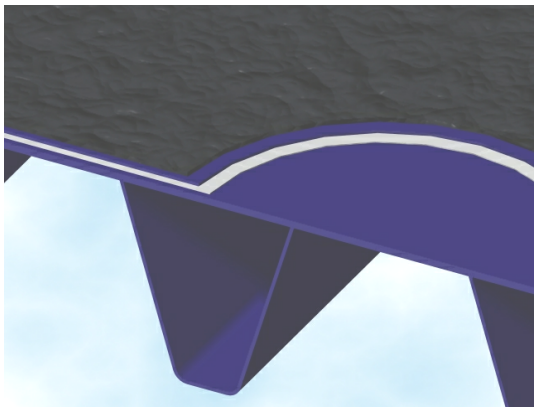

Figure 7-1: Bonding a second steel deck plate

Adding a second steel deck plate on a movable bridge deck is divided in several phases. The application is more or less comparable to the application process of a RHPC surfacing on fixed bridges, see paragraph 6.2. First the existing epoxy surfacing has to be removed. Then the deck plate is subjected to an inspection to detect all the fatigue cracks, which have to be repaired if they are bigger than the repair criterion. The next step is to shot blast the surface of the steel deck plate to Sa 2.5 to achieve a optimum bonding condition. Then the adhesive

layer and the second steel deck plate of approximately 6 mm are applied. Lastly a normal epoxy surfacing sprinkled with aggregates should be applied as a wearing course. When these steps have been completed the bridge deck is ready for traffic again. The development of this renovation technique started after the fatigue problems with the Van Brienenoord Bridge in 1997. Within the research of this renovation method, the thickness of the additional steel deck plate is maximal 6 mm, due to weight restrictions.

7.2.2 Adhesive layer & Application method

Two different bonding technologies were researched.

1. The adhesive is applied to the original deck plate and the second steel deck plate is placed in the wet adhesive (Nagtegaal, 2002-a)
2. First the second plate is placed over the original steel deck plate separated by vertical spacers. Vacuum is then used to draw the adhesive into the space between the old and new deck plates (Labordus, 2004, 2005, 2006).

The first technology was developed first. At the end of the development stage a fatigue test on a full-scale bridge deck test panel was performed. During this test delamination occurred between the old and the new deck plates. It is thought that this delamination was partly due to the air inclusions in the adhesive layer. This fatigue failure necessitated a different way of bonding the two plates. The second method is the result of this new adhesive layer development phase. It made possible the creation of an adhesive layer without air inclusions.

7.2.2.1 Bonding material

Both for application method 1 and 2 literature surveys were performed to select an appropriate bonding system. The main requirements of the various adhesives are:

- Mechanical properties
- Application properties
- Durability properties
- Experience with the adhesive

Bonding material for application method 1

Nagtegaal performed a literature survey on adhesive layers for the first application method (Nagtegaal, 2002-b). The purpose of this survey was to select a few bonding systems that were suitable for this application. Based on the survey three different adhesives were selected that were probably appropriate for the adhesive layer between old and new steel deck plate. These three are:

- Sikadur 30 from the firm Sika (Youngs' modulus E = 12800 MPa)
- Araldite 2015 from the firm Ciba (Youngs' modulus E = 2000 MPa)

- Edilon 900108A from the firm Edilon (Youngs' modulus E = 4500 MPa)

The reduction in the stress ranges, and thus the effect of this renovation method on the fatigue life depends both on the thickness of the additional steel deck plate and on the shear stiffness, and thus on the Youngs' modulus, of the adhesive. A higher Youngs' modulus leads to a higher stress range reduction.

Bonding material for application method 2

For the second application method in which the adhesive is infused by a vacuum between old and new steel deck plate, the viscosity of the adhesive is important for a successful application process. The viscosity should be low enough to facilitate the liquid flow into the space between the two steel plates. Labordus performed a literature survey on adhesive layers for the vacuum infusion bonding method (Labordus, 2005). The purpose of this survey was to select a few adhesive types that are suitable for this application. Based on the survey four different epoxy adhesive systems that are probably appropriate were selected. These four are:

- System 1: EPR 4908A + EPH 4908B (mix proportion 100:30, pot life 300 to 360 minutes) from the firm Brands Structural Products
- System 2: EP hars + EH 50 (mix proportion 100:50, pot life 60 minutes) from the firm Gouda Chemiebouw
- System 3: EPR 275 + EPR 307 + H545 (mix proportion 25:75:46.7, pot life 45 minutes) from the firm Brands Structural Products
- System 4: EPR 307 + DPTA + Jeffamine D230 (mix proportion 100:10:10, pot life 45 minutes) from the firm Brands Structural Products

Mechanical tests were performed on small coupons for all four systems, see (Labordus, 2005) for a description of the tests. System 1 had the highest elasticity and rupture strength (E = 4900 MPa and f_t = 77 MPa). Therefore system 1 was the selected epoxy adhesive system for the infusion bonding process.

7.2.2.2 Application method 1

In the first application method the adhesive was applied to the old steel deck plate then the second steel deck plate was placed on the adhesive layer. Figure 7-2 shows the application of the adhesives on both steel plates (Hechtings Instituut, 2002-a). For test purposes small square steel plates were used. At first the adhesive was applied with a glue comb on the lower plate that would be in bridge structure the original deck plate. Subsequently for this specific adhesive a thin layer was also applied on the top plate, that is the new second steel deck plate. Figure 7-2 shows the application of the Araldite 2015 adhesive on test specimen.

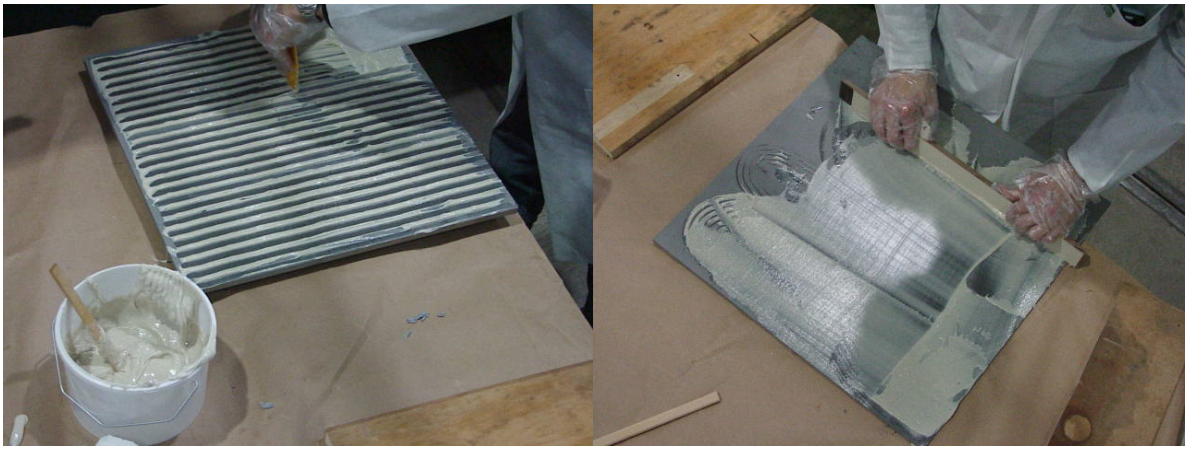

Figure 7-2: Method 1 - adhesive applied on lower plate (left) and top plate (right)

Figure 7-3 shows the Sikadur 30 adhesive on the lower plate. After the application of the adhesives on the steel plates, the top steel plate was laid on the lower steel plate. To improve the squeeze-out of the adhesive layer heavy steel plates were laid out on top of the upper steel plate.

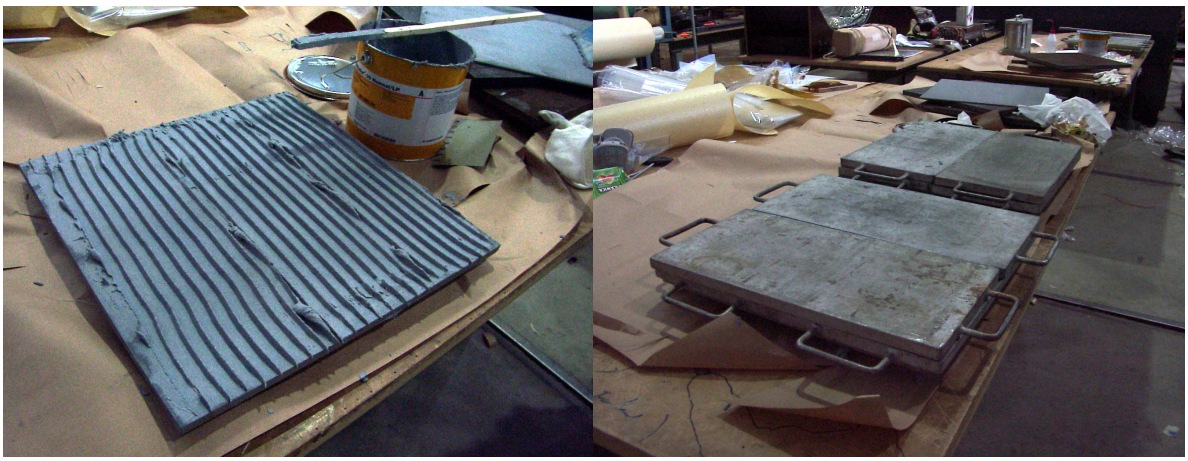

Figure 7-3: Method 1 – Sikadur 30 applied (left) and dead load on bonding (right)

Plate division

If the steel plates are bonded on movable bridge decks the dimensions are much larger. The complete area of the heavy vehicle lane on a movable bridge should be provided with the second steel deck plate. In general this lane is approximately 3.5 m wide and the length varies between approximately 8 and 60 m. It is impossible the cover such an area with one single steel deck plate. The second steel deck plate has to be divided in several parts. The dimensions of the separate parts of the second steel deck plate should be chosen so that it is appropriate in practical situations, for instance plates with a length of 3.5 m and a width of 3.5

m. The divisions between the separate plates have to be located at a place where stresses in the longitudinal direction are minimal, which is approximately the same location as the stiffener splice joint, see Figure 2-18. Figure 7-4 shows an example of the division of the second steel deck plate on top of the movable bridge deck.

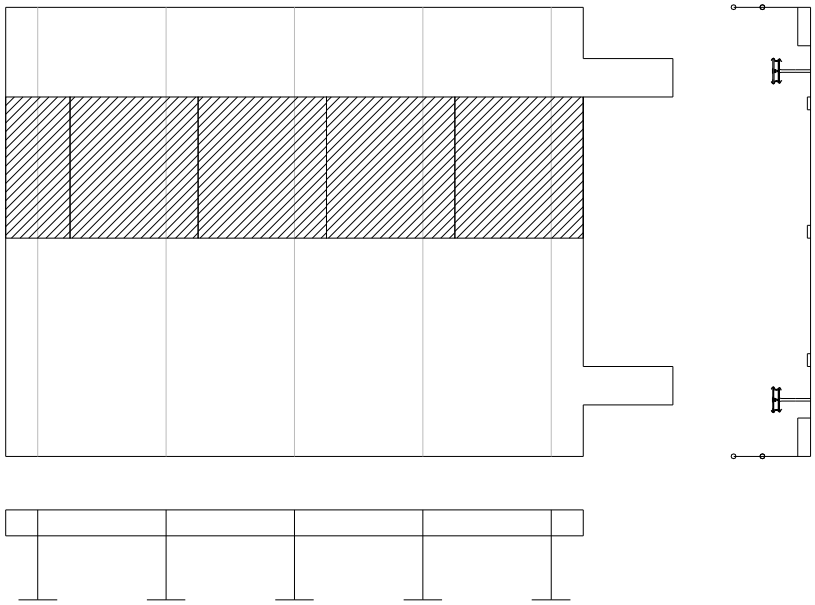

Figure 7-4: Top view of division in several plates on movable bridge deck

The separate plates have to be connected to each other to prevent high stress concentrations at the plate division. For the plate division there are basically two options: welding the plates together or an indirect bonded connection, see Figure 7-5. The indirect bonded connection can be made in different ways as the figure shows.

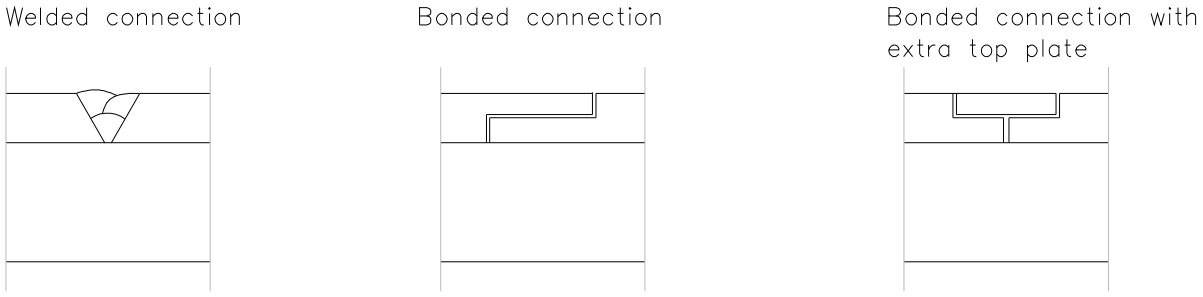

Figure 7-5: Connection between plates at the plate division

Tests were performed to determine how a good welded connection between the two plates could be made (Hechtings Instituut, 2002-b). The first test comprised a continuous adhesive

layer between the old bottom steel deck plate and the new additional plate. There was no interruption in the adhesive layer at the weld location. The weld was applied after the plates had been bonded together and the adhesive was hardened. It became clear that the adhesive at the weld location burns during welding, and that a poor weld-quality was achieved due to gas formation. It was impossible to weld the plates together with a continuous adhesive layer. Therefore the solution was to interrupt the adhesive layer at the location where the weld had to be made. This was achieved by attaching two bars on top of the original steel deck plate which retained the adhesive between them. In this way a weld without air inclusions could be made. Figure 7-6 shows a weld with the bars without air inclusions.

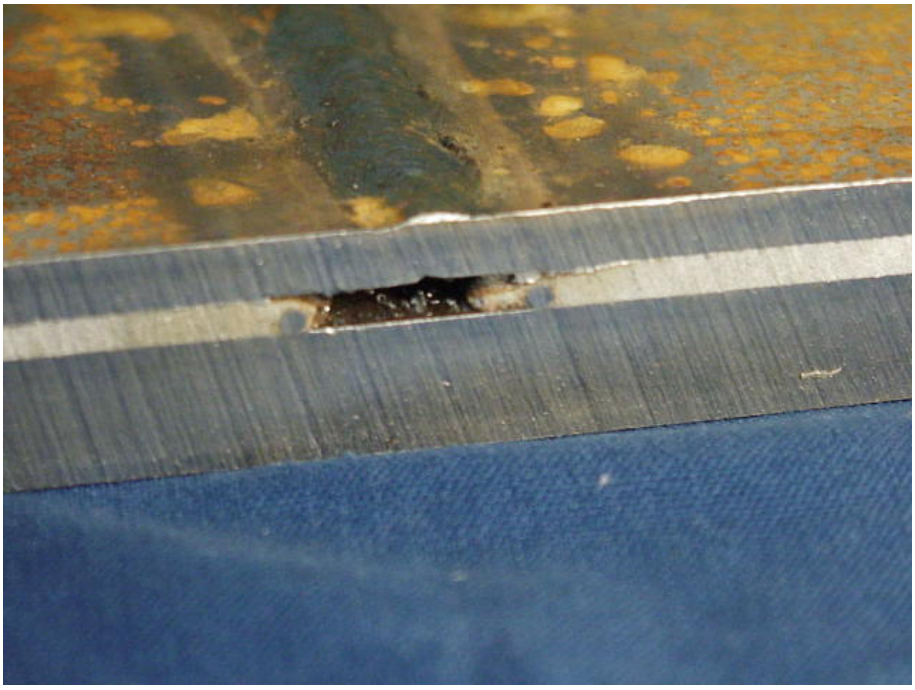

Figure 7-6: Good weld quality at plate division due to bar material

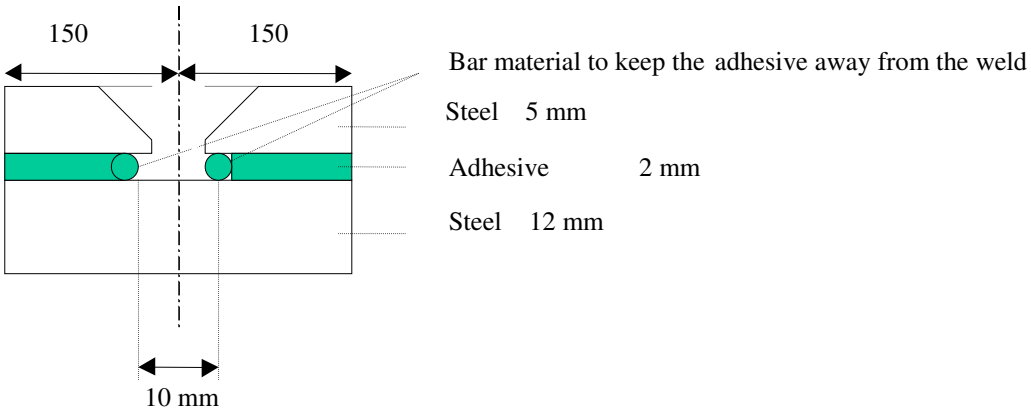

Figure 7-7: Solution to keep adhesive away from the weld (not on scale)

However although it is possible to make a weld without air inclusions in this way, in practice it is not thought to be a good connection method for bridges. Due to the sizable gap between the two upper plates, a lot of weld metal has to be added, leading to sizable weld shrinkage. Although this solution is suitable for laboratory conditions it is thought to be vulnerable when applied on a real bridge. Therefore a bonded connection is preferred.

Large scale application test

Before adopting this system on a bridge deck in a motorway it should be proved that it is appropriate for such an application. For that reason the laboratory tests and calculations described in this paragraph were performed. Besides the calculations and laboratory research there are also aspects, related to the application and execution on a larger scale. To research these aspects a large application test was performed. The test was made on a removed part of the old Van Brienenoord bascule bridge. The test is described in (Nagtegaal, 2002-a). Figure 7-8 shows the result of the application test on the old bridge deck.

Figure 7-8: Application test bonded second steel plate

The test area was made in December 2001. The area of the test surface was 27.5 m^2 (2.75 x 10 m) divided into three sections. Two plates 2.75 x 4.0 m and 1 plate 2.75 x 2.0 m were bonded to the bridge deck. The steel deck plate was shot blasted to Sa 2.5. and the plates bonded together with Sikadur 30 adhesive. One side the adhesive was applied with a glue comb and on the other side a thin flat layer of adhesive was applied. The connection between the plates

is a bonded indirect connection. The application test was performed in a factory hall, because of the bad weather conditions. During the bonding process no difficulties were observed. After the application process some specimen were cut out from the bridge deck. From these specimens it became clear that at many locations the bonding was inadequate because there were many air inclusions in the adhesive layer.

Tests were performed to discover the reasons for the unsatisfactory bonding in the test area. A few laboratory experiments were performed (Hechtings Instituut, 2002-a). From this tests a few conclusions can be drawn.

- To avoid air inclusions it is important to apply the adhesive to the steel deck plate with a coarse glue comb, which makes wide gaps between the adhesive thus facilitating the flow of air out of the interface.
- The second steel deck plate should be placed in contact at one edge of the old steel deck plate and then slowly rolled onto the deck plate, see Figure 7-18.

7.2.2.3 Application method 2

The second application method was developed at the laboratory of TNO in conjuntion with the Center of Lightweight Structures (Labordus, 2004, 2005, 2006). The main difference between the two application methods is that in the second application method the additional steel plate is located on top of the original steel deck plate before the application of the adhesive layer. The adhesive is then vacuum infused into the small space between the two steel plates Figure 7-9 shows this diagrammatically.

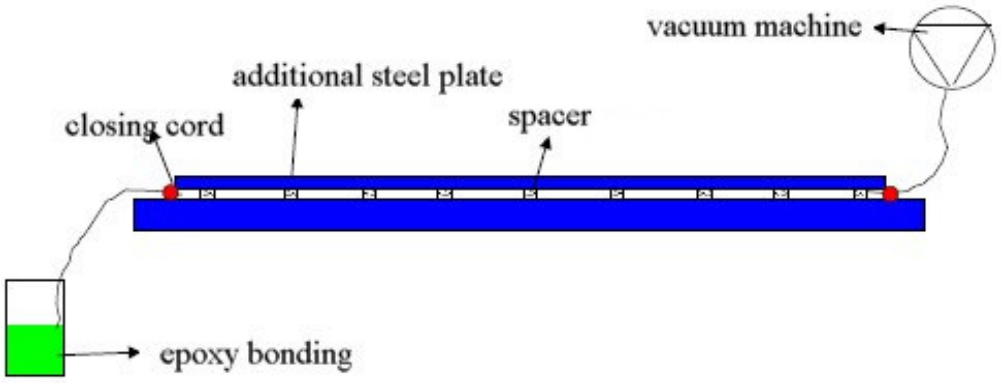

Figure 7-9: Vacuum infusion of bonded connection

The distance between the two steel plates is 2 mm and the vacuum infusion technique requires spacers between the original and the additional steel deck plate to maintain this gap. The rings as shown in Figure 7-10 were chosen as spacers, because the profile of the ring enables a good flow of the epoxy in and around it. Sealing cords around the additional steel deck plate are necessary to prevent leakage around the edges.

Figure 7-10: Spacer ring

From primary flow simulations is known that this vacuum infusion technique is probably a good technique, see (Labordus, 2004, 2005) for an elaborate description of these primary flow simulation. Subsequent strip infusion tests over a length of 3.5 m showed no problems in filling the complete gap between the bridge deck and the reinforcing plate. See Figure 7-11 for this test. A fill time of less than 3.5 minutes was measured. The epoxy is added at one side of the strip and the vacuum is applied at the other side.

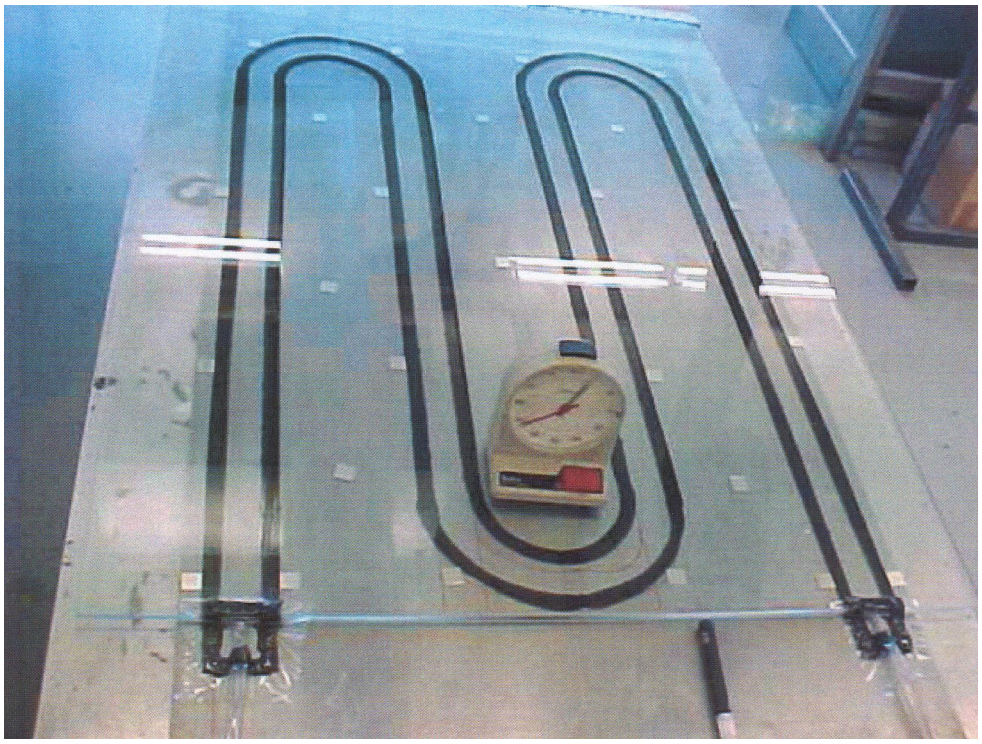

Figure 7-11: Strip infusion test

Flow simulation software was used to determine the optimum infusion strategy for a practical infusion of a 10 x 3.5 m infusion area. This area is more like the dimensions on real bridges. Figure 7-12 shows the flow simulation of a 30 x 3.5 m infusion area. The vast majority of the movable bridges are up to a length of 30 m. Visible at the lower side in the figure are the three-points where the epoxy adhesive is added and at the upper side the four-points where the vacuum is created. From flow simulations it became clear that it would be possible to fill this area in a few minutes.

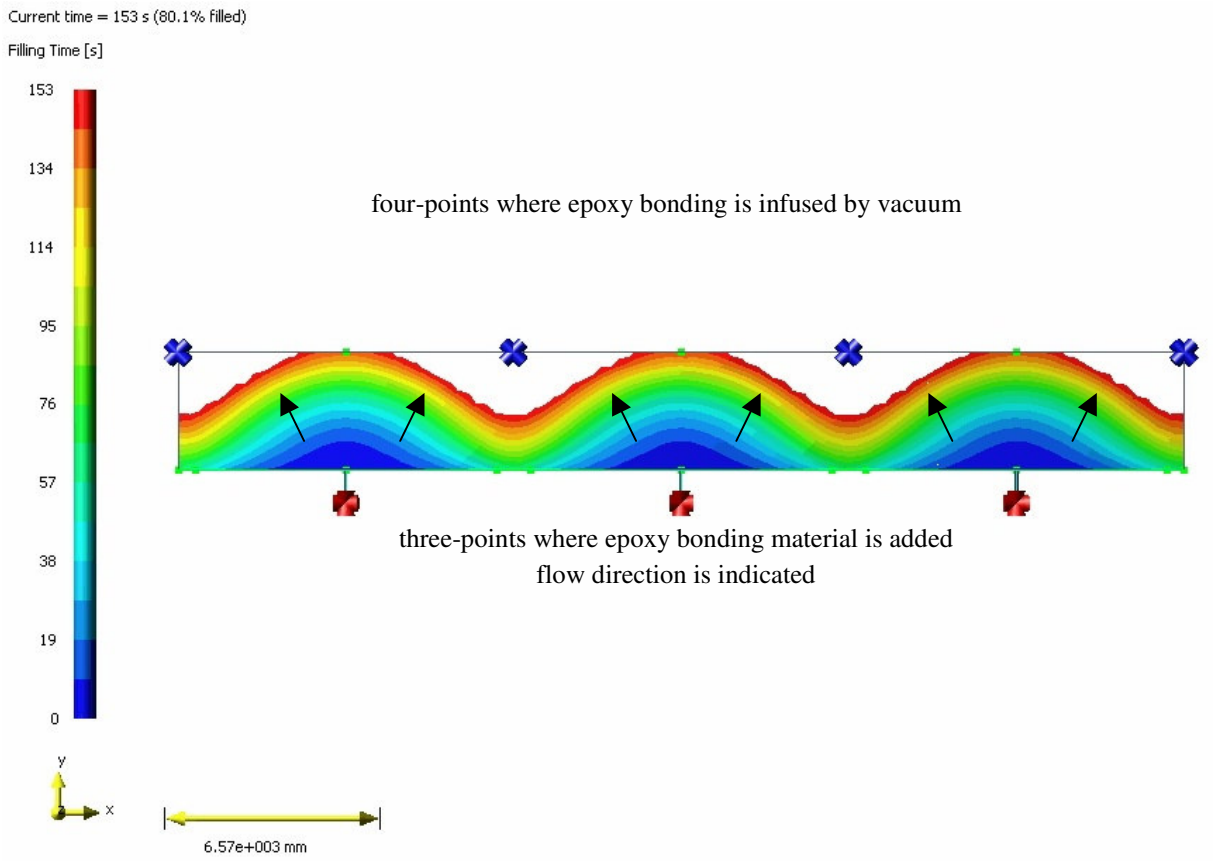

Figure 7-12: Flow simulation real bridge dimension

Large scale application test

Besides the flow simulation an additional steel plate 10 x 3.5 m was bonded to the original steel deck plate by the vacuum infusion technique in a practical test (Labordus, 2006). Figure 7-13 shows the vacuum infusion test on an old removed part of the van Brienenoord bascule bridge. The additional steel deck plate was welded together from several plates. Due to the welding shrinkage some deformation occurred and at some locations the distance between the original steel deck plate and the additional plate was more than 2 mm. Therefore the additional steel deck plate was loaded with some dead weight to guarantee the 2 mm

separation. Provisions to prevent leakage are clearly visible at the edges around the additional steel deck plate.

The time needed to achieve a complete fill in the test was significantly more than in the flow simulation. This was due to the temperature. In the test the temperature was about 8 °C and in the simulation 20 °C. The lower temperature was responsible for a higher viscosity, which slows down the flow. After the vacuum infusion test parts were cut out of the deck plate at four-points. At all these points full adhesion between the epoxy adhesive and both steel plates was observed. The adhesion strength at all 4 points was more than 20 MPa.

From this tests a few conclusions can be drawn.

- In practical situations the minimum temperature should be 15 °C – 20 °C to ensure easy flow of the epoxy adhesive. This means that this kind of renovation should be scheduled in the summer.
- A good bonding strength is achieved with this vacuum infusion method
- To verify if this is a method suitable for bridges a fatigue test should be performed on the bridge deck section.

Figure 7-13: Vacuum infusion test on bridge deck section

7.2.3 Numerical research and results

Pover has performed extensive Finite Element calculations (Pover, 2002, 2004). Chapter 6 has already given a thorough description of the different FE-models. In chapter 6 the models were pointed towards renovation with RHPC. Besides the FE-models provided with asphalt and concrete FE-models with a second steel deck plate bonded to the original steel deck plate were also made. For these models also the general purpose was to quantify the stress range reduction, in the deck plate at the fatigue prone locations, due to the renovation method. This paragraph reports in brief the results of the FE-models with a second steel deck plate.

Unlike the FE-models made for the RHPC surfacing only two types of FE-models were made for the renovation method with a second steel plate all with solid elements. These two types were:

- FE-models representing both local deck plate behaviour and crossbeam behaviour at the crossbeam location
- FE-models only representing local deck plate behaviour between two crossbeams

Unfortunately no FE-models representing only local deck plate behaviour at the crossbeam location were made.

7.2.3.1 FE-models - local deck plate behaviour and crossbeam behaviour

For the description of the FE-models representing both local deck plate and crossbeam behaviour at the crossbeam location and for an interpretation of the calculated stresses, see paragraph 6.3.1.2. The main interest is the stress reduction factor at the underside of the steel deck plate. Table 7-1 gives the numerical results of the calculations for the stresses in x-direction for the different load cases at the crack location along line 1, at the root of the weld.

Table 7-1: Stress σ_{xx} - underside deck plate along line 1 (MPa)

Stress underside deck plate in x-direction (MPa)	LC 5	LC 6	LC 7	LC 8
Standard model (No. 1 – STD)	-124	-86	-45	-4
Additional steel plate bonded	-59.3	-45	-29.4	-18
Stress reduction factor	0.48	0.52	0.65	

The shear stress σ_{yx} was also calculated at two interfaces, at the top surface and the underside of the epoxy adhesive layer at the interface with the steel deck plate. The maximum calculated shear stress was 4.35 MPa, which is relatively low compared to the shear capacity. From the FE-models it is clear that a reduction factor of approximately 0.5 to 0.6 is possible, dependent on the location of the local wheel load.

7.2.3.2 FE-models - local deck plate behaviour between crossbeams

For the description of the FE-models representing local deck plate behaviour between two crossbeams and for an interpretation of the calculated stresses, see paragraph 6.3.1.3. The main interest is the stress reduction factor at the underside of the steel deck plate. Table 7-2 gives the numerical results of the calculations for the stresses in x-direction for the different load cases at the crack location along line 1, at the root of the weld.

Table 7-2: Stress σ_{xx} - underside deck plate along line 1 (MPa)

Stress (MPa)	LC5	LC5	LC6	LC6	LC7	LC7
Location	crack	midspan	crack	maximum	crack	maximum
Standard model	-212	323	-120	120	-345	321
Steel plate	-59	150	-61	74	-141	134
Reduction factor	0.27	0.46	0.51	0.62	0.41	0.42

Reductions for stresses in the trough web were also calculated as these stresses in the trough web are responsible for fatigue crack growth in the longitudinal weld between trough web and deck plate. The application of an additional steel deck plate also reduces these stresses. Table 7-3 gives the calculated principal stresses in the trough web at the connection with the longitudinal weld. Local stress concentration effects are not included in this principal stress. The stress reduction factor is calculated for the stress at the inside of the trough web because the fatigue crack in the longitudinal weld initiates from the inner side of the trough web.

Table 7-3: Principal stress in trough web at longitudinal weld (MPa)

Principal Stress trough web (MPa)	LC5	LC5
	Outside trough web	Inside trough web
Standard model	135.7	-162.9
Steel plate	43	-73
Stress reduction factor (Steel/STD)	x	0.45

It is difficult to draw conclusions from the FE-models representing the local deck plate behaviour between the crossbeams. Table 7-2 shows that a reduction factor of 0.4 to 0.6 is possible for the stress in the deck plate depending on the location of the local wheel load. For the stress in the trough web a reduction factor of approximately 0.45 was derived from the FE-calculations.

7.2.4 Static testing program

7.2.4.1 Small test specimens

Some small test specimens were made for static testing (Poulis, 2000-a). For the tests the thickness of the adhesive layer was 2 mm. The dimensions of the lower original steel deck plate were 100 x 250 x 12 mm and the dimensions of the additional top plate were 100 x 250 x 5 mm. The steel plates were shot blasted to Sa 2.5 and the adhesive was applied within 60 minutes of shot blasting. Test specimens were made with the three selected types of adhesives: Sikadur 30, Araldite 2015 and Edilon NEX. Three specimens were made with each adhesive i.e.in total 9 test specimen were available. The test specimens were made from S355 steel and each was subjected to a three-point bending test, in order to determine the static strength of the adhesive layer. Figure 7-14 shows the test set-up. Figure 7-15 gives an overview and a detail photograph of the test up.

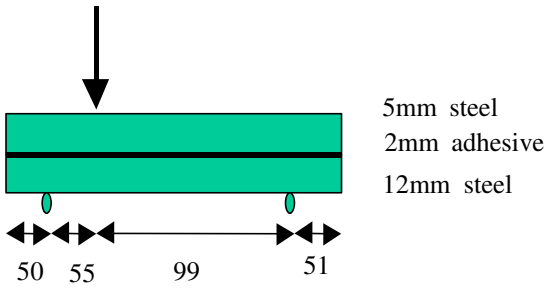

Figure 7-14: Test dimensions three-point bending tests (not on scale)

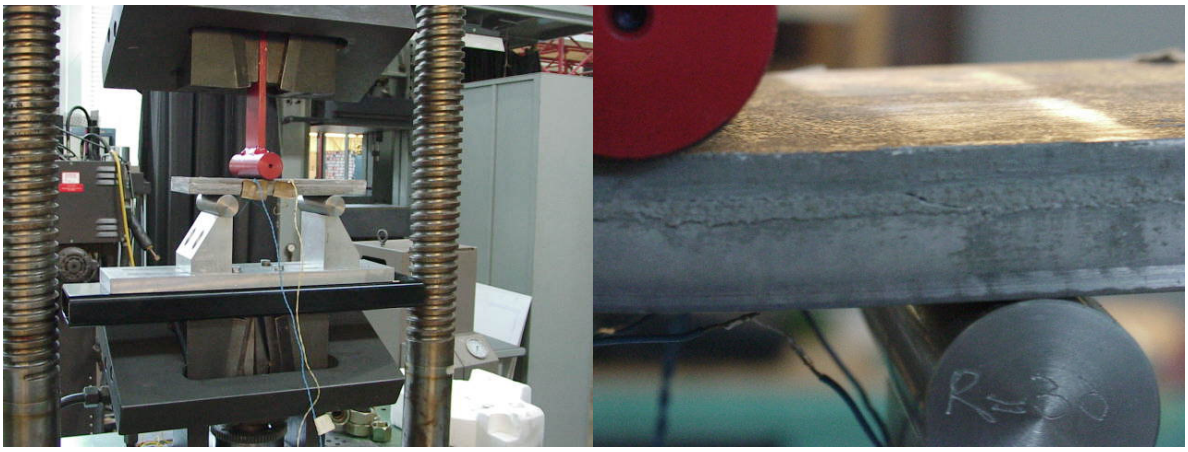

Figure 7-15: Three-point bending tests - bonded steel plate

Figure 7-16 shows a deformed test specimen after the test. Failure in the test specimen was a

combination of delamination at the interfaces between steel and the adhesive layer and plastic deformation of the steel plates. Delamination was not observed before the plastic deformation of the steel parts occurred. This means that the shear strength in the interfaces between steel and adhesive is sufficient. The ultimate static capacity of the three specimens for each adhesive type was about the same.

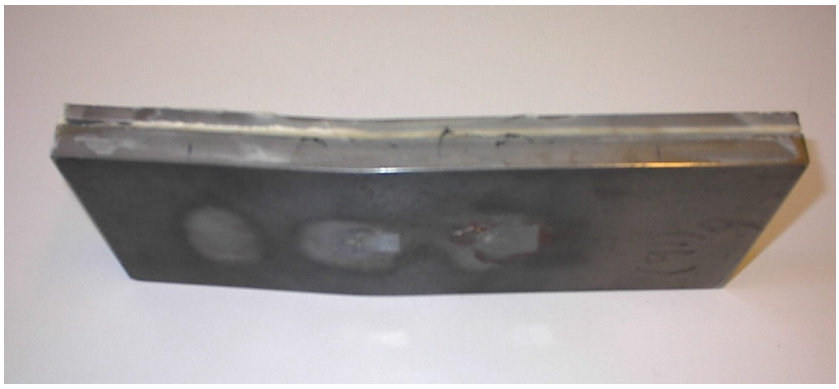

Figure 7-16: Deformation after 3-point bending test

Figure 7-17 shows the results of the three-point bending tests for all 9 specimens.

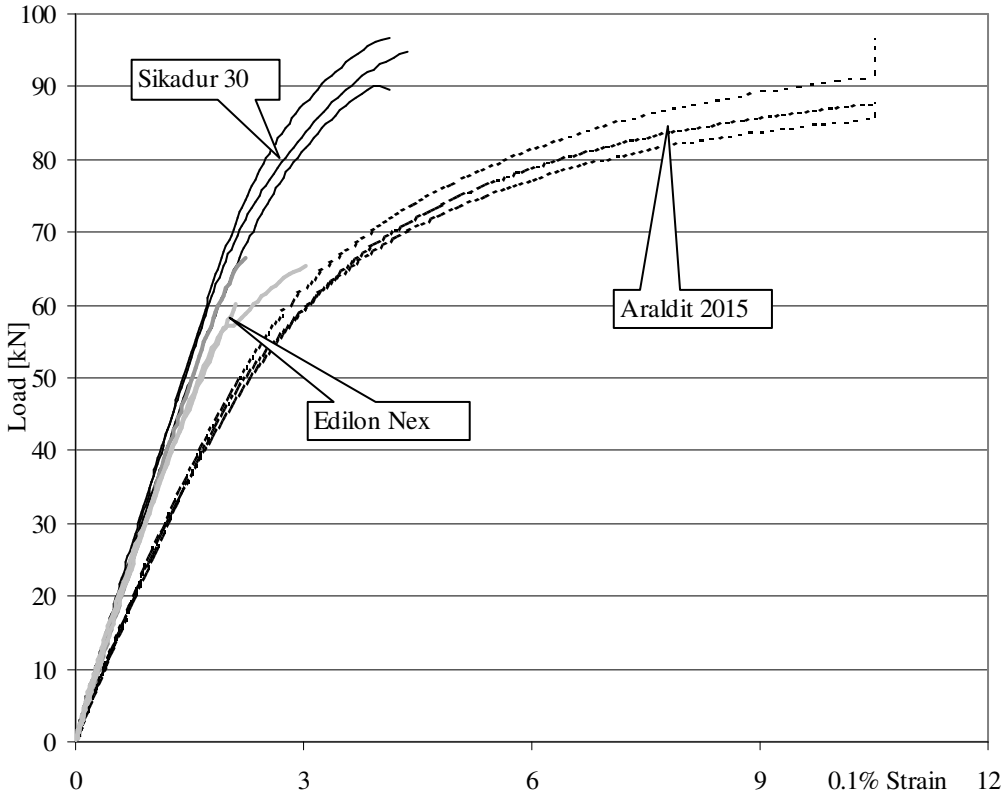

Figure 7-17: Results 3-point bending tests

The static strength of the Sikadur 30 and the Araldite 2015 were about the same. The strength of the Edilon NEX was much lower. The stiffnesses of Sikadur 30 and Edilon NEX were about the same and higher than the stiffness of the Araldite 2015. From the tests a shear capacity of 25 to 30 MPa was calculated back for the Sikadur 30 and the Araldite 2015 and a shear capacity about 20 MPa for the Edilon NEX (Nagtegaal, 2002-c).

In addition to these tests some static tests were also performed on test specimen with an division between the steel plates (Hechtings Instituut, 2002-b). Both a welded connection and a bonded connection between the two upper plates were tested, see Figure 7-5.

Three-point bending tests were performed on the welded connection. The test set-up is identical to the tests described above. The three-point bending tests were intended to determine the shear strength of the adhesive layer at the location where a connecting weld between two upper plates had been made. These tests were intended to determine the shear strength of the adhesive layer. From the three-point bending tests it was clear that the connection between the two upper plates had only a slight influence on the shear strength of the bonded connection, and that the steel parts were already yielding before delamination in the interface between steel and adhesive occurred (Nagtegaal, 2002-d). These small static tests revealed that the welded and bonded connections are comparable to each other but the bonded connection is preferred because the welded connection is not suitable for real bridge conditions.

7.2.4.2 Bridge panel TNO

Tests were also performed on a full-scale bridge deck test panel with a second steel deck plate bonded to the original steel deck plate. This panel is called TNO panel because this panel was subjected to tests at the laboratory of TNO. The test panel was subjected to static and fatigue tests. The fatigue tests are described in paragraph 7.2.5.2.

Test panel

The test panel was not cut from the test panel depicted in Figure 7-8, because the adhesion achieved in this test was unsatisfactory. A new test panel was made in the laboratory of TNO. Therefore a part of the old Van Brienenoord bascule bridge was transported to the TNO laboratory. In the laboratory, the second steel deck plates were bonded to this bridge deck panel, see Figure 7-18.

The applied steel deck plates were 6 mm thick and the adhesive used was again Sikadur 30. The adhesive was carefully applied to the steel deck plate and the additional plates were rolled on to prevent air inclusions. The plates that were bonded to the steel deck were also weighted in order to achieve a satisfactory squeeze out of the adhesive layer, see Figure 7-19.

This test panel was used for the tests at TNO. The static and fatigue tests are extensively reported by Van Straalen (Van Straalen, 2003-a). Figure 7-20 shows the test panel that was used for the tests at TNO. The division between two plates is covered with an extra top plate with a thickness of 2 mm. Figure 7-5 shows this solution in the right figure.

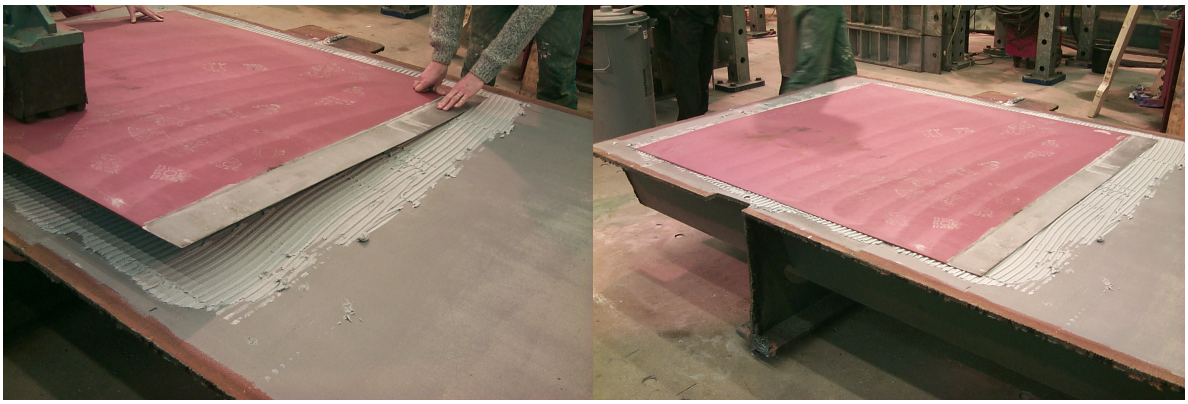

Figure 7-18: Bonding steel deck plate to TNO test panel

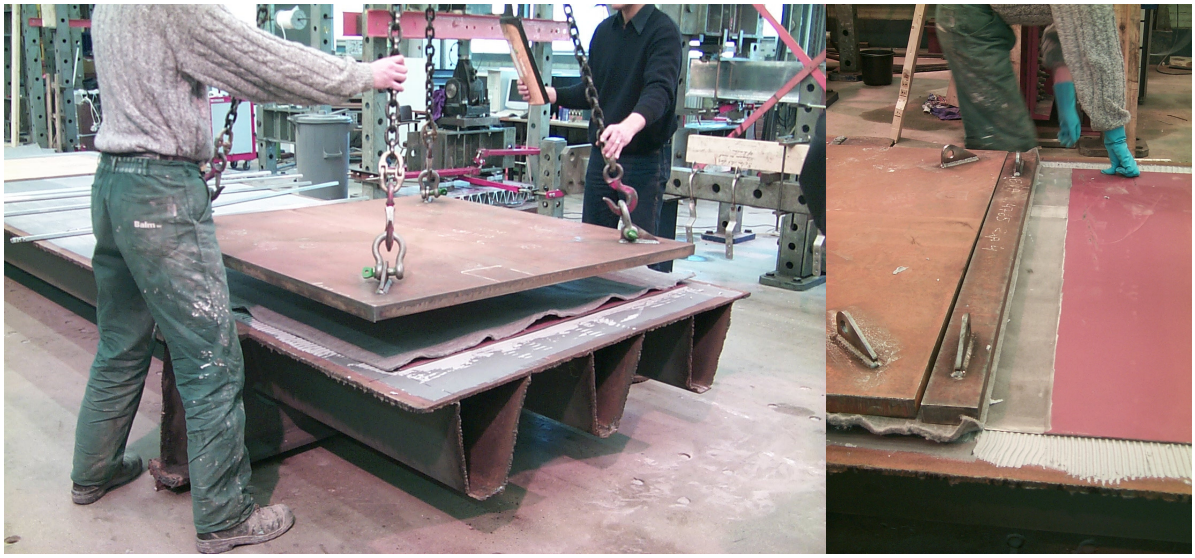

Figure 7-19: Ballast to facilitate squeeze out of the adhesive between steel plates

The wheel load is placed on an area of 270 mm wide and 320 mm long, which is the super single tyre (type C) according to the Eurocode, see paragraph 3.2.1. Figure 7-21 shows this load set-up. This load is placed at two locations, for two different fatigue tests:

- Above the crossing of the middle trough and the crossbeam.
- Above the crossing of the middle trough and the plate connection

The footprint differs from the footprint on the FE-models, which was the single tyre (type A, 220 mm wide). In paragraph 6.6.1 it has already been argued that it is possible to compare the results of the models and the measurements.

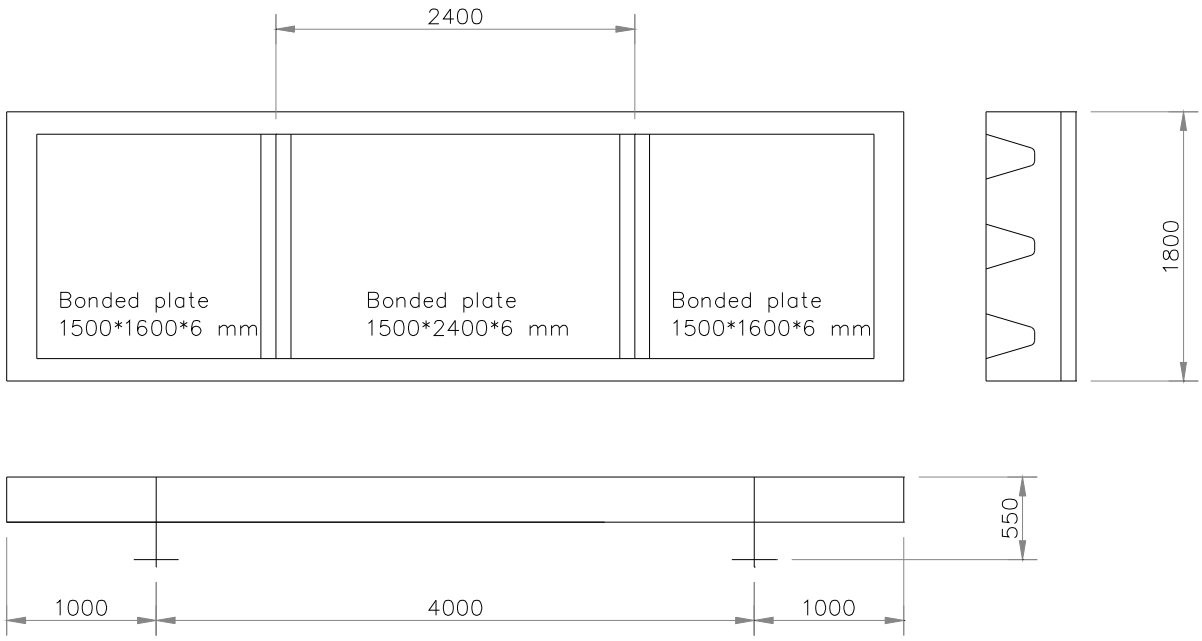

Figure 7-20: TNO panel for static and fatigue tests with bonded second steel plate

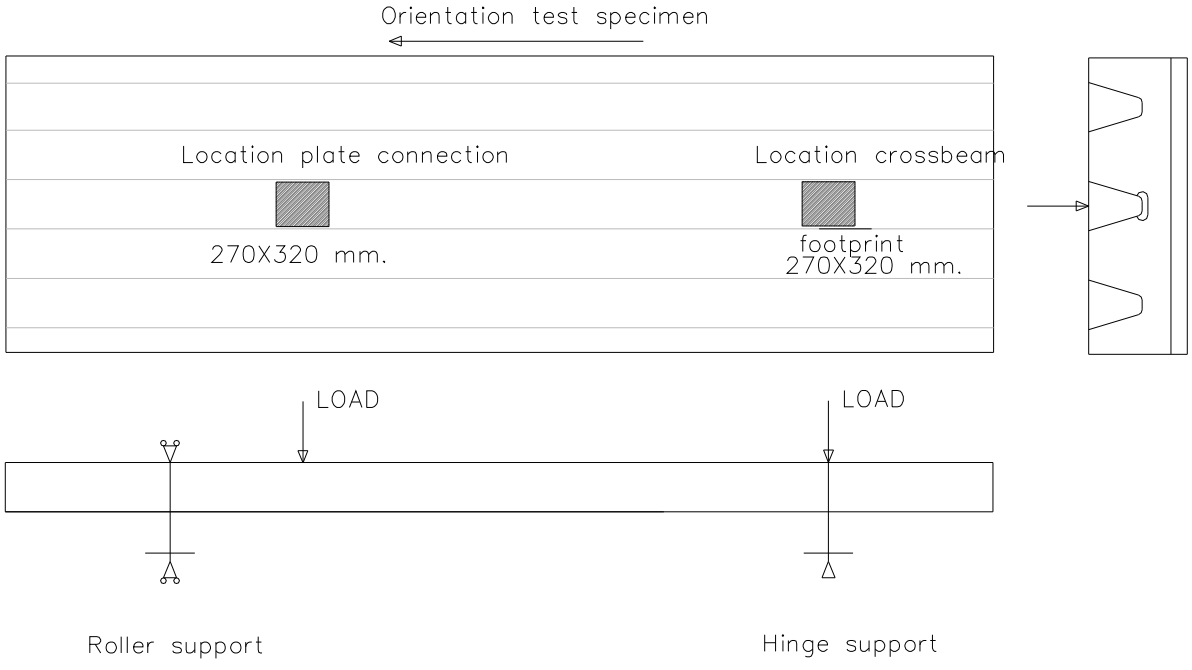

Figure 7-21: Location wheel load on TNO panel

Strain gauges

Strain gauges were applied on the bridge deck at both locations tested.
The strain gauges at the crossbeam are shown in three figures:

- Figure 7-22 - a cross-section of the gauges
- Figure 7-23 - a top view of the gauges at the underside of the deck and trough web
- Figure 7-24 - a top view of the gauges at the top side of the second steel plate.

The strain gauges at the plate connection are given in three figures:

- Figure 7-22 - a cross-section of the gauges
- Figure 7-25 - a top view of the gauges at the underside of the deck and trough web
- Figure 7-26 - a top view of the gauges at the top side of the second steel plate.

Strain gauges were also applied to the underside of the steel deck plate, both at the crossbeam location and on the plate division location. To create accessibility at both locations parts of the troughs were cut out, just as in other test specimen, see Figure 6-31. The pieces that were cut out were welded back in the troughs after the application of the strain gauges and before testing. Note that these figures are not on scale. The strain gauges all measure in transverse direction.

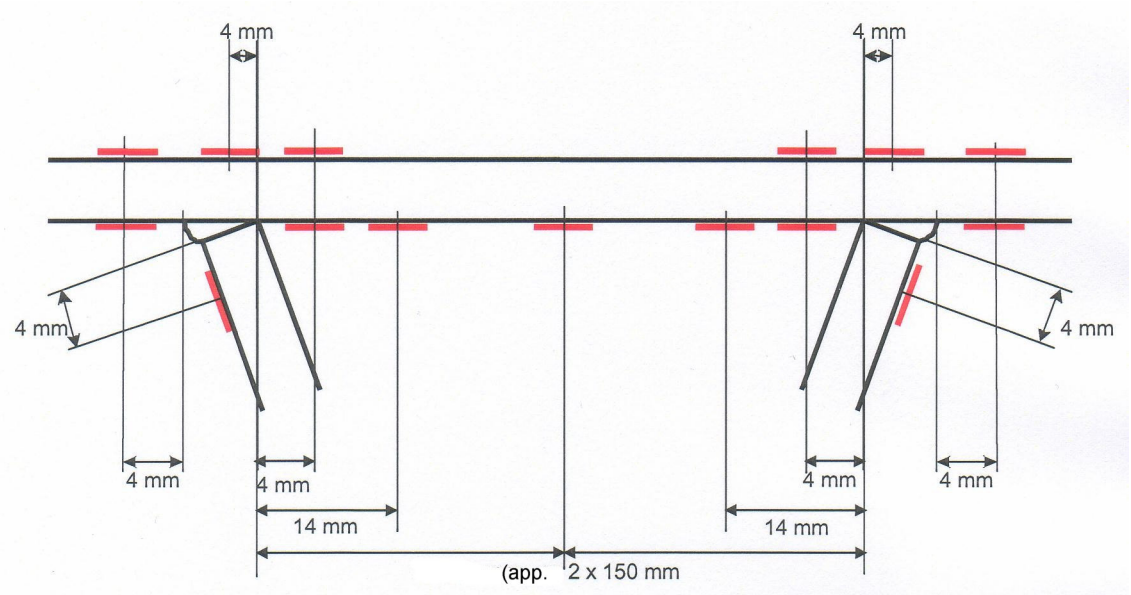

Figure 7-22: Cross-section strain gauges

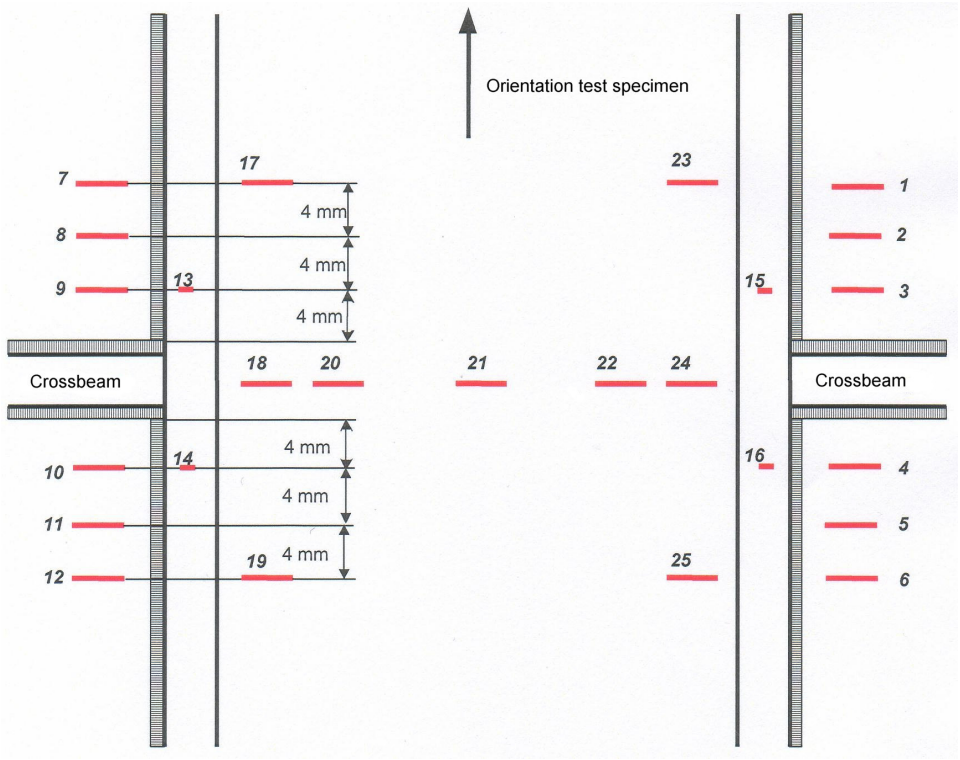

Figure 7-23: Top view of strain gauges at underside deck plate and trough web at crossbeam

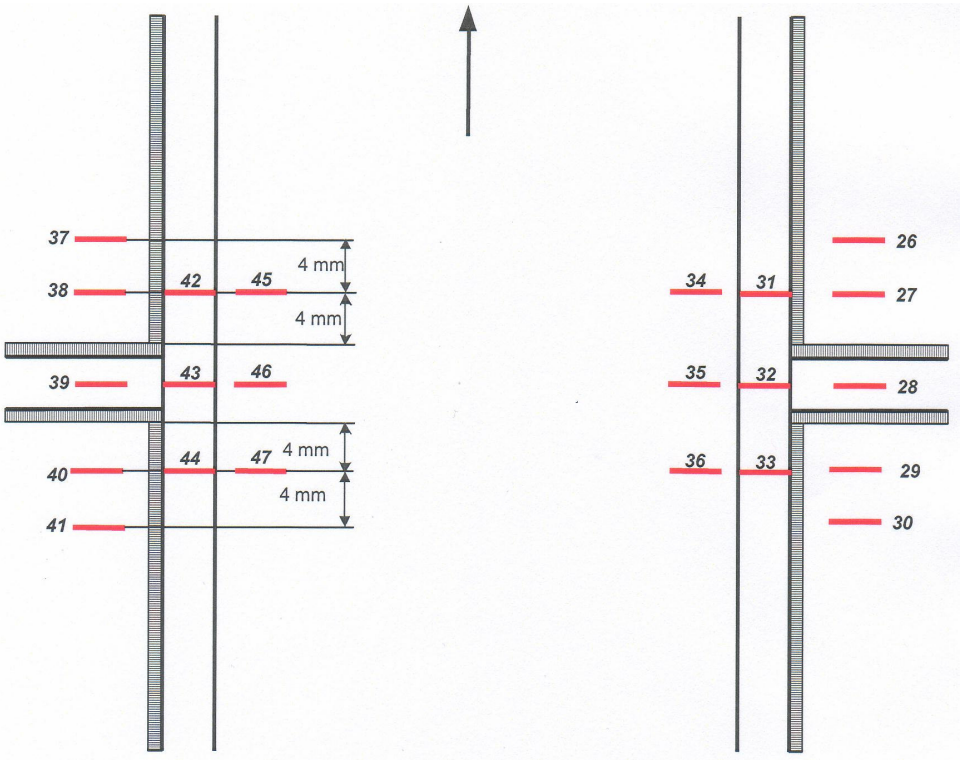

Figure 7-24: Top view of strain gauges at top side of second steel deck plate at crossbeam

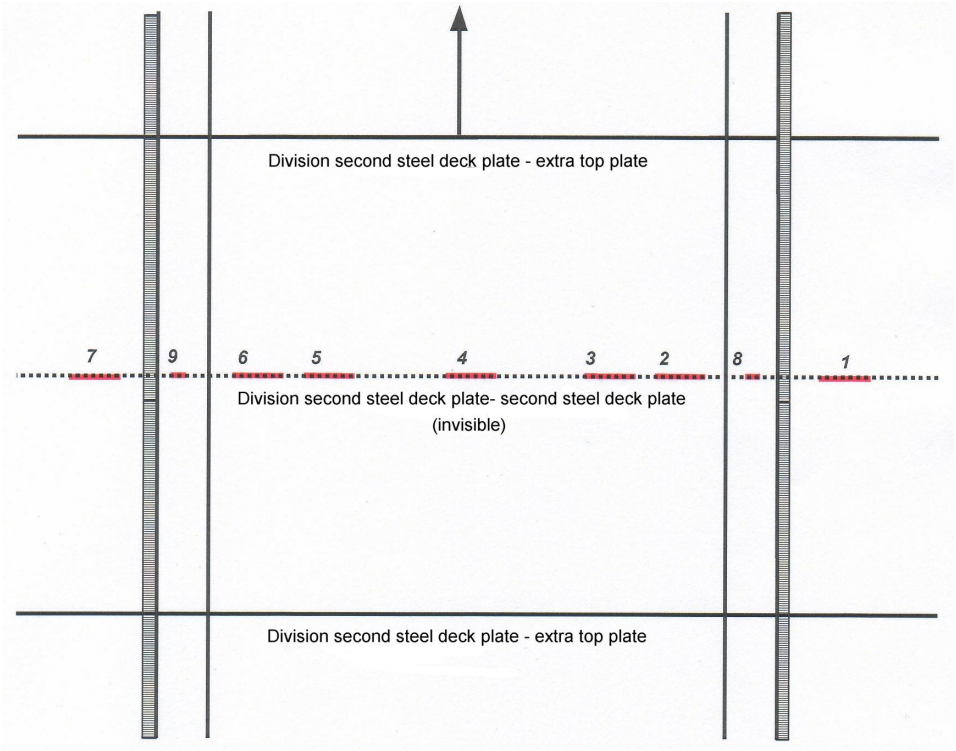

Figure 7-25: Top view of gauges at underside deck plate and trough web at plate connection

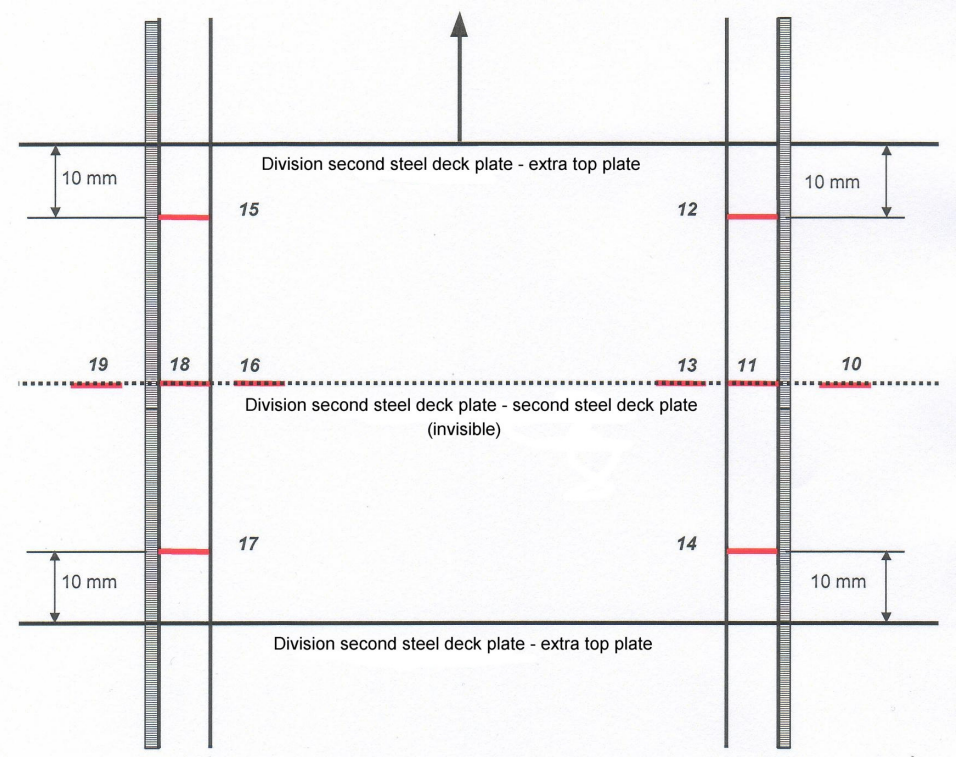

Figure 7-26: Top view of gauges at top side of second steel deck plate at plate connection

Measurements at crossbeam

The most relevant strain gauges for the determination of the stress reduction at the fatigue prone location are those that are attached to the underside of the deck plate, within the trough web and in line with the crossbeam. These strain gauges are numbered 18, 20, 21, 22 and 24. On the top of the additional steel deck plate the most relevant strain gauges are 28, 32, 35, 39, 43 and 46.

A load of 117 kN was applied in 5 equal load cycles. In one cycle the load is increased and decreased in 5 equal steps set from 12 kN to the maximum load of 117 kN (12 – 33 – 54 – 75 – 96 – 117 – 96 – 75 – 54 – 33 – 12 kN). The results of these 5 load cycles are given in Table 7-4, for the strain gauges 18, 20, 21, 22 and 24. This table gives the measured strain range in the load range (ΔF) of 105 kN. To get a more complete overview of the strains the results of the strain ranges on top of the second steel deck plate have been tabulated, see Table 7-5.

Table 7-4: Strain range underside ($\Delta\varepsilon$ x10^{-6}) at ΔF 105 kN (12-117 kN) at crossbeam

Gauge	18	20	21	22	24
Average	-609	-402	365	-376	-625

Table 7-5: Strain range top side ($\Delta\varepsilon$ x 10^{-6}) at ΔF 105 kN (12-117 kN) at crossbeam

Gauge	28	32	35	46	43	39
Average	251	411	392	360	410	270

Measurement at plate division

The same static test procedure was also applied at the plate division. The most relevant strain gauges are numbered 1, 2, 3, 4, 5, 6 and 7, see Figure 7-25. On top of the additional steel deck plate at the location of the plate division the most relevant strain gauges are 10, 11, 13, 16, 18 and 19, see Figure 7-26.

Table 7-6: Strain range underside ($\Delta\varepsilon$ x10^{-6}) at ΔF 105 kN (12-117 kN) at plate division

Gauge	1	2	3	4	5	6	7
Average	389	357	202	766	141	289	382

Table 7-7: Strain range top side ($\Delta\varepsilon$ x 10^{-6}) at ΔF 105 kN (12-117 kN) at plate division

Gauge	10	11	13	16	18	19
Average	101	74	47	153	200	205

Evaluation measurements

A few comments on the results of the measurements at the crossbeam location:

- The difference between gauges 18 and 20 is relatively large, as is the difference between the gauges 22 and 24. Considering the distance of 10 mm between 18 and 20 and between 22 and 24, it can be concluded that there is a high strain gradient.
- The strain gradient between the gauges 18 and 20 is 20.7×10^{-6}/mm. The strain gradient between the gauges 22 and 24 is 24.9×10^{-6}/mm.
- Linear extrapolation of the strains to the crack locations leads to a strain of -692×10^{-6} at the side of gauges 18 and 20 and to a strain of -725×10^{-6} at the side of the gauges 20 and 22.

A few comments on the results of the measurements at the plate division:

- Contrary to expectation there is a big difference between the strain gauges 10-11-13 at one side and 16-18-19 at the other side. Based on symmetry conditions approximately the same results were expected at both sides.
- The differences between the left and right gauges on the underside of the steel deck plate are not so clear. The difference between 2 and 6 and the difference between 3 and 5 is significant.

7.2.5 Fatigue testing program

7.2.5.1 Small test specimens

The test specimens with the three different adhesives (Sikadur 30, Araldite 2015 and Edilon NEX) were subjected to some fatigue tests (Poulis, 2000-a). The tests specimens had the same dimensions as the specimens that were used for the static tests and described in paragraph 7.2.4.1.

In the fatigue tests each specimen was subjected to 1 million cycles with a range of ΔF = 10 kN and subsequently to 1 million cycles with ΔF = 20 kN. During the fatigue tests the strain ranges did not change. After the fatigue tests the specimen were subjected to identical static tests. The results of these static tests show that the strength and stiffness of the adhesive layers was the same as before the fatigue test. An extensive description of the fatigue on the small laboratory specimens can be found in (Poulis, 2000-a)

7.2.5.2 Bridge panel TNO

After the static test, reported in paragraph 7.2.4.2 two fatigue tests were performed, one test at the crossbeam location and one test at the plate connection. The fatigue tests were performed in the laboratory of TNO. The test data were reported by Van Straalen (Van Straalen, 2003-a).

The wheel load (270 x 320 mm, width x length) is again centered above the trough at the location of the crossbeam or the plate connection, see Figure 7-21. Figure 7-27 gives a photograph of the fatigue test at the location of the plate division.

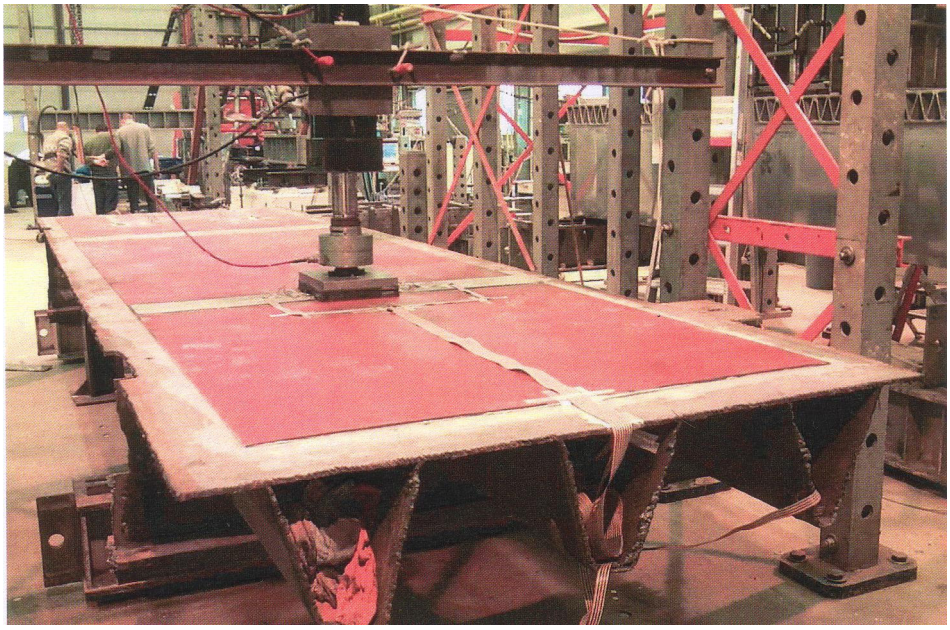

Figure 7-27: Full-scale fatigue test at bonded steel deck plate at location plate division

The following load cycles were applied:

- At the crossbeam location: 8.4x 10^6 cycles with a range of 105 kN (12 kN - 117 kN)
- At the plate division: 4.2x10^6 cycles with a range of 105 kN (12 kN - 117 kN)

Calculations (De Jong, 2006-b) have shown that for this number of cycles at the crossbeam location this load set-up is equivalent to :

- 24 years of fatigue according to fatigue load model 4 from Eurocode 1991 - Part 2
- 21 years of heavy vehicle traffic on the Moerdijk Bridge, with respect to fatigue of the steel deck plate. The Moerdijk Bridge is the most heavy loaded bridge deck in the Netherlands.

For the test at the plate division it equals 12 years for both Eurocode and Moerdijk load spectra.

Strain ranges at crossbeam location

During the fatigue test the static loading procedure was repeated 108 times. Figure 7-28 shows the measured strain ranges at the underside of the original steel deck plate at the load range of 105 kN for these static loading procedures. Figure 7-29 gives the strain ranges at the top side of the additional steel deck plate.

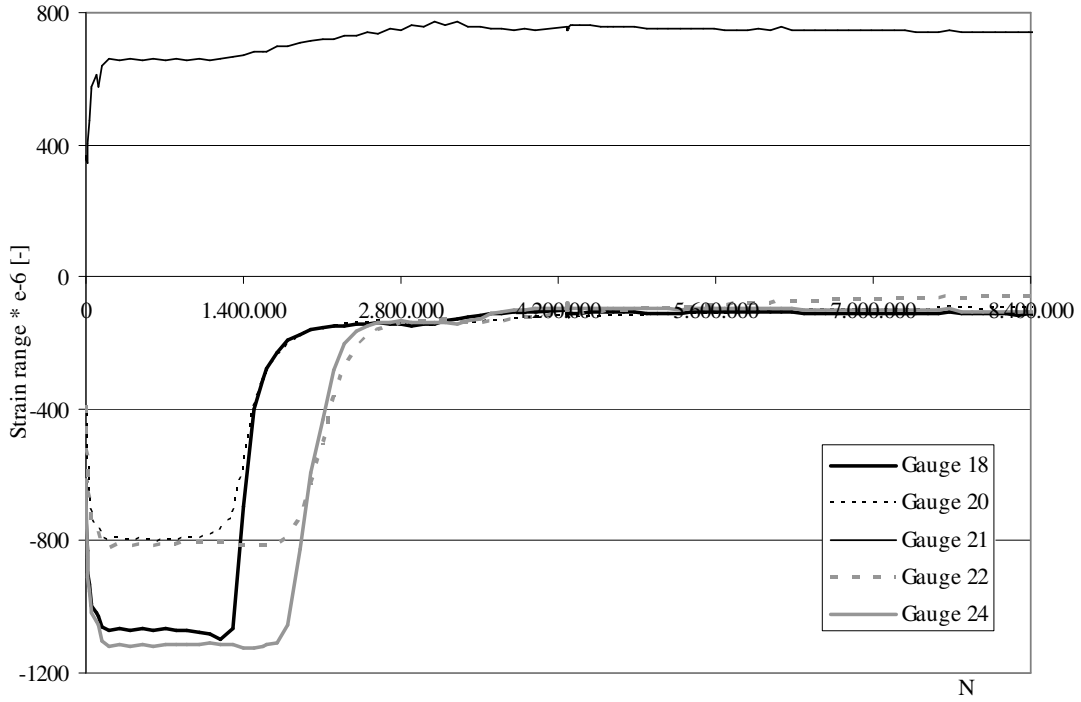

Figure 7-28: Strain ranges at bottom steel during fatigue test at TNO panel at crossbeam

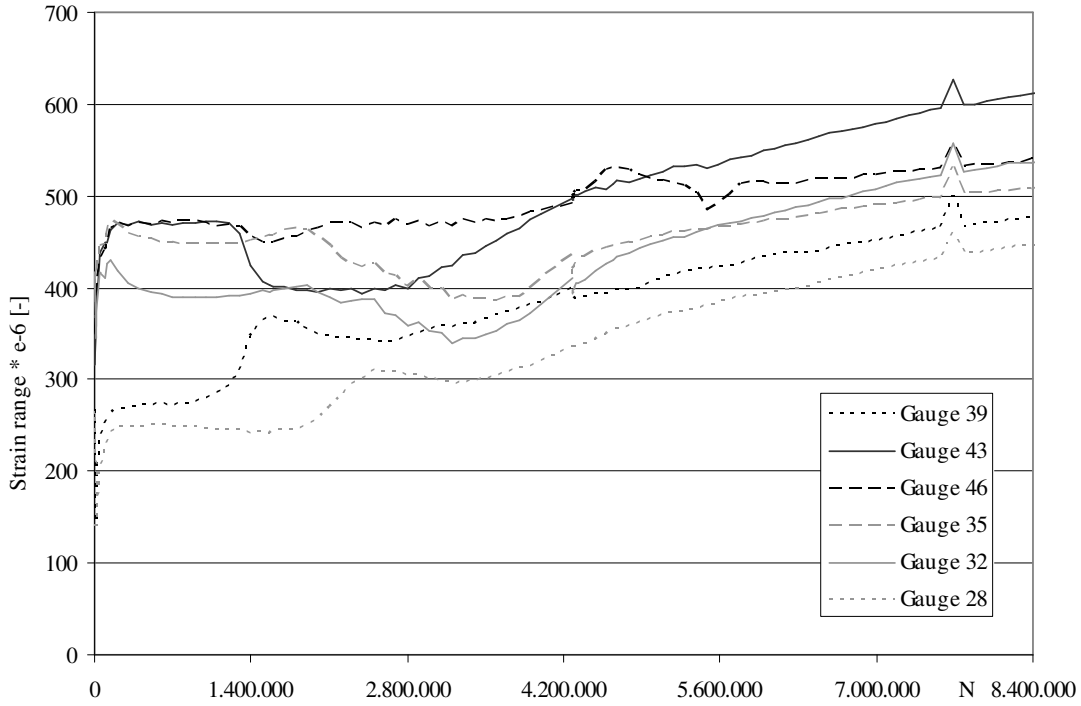

Figure 7-29: Strain ranges at top additional steel plate during fatigue test at TNO panel at crossbeam

Some remarks on these two figures:

- A major change is clearly visible in the measured strain ranges at approximately 1 million cycles. The strain ranges at the underside decrease dramatically, the strain ranges at the top side however increase or decrease only slightly.
- The strain range at gauge 21 midspan between the two trough webs hardly increases, whereas the ranges of the four gauges at the trough web connection decrease dramatically.
- This suggests that fatigue cracks in the steel were growing or that the adhesive layer has delaminates. During the fatigue test at the crossbeam location however this was not noticed. Inspection after the test showed that delamination had occurred, see paragraph 7.2.6.

Strain ranges at plate division

During the fatigue test the static loading procedure was repeated 77 times. Figure 7-30 shows the measured strain ranges at the load range of 105 kN for these static loading procedures on the underside of the original steel deck plate. Figure 7-31 gives the strain ranges at the top side of the additional steel deck plate.

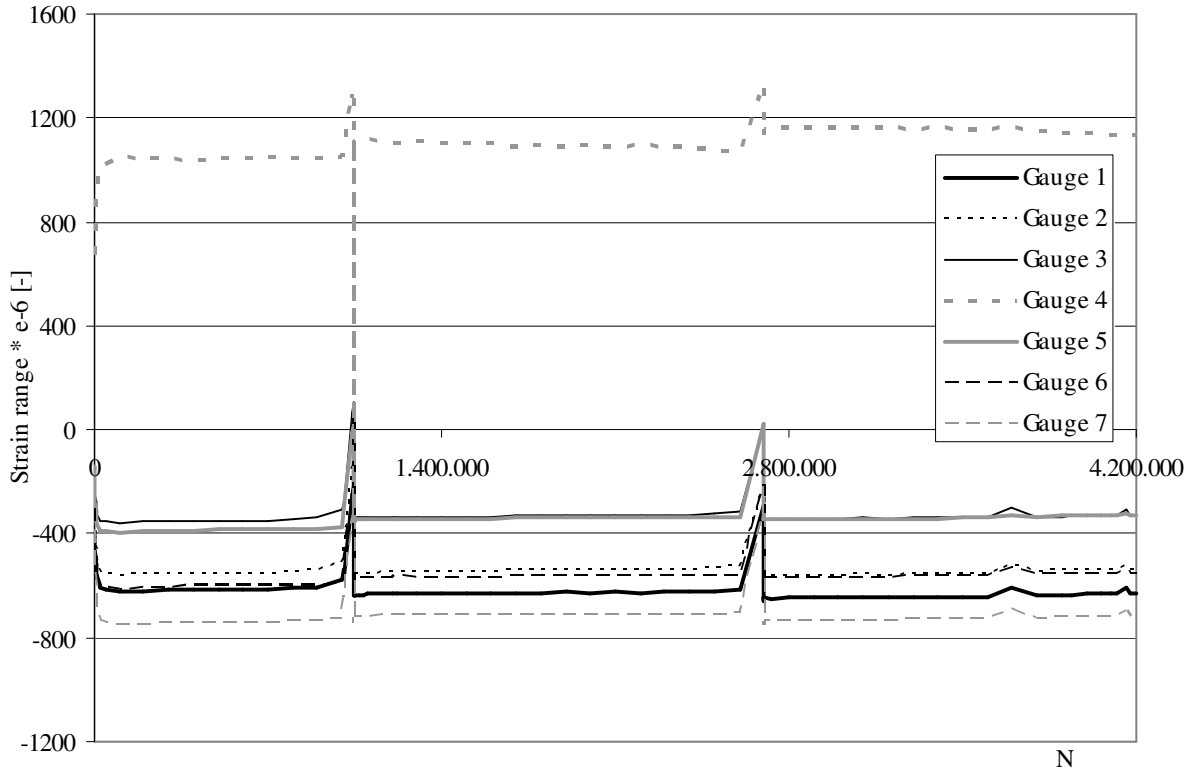

Figure 7-30: Strain ranges at bottom steel during fatigue test at TNO panel at plate division

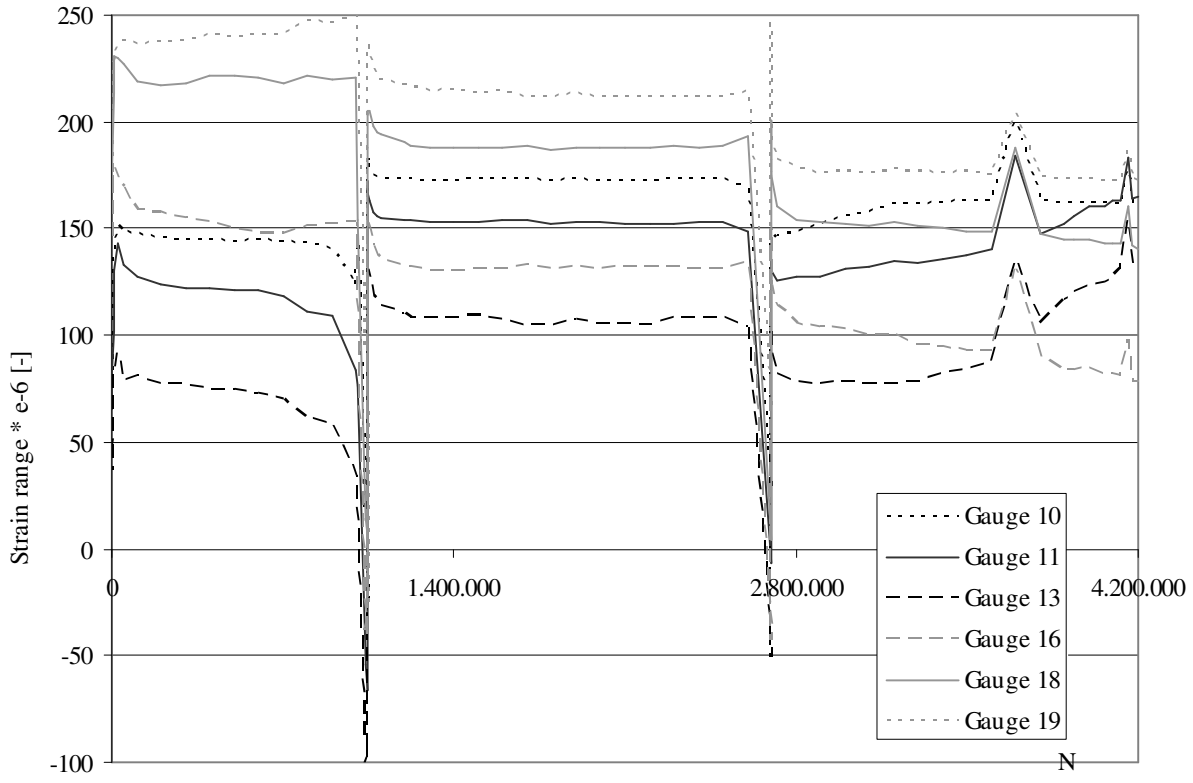

Figure 7-31: Strain ranges at top additional steel plate during fatigue test at TNO panel at plate division

Some remarks at these two figures:

- During the fatigue test at the plate division location no fatigue cracks in the steel were detected.
- After the fatigue test delamination in the adhesive layer was detected, because it was possible to insert a plastic card completely between the adhesive layer and the extra top plate at the plate division, see Figure 7-5.
- To attach the strain gauges to the underside a part of the trough was cut out and welded back, see figure 6-33. During the fatigue test in two places a fatigue crack was observed in this weld, at N = 1.046.475 and at N = 2.695.310 cycles. Both times the crack was repaired by welding and the fatigue test was continued. These two occurrences are clearly visible in Figure 7-30 and Figure 7-31.
- During the fatigue test the measured strain ranges for the gauges attached to the underside of the steel deck plate hardly change and for the gauges attached to the top of the extra steel plate the changes are limited. The moment of the delamination cannot be detected from the measured strain ranges.

7.2.6 NDT inspection bridge panel TNO

Ultrasonic inspections of the adhesive layer between the additional steel plate and the original steel plate were performed (Bakker, 2003-b, 2004). This paragraph describes those tests which were performed in addition to the visual inspections during the fatigue test. The quality of the adhesive layer is fundamental to the durability of this renovation method. Therefore the ultrasonic inspection was performed twice:

- Before the fatigue tests at crossbeam location and plate division on 4 June 2003
- After both fatigue tests on 3 February 2004

It is possible to detect delaminated areas with this type of inspection. The inspections were carried out from the top surface of the additional steel plates. The adhesion at the upper interface between the additional top plate and the adhesive layer was inspected ultrasonically but that at the bottom interface between original steel deck plate and the adhesive layer or fatigue cracks in the original steel deck plate were not inspected. It may be assumed that the adhesion between the adhesive layer and the original steel deck plate was good because the adhesive layer was applied to this original steel deck plate with a glue comb.

In total 6 locations were inspected before the fatigue tests. These locations are labelled A to F, see Figure 7-32. The O in this figure is the origin of each measurement location. In total 2 locations were inspected after the fatigue tests. These are the location of the fatigue test at the intersection of crossbeam and trough, labelled A, and the location of the fatigue test at the plate division, labelled C.

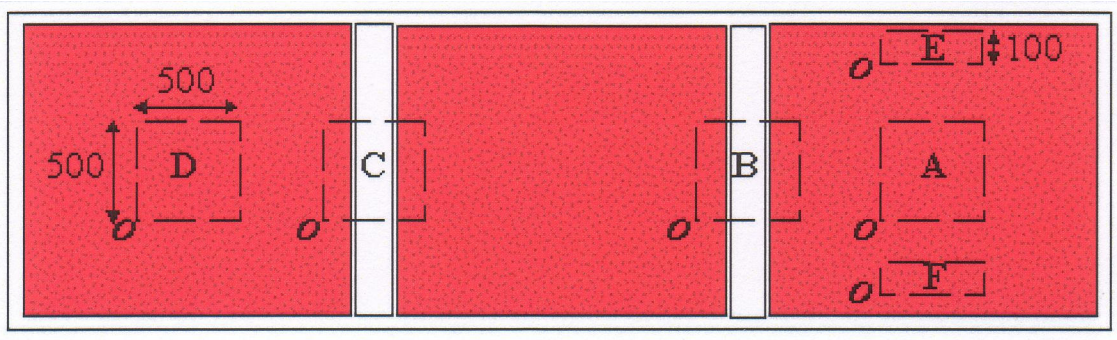

Figure 7-32: Locations ultrasonic inspection

The locations A, B, C and D are 500 x 500 mm. The locations E and F were 500 x 100 mm. The ultrasonic inspections were performed on a measurement grid with a mesh dimension of 50 mm in both directions. This meant that 11 x 11 spots were inspected for A to D and 11 x 3 spots for E and F.

The ultrasonic inspection before the fatigue tests detected no relevant indications of delaminated areas. Only a few indications slightly above detection level were observed. No indications were found at the plate division (C and B) and at E and F.

The second inspection in February 2004 after the fatigue tests however shows significant delaminations in the adhesive between the top plate and the adhesive layer. These delaminations were observed both at the crossbeam location (A) and at the plate division location (C). Figure 7-33 and Figure 7-34 show the delamination detected at the crossbeam location for two different measurement frequencies. Figure 7-35 shows the delamination detected at the plate division location for two different measurement frequencies. Table 7-8 provides the chart legend.

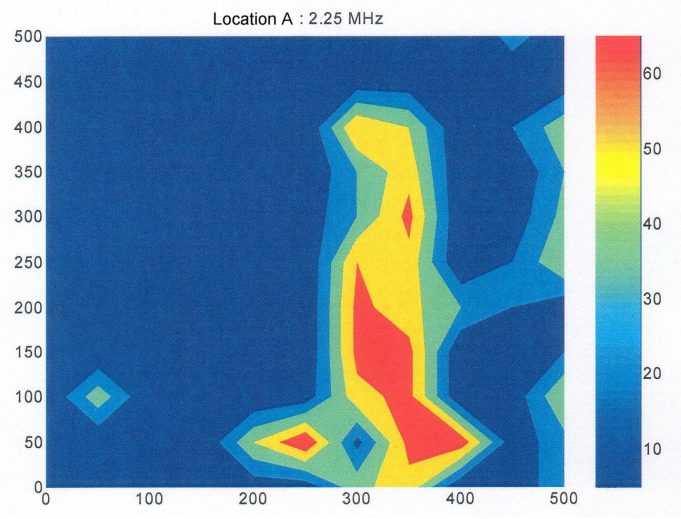

Figure 7-33: Delaminations at location A at 2.25 MHz

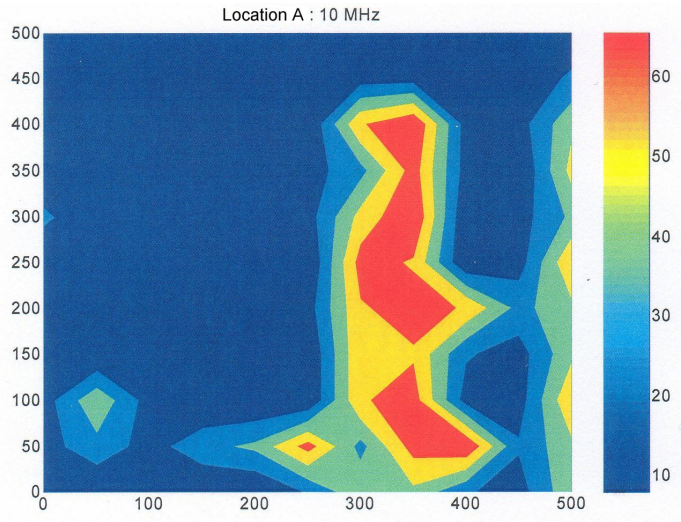

Figure 7-34: Delaminations at location A at 10 MHz

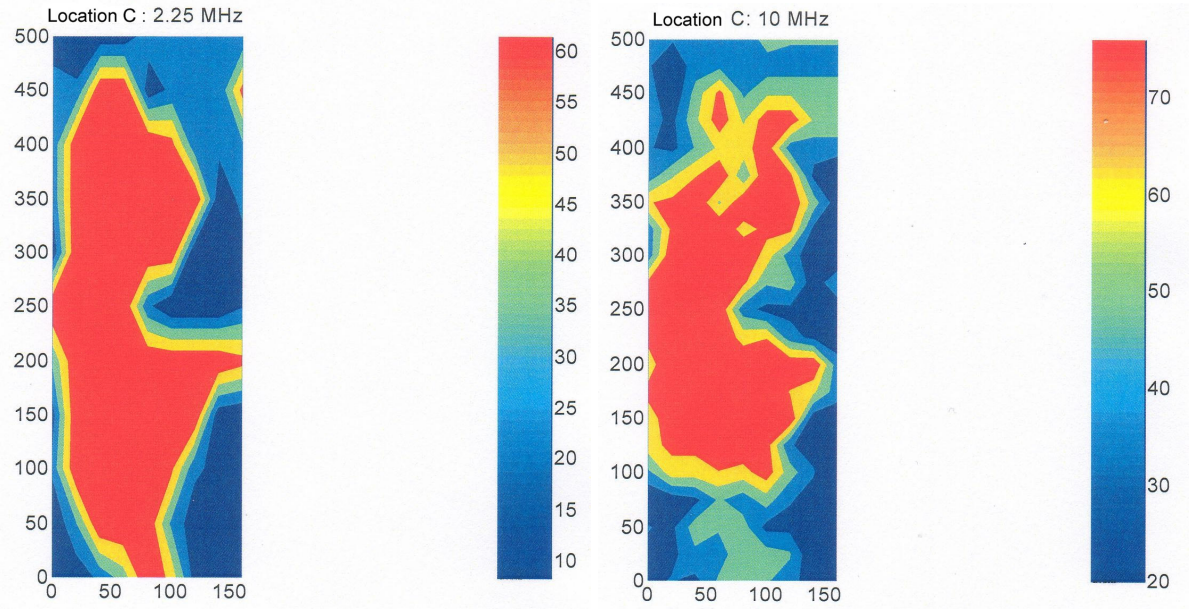

Figure 7-35: Delaminations at location C at 2.25 MHz (left) and 10 MHz (right)

Table 7-8: Interpretation and presentation of amplitude level

Amplitude level	Damping [dB]	Interpretation	Color
0 - 10%	<= 18	Good bonding	
10 - 32%	12 - 18	Good bonding to ¼ delaminated	
32 - 40%	6 - 12	¼ to ½ delaminated	
40 - 80%	0 - 6	½ to full delamination	
>= 80%	0	Full delamination	

Due to the fatigue test significant delaminations developed in the adhesive layer. The strain signals during the fatigue test suggest that these delaminations at the crossbeam location developed at an early stage of the fatigue test, see Figure 7-28. The strain signals for the plate division location give no indication when this delamination occurred. Therefore the conclusion is that the additional steel plate bonded in this way is not a suitable solution for enhancing the lifetime of steel bridge decks. Although the fact that the stresses in the original steel deck are reduced, the lifetime of the renovation technique is limited. Further research should be focused on an adhesive layer with a longer lifetime.

7.2.7 Concluding remarks

Some concluding remarks can be drawn at the end of this part about bonding additional steel plates:

- Bonding additional steel plates reduces stresses in the deck plate significantly. A rough estimation of the stress reduction factor is 0.5, both for stresses in the deck plate and in the trough web.
- These reduction factors were not calculated with an FE-model, which only represented the deck plate behaviour. It is not necessary to do this yet, because it is not expected to give more relevant insight.
- This stress reduction factor results theoretically in a significant extension of the lifetime of the bridge deck structure
- However in the fatigue test structural failure is observed as delamination occurred in the adhesive layer.
- A new application method, the vacuum infusion technique, leads to a fully bonded connection. Possibly this is a more robust adhesive layer, with respect to fatigue. This should be demonstrated in a fatigue test.
- At this moment the conclusion is that bonding an additional steel plate is still a candidate renovation technique with respect to the lifetime of the steel structure, provided that the fatigue properties of the adhesive can be improved.

7.3 Filling troughs with polyurethane

7.3.1 Introduction

To prevent fatigue in the deck plate, stress ranges in the deck plate have to be reduced. Bonding an additional steel plate on top of the existing steel deck plate leads to an increase in the deck plate stiffness.

Another renovation method is to fill the troughs under the wheel tracks with polyurethane. If the troughs are filled with a material with sufficient stiffness, the deck plate is quasi-continuously supported. The spring stiffness of this support depends on the stiffness of the filling material, the stiffer the material the greater the stress reduction in the deck plate.

The advantage of this method is that it requires no additional components etcetera on top of the existing steel deck plate. One disadvantage with this method is that the spring support only acts at the inside of the trough and the deck plate between two troughs is not supported. Another disadvantage is that when the troughs are filled the positions of the wheel tracks become fixed on the bridge deck and changing lanes is no longer an option without losing the effectiveness of the trough filling.

7.3.2 Filling material & application method

7.3.2.1 Filling material

The first step in the development of this renovation technique is a literature survey to determine the materials that are appropriate for filling the troughs (Nagtegaal, 2002-e). The main relevant considerations in making a choice from various possible materials are:

- Mechanical properties, especially the stiffness and the thermal coefficient.
- Chemical properties, especially the exothermic reaction and the shrinkage. If shrinkage occurs, the filling material gives less support to the deck plate and the effectiveness of the renovation is low.
- Application properties

Based on the survey two different filling materials were selected. These two were:

- Epoxy foam from the firm Gouda Chemiebouw
- A polyurethane from the firm Gijsman Epoxy Producten

These two materials were subjected to laboratory test to determine the mechanical properties (De Kanter, 2000-a, 2000-b). Small cylindrical test specimens with a diameter of 30 mm were loaded in compression. Figure 7-36 shows the test specimen for both materials before and after the compression test.

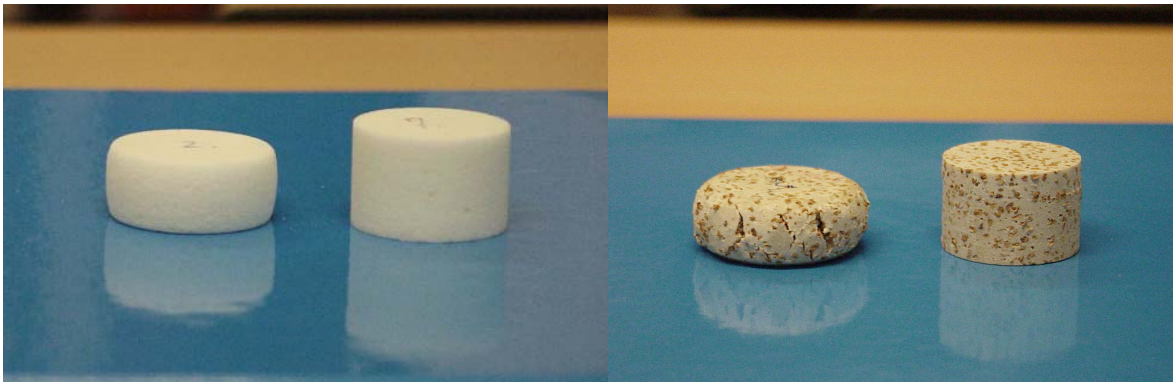

Figure 7-36: Test specimen epoxy foam (left) and polyurethane (right)

De test results are (De Kanter, 2000-a, 2000-b):

- Epoxy foam: Young's modulus E = 279 MPa, yield strength in compression $f_{y;c}$ = 7.2 MPa and density ρ = 397 kg/m^3
- Polyurethane: Young's modulus E = 674 MPa, yield strength in compression $f_{y;c}$ = 32.8 MPa and density ρ = 1068 kg/m^3

The difference in stiffness led to the decision to only continue the development of this renovation method with the polyurethane filling material.

7.3.2.2 Application method

Before filling the troughs of a bridge deck in a motorway it should be proved that this system is appropriate for such an application. For that reason the tests and calculations were performed, that are described in this paragraph. Besides the calculations and laboratory research there are also aspects related to the application and execution on a larger scale. To investigate these aspects two application tests were performed.

Application test 1

First a large application test was performed. The test was made on a part removed from the old Van Brienenoord bascule bridge. The test is described in (Nagtegaal, 2002-f).

One 17 m long trough was filled with polyurethane. In order to carry out this filling process threaded boreholes 24 mm diameter were made in the deck plate every 0.8m. One borehole, at the end of the 17 m, was used to insert the polyurethane into the trough from the top of the deck plate, the others were to avoid air inclusions in the trough. When the polyurethane flowed out of a borehole complete filling of the trough at that location was guaranteed and the borehole was blocked with a screw. It became clear from the test that the number of boreholes was far more than necessary. In reality boreholes spaced at 3 or 4 m would be adequate. Boreholes generate a stress concentration effect in the deck plate but the risk of fatigue cracks occurring at them is thought to be low because the stress ranges are low.

A short length of approximately 1 meter was cut from this filled trough for testing. Visual examination showed that there were no air inclusions and that the filling material was directly in contact with the steel parts.

Application test 2

In a significant number of bridges in the Netherlands a small steel plate is fitted in the trough at the location of the crossbeam. Figure 7-37 shows this plate.

This plate is added to the trough during the fabrication of the bridge deck before attaching the trough to the deck plate and is therefore only welded to the trough webs and not to the deck plate. It provides torsional rigidity to the trough, which is desirable for its accurate positioning, see Figure 7-37. This plate is a discontinuity in the trough and possibly disturbs the flow of the polyurethane. The second application test was performed to research the effects of this small steel plate.

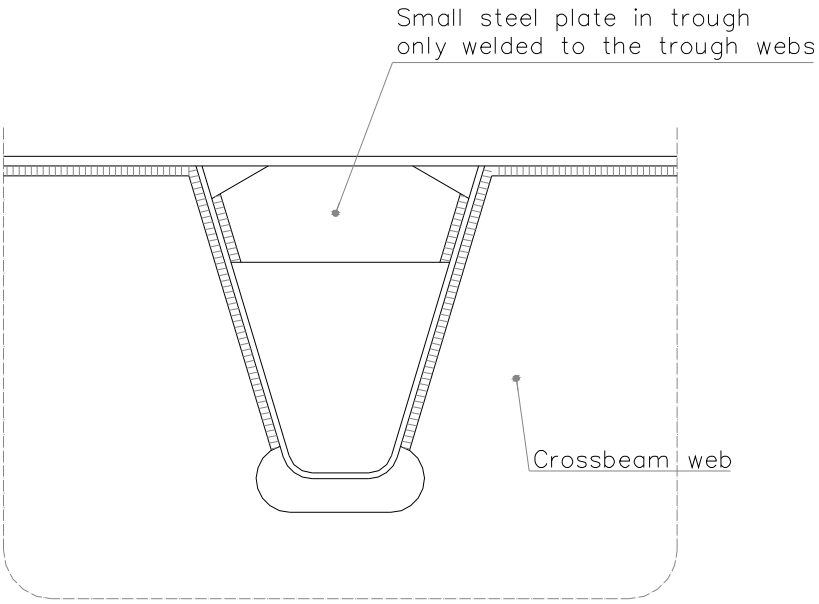

Figure 7-37: Small steel plate in trough

This application test is extensively described in (van der Leest, 2003). A trough of approximately 2 m was built from clear plastic with the small plate added in the trough thus the flow of the polyurethane in the trough and around the small plate is visible. Figure 7-38 shows a part of the trough and the filling point.

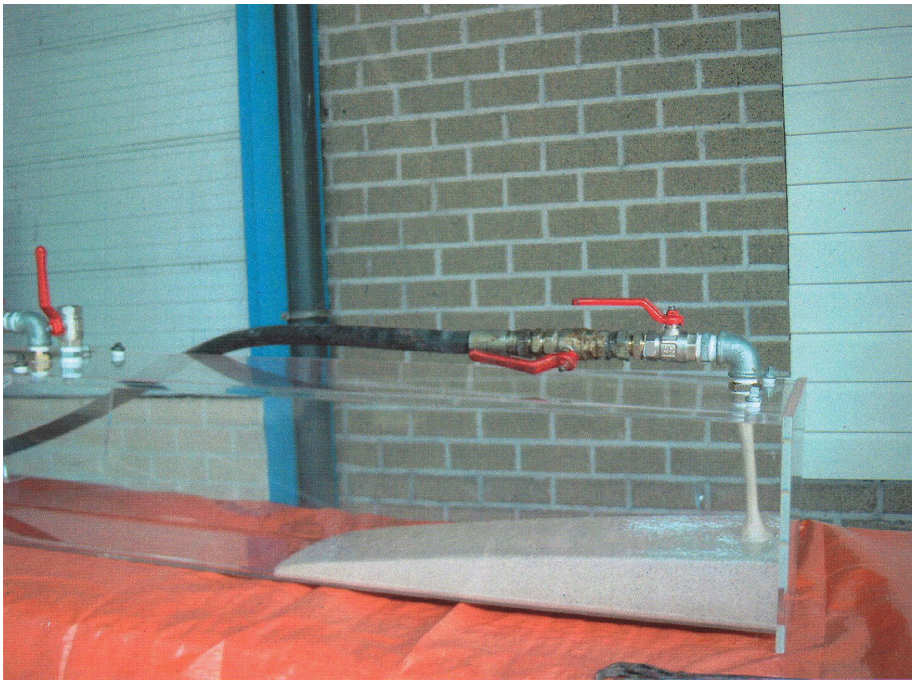

Figure 7-38: Trough with filling point

Figure 7-39 shows the trough completely filled. The location of the small internal plate in the trough is clearly visible and it is apparent that this plate has not disturbed the flow of the polyurethane.

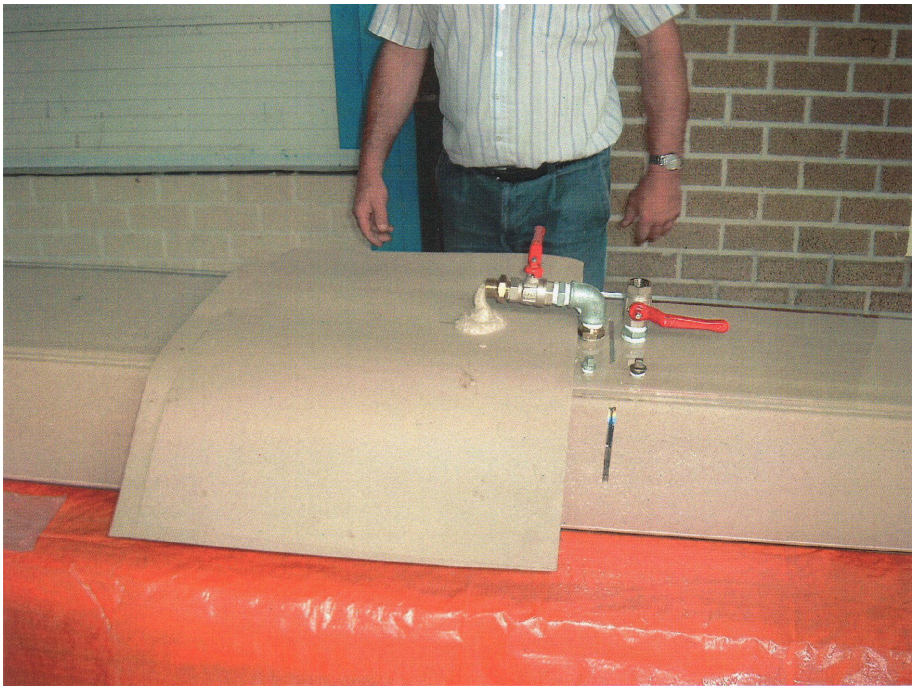

Figure 7-39: Filled trough at small internal plate at crossbeam location

7.3.3 Numerical research and results

Pover has performed extensive Finite Element calculations (Pover, 2002, 2004). Chapter 6 has already given a thorough description of the different FE-models. In chapter 6 the models were directed towards renovation with RHPC. Besides the FE-models provided with asphalt and concrete FE-models with a trough filled with polyurethane were also made. Again for these models the general purpose was to quantify the stress range reduction in the deck plate at the fatigue prone locations due to the renovation method. This paragraph reports in brief the results of the FE-models with troughs filled with polyurethane.

Contrary to the FE-models made for the RHPC surfacing only two types of FE-models were made for the renovation method with troughs filled with polyurethane both with solid elements. These two types are:

- FE-models representing both local deck plate behaviour and crossbeam behaviour at the crossbeam location
- FE-models only representing local deck plate behaviour between two crossbeams

Unfortunately no FE-models representing only local deck plate behaviour at the crossbeam location were made.

7.3.3.1 FE-models - local deck plate behaviour and crossbeam behaviour

For the description of the FE-models representing both local deck plate and crossbeam behaviour at the crossbeam location and for an interpretation of the calculated stresses, see paragraph 6.3.1.2. The main interest is the stress reduction factor at the underside of the steel deck plate. Table 7-9 gives the numerical results of the calculations for the stresses in x-direction for the different load cases at the crack location along line 1, at the root of the weld. A distinction is made between FE-models in which there was and was not adhesion between the steel and polyurethane.

Table 7-9: Stress σ_{xx} - underside deck plate along line 1 (MPa)

Stress underside deck plate X-direction (MPa)	LC 5	LC 6	LC 7	LC 8
Standard model (No. 1 – STD)	-124	-86	-45	-4
Troughs filled with adhesion	-66	-48	-46	-15
Troughs filled without adhesion	-96	-69	-56	-16
Stress reduction factor	0.77	0.80	1.24	x

For the calculation of the reduction factors in this table the calculated stress without adhesion is used. Trough filling is intended to be used in existing bridges. Normally the inside of the trough is not painted, thus at the inner side of the trough there is some corrosion and also mill scale. Thus it is unlikely that a good adhesion between the steel and the polyurethane can be achieved.

From the FE-models is clear that a reduction factor of approximately 0.7 to 0.8 is possible, if the wheel load is located above the trough filled with polyurethane (load case 5). It is also clear from the reduction factors that if the wheel load is placed outside the filled trough no stress reduction is achieved.

7.3.3.2 FE-models - local deck plate behaviour between crossbeams

For the description of the FE-models representing local deck plate behaviour between two crossbeams and for an interpretation of the calculated stresses, see paragraph 6.3.1.3. The main interest is the stress reduction factor at the underside of the steel deck plate. Table 7-10 gives the numerical results of the calculations for the stresses in x-direction for the different load cases at the crack location along line 1, at the root of the weld and also the maximum tensile stress.

Table 7-10: Stress σ_{xx} - underside deck plate along line 1 (MPa)

Stress (MPa)	LC5	LC5	LC6	LC6	LC7	LC7
Location	crack	midspan	crack	maximum	crack	maximum
Standard model	-212	323	-120	120	-345	321
Troughs filled with adhesion	-36	63	-65	99	-207	303
Troughs filled without adhesion	-66	106	-64	91	-175	312
Stress reduction factor	0.31	0.33	0.53	0.76	0.51	0.97

Stress reduction factors for the stress range in the trough web are also calculated as these stresses in the trough web are responsible for fatigue crack growth in the longitudinal weld between trough web and deck plate. The application of a polyurethane trough filling also reduces these stresses. Table 7-3 gives the calculated principal stresses in the trough web at the connection with the longitudinal weld. Local stress concentration effects are taken out of this principal stress. The reduction factor is calculated for the stress at the inside of the trough web as the fatigue crack in the longitudinal weld initiates from the inner side of the trough web.

Table 7-11: Principal stress in trough web at longitudinal weld (MPa)

Principal stress trough web (MPa)	LC5	LC5
	Outside trough web	Inside trough web
Standard model	135.7	-162.9
Troughs filled with adhesion	+59	-77
Troughs filled without adhesion	+74	-112
Reduction factor (Steel/STD)	0.54	0.69

It is difficult to draw conclusions from the FE-models representing the local deck plate behaviour between the crossbeams Table 7-10 shows that a reduction factor of 0.3 to 0.7 is possible for the stress in the deck plate. It also shows that the reduction factor is very sensitive to the location of the wheel load in the transverse direction. For the stress in the trough web a reduction factor of approximately 0.7 was derived with the FE-calculations.

7.3.4 Static testing program

7.3.4.1 Small test specimen

Kolstein has performed some tests on small test specimen (Kolstein, 2001-b). A section at the crossbeam location approximately 1 meter long was cut from the application test on an old part of the Van Brienenoord Bridge and another section 1 meter long was cut from a trough

without filling.

Basically four static tests were performed on these two test specimen:
1. Static test on trough 1 with filling before short fatigue test
2. Static test on trough 1 with filling after short fatigue test
3. Static test on trough 2 without trough filling
4. Static test on trough 2 with filling before short fatigue test

Figure 7-40 shows the process of filling trough 2 after which the initial static test, no.3 was performed. Because the test specimen was relatively small, it was possible to orientate the trough in vertical direction, which was thought to be good for the flow of the polyurethane and thus for a good adhesion between the filling and the underside of the deck plate. Figure 7-41 shows the test set-up in two photographs.

Figure 7-40: Filling procedure trough 2 after static test no. 3 and before test no. 4

The short fatigue tests comprise only 10.000 cycles, and are described in paragraph 7.3.5.1. Both test specimens were provided with five strain gauges on top of the steel deck plate. Figure 7-42 shows schematically the test specimen and the location of the five strain gauges. All strain gauges measure in transverse direction.

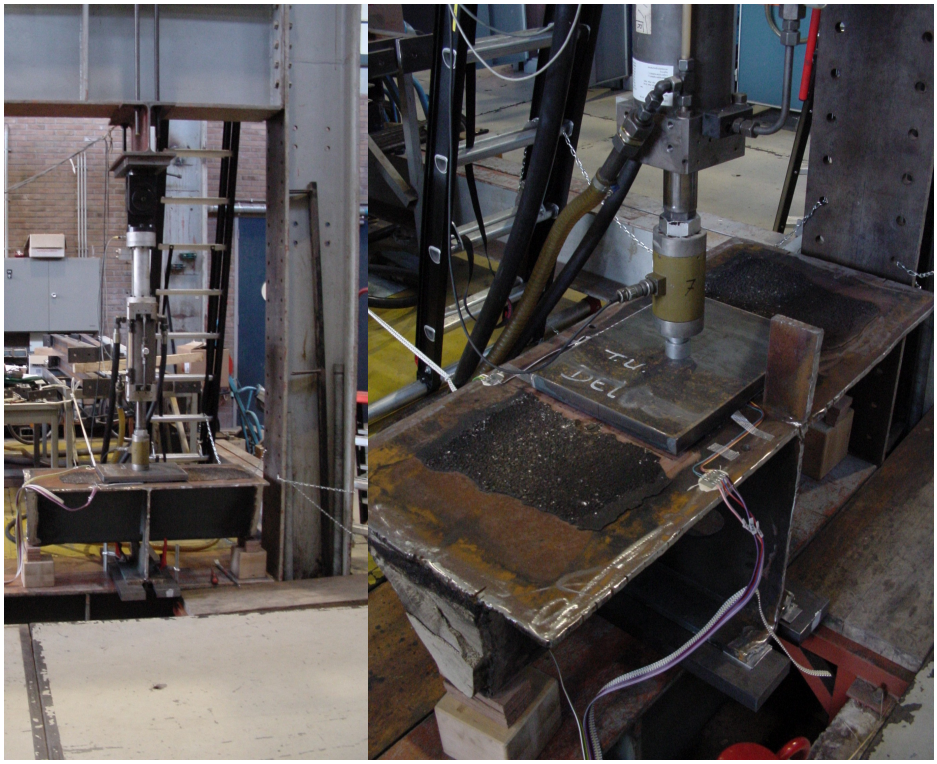

Figure 7-41: Test set-up small test specimen

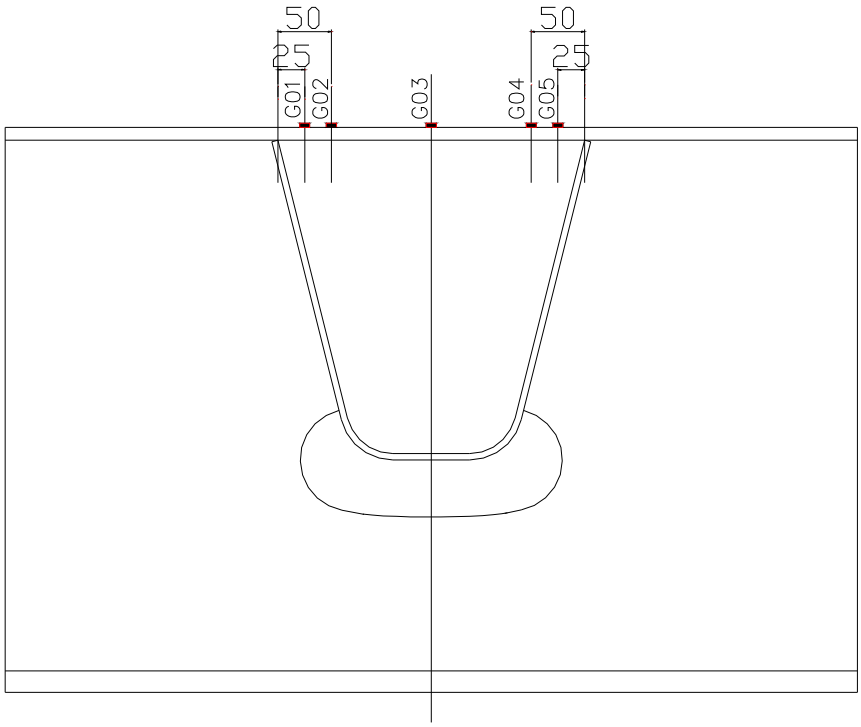

Figure 7-42: Strain gauges small trough test specimen

For the static test the centre of the wheel footprint was located on the intersection of crossbeam web and longitudinal symmetry axis. The wheel footprint used in the test was 320 mm long and 270 mm wide, and the load was 100 kN. This is wheel type C, the so-called super single, from Eurocode 1 – Part 2, see paragraph 3.2.

No strain gauges were attached to the top side of the deck plate immediately above the root of the weld. This an interesting location as the fatigue crack originates there. Therefore the measured strains were linearly extrapolated to this location. Linear interpolation probably leads to a relatively small underestimation of the strains at the crack location, see Figure 4-6. Table 7-12 summarizes the measured strains at the strain gauges 1, 2, 4 and 5 and the extrapolated strains at the crack location, for the four static tests at the two test specimen.

Table 7-12: Measured strains small test specimens with trough filling at static tests

Static test no.	ε_{crack} ($x10^{-6}$)	ε_{G01} ($x10^{-6}$)	ε_{G02} ($x10^{-6}$)	ε_{G04} ($x10^{-6}$)	ε_{G05} ($x10^{-6}$)	ε_{crack} ($x10^{-6}$)
1 - at trough 1 with filling before fatigue test	329	90	-149	-8	100	208
2 – at trough 1 with filling after fatigue test	288	68	-152	-29	78	185
3 – at trough 2 without filling	1085	485	-115	-100	387	874
4 – at trough 2 with filling before fatigue test	219	58	-103	-81	8	97

A few remarks on the measured strains:

- A significant stress reduction due to the trough filling is observed, when test 3 and 4 are compared.
- There are major differences between strains left and right, where theoretically identical strains are expected.
- The change in measured strains after a small fatigue test with only 10,000 cycles is significant. This is obvious from a comparison of tests 1 and 2.
- The tests 1, 2 and 4 were all performed on troughs with filling. Therefore 6 times the same measured strains were expected, in reality however, the minimum measured strain is 97 $x10^{-6}$ and the maximum measured strain is 329 $x10^{-6}$.

7.3.4.2 Bridge panel TNO

Besides the FE-models and the tests on small specimen, tests were performed on two full-scale bridge deck test panels both with a trough filled with polyurethane. These panels are called TNO panel 1 and 2, they were both subjected to tests at the laboratory of TNO. Both

tests panel were subjected to static tests and fatigue tests. The fatigue tests are described in paragraph 7.3.5.2.

The static and the fatigue tests on test panel 1 are extensively reported by Van Straalen (Van Straalen, 2002-b) and the tests on panel 2 by Van Straalen (Van Straalen, 2003-b). Figure 7-43 shows the test panels that were used for the tests at TNO. As test panel 1 and 2 were identical, only one figure is given. In both panels the middle trough is filled with polyurethane.

Again two sections from the old Van Brienenoord Bascule Bridge were used as the test panel. Both panels had a filled trough. Test panel 1 was subjected to the static and the fatigue test. In the fatigue test at panel 1 two large cracks grew. At that point the decision was taken to test a second panel.

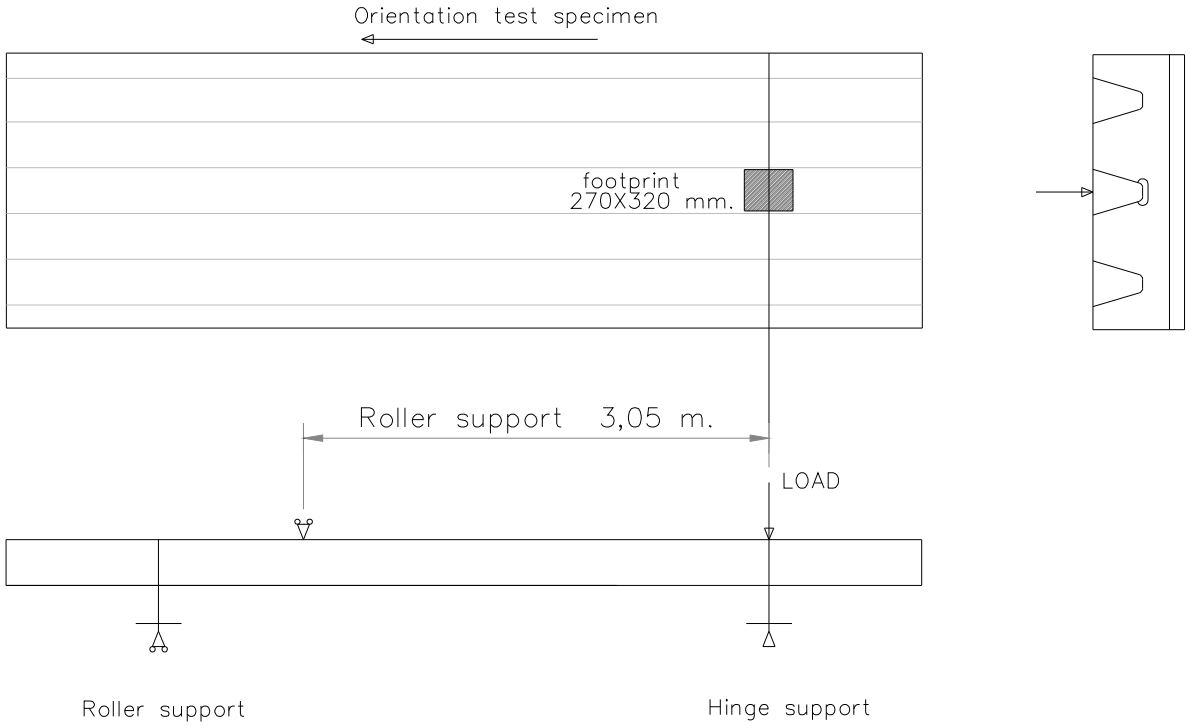

Figure 7-43: TNO panels for static and fatigue tests with trough filled with polyurethane

The wheel load was placed on an area of 270 mm width and 320 mm long, which is the super single tyre (type C) according to the Eurocode, see paragraph 3.2.1. This load was placed at the crossing of the middle trough and the crossbeam. Figure 7-43 shows this load set-up. The footprint differs from the footprint on the FE-models, which was the footprint of the single (220 mm). In paragraph 6.6.1 it has already been argued that it is possible to compare the results of the models and the measurements.

Strain gauges

Strain gauges were applied to both test panels. Due to the fact that the troughs were filled, no strain gauges could be attached to the underside of the deck plate inside the trough.

The strain gauges on test panel 1 are given in three figures:

- Figure 7-44 – a cross-section of the strain gauges
- Figure 7-45 – a top view of the gauges at the underside of the deck plate and trough web
- Figure 7-46 – a top view of the gauges at the top side of the deck plate

The strain gauges on test panel 2 are given in three figures:

- Figure 7-47 – a cross-section of the strain gauges
- Figure 7-48 – a top view of the gauges at the underside of the deck plate and trough web
- Figure 7-49 – a top view of the gauges at the top side of the deck plate

Be aware that these figures are not on scale. The strain gauges all measure in the transverse direction.

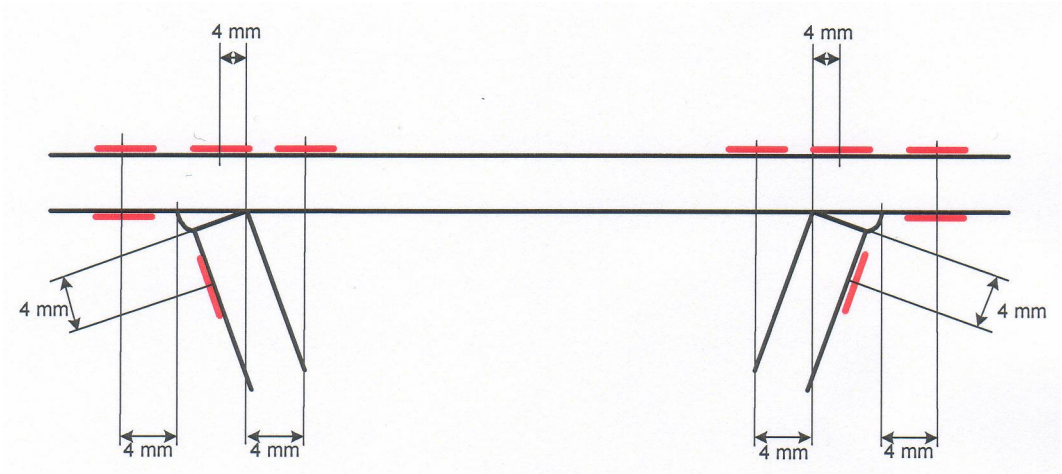

Figure 7-44: Cross-section strain gauges panel 1

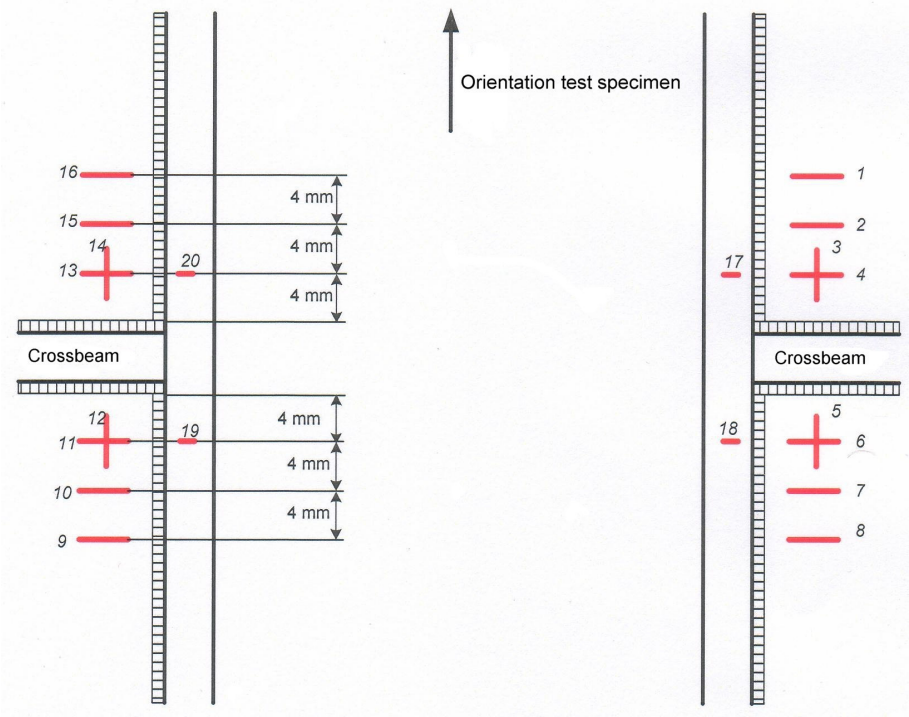

Figure 7-45: Top view of strain gauges on underside deck plate and trough web on panel 1

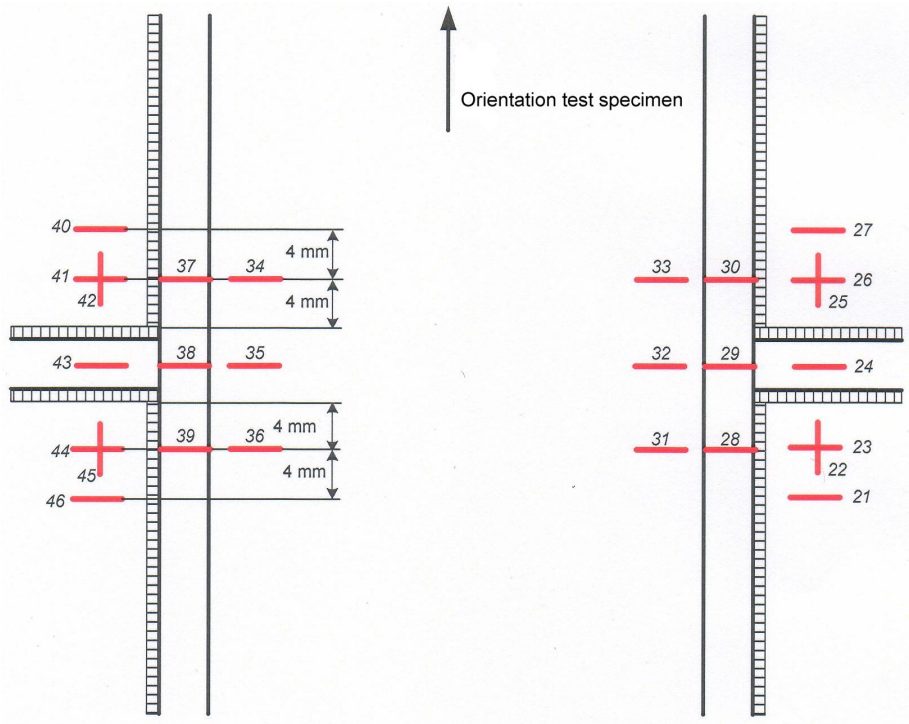

Figure 7-46: Top view of strain gauges on top side of steel deck plate on panel 1

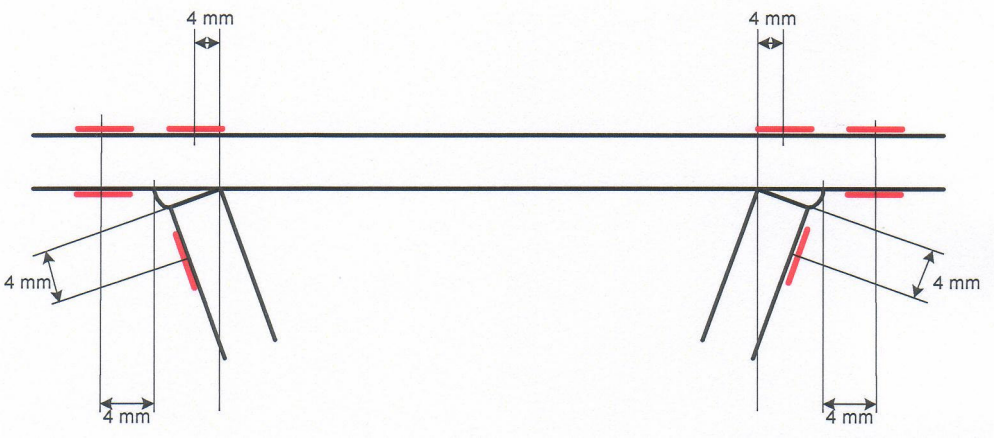

Figure 7-47: Cross-section strain gauges panel 2

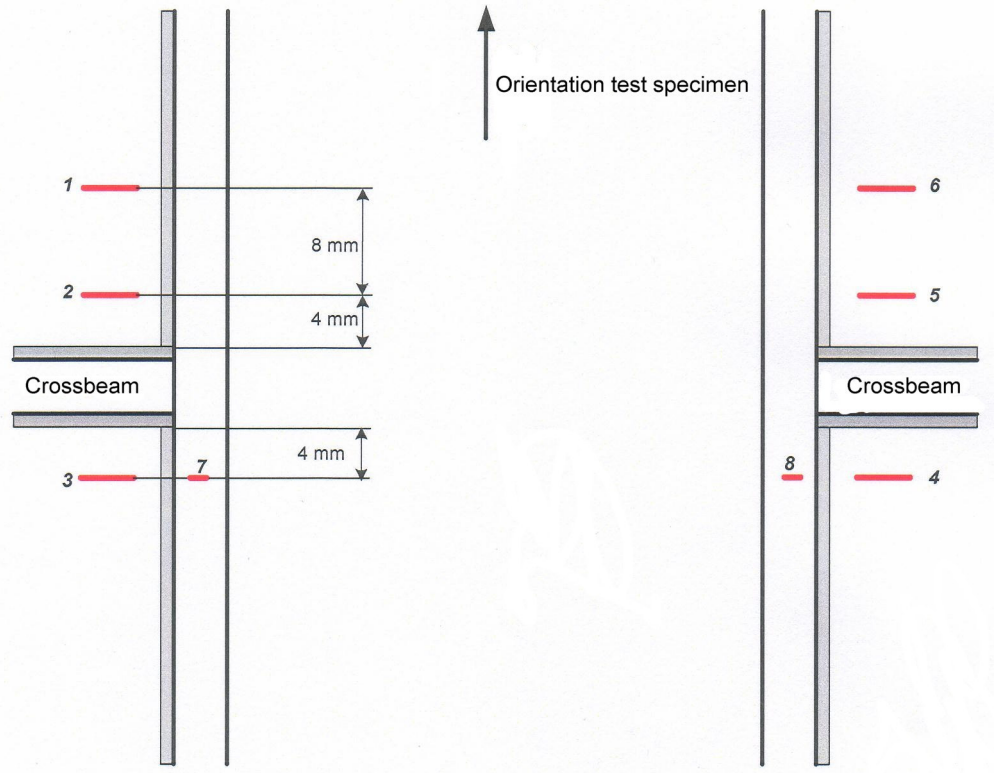

Figure 7-48: Top view of strain gauges on underside deck plate and trough web on panel 2

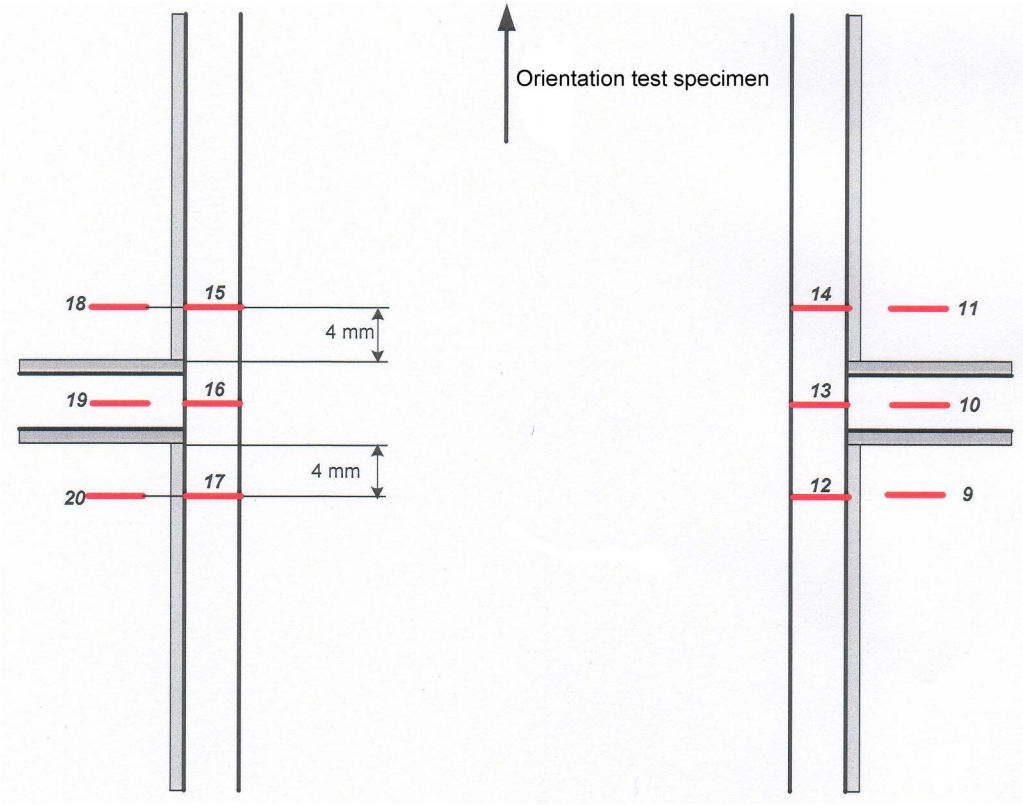

Figure 7-49: Top view of strain gauges on top side of steel deck plate on panel 2

Measurement results

Measurement of the stress on the underside of the deck plate near the crack location is the best indication of the effect of this renovation method. But because of the impossibility of attaching strain gauges at this location, the interesting gauges for these two test panels are on top of the deck plate. The most relevant strain gauges for the determination of the stress reduction at the fatigue prone location are those that are attached at the top side of the deck plate, in line with the crossbeam. These strain gauges are numbered 24, 29, 32, 35, 38 and 43 for panel 1, and 10, 13, 16 and 19 for panel 2.

A load of 117 kN was applied in 5 equal load cycles. In one cycle the load is increased and decreased in 5 equal steps set from 12 kN to the maximum load of 117 kN (12 – 33 – 54 – 75 – 96 – 117 – 96 – 75 – 54 – 33 – 12 kN).

The results of these 5 load cycles are given in Table 7-13, for test panel 1, for the strain gauges 24, 29, 32, 35, 38 and 43, and in Table 7-14, for test panel 2, for the strain gauges 10, 13, 16 and 19. These tables gives the measured strain range ($\Delta\varepsilon$) at the load range (ΔF) of 105 kN.

Table 7-13: Strain range top side of panel 1($\Delta\varepsilon$ x 10^{-6}) at ΔF 105 kN (12-117 kN)

Gauge	24	29	32	35	38	43
Average	389	893	868	1059	585	278

Table 7-14: Strain range top side panel 2($\Delta\varepsilon$ x 10^{-6}) at ΔF 105 kN (12-117 kN)

Gauge	10	13	16	19
Average	71	441	425	77

Evaluation measurements

A few comments on the results of the measurements at panels 1 and 2:

- The difference between the measured strains on the two panels was very large, in fact it was so large that it suggests that the trough on panel 1 was not completely filled, and that the polyurethane filling was not acting as a spring support for the deck plate.
- A comparison with test BA1_S8 from paragraph 4.2.2.2 shows that the strains in that test were at the same level as in panel 1, however with a test load of 49 kN, instead of the 105 kN on panel 1. This however suggests that the trough filling did have an effect.
- Also the differences between the strains at the both sides of test panel 1 are relatively large, compare for instance the strains of gauges 29 and 38, which should be equal.
- It is difficult to derive a strain range at the crack location by linear extrapolation from the inner side of the trough, because only one strain gauge was mounted inside the trough webs.
- For panel 1, linear interpolation of the strains to the crack location from the outer side of the trough leads to a strain range of 1095x10^{-6} at the side of gauges 24 and 29 and to a strain range of 831x10^{-6} at the side of gauges 38 and 43. This last extrapolated strain range however is lower than the measured strain range in gauge 35 (1059x10^{-6})
- For panel 2, linear interpolation of the strain ranges to the crack location leads to a strain range of 737x10^{-6} at the side of gauges 10 and 13 and to a strain range of 703x10^{-6} at the side of gauges 16 and 19.

7.3.5 Fatigue testing program

7.3.5.1 Small test specimen

Two short fatigue tests were performed on test specimen trough 1 and trough 2 that are described in paragraph 7.3.4.1. The footprint of the applied load was again 270 mm wide by 320 mm long. The load alternated between 5 kN and 100 kN, so the load range is 95 kN. Figure 7-50 shows the measured strain ranges during the small fatigue test at trough 1. Figure 7-51 shows the measured strain ranges during the small fatigue test at trough 2.

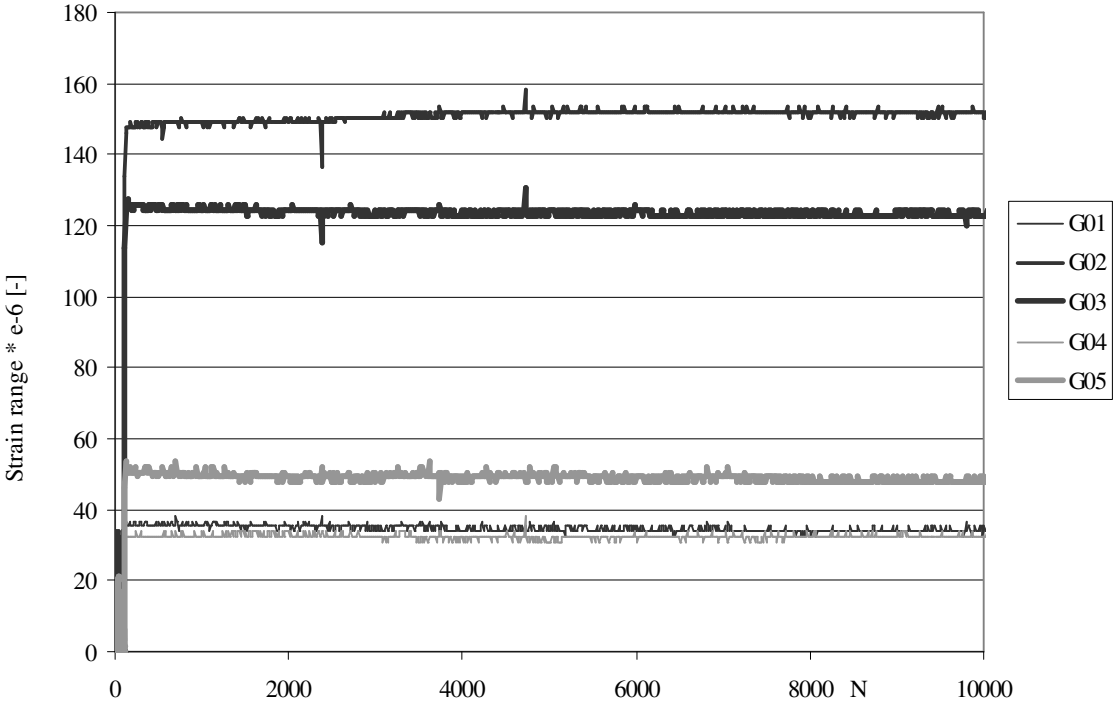

Figure 7-50: Strain ranges on top of steel plate during fatigue test on small test trough 1

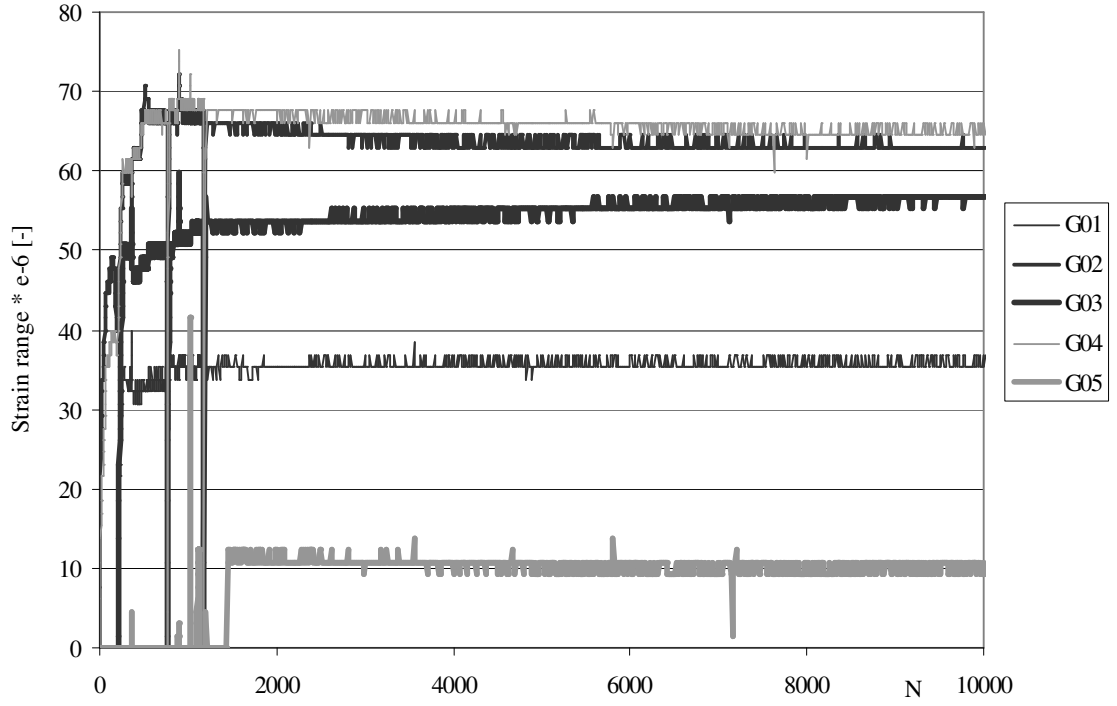

Figure 7-51: Strain ranges on top of steel plate during fatigue test on small test trough 2

Table 7-15 gives the strain ranges during the fatigue tests for the strain gauges 1, 2, 4 and 5. For the extrapolation to the crack location it was assumed that same signs (positive or negative) apply as for the static tests, see Table 7-12. Based on this assumption the strains have been linearly extrapolated to the crack location.

Table 7-15: Measured strain ranges small laboratory specimens with trough filling in fatigue tests

Static test no.	ε_{crack} ($x10^{-6}$)	ε_{G01} ($x10^{-6}$)	ε_{G02} ($x10^{-6}$)	ε_{G04} ($x10^{-6}$)	ε_{G05} ($x10^{-6}$)	ε_{crack} ($x10^{-6}$)
Fatigue test at trough 1	215	32	(-)151	(-)32	48	128
Fatigue test at trough 2	133	35	(-)63	(-)65	11	87

A few remarks on the results:

- Strain ranges for the fatigue test are significantly smaller than the strain ranges for the static test.
- Again major differences between both sides and both test specimen are seen
- The measured strain ranges are constant during the fatigue test, except for the start of the test on trough 2, but there the load ranges were also not stable at 95 kN.

7.3.5.2 Bridge panel tests TNO

After the static tests, reported in paragraph 7.3.4.2 two fatigue tests were performed, one test on each test panel. The fatigue tests were performed in the laboratory of TNO. The test data were reported by Van Straalen (Van Straalen, 2002-b, 2003-b). Figure 7-43 shows the location of the wheel load (270 x 320 mm, width x length) above the filled trough at the location of the crossbeam. Figure 7-52 gives a photograph of the fatigue test.

The following load cycles were applied:

- On test panel 1: $4.2x10^6$ cycles with a range of 105 kN (12 kN - 117 kN)
- On test panel 2: $4.2x10^6$ cycles with a range of 105 kN (12 kN - 117 kN)

Calculations (De Jong, 2006-b) have shown that this load set-up is equivalent to:

- 12 years of fatigue according to fatigue load model 4 from Eurocode 1991 – Part 2
- 12 years of heavy vehicle traffic on the Moerdijk Bridge, with respect to fatigue of the steel deck plate. The Moerdijk Bridge is the most heavy loaded bridge deck in the Netherlands.

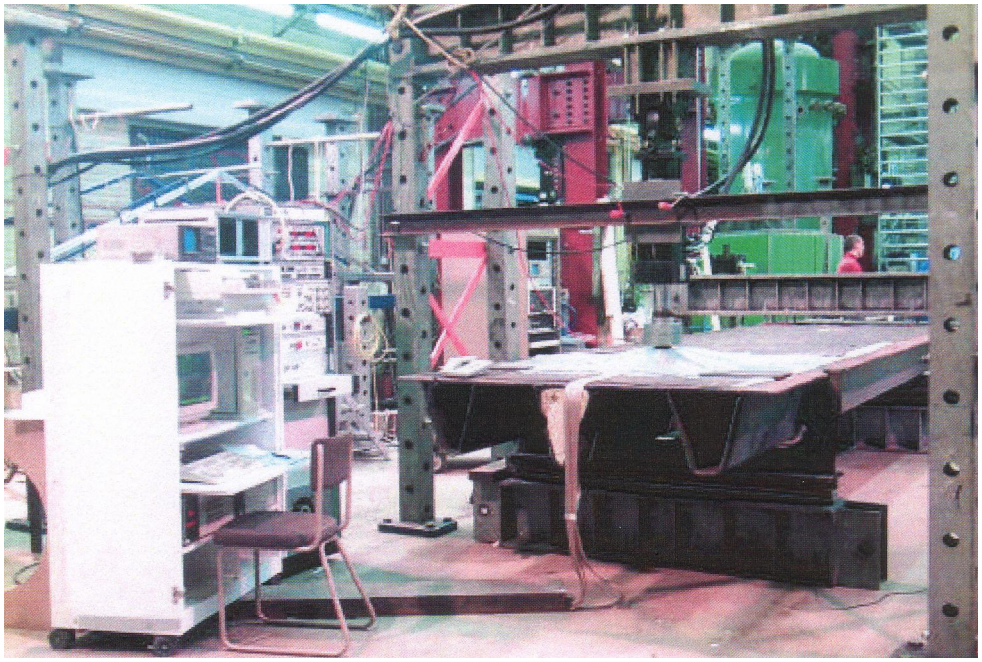

Figure 7-52: Full scale fatigue test on test panel with trough filling

Strain ranges

During the fatigue tests the static loading procedure as described in paragraph 7.3.4.2 was repeated 93 times for test panel 1 and 66 times for test panel 2. Figure 7-53 shows the measured strain ranges at the load range of 105 kN for these static loading procedures at the top surface of the steel deck plate for test panel 1. Figure 7-54 depicts the measured strain ranges for test panel 2.

Some remarks at these two figures:

- Particularly the strain ranges at panel 1 showed large fluctuations right from the start during the fatigue test.
- Up to approximately 1 million cycles the measured strain ranges for panel 1 are large, and after 1 million cycles all the strain ranges reduced to approximately $100x10^{-6}$.
- The strain ranges for panel 2 increase in a more step by step manner. For strain gauge 16 there is a clear reduction of the measured strain range at around 1 million cycles.
- This suggests that in both panels fatigue cracks were growing. Besides that the measured strain ranges fluctuate a lot, which means that the achieved stress reduction due to the renovation method is indistinct. With an indistinct stress reduction a reliable fatigue lifetime calculations is difficult.

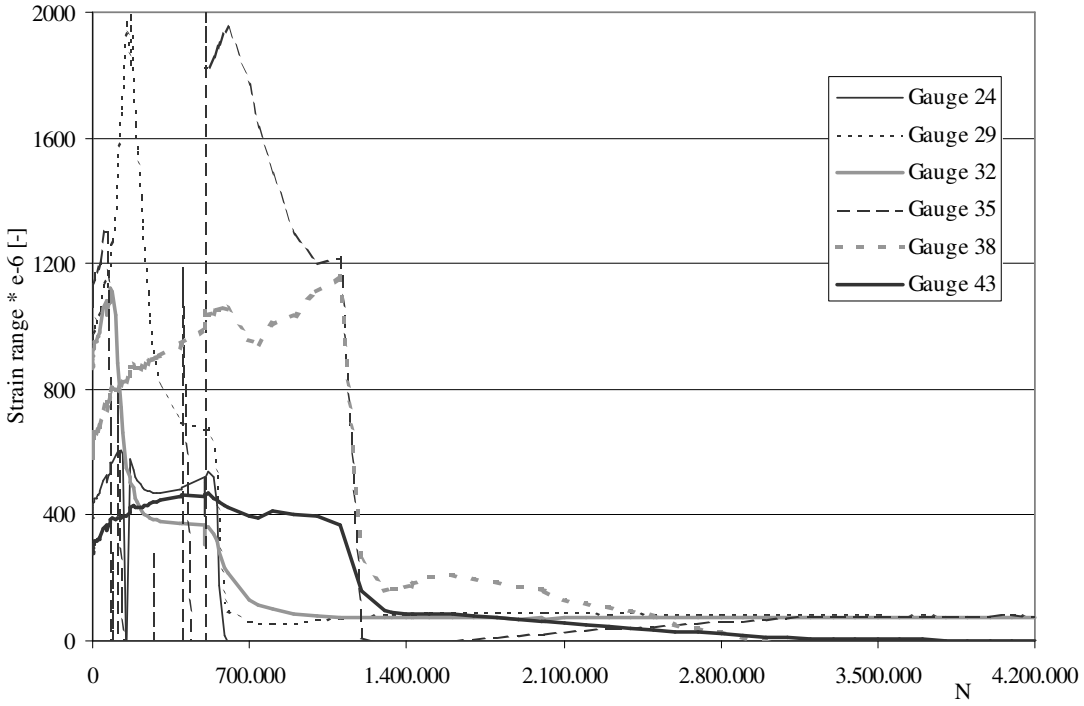

Figure 7-53: Strain ranges on top steel deck plate during fatigue test on TNO test panel 1

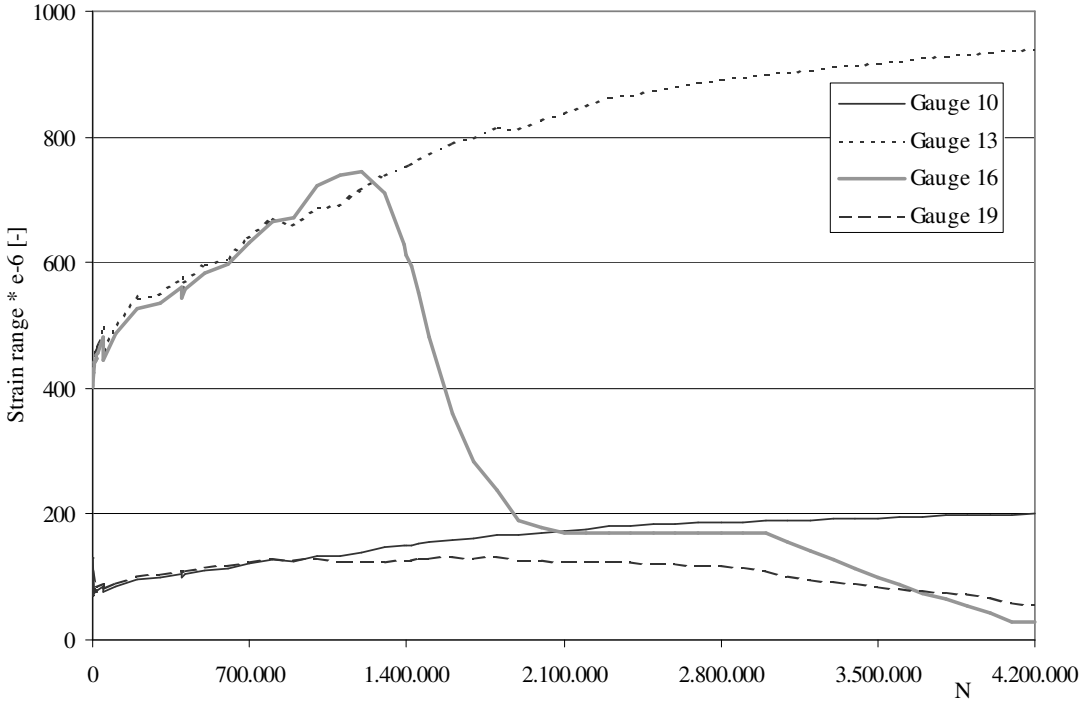

Figure 7-54: Strain ranges on top steel deck plate during fatigue test on TNO test panel 2

Visual observations at test panels

In test panel 1 are after 2.017.004 cycles two fatigue cracks were observed by visual inspection. Between the gauges 24 and 29 there was a crack of approximately 210 mm, and between the gauges 38 and 43 a crack of approximately 130 mm. It was difficult to detect these cracks between the gauges and it is likely that the cracks had already grown through the deck plate long before the moment that they were observed. This is plausible because of the large length of the cracks at the first observation and because of the measured strain ranges during the fatigue test, see Figure 7-53. After the first observation the crack growth could not be monitored because the crack tips disappeared under the rubber footprint of the load. Figure 7-55 shows the cracks at the end of the test after 4.200.000 cycles, made visible by a dye penetrate liquid. At the end of the fatigue test the cracks in panel 1 had reached a length of approximately 25 to 30 cm.

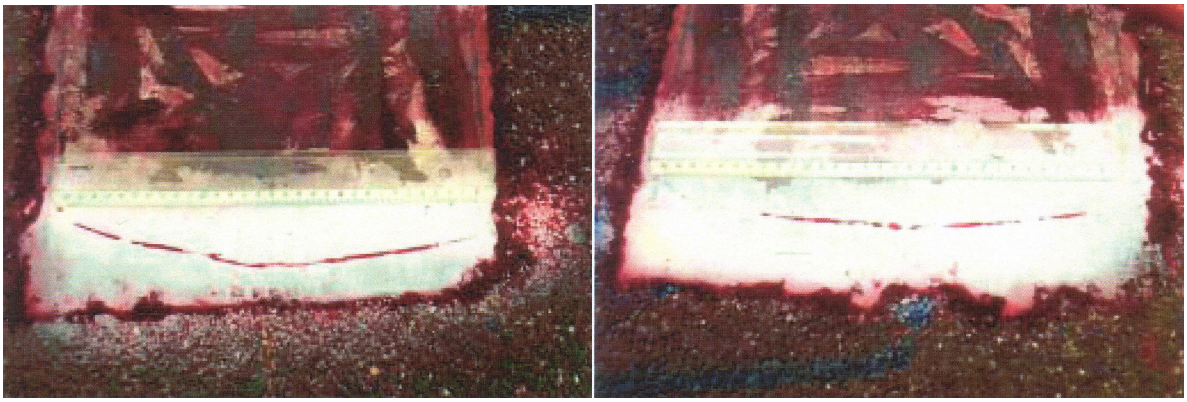

Figure 7-55: Cracks in panel 1 after fatigue test between gauges 24-29 (left) and 38-43 (right)

In test panel 2 after 3.193.910 cycles a crack 15 mm long was observed, between strain gauges 16 and 17. This crack had grown to 44 mm by the end of the fatigue test at 4.200.000 cycles.

7.3.6 Comparison calculations with tests

Some concluding remarks can be made at the end of this section about filling the troughs with polyurethane.

- Tests showed that in general filling the troughs with polyurethane causes significant lower stresses in the deck plate.
- The differences between the measured stress reductions are very large; however the measured stress reduction factor are in all cases higher than the stress reduction factor calculated with FE-models.
- These differences mean that the effectiveness of the trough filling is not always the same,

which could be due to differences in adhesion between filling material and the underside of the deck plate.

- The reduction factors with an FE-model only representing the deck plate behaviour are not calculated. It is not necessary to do this yet, because it is not expected to give more relevant insight. Besides that this renovation method has not given the expected extension of the lifetime, which makes additional numerical research unnecessary.
- The high strains measured for TNO test panel 1 in combination with the two large fatigue cracks in that panel tends even more towards the conclusion that there was either no or limited adhesion between the filling material and underside of the steel deck plate.
- Following the appearance of the fatigue cracks in TNO test panel 1 it was decided to test a second identical panel. A comparison of the strains in the static tests, see Table 7-13 and Table 7-14, shows that strains in the second panel are much smaller than in the first test panel. This is more evidence that the adhesion in panel 1 was of poor quality in comparison to panel 2.
- With respect to the fatigue tests on the two larger TNO panels it can be said that fatigue cracks grew in the deck plate in both panels but in panel 2 only a relative short crack was observed.
- The final conclusion therefore must be that this method does not lead to the required significant extension of the lifetime of the deck structure. This might be due to the lack of adhesion between filling material and underside deck plate. In addition to this there is the disadvantage that this renovation method does not strengthen the deck plate between the troughs.

7.4 Reinforced ultra high performance concrete

7.4.1 Introduction

The development of the renovation methods described in the previous paragraphs, bonding additional steel plates and filling the troughs, has led to solutions, which are not as durable as the RHPC surfacing for fixed bridges described in chapter 6. Because of that research investigation was started into the possibility of replacing the existing epoxy layer on the bridge decks with a thin concrete layer. This research was started after the development phase of the trough filling and bonding additional steel plates and was carried out by Schrieks. The research is extensively described in (Schrieks, 2006)

The purpose is the design of a thin concrete layer intended to extend the lifespan of the orthotropic steel deck of a movable bridge by replacing the epoxy surface on this deck by this thin concrete layer.

The main project approach was as follows. Concepts were formulated on the basis of the initially formulated boundary conditions and the demands on the renovation method. These concepts were subjected both to laboratory tests and to computations, which were needed to select the appropriate concepts. Tests and computations lead to alternatives that are appropriate for further research.

The very small thickness of the concrete layer results in the need for very effective reinforcement. This implies that the reinforcement has to be very dense and stiff, and the internal lever arm between steel deck plate and reinforcement has to be as large as possible.

This can be achieved by reducing the concrete cover depth and the bar spacing. The use of ultra high performance concrete and non-corroding reinforcement materials is a promising option. However, such a design cannot be based on normal standards. Therefore, tests have to be performed in order to research the design possibilities and verify the assumptions made. Repair thicknesses of 25 and 30 mm were investigated by Schrieks. The reinforcement alternatives, which were considered for the design were:

- Smooth stainless steel bars
- Ribbed stainless steel bars
- Carbon fibre reinforced polymer (CFRP) bars, sprinkled with sand
- CFRP laminates, glued on top of the concrete layer

Two types of experiments were performed. Pull-out tests to study the bond behaviour between concrete and reinforcement and to obtain information about the minimum concrete cover required to prevent splitting of the concrete and bending tests to obtain more knowledge about the actual bending behaviour (stiffness, cracking behaviour) of steel plates covered with various repair alternatives.

7.4.2 Boundary conditions, assumptions and demands

In case of movable bridges weight restrictions limit the repair thickness. For fixed bridges a concrete layer thickness of 50-60 mm was developed. However, that is not acceptable in case of movable bridges. The maximum weight for movable bridges results in applicable concrete layer thicknesses up to 25-30 mm in general. This layer can only be placed on the heavily loaded lanes, due to the weight restrictions.

The very small thickness of the concrete layer results in the need for a very effective reinforcement. This implies that the reinforcement has to be very dense and stiff, and the internal lever arm between steel deck plate and reinforcement has to be as large as possible.
The stress reduction in the steel deck plate results from the increased moment capacity of the

deck. Most cracks occur due to a hogging moment at the connection of the deck plate to the trough. At that location the steel deck is loaded in compression and the concrete layer in tension. Hence, the effectiveness of the replacement is mainly dependent on the reinforcement of the concrete layer. Thus a good shear bond between concrete and steel is a requirement for a full composite action between concrete and steel. A two-component epoxy layer sprinkled with calcinated bauxite aggregate is needed to bond the concrete to the steel, as illustrated in Figure 7-56, and similar to the intermediate epoxy layer for fixed bridges. Part of the bauxite aggregate can be assumed to contribute to the moment resistance in the same way as the concrete. The thickness of this epoxy layer is 4 mm.

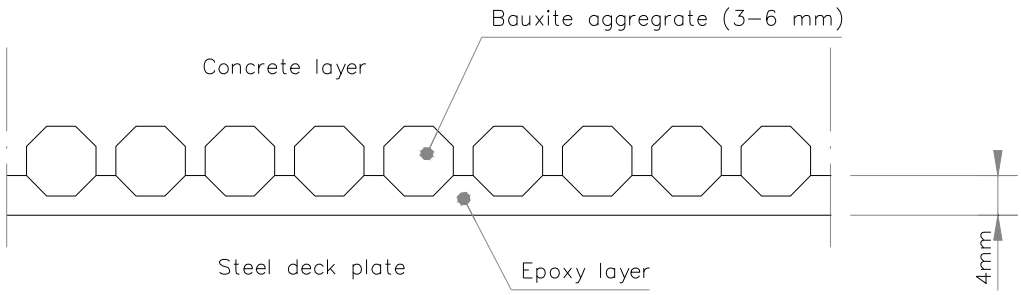

Figure 7-56: Schematic overview of the interface between steel deck and concrete layer

Some more demands and assumptions on this renovation method are:

- The maximum crack width in the concrete is 0.2 mm
- The skid resistance of the surface has to be adequate. It was assumed that sprinkling with aggregate would give the surface layer an adequate skid resistance. The extra thickness of the grains, which form the surface layer, is 2 mm. If the skid resistance of this layer is doubted tests are recommended.

7.4.3 Reinforcement concepts

The thin concrete layer has to be reinforced, to achieve a significant stress reduction. Different ways of reinforcing the concrete layer were researched. These are:

- Fibre reinforced polymer bars
- Fibre reinforced polymer grids
- Fibre reinforced polymer laminates
- Carbon braids
- Stainless steel bars
- Steel plates
- Combinations of reinforcements

In case of the FRP alternatives, four fibre materials were considered, namely glass, aramide, basalt and carbon. From these alternatives carbon FRP is the most appropriate material, because of the high stiffness, the alkali resistance and the fatigue behaviour. Therefore only CFRP material is considered for this design. With CFRP material bars, grids and laminates are possible solutions. Schrieks argues that grids and laminates are not appropriate for thin concrete layers on movable bridges. Therefore only CFRP bars were considered.

The following aspects, which could possibly influence the effectiveness of the reinforcement needed to be considered if CFRP bar reinforcement was to be used to reinforce the concrete layer:

- Required concrete cover
- Minimum distance between bars
- Need for longitudinal reinforcement

These aspects define the possible reinforcement configurations. When the concrete cover can be minimised, the effectiveness of the reinforcement will increase. If the minimum distance between reinforcing bars decreases, the possible amount of reinforcement increases. The same holds true for the situation where no longitudinal reinforcement is required.

For conventional steel reinforced concrete the required amount of concrete cover is prescribed by the environmental attacks on the concrete. Because of the capacity of CFRP to withstand all environmental attacks these attacks give no requirements to the cover. Hence the concrete cover is only needed to avoid the occurrence of splice cracks in the concrete. Splice cracks occur if the stress transferred from the reinforcement steel to the concrete results in a tensile stress in the concrete that exceeds its tensile capacity. Two different concrete covers were researched:

- 0.5 x ∅, plus an additional 3 mm construction tolerance
- 1.0 x ∅, plus an additional 3 mm construction tolerance

Schrieks concluded that concrete could be poured down to a grid spacing of 2 by 2 mm. In addition, based on calculations he concluded that no longitudinal reinforcement was required, because the calculated crack width was below the maximum allowed crack width of 0.2 mm. Because no longitudinal reinforcement is required, only one reinforcement layer is necessary in the small thickness of the concrete layer. Various bar diameters were considered from 3 to 10 mm, which results, together with the two cover depth alternatives and the two concrete layer thickness alternatives (25 and 30 mm), in a considerable number of bar reinforcement configurations.

The stress reduction factor at the crack location, due to the application of this reinforcement,

is compared to the situation of a steel deck plate without any surfacing. The stress reduction factor is computed using the Euler-Bernoulli theory, assuming full composite action between steel and concrete. The stresses and strains in the longitudinal section are illustrated in Figure 7-57. The calculation of the stress reduction, leads to high stress reduction factors, from 0.2 up to 0.45 (Schrieks, 2006, §6.3).

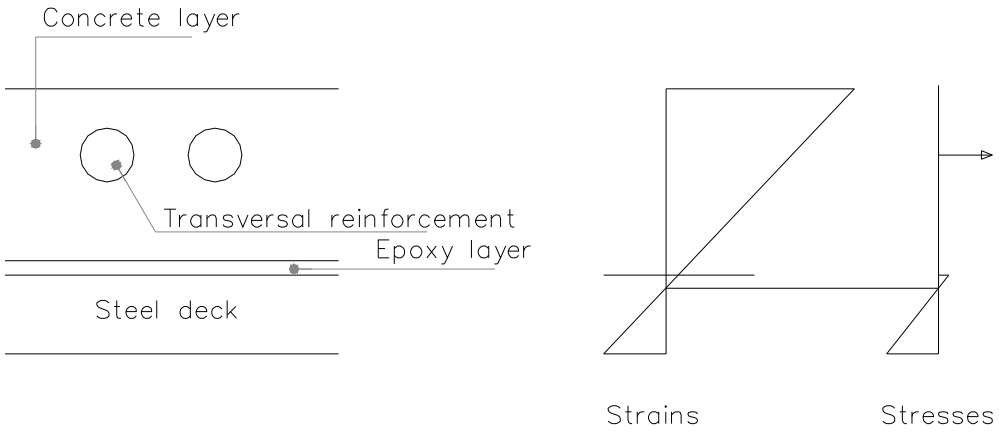

Figure 7-57: Scheme of stresses and strains in deck and concrete in transverse direction

CFRP grids are a common reinforcement for asphalt and small concrete structures such as stairs. It was doubted whether the use of grids was practical for this design, because of the lack of need for longitudinal reinforcement. Therefore grids were not considered.

As an alternative to bars or grids, CFRP can also be used as a laminate to reinforce concrete. Laminates are more commonly used on the outside as a repair to strengthen concrete. If a thick laminate is used a large amount of reinforcement can be achieved with a relatively large internal lever arm, which seems ideal in this situation. The laminate can be glued on to the concrete as strips of CFRP.

The effectiveness of the strip reinforcement depends on the amount that can be placed on the concrete. A CFRP laminate usually has a thickness of 1.0 or 1.4 mm and a width up to 120 mm. Calculation of the stress reduction, leads to reduction factors, from 0.14 up to 0.3 (Schrieks, 2006, §6.5). Figure 7-58 shows a cross-section of a deck with concrete and CFRP laminates.

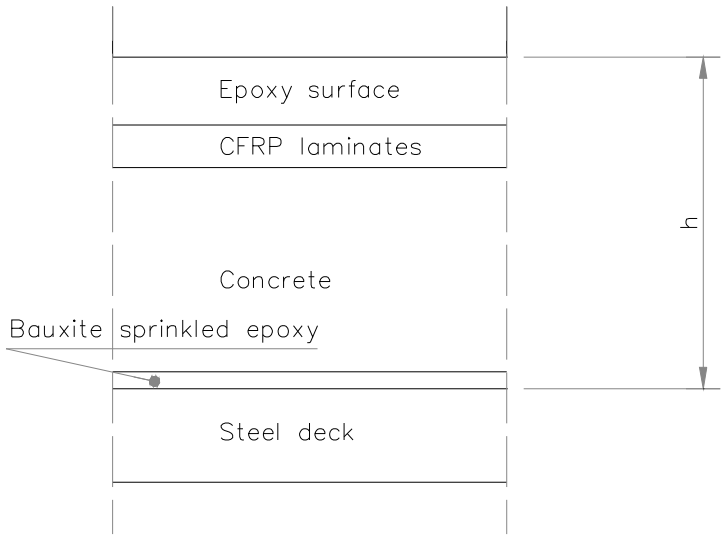

Figure 7-58: Cross-section of deck with CFRP laminate

A carbon braid is braided carbon fibres without epoxy material. Since the material is composed only of carbon fibres, a higher stiffness of about 230 GPa can be reached. However, by braiding the fibres the direction of each fibre is not fully in line with the tensile stress. A certain threshold deformation is required to make use of the stiffness. In order to achieve a considerable stiffness the braids need to be pretensioned, which makes too many complications for the construction. Therefore carbon braids are not considered to be an appropriate alternative for the design.

Stainless steel is less sensitive to corrosion than the commonly used carbon steel but as some corrosion can still occur, a minimum cover is required. However the concrete cover needed to prevent corrosion is less than that needed to resist bond-splitting forces. Therefore stainless steel is considered to be totally corrosion resistant for this design.

Schrieks concluded that the most appropriate reinforcement alternatives are:
- CFRP bars
- CFRP laminates
- Stainless steel bars, smooth and ribbed

7.4.4 Pull-out tests

Tests need to be performed to obtain knowledge about the uncertain aspects and the actual structural behaviour. In order to make this design pull-out and bending tests were performed, see paragraph 7.4.5.

Bond behaviour between high strength concrete and reinforcing bars is not dealt with in standards, neither bond characteristics of special types of reinforcement such as ‘sprinkled with sand’ CFRP nor smooth stainless steel, especially not for the small depths of concrete cover as considered for the bridge deck repair. The pull-out tests provide understanding of the bond behaviour between high strength concrete and reinforcing bars with small depths of concrete cover. In particular for the design of the bridge deck repair, pull-out tests have to be performed to quantify the minimum concrete cover on the bars and their spacing. Since these are two important parameters in the design of the reinforcement, the results of the pull-out tests might have a considerable influence on the design of the concrete layer and moreover on the effectiveness of the surface layer replacement.

Splitting of the concrete is a result of bond between reinforcing bars and concrete. In the past many investigations were carried out in order to quantify bond stresses. According to (Malvar, 1992), (Cairns, 1995, 1996-a, 1996-b) and (Lees, 1999) the bond behaviour can be divided in three basic mechanisms:

- Chemical adhesion
- Friction
- Mechanical interlock

Chemical adhesion is present before slip occurs. At that stage it is the only bond mechanism acting. When a rebar is subjected to a tensile force larger than the chemical adhesion, slip occurs and the mechanisms of friction and mechanical interlock are activated. Friction depends on the surface characteristics of a rebar. The mechanical interlock is a result of the surface profile of the reinforcing bars.

The test specimens consisted of a concrete block with several bars sticking out. The bars were fixed in the mould before the concrete was cast. Three types of bars were used:

- Ribbed ‘standard’ reinforcement steel bars
- Smooth stainless steel bars
- ‘Sprinkled with sand’ CFRP bars

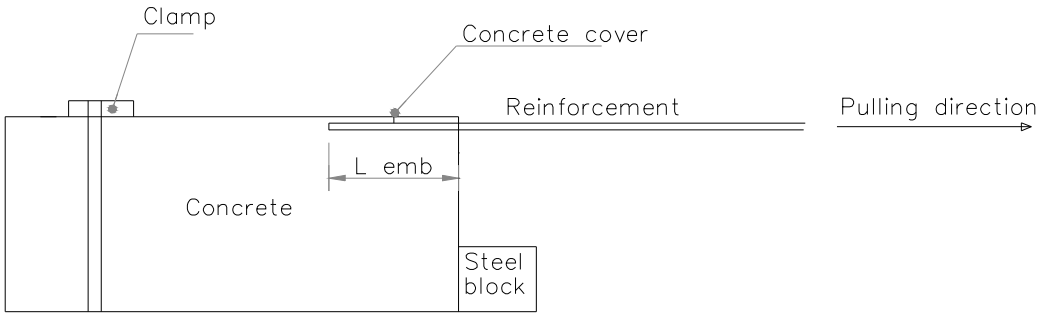

Figure 7-59: Schematic diagram of the pull-out tests

The pull-out tests were done in order to quantify the minimum concrete cover on the rebars, but along with this parameter the concrete strength and the embedment length were also investigated for the different types of reinforcement. This results in a total of four varied parameters:

- Type of reinforcement
- Concrete cover (3, 6, 9 mm)
- Concrete strength (C100 and C200)
- Embedment length of the rebar (30, 50, 80, 100, 232 mm)

The slip of the rebar is measured by an LVDT, which is located at the position where the rebar protrudes from the concrete. The pull-out tests result in forces and corresponding slip of the reinforcement bar. Thereby an observation of the failure mechanism is possible. Three main types of failure mechanisms occurred during the tests:

- Slip of a bar through the concrete
- Splitting of the concrete
- Failure of a bar before slipping or splitting occurred

For all smooth stainless steel bars, slipping occurred. Ribbed ‘standard’ reinforcement steel bars showed all three types of failure mechanism. Tests with a large embedment length and the use of C200 concrete resulted in yielding of the rebar. In the case of tests with smaller embedment lengths or the use of C100, the failure mode depended on the concrete cover depth. In case of a small concrete cover splitting failure occurred, as shown in Figure 7-60.

Figure 7-60: Splice failure of ribbed steel bar in C100, 3 mm concrete cover

Failure of a CFRP reinforcing bar occurred due to shear failure of the resin that glued the sand grains to the CFRP bar. As can be seen in Figure 7-61, the sand grains were stripped from the part of the CFRP bar, which has slipped through the concrete, and only the bare bar remained.

Figure 7-61: Slip failure of CFRP bar in C200, 3 mm concrete cover

This paragraph has only given a brief qualitative outline of the pull-out tests. For more details, quantitative test results etc., see (Schrieks, 2006).

7.4.5 Static bending tests

In order to obtain more knowledge on the actual behaviour of combinations of a steel deck covered with various repair alternatives, bending tests were performed on these alternatives. The most interesting bending property is the section modulus of the total deck plate structure after the repair. This parameter mainly determines the steel stress level at the bottom of the steel deck plate and therefore the expected lifespan of the deck plate. Next to the section modulus, the deflection of the structure and the relation between bottom and top strain provide better understanding of the bending behaviour. Finally the distance between the cracks in the concrete, which can be measured in the bending tests, is important concerning the cracking behaviour of the structure.

Because the behaviour of the rebars and laminates bond to concrete is unknown, unexpected premature failure mechanisms can occur during testing. These failures are used to calculate the maximum bond stress. As the deck plate in bridge decks is bent in two directions, the bending behaviour in both directions is researched.

To simulate the behaviour of the bridge deck plates with the alternative repairs, beams with a width of 120 mm were produced. An example of such a beam is depicted in Figure 7-62 and in Figure 7-63. The length of the beam was 600 mm. All beams consisted of the following elements:

- Steel strip, S235, 120 mm x 12 mm x 600 mm
- Epoxy resin, 120 mm x 3 mm x 600 mm
- Concrete layer, Contec Ferroplan C100/C200, 120 mm x $h_{concrete}$ x 600 mm
- Four types of reinforcement:
    - CFRP bars sprinkled with sand, ø = 5.4 mm
    - Smooth stainless steel bars, ø = 6.0 mm
    - Ribbed 'standard' reinforcing steel bars, ø = 6.0 mm
    - CFRP laminates, 120 mm x h_{lamel} x 600 mm

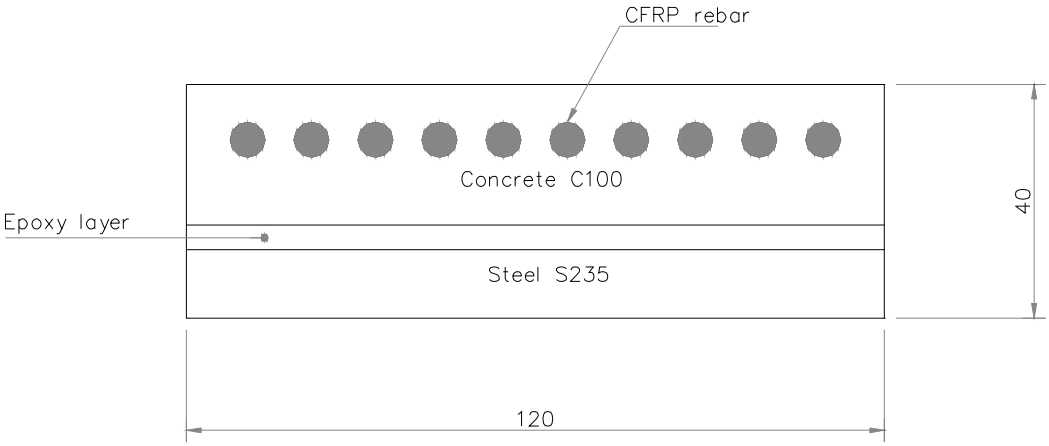

Figure 7-62: Cross-section of a test strip with CFRP rebars, $h_{concrete}$ is 25 mm

Figure 7-63: CFRP reinforced beam

An overview of the experimental program is given in (Schrieks, 2006). A total of 39 specimens were tested, with four aspects varied:

- Concrete type (C100 and C200)
- Type of reinforcement
- Total thickness of repair (25 or 30 mm)
- Reinforcement configuration

The test specimens were statically loaded in a four-point bending test device, as shown in Figure 7-64. The steel strain measured was used to control the applied force. This was done in order to prevent the steel plate from yielding, so the test specimens could be used for future research. As the actual bridge deck plate bends in two directions the strips in the tests were also loaded by a hogging and a sagging moment. In order to change the moment type the test specimens were turned upside down.

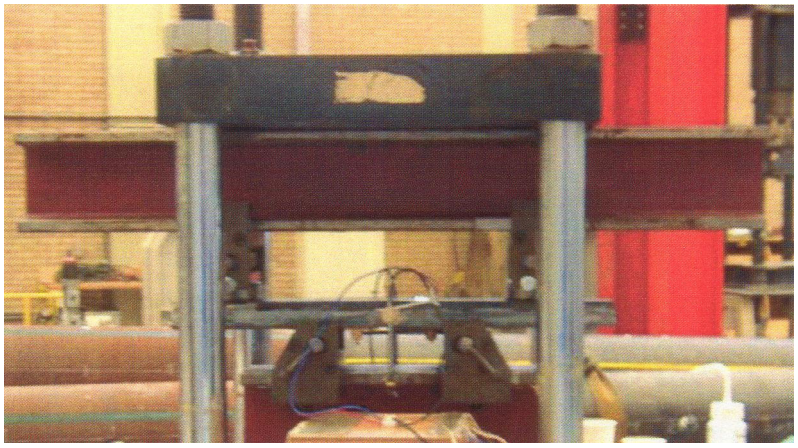

Figure 7-64: Bending test device

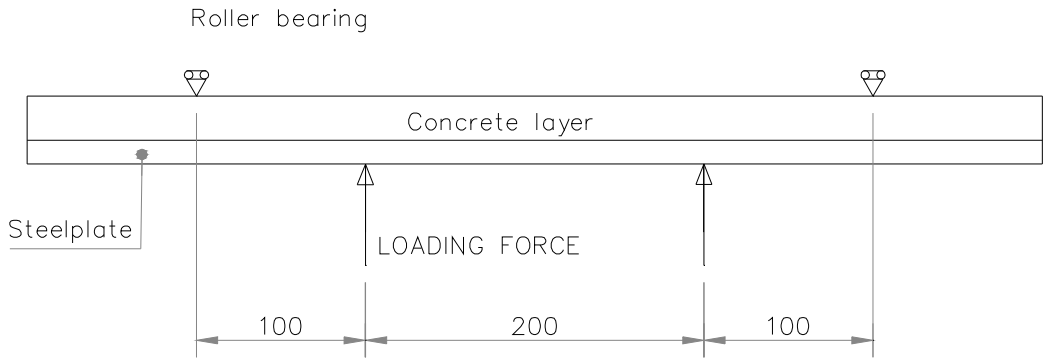

Figure 7-65: Scheme of four-point bending test

The measuring system consisted of a strain gauge and three LVDTs. The strain gauge was used to measure the strain at the steel surface. This was done in the middle of the beam in longitudinal direction. The strain gauge had a measuring length of 10 mm. The displacement at a distance of 10 mm from the concrete surface, the top surface in case of a hogging moment, was measured by means of an LVDT, located in the middle of the beam in longitudinal direction. The deflection in the middle of the beam was measured by two LVDTs, one on each side of the beam. Figure 7-66 shows the LVDTs.

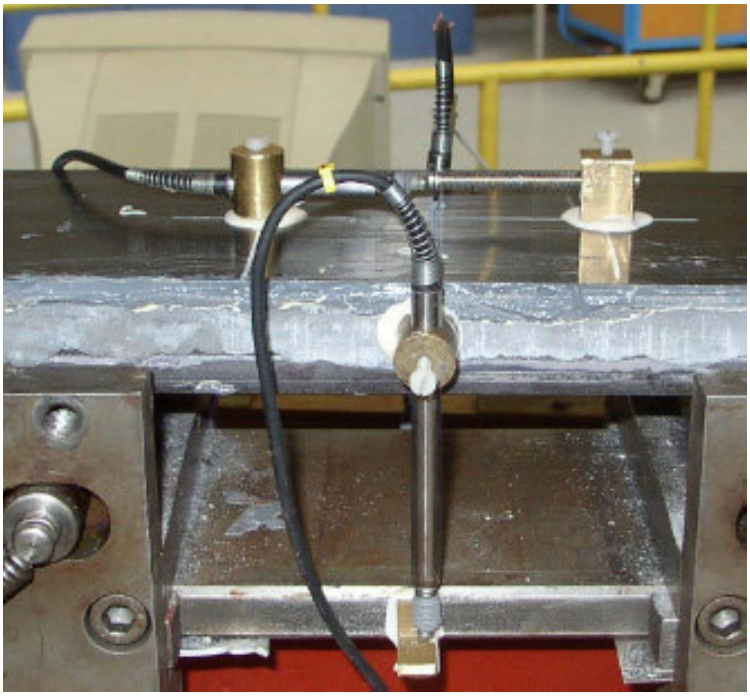

Figure 7-66: Location LVDT's during bending tests

A calculation of the stress reduction factor was made for each alternative, based on Euler-Bernoulli theory. This theory is based on the assumption that plane sections remain plane. Along with the use of the Euler- Bernoulli theory, it is assumed that in the case of a hogging moment, with the concrete loaded in tension, the concrete does not contribute to the moment resistance. A scheme of the stresses and strains in the section based on these assumptions is shown in Figure 7-57. Based on this theory the section modulus is calculated for each alternative. The stress reduction factor is again stress with renovation method divided by the stress without renovation method. This is equivalent to the section modulus for a bare steel plate divided by the section modulus of a steel plate with concrete and reinforcement.

The bending tests were intended to verify these calculations. From the bending tests an indication of the stress reduction factor for real bridges can be derived. For an extensive description of the bending tests, see (Schrieks, 2006). Some examples of premature failure occurred during the tests. Some shear bond failure of CFRP laminates occurred where the bond strength of the adhesive applied to bond laminate and concrete is less than the shear stress in this interface layer. In two cases the reinforcing bar slipped through the concrete. This occurred with smooth reinforcing bars embedded in C100.

From the test results it can be concluded that the equations used to calculate the hypothesis give a reasonably good estimate of the section modulus. Hence the Euler-Bernoulli theory can

be used to calculate the stress in the steel deck. Figure 7-67 illustrates this in a graph where the analytical bending stiffness is related to the measured bending stiffness. This conclusion is valid both for a positive as well as for a negative moment.

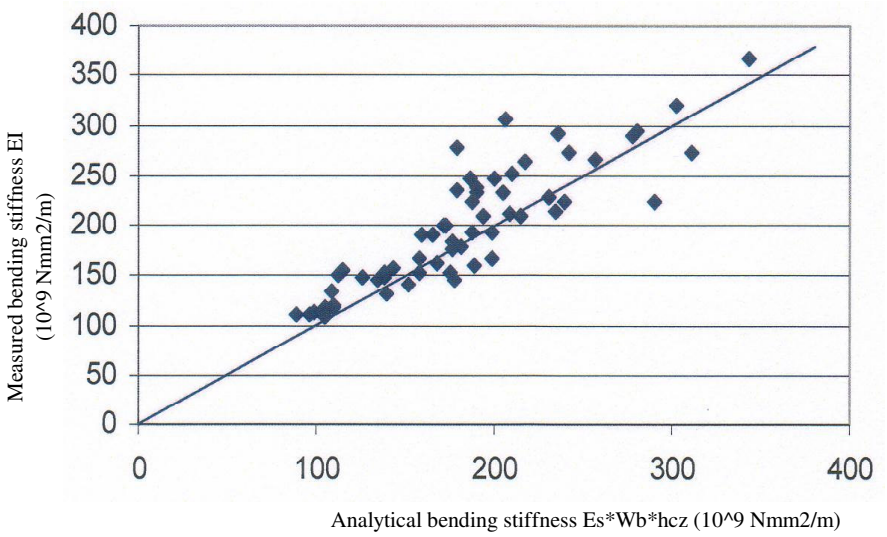

Figure 7-67: Results measurements against calculation for 4-point bending tests

7.4.6 Fatigue analysis

Schrieks has performed a concise fatigue analysis of the renovation method with a thin layer of reinforced high performance concrete on a steel bridge deck. He performed fatigue analyses of various aspects: the steel deck plate, the reinforcement, the concrete layer, the bond between concrete and reinforcement and the bonding of the epoxy layer. For the fatigue analysis of the deck plate see Chapter 8.

To check the fatigue lifespan of the reinforcement, first the stresses acting in the reinforcement are computed. These are compared with the fatigue curves for the reinforcement types, after which the lifespan can be computed. The critical fatigue stress for a CFRP material is considerably higher than that of reinforcement steel. Since this is not the case for the stresses acting on the CFRP reinforcement, it is concluded that a fatigue check of the CFRP material is not necessary. As the maximum stress in the steel reinforcement for a repair occurs with a 20 mm concrete overlay and a centre-to-centre spacing of the rebars of 18 mm, the fatigue check can be limited to checking the design fatigue lifespan of this alternative. The calculation is described in (Schrieks, 2006) from which it is concluded that the lifespan of the reinforcement is not critical for the design.

7.4.7 Alternatives

In this paragraph repair alternatives are presented as a result of the calculations, which were carried out and on the results of the pull out tests, the bending tests and the fatigue calculations. For the alternatives the most important properties considering the design are listed. Based on these properties a conclusion can be drawn on which alternative is the most appropriate deck plate renovation technique.

With respect to the bar diameter:

- From the results it is concluded that a rebar diameter of 6 mm leads, in case of all rebar configurations, to a stress reduction, which is close to the maximum possible. Therefore it is concluded that, for this design, in the case of all bar reinforcement materials a bar diameter of 6 mm is the most appropriate diameter.

With respect to the concrete cover:

- The tests showed that in the case of smooth steel bars and 'sprinkled with sand' CFRP bars, for the tested concrete cover depths, slip failure will occur before the concrete cover splits. Therefore it is concluded that for these rebar types the concrete cover depth to avoid splitting can be limited to 0.5 Ø, which results in a total concrete cover depth of 6 mm, because of the 3 mm construction tolerance.
- The same holds for ribbed stainless steel bars.

With respect to the minimum distance between reinforcement bars:

- A rebar spacing of 12 mm can be used in all cases as well. This results in a distance between the rebars of 6 mm.

With respect to the type of reinforcement:

- Smooth reinforcement cannot be used to reinforce the concrete on the repair, because smooth reinforcement requires long effective bond lengths, which cannot be attained on the deck plate.
- To prevent shear bond failure the application of laminate reinforcements are not recommended on bridge deck plate repairs.

Based on these considerations appropriate alternatives for renovations are:

- Repair thicknesses of 25 and 30 mm (h_{total})
- Ribbed stainless steel (RS) and 'sprinkled with sand' CFRP reinforcing bars are appropriate to reinforce the concrete layer. These bars can be applied with 6 mm concrete cover (c) and 12 mm centre spacing.

The alternatives appropriate to apply for the repair of steel bridge decks of movable bridges are listed in Table 7-16.

Table 7-16: Alternatives for RHPC on movable bridges decks (Schrieks, 2006)

Code	h_{total} (mm)	$h_{concrete}$ (mm)	Type of reinforcement	Spacing rebars (mm)	c (mm)
RS-25	25	20	Ribbed stainless steel	12	6
CFRP-25	25	20	'Sprinkled with sand' CFRP	12	6
RS-30	30	25	Ribbed stainless steel	12	6
CFRP-30	30	25	'Sprinkled with sand' CFRP	12	6

The alternatives are compared against the following characteristics, as shown in Table 7-17.

- Stress reduction factor (concerning local stresses and a hogging moment)
- Theoretical lifespan expectation (based on Moerdijk Bridge load spectrum and mean lifespan)
- Weight added to the bridge deck
- Thickness difference between two lanes

Table 7-17: Characteristics of alternatives (Schrieks, 2006)

Repair code	RS-25	CFRP-25	RS-30	CFRP-30
Stress reduction factor	0.24	0.28	0.18	0.20
Lifespan expectation (year)	416	261	1148	748
Weight added (kg/m^2)	63	49	76	62
Thickness difference	18	18	23	23

7.4.8 Conclusions and recommendations

7.4.8.1 Conclusions

Conclusions based on the research Schrieks performed are:

- Repair thicknesses up to approximately 30 mm are possible on the bridge deck giving due consideration to repair weight and repair thickness.
- CFRP is a more favourable reinforcement material than GFRP, AFRP and BFRP.
- Longitudinal reinforcement is not required for the bridge deck repair.
- A grid reinforcement is not appropriate for the design.
- Carbon braids cannot be used to reinforce the concrete overlay.
- Smooth stainless steel bar reinforcement is inappropriate to reinforce the concrete layer.
- CFRP laminate can not be used to reinforce the concrete surfacing.

- For smooth steel bars embedded in C100 or C200 pull-out failure mechanism is slip of the bar through the concrete.
- For ribbed bars embedded in C100 or C200 two types of pull-out failure can occur, depending on the concrete cover depth and the concrete strength, these are splitting of the concrete cover and slip of the bar through the concrete.
- For 'sprinkled with sand' CFRP bars embedded in C100 or C200 slip of the bars through the concrete is the main failure mechanism.
- The required minimum concrete cover depth is 6 mm, made up of 3 mm in order to avoid splitting of the cover and 3 mm casting tolerance.
- The use of the Euler-Bernoulli theory and the assumption that concrete loaded in tension is fully cracked results in reasonably good values for the section modulus and thus for the stress reduction factor, both for positive and negative moments.
- CFRP bar reinforcement is an appropriate reinforcement for the concrete overlay. A CFRP reinforced concrete overlay results in a stress reduction factor of 0.28 for a 25 mm renovation thickness and a stress reduction factor of 0.20 for a 30 mm renovation thickness.
- Ribbed stainless steel bar reinforcement is an appropriate reinforcement for the concrete layer. In C100 concrete stainless steel can be considered corrosion resistant for concrete cover depths of at least 2 mm. A stainless steel reinforced concrete overlay results in a stress reduction factor of 0.24 for a 25 mm renovation thickness and a stress reduction factor of 0.18 for a 30 mm renovation thickness.
- The minimum possible thickness of the bridge deck repair layer is 20 mm, consisting of 3 mm epoxy resin, 3 mm sprinkled bauxite layer, 6 mm rebar diameter, 6 mm concrete cover and 2 mm surface layer grains.

7.4.8.2 Recommendations

The research of Schrieks comprised a literature review, stress reduction calculations, pull-out tests, static bending tests on small beam specimen and fatigue calculations. Based on this research it can be concluded that significant stress reductions in the steel deck plate of real bridges are achievable. Therefore this renovation method is concluded to be a promising solution. Before application on a real bridge with traffic the following supplementary research should be performed:

- Bending fatigue tests on beams. In addition to the static tests that have already been performed on the small beam specimens, fatigue tests should be performed on these specimens. These tests will give insight in the fatigue properties of the various alternatives.
- Application test on a real bridge deck test panel, out of service. In this test all questions related to the application process should be answered. A major topic in this test is the

construction tolerance that is necessary. The alternatives were researched with the assumption that 3 mm construction tolerance is enough. This assumption should be verified in the application test.

- Static tests on part of a bridge deck. If a part of a bridge deck with common dimensions is provided with a thin concrete surfacing and loaded with simulated real wheel loads, a better insight into stress patterns will be achieved.
- Fatigue tests on part of a bridge deck. Subsequently the bridge deck part that has been loaded with a static load, can be subjected to a fatigue test. In this fatigue test a footprint with real dimensions can be used, and traffic flow of heavy vehicles on motorways can be simulated.
- Durability and environmental influences should be researched in more detail
- A solution is required for the transition between the edges of the concrete layer and the adjacent traffic lanes and at the expansion joints where a thickness difference occurs . In the research it was assumed that a transition could be solved in a satisfactory way. This should be designed.
- The absolutely minimum thickness of such a thin concrete surfacing should be determined by research together with the stress reduction factor that can be achieved with that thickness.

7.5 Concluding remarks

Three possible renovation methods for movable steel bridge decks were researched: bonding on an additional steel plate, filling the troughs with polyurethane and a thin surfacing of reinforced high performance concrete. At the end of this chapter some concluding remarks can be drawn with respect to the behaviour of the researched renovation methods. Table 7-18 gives a summary of the main results of this chapter. SRF stands for stress reduction factor.

Table 7-18: Summary of main results

Method	SRF	Fatigue	Conclusion
Bonding steel plates	≈ 0.5	Failure	Possible renovation technique if infusion technique leads to good fatigue behaviour of adhesive layer.
Trough filling	≈ 0.12 up to 0.8	Failure	Unreliable renovation technique, no further research
Thin RHPC	≈ 0.18 up to 0.28	Not tested	Promising solution, but a lot more research is necessary.

Bonding additional steel plates reduces stresses in the deck plate significantly. The stress reduction factor is approximately 0.5. This stress reduction factor results theoretically in a significant extension of the lifetime of the bridge deck structure. However in the fatigue test structural failure is observed as delamination occurred in the adhesive layer. A new application method, the vacuum infusion technique, has probably better fatigue properties. At this moment the conclusion is that bonding steel plates is still a candidate renovation technique with respect to the lifetime of the steel structure. But before application on a real bridge the fatigue properties of the adhesive layer and the steel deck should be tested with a good result.

Filling the troughs with polyurethane causes in general lower stresses in the deck plate. Differences between measurements however are very large. These differences mean that the effectiveness of the trough filling is not always the same, which could be due to differences in adhesion between filling material and the underside of the deck plate. In two fatigue tests on bridge samples three fatigue cracks grew in the deck plate. A significant improvement in this renovation method cannot be envisaged without changing the total concept of the method. The final conclusion therefore must be that this method does not lead to the required significant extension of the lifetime of the deck structure. This is probably be due to the lack of adhesion between filling material and underside deck plate. Besides this there is also the disadvantage that this renovation method does not strengthen the deck plate between the troughs.

A thin reinforced high performance layer up to 30 mm thick causes stress reduction factors, depending on the thickness and reinforcement, from 0.18 up to 0.28. These are significant stress reduction factors, which can lead to a significant increase of the lifespan of movable bridges. This stress reduction however is only based on calculation and verified with small static tests. At this moment the conclusion is that this is a promising solution for lifespan extension of movable bridges, but extensive supplementary research is necessary before it can be concluded that it can be applied on a real bridge. This additional research should at least comprise bending fatigue tests on beams, an application test on a real bridge deck panel, out of service, static and fatigue tests on a part of a bridge deck. Also durability and environmental influences should be researched in more detail and a proper solution to the thickness transition differences should be designed.

The general conclusion is that the researched renovation techniques for movable bridge decks have not yielded the significant extension of the lifetime that is required. Besides that with these renovation techniques new durability problems are introduced on the bridge. For two techniques: bonding steel plates and the reinforced high performance concrete layer additional research is recommended.

With this conclusion in mind, consideration should be given to building a new bridge as a better alternative to renovating an old one with fatigue cracks. The technical disadvantages are obvious, and in that case the financial implications of building a new bridge can be accepted.

8. Design and maintenance philosophy

8.1 Introduction

Previous chapters in this thesis are mainly focussed on the behaviour of existing bridges and the development of renovation techniques. This chapter deals with other subjects the consideration of which are also necessary for a successful maintenance philosophy.

Paragraph 8.2 gives a description of the maintenance philosophy that is proposed for orthotropic bridges with fatigue problems. Besides renovation techniques, lifetime calculations and inspection techniques are necessary.

Paragraph 8.3 with the title probabilistic maintenance describes the background of the proposed maintenance strategy.

Paragraph 8.4 contains a description of the systematic lifetime calculations for steel bridge deck plates. These lifetime calculations are also probabilistic and are essential for the successful implementation of such a probabilistic maintenance strategy. Also within this paragraph is a part about the influence of asphalt surfacings on the lifetime of bridge decks.

Paragraph 8.5 briefly describes several inspection methods. Although the development of inspection techniques is outside the scope of the thesis, inspection techniques are of course also necessary for a successful implementation of the proposed strategy.

Paragraph 8.6 is the last paragraph in this chapter with some concluding remarks.

8.2 Maintenance philosophy

8.2.1 Introduction

A usual maintenance strategy for orthotropic steel bridge decks is formed by time-based inspections of the bridge structure and the replacement of parts of the structure when these parts are at the end of their lifetime. Up to the time of the observed fatigue problems on the Van Brienenoord bascule bridge (De Jong, 2003, 2004-a, 2004-b) this meant that for example

once in five years an extensive visual inspection of the total structure was performed (asphalt surfacing, deck structure, crossbeams, main girders, structural bearings, coating etc.). The elements that were replaced on regular basis were, up to the Van Brienenoord case, mainly the asphalt surfacing, the structural bearings and the protection coating. This maintenance strategy is characterized as conventional maintenance.

After the problem with the Van Brienenoord Bridge was solved two questions had to be answered in relation to the maintenance philosophy:

- What are possible repair techniques for observed fatigue cracks, which need to be repaired very quickly? These local repair techniques are necessary up to the moment that a total renovation is carried out.
- What renovation techniques are there to enhance the lifetime of the total bridge deck structure?

8.2.2 Conventional maintenance

As stated before practice up to now has been conventional maintenance. Conventional maintenance is formed by time-based inspections of the bridge structure and the replacement of parts of the structure when these parts are at the end of their lifetime. The inspections are intended to enable decisions to be made about replacement of parts of the structure. Figure 8-1 gives a model of this kind of maintenance. This kind of maintenance is appropriate, provided that the time based interval is long and failure of elements within this interval doesn't cause structural failure.

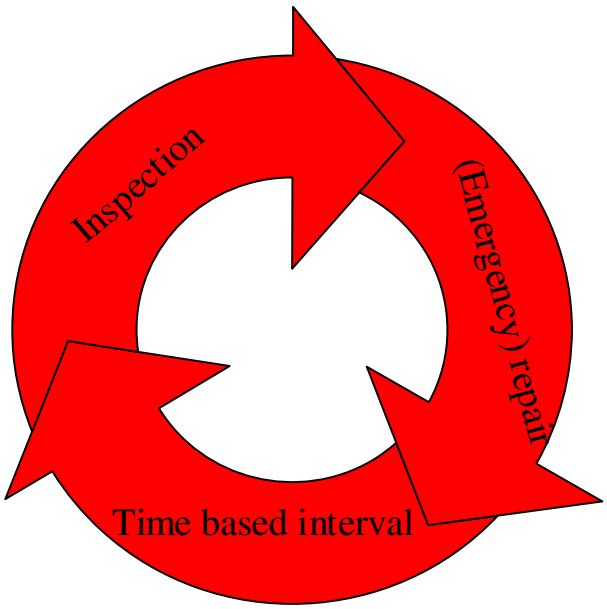

Figure 8-1: Conventional maintenance strategy

In the case of the fatigue problems on orthotropic steel bridge decks both requirements are not met. Experiences on steel bridges in the Netherlands have shown that monthly visual inspection of the steel bridge deck structure is necessary on the most heavily loaded bridge structures with fatigue cracks, i.e. the Caland Bridge. Besides these expensive inspections expensive emergency repairs of the deck structure are also needed when severe fatigue cracks are observed in the deck plate.

Due to the nature of the fatigue phenomenon we can expect that the number of inspections and repairs will continue to increase. Therefore the conclusion must be that this conventional maintenance strategy is no longer appropriate and that the maintenance philosophy has to be changed to another strategy.

8.2.3 Risk based maintenance

In changing from a conventional maintenance strategy to a more sophisticated one two major changes can be observed. At first the maintenance strategy should be more focussed on the control of risks. The time based inspection interval has to be replaced by an interval based on a lifetime calculation. Systematic lifetime calculations for fatigue cracks are very important for a risk-based strategy and local (emergency) repairs have to be replaced by renovation of the total bridge deck structure or by a new bridge deck. These renovations have been described in chapters 6 and 7. Figure 8-2 depicts this strategy schematically.

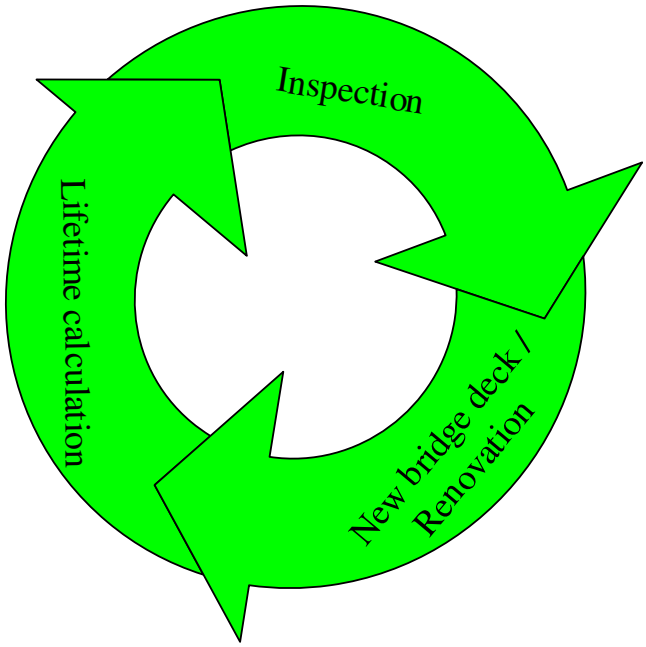

Figure 8-2: Risk-based maintenance strategy

A risk-based maintenance philosophy consists of three parts:

- Lifetime calculations – to schedule inspections
- Inspection methods – for an inventory of the fatigue that is necessary before deciding if a renovation is necessary
- Renovation techniques – to rehabilitate the total deck structure

The objective of the philosophy is to guarantee the safety of the structure with a required safety level described as the reliability index β. Paragraph 8.3 describes in more detail probabilistic maintenance and its theoretical background.

8.3 Probabilistic maintenance

8.3.1 Probabilistic theory

Van Straalen has given an overview of the development of probabilistic design rules (Van Straalen, 1999, 2001). In this paragraph a summary of the overview written by Van Straalen is given. This summary gives the background to the probabilistic theory; see also Annex C of Eurocode 0 (Eurocode 0, 2002). The limit state is defined as the condition in which the structure is no longer capable of fulfilling its function under given actions. In practice this means that the structure collapses or that the structure can not be used normally. A mathematical representation is given by the limit state function defined as the difference between the resistance (R) and the action effect (S):

$$Z = R - S$$

As long as $Z > 0$ no failure will occur, while for $Z < 0$ the structure fails; the limit state is reached when $Z = 0$. Both the resistance and the action effects are regarded as stochastic variables, which can be represented by their probability density functions $f_R(r)$ and $f_S(s)$ respectively. When the resistance and the action effects are statistically independent, their combined probability function is defined as $f_R(r) \cdot f_S(s)$. This function can be graphically presented by contours in its R-S plane, see Figure 8-3.

Instead of presenting the results of the probabilistic reliability methods in terms of probability of failure, the reliability index β is commonly used in simplified probabilistic analyses at level II. The relation between the probability of failure $P(Z < 0)$ and the reliability index β is given by:

$$P(Z < 0) = \Phi(-\beta)$$

Where Φ is the cumulative distribution function of the standardized normal distribution. If the limit state function Z is normally distributed, the reliability index is defined as:

$$\beta = \frac{\mu}{\sigma}$$

Where μ is the mean value of the limit state function and σ its standard deviation.

Target values for the reliability index β are given in the European as well as in the national Dutch standard (Eurocode 0, 2002), (NEN 6700, 2005).

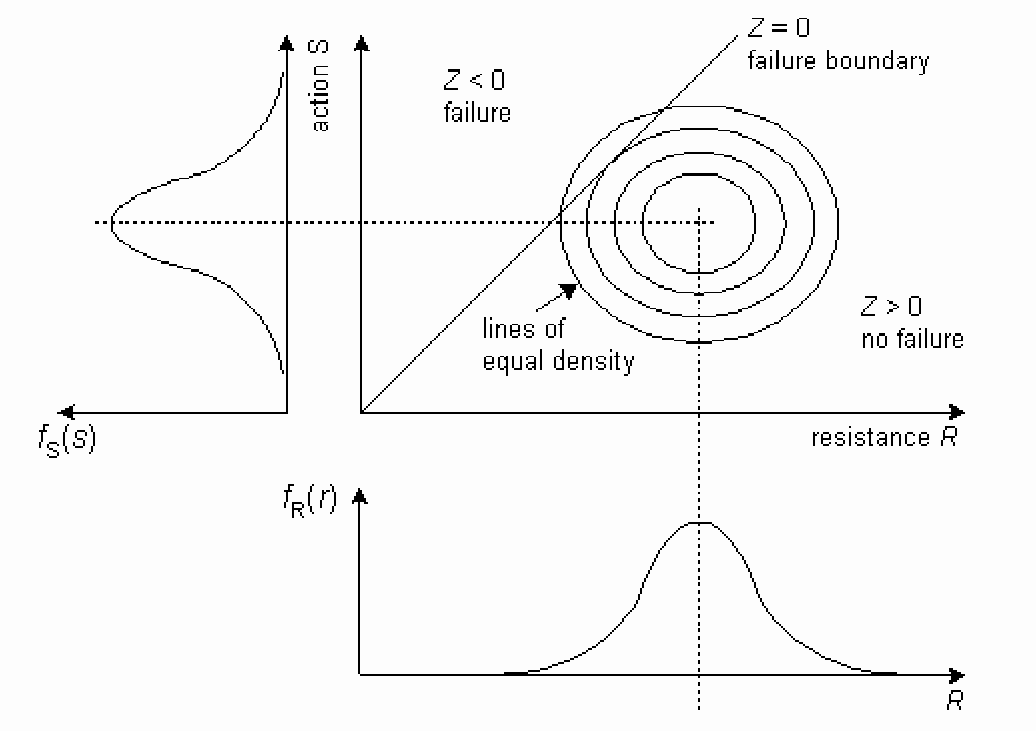

Figure 8-3: Failure function Z in R-S plane (Van Straalen, 1999)

Table 8-1: Target reliability index β

Limit state	Eurocode 0	NEN 6700
Ultimate	3.8	3.6
Fatigue	1.5 to 3.8	
Serviceability	1.5	1.8

The target reliability index for fatigue in the Eurocode depends on the degree of inspectability, repairability and damage tolerance. The NEN 6700 does not define a target

reliability index for fatigue. Note that the tabulated values of the reliability index are for a standard reference period of 50 years. Generally bridges are designed with a longer reference period, which means that the reliability index should be slightly higher.

The most convenient structural reliability method for daily design practice is the partial safety factor approach, also known as the level I method. The reliability of a structure or component with respect to failure is checked on the basis of the limit state function in combination with design values for the action and the resistance. These design values follow from so-called characteristic values combined with matching partial safety factors. Within the partial safety factor approach the safety of a structure or component has to be validated by comparing the so-called characteristic values for the action S_k and the resistance R_k:

$$\gamma_S \cdot S_k \leq \frac{R_k}{\gamma_R}$$

Where is γ_S and γ_R are the partial safety factors for the action effects and the resistances respectively.

To combine the partial safety factor approach with probabilistic techniques, a relationship between level I and II methods is worked out. The key to this relationship is the level II design point, defined as the point of the limit state $Z = 0$ with the highest probability. Figure 8-4 defines the design point (R_d, S_d) in the case of normal probability distributions. Due to the fact that in this graph for both axes S and R are divided by their standard deviations, the meanings of the reliability index β and the weighting factors α become clear. The reliability index β is equal to the number of standard deviations between the mean value of the limit state function Z and the design point, while the weighting factors α_S and α_R indicate which part of the reliability index counts for the action and for the resistance respectively. α_S and α_R are the values of the sensitivity factors. The value of α is negative for unfavourable actions and actions effects and positive for resistances. This leads to:

$$P(S > S_d) = \Phi(-\alpha_S \beta)$$

$$P(R \leq R_d) = \Phi(\alpha_R \beta)$$

α_S and α_R may be taken as -0.7 and 0.8 respectively. These values are given for dominating variables and seem to be valid for a wide field of applications. When an action or resistance model contains more basic variables, the values of α_S and α_R for additional non-dominating variables have to be multiplied with a factor 0.4.

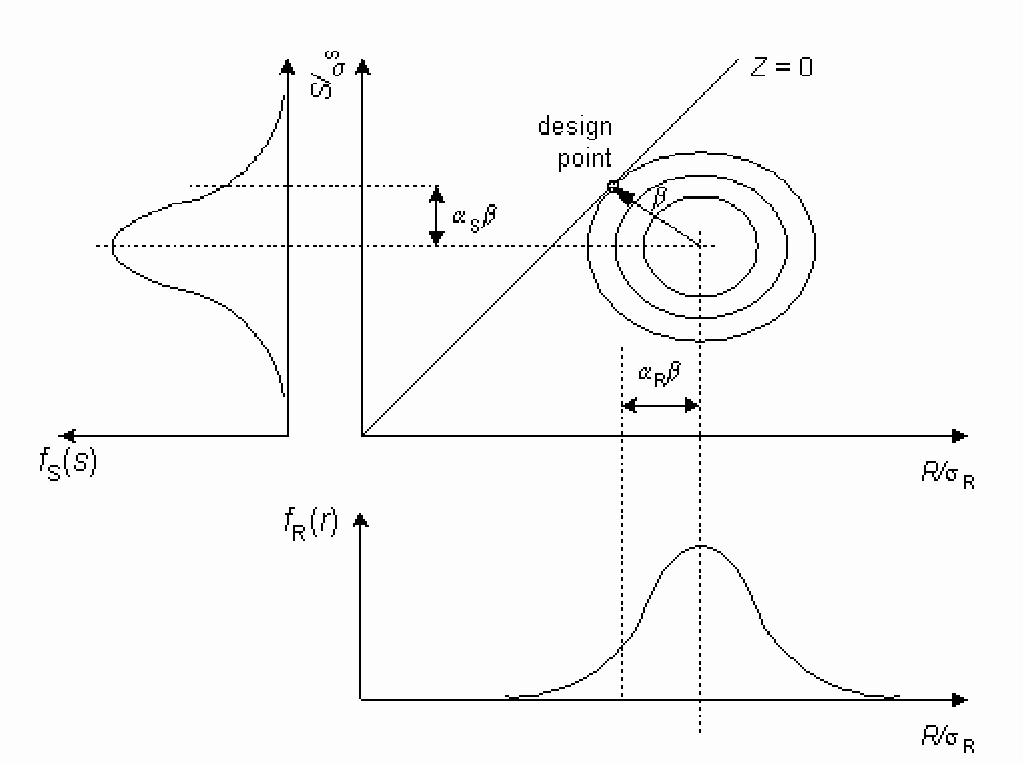

Figure 8-4: Location of the design point on the failure boundary $Z = 0$ (Van Straalen, 1999)

Expressions for the design values of variables are given in Annex C of Eurocode 0 (Eurocode 0, 2002) for several probability distributions. Table 8-2 gives the expression for the normal and the lognormal distribution.

Table 8-2: Design values for two distribution functions

Distribution	Design values
Normal	$\mu - \alpha\beta\sigma$
Lognormal	$\mu\exp(-\alpha\beta V)$

Once the design values are known, the relevant partial factors can be calculated from the design value and its relevant representative or characteristic value.

8.3.2 Target reliability index for fatigue in deck plates

In the previous paragraph the target values of the reliability index β both for the European and Dutch code are given. For fatigue verifications the target value is indistinct: between 1.5 and 3.8 in the Eurocode and the NEN 6700 provides no target value. Setting a successful

functioning maintenance strategy on a probabilistic basis requires the definition of a more specific target value for the reliability. The setting of a target reliability index is especially necessary when dealing with the crack in the deck plate at the crossbeam location, see Figure 2-9.

Therefore it is profitable to go more deeply into the definition of limit states. Ultimate limit states are concerned with the safety of people, the safety of the structure, loss of human lives, loss of equilibrium of the structure or parts of it. Serviceability states are concerned with the comfort of people, functioning of the structure under normal use etc. (Eurocode 0, 2002)

An essential part of the probabilistic approach to fatigue phenomena in orthotropic steel bridge decks is the definition of failure. Which crack dimension is considered as failure of the structure? For deck plate cracks, the question is then: which crack length corresponds to the description of the limit states. The definition of failure should correspond to the description of ultimate or serviceability limit states. For the fatigue calculation based on Miners rule the detail classification should also be taken at that defined failure point.

In paragraph 4.2.4 a test is reported to determine the ultimate static capacity of the deck plate with fatigue cracks. From this test it becomes clear that longer crack lengths up to approximately 50 cm only cause an indentation in the deck plate. Therefore it can be argued that a crack length in excess of 50 cm in the longitudinal direction should be defined as ultimate limit state failure. To calculate appropriate inspection intervals a detail classification or crack growth model of this crack length should be available. Both however are not available at the moment.

On the other hand the detail classification of 91 MPa, see paragraph 4.3.2.3, based on fracture mechanics, or 113 MPa, see paragraph 4.3.3.3, based on fatigue tests both at 10^7 cycles according to the NEN 2063 format (NEN 2063, 1988), are for a crack, which has just grown through the deck plate and has no length at the top surface of the deck plate. With the definition from the standards in mind, a deck plate crack with this dimension should be classified as serviceability limit state.

This difference is also the case for other crack types. For example, for the trough splice weld, see Figure 2-18 and Figure 2-19, the definition of failure on which the detail classification is based is a small crack, which is just visible. This crack dimension defines the serviceability limit state. However if the splice weld is fully cracked, from the deck plate around the trough to the deck plate on the other side, it can be argued that even this is not an ultimate limit state because there is the possibility of redistribution of loads to the adjacent troughs.

This means that there are two options:

- Ultimate limit state, $\beta = 3.6$ or 3.8 combined with a detail classification for a 'long' crack
- Serviceability limit state, $\beta = 1.8$ combined with a detail classification for a 'small' crack

A choice has to be made between these two options, but in principle it can also be argued that the fatigue verifications have to be done for both limit states, to determine which is critical.

For a fatigue verification at the ultimate limit state level it is essential to have a detail classification or crack growth model for these long cracks in order to calculate appropriate inspection intervals. For the deck plate crack and other crack types only detail classifications at serviceability level are available, it is very costly and a time-consuming activity to derive detail classifications for ultimate limit states.

To handle this problem it is better to use the available detail classifications from chapter 4 with small crack dimensions and make a calculation for the serviceability limit state and its target reliability index $\beta = 1.8$. In that case it must be assumed that the serviceability limit state is decisive and to treat the calculated inspection interval as that which is necessary to guarantee that no ultimate limit state will occur with the required probability on the reliability level at $\beta = 3.6$. This assumption can be partly validated, as there are fatigue detail classifications for crack lengths up to 100 mm available from chapter 4.

The conclusion of this paragraph is that the target reliability index is that of serviceability limit states, $\beta = 1.8$ both for the European as well as for the Dutch standard.

8.3.3 Safety factors for lifetime calculations

In the fatigue lifetime calculation three safety factors have been used:

$\gamma_{S\text{-}N}$ safety factor on the detail classification

γ_n safety factor for the number of stress cycles

$\gamma_{\Delta\sigma}$ safety factor for the stress ranges

Table 8-3 gives the values of these safety factors. These values are derived in a comparable way to the calculation of safety factors in (Vrouwenvelder, 2000-b).

Table 8-3: Safety factors for lifetime calculations

Safety factor	$\beta = 0$	$\beta = 1.8$	$\beta = 3.6$
$\gamma_{S\text{-}N}$	1.0	1.246	1.552
γ_n	1.0	1.199	1.423
$\gamma_{\Delta\sigma}$	1.0	1.287	1.655

It should be noted that these safety factors, all have to be used in combination with the mean value and not with the characteristic value.

8.4 Systematic lifetime calculations for steel bridge deck plates

8.4.1 Introduction

In general two types of lifetime calculations have been made.

- Expected lifetime, without partial safety factors. This type of calculation is totally based on mean values, which means that the reliability index used is $\beta = 0$. All safety factors in this calculation are 1.0. This calculation is intended to calibrate the lifetime calculation model.
- Design lifetime, with partial safety factors. In this calculation safety factors larger than 1.0 are used. The values of the safety factors are based on a probabilistic approach as described earlier in this chapter.

Another distinction is also possible. The lifetime calculations are useful for the calculation of the fatigue lifetime of the bridge deck plate in several situations:

- An unrenovated bridge deck with as the starting point the building year. The calculation then starts with an initial damage $D = 0$.
- An unrenovated bridge deck with a result of an inspection as the starting point. The calculation then starts with an initial damage D where $0 < D < 1$.
- A renovated bridge deck with as starting point the building year. The calculation then starts with an initial damage $D = 0$ and the effects of the renovation technique are taken into account.
- A renovated bridge deck with a result of an inspection as the starting point. The calculation then starts with an initial damage D where $0 < D < 1$ and takes into account the effects of the renovation technique.

Figure 8-5 illustrates this. The calculation starts with a damage $D = 0$ in the building year. The result of this calculation, with partial safety factors, is a year in which the expectation for damage $D = 1$. The first inspection has to be performed in this year. Because the lifetime calculation to schedule the inspection has been performed with partial safety factors it is likely that the damage D found with an inspection is smaller: $D < 1$. In that case a new fatigue lifetime calculation can be performed to schedule the second inspection. If the inspection is not combined with a renovation technique the calculated crack growth rate will be the same as in the first calculation. If the inspection is combined with an renovation technique the stress ranges reduce, thus lowering the crack growth rate. This is visible after the second inspection.

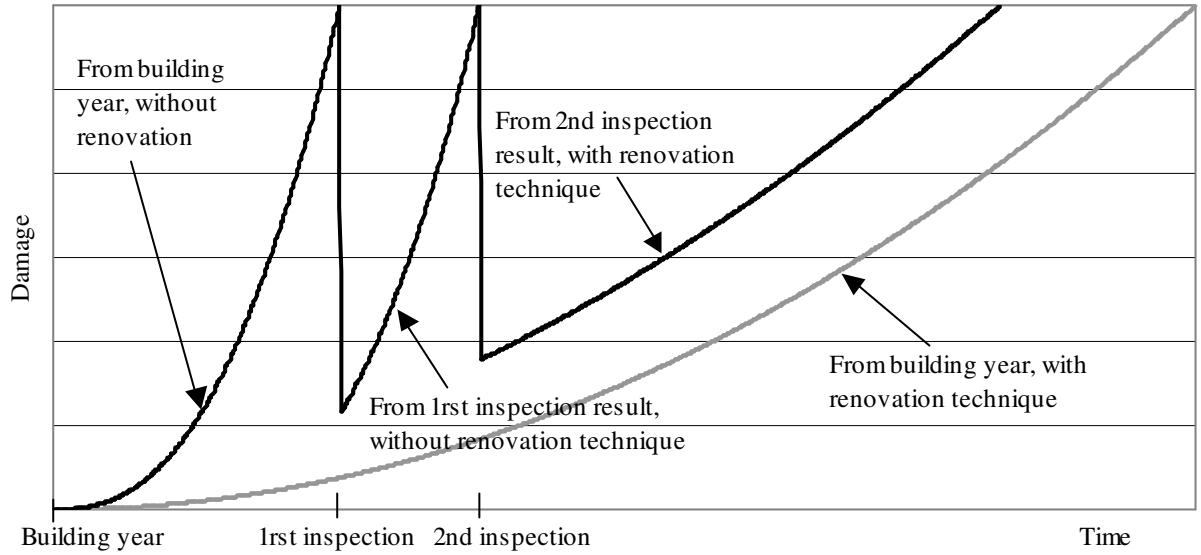

Figure 8-5: Lifetime calculations

8.4.2 Calculation procedure

Reliable lifetime calculations are important. This paragraph gives a formal model to calculate the fatigue damage for the deck plate crack at the location of the crossbeam. The given numerical values are valid for motorway bridges in the Netherlands. For other countries these values may differ. The total fatigue damage is given by:

$$D_{total} = \sum_{i=A,B,C} \iiint D(t,x,Q)\, dt\, dx\, dQ$$

with:

D	Fatigue damage
i	Wheel type; A = single, B = double, C = super single
t	Time [hours]
x	Position in transverse direction
Q	Wheel load [kN]

The fatigue damage D is given by:

$$D(t,x,Q) = \frac{n_i}{N_i}$$

with:

N_i Number of axle loads at $D = 1$
n_i Number of axle loads given by:

$$n_i = f(Q) \cdot f(x) \cdot f(t) \cdot n_{axle/lorry}$$

with:
$f(Q)$ Lognormal distribution function of the wheel loads
$f(x)$ Normal distribution of the location of the wheel in transverse direction, with σ = 150 mm. This distribution is based on measurements described in (Vrouwenvelder, 1998), see also paragraph 3.3.3
$f(t)$ Distribution function for the traffic over the time
$n_{axle/lorry}$ Average number of axles per lorry, for motorway bridges in the Netherlands $n_{axle/lorry}$ = 4.15. This value is based on fatigue load model 4, traffic type long distance (from Eurocode 1991 – part 2, 2003), see paragraph 3.4.2

The lognormal distribution of the wheel loads is given by:

$$f(Q_i) = \frac{1}{\sqrt{2\pi}} \frac{1}{\sigma_i} \frac{1}{Q_i} \exp\left(\frac{-(\ln(Q_i) - \mu_i)^2}{2\sigma_i^2} \right)$$

with:
Different values for μ_i and σ_i for the three different wheel types given by:
μ_A = 3.22 and σ_A = 0.240 for wheel type A (single)
μ_B = 3.40 and σ_B = 0.475 for wheel type B (double)
μ_C = 3.22 and σ_C = 0.375 for wheel type C (super single)
The distribution type and the parameters have been measured on several Dutch motorway bridges; see paragraph 3.3.2 (Vrouwenvelder, 2000-a and 2000-b).

The distribution function for the traffic over the time is given by:

$$f(t) = f_{day}(t) \cdot n_{lorry/day} \cdot (1+g)^{(t-t0)} \cdot p_i \cdot \gamma_n$$

with:
f_{day} Distribution function for the traffic flow over 24 hours
$n_{lorry/day}$ Number of lorries in 24 hours at the reference time t_0
g Growth of the traffic volume, on Dutch bridges 2-4 % per year
p_i Part of the traffic for the three wheel types. On Dutch bridges $p_A \approx 0.3$, $p_B \approx 0.4$

and $p_C \approx$ 0.3, see paragraph 3.3.2

γ_n Safety factor for the number of stress cycles

The distribution of the traffic flow over 24 hours is based on several measurements on the Dutch motorways, see paragraph 3.4.3 and given by:

$$f_{day}(t) = \frac{1}{hrs_{day}} + 0.03 \cdot \sin\left(\frac{t \cdot 2\pi}{hrs_{day}} - \frac{\pi}{2}\right) - 0.005 \cdot \sin\left(\frac{t \cdot 6\pi}{hrs_{day}} - \frac{\pi}{2}\right)$$

with:

hrs_{day} Number of hours in one day (24)

The number of axle loads at D = 1 is given according to Eurocode 3 – Part 1-9 (Eurocode 3-1-9, 2005) by:

$$N_i = N_c \cdot \left(\frac{\Delta\sigma_{c;d}}{\Delta\sigma_{i;d}}\right)^m$$

with:

N_c $2x10^6$ conforming to Eurocode 3-1-9

$\Delta\sigma_{c;d}$ Detail classification

$\Delta\sigma_{i;d}$ Actual stress

m Slope of the fatigue detail curve

The detail classification $\Delta\sigma_c$ for the deck plate crack at the location of the crossbeam is derived by crack growth calculations based on fracture mechanics and on fatigue tests. The crack growth calculations have resulted in a classification of 115/156 MPa for design/mean value, see paragraph 4.3.2.3. The fatigue tests have resulted in a classification of 147/197 MPa for the same crack dimension, see paragraph 4.3.3.3, all at $2x10^6$ cycles according to Eurocode format. At this dimension the crack depth just equals the deck plate thickness and the length at the top side of the deck plate is 0 mm.

$$\Delta\sigma_{c;d} = \frac{\Delta\sigma_c}{\gamma_{S-N}}$$

$$m = \begin{cases} 3 & for \quad \Delta\sigma_{i;d} > \Delta\sigma_{c;d} \\ 5 & for \quad 0.55 \cdot \Delta\sigma_{c;d} < \Delta\sigma_{i;d} < \Delta\sigma_{c;d} \\ \infty & for \quad \Delta\sigma_{i;d} < 0.55 \cdot \Delta\sigma_{c;d} \end{cases}$$

The actual stress $\Delta\sigma_i$ is given by:

$$\Delta\sigma_{i;d} = \frac{M_L(x)}{W_{steel}} \cdot f_{dyn} \cdot f_{renovation} \cdot r(t) \cdot \gamma_{\Delta\sigma}$$

with:

m	Slope of the fatigue detail curve
$M_L(x)$	Moment at the crack location
W_{steel}	Section modulus steel deck plate for a unit thickness of 1 mm
f_{dyn}	Dynamic factor with value 1.1 (Vrouwenvelder, 2000-a, 2000-b)
$f_{renovation}$	Stress reduction factor for the renovation technique, see chapters 6 and 7
$r(t)$	Reduction factor on the stress for the stress reduction in the steel deck plate due to asphaltic surfacings, see paragraph 8.4.3. Per definition r(t) = 1 for movable bridges without asphalt surfacing. For renovated bridges r(t) can also be taken at 1.
$\gamma_{\Delta\sigma}$	Safety factor for the stress ranges

Figure 4-1 gives the mechanical model for the stress calculation. The moment at the crack location, location L, is described, according to paragraph 4.2.2.1 with:

$$M_L(x) = \frac{qc}{24l}\left(24\frac{d^3}{l} - 6\frac{bc^2}{l} + 3\frac{c^3}{l} + 4c^2 - 24d^2\right)$$

with:

$$a = \begin{cases} 0 & for \quad x \le w \\ x - w & for \quad w < x < l + w \\ l & for \quad l < x \end{cases}$$

$$b = \begin{cases} x & for \quad x < l \\ l & for \quad x \ge l \end{cases}$$

$$c = \begin{cases} b & for \quad x \le w \\ w & for \quad w < x \le l \\ l - a & for \quad l < x \end{cases}$$

$$d = l - \frac{a}{2} - \frac{b}{2}$$

$$q = \frac{Q}{w_t \cdot l_t}$$

with:

q	Uniformly distributed wheel load
w_t	Width of the tyre
l_t	Length of the tyre. Formulas for the footprint length (l_t) were derived in paragraph 3.2.4.

With these formulas the stress at the crack location can be calculated for each location of the wheel load in transverse x-direction.

8.4.3 Stress reductions due to surfacing

The usually applied mastic asphalt layer of 50 mm on fixed bridges reduces the stress ranges in the deck plate. Modelling this effect is necessary to obtain accurate lifetime calculations. The mechanical modelling is difficult because the behaviour of the bituminous asphalt layer is strongly temperature dependent.

Because the asphalt models are necessary for lifetime calculations of the steel deck plate the first interest is in its effect on stress reduction in the steel deck plate and consequently strains, stresses and displacements in the asphalt surfacing are less important. The modelling of the stress reduction effect of the asphalt layer is split up into three parts.

1. What are the temperatures of the asphalt layer on steel bridge decks as function of the time, sun and air temperature?
2. What is the stiffness (E-modulus) of the asphalt material as function of the asphalt temperatures and loading frequencies?
3. What are the stress reduction factors, based on calculations of the clamped beam model, with and without asphalt surfacing?

8.4.3.1 Temperatures of the asphalt layer (part 1)

The assumption is that the temperature of the asphalt is a function of the air temperature, the time of day and sunshine. From measurements of the KNMI, the royal Dutch meteorological institute, the average daily minimum, maximum and average air temperature and also the average hours of sun and daylight are known for every month (KNMI, 2000), for this information see Table 8-4.

Table 8-4: Averages daily minimum, maximum and average temperature and average daily hours sunshine and hours daylight in the Netherlands

Month	Min T (°C)	Max T (°C)	Avg T (°C)	Avg sun (hrs)	Avg day (hrs)
January	0.1	5.1	2.8	1.44	8
February	-0.1	5.8	2.9	2.47	9.5
March	2	9.2	5.6	3.34	11.5
April	3.6	12.5	8.1	5.00	13.5
Mai	7.5	17.1	12.5	6.36	15.5
June	10.3	19.4	15	6.44	16.5
July	12.5	21.6	17.2	5.92	16
August	12.3	21.9	17.1	5.95	14.5
September	10	18.4	14.2	4.38	12.5
October	6.7	14	10.4	3.26	10.5
November	3.4	9	6.3	1.79	8.5
December	1.4	6.3	4	1.35	7.5

Based on this measured temperatures functions have been derived, which describe the air temperature.

$$T_{air}(t) = A(t) + B(t) \cdot C(t)$$

Part A is a sine function with a period of one year and describes the average temperature over the year. Part C is a sine function with a period of 24 hours and describes the temperature over one day. The amplitude of part C is the difference between the average daily minimum and average daily maximum. This amplitude is described by part B.

$$A(t) = 9.68 + 7.32 \cdot \sin\left(t \cdot \left(\frac{2\pi}{hrs_{year}} \right) - 0.62\pi \right)$$

$$B(t) = 7.55 + 2.2 \cdot \sin\left(t \cdot \left(\frac{2\pi}{hrs_{year}} \right) - 0.48\pi \right) - 0.58 \cdot \sin\left(t \cdot \left(\frac{5\pi}{hrs_{year}} \right) \right)$$

$$C(t) = \sin\left(t \cdot \left(\frac{2\pi}{hrs_{day}} \right) - \frac{2\pi}{3} \right)$$

with:

hrs_{day}	Number of hours in one day (24)
hrs_{year}	Number of hours in one year (8760)

Both the air and the asphalt temperatures as functions of time are known from measurements on the Moerdijk Bridge (Huisman, 1992). The measurements were performed from July to September, they show that there is a difference between asphalt temperature and air temperature, which is due to the effect of the sun. It is assumed that the asphalt temperature is the air temperature with an additional component and it is assumed that this component of the temperature is a function of the average hours of sun per day and the average hours of daylight per day. This can be described with the formula:

$$T_{asphalt}(t) = T_{air}(t) + g(t) \cdot H_{sun}(t) \cdot H_{day}(t)$$

with:

g(t):	a function which fits calculated asphalt temperatures to the measured asphalt temperatures.

$$g(t) = \frac{0.5 + 0.5 \cdot \sin\left(t \cdot \left(\frac{2\pi}{hrs_{day}} \right) - \frac{5\pi}{3} \right)}{12}$$

The average hours of sun and the average hours of daylight can be described with sine functions.

$$H_{sun}(t) = 3.975 + 2.63 \cdot \sin\left(t \cdot \left(\frac{2\pi}{hrs_{year}} \right) - 0.46\pi \right)$$

$$H_{day}(t) = 12 + 4.52 \cdot \sin\left(t \cdot \left(\frac{2\pi}{hrs_{year}} \right) - 0.45\pi \right)$$

The calculated values are averages, for cloudy days the difference between asphalt and air temperature is smaller and for sunny days the temperature of the asphalt can reach the 50 °C. However because those major differences from the averages values are realistic, this modelling turns out to be appropriate with respect to the fatigue life calculation of the steel deck plate (De Jong, 2003).

8.4.3.2 Stiffness of the asphalt material (part 2)

The stiffness of asphalt materials is dependent on temperature and loading frequencies. To examine the material properties for the asphalt mixes used on orthotropic steel bridge decks 4-point bending tests were performed (Verburg, 1996). These tests were done for two materials: mastic asphalt and ZOAB. ZOAB is an open graded asphalt mix, which is used on only a few steel bridge decks in the Netherlands. The stiffness is determined for a wide variety of temperatures and loading frequencies. Figure 8-6 shows the results of these tests. The loading frequencies are depicted as velocity of the heavy vehicles. The velocity of 25 km/h is equivalent to a loading frequency of 6 Hz and a velocity of 125 km/h a frequency of 30 Hz.

Based on the 4-point bending tests a few conclusions can be drawn. Mastic asphalt is much stiffer than ZOAB, the influence of the temperature is very significant and the influence of the loading frequency is limited. Extrapolation of the results to approximately 30-40 °C shows that at these temperatures the asphalt looses practically all its stiffness, which is in accordance with the Lintrack measurements, see chapter 4. Based on these tests formulas for the asphalt stiffness as a function of the temperature have been derived. These functions have been derived for a velocity of 85 km/h assuming that the majority of the lorries are travelling at this speed. The functions do not describe the stiffness at higher temperatures. In that case a minimum value of 50 MPa for the asphalt stiffness is appropriate.

$$E_{mastic.asphalt}(T_{asphalt}) = 16956 - 589 \cdot T_{asphalt}$$

$$E_{ZOAB}(T_{asphalt}) = 8821 - 295 \cdot T_{asphalt}$$

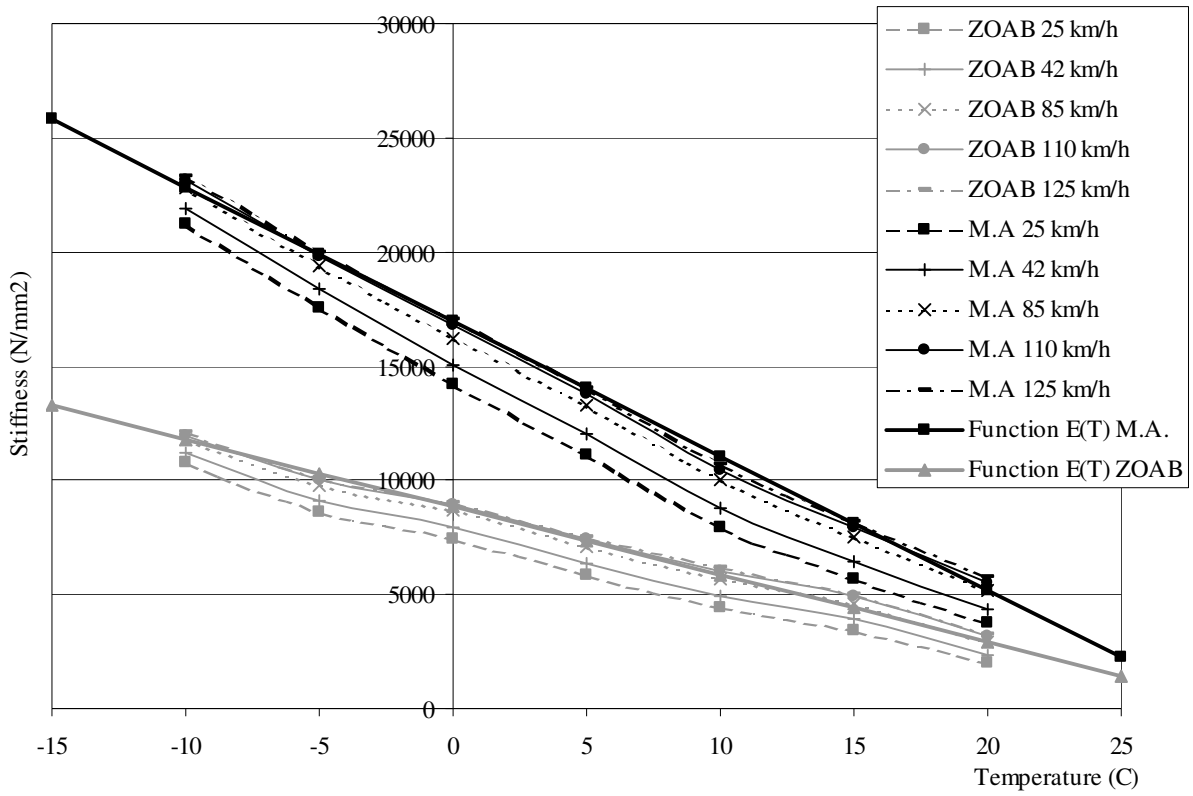

Figure 8-6: Stiffness asphalt mixes

8.4.3.3 Stress reduction factors for asphalt (part 3)

The mechanical model depicted in Figure 4-1 is used to calculate the stress in the steel deck plate. To calculate the stress in the steel deck plate surfaced with an asphalt layer, the same mechanical model is used. From chapter 4 became clear that there is no effective composite action between asphalt and steel, due to the very low stiffness of the 2 mm intermediate bituminous layer. The calculation of stresses is therefore based on a model of two beams, one steel and one asphalt, with the same deflection. For each stiffness of the asphalt layer the reduction factor *r(t)* can be calculated. This reduction factor is defined as the ratio of the stress in the steel deck plate with asphalt surfacing and the stress in the steel deck plate without asphalt surfacing. This is given by the formula:

$$r(t) = \frac{\frac{EI_{steel}}{EI_{asphalt}}}{\left(1 + \frac{EI_{steel}}{EI_{asphalt}}\right)}$$

8.4.4 Calculation after inspection

As already described in paragraph 8.4.1 and depicted in Figure 8-5 lifetime calculations can be performed after an inspection of the bridge deck. A theoretical model to handle inspections is formulated by Vrouwenvelder (Vrouwenvelder, 2000-b).

The probability of detecting fatigue cracks depends on the inspection method and the accessibility of the structure. Larger cracks will be found more easily than small ones and small cracks will never be found. The detectability increases with increasing crack dimension. The relationship between the probability of detection is generally given as a POD (Probability Of Detection) curve. In general the following expression for the POD curve is used

$$POD = 1 - \exp\left(\frac{-(a - \alpha_{POD})}{\beta_{POD}}\right)$$

with:

POD	Probability of Detection
a	crack dimension
α_{POD}	smallest crack dimension found
β_{POD}	shape parameter of POD curve

Figure 8-7 shows for example two different fictitious POD curves.

The inspection results leads to two possible situations:
1. No crack is found
2. A crack is found with crack dimension a_{det} or c_{det}

The POD-curve is thought to be the cumulative distribution of the cracks to be discovered. With this the distribution of the cracks to be discovered is an exponential function. With a probabilistic analysis on level II, the inspection interval till the next inspection can be calculated for both situations (Vrouwenvelder, 2000-b).

For a more simple approach on probabilistic level I, the lifetime calculation for the situation where a crack is found, starts with detected crack dimension a_{det} or c_{det}. If the inspection has not detected a crack, the unknown dimension of the undetected crack can be determined with the conservative approximation that the relevant reliability index β and the sensitivity factor α determine the unknown crack dimension. Thus this crack dimension can be determined with:

$$POD = \Phi(-\alpha\beta)$$

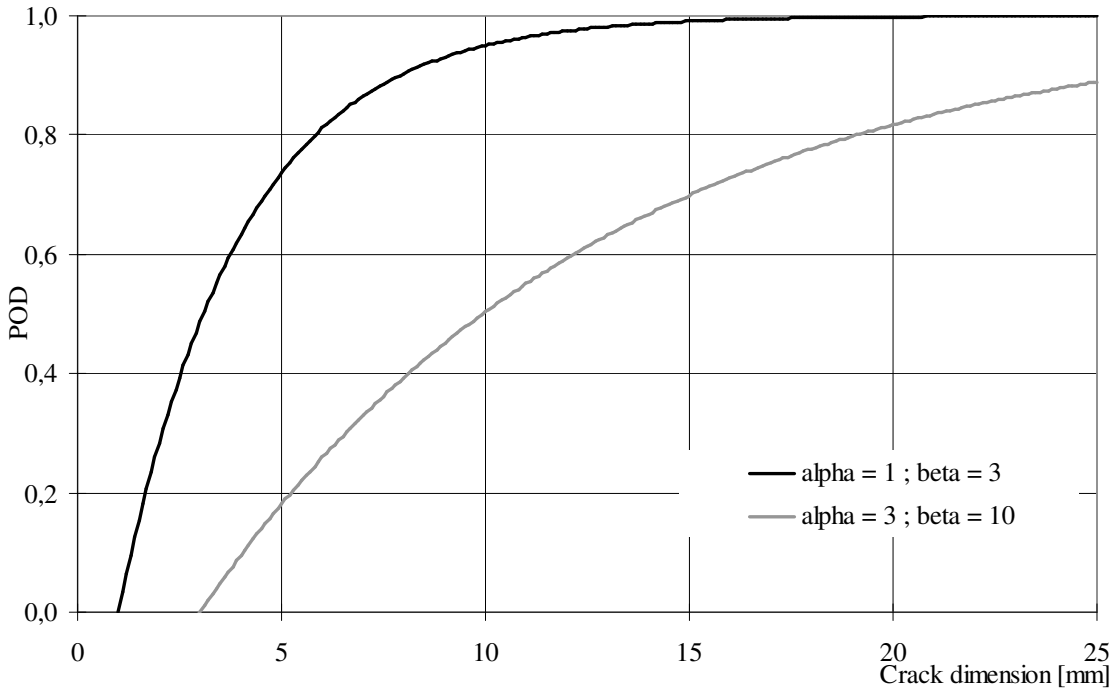

Figure 8-7: POD curve format

Assuming that the crack dimension is not the dominating parameter in the analysis, the sensitivity factor α = -0.4 x 0.7. The POD for different values of the target reliability index β are:

POD = 0.5 with reliability index $\beta = 0$
POD = 0.69 with reliability index $\beta = 1.8$

An estimation of the unknown crack dimension "a" is then:

$$a_{insp} = \alpha_{POD} - \beta_{POD} \ln(1-0.5) = \alpha_{POD} + 0.69\beta_{POD} \quad \text{for reliability index } \beta = 0$$
$$a_{insp} = \alpha_{POD} - \beta_{POD} \ln(1-0.69) = \alpha_{POD} + 1.18\beta_{POD} \quad \text{for reliability index } \beta = 1.8$$

For each situation a crack is either found or not, a crack dimension a_{insp} is defined as the basis for the subsequent lifetime calculation. There are basically two methods for a new fatigue calculation if a crack a_{insp} is detected or assumed:

- Calculate with a lower detail classification $\Delta\sigma_k$ adjusted to a_{insp}, for this calculation D = 0
- Calculate with the original detail classification combined with a $D_{start} > 0$ dependent on the specific crack size a_{insp}

Dijkstra has proposed that the D_{start} method probably leads to non-conservative results. Therefore the first method with reduced detail classifications $\Delta\sigma_k$ is preferred (Dijkstra, 2003).

Dijkstra has performed several analyses, and calculated reduced detail classifications (Dijkstra, 2001). These are related to the crack growth model described in paragraph 4.3.2.3. A few modifications on the calculated reduced detail classifications have been made:

- They are given in Eurocode format instead of NEN 2063 format
- The classification for $a_{insp} = 0$ is taken according to the tests results described in paragraph 4.3.3.2, instead of the classification from the crack growth calculation. For $a_{insp} > 0$ this modification has also been calculated.

Table 8-5 tabulates the reduced detail classifications. T is the deck plate thickness. The given classifications are valid for a deck plate thickness of 10 to 14 mm. For intermediate values of a_{insp}/T a linear interpolation should be performed.

Table 8-5: Detail classification for initial damage a_{insp} from inspection result

a_{insp}/T	D_{start}	$\Delta\sigma_k$ - *mean*	$\Delta\sigma_k$ - *design*
0.00	0.00	197	147
0.25	0.29	175	131
0.50	0.60	145	108
0.75	0.94	78	58
1.00	1.00	0	0

8.4.5 Calculation results

A computer program has been developed for lifetime calculations for bridge decks in the Netherlands. The basis of the calculation procedure in this computer program is the presented formal model. There are a few differences between the formal model and the computer program. In general based on measurements functions were derived, for instance for the load distribution, where the measurements are presented in Figure 3-4 and the function based on these measurements is lognormal, see Table 3-3. In the computer program mainly measurement results are incorporated instead of the functions. This can cause differences between the formal model and the computer program. With this computer program lifetime calculations for several Dutch bridges have been performed. Table 8-6 gives the calculation results for some major bridges in the Dutch infrastructure. The table is based on calculation without safety factors. The table shows that the calculated lifetimes for the deck plate crack for some bridges are somewhat too long and for other bridges somewhat too short. Because

the observations are roughly in accordance with the calculated lifetime, we can conclude that we have a reliable calculation model for fatigue damage at our disposal. The calculation results are accurate, both for the movable bridges with a thin epoxy surfacing and for the fixed bridges with mastic asphalt surfacing. This means that an accurate modelling of the behaviour of asphalt surfacings with respect to the stresses in the steel construction is obtained. Based on this lifetime calculation system inspection programs can be made.

Table 8-6: Results fatigue lifetime calculations for deck plate crack at crossbeam

Bridge	Built	First visual observed fatigue crack	Lifetime calculation – mean values $\beta = 0$
Ketel Bridge, movable	1968	1998	2002
Scharsterrijn, movable	1972	2002	2004
Van Brienenoord, movable	1990	1997	1996
Caland Bridge, movable part	1969	1998	1991
Bridge Zijkanaal C, movable	1969	2003	2000
Caland Bridge, fixed part	1969	2002	2003
Bridge Hagestein, fixed	1980	2002	2006
Galecopper Bridge, fixed	1971	2002	1996
Juliana Bridge, movable	1966	2001	1997
Moerdijk Bridge, fixed	1976	2001	1998
Tied arch Bridge Beek	1968	2004	2007

8.5 Inspections methods

Within the framework of the research presented in this thesis, hardly any research has been done in the field of the inspection techniques. Development of inspection techniques was not the scope of the research project; however they are important to the implementation of a successful maintenance strategy as depicted in Figure 8-2. Several inspection techniques have been developed, or have been made useful for inspection of orthotropic steel bridge decks in a research project at the ministry of Transport. Den Besten has described these techniques (Den Besten, 2005).

This paragraph gives a brief overview of the inspection techniques for orthotropic bridge decks. There is a short description of each technique, and a summary of the advantages and disadvantages of that technique. If possible the parameters α_{POD} and β_{POD} of the POD curve are also given. More technical information on the inspection techniques is not given, as it is outside the scope of this thesis.

8.5.1 Visual

Chapter 2 has already described this inspection technique in brief. In that chapter several photographs of possible visual observations are given. For more background information see chapter 2.

In general it can be said that the visual inspection technique is appropriate for movable bridge decks with a thin epoxy surfacing. For fixed bridges with a thick asphaltic surfacing visual observations are unreliable, which makes this technique less appropriate for fixed bridges. A visual observation of a fixed bridge gives in the first place information on the degradation of the asphalt surfacing. The relationship between degradation of the surfacing and fatigue crack growth in the steel deck plate is indistinct. Degradation of the surfacing can be the motivation for further inspection of the steel deck.

The advantages of visual observation are:
- Quick execution
- The surfacing remains intact
- It is a relatively cheap method

The disadvantages of visual observation are:
- Traffic disruption is necessary because visual inspection is carried out from the top side of the deck.
- Only long cracks, through the deck plate with a length of app. 100 to 200 mm are revealed
- Experiences on the Caland Bridge have shown that long cracks (app. 50 cm in that case) in the steel are possible without any damage in the asphaltic surfacing.

A rough estimation, based on practical experience, of the parameters α_{POD} and β_{POD} of the POD curve are:

If the epoxy surfacing is removed locally for the inspection:
- α_{POD} = 75 mm (length at the top surface of the deck plate)
- β_{POD} = 25

This means that the probability of detection of a crack of 150 mm on top side of the deck plate is 95%.

If the epoxy surfacing is not removed locally for the inspection:
- α_{POD} = 100 mm (length at the top surface of the deck plate)
- β_{POD} = 50

This means that the probability of detection of a crack of 250 mm on top side of the deck plate is 95%.

8.5.2 Time of flight diffraction (TOFD)

A TOFD inspection (Time of Flight Diffraction) is an ultrasonic inspection technique with a very high accuracy (Liefting, 1997). This technique is executed with two probes and the basis is that differences in time of flight of the signal between the two probes can be calculated back to the defect size. If a defect is detected the location of this defect can be calculated. Figure 8-8 shows the basics of the TOFD technique.

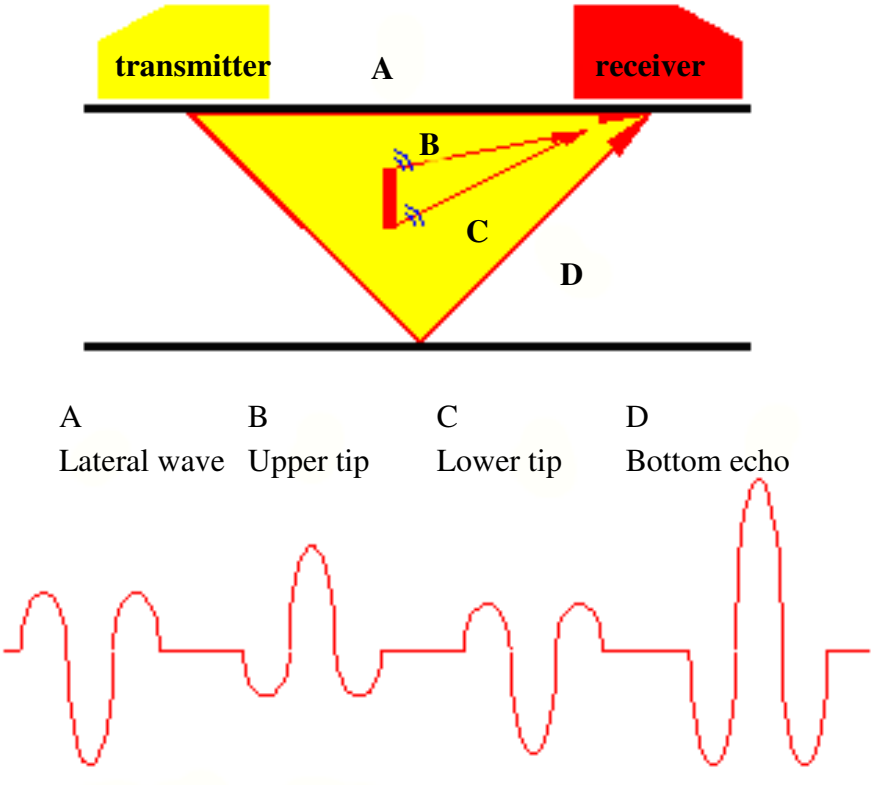

Figure 8-8: Basic principle of TOFD inspection technique

TOFD inspections are performed on the top surface of the steel deck plate. Acoustic coupling of the probe with the steel deck plate is necessary therefore the surfacing layer has to be removed. For that reason this inspection method generates considerable traffic disruption. In addition to that it is also an expensive technique due to the costs of a new surfacing. Figure 8-9 shows a TOFD inspection of a bridge. The scanner is shown in the right hand photograph and the two probes can be seen at the left hand end. Figure 8-10 shows two typical results of a TOFD scan. In the left hand photograph there is no defect in the steel plate. In the right hand photograph a crack that has grown through the deck plate has been detected.

Figure 8-9: TOFD inspection (left), TOFD scanner (right)

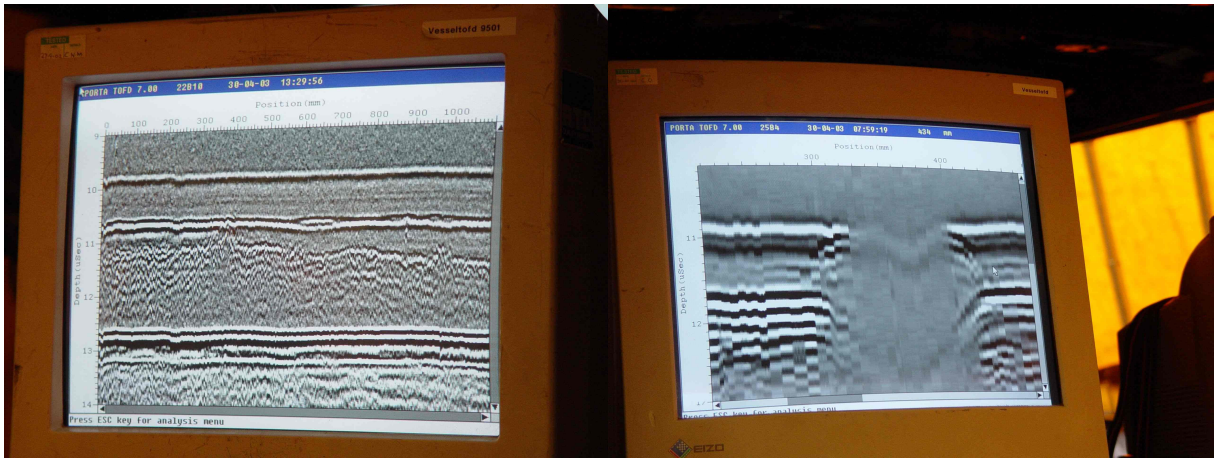

Figure 8-10: Result TOFD scan - no defect (left), Result TOFD scan with defect (right)

The advantages of the TOFD technique are:

- Very small cracks can be detected

The disadvantages of the TOFD technique are:

- The probes have to make an acoustic coupling with the steel deck plate, which necessitates removal of the surfacing
- It is an inspection technique, which causes much traffic disruption
- It is an expensive and time consuming technique due the removal and replacement of the surfacing

There is a lot of experience with this inspection technique on steel bridge decks in the Netherlands. Based on this experience a rough estimation of the parameters α_{POD} and β_{POD} of

the POD curve are:
α_{POD} = 1.5 mm (crack height *a* measured from bottom of the deck plate)
β_{POD} = 0.5
This means that the probability of detection of a crack of with a height of 3 mm.

8.5.3 Ultrasonic Testing (UT)

The ultrasonic testing inspection method works with a scanner with several probes. The scanner is located at the underside of the deck plate, see Figure 8-11. The fact that this inspection technique works from the underside of the deck plate is it's main advantage, because it causes no traffic disruption.

With the scanner it is possible to inspect the deck plate between the two crossbeams. Due to the dimensions of the scanner, the inspection can only start at approximately 30 mm from the crossbeam web, which means that there is an uninspectable zone of approximately 70 mm long (twice these 30 mm plus 10 mm crossbeam web thickness). This is the main disadvantage of this technique. The UT inspection technique for bridges is extensively described in (Terpstra, 2000-a)

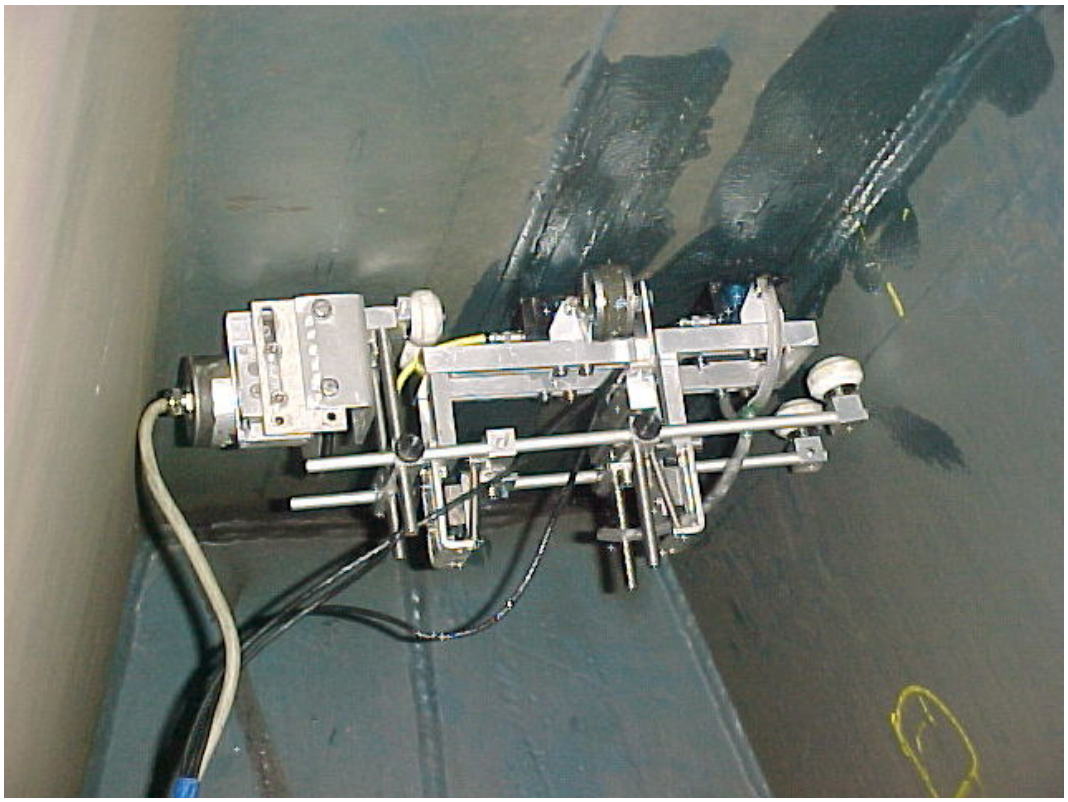

Figure 8-11: Mechanised scanner with UT inspection probes

The advantages of UT inspections are:

- The inspection can be performed from the underside of the deck plate so traffic disruption can be avoided
- The probes are able to inspect through the paint on the steel parts

The disadvantages of UT inspections are:

- UT cannot inspect the most critical location for deck plate cracks at the crossbeam location
- Access to the underside of bridges is often difficult, which makes it an expensive and time consuming technique
- The probes cannot inspect through a bituminous corrosion protection system
- With the mechanised scanner only indications with a height of approximately 6 mm or higher can be detected. The scanner only indicates whether there is a crack or not, no information is given about the crack size.

With this method crack of approximately a = 6 mm high can be detected. This means that α_{POD} = 6 mm. It is not possible to derive the other parameter β_{POD} of the POD curve, due to a lack of experience with this method.

8.5.4 Slofec

Slofec is an abbreviation of Saturated Low Frequency Eddy Current. It is an eddy current technique, which has proved useful for orthotropic steel bridge decks. With a so-called “lift-off” up to 10 mm, which is the distance between measuring device and the upper side of the steel deck plate, it is possible to inspect through a thin epoxy surfacing. That makes this technique suitable for movable bridges. The technique cannot be used to inspect through thick surfacings on fixed bridges. The development of this technique is extensively described in (Terpstra, 2000-b) and (Kronemeijer, 2003-a, 2003-b). This technique works with a scanner on top of the epoxy surfacing that is moved in the transverse direction of the bridge. Figure 8-12 shows a photograph of this technique being used.

The advantages of SLOFEC inspection are:

- The possibility of inspection through the epoxy surfacing
- Relatively quick operation

The disadvantages of SLOFEC inspection are:

- Only cracks, which have grown through the deck plate with a length of approximately 40 mm on top surface of the deck plate, are detectable. This means that α_{POD} = 40 mm

(length at the top surface of the deck plate). It should be noted that this α_{POD} is only slightly smaller as that of visual observation with local removal of the epoxy surfacing.

- Traffic disruption is necessary because a SLOFEC inspection is carried out from the top surface of the surfacing. The scanner moves in the transverse direction and because of that the width of closure is probably wider, thus causing more traffic disruption.

It is not possible to derive the other parameter β_{POD} of the POD curve, due to a lack of experience with this method.

Figure 8-12: SLOFEC inspection being carried out on Caland Bridge

8.5.5 Crack PEC

Crack PEC is an abbreviation of Crack Pulsed Eddy Current. Non destructive inspections such as the TOFD technique require removal of the surfacing, because the probes have to make direct contact with an electrically conductive material (such as steel). Access to the underside of the steel deck plate is very restricted and therefore not always a practical option. Therefore, non-destructive tests, which can detect cracks in the steel deck plate through the asphalt layer could reduce inspection time, traffic disruption and costs. The crack PEC inspection technique is capable of detecting cracks in the steel deck plate from the top side of the bridge without having to remove asphalt surfacing on fixed bridges. Because it is possible to inspect through thick asphaltic surfacing with the technique it is very suitable for fixed bridges, where the visual inspection technique is unreliable. The development of this technique is extensively described by Overduin (Overduin, 2003).

Eddy current testing is an electromagnetic technique and can only be used on electrically conductive materials. Its applications range from crack detection to the rapid sorting of small components for either flaws or size and material variations (thickness and properties). PEC is widely used in the aerospace, automotive, marine and manufacturing industries. The

technique uses pulsed magnetic fields to generate eddy currents in the steel. To this end, a probe containing excitation and receiver coils is placed above the test specimen. The measurement has two phases. In the first phase an electrical current is sent through the excitation coils to generate a field that magnetises the steel underneath. The current is switched off in the second phase. The sudden drop in magnetic field induces eddy currents in the steel test specimen. The eddy currents in turn induce an electrical signal in the receiver coils, which is recorded and analysed by a dedicated PEC instrument.

For the crack PEC inspection technique the “insPECteur” has been developed. This is a measurement car with 8 PEC probes installed on it. Four probes are available for both wheel tracks. Figure 8-13 shows the insPECteur and the 4 probes for each wheel track and of course the probes have an intermediate distance of 300 mm, which is the distance between the trough webs.

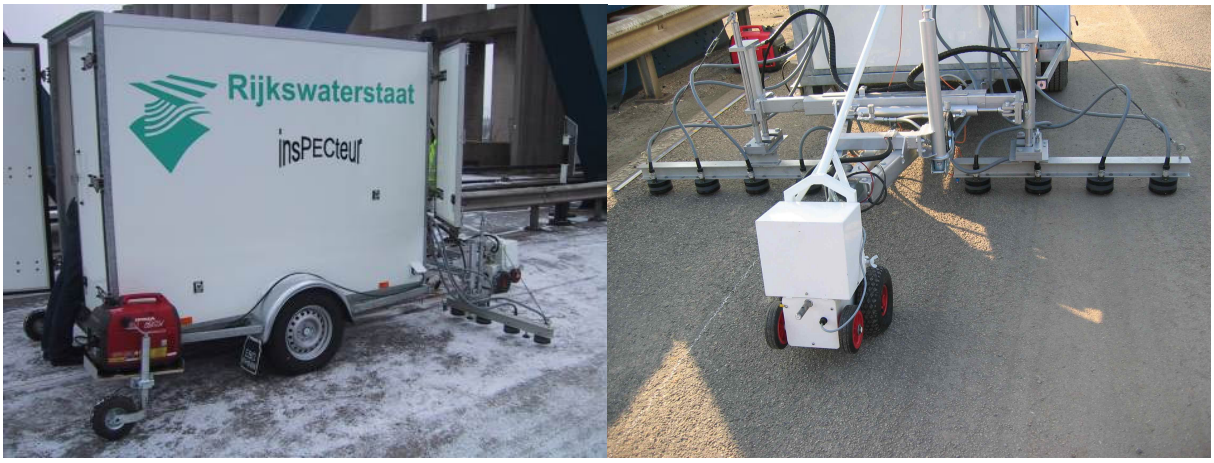

Figure 8-13: InsPECteur (left), 4 probes per wheel track (right)

For an inspection of a bridge deck a measurement grid should be defined on the deck. This enables a quick execution of the inspection. The measurement grid is likely to focus on the locations of the crossbeams and gives the locations where the inspection will be carried out. At each measurement point on the grid the inspected area per trough web is approximately the diameter of the probe, 100 mm. In practice often a measurement grid of 7 points with an intermediate distance of 100 mm is used. If the grid is symmetrically located around the crossbeam (-300 mm, -200 mm, -100 mm, 0 mm, 100 mm, 200 mm, 300 mm) The inspected length is approximately 700 mm around the crossbeam.

The advantages of Crack PEC inspection are:

- It is a relatively quick method
- The possibility of inspection through a thick asphaltic surfacing

The disadvantages of the Crack PEC inspection are:

- The technique uses a measurement grid. Locations outside the grid are not inspected. This means that the grid should be defined with great care.
- Only cracks that have already grown through the deck plate and have a length of app. 100 mm on top surface of the deck plate are detected.

It is not possible to derive the parameters α_{POD} and β_{POD} of the POD curve, due to a lack of experience with this method.

8.5.6 Concluding remarks

Several inspection techniques with different characteristics for orthotropic steel bridge decks have been described in this paragraph. The three frequently used inspection techniques are:

- Visual inspection
- TOFD inspection
- Crack PEC inspections

The use of three techniques can be explained if we look at the situation of the steel bridges on the motorways in the Netherlands. Many bridges are suffering from fatigue cracks in the deck plate. For these bridges it is evident that the safety must be guaranteed. The quickest method of guaranteeing safety for movable bridges is a visual inspection. As this method is unreliable for fixed bridges with a thick asphaltic surfacing the Crack PEC inspection technique is available, for these bridges. Both visual inspection and Crack PEC inspection detect cracks very late in the crack growth process, in the third crack growth phase when the cracks have already grown through the deck plate, see Figure 2-10. Although it is in the last phase of the crack growth process, it is early enough with respect to safety, because only very long cracks, more than 50 cm, are a probable threat to traffic safety, see paragraph 4.2.4.

At the point when the existing surfacing on a bridge deck must be renewed, due to degradation, or because of the application of a renovation technique a TOFD inspection is the most suitable technique. From this the most accurate crack information can be obtained, which is relevant to the lifetime of the bridge after the renovation. If a renewal of the surfacing is combined with a TOFD inspection the renewal of the surfacing can no longer be considered as a disadvantage of the TOFD inspection.

Regarding traffic safety, up to the moment of a renovation of the bridge, visual and Crack PEC inspection are the appropriate techniques, during a renovation technique TOFD is the most appropriate.

8.6 Concluding remarks

This chapter of this thesis has dealt with some important additional subjects for a state of the art maintenance philosophy of orthotropic steel bridge decks. It has been stated that such a philosophy guarantees the safety of the structure with the required safety level, described with the reliability index β. This makes this maintenance philosophy a probabilistic method consisting of three parts: lifetime calculations, renovation techniques and inspection methods. This chapter has also argued that the target reliability index for fatigue deck plate cracks should be at the level of serviceability limit state, $\beta = 1.8$ both for the European and for the Dutch standard. With this target reliability index an approach to bridges, which is too conservative can be avoided.

As stated before an important tool in the maintenance philosophy is a lifetime calculation model with respect to deck plate cracks. A reliable calculation model for fatigue damage has been presented. The calculation results are accurate, both for the movable bridges with a thin epoxy surfacing and for the fixed bridges with mastic asphalt surfacing. This means that an accurate modelling of the behaviour of asphalt surfacings with respect to the stresses in the steel construction is obtained. Based on this lifetime calculation system inspection programs can be made. This lifetime calculation is valid for existing bridges with fatigue damage but can also be used for the design of new bridge decks.

Several inspection techniques have been presented briefly. For safety up to the point of renovation of the bridge, visual and Crack PEC inspection are the appropriate techniques, and during a renovation TOFD is the most appropriate inspection technique.

9. Conclusions, future research and recommendations

9.1 Conclusions

In this paragraph conclusions are presented.

With respect to the fatigue problems in orthotropic steel bridge decks the following conclusions can be drawn:

1. Several types of fatigue cracks have been described. Particularly discussed are the cracks at deck plate level, which are cracks in the deck plate itself and cracks in the longitudinal weld between deck plate and trough web.
2. These cracks grow due to the amplitude and the number of the stress cycles in the bridge deck structure. The heavy vehicles and its axle loads induce these stress cycles.
3. Bridge owners must expect a lot of bridges with fatigue cracks at deck plate level in the future.
4. The fatigue cracks possibly threaten the safety of the bridge structure. Therefore, if a crack is observed on a bridge structure repairs at the cracks locations are necessary to solve the local problem.
5. There is an obvious need for renovation techniques for orthotropic steel bridge decks with fatigue cracks. These techniques should be applied to the bridge deck to reduce the stress ranges.

Several aspects of traffic loads have been researched. With respect to bridge loading, which is relevant for fatigue phenomena at deck plate level, the following important conclusions can be drawn:

1. Footprint sizes vary with wheel load and inflation pressure. The smaller the load, the smaller the footprint. The higher the inflation pressure, the smaller the footprint size.
2. Axle load spectra are given based on measurements on the Moerdijk Bridge. There is a significant difference between the measured axle load spectra and that according to the Eurocode 1 – Part 2. Due to this fatigue verifications with measured axle load spectra give more accurate results for fatigue at deck plate level. The measured axle load spectra should be used with partial safety factors.

3. Relevant traffic volume properties are the number of lorries, the average number of axles per lorry and the distribution of the lorries over the day. With a finely meshed measurement network these traffic volume properties are available for almost every bridge on the network of motorways in the Netherlands. For the bridges with the highest flow of heavy vehicles the present traffic flow already exceeds the design values of the Eurocode 1 – Part 2.

With respect to the calculation of local stresses at the crack location in the deck plate due to wheel loading these conclusions can be drawn:
1. For fatigue verifications of deck plate cracks the stress calculations can be based on a clamped beam model.
2. For this calculation the wheel load can be modelled as a uniformly distributed load and the span of the clamped beam can be taken as 290 mm.

With respect to the fatigue behaviour of deck plates:
1. Based on fatigue tests detail classifications have been derived for several cracks lengths.
2. These classifications are proposed for fatigue calculations.

With respect to the ultimate load capacity of the deck plate with fatigue cracks:
1. Long cracks (up to 50 cm) do not threaten the safety

With respect to the effects of asphalt surfacing:
1. The stress reduction in the steel due to surfacing is for the most part the effect of the pavement acting as a beam.
2. A comparison of theoretical and numerical analysis with both field measurements on bridges and tests in the Lintrack points towards a modelling with a flexible interface for fixed bridges.

With respect to the development of the submerged arc welding process for crack repair:
1. Submerged arc welding is a good repair method for detected cracks. The three advantages of SAW-welding are: the speed of execution is high, the welding only takes place from the top of the deck plate and the weld shrinkage is relatively limited.
2. Parameter settings for the welding process have been determined with research. The current is the most important parameter in determining the depth of penetration.
3. The maximum depth of penetration that can be achieved without a burn through is approximately between 65% and 75% of the deck plate thickness
4. The detail classification of a deck plate with a SAW repaired crack is only slightly lower than the detail classification for the uncracked situation with parent material. 97 MPa instead of 113 MPa according to the NEN format.

With respect to the requirements of renovation techniques, the two major requirements are:

1. That the existing bridge deck remains undisturbed as much as possible.
2. Effective lifetime extension. Increasing the total stiffness of the deck plate structure is one of the main criteria. The stiffness of the deck plate should be increased as much as possible.

With respect to possible renovation techniques:

1. Several ideas for possible renovation techniques have been briefly described. From these a limited number of techniques have been selected for further research. These are the alternatives:
    a. High performance concrete on fixed bridges
    b. Bonding on a second steel deck plate for movable bridges
    c. Trough filling for movable bridges
2. Renovation techniques with bolted connections were not selected for further research because it was thought that bolted connections could not give satisfactory durability.
3. Renovation techniques with prefabricated panels were not selected for further research mainly because of the problems that were foreseen with respect to the tolerances.
4. In addition to these a few renovation methods were not selected due to the fact that severe problems with the corrosion protection of the steel bridge deck were expected.

With respect to the renovation method for fixed bridges:

22. The replacement of the asphalt surfacing with a reinforced high performance concrete surfacing (RHPC) is a good solution for the fatigue problems on steel bridge decks. It significantly reduces the stresses in the deck plate and trough web, hence it greatly extends the lifetime.
23. An epoxy interface layer between steel and concrete provides sufficient shear strength and capacity. This makes composite action between steel and RHPC possible.
24. Filling troughs in addition to the application of the RHPC surfacing layer is unnecessary, as it does not lead to extra reduction in the stresses.
25. With respect to the application process of this method:
    a. It is important that sufficient vibration energy is applied to the concrete in order to achieve a good compaction and avoid air inclusions.
    b. The mesh dimensions of the reinforcement should be produced exactly at the nominal value in order to avoid problems with the placing of the mesh reinforcement and problems with the compaction at mesh overlap locations.
26. With respect to the reduction of the stresses:
    a. If the asphalt surfacing is replaced by a RHPC surfacing the stresses are greatly reduced.

b. However; from the various FE-models and measurements no clear reduction factor appears.
c. The calculated and measured stress reduction factors for the deck plate vary between 0.08 and approximately 0.4 for deck plate cracks.
d. The measured reduction factors are in general smaller than the reduction factors calculated with the FE-models.
e. Especially for the FE-model representing local deck plate behaviour and crossbeam behaviour at the crossbeam location, and for the FE-model representing local deck plate behaviour between the crossbeams, it is clear that the applied boundary constraints in these models lead to conservative calculated reduction factors. Therefore it is reasonable to rely more on the measured stress reduction factors.
f. It is not possible to derive separate stress reduction factors for the stress due to crossbeam behaviour from the FE-models.
g. The measurements on the Caland Bridge show no distinct crossbeam behaviour.
h. Therefore the measured stress reduction factors at the Caland Bridge in the field between the crossbeams, as well as the results of the models and test that only comprise local deck plate behaviour are appropriate for the crossbeam location.
i. A stress reduction factor for the stress in the deck plate of 0.2 and a stress reduction factor of 0.4 for the stress in the trough web are proposed.
j. The measured strains on test panel A with unrepaired fatigue cracks are about the same as the strains in the TNO panel with no cracks in the deck plate. It might be concluded that with respect to the static strains it is not necessary to repair deck plate fatigue cracks, up to a length of approximately 100-150 mm.

27. With respect to the fatigue behaviour:
a. Fatigue tests were successfully applied to the TNO panel and to test panel A. The applied loading sequence represents more than 50 years of heavy traffic for each test.
b. The measured strain ranges are mostly constant or only minor changes were measured, during the whole test.
c. No fatigue crack growth was observed during the fatigue tests.
d. The measured strain ranges on test panel A with unrepaired fatigue cracks are about the same as the strains in the TNO panel without any crack in the deck plate. During the fatigue test no crack growth was observed in either test panels. It might be concluded that it is not necessary to repair fatigue cracks in the deck plate, up to a length of 100-150 mm.
e. A simple conservative approach to the lifetime enhancement uses the regular slope $m = 3$ of the fatigue detail curves. The lifetime enhancement factor in this simple approach is $1/(0.2^3) = 125$ for fatigue cracks in the deck plate and $1/(0.4^3) = 16$ for

fatigue cracks in the longitudinal weld between trough web and deck plate.

f. Due to the large reduction in the stresses in deck plate and trough web, a significant part of the stress ranges is in the region of the slope $m = 5$ or even below the fatigue limit. These stress ranges give only a small contribution to the fatigue damage.

With respect to the renovation methods for movable bridges a general conclusion can be drawn:

1. Three techniques were researched. This has not yet led to an appropriate renovation technique. It is debatable whether a movable bridge deck with fatigue cracks should be replaced by a new deck, or renovated with one of these renovation methods.
2. With respect to the renovation method with bonded steel plates
    a. Bonding additional steel plates reduces stresses in the deck plate significantly. The stress reduction factor is approximately 0.5. This stress reduction factor results theoretically in a significant extension of the lifetime of the bridge deck structure.
    b. However in the fatigue test structural failure is observed as delamination occurred in the adhesive layer. A new application method, the vacuum infusion technique, probably yields better fatigue properties.
    c. At this moment the conclusion is that bonding steel plates is still a candidate renovation technique with respect to the lifetime of the steel structure, because of the stress reduction. But before application on a real bridge the fatigue properties of the adhesive layer and the steel deck should be tested with a good result.
3. With respect to the renovation method by filling the troughs:
    a. Filling the troughs with polyurethane causes in general significantly lower stresses in the deck plate. However; differences between measurements are very large meaning that the effectiveness of the trough filling is not consistent. This could be due to differences in adhesion between filling material and the underside of the deck plate.
    b. In two fatigue tests on bridge samples three fatigue cracks grew in the deck plate.
    c. Besides this there is also the disadvantage that this renovation method does not strengthen the deck plate between the troughs.
    d. A significant improvement in this renovation method cannot be envisaged without changing the whole concept.
    e. The final conclusion therefore must be that this method does not lead to the required significant extension of the lifetime of the deck structure.
4. With respect to the renovation method with a thin layer of high performance concrete:
    a. A thin reinforced high performance layer up to 30 mm repair heights gives, depending on the thickness and reinforcement, stress reduction factors of from 0.18 up to 0.28.

b. This is a significant stress reduction factor, which can lead to an enormous increase in the lifespan of movable bridges.
c. This stress reduction however is only based on calculations verified with small static tests.
d. At this moment the conclusion is that this is a promising solution for lifespan extensions of movable bridges. But many more research is needed.

With respect to the maintenance philosophy:

1. The framework of a probabilistic maintenance philosophy has been given. The safety of the deck structure is guaranteed with the required safety level, described with the reliability index β.
2. This maintenance philosophy consists of three parts: lifetime calculations, inspection methods and renovation techniques.
3. The target reliability index for fatigue deck plate cracks should be at the level of serviceability limit state, $\beta = 1.8$ both for the European and for the Dutch standard. With this target reliability index an approach to bridges, which is too conservative can be avoided.

With respect to lifetime calculations:

1. An important tool in the maintenance philosophy is a lifetime calculation model with respect to deck plate cracks.
2. A reliable calculation model for fatigue damage in the deck plate has been presented. The calculation results are accurate, both for the movable bridges with a thin epoxy surfacing and for the fixed bridges with mastic asphalt surfacing.
3. An accurate modelling of the behaviour of asphalt surfacing with respect to the stresses in the steel construction is obtained.
4. Based on this lifetime calculation system inspection programs can be prepared.
5. This lifetime calculation is valid for existing bridges with fatigue damage but can also be used for the design of new bridge decks.

With respect to inspection techniques:

1. Several inspection techniques have been presented briefly.
2. For guaranteeing traffic safety up to the point of renovation of the bridge, visual and Crack PEC inspection are the appropriate techniques
3. During renovation TOFD is the appropriate inspection technique.

9.2 Recommendations and future research

Recommendations for future research:

1. The RHPC surfacing for movable steel bridges should be researched further. Extensive supplementary research is necessary before it can be concluded that this renovation method can be applied on a real bridge. This additional research should at least comprise bending fatigue tests on beams, an application test on a real out of service bridge deck, static and fatigue tests on part of a bridge deck. Durability and environmental influences should be researched in more detail and a satisfactory solution for transition between the different heights should be designed.
2. For the renovation method with bonded steel plate, a new application method, the vacuum infusion technique, leads to a fully bonded connection. Possibly this is a more robust adhesive layer, with respect to fatigue and this should be proven in fatigue tests.

Recommendations for changes in Eurocode 1991- Part 2 Traffic loads on bridges:

1. A comparison of the measured footprint sizes with the footprint sizes according to Eurocode 1 – Part 2, table 4.8 showed that the Eurocode gives footprint sizes related to very high loads. Because stresses in e.g. the deck plate due to local wheel loads are sensitive to the footprint size, smaller footprints, dependent on the load level, should be considered for fatigue verifications.
2. The intensity of heavy vehicles on the Moerdijk Bridge on the motorway A16 is approximately 2.5×10^6 per slow lane per year. This is already more than the 2×10^6 lorries indicated for fatigue design in Eurocode 1 – Part 2, table 4.5. For fatigue verifications the predefined number of lorries should be higher to be on the safe side.
3. The load dispersal model in paragraph 4.3.6 in Eurocode 1 – Part 2 overestimates the stress reducing effects of the surfacing. The dispersal model in the Eurocode is useless for accurate fatigue verifications of deck plate cracks. The stress in the deck plate depends on the stiffness of the surfacing material. This stiffness is not taken into account in the Eurocode model.

Recommendations for changes in Eurocode 1993- Part 1.9 Fatigue:

1. A fatigue detail classification of a crack in the deck plate at the crossbeam location should be incorporated in the Eurocode. From the performed fatigue testing program a detail classification design value of 147 MPa is calculated. Therefore it is recommended to use fatigue detail category 140.

References

AVV, www.rws-avv.nl, Internet application MTR+ / Wegwerk, 18-02-2005 (in Dutch)

Bakker, M.C.M., F.B.P. de Jong, Ultrasonic underside inspection for fatigue cracks in the deck plate of a steel orthotropic bridge deck, Heron, volume 48, no.4, 2003-a

Bakker, M.C.M., S.C.H.van Meer, Ultrasone Inspectie van de lijmverbinding tussen een stalen bovenplaat en de stalen dekplaat van een orthotroop brugdek, Rapport HI 2197, Delft, 2003-b (in Dutch)

Bakker, M.C.M., S.C.H.van Meer, Ultrasone Inspectie van de vermoeide lijmverbinding tussen een stalen bovenplaat en de stalen dekplaat van een orthotroop brugdek, Rapport HI 2218, Delft, 2004 (in Dutch)

Beales, C., Severn/Wye Bridge Project – Tests on cross-beam joints, Crowthorne 1979

Beer, M. de, Measurement of tyre/pavement interface stresses under moving wheel loads', Heavy Vehicle Systems, Special Series, Int. J. of Vehicle Design, Vol. 3, Nos 1-4, pp. 97-115, 1996

Besten, C.M. den, Problematiek Stalen Rijdekken, Onderzoeksmethodenblad DPS01/02, Capelle aan de IJssel, 2005 (in Dutch)

Blab, R., Die Rahrspurverteilung als Einflussgröße bei die Bemessung des Strassenoberbaus, Mitteilungen des Institutes fuer Stassenbau und Strassenerhaltung, TU Wien, Heft 5, Istu 1995

Bignonnet, A. B.Jacob, J.Caracilli, M.LaFrance, Fatigue Resistance of Orthotropic Steel Bridge Decks, IABSE Volume 59: Remaining Fatigue Life of Steel Structures, p 227-236, Zürich, 1990

Boersma, P.D., F.B.P. de Jong, Techniques & solutions for rehabilitation of orthotropic steel bridge decks in the Netherlands, Conference Proceedings 10th International Conference on Structural Faults and Repair, London 2003

Borger, D., J.A.Poulis, Het verlijmen van beton op staalplaten ten behoeve van brugdek versteviging, Rapport HI 2064, Delft, 2000 (in Dutch)

Braam, C.R., R.Mulder, Contec – Onderzoek kubussen en prisma's, Bepaling druksterkte en elasticiteitsmodulus, Rapport 25.5-02-12, Delft, 2002-a (in Dutch)

Braam, C.R., F.J.P.Schilperoort, Contec – Onderzoek hechting staal-beton, Trek- en buigproeven, Rapport 25.5-02-18, Delft, 2002-b (in Dutch)

Braam, C.R., A.van Rhijn, Contec – Onderzoek krimp verhardend beton, Bepaling invleod wapening en nabehandeling, Rapport 25.5-02-15, Delft, 2002-c (in Dutch)

Braam, C.R., F.J.P.Schilperoort, Contec – Onderzoek naar de invloed van het vlinderen van platen, Krimp en buigtreksterkte, Rapport 25.5-02-20, Delft, 2002-d (in Dutch)

Braam, C.R., R.van der Baars, Contec – Onderzoek naar de langeduur krimp van prisma's, Rapport 25.5-02-21, Delft, 2002-e (in Dutch)

Braam, C.R., F.J.P.Schilperoort, Contec – Onderzoek naar de buigtreksterkte, Invloed van liggerhoogte en aanwezigheid zaagsnede, Rapport 25.5-02-22, Delft, 2002-f (in Dutch)

Braam, C.R., Contec – Ferroplan als brugdekoverlaging, Technologische- constructieve- en duurzaamheidsaspecten, Rapport 25.5-02-46, Delft, 2002-g (in Dutch)

Braam, C.R., N.Kaptijn, P.Buitelaar, Hogesterktebeton als brugdekoverlaging. Technologische-, constructieve- en duurzaamheidsaspecten, Cement 1/2003-a (in Dutch)

Braam, C.R., E.M. Horeweg, Contec – Onderzoek vorst-dooizout bestandheid, Bepaling gewichtsverlies, Rapport 25.5-02-44, Delft, 2003-b (in Dutch)

Braam, C.R., P.Wardenier, Contec – Onderzoek chloride-indringing, Bepaling chloridegehalte na 1,6 en 12 maanden expositie in een zoutoplossing, Rapport 25.5-03-14, Delft, 2003-c (in Dutch)

Bridgestone, www.bridgestone.com, 10-12-2004

Bruls, A., Assessment of Fatigue Life of Orthotropic Steel Decks, IABSE Volume 59: Remaining Fatigue Life of Steel Structures, p 259-270, Zürich, 1990-a

Bruls, A. Measurements and interpretation of dynamic loads in bridges, Phase 3: Fatigue behaviour of orthotropic steel decks. Common synthesis report, 1990-b

Buitelaar, P., Ultra thin white toppings using high strength high performance concretes, Cement no. 7, 1999 (in Dutch).

Buitelaar, P., Problematiek Stalen Rijdekken, Uitvoering Contec Ferroplan Systeem, 2002 (in Dutch)

Buitelaar, P., Ultra Thin Heavy Reinforced High Performance Concrete Overlays. 6th International Symposium on Utilization of High Strength / High Performance Concrete, Leipzig, 2002

Buitelaar, P., C.R.Braam, N.Kaptijn, Reinforced high performance concrete overlay system for steel bridges, Conference proceedings 5th International CROW-workshop on fundamental modelling of the design and performance of concrete pavements 1&2, Istanbul, 2004-a

Buitelaar, P., C.R.Braam, N.Kaptijn, Reinforced High Performance Concrete Overlay System for Rehabilitation and Strengthening of Orthotropic Steel Bridge Decks, Conference Proceedings Orthotropic Bridge Conference 2004, Sacramento, 2004-b

Cairns, J., K. Jones, The splitting forces generated by bond, Magazine of concrete research 47 (1995) 153 – 165, 1995

Cairns, J., K. Jones, An evaluation of the bond-splitting action of ribbed bars, ACI materials

journal January/February 1996 10 – 19, 1996-a

Cairns, J., R. Bin Abdullah, Bond strength of black and epoxy-coated reinforcement – a theoretical approach, ACI materials journal July/August 1996 1 – 9, 1996-b

Corte, W. de, Vermoeiingsgedrag van stalen orthotrope rijvloeren onderworpen aan verkeersbelasting, Gent, 2005

Cullimore, M.S.G., J.W.Smith, Local Stresses in Orthotropic Steel Bridge Decks Caused by Wheel Loads, Journal of Constructional Steel Research, Vol 1., no.2, January 1981

Cunningham, J.R., C.Beales, Fatigue Crack Locations in orthotropic Steel Decks, Proceedings IABSE Workshop Remaining Fatigue Life of Steel Structures, p.133-146, Lausanne, 1990

Dijkstra, O.D., Vrouwenvelder, A.C.W.M., Vermoeiing verkeersbruggen met orthotrope dekplaat. Case Brienenoord, TNO-report 98-CON-R0714, Delft, 1998 (in Dutch)

Dijkstra, O.D, Vrouwenvelder, A.C.W.M., Vermoeiing stalen rijdekken, Praktijk S-N lijnen voor dekplaat scheur, TNO-report 2001-CON-BS-R6024, Rijswijk, 2001 (in Dutch)

Dijkstra, O.D., Vermoeiing orthotrope stalen rijdekken, Toetsing RWS programma, TNO report 2003-BC-R0061, Delft, 2003 (in Dutch)

Erkens, S.M.J.G., Asphalt Concrete Response (ACRe), -Determination, modeling and prediction- , dissertation, Delft University of Technology, Delft, 2002

Eurocode 0: Basis of structural design, EN 1990:2002

Eurocode 1: Actions on structures – Part 2: Traffic loads on bridges, EN 1991-2, 2003

Eurocode 3: Design of steel structures, Part 1.9: Fatigue strength of steel structures, EN 1993-1-9, 2005

Friedrich, H., G. Sedlacek, M. Paschen, Deep Improvement of the Fatigue Behaviour of Orthotropic Steel Decks with Consideration of the Asphalt Layer, 6th Japanese German Bridge Symposium, Munich, 2005

Fujino, Y., Vibration, control and monitoring of long-span bridges—recent research, developments and practice in Japan, Journal of Constructional Steel Research 58 p. 71–97, 2002-a

Fujino, Y., Y.Yoshida, Wind-Induced Vibration and Control of Trans-Tokyo Bay Crossing Bridge, Journal of Structural Engineering, p.1012-1025, August 2002-b

Groenendijk, J., Accelerated testing and surface cracking of asphaltic concrete pavements, dissertation, Delft University of Technology, Delft 1998

Günther, G.H., S.Bild, G.Sedlacek, Zur Frage der Haltbarkeit von Fahrbahnbelägen auf stählernen Strassenbrücken, Der Stahlbau, p.336-342, 11/1985,

Gurney, T.R., S.J. Maddox, Fatigue Tests on Joints in Orthotropic Decks, Proceedings Fatigue of Welded Structures, The Welding Institute, p. 64/1-64/20, Cambridge, 1987

Gurney, T.R., Fatigue of Steel Bridge Decks,Transport Research Laboratory, Department of Transport, HMSO Publication Centre, London, 1992

Haibach, E., I. Plasil, Untersuchungen zur Betriebsfestigkeit von Stahlleichtfahrbahnen mit

Trapezhohlsteifen in Eisenbrückenbau, Der Stahlbau, Wilhelm Ernst und Sohn, 1983

Hamaue, G., C.Puch, A.M.Ajour, Comportement à la fatigue en flexion sous moment négatif," (in French), Revêtements de Chaussées sur Platelages Métalliques, Bulletin de Liaison des Laboratoires des Ponts et Chaussées, Paris, 1981.

Hechtings Instituut, Onderzoek naar verlijming van vlakke plaat met een minimum aan luchtinsluiting, HI rapport 2123, Delft, 2002-a (in Dutch)

Hechtings Instituut, Statische en dynamische testen van zowel verlijmde als verlijmde en gelaste staalplaten, HI rapport 2093, Delft, 2002-b (in Dutch)

Hemmert-Halswick, A., Dokumentation über Schäden an Stahlbrücken, Bericht Bundesanstalt für Strassenwesen, Bergisch Gladbach, 2001

Henny, R.J., Samenvatting Aslastmetingen 1978-1994, DWW Report IB-R-95-05, Delft, 1995 (in Dutch)

Hobbacher, A., Recommendations for Fatigue Design of Welded Joints and Components, International Institute of Welding, doc. XIII-1965-03/XV-1127-03, Paris, 2003

Honshu Shikoku Bridge Authority (2005), www.hsba.go.jp, 17-01-2005

Huisman, J.G., Temperatuurmetingen aan de brug over het Hollandsch Diep te Moerdijk, RTD report INS 9042, Rotterdam, 1992

Huurman, M., T.O.Medani, A.Scarpas, C.Kasbergen, Development of a 3D-FEM for Surfacings on Steel Deck Bridges ICCES 2003, Advances in Computational & Experimental Engineering & Sciences, Corfu, Greece, 2003

Huurman, M., T.O.Medani, A.A.A.Molenaar, C.Kasbergen, A.Scarpas, APT Testing and 3D Finite Element Analysis of Asphalt Surfacings on Orthotropic Steel Deck Bridges 83rd Annual TRB Meeting, Washington, USA, 2004

Janss, J, Fatigue of Welds in Orthotropic Bridge Deck Panels with Trapezoidal Stiffeners, Journal of Constructional Steel Research 9, p 147-154, 1988

Jong, F.B.P.de, Numeriek onderzoek spreiding in asfalt, Internal report Ministry of Transport, Public Works and Water Management (in Dutch), Zoetermeer, 2001

Jong, F.B.P.de, M.H.Kolstein, F.S.K.Bijlaard, Development of long term renovation techniques for bridge decks with fatigue cracks, Conference proceedings Third International Conference on Steel Structures (Eurosteel 2002), Coimbra, 2002

Jong, F.B.P. de, Boersma, P.D., Lifetime calculations for orthotropic steel bridge decks, Conference Proceedings 10th International conference on Structural Faults and Repair on steel structures, London, 2003

Jong, F.B.P. de, M.H. Kolstein, F.S.K. Bijlaard, Strain measurement tests at orthotropic steel bridge decks with a heavy vehicle simulator, Stresses due to real moving wheel loads in deck plate, trough wall and surfacing, Conference Proceedings 10th Nordic Steel Construction Conference, Copenhagen, 2004-a

Jong, F.B.P. de, Overview Fatigue phenomenon in orthotropic bridge decks in the Netherlands, Conference Proceedings Orthotropic Bridge Conference 2004,

Sacramento, 2004-b

Jong, F.B.P. de, M.H.Kolstein, F.S.K.Bijlaard, Research project TU Delft; behaviour conventional bridge decks & development of renovation techniques, Conference Proceedings Orthotropic Bridge Conference 2004, Sacramento, 2004-c

Jong, F.B.P. de, P.D.Boersma, Maintenance philosophy and Systematic lifetime assessment for decks suffering from fatigue, Conference Proceedings Orthotropic Bridge Conference 2004, Sacramento, 2004-d

Jong, F.B.P. de, M.H.Kolstein, Strengthening a bridge deck with high performance concrete, , Conference Proceedings Orthotropic Bridge Conference 2004, Sacramento, 2004-e

Jong, F.B.P. de, Optimalisatie OP-lassen, Dekplaatscheuren repareren door onder poederdek lassen, Zoetermeer, 2004-f (in Dutch)

Jong, F.B.P. de, Plan Lintrack reference experiments on conventional orthotropic steel bridge decks with surfacings, Stevin Report 6.03.6, Delft, 2005-a

Jong, F.B.P. de, Data processing & Results Lintrack reference experiments on conventional orthotropic steel bridge deck with surfacings, Stevin Report 6.03.7, Delft, 2005-b

Jong, F.B.P. de, Stress distribution in orthotropic steel bridge decks, Measurements and calculations for the crossing trough-crossbeam, Stevin Report 6.04.3, Delft, 2005-d

Jong, F.B.P. de, Fatigue tests for deck plate cracks in orthotropic bridge decks, Stevin Report 6.04.4, Delft, 2005-e

Jong, F.B.P. de, Static and Fatigue tests on orthotropic bridge deck with fatigue cracks and RHPC surfacing, Stevin Report 6.05.2, Delft, 2006-a

Jong, F.B.P. de, Fatigue test loading related to measured traffic loads, Delft, 2006-b

Kanter, J.L.C.G. de, Mechanische eigenschappen Epoxy-schuim op druk, Test rapport B2V-00-69, Delft University of Technology, Faculty of Aerospace Engineering, Structures & Materials Laboratory, Delft, 2000-a

Kanter, J.L.C.G. de, Mechanische eigenschappen Kurk gevuld Polyurethaan op druk, Test rapport B2V-00-70, Delft University of Technology, Faculty of Aerospace Engineering, Structures & Materials Laboratory, Delft, 2000-b

KNMI, Koninklijk Nederlands Meteorologisch Instituut, www.knmi.nl, 2000

Kolstein, M.H., J.de Back, Measurements and interpretation of dynamic loads on bridges – Phase 1 – ECSC contractnr. 7210-KD/6/606, Stevin reports, 6-79-5, 6-79-6, 6-79-7, Delft University of Technology, Stevin Laboratory, Steel Structures, Delft, 1979

Kolstein, M.H., J.de Back, Measurements and interpretation of dynamic loads on bridges – Phase 2 – ECSC contractnr. 7210-KD/6/606, Stevin reports, 6-83-6, Delft University of Technology, Stevin Laboratory, Steel Structures, Delft, 1983

Kolstein, M.H., A review of vehicle-type counting and measurement of axle loads on highways 1978 until 1990, Stevin Report 25.6.90.26 A2/22.06, Delft 1990

Kolstein, M.H., J. Wardenier, Fatigue strength of welded joints in Orthotropic Steel Bridge Decks, Welding in the World/Le Soudage dans le Mode, Vol. 38, pp.175-194,

Budapest, 1996

Kolstein, M.H., J. Wardenier, H.van der Weijde, A new type of fatigue failures in steel orthotropic bridge decks, Proceedings of Fifth Pacific Structural Steel Conference, pp. 483-488, Techno Press, Korea, 1998

Kolstein, M.H., Laboratory tests of the deck plate weld at the intersection of the trough and the crossbeam of steel orthotropic bridge decks, Conference proceedings Eurosteel Conference 1999, p.411-414, Prague, 1999-a

Kolstein, M.H., J.Wardenier, Evaluation of Recently Observed Fatigue Cracks in the Stiffener to Deck Plate Joint of Orthotropic Bridge Decks, Proceedings international Conference on Bridge Design, Construction and Maintenance, Singapore, 1999-b

Kolstein, M.H., Laboratory test orthotropic deck bascule bridge van Brienenoord, Stevin Report 6-98-15, Delft, 2000-a

Kolstein, M.H., J.Wardenier, Fatigue Analysis of a cracked steel deck using measured stress spectra and full-scale laboratory tests, Proceedings Bridge Management 4 – Inspection, maintenance, assessment and repair, Thomas Telford Publishing, ISBN 0 7277 28547 p. 584-591, London, 2000-b

Kolstein, M.H., J.S.Leendertz, Measurements and interpretation of dynamic loads on bridges (fourth phase: fatigue design of European orthotropic steel bridges deck), Brussels, 2001-a

Kolstein, M.H., L.Eekhout, Resultaten statische – en dynamische proeven op (on)gevulde troggen, Delft, 2001-b (in Dutch)

Kolstein, M.H., Strain Measurements Caland Bridge 2003, Stevin Report 6-03-13, Delft, December 2003

Kolstein, M.H., European Research on the Improvement of the Fatigue Resistance and Design of Steel Orthotropic Bridge Decks, Conference Proceedings Orthotropic Bridge Conference 2004, Sacramento, 2004-a

Kolstein, M.H., The Role of Site Measurements to improve the Knowledge about the Fatigue Behaviour of Steel Orthotropic Bridges, Conference Proceedings Orthotropic Bridge Conference 2004, Sacramento, 2004-b

Kolstein, M.H., Stress reduction due to surfacing on orthotropic steel decks, Conference Proceedings 10th Nordic Steel Construction Conference, Copenhagen, 2004-c

Kolstein, M.H., Rapportage rekmetingen hoge-sterkte beton brug Hagestein, 2006-a

Kolstein, M.H., Rapportage vermoeiingsproeven onder poederdek gelaste brugdekplaten 2e serie, Delft, 2006-b

Kronemeijer D.A., C.M. Schipper, Technical Specification for the inspection of steel bridges using the SLOFEC system for the presence of cracks emanating from the welded connection between trogbeen and deck plate in the presence of a ‘thin’ wear layer as typical on movable parts of steel bridges in the Netherlands, Specification No. : TS–ET 02-03, Revision : 0, Amsterdam, 2003-a

Kronemeijer, D.A., C.M.Schipper, Niet destructief onderzoek aan het rijdek van stalen bruggen op de aanwezigheid van rijdekplaatscheuren, Deel 6: Praktijk gereed maken van het SLOFEC inspectiesysteem voor de toepassing door een “dunne” epoxy slijtlaag, report nr. OG.03.20643, Amsterdam, 2003-b (in Dutch)

Labordus, M., Vacuüminjectie als lijmmethode, TNO-report, Delft, 2004 (in Dutch)

Labordus, M., W.Souren, R.Janssen, E.van Herpt, Vacuüminjectie als lijmmethode – fase 3, TNO-report, Delft, 2005 (in Dutch)

Labordus, M., Injectie als lijmmethode – fase 4: Validatie aan een brugdek segment, TNO-report 2005046MLR-1, Delft, 2006 (in Dutch)

Leendertz, J.S., M.H.Kolstein, J.Wardenier, The Behaviour of Trough Stiffener to Crossbeam Connections in Orthotropic Steel Bridge Decks, Heron vol. 40, pp. 217-259, Delft 1995

Leendertz, J.S., F.B.P.de Jong, Fatigue Aspects of Orthotropic Steel Decks, Conference Proceedings Lightweight Bridge Decks, European Bridge Engineering Conference, Paper no. 14, Rotterdam, 2003

Lees, J.M., C.J. Burgoyne, Transfer bond stresses generated between FRP tendons and concrete, Magazine of concrete research 51 (1999) 229 - 239, 1999

Leest, M.C.van der, Proefvulling trogprofiel, report A03156 werkplaats Frans Nooren b.v., Stadskanaal, 2003

Liefting, KINT Project “Development of Acceptance Criteria fro TOFD Examination Method”, Part C: Probabilistic Fracture Mechanics Evaluation of Draft Acceptance Criteria, Partial report on determination of input data, TNO report TO 97-29, Apeldoorn, 1997

Machida, F., T.Yuge, C.Miki, E Yamaguchi, T.Shimozata, T.Masui, Stress Measurements on Fatigue-Damaged Structures with Orthotropic Steel Decks in Summer and Winter, Conference Proceedings Orthotropic Bridge Conference 2004, Sacramento, 2004

Malvar, L.J., Bond of reinforcement under controlled confinement, ACI materials journal November/December 1992 593 – 601, 1992

Medani, T.O. Asphalt Surfacing Applied to Orthotropic Steel Bridge Decks, a Literature Study Report 7-01-127-1, Road and Railway Research Lab. Delft University of Technology, the Netherlands, 2001-a

Medani, T.O. Towards a New Design Philosophy for Surfacings on Orthotropic Steel Bridge Decks Report 7-01-127-2 Road and Railway Research Lab. Delft University of Technology, the Netherlands, 2001-b

Medani, T.O., M.H.Kolstein, A.Scarpas, A.Bosch, A.A.A.Molenaar, Material Behaviour of Mastic Asphalt for Orthotropic Steel Deck Bridges CROW, Wegbouwkundige Werkdagen, Ede, 2002-a

Medani, T.O., A.Scarpas, M.H.Kolstein, A.Bosch, A.A.A.Molenaar, Estimation of the ACRe material model's parameters of mastic asphalt for orthotropic steel deck bridges

CROW, Wegbouwkundige Werkdagen, Ede, 2002-b

Medani, T.O., A.Scarpas, M.H.Kolstein, A.A.A.Molenaar, Design Aspects for Wearing Courses on Orthotropic Steel Bridge Decks ISAP 2002, Copenhagen, Denmark, 2002-c

Medani, T.O. and M.Huurman, Constructing the Stiffness Master Curves for Asphaltic Mixes Report 7-10-127-3, Faculty of Civil Engineering and Geosciences, Delft University of Technology, 2003

Medani, T.O., M.Huurman, A.A.A.Molenaar, On the constructing of master curves for bituminous mixes Proceedings 3rd EuroBitume Congress, Vienna, Austria, 2004-a

Medani, T.O., M.Huurman, L.J.M.Houben, A.A.A.Molenaar, A proposed Fatigue Based Design Methodology for Asphaltic Mixes Applied on Orthotropic Steel Bridges Proceedings 5th RILEM International Conference, Limoges, France, 2004-b

Medani, T.O., Design Principles of Surfacings on Orthotropic Steel Bridge Decks, dissertation, Delft University of Technology, Delft, 2006

Michelin, www.michelintransport.com, 10-12-2004

Miki, C., Fatigue Damage in Orthotropic Steel Bridge Decks and Retrofit Works, Steel Structures 6, p.255-267, 2006

Nagtegaal, G., Problematiek stalen rijdekken, Levensduur verlengende oplossingen, Errata bij het rapport “Resultaten statische en dynamische proeven op (on)gevulde troggen”, Zoetermeer, 2001 (in Dutch)

Nagtegaal, G., Problematiek stalen rijdekken, Deel 6.2.3, Levensduurverlengende oplossingen, Het verlijmen van staalplaten, Zoetermeer, 2002-a (in Dutch)

Nagtegaal, G., Problematiek stalen rijdekken, Levensduurverlengende oplossingen, Selectie van lijmen, Zoetermeer, 2002-b (in Dutch)

Nagtegaal, G., Problematiek stalen rijdekken, Levensduurverlengende oplossingen, Validatie testen aan diverse verlijmde materialen, Errata bij rapport “Het verlijmen van diverse materialen op staalplaten ten behoeve van brugdekversteviging”, Zoetermeer, 2002-c (in Dutch)

Nagtegaal, G., Problematiek stalen rijdekken, Levensduurverlengende oplossingen, Validatie testen aan delingen in verlijmde staalplaten, Errata bij rapport “Statische en dynamische testen van zowel verlijmde als verlijmde en gelaste platen”, Zoetermeer, 2002-d (in Dutch)

Nagtegaal, G., Problematiek stalen rijdekken, Deel 6.2.4., Levensduurverlengende oplossingen, Het vullen van de troggen, Zoetermeer, 2002-e (in Dutch)

Nagtegaal, G. Injecteren van stalen rijdekken, Zoetermeer, 2002-f (in Dutch)

Nagtegaal, G., Problematiek stalen rijdekken, Levensduur verlengende oplossingen, Brainstormsessies, Zoetermeer, 2002-g (in Dutch)

Nagtegaal, G., Problematiek stalen rijdekken, Levensduurverlengende oplossingen, Zoetermeer, 2003 (in Dutch)

NEN 6700, Technische grondslagen voor bouwconstructies, Algemene basiseisen, Delft, 2005 (in Dutch)

NEN 6788, Het ontwerpen van stalen bruggen, basiseisen en eenvoudige rekenregels (VOSB 1995), Delft, 1995

NEN 2063:1988, Arc welding; Fatigue loaded structures; Calculation of welded joints in unalloyed and low-alloy steel up to and including Fe 510 (Fe 52) (in Dutch)

Nieuwsma, R., Moerdijkbrug eindrapportage aslastmeetresultaten, DWW report, IB-R-98-47, Delft 1999 (in Dutch)

Nordtest, Concrete hardened: accelerated chloride penetration. NT Build 443, Nordtest, Espoo, 1995

Nunn, D.E., J.R.Cunninghame, Stresses under Wheel loading in steel orthotropic decks with trapezoidal stiffeners, Transport and Road Research Laboratory, TRRL Supplementary Report 53, Crowthorne, 1974

Overduin, L., Deklaagsystemen voor stalen bruggen, M.Sc. thesis Delft University of Technology, Delft, 1999

Overduin, L., CrackPEC: Detection of cracks in steel bridges by directional Pulsed Eddy Current, internal report, Capelle aan den IJssel, 2003

Paschen, M., Untersuchungen zu Schäden an Stahlbrücken, Lehrstuhl für Stahlbau der RWTH Aachen, Aachen, 1995

Pottinger, M.G., The Three-Dimensional Contact Patch Stress Field of Solid and Pneumatic Tires, Tire Sceince and Technology, TSTCA, Vol. 20, No. 1, pp. 3-32, January-March 1992

Poulis, J.A., D.P.Borger, P.de Regt, Metingen Rijkswaterstaat, Het verlijmen van diverse materialen op staalplaten ten behoeve van brugdekversteviging, Delft, Rapport HI 2079, 2000-a (in Dutch)

Poulis, J.A., Het storten van beton op staal, Rapport HI 2081, Delft, 2000-b (in Dutch)

Pover, J., Rapportage mbt uitgevoerde analyses tbv levensduurverlengende oplossingen in het kader van het PSR-project (Problematiek Stalen Rijdekken), Concept d.d. 25 april 2002, Zoetermeer, 2002 (in Dutch, internal publication)

Pover, J., Rapportage mbt uitgevoerde analyses tbv levensduurverlengende oplossingen in het kader van het PSR-project (Problematiek Stalen Rijdekken), Deel DPS02-scheur, Concept d.d. 19 maart 2004, Zoetermeer, 2004 (in Dutch, internal publication)

RILEM, CDF Test – Test method for the freeze-thaw resistance of concrete – test with sodium chloride solution. RILEM, Materials and structures, vol. 29, 1996

Schat, F., Onderzoek aan TU-Proefstuk, TNO-report 97MI-00970/SCA/VIS, Apeldoorn, 1997-a

Schat, F., J.Vuik, Onderzoek aan proefstuk met scheurafkomstig van de “Van Brienenoord brug”, TNO-report97 MI-00990/SCA/VIS, Apeldoorn ,1997-b

Schat, F., J.Vuik, Onderzoek aan 2e proefstuk met scheurafkomstig van de “Van Brienenoord

brug", TNO-report97 MI-00969/SCA/VIS, Apeldoorn ,1997-c

Schrieks, M.C., Lifespan enlargement of deck plates of movable steel bridges, M.Sc. Thesis Delft University of Technology, Faculty of Civil Engineering and Geosciences, Delft, 2006

Sedlacek, G., Orthotropic Plate Bridge Decks, Paper and presentation at First World conference on constructional Steel Design. Constructional Steel Design Guide, Chapter 2.10, 1992

Sika, www.sika.nl/tds_sikadur30_nl.pdf, 13-01-2006 (in Dutch)

Straalen, van, IJ.J., Development of design rules, www.dogma.org.uk/vtt/design/cases/developmentofdesignrules.html, 1999

Straalen van, IJ.J., Development of Design Rules for Structural Adhesive Bonded Joints, A Systemaric Approach, PhD dissertation, Delft University of Technology, Delft, 2001

Straalen, van, IJ.J., R. Vis, Proeven op stalen rijdekken - Levensduurverlengende oplossing met een 5 cm dikke laag beton op het rijdek, TNO-report 2002-BC-R0023, Delft 2002-a (in Dutch)

Straalen, van, IJ.J., R. Vis, Proeven op stalen rijdekken - Levensduurverlengende oplossing met een trog gevuld met polyurethaan, TNO-report 2002-BC-R0026, Delft, 2002-b (in Dutch)

Straalen, van, IJ.J., R.Vis, Proeven op stalen rijdekken - Levensduurverlengende oplossing met een 5 cm dikke laag beton op het rijdek: aanvullende proef, TNO-report 2002-BC-R0030, Delft, 2002-c (in Dutch)

Straalen, van, IJ.J., H.Botter, Review van de resultaten van het deelproject "Het verlijmen van staalplaten" in het kader van het Bouwdienst RWS-project "Problematiek Stalen Rijdekken", TNO-report 2002-BC-R0025, Delft, 2002-d (in Dutch)

Straalen, van, IJ.J., G.J.Hagen, Proeven op stalen rijdekken - Levensduurverlengende oplossing met een 6 mm dikke staalplaat gelijmd op het rijdek, TNO-report 2003-BC-R0062, Delft, 2003-a (in Dutch)

Straalen, van, IJ.J., Proeven op stalen rijdekken - Levensduurverlengende oplossing met een trog gevuld met polyurethaan: 2e proef, TNO-report 2003-BC-R0002, Delft, 2003-b (in Dutch)

Terpstra, S., A.Visser, Niet destructief onderzoek aan het rijdek van stalen bruggen op de aanwezigheid van rijdekplaatscheuren, Deel 2A: Periodiek ultrasoon onderzoek van af de onderkant van het rijdek, report nr. OP.00.20357, Amsterdam, 2000-a (in Dutch)

Terpstra, S., A.Visser, D.A.Kronemeijer, Niet destructief onderzoek aan het rijdek van stalen bruggen op de aanwezigheid van rijdekplaatscheuren, Deel 2B: Onderzoek vanaf de bovenkant van het rijdek door een "dunne" epoxy-slijtlaag, report nr. OP.00.20348, Amsterdam, 2000-b (in Dutch)

The Welding Institute, www.twi.co.uk/j32k/protected/band_3/jk5.html, 26-06-2006

Tielking, J.T., M.A. Abraham, Measurements of Truck Tire Footprint Pressures,

Transportation Research Record 1435, pp. 92-99, 1994

Verburg, H.A., F. Van Gogh, Bepaling dynamische stijfheidsmoduli en fasehoeken van zeer open asfalt beton en gietasfalt, DWW Report nr. IR-R-96.042, Delft, 1996 (in Dutch)

Virlogeux, M., The Viaduct over the River Tarn, Conference Proceedings Steelbridge 2004, 23-25 June 2004, OTUA, Paris, p. 145-164, 2004-a

Virlogeux, M., French Experience with Long-Span Cable-Stayed Bridges with Orthotropic Deck, Conference Proceedings Orthotropic Bridge Conference 2004, Sacramento, 2004-b

Vogelzang, C.H., M.H. Kolstein, Vermoeiingsterkte Reparatielas, Stevin Report 6-03-14, Delft, 2003 (in Dutch)

Vrouwenvelder, A.C.W.M., P.H.Waarts, S.de Wit, Algemene veiligheidsbeschouwing en modellering van wegverkeersbelasting voor brugconstructies, TNO-rapport 98-CON-R1813, Delft, 2000-a (in Dutch)

Vrouwenvelder, A.C.W.M., O.D.Dijkstra, R.J.van Foeken, Basisfilosofie voor het ontwerpen van verkeersbruggen, Onderdeel: Vermoeiing stalen rijdekken, Probabilistische ontwerpfilosofie, TNO-rapport 99-CON-DYN-R0108, Delft, 2000-b (in Dutch)

Waarts, P.H., Axle loads on bridges. Results of measurements in 1994, 1996 and 1997, TNO-report 98-CON-R1741, Delft, 1998 (in Dutch)

Weijde, H.van der, Van Brienenoordbrug: Vermoeiing beweegbare brug, oorzaak en oplossing, Syllabus nr 20, Staalbouwkundig Genootschap, Rotterdam, 1998 (in Dutch)

Weijde, H.van der, Reparatie Van Brienenoordbrug, Rotterdam, Val vervangen wegens vermoeiing, Bouwen met Staal 146, p.40-44, 1999 (in Dutch)

Weitz, F.R., Neuzeitliche Gesichtspunkte im schweißenden Brückenbau, Der Stahlbau 3, p.73-81, 1974 (in German)

Weitz, F.R., Die Komplexität von Konstruktionssystemen und Fertigungstechniek am Beispeil der Stahlbrückenmontage, Bauingenieur 54, p. 355-364, 1979 (in German)

Wolchuk, R., Design Manual for Orthotropic Steel Plate Deck Bridges, American Institute of Steel Construction, Chicago, 1963

Yuge, T., F.Machida, H.Morikawa, C.Miki, T.Kamiki, T.Masui, Analysis of fatigue damage patterns in orthotropic steel deck of Tokoy Metropolitan Expressways, Conference Proceedings Orthotropic Bridge Conference 2004, Sacramento, 2004

Annex A – Footprints

An accurate prediction of the stresses is important in order to achieve accurate fatigue calculations. One of the major aspects influencing the stress is the size of the footprint. Accurate knowledge about the footprints is very important in order to accurately predict stresses in the bridge deck structure. Some tests were performed to show the dimensions of the footprints of the tyres at different loads and inflation pressure. For the reported tests a print of the contact area has been made. The procedure was:

- Paint the tyre
- Lower and load the tyre on a plain white paper
- Unload and lift the tyre from the white paper

The applied load was measured with a measuring unit below the white paper. Figure 3-3 gives an overview of the contact area measurements. The tests were performed with the Lintrack apparatus, a heavy vehicle simulator originally built up for pavement testing. The Lintrack is described more in detail in chapter 4 and (Groenendijk, 1998). The tyres, which were used for these tests, were also used in the test series in the Lintrack, which are reported in chapter 4. These tests were also intended to check if the formulas derived by Groenendijk were also valid for these tyre types.

Figure A-14: Contact area measurements

The tests were carried out for the four tyre types, but especially for the double (type B) and the super single (type C), because these are common tyre types on heavy vehicles with the highest loads, thus causing the major part of the fatigue damage in the steel structure. In total 21 footprints were created see Table A-1. For the single (type A) and the double (type B) 315/80R22.5 tyres were used, for the super single (type C) a 385/65R22.5 was used, and for the extra wide base (type D) the 495/45R22.5 was used.

Table A-1: Footprint measurements

Test no.	Tyre	p (MPa)	F (kN)
1	A	0,9	25
2	A	0,9	50
3	B	0,7	25
4	B	0,7	50
5	B	0,7	80
6	B	0,7	90
7	B	0,9	25
8	B	0,9	50
9	B	0,9	80
10	B	0,9	90
11	C	0,9	25
12	C	0,9	28
13	C	0,9	25
14	C	0,9	50
15	C	0,9	52
16	C	0,9	80
17	C	0,9	79
18	C	0,9	90
19	C	0,9	88,5
20	D	0,9	50
21	D	0,9	90

Photographs of the footprints are given in this annex. The width and the length of the footprints were measured. These results are given in Table A-2 and Table A-3 for tyre types B and C. For almost every footprint, the area can be modelled as a square. The single (type A) at 25 kN, and the double (type B) at 50 kN, both at 0.9 MPa inflation pressure, resulted in a circular footprint. The average contact stress in the footprint was calculated by dividing the applied load by the total contact area. These contact stresses are also given in the tables.

Table A-2: Footprint dimensions double (type B)

			Left tyre		Right tyre		Contact stress
Test	F (kN)	p (Mpa)	w (mm)	l (mm)	w (mm)	l (mm)	σ (MPa)
	measured	measured	measured	measured	measured	measured	calculated
3	25	0.7	172	163	170	174	0.43
4	50	0.7	251	215	250	228	0.45
5	80	0.7	252	261	253	277	0.59
6	90	0.7	251	285	253	304	0.61
7	25	0.9	169	153	170	161	0.47
8	50	0.9	246 (diameter)	circular	256 (diameter)	circular	0.51
8	50	0.9	248	207	246	233	0.46
9	80	0.9	254	252	254	284	0.59
10	90	0.9	253	270	253	288	0.64

Table A-3: Footprint dimensions super single (type C)

no.	F (kN)	p (MPa)	w (mm)	l (mm)	Contact stress σ (MPa)
	measured	measured	measured	measured	calculated
11	25	0.9	274	187	0.49
12	28.00	0.9	275	185	0.55
13	25.00	0.9	276	180	0.50
14	50.00	0.9	282	242	0.73
15	52.00	0.9	282	246	0.75
16	80.00	0.9	283	321	0.88
17	79.00	0.9	283	322	0.87
18	90.00	0.9	282	345	0.93
19	88.50	0.9	282	342	0.92

The contact stresses in the edge zones and the middles zone were also calculated with the formulas derived by Groenendijk. Subsequently the length of the footprint was calculated. These values are given in Table A-4 and Table A-5. Because the Groenendijk formulas represent the situation under the tread blocks and not over the entire footprint the areas of tread and grooves were determined. The average width of the tread blocks on the double (type B) was 39 mm and the average groove between the tread blocks on the double (type B) was 3.8 mm. The average length of the tread blocks was 29 mm and the average width of the grooves between the tread blocks was 5.5 mm. The tread block area was only 77% of the total

area including the grooves between the tread blocks. For the super single (type C) only the middle zone was grooved. The average width of the grooves was 12.3 mm and the average width of the treads was 29 mm. The tread area was only 70% of the total area including the grooves between the treads.

Table A-4: Calculated contact stresses and footprint length double (type B)

Test	F (kN)	p (MPa)	$\sigma_{z;ave;middle}$ (MPa)	$\sigma_{z;ave;edge}$ (MPa)	l (mm)
	measured	measured	calculated	calculated	calculated
3	25	0.7	0.70	0.52	151
4	50	0.7	0.75	0.75	173
5	80	0.7	0.81	1.03	229
6	90	0.7	0.83	1.12	245
7	25	0.9	0.79	0.58	136
8	50	0.9	0.86	0.81	154
8	50	0.9	0.86	0.81	157
9	80	0.9	0.95	1.09	204
10	90	0.9	0.98	1.18	218

Table A-5: Calculated contact stresses and footprint length super single (type C)

Test	F (kN)	p (MPa)	$\sigma_{z;ave;middle}$ (MPa)	$\sigma_{z;ave;edge}$ (MPa)	l (mm)
	measured	measured	calculated	calculated	calculated
11	25	0.9	0.79	0.58	163
12	28.00	0.9	0.79	0.61	177
13	25.00	0.9	0.79	0.58	161
14	50.00	0.9	0.86	0.81	259
15	52.00	0.9	0.86	0.83	266
16	80.00	0.9	0.95	1.09	340
17	79.00	0.9	0.94	1.08	337
18	90.00	0.9	0.98	1.18	362
19	88.50	0.9	0.97	1.17	359

This annex gives photographs of the footprints. Each photograph contains a header above the photograph. The structure of the header is: Test no. – Wheel type – Inflation pressure – Wheel load. The width and the length of the footprints are given. The width is horizontal and the length is vertical on the paper. Traffic drives in longitudinal direction. The photographs are not presented on the same scale.

Test no. 1 Wheel type A (Single) 315/80R22.5 Inflation pressure 0.9 MPa Wheel load 25 kN Circle diameter = 236 mm A little bit flattened at front and rear	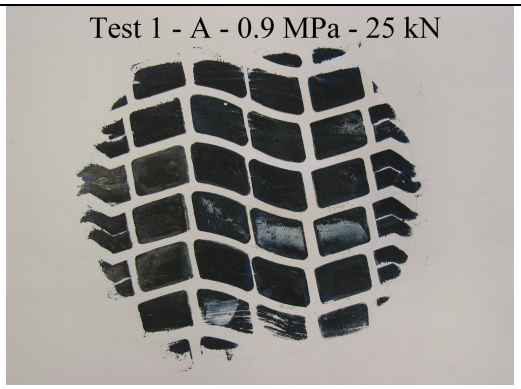
Test no. 2 Wheel type A (Single) 315/80R22.5 Inflation pressure 0.9 MPa Wheel load 50 kN Width x Length = 250 x 283 mm	

Test no. 3 Wheel type B (Double) 315/80R22.5 Inflation pressure 0.7 MPa Wheel load 25 kN Left tyre: Width x Length = 172 x 163 mm Right tyre: Width x Length = 170 x 174 mm	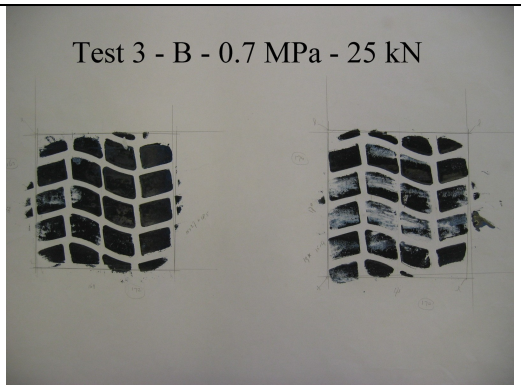
Test no. 4 Wheel type B (Double) 315/80R22.5 Inflation pressure 0.7 MPa Wheel load 50 kN Left tyre: Width x Length = 251 x 215 mm Right tyre: Width x Length = 250 x 228 mm	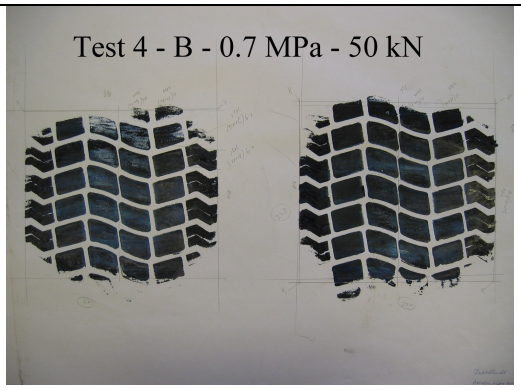
Test no. 5 Wheel type B (Double) 315/80R22.5 Inflation pressure 0.7 MPa Wheel load 80 kN Left tyre: Width x Length = 252 x 261 mm Right tyre: Width x Length = 253 x 277 mm	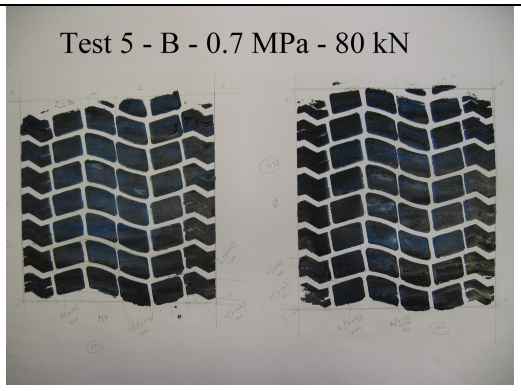
Test no. 6 Wheel type B (Double) 315/80R22.5 Inflation pressure 0.7 MPa Wheel load 90 kN Left tyre: Width x Length = 251 x 285 mm Right tyre: Width x Length = 253 x 304 mm	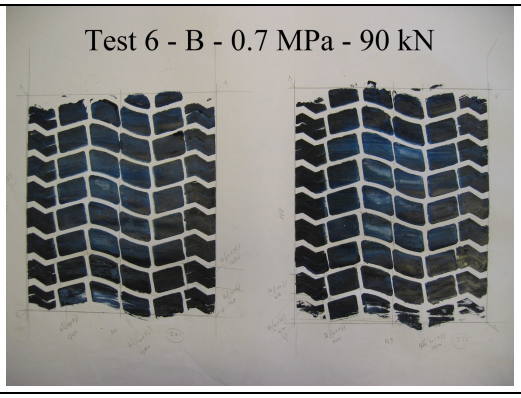

Test no. 7 Wheel type B (Double) 315/80R22.5 Inflation pressure 0.9 MPa Wheel load 25 kN Left tyre: Width x Length = 169 x 153 mm Right tyre: Width x Length = 170 x 161 mm	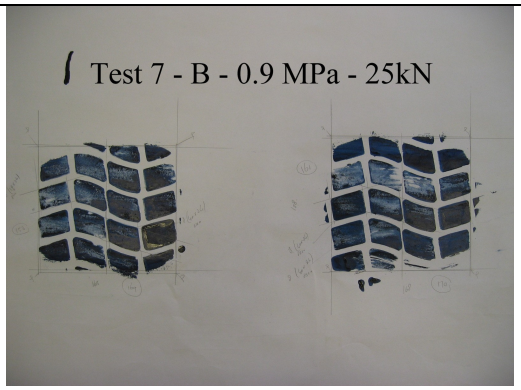
Test no. 8 Wheel type B (Double) 315/80R22.5 Inflation pressure 0.9 MPa Wheel load 50 kN Left tyre: Circle diameter = 246 mm Right tyre: Circle diameter = 256 mm Circles are a bit flattened at front and rear Left tyre: Width x Length = 248 x 207 mm Right tyre: Width x Length = 246 x 233 mm	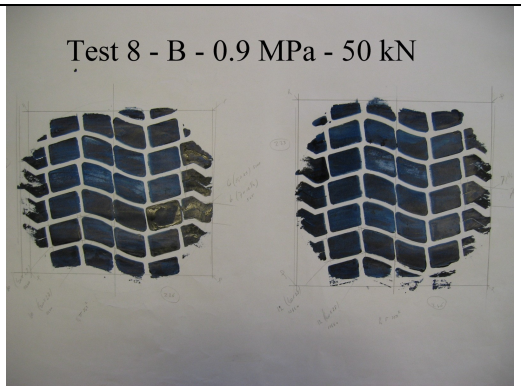
Test no. 9 Wheel type B (Double) 315/80R22.5 Inflation pressure 0.9 MPa Wheel load 80 kN Left tyre: Width x Length = 254 x 252 mm Right tyre: Width x Length = 254 x 284 mm	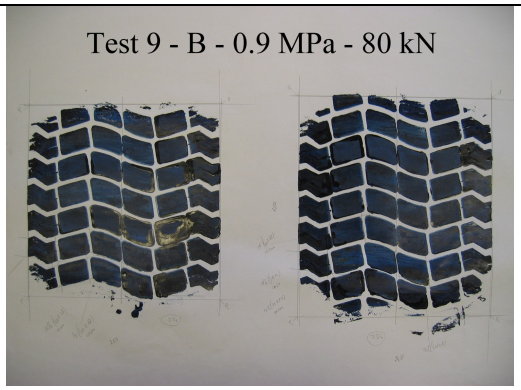
Test no. 10 Wheel type B (Double) 315/80R22.5 Inflation pressure 0.9 MPa Wheel load 90 kN Left tyre: Width x Length = 253 x 270 mm Right tyre: Width x Length = 253 x 288 mm	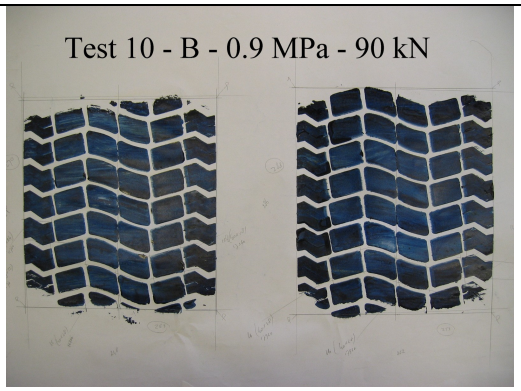

Test no. 11 Wheel type C (Super single) 385/65R22.5 Inflation pressure 0.9 MPa Wheel load 25 kN Width x Length = 274 x 187 mm	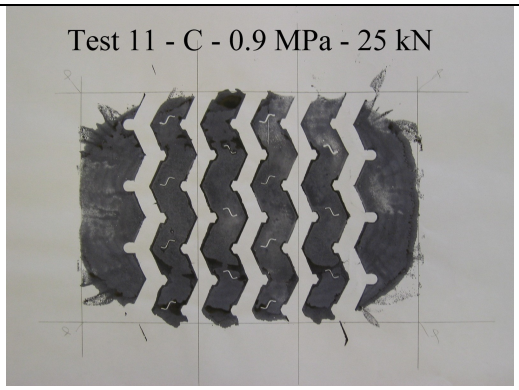
Test no. 12 Wheel type C (Super single) 385/65R22.5 Inflation pressure 0.9 MPa Wheel load 28 kN Width x Length = 275 x 185 mm	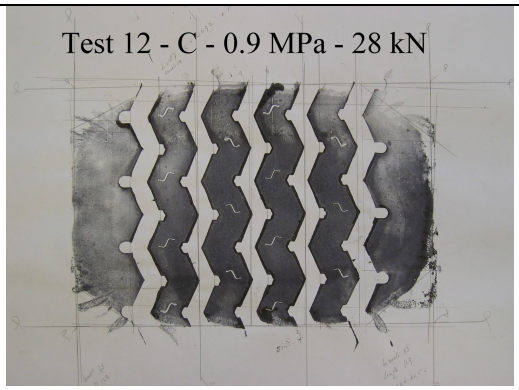
Test no. 13 Wheel type C (Super single) 385/65R22.5 Inflation pressure 0.9 MPa Wheel load 25 kN Width x Length = 276 x 180 mm	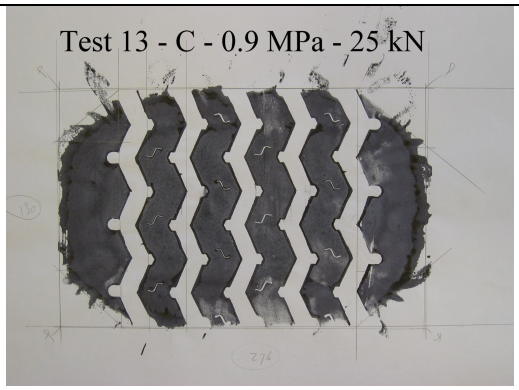
Test no. 14 Wheel type C (Super single) 385/65R22.5 Inflation pressure 0.9 MPa Wheel load 50 kN Width x Length = 282 x 242 mm	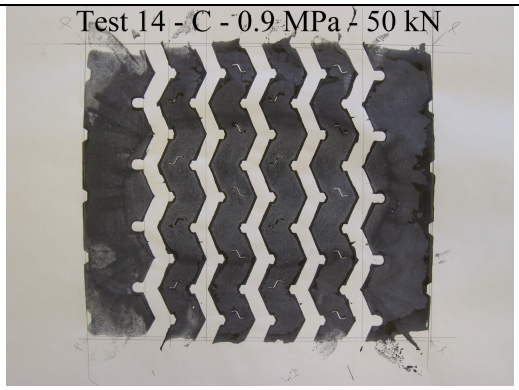

Test no. 15 Wheel type C (Super single) 385/65R22.5 Inflation pressure 0.9 MPa Wheel load 52 kN Width x Length = 282 x 246 mm	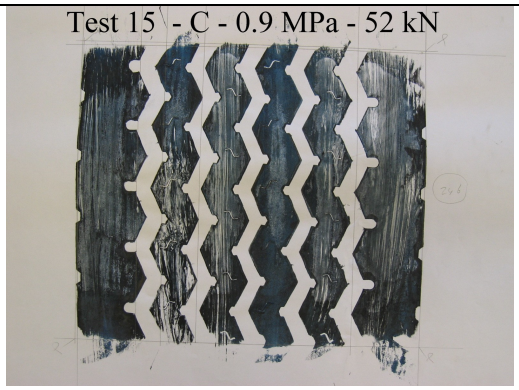
Test no. 16 Wheel type C (Super single) 385/65R22.5 Inflation pressure 0.9 MPa Wheel load 80 kN Width x Length = 283 x 321 mm	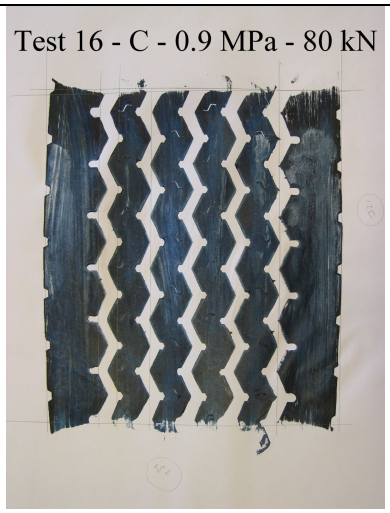
Test no. 17 Wheel type C (Super single) 385/65R22.5 Inflation pressure 0.9 MPa Wheel load 79 kN Width x Length = 283 x 322 mm	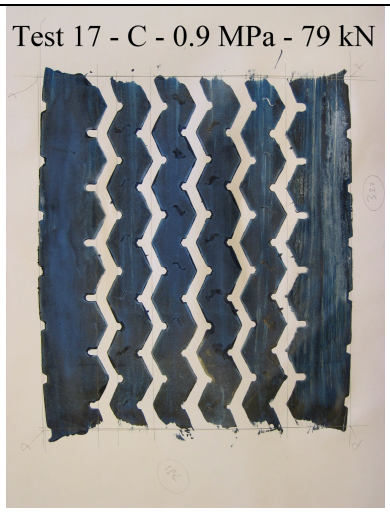

Test no. 18 Wheel type C (Super single) 385/65R22.5 Inflation pressure 0.9 MPa Wheel load 90 kN Width x Length = 282 x 345 mm	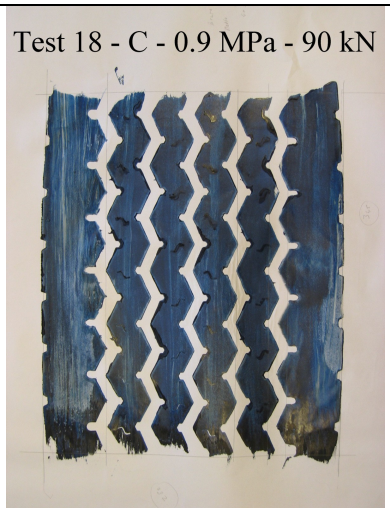
Test no. 19 Wheel type C (Super single) 385/65R22.5 Inflation pressure 0.9 MPa Wheel load 88.5 kN Width x Length = 282 x 342 mm	

Test no. 20 Wheel type D (Extra wide base) 495/45R22.5 Inflation pressure 0.9 MPa Wheel load 50 kN Width x Length = 430 x 165 mm	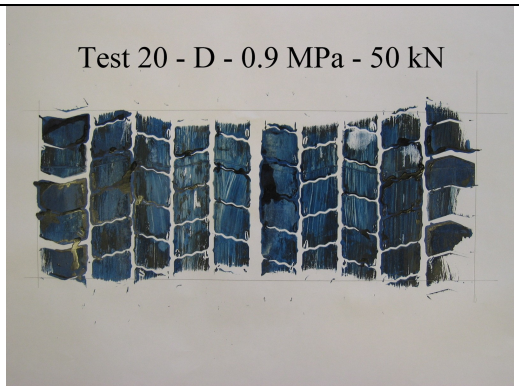
Test no. 21 Wheel type D (Extra wide base) 495/45R22.5 Inflation pressure 0.9 MPa Wheel load 90 kN Width x Length = 430 x 240 mm	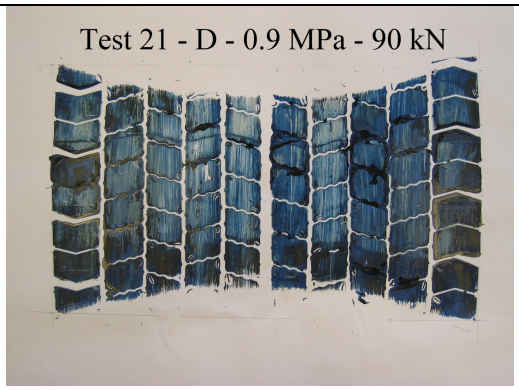

Annex B – Axle load model

This annex contains the result of the axle load measurements on the Moerdijk Bridge in 1998 and the graphical presentation of the lognormal functions that are based on the measurements.

This annex contains 12 figures:

1. The distribution functions for the single (type A), both measurement and lognormal
2. The distribution functions for the double (type B), both measurement and lognormal
3. The distribution functions for the super single (type C), both measurement and lognormal
4. The distribution functions for the total (30% A + 40% B + 30 % C), both measurement and lognormal
5. The distribution functions for the single (type A), double (type B), super (type C) and total (30% A + 40% B + 30 % C), lognormal
6. The distribution functions for the single (type A), double (type B), super (type C) and total (30% A + 40% B + 30 % C), measurement
7. The cumulative distribution functions for the single (type A), both measurement and lognormal
8. The cumulative distribution functions for the double (type B), both measurement and lognormal
9. The cumulative distribution functions for the super single (type C), both measurement and lognormal
10. The cumulative distribution functions for the total (30% A + 40% B + 30 % C), measurement, lognormal, fatigue load model 4 EN 1991-2
11. The cumulative distribution functions for the single (type A), double (type B), super (type C) and total (30% A + 40% B + 30 % C), lognormal, fatigue load model 4 EN 1991-2
12. The cumulative distribution functions for the single (type A), double (type B), super (type C) and total (30% A + 40% B + 30 % C), measurement, fatigue load model 4 EN 1991-2

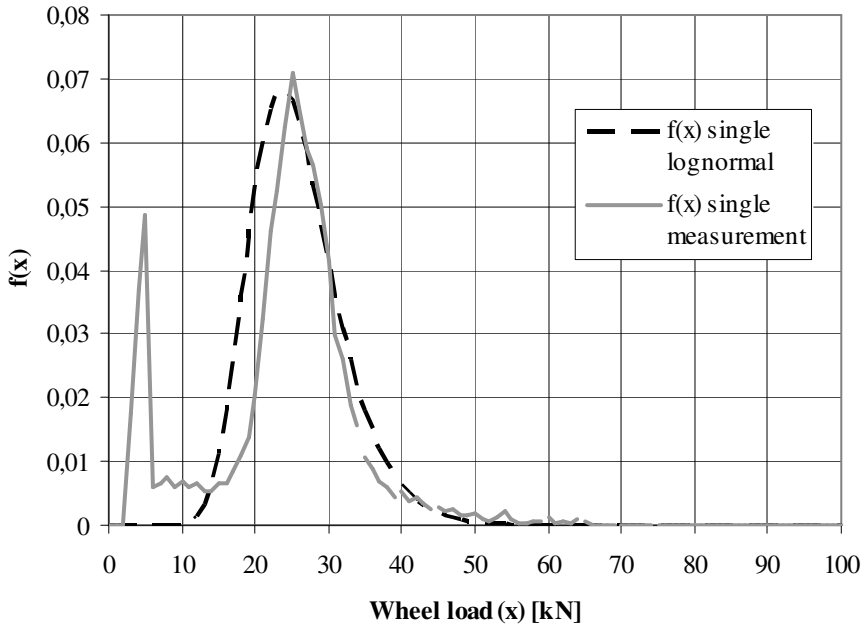

Figure B - 1: The distribution functions for the single (type A), both measurement and lognormal

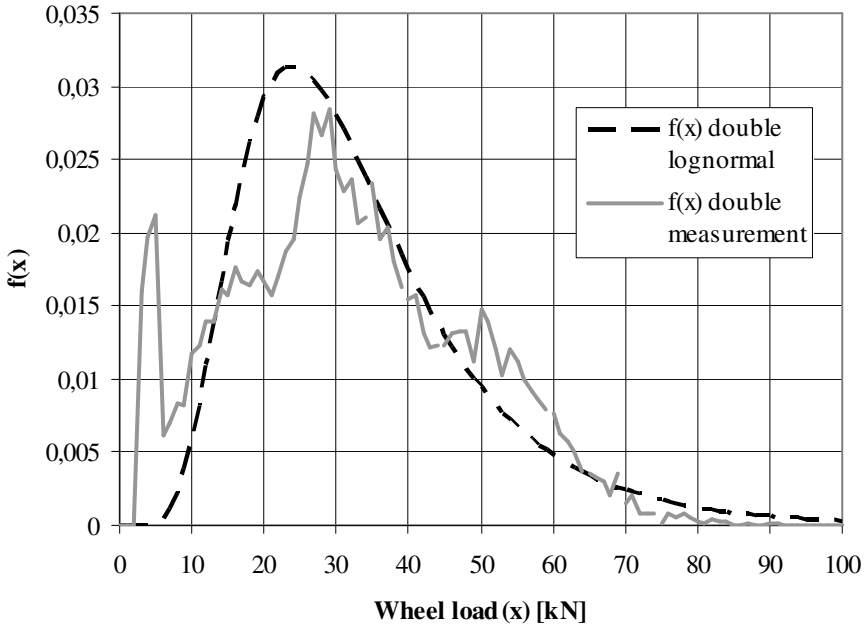

Figure B - 2: The distribution functions for the double (type B), both measurement and lognormal

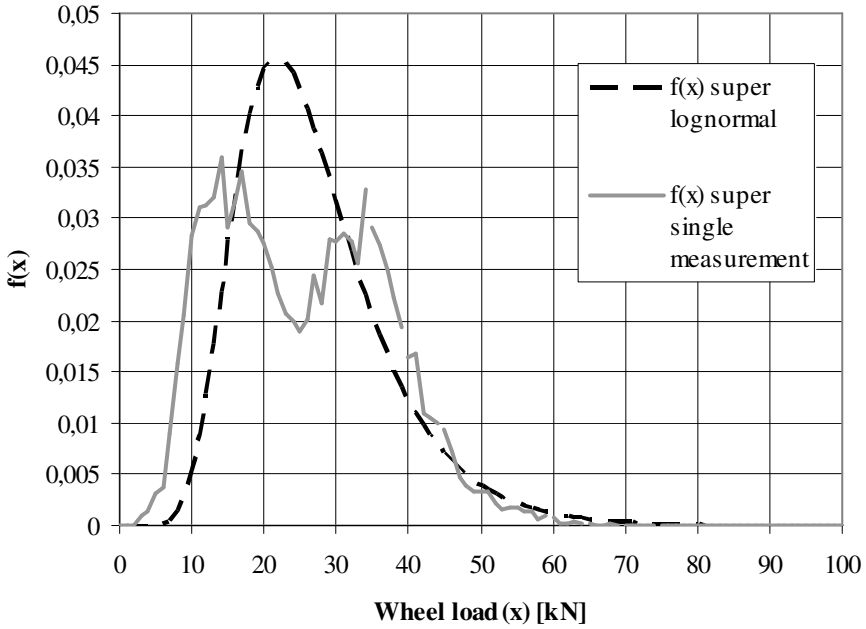

Figure B - 3: The distribution functions for the super single (type C), both measurement and lognormal

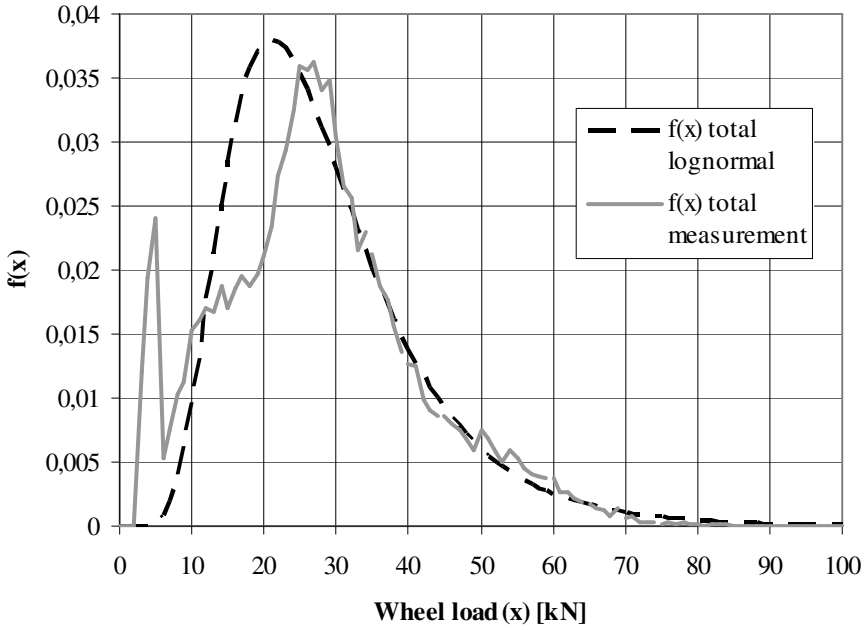

Figure B - 4: The distribution functions for the total (30% A + 40% B + 30 % C), both measurement and lognormal

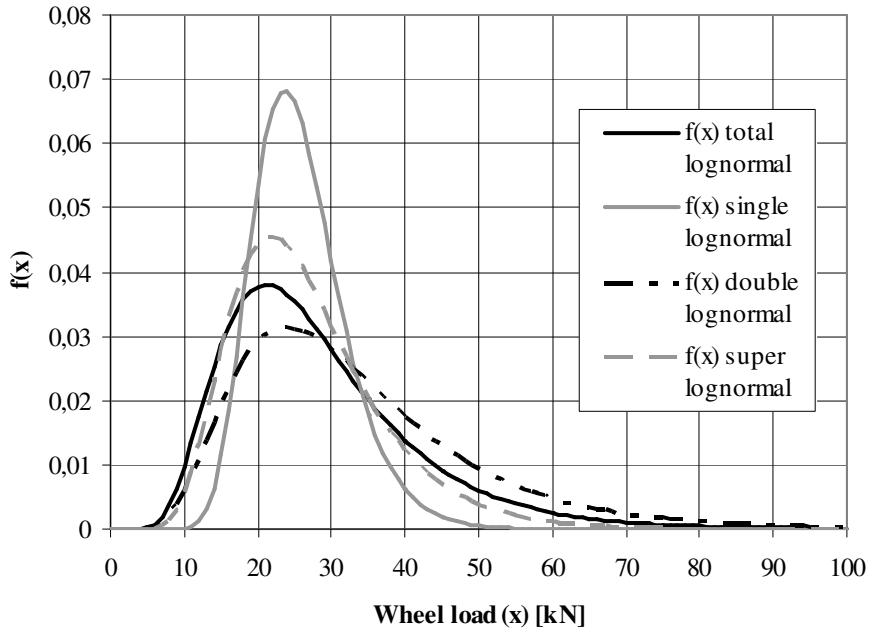

Figure B - 5: The distribution functions for the single (type A), double (type B), super (type C) and total (30% A + 40% B + 30 % C), lognormal

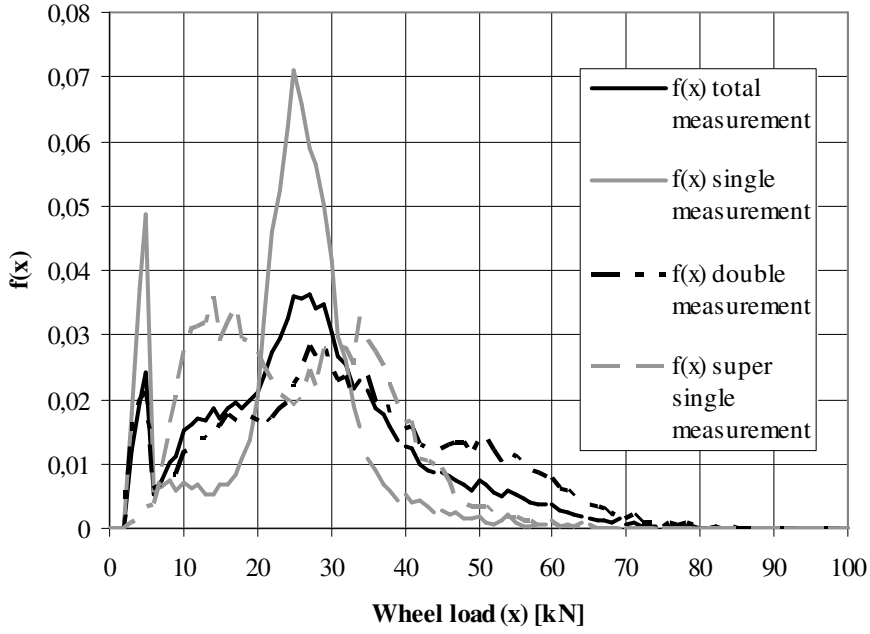

Figure B - 6: The distribution functions for the single (type A), double (type B), super (type C) and total (30% A + 40% B + 30 % C), measurement

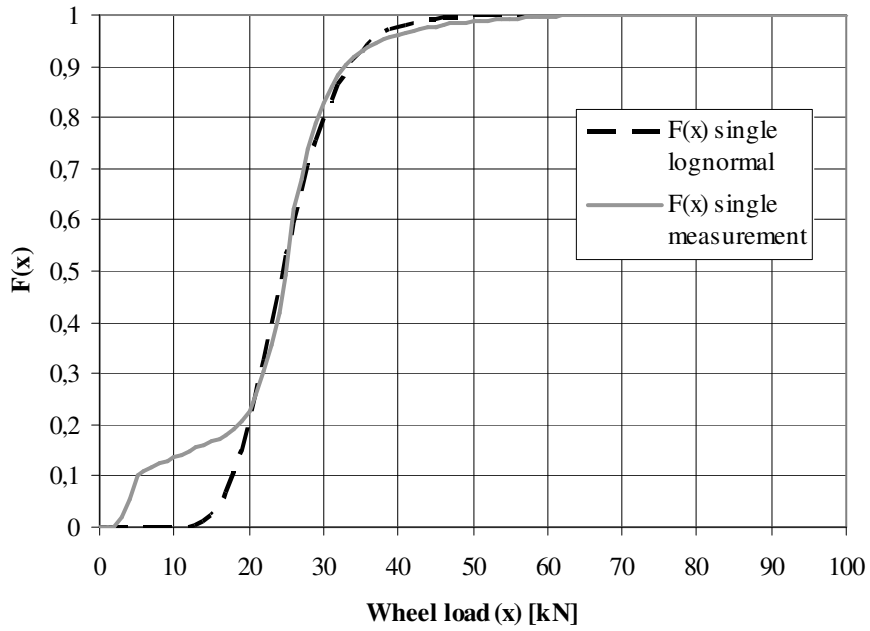

Figure B - 7: The cumulative distribution functions for the single (type A), both measurement and lognormal

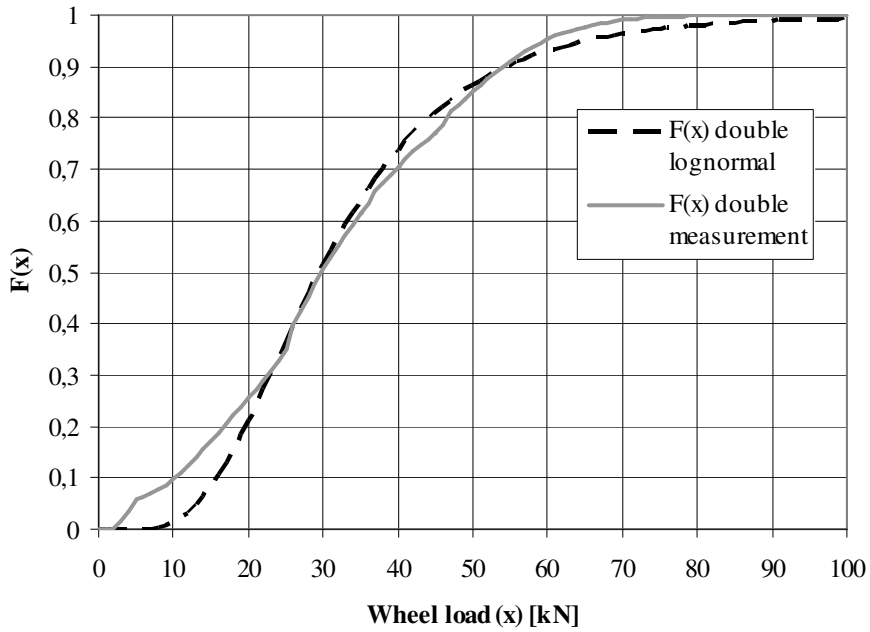

Figure B - 8: The cumulative distribution functions for the double (type B), both measurement and lognormal

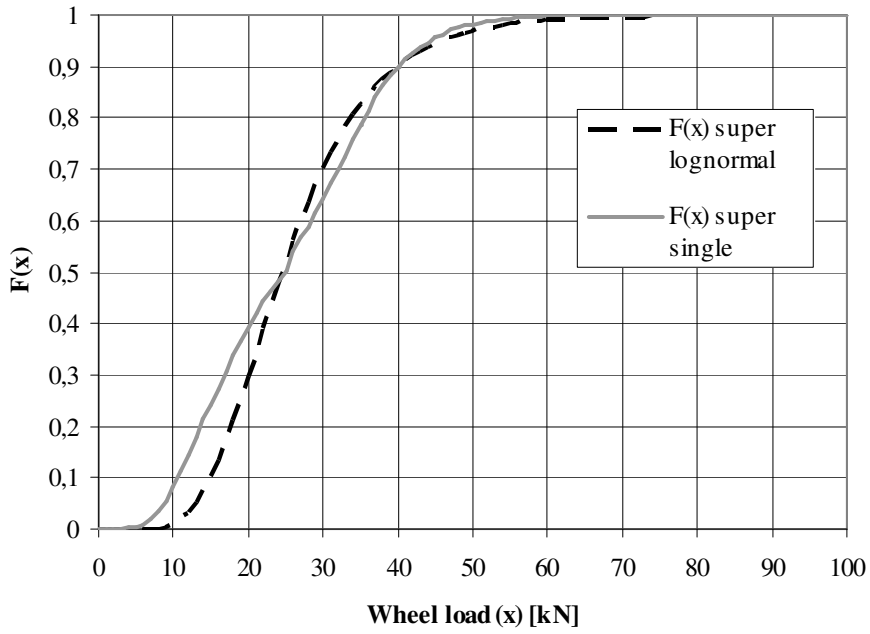

Figure B - 9: The cumulative distribution functions for the super single (type C), both measurement and lognormal

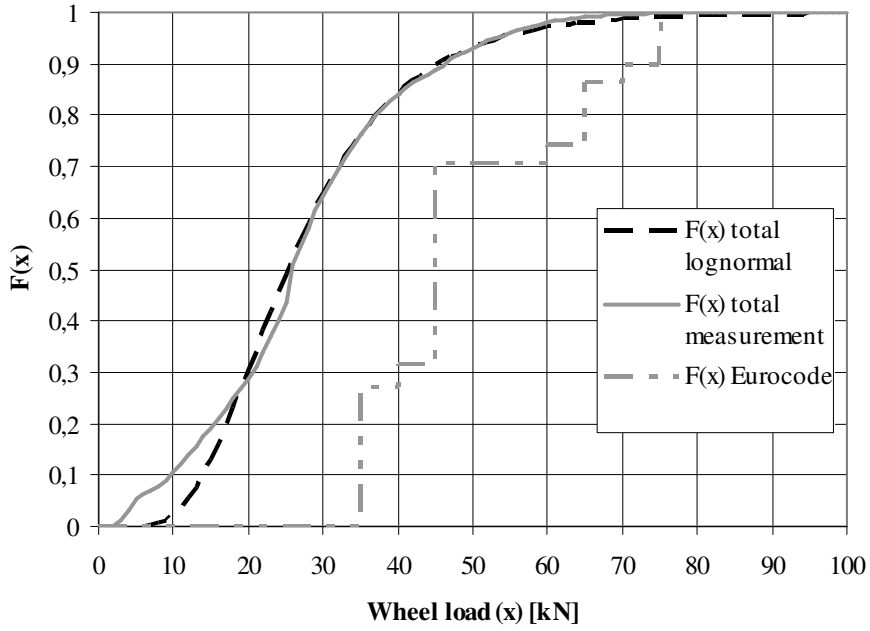

Figure B - 10: The cumulative distribution functions for the total (30% A + 40% B + 30 % C), measurement, lognormal, fatigue load model 4 EN 1991 – Part 2

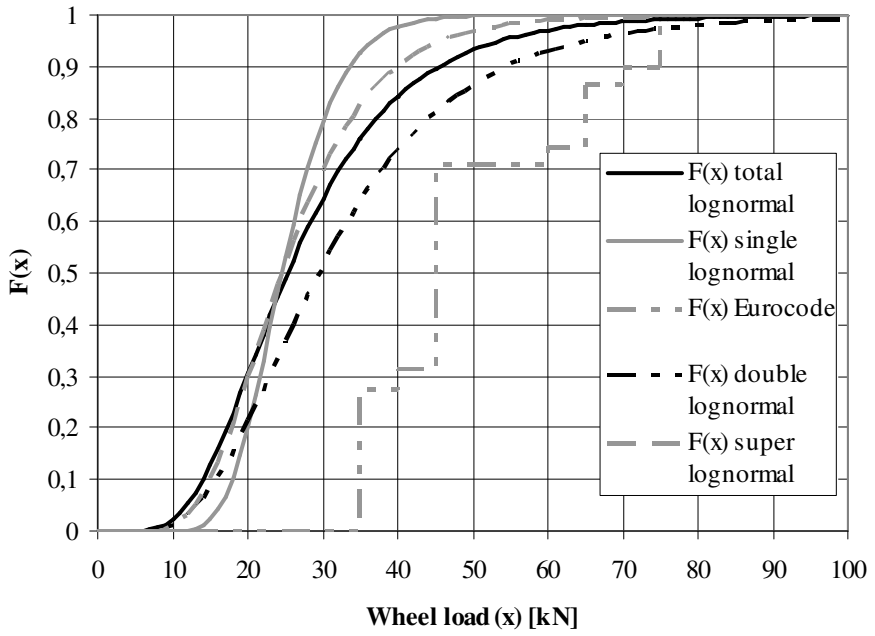

Figure B - 11: The cumulative distribution functions for the single (A), double (B), super (C) and total (30% A + 40% B + 30 % C), lognormal, fatigue load model 4 EN 1991 – Part 2

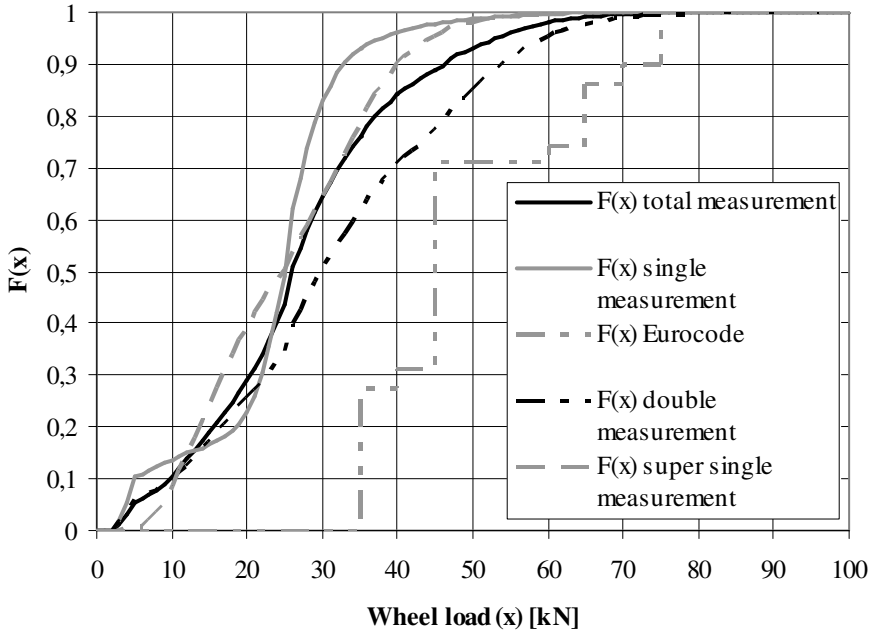

Figure B - 12: The cumulative distribution functions for the single (A), double (B), super (C) and total (30% A + 40% B + 30 % C), measurement, fatigue load model 4 EN 1991 – Part 2

Annex C – Strain gauges test panel A phases 1 and 2

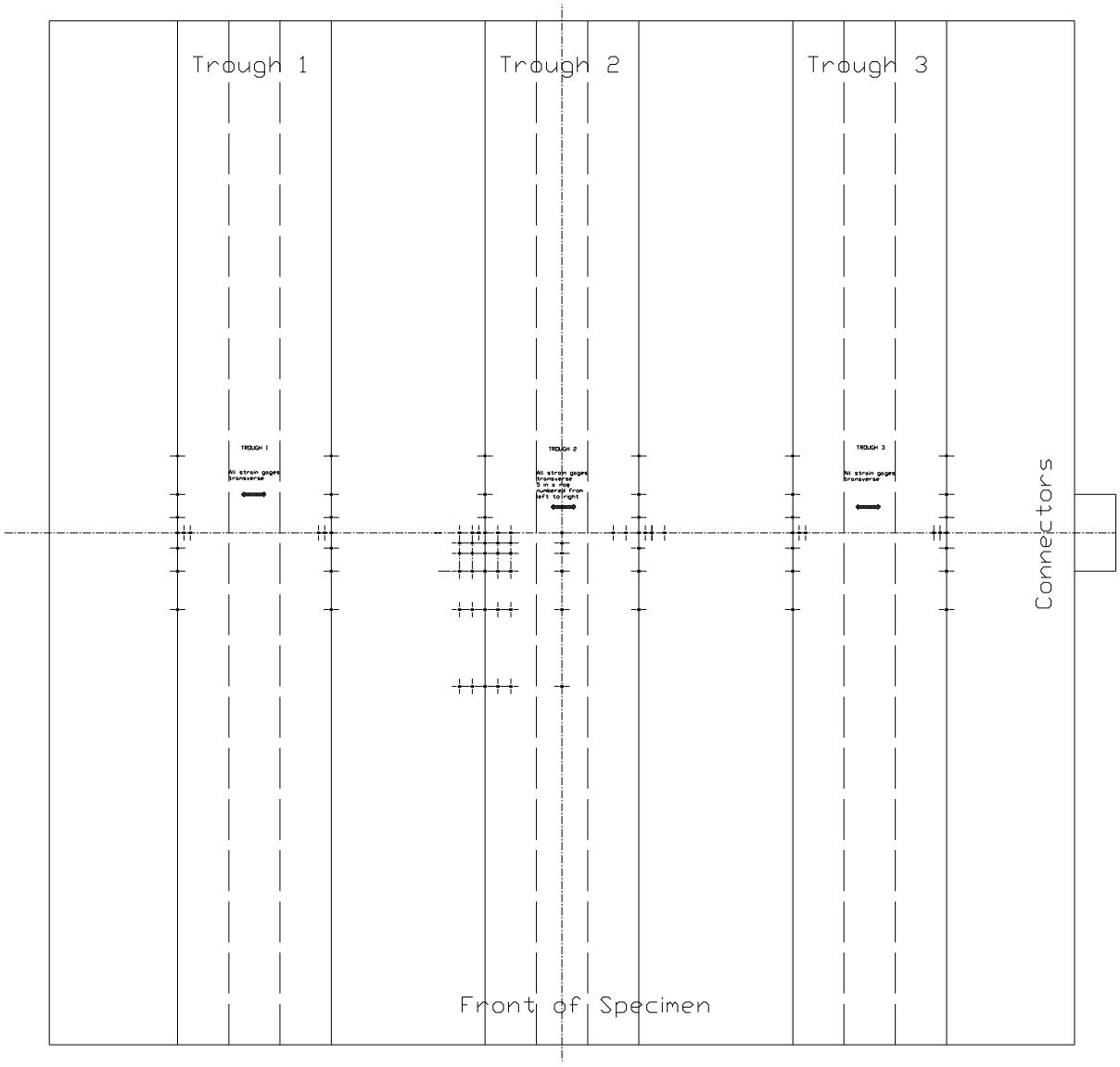

Figure C-1: Total overview applied strain gauges

Only locations are indicated. See figures C-2 to C-5 for more details. All gauges measure in transverse direction.

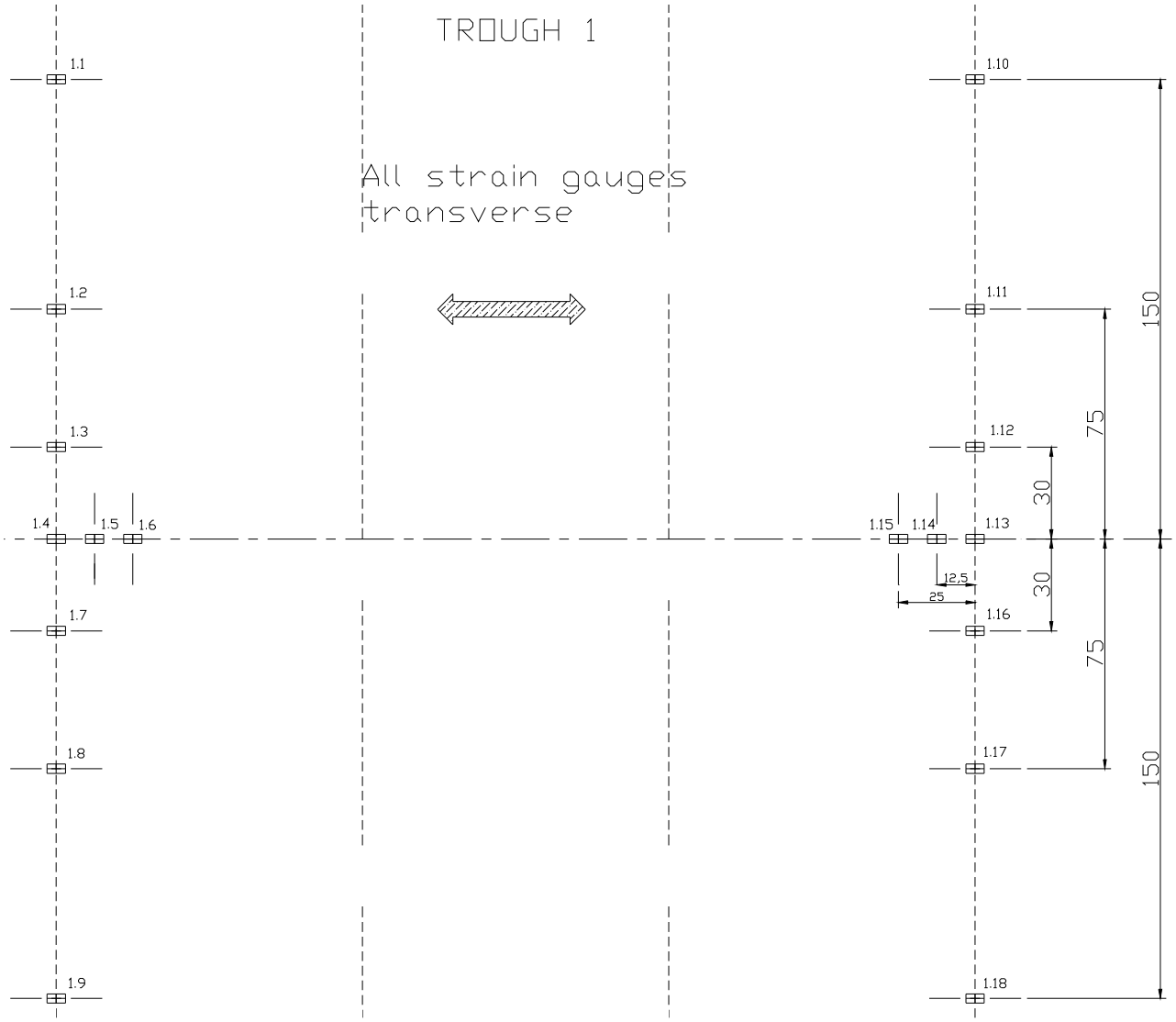

Figure C-2: Strain gauges trough 1

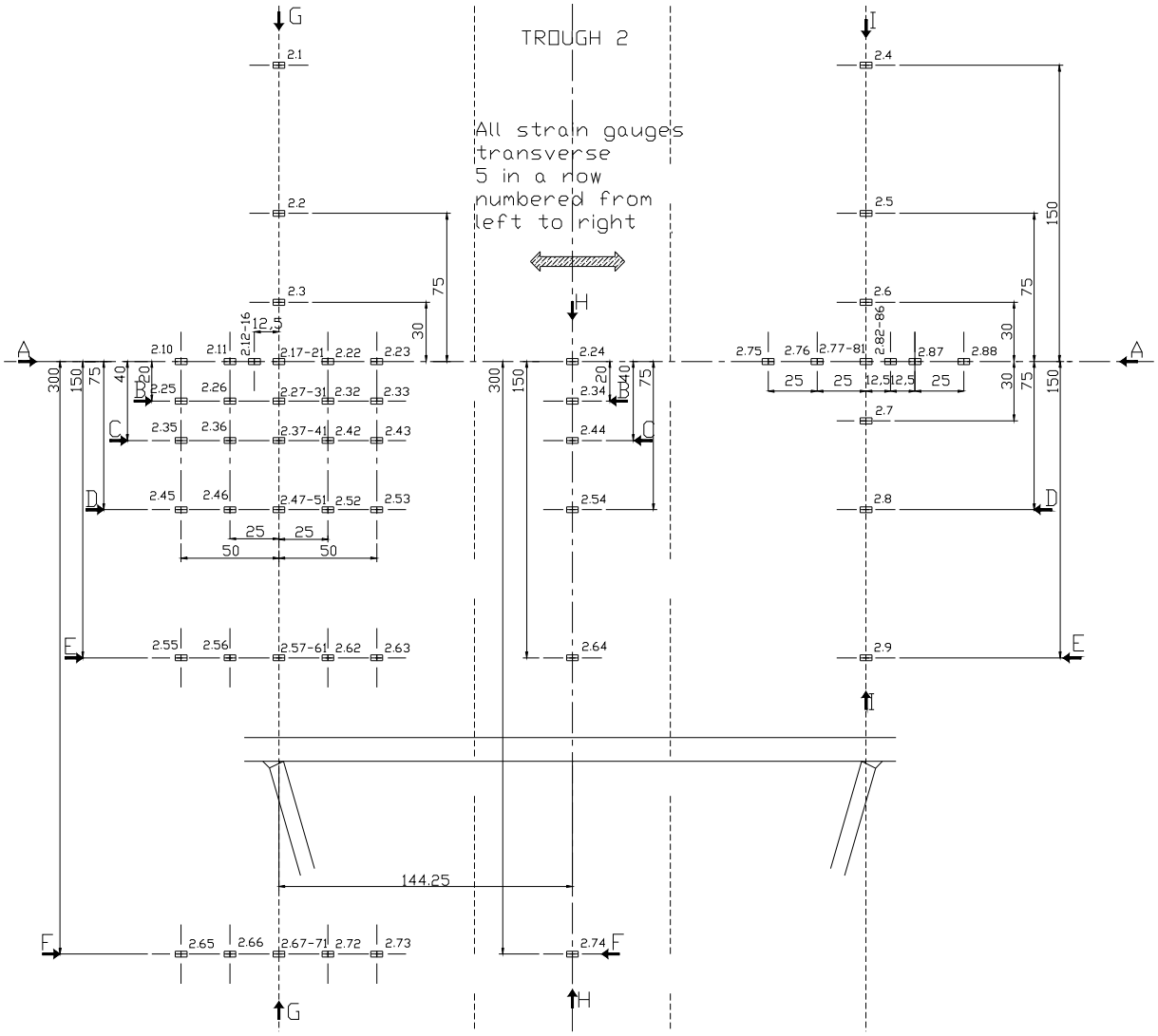

Figure C-3: Strain gauges trough 2

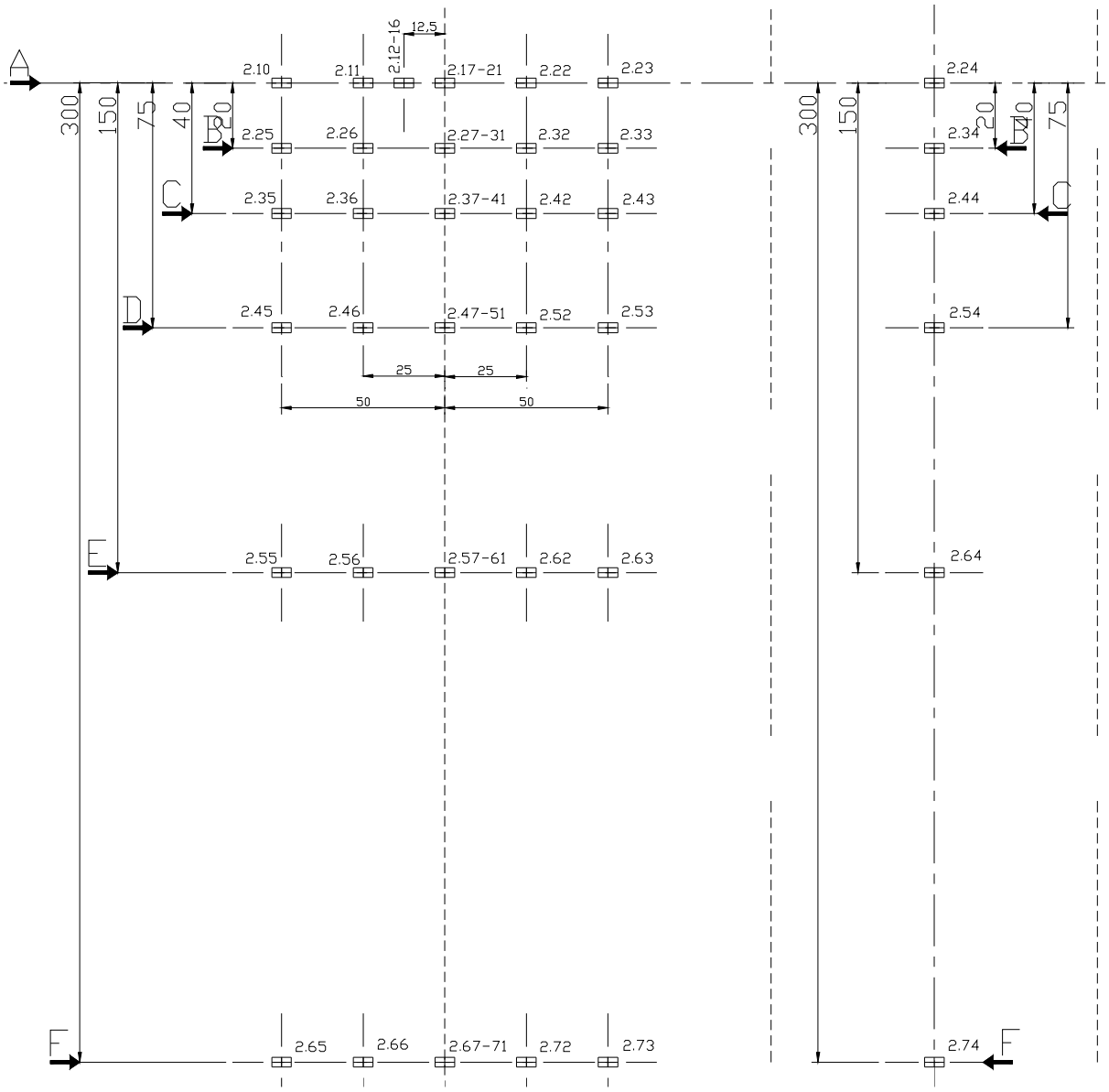

Figure C-4: Detail view strain gauges trough 2

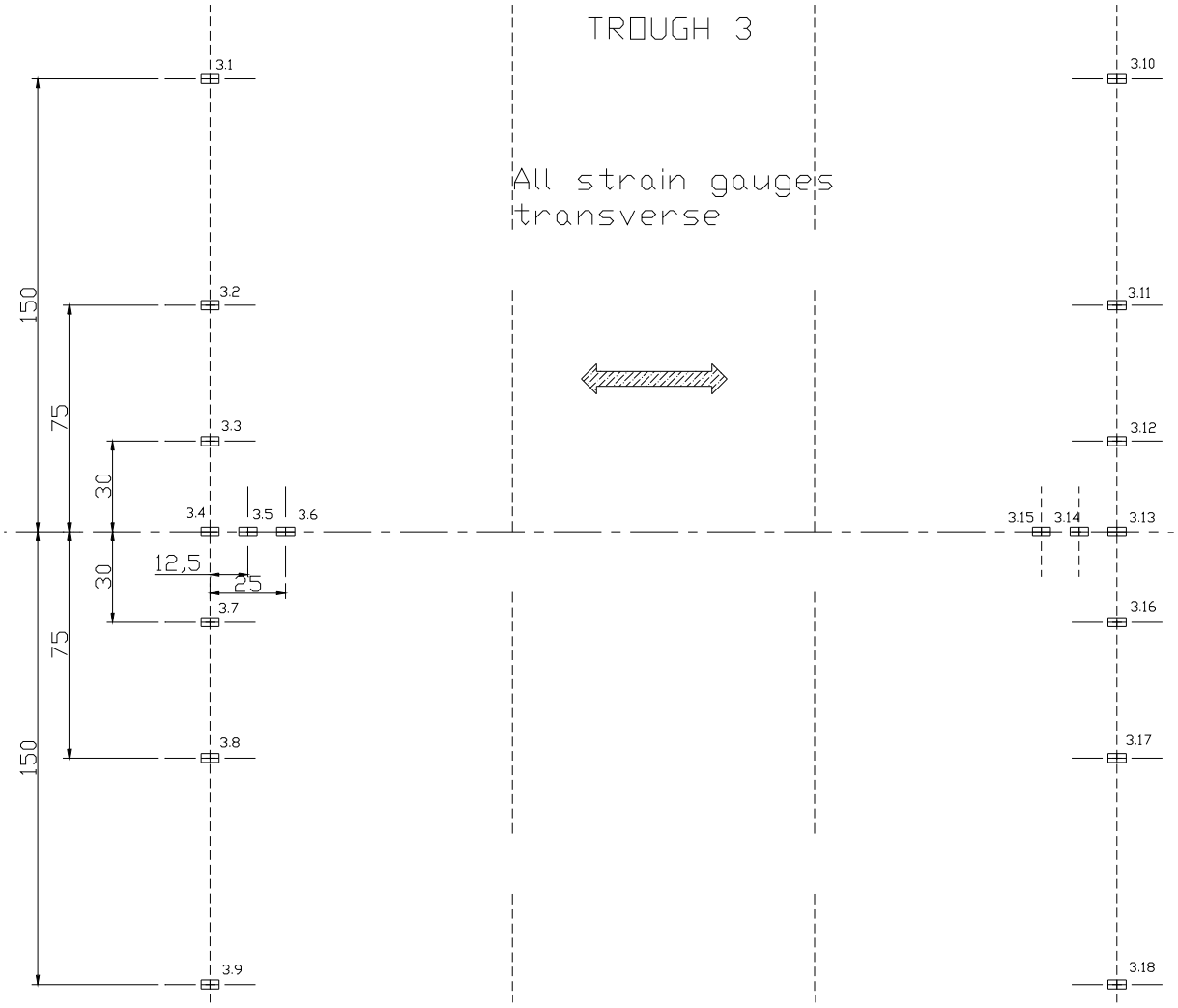

Figure C-5: Strain gauges trough 3

Annex D – Strain gauges Lintrack test panel

Strain gauges section 1 trough 2

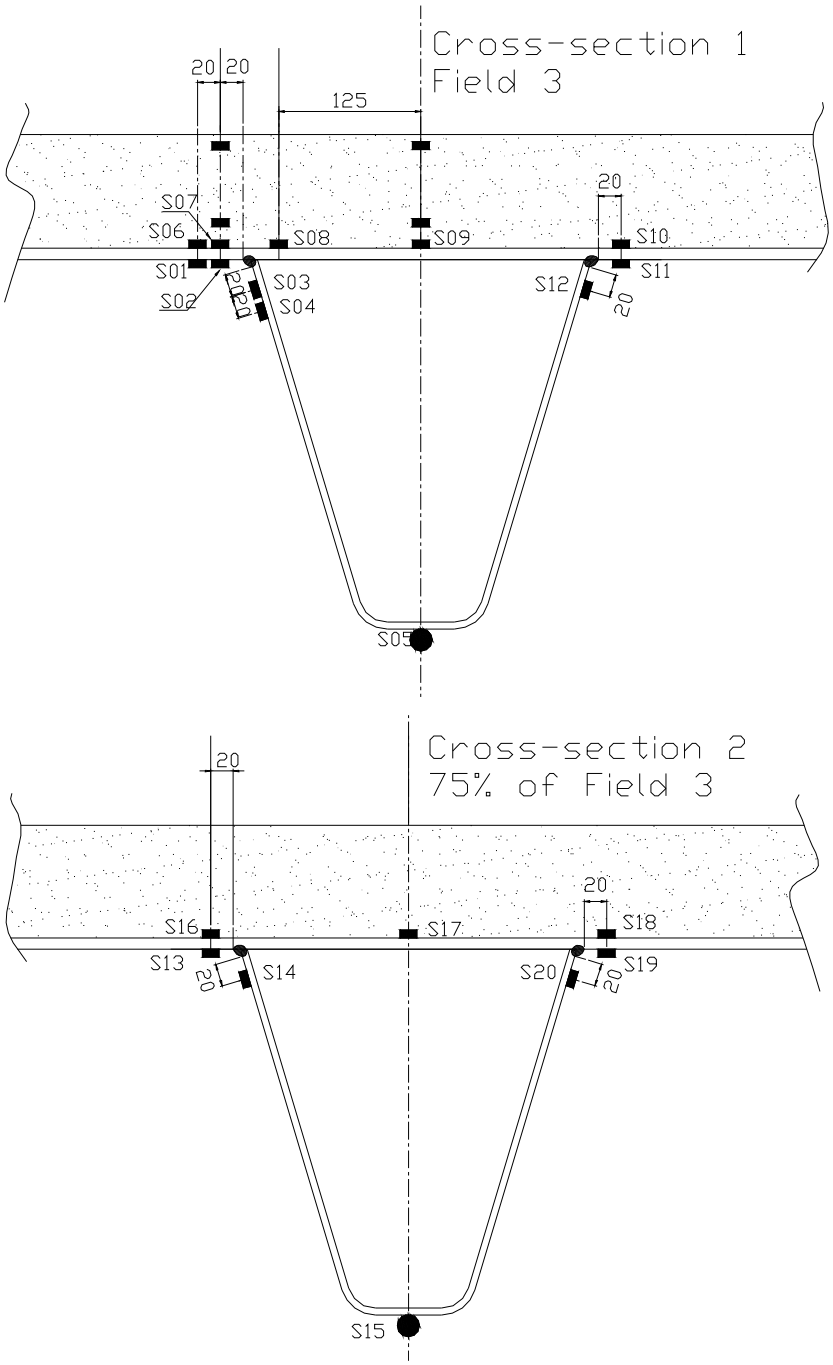

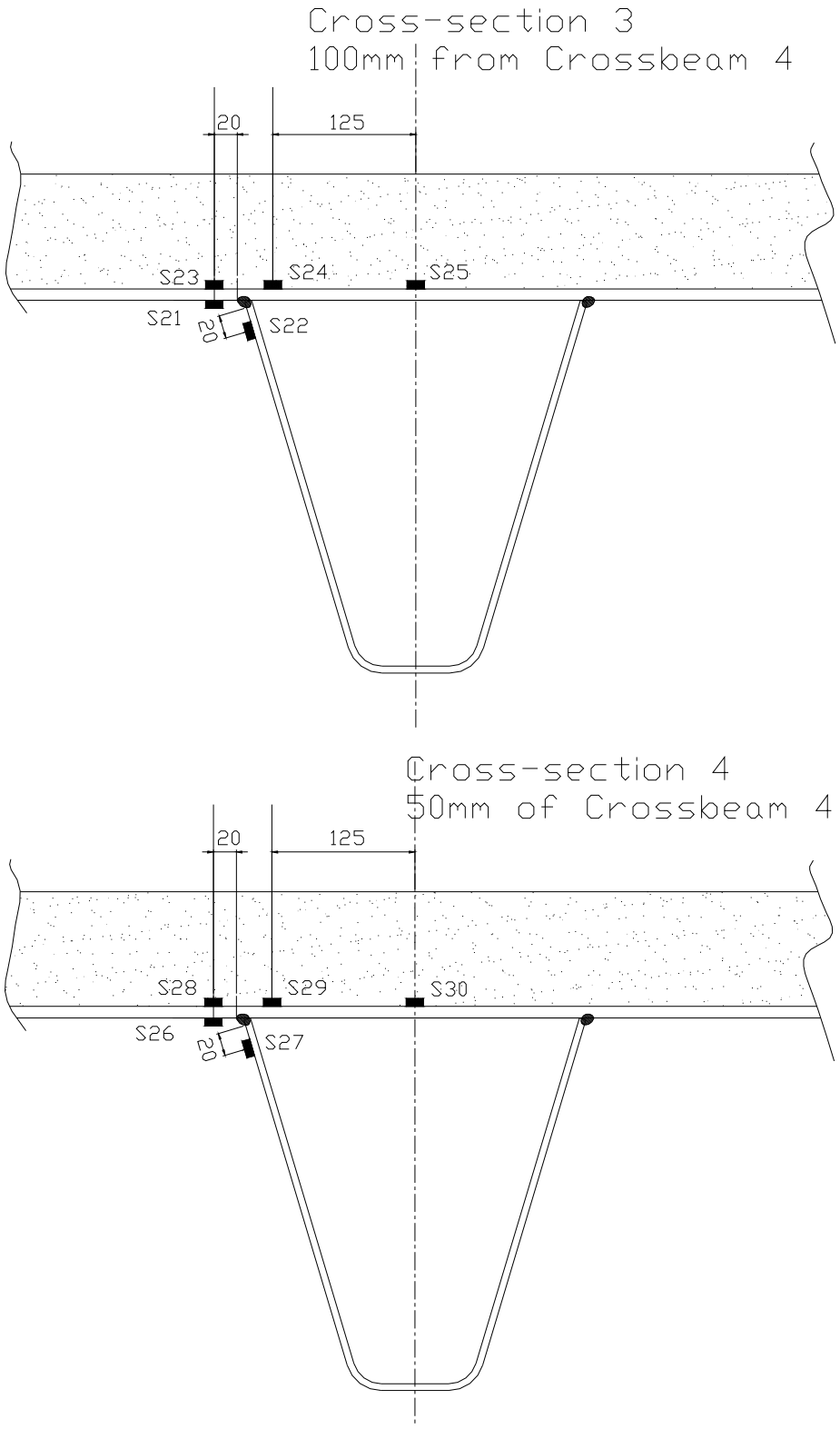
Cross-section 3
100mm from Crossbeam 4
20
125
S23
S24
S25
S21
20
S22
Cross-section 4
50mm of Crossbeam 4
20
125
S28
S29
S30
S26
20
S27

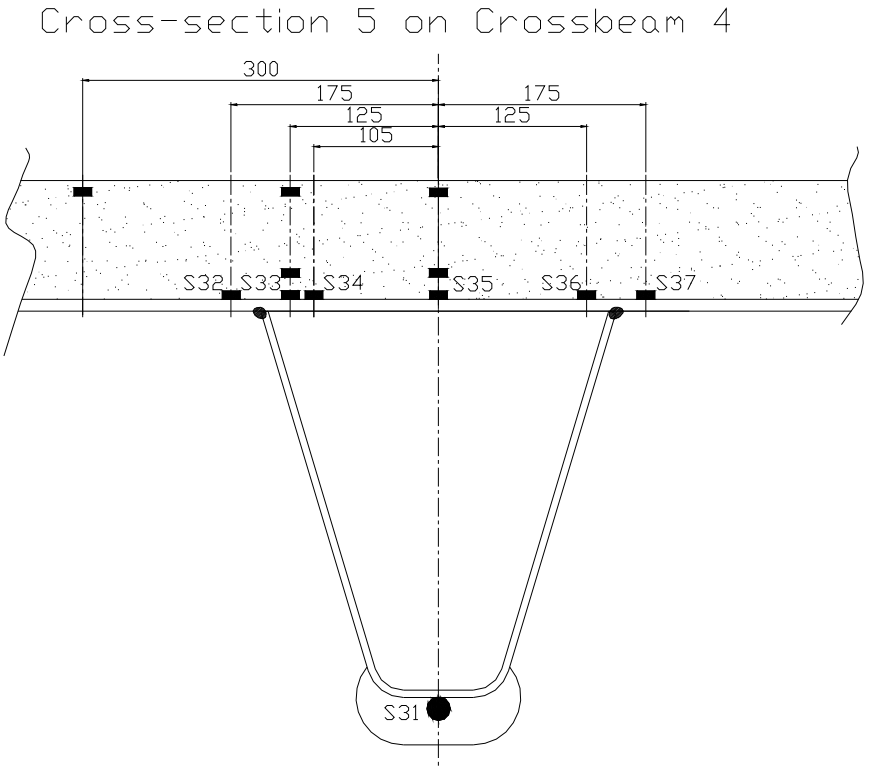
Cross-section 5 on Crossbeam 4
300
175
175
125
125
105
S32
S33
S34
S35
S36
S37
S31

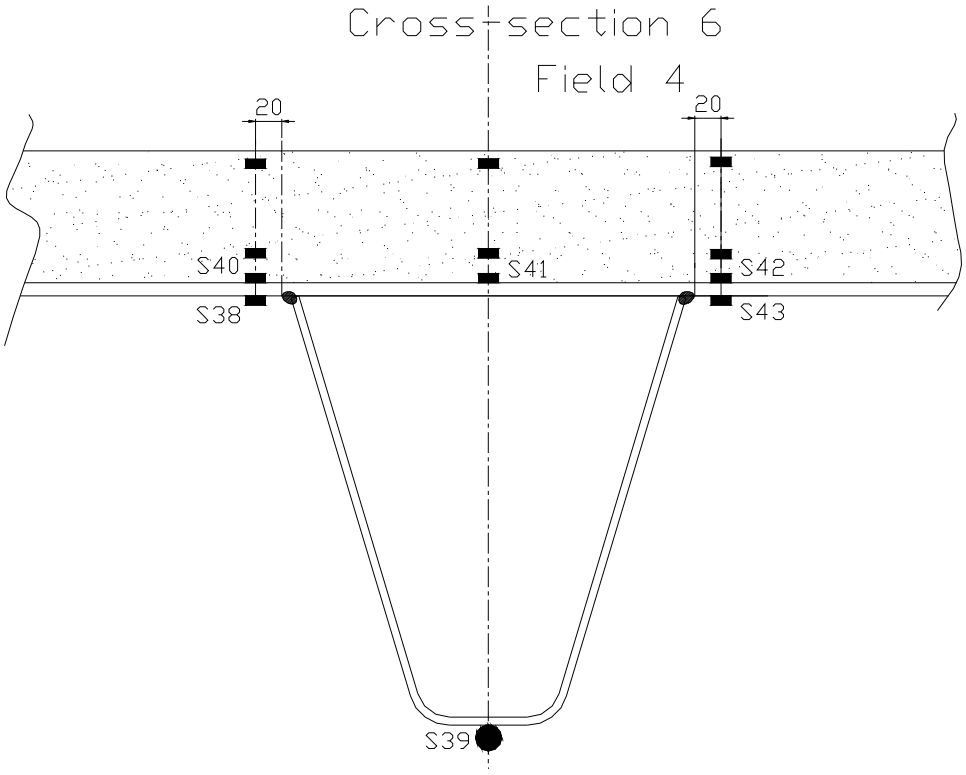
Cross-section 6
Field 4
20
20
S40
S41
S42
S38
S43
S39

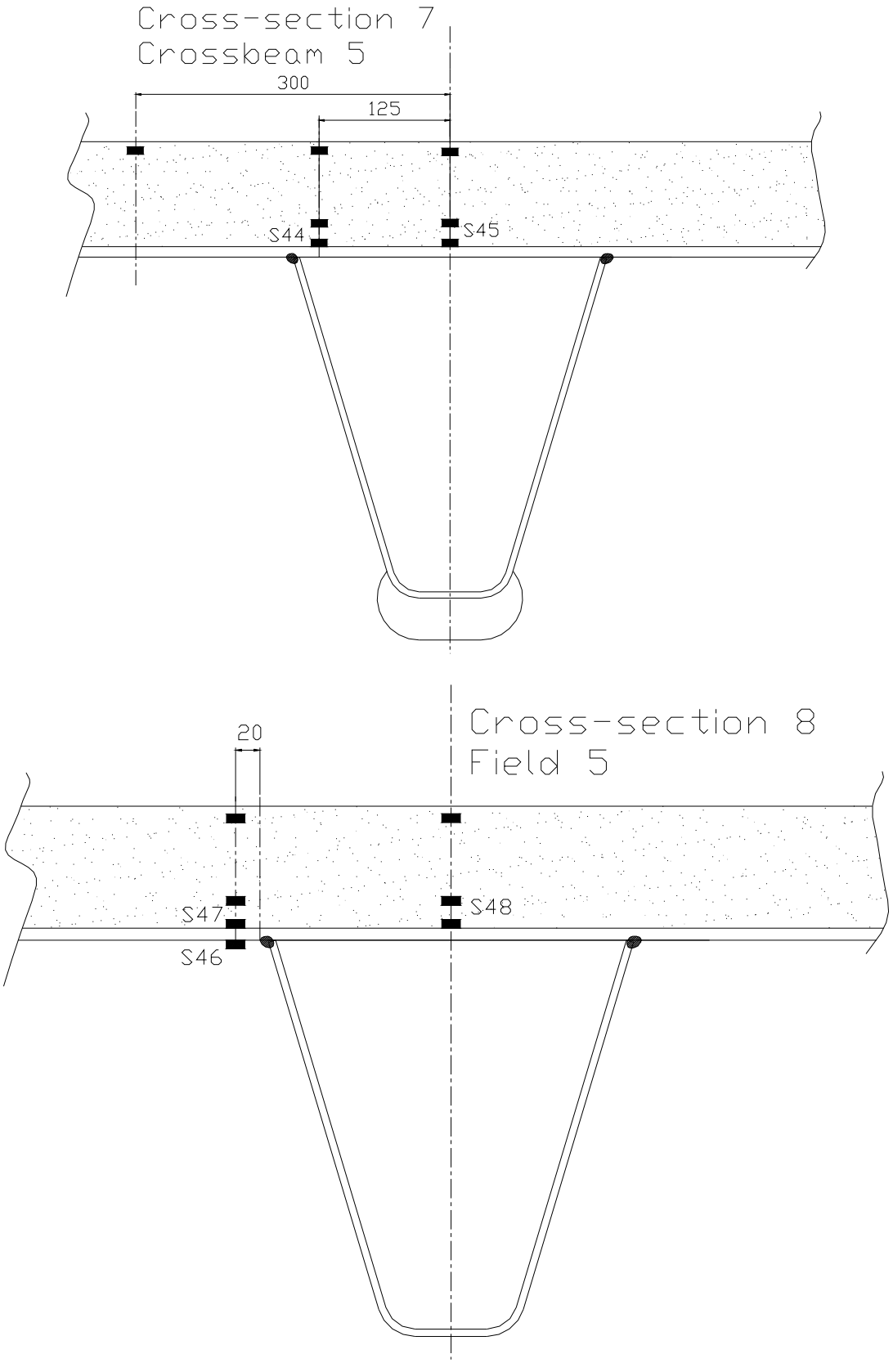
Cross-section 7
Crossbeam 5
300
125
S44
S45
Cross-section 8
Field 5
20
S47
S46
S48

Strain gauges section 2 trough 5

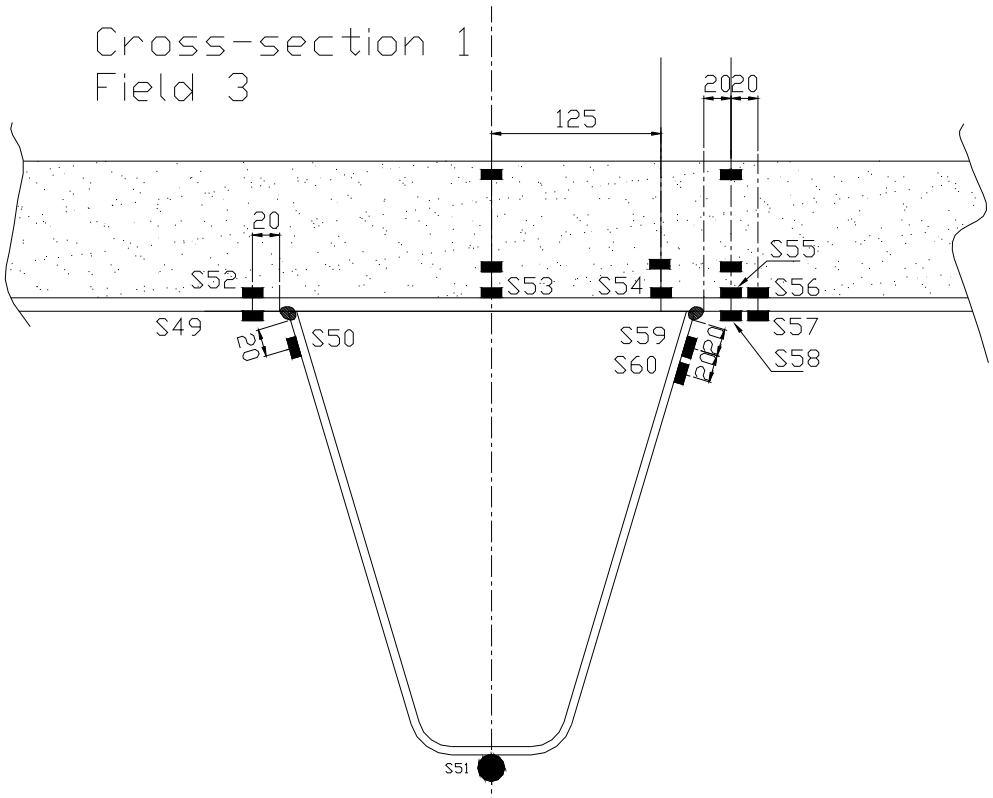

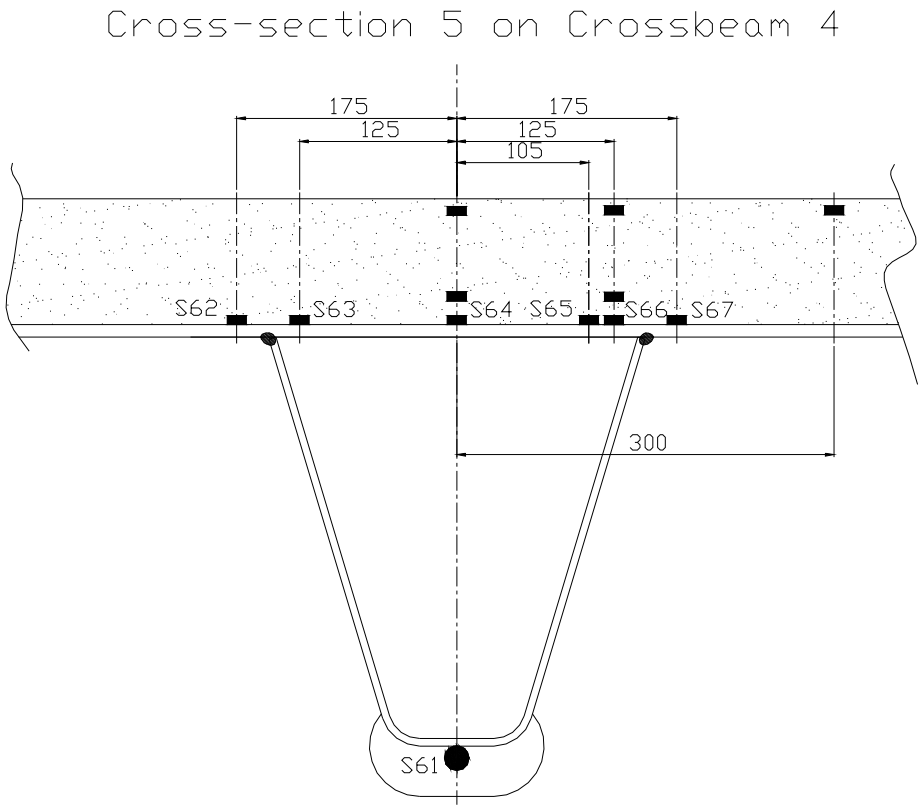

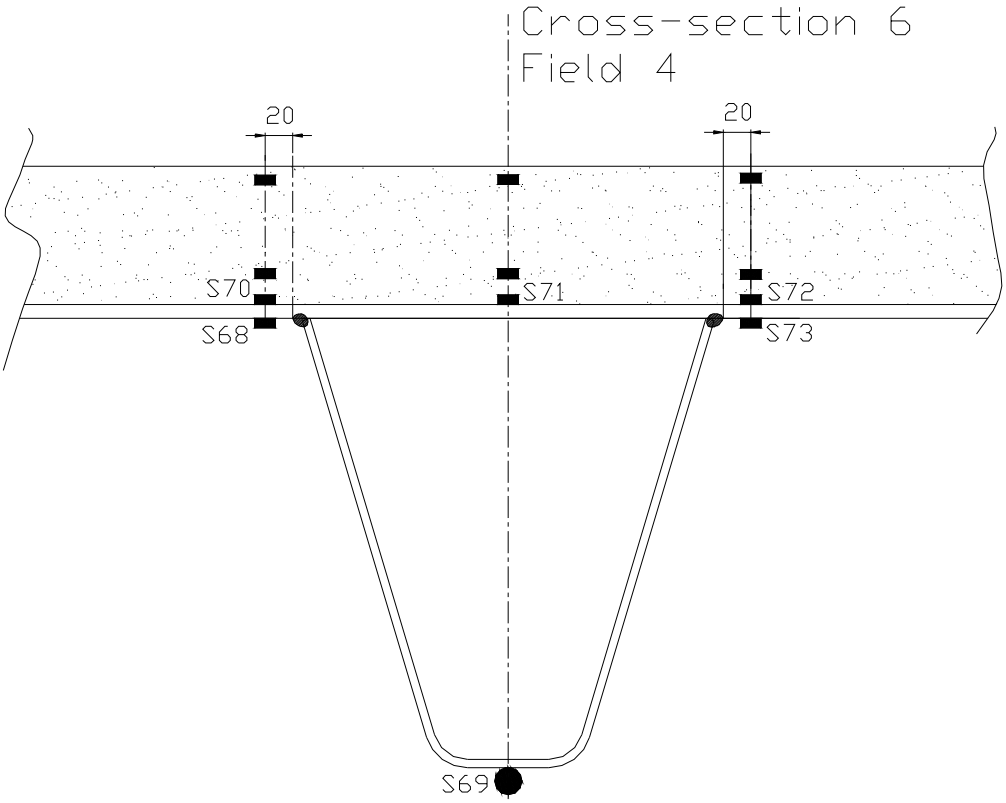
Cross-section 6
Field 4
20
20
S70
S71
S72
S68
S73
S69

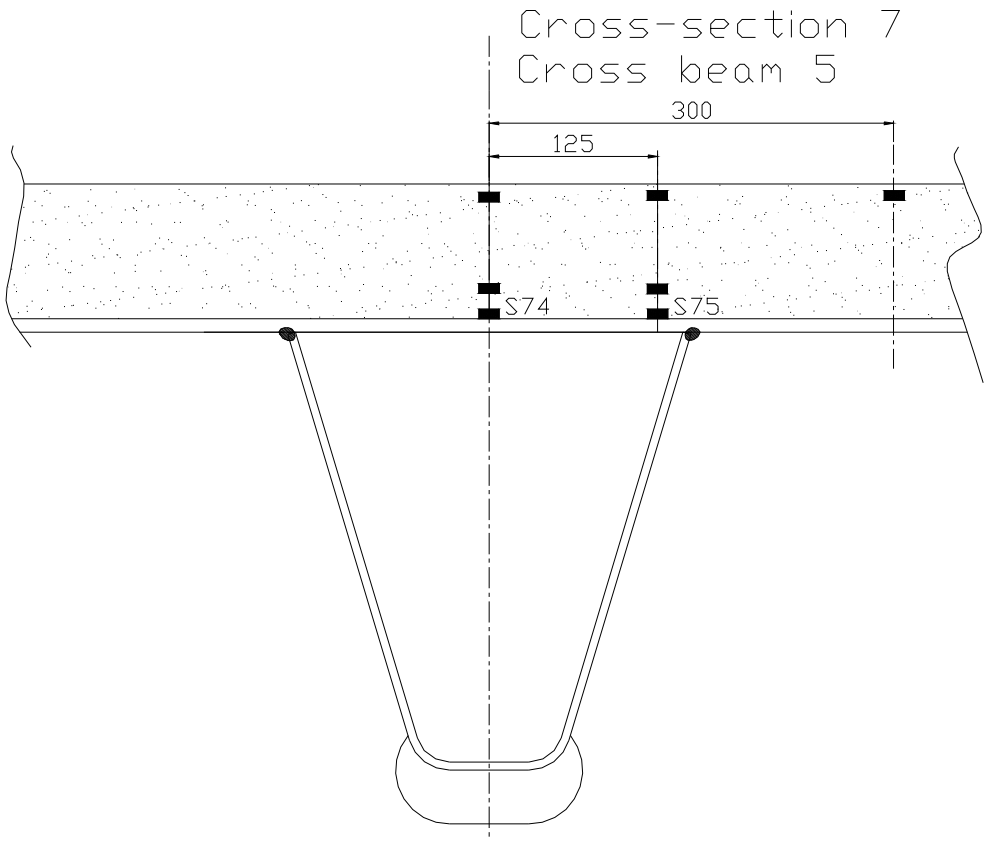
Cross-section 7
Cross beam 5
300
125
S74
S75

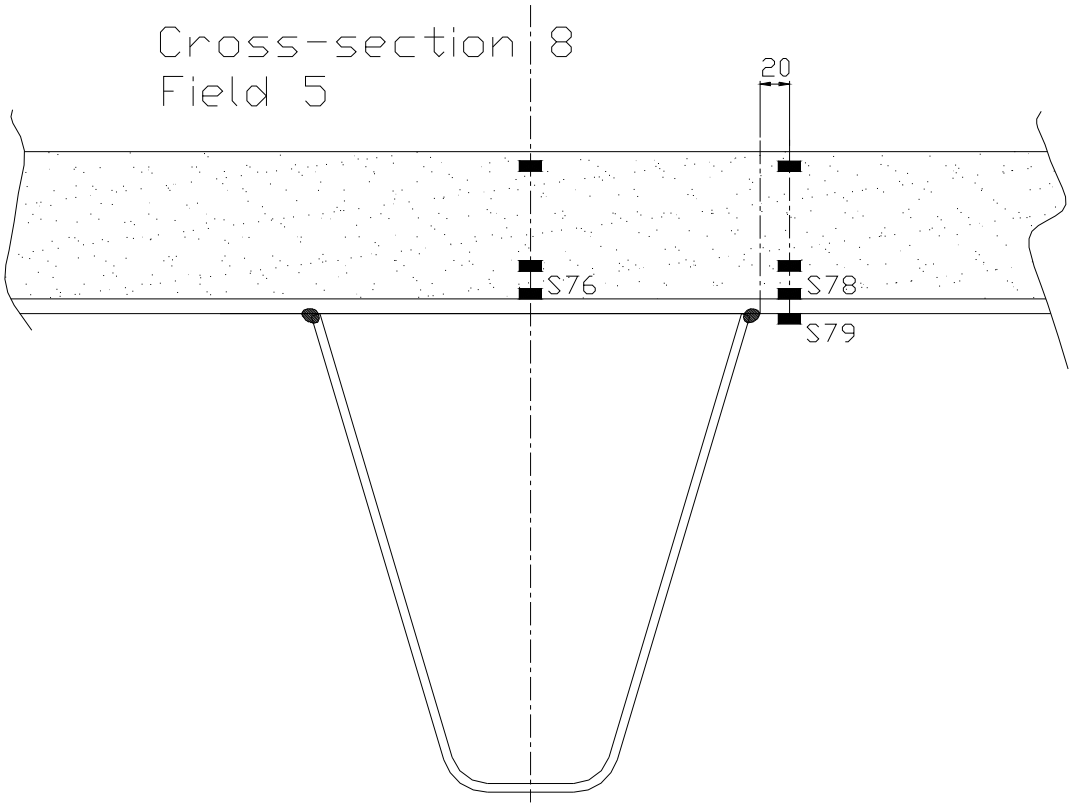
Cross-section 8
Field 5
20
S76
S78
S79

Annex E –Measured strains Lintrack test panel

Table E - 1: Strains for some gauges at the steel deck plate at deck plate crack location

No..	Location	Gauge	Section	Surfacing	Wheel	F (kN)	V (km/h)	Remarks	Max/min ($x10^{-6}$)
C001	Cross beam 4	S33	S1	No	C	50	02	Reference, deck plate crack	455
C002	Cross beam 4	S36	S1	No	C	50	02	Analogous strain gauge	472
C003	Cross beam 5	S44	S1	No	C	50	02	Analogous strain gauge	489
C004	Cross beam 4	S33	S1	MA 0 °C	C	50	02	Variation surfacing temperature	108
C005	Cross beam 4	S33	S1	MA 15 °C	C	50	02	Variation surfacing temperature	382
C006	Cross beam 4	S33	S1	MA 30 °C	C	50	02	Variation surfacing temperature	429
C007	Cross beam 4	S33	S1	No	C	25	02	Variation wheel load	282
C008	Cross beam 4	S33	S1	No	C	50	20	Variation velocity	479
A001	Cross beam 4	S33	S1	No	A	50	02	Variation wheel type	454
B001	Cross beam 4	S33	S1	No	B	50	02	Variation wheel type	312
D001	Cross beam 4	S33	S1	No	D	50	02	Variation wheel type	311
A004	Cross beam 4	S33	S1	MA 0 °C	A	50	02	Variation wheel type	177
B004	Cross beam 4	S33	S1	MA 0 °C	B	50	02	Variation wheel type	86
D004	Cross beam 4	S33	S1	MA 0 °C	D	50	02	Variation wheel type	81
A007	Cross beam 4	S33	S1	No	C	25	02	Variation wheel type	318
B007	Cross beam 4	S33	S1	No	C	25	02	Variation wheel type	193
D007	Cross beam 4	S33	S1	No	C	25	02	Variation wheel type	194
C011	Cross beam 4	S66	S2	No	C	50	02	Reference, deck plate crack	466
C014	Cross beam 4	S66	S2	ZOK 0 °C	C	50	02	Variation surfacing temperature	63
C015	Cross beam 4	S66	S2	ZOK 15 °C	C	50	02	Variation surfacing temperature	165
C016	Cross beam 4	S66	S2	ZOK 30 °C	C	50	02	Variation surfacing temperature	226
C019	Cross beam 4	S35	S1	No	C	50	02	Reference, above trough	-566
C021	Cross beam 4	S35	S1	MA 0 °C	C	50	02	Variation surfacing temperature	-159
C022	Cross beam 4	S35	S1	MA 15 °C	C	50	02	Variation surfacing temperature	-478
C023	Cross beam 4	S35	S1	MA 30 °C	C	50	02	Variation surfacing temperature	-530
C028	Cross beam 4	S64	S2	No	C	50	02	Reference, above trough	-588
C030	Cross beam 4	S64	S2	ZOK 0 °C	C	50	02	Variation surfacing temperature	-67
C031	Cross beam 4	S64	S2	ZOK 15 °C	C	50	02	Variation surfacing temperature	-173
C032	Cross beam 4	S64	S2	ZOK 30 °C	C	50	02	Variation surfacing temperature	-245

Table E - 2: Strains for some gauges at the membrane layer at crossbeam location

No..	Location	Gauge	Section	Surfacing	Wheel	F (Kn)	v (km/h)	Remarks	Max/min ($x10^{-6}$)
C035	Cross beam 4	M33	S1	MA 15 °C	C	50	02	Reference, deck plate crack	X
C036	Cross beam 5	M44	S1	MA 15 °C	C	50	02	Analogous strain gauge	-758
C037	Cross beam 4	M33	S1	MA 0 °C	C	50	02	Variation surfacing temperature	-348
C038	Cross beam 4	M33	S1	MA 30 °C	C	50	02	Variation surfacing temperature	X
C039	Cross beam 4	M33	S1	MA 15 °C	C	25	20	Variation wheel load & velocity	-387
C040	Cross beam 4	M33	S1	MA 15 °C	C	50	20	Variation velocity	-659
C041	Cross beam 4	M66	S2	ZOK 15 °C	C	50	02	Reference, indicative for crack	X
C043	Cross beam 4	M66	S2	ZOK 0 °C	C	50	02	Variation surfacing temperature	X
C044	Cross beam 4	M66	S2	ZOK 30 °C	C	50	02	Variation surfacing temperature	X
C047	Cross beam 4	M35	S1	MA 15 °C	C	50	02	Reference, above trough	516
C049	Cross beam 4	M35	S1	MA 0 °C	C	50	02	Variation surfacing temperature	267
C050	Cross beam 4	M35	S1	MA 30 °C	C	50	02	Variation surfacing temperature	481
C053	Cross beam 4	M64	S2	ZOK 15 °C	C	50	02	Reference, above trough	X
C055	Cross beam 4	M64	S2	ZOK 0 °C	C	50	02	Variation surfacing temperature	-106
C056	Cross beam 4	M64	S2	ZOK 30 °C	C	50	02	Variation surfacing temperature	X

Table E - 3: Strain for some gauges at the top of the surfacing at crossbeam location

No..	Location	Gauge	Section	Surfacing	Wheel	F (kN)	v (km/h)	Remarks	Max/min ($x10^{-6}$)
C059	Cross beam 4	D33	S1	MA 15 °C	C	50	02	Reference, deck plate crack	1215
C060	Cross beam 5	D44	S1	MA 15 °C	C	50	02	Analogous strain gauges	X
C061	Cross beam 4	D33	S1	MA 0 °C	C	50	02	Variation surfacing temperature	313
C062	Cross beam 4	D33	S1	MA 30 °C	C	50	02	Variation surfacing temperature	X
C063	Cross beam 4	D33	S1	MA 15 °C	C	25	20	Variation wheel load & velocity	582
C064	Cross beam 4	D33	S1	MA 15 °C	C	50	20	Variation velocity	913
C065	Cross beam 4	D66	S2	ZOK 15 °C	C	50	02	Reference, deck plate crack	X
C067	Cross beam 4	D66	S2	ZOK 0 °C	C	50	02	Variation surfacing temperature	96
C068	Cross beam 4	D66	S2	ZOK 30 °C	C	50	02	Variation surfacing temperature	349
C071	Cross beam 4	D35	S1	MA 15 °C	C	50	02	Reference, above trough	X
C073	Cross beam 4	D35	S1	MA 0 °C	C	50	02	Variation surfacing temperature	-424
C074	Cross beam 4	D35	S1	MA 30 °C	C	50	02	Variation surfacing temperature	X
C077	Cross beam 4	D64	S2	ZOK 15 °C	C	50	02	Reference, above trough	X
C079	Cross beam 4	D64	S2	ZOK 0 °C	C	50	02	Variation surfacing temperature	-347
C080	Cross beam 4	D64	S2	ZOK 30 °C	C	50	02	Variation surfacing temperature	-927

Table E - 4: Strains for some gauges at longitudinal weld trough-deck plate

No..	Location	Gauge	Section	Surfacing	Wheel	F (kN)	v (km/h)	Remarks	Max/min ($x10^{-6}$)
C172	Field 3	S03	S1	No	C	50	02	Reference, weld crack	-439
C173	Field 3	S12	S1	No	C	50	02	Analogous strain gauge	-413
C176	Field 3	S03	S1	MA 0 °C	C	50	02	Variation surfacing temperature	-197
C177	Field 3	S03	S1	MA 15 °C	C	50	02	Variation surfacing temperature	-341
C178	Field 3	S03	S1	MA 30 °C	C	50	02	Variation surfacing temperature	-376
C179	Field 3	S03	S1	No	C	25	02	Variation wheel load	-293
C180	Field 3	S03	S1	No	C	50	20	Variation velocity	-449
A172	Field 3	S03	S1	No	C	50	02	Variation wheel type	-435
B172	Field 3	S03	S1	No	C	50	02	Variation wheel type	-240
D172	Field 3	S03	S1	No	C	50	02	Variation wheel type	-282
C181	Field 3	S59	S2	No	C	50	02	Reference, weld crack	-387
C182	Field 3	S50	S2	No	C	50	02	Analogous strain gauge	-355
C183	Field 3	S59	S2	ZOK 0 °C	C	50	02	Variation surfacing temperature	-94
C184	Field 3	S59	S2	ZOK 15 °C	C	50	02	Variation surfacing temperature	-186
C185	Field 3	S59	S2	ZOK 30 °C	C	50	02	Variation surfacing temperature	-228
C186	Field 3	S59	S2	No	C	25	02	Variation wheel load	-248
C187	Field 3	S59	S2	No	C	50	20	Variation velocity	-395
A181	Field 3	S59	S2	No	C	50	02	Variation wheel type	-395
B181	Field 3	S59	S2	No	C	50	02	Variation wheel type	-212
D181	Field 3	S59	S2	No	C	50	02	Variation wheel type	-261

Table E - 5: Strain at cross-section in section 1, field 3

	(0 °C)	(15 °C)	(30 °C)
	+ 150 mm	+ 150 mm	+ 150 mm
S1	-72	-185	-271
S2	-116	-311	-361
S3	34	92	128
S4	22	71	103
S5	135	152	156
S6	86	221	310
S7	124	350	414
S8	107	317	294
S9	-153	-504	-603
S10	101	281	394
S11	-90	-261	-364
S12	-15	109	198
M07	X	X	X
M09	90	23	94
D07	240	637	X
D09	-619	-1170	X

Table E - 6: Strain at cross-section in section 1, crossbeam 4

	(0 °C)	(15 °C)	(30 °C)
	+ 150 mm	+ 150 mm	+ 150 mm
S32	62	112	160
S33	96	345	405
S34	-31	49	26
S35	-157	-448	-529
S36	91	401	510
S37	40	95	132
M33	-313	-595	-298
M35	136	163	20
D80	-5	-258	-989
D33	287	546	X
D35	-412	-647	X

Table E - 7: Strain at cross-section in section 1, field 4

	(0 °C)	(15 °C)	(30 °C)
	+ 150 mm	+ 150 mm	+ 150 mm
S38	-98	-292	-383
S39	144	159	164
S40	134	352	445
S41	-157	-502	-611
S42	98	277	409
S43	-87	-267	-385
M40	-40	69	-319
M41	405	447	X
M42	-49	X	X
D40	347	844	X
D41	-634	X	X
D42	302	1050	X

Table E - 8: Strain at cross-section in section 1, crossbeam 5

	(0 °C)	(15 °C)	(30 °C)
	+ 150 mm	+ 150 mm	+ 150 mm
S44	99	376	459
S45	-142	-449	-546
M44	-184	-523	X
M45	221	239	X
D44	X	X	X
D45	-584	-1036	X
D81	X	X	X

Table E - 9: Strain at cross-section in section 1, field 5

	(0 °C)	(15 °C)	(30 °C)
	+ 150 mm	+ 150 mm	+ 150 mm
S46	X	X	X
S47	X	X	X
S48	X	X	X
M47	X	X	X
M48	X	X	X
D47	X	X	X
D48	X	X	X

Table E - 10: Strain at cross-section in section 2, field 3

	(0 °C)	(15 °C)	(30 °C)
	+ 150 mm	+ 150 mm	+ 150 mm
S49	-45	-123	-153
S50	0	15	22
S51	73	149	151
S52	60	162	200
S53	-61	-159	-225
S54	46	104	134
S55	84	193	246
S56	35	94	145
S57	-23	-60	-95
S58	-60	-138	-177
S59	0	18	57
S60	-6	5	32
M53	X	X	X
M55	89	X	545
D53	-450	X	-1659
D55	X	X	X

Table E - 11: Strain at cross-section in section 2, crossbeam 4

	(0 °C)	(15 °C)	(30 °C)
	+ 150 mm	+ 150 mm	+ 150 mm
S61	0	0	13
S62	12	41	55
S63	33	128	179
S64	-64	-170	-245
S65	-37	X	0
S66	57	159	226
S67	24	56	78
M64	-100	X	X
M66	X	X	163
D64	-335	X	-865
D66	49	X	349
D82	21	X	X

Table E - 12: Strain at cross-section in section 2, field 4

	(0 °C)	(15 °C)	(30 °C)
	+ 150 mm	+ 150 mm	+ 150 mm
S68	-40	-111	-134
S69	78	151	150
S70	43	130	162
S71	-48	-119	-184
S72	56	141	175
S73	-52	X	-151
M70	X	X	X
M71	X	X	X
M72	X	X	X
D70	X	X	X
D71	X	X	X
D72	158	X	X

Table E - 13: Strain at cross-section in section 2, crossbeam 5

	(0 °C)	(15 °C)	(30 °C)
	+ 150 mm	+ 150 mm	+ 150 mm
S74	-67	-171	-214
S75	82	211	262
M74	-119	X	X
M75	27	X	-953
D74	-306	X	X
D75	61	X	X
D83	32	X	X

Table E - 14: Strain at cross-section in section 2, field 5

	(0 °C)	(15 °C)	(30 °C)
	+ 150 mm	+ 150 mm	+ 150 mm
S76	-75	-197	-235
S77	39	122	145
S78	-50	-126	-147
M76	-131	X	-58
M78	X	X	X
D76	-471	X	-935
D78	X	X	X

Annex F – Strain gauges test panel A with RHPC surfacing

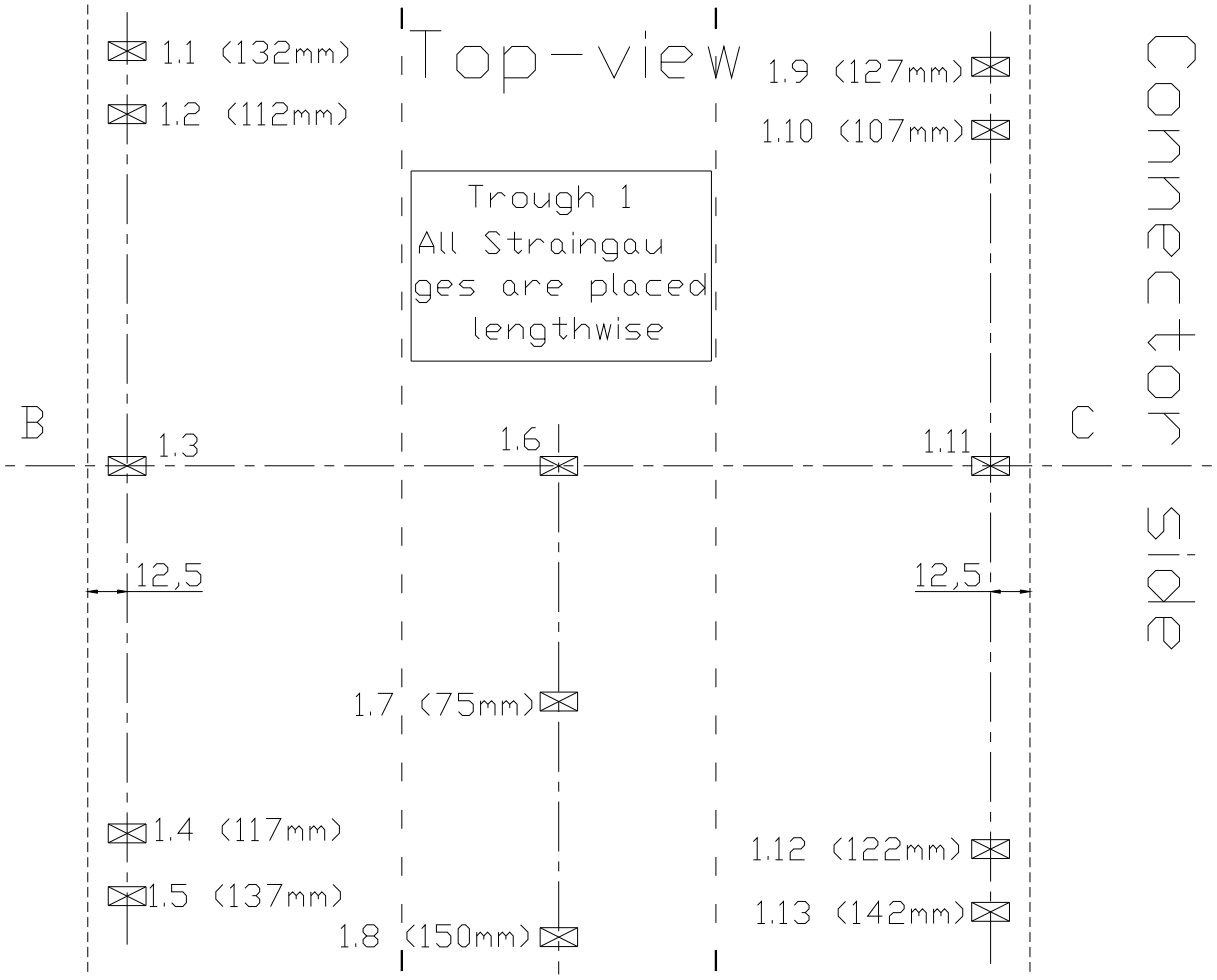

Figure F-1: Top view of strain gauges at bottom side deck plate at trough 1

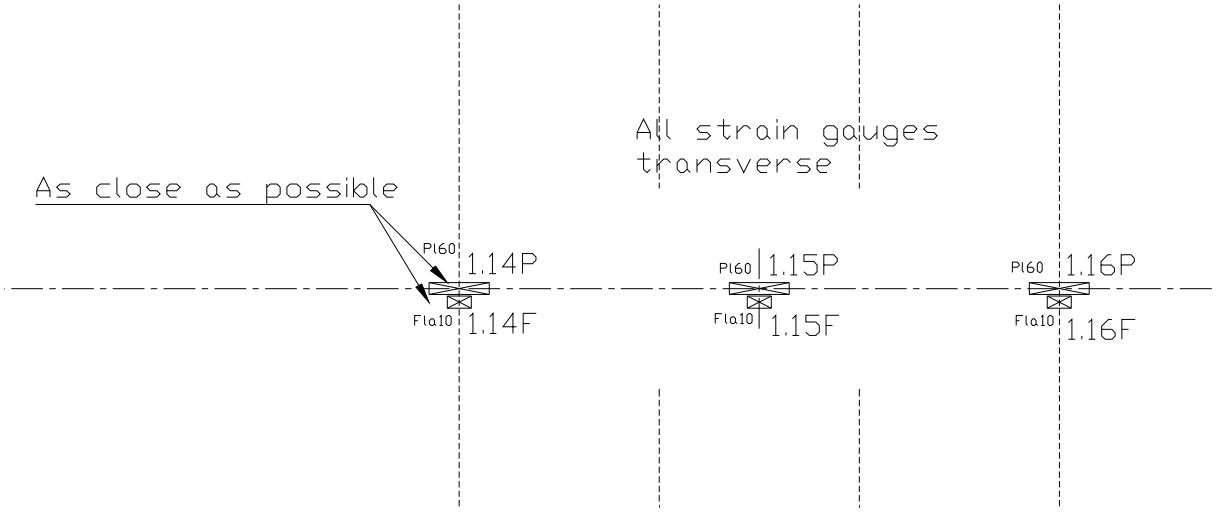

Figure F-2: Top view of strain gauges at top side RHPC surfacing at trough 1

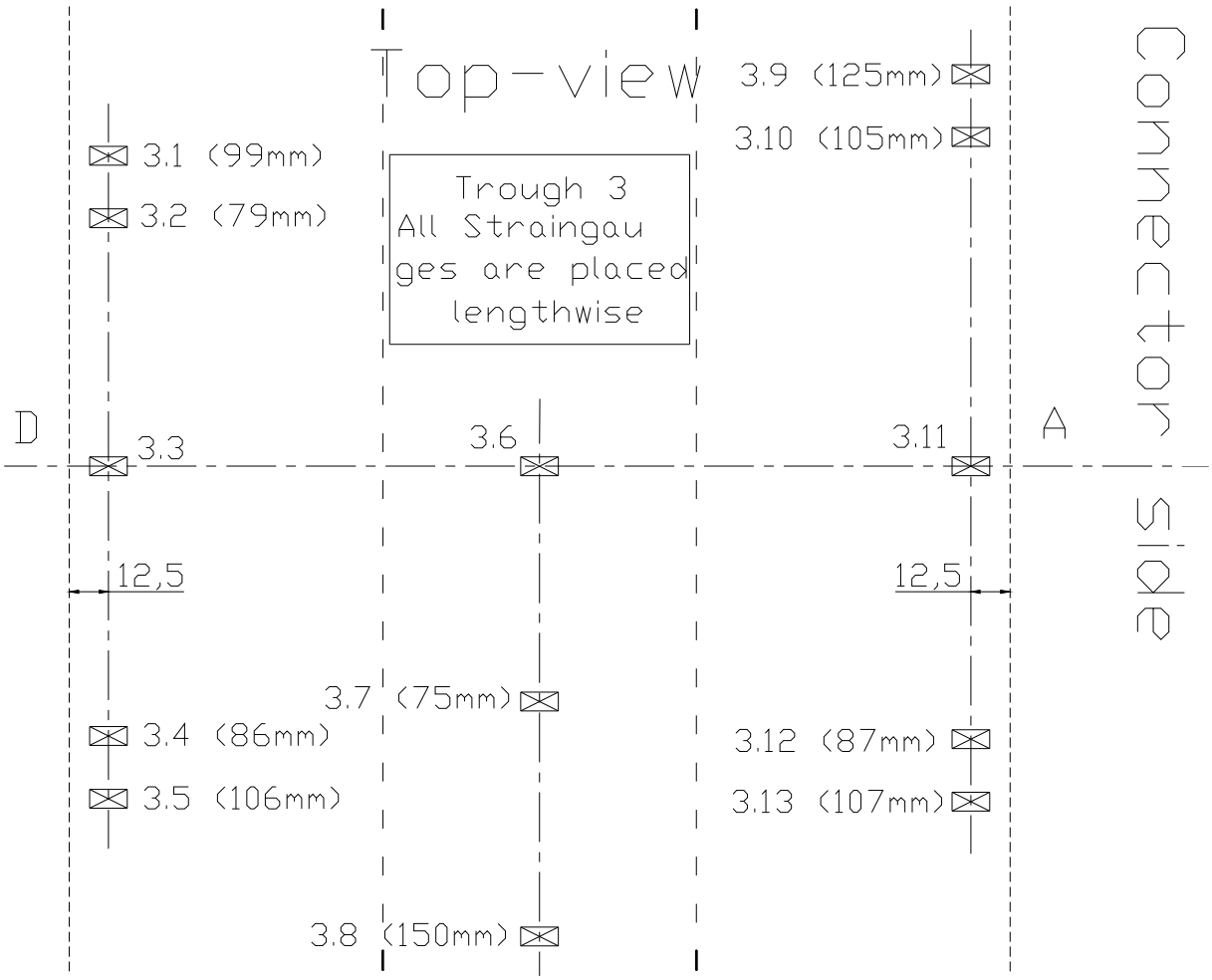

Figure F-3: Top view of strain gauges at bottom side deck plate at trough 3

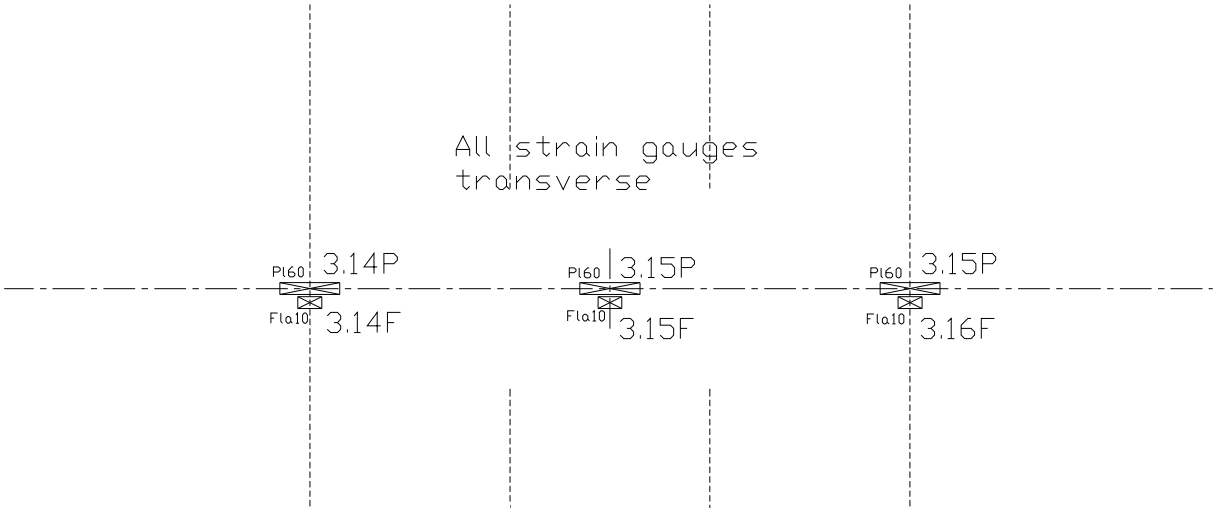

Figure F-4: Top view of strain gauges at top side RHPC surfacing at trough 3

Annex G – Comparison stresses with RHPC overlay

G.1. FE-models only representing local deck plate behaviour at the crossbeam location

Footprint 220 x 320 mm - Model load 117 kN
Calculated reduction factor (No. 4. BET/ASF) 0.20
Calculated reduction factor (No. 5. BET/ASF) 0.22
Calculated reduction factor (No. 6. BET/ASF) 0.13

Results at x = 0 mm crack location for LC 5 above trough

Description	Original		Comparison	
No. 1 (STD)	-483	MPa	-412.8	MPa
No. 3 (ASF_50_12)	-250	MPa	-213.7	MPa
No. 4 (BET_50_12)	-49.7	MPa	-42.5	MPa
No. 5 (BET_50_10)	-55	MPa	-47.0	MPa
No. 6 (BET_80_10)	-32.2	MPa	-27.5	MPa

Results at midspan x = 150 mm for LC 5 above trough

Description	Original		Comparison	
No.1 (STD)	228.00	MPa	194.9	MPa
No. 4 (BET_50_12)	22.00	MPa	18.8	MPa

G.2. FE-models representing both local deck plate behaviour and crossbeam behaviour

Footprint 220 x 320 mm - Model load 35 kN

Results at x = 0 mm crack location for LC 5 above trough

Description	Original		Comparison	
No. 1 (STD)	-124	MPa	-354.3	MPa
No. 2 (BET_50_12)	-26.5	MPa	-75.7	MPa

Results at x = 0 mm crack location for LC 6 not exactly above trough

Description	Original		Comparison	
No. 1 (STD)	-86	MPa	-245.7	MPa
No. 2 (BET_50_12)	-24	MPa	-68.6	MPa

Results at x = 0 mm crack location for LC 7 not exactly above trough

Description	Original		Comparison	
No. 1 (STD)	-45	MPa	-128.6	MPa
No. 2 (BET_50_12)	-18	MPa	-51.4	MPa

Results at x = 0 mm crack location for LC 8 not exactly above trough

Description	Original		Comparison	
No. 1 (STD)	-4	MPa	-11.4	MPa
No. 2 (BET_50_12)	-12	MPa	-34.3	MPa

G.3. FE-models representing local deck plate behaviour between two crossbeams

Footprint 220 x 320 - Model load 117 kN

Results at x = 0 mm crack location for LC5 above middle trough
Calculated reduction factor (BET/ASF) 0.30

Description	Original		Comparison	
No. 1 STD	323	MPa	276.1	MPa
No. 2 BET	37	MPa	31.6	MPa
No. 3 ASF	123	MPa	105.1	MPa

Results at x = 0 mm crack location for LC6 above left web of middle trough
Calculated reduction factor (BET/ASF) 0.39

Description	Original		Comparison	
No. 1 STD	120	MPa	102.6	MPa
No. 2 BET	28	MPa	23.9	MPa
No. 3 ASF	72	MPa	61.5	MPa

Results at x = 0 mm crack location for LC7 above left trough
Calculated reduction factor (BET/ASF) 0.27

Description Description	Original		Comparison	
No. 1 STD	321	MPa	274.4	MPa
No. 2 BET	31	MPa	26.5	MPa
No. 3 ASF	113	MPa	96.6	MPa

G.4. Static tests at TNO panel with RHPC

Footprint 270 x 320 mm - Test load: F_{min} = 12 kN, F_{max} = 117, ΔF = 105 kN
Strain ranges $\Delta\varepsilon$ (at ΔF) are given in the table below - Strains are given as microstrains (x10^{-6})

Description	Original		Comparison	
Strain at crack location left (crack-16-17)	-197	[-]	-39,4	MPa
Strain at 12.5 mm (16-location-17)	-68	[-]	-13,6	MPa
Strain midspan (gauge 19)	77	[-]	15,4	MPa
Strain at 12.5 mm (20-location-22)	-88	[-]	-17,6	MPa
Strain at crack location right (20-22-crack)	-230	[-]	-46,0	MPa

G.5. Static tests at test panel A with RHPC

Footprint 270x 320 mm - Test load: F_{min} = 0 kN, F_{max} = 150, ΔF = 150 kN
Strains are given as microstrains (x10^{-6})

Trough 1

Description	Original		Comparison	
Strain at gauge 1.03 at 12.5 mm	-74	[-]	-10.4	MPa
Strain at gauge 1.06 at 150 mm	192	[-]	26.9	MPa
Strain at gauge 1.11 at 287.5 mm	-71	[-]	-9.9	MPa

Trough 2

Description	Original		Comparison	
Strain at gauge 2.03 at 12.5 mm	-66	[-]	-9.2	MPa
Strain at gauge 2.06 at 150 mm	127	[-]	17.8	MPa
Strain at gauge 2.11 at 287.5 mm	-61	[-]	-8.5	MPa

Trough 3

Description	Original		Comparison	
Strain at gauge 3.03 at 12.5 mm	-74	[-]	-10.4	MPa
Strain at gauge 3.06 at 150 mm	183	[-]	25.6	MPa
Strain at gauge 3.11 at 287.5 mm	-29	[-]	-4.1	MPa

G.6. Fatigue test at TNO panel

Footprint 270 x 320 mm - Strains are given as microstrains ($x10^{-6}$)

Step 1 ΔF = 105 kN (12-117)

Description	Original		Comparison	
Strain at crack location left (crack-16-17)	-230	[-]	-46.0	MPa
Strain at 12.5 mm (16-location-17)	-89	[-]	-17.8	MPa
Strain at mid span gauge 19	81	[-]	16.2	MPa
Strain at 12.5 mm (20-location-22)	-103	[-]	-20.7	MPa
Strain at crack location right (20-22-crack)	-247	[-]	-49.4	MPa

Step 2 ΔF = 137 kN (15-152)

Description	Original		Comparison	
Strain at crack location left (crack-16-17)	-319	[-]	-48.8	MPa
Strain at 12.5 mm (16-location-17)	-126	[-]	-19.3	MPa
Strain at mid span gauge 19	76	[-]	11.6	MPa
Strain at 12.5 mm (20-location-22)	-131	[-]	-20.1	MPa
Strain at crack location right (20-22-crack)	-307	[-]	-47.1	MPa

Step 3 ΔF = 168 kN (19-187)

Description	Original		Comparison	
Strain at crack location left (crack-16-17)	-410	[-]	-51.3	MPa
Strain at 12.5 mm (16-location-17)	-169	[-]	-21.1	MPa
Strain at mid span gauge 19	110	[-]	13.8	MPa
Strain at 12.5 mm (20-location-22)	-179	[-]	-22.3	MPa
Strain at crack location right (20-22-crack)	-401	[-]	-50.2	MPa

Step 4 ΔF = 210 kN (23-233)

Description	Original		Comparison	
Strain at crack location left (crack-16-17)	-598	[-]	-59.8	MPa
Strain at 12.5 mm (16-location-17)	-261	[-]	-26.1	MPa
Strain at mid span gauge 19	164	[-]	16.4	MPa
Strain at 12.5 mm (20-location-22)	-283	[-]	-28.3	MPa
Strain at crack location right (20-22-crack)	-570	[-]	-57.0	MPa

G.7. Fatigue test at test panel A with RHPC

Footprint 270 x 320 mm - Test load ΔF = 150 kN (first part of test)
Strains are given as microstrains ($x10^{-6}$)

Trough 1

Description	Original		Comparison	
Strain at gauge 1.03 at 12.5 mm	-91	[-]	-12.7	MPa
Strain at gauge 1.06 at 150 mm	168	[-]	23.5	MPa
Strain at gauge 1.11 at 287.5 mm	-145	[-]	-20.3	MPa

Trough 2

Description	Original		Comparison	
Strain at gauge 2.03 at 12.5 mm	-80	[-]	-11.2	MPa
Strain at gauge 2.06 at 150 mm	110	[-]	15.4	MPa
Strain at gauge 2.11 at 287.5 mm	-153	[-]	-21.4	MPa

Trough 3

Description	Original		Comparison	
Strain at gauge 3.03 at 12.5 mm	-102	[-]	-14.3	MPa
Strain at gauge 3.06 at 150 mm	175	[-]	24.5	MPa
Strain at gauge 3.11 at 287.5 mm	-95	[-]	-13.3	MPa

G.8. Static tests at end fatigue test at test panel A

Footprint 270x 320 - Test load ΔF = 150 kN
Strains are given as microstrains ($x10^{-6}$)

Trough 1

Description	Original		Comparison	
Strain at gauge 1.03 at 12.5 mm	-106	[-]	-14.8	MPa
Strain at gauge 1.06 at 150 mm	174	[-]	24.4	MPa
Strain at gauge 1.11 at 287.5 mm	-154	[-]	-21.6	MPa

Trough 2

Description	Original		Comparison	
Strain at gauge 2.03 at 12.5 mm	-89	[-]	-12.5	MPa
Strain at gauge 2.06 at 150 mm	109	[-]	15.3	MPa
Strain at gauge 2.11 at 287.5 mm	-163	[-]	-22.8	MPa

Trough 3

Description	Original		Comparison	
Strain at gauge 3.03 at 12.5 mm	-109	[-]	-15.3	MPa
Strain at gauge 3.06 at 150 mm	186	[-]	26.0	MPa
Strain at gauge 3.11 at 287.5 mm	-104	[-]	-14.6	MPa

Annex H - Submerged Arc Welding Tests

H.1. Execution specimen 4

Figure H-1 shows a photograph of the topside of specimen 4 after the fabrication of the SAW-weld. The weld was made from right to left. The first half was made with a travel speed of 450 mm/min (18 inch/min). The second half was made with a travel speed of 600 mm/min (24 inch/min). The SAW-weld was continuous at this location. During the welding process there were no unusual observations.

The properties of the welds were as follows:

Left:
t = 12 mm
v = 600 mm/min
I = 650 Amp
V = 30 Volt
Weld quality = good

Right:
t = 12 mm
v = 450 mm/min
I = 650 Amp
V = 30 Volt
Weld quality = good

The locations of macros 4 and 5 were marked at the topside of the deck plate after the welding process.

Welding direction: ←

Small gap between plate halves No gap

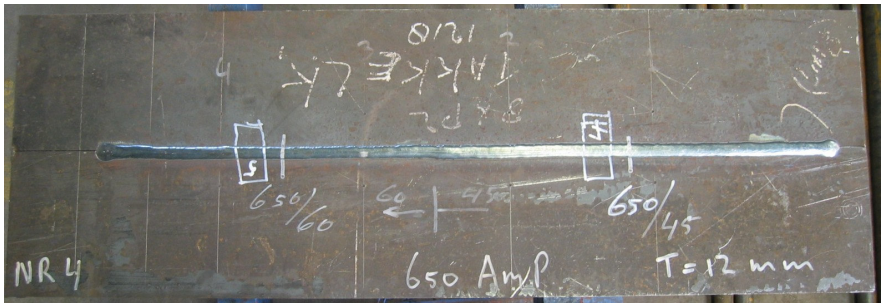

Figure H-1: Topside specimen 4 after welding

H.2. Execution specimen 5

Figure H-2 shows a photograph of the topside of specimen 5 after the SAW-welding process. The weld was made from right to left in the photograph.
At the start of the welding process there was immediately a burn through the deck plate. The current was too high. Therefore the current was decreased, which led to a good weld at the left side of the plate.

The properties of the welds were as follows:

Left:	Right:
t = 12 mm	t = 12 mm
v = 600 mm/min	v = 450 mm/min
I = 730 Amp	I = 800 Amp, later 730 Amp
V = 30 Volt	V = 30 Volt
Weld quality = good	Weld quality = burn through

The location of macro 7 was marked at the topside of the deck plate after the welding process.

Welding direction: ←

No gap Small gap between plate halves

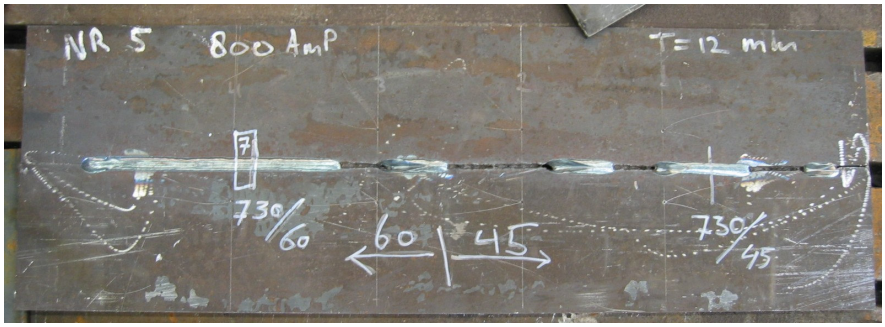

Figure H-2: Topside specimen 5 after welding

H.3. Execution specimen 8

Figure H-3 shows a photograph of the topside of specimen 8 after the SAW-welding process. The weld was made from left to right in the photograph. The first half was made with a travel speed of 450 mm/min (18 inch/min). The second halve was made with a travel speed of 600 mm/min (24 inch/min).). The SAW-weld was continuous at this location. During the welding process there were no unusual observations.

The properties of the welds were as follows:

Left:
T = 14 mm
v = 450 mm/min
I = 800 Amp
V = 35 Volt
Weld quality = good

Right:
T = 14 mm
v = 600 mm/min
I = 800 Amp
V = 35 Volt
Weld quality = good

The location of macro 10 was marked at the topside of the deck plate after the welding process.

Welding direction: ⟶

No gap No gap

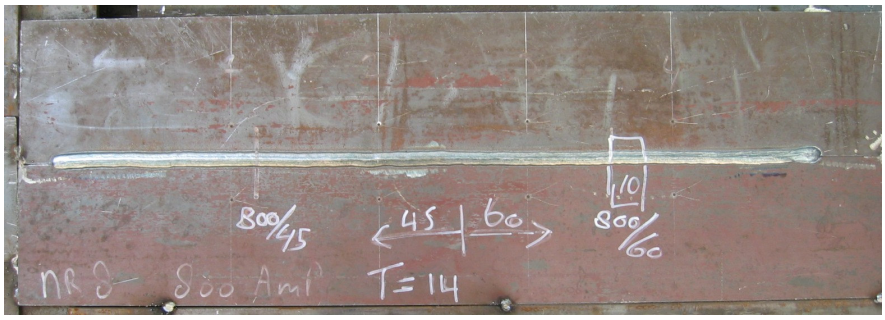

Figure H-3: Topside specimen 8 after welding

H.4. Execution specimen 9

Figure H-4 shows a photograph of the topside of specimen 9 after the SAW-welding process. The weld was made from right to left in the photograph. The first half was made with a travel speed of 450 mm/min (18 inch/min). The second halve was made with a travel speed of 600 mm/min (24 inch/min). The SAW-weld was continuous at this location.
At the start of the welding process there was immediately a burn through the deck plate. The current was too high. Therefore the current was decreased, which led to a good weld at the left side of the plate.
The test plate has a gap of approximately 2 mm in the first 300 mm. At 800 Amps there was immediately a burn through at this location. In the last 300 mm there was no gap and at that location a current of 840 Amps results in a good weld.

The properties of the welds were as follows:

Left:
t = 14 mm
v = 600 mm/min
I = 840 Amp
V = 35 Volt
Weld quality = good

Right:
t = 14 mm
v = 450 mm/min
I = 950 Amp, later 800 Amp
V = 35 Volt
Weld quality = burn through

Welding direction: ←

No gap Small gap between plate halves

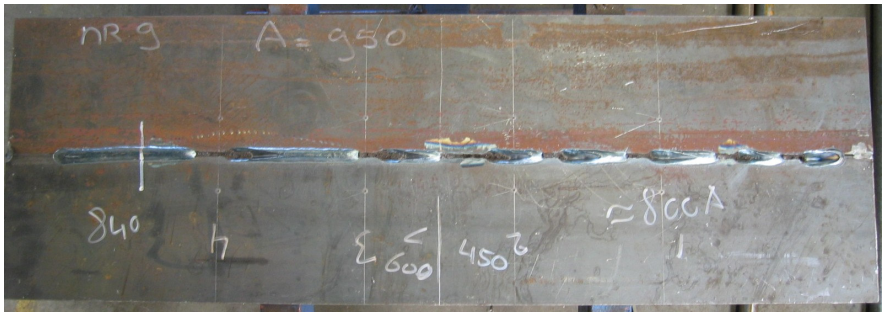

Figure H-4: Topside specimen 9 after welding

H.5. Execution specimen 6

Figure H-6 shows a photograph of the topside of specimen 6 after the SAW-welding process. The weld was made from left to right in the photograph. This weld was made with an eccentricity of 4 mm, measured from the crack to the adjacent side of the wire. The eccentricity was at the inner side of the trough. All other specimens were welded with an eccentricity of 0 mm. Figure H-5 shows this eccentricity. At the start of the welding process there was immediately a burn through the deck plate. The current was too high. Therefore the current was decreased, which led to a good weld at the right side of the plate.

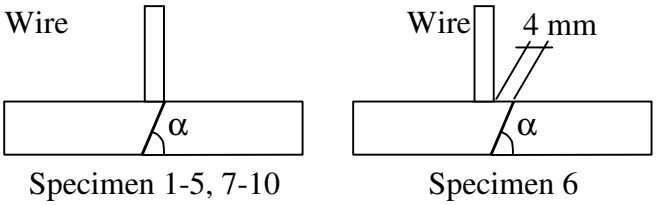

Figure H-5: Eccentricity weld specimen 6

The properties of the weld was as follows:

Left:	Right:
t = 12 mm	t = 12 mm
v = 450 mm/min	v = 600 mm/min
I = 800 Amp	I = 720 Amp
V = 30 Volt	V = 30 Volt
Eccentricity = 4 mm	Eccentricity = 4 mm
Weld quality = burn through	Weld quality = good

The location of macro 6 was marked at the topside of the deck plate after the welding process.
Welding direction: ⟶
No gap Small gap between plate halves

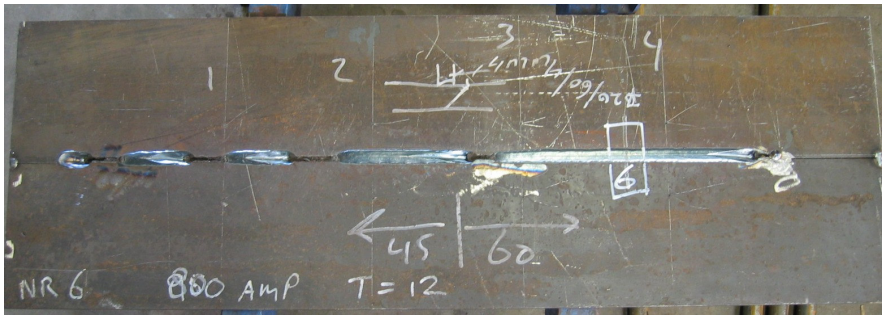

Figure H-6: Topside specimen 6 after welding

H.6. Execution specimen 1

Figure H-7 shows a photograph of the topside of specimen 1 after the SAW-welding process. The weld was made from right to left in the photograph. The first half was made with a travel speed of 450 mm/min (18 inch/min). The second halve was made with a travel speed of 600 mm/min (24 inch/min). The SAW-weld was continuous at this location.

The properties of the welds were as follows:

Left:	Right:
t = 10 mm	t = 10 mm
v = 600 mm/min	v = 450 mm/min
I = first 500, later 550 Amp	I = 500 Amp
V = 25 Volt	V = 20 Volt
Weld quality = good	Weld quality = good

The location of macro 1 was marked at the topside of the deck plate after the welding process.

Welding direction: ←

Small gap between plate halves No gap

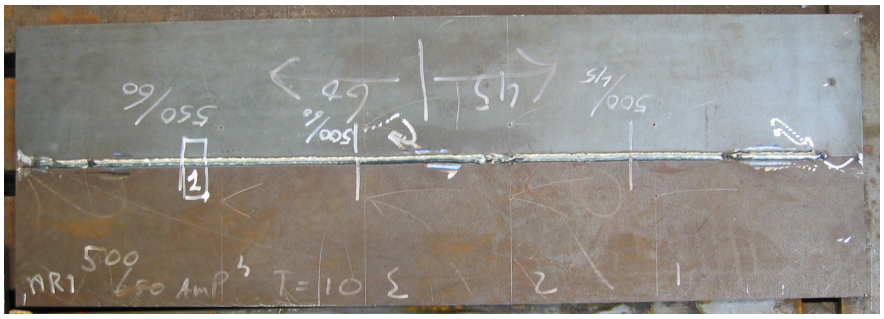

Figure H-7: Topside specimen 1 after welding

H.7. Execution specimen 2

Figure H-8 shows a photograph of the topside of specimen 2 after the SAW-welding process. The weld was made from left to right in the photograph. The travel speed was 600 mm/min (24 inch/min) from start to end. The current in the first quarter was 600 Amp. The current in the second quarter was increased to 650 Amp. Halfway the plate the current was increased to 700 Amp, which led to a burn through. The current was then decreased to 650 Amp.

The properties of the welds were as follows:

Left, 1st quarter:	Left, 2nd quarter:	Right 3rd quarter:	Right, 4th quarter
t = 10 mm	t = 10 mm	t = 10 mm	t = 10 mm
v = 600 mm/min	v = 600 mm/min	v = 600 mm/min	v = 600 mm/min
I = 600 Amp	I = 650 Amp	I = 700 Amp	I = 650 Amp
V = 25 Volt	V = 25 Volt	V = 25 Volt	V = 25 Volt
Weld quality = good	Weld quality = good	Weld quality = burn through	Weld quality = good

The location of macro 2 was marked at the topside of the deck plate after the welding process.

Welding direction: ⟶

Small gap between plate halves No gap

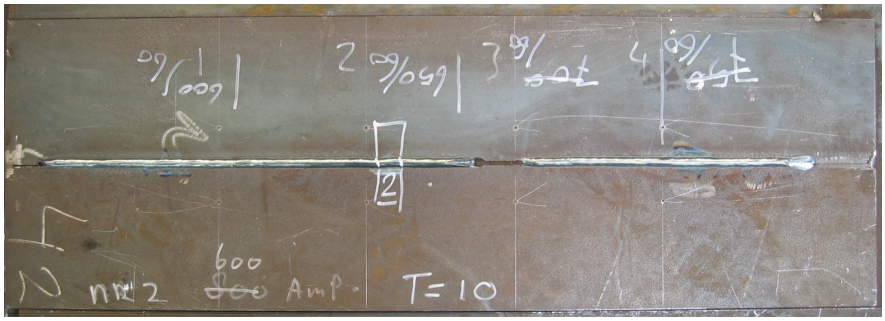

Figure H-8: Topside specimen 2 after welding

H.8. Execution specimen 3

Figure H-9 shows a photograph of the topside of specimen 3 after the SAW-welding process. The weld was made from right to left in the photograph. The travel speed was 600 mm/min (24 inch/min) from start to end. Specimen 3 had a backing strip to simulate the trough web. see Figure H-10.

The properties of the welds were as follows:

Left, 1st and 2nd quarters:	Right, 3rd quarter:	Right, 4th quarter:
t = 10 mm	t = 10 mm	t = 10 mm
v = 600 mm/min	v = 600 mm/min	v = 450 mm/min
I = 700 Amp	I = 650 Amp	I = 600 Amp
V = 25 Volt	V = 25 Volt	V = 25 Volt
Weld quality = burn through	Weld quality = good	Weld quality = good

The location of macro 3 was marked at the topside of the deck plate after the welding process.

Welding direction: ←

No gap No gap

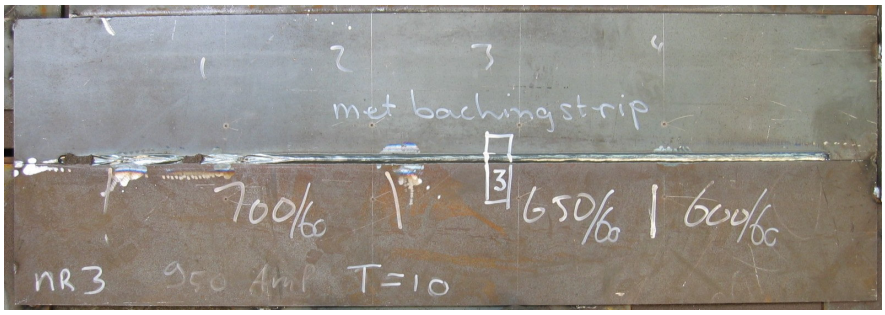

Figure H-9: Topside specimen 3 after welding

Figure H-10: Backing strip, simulating trough web at crack location

H.9. Execution specimen 7

Figure H-11 shows a photograph of the topside of specimen 7 after the SAW-welding process. The weld was made from right to left in the photograph. The travel speed was 450 mm/min (24 inch/min) from start to end.
Instead of a backing strip this test specimen was laid directly on the working table. So there was no space under the plate. This probably prevented a burn through.

The properties of the welds were as follows:

Left, 1st quarter:	Left, 2nd quarter:	Right, 3rd quarter:	Right, 4th quarter:
t = 14 mm	t = 14 mm	t = 14 mm	t = 14 mm
v = 450 mm/min	v = 450 mm/min	v = 450 mm/min	v = 450 mm/min
I = 950 Amp	I = 900 Amp	I = 850 Amp	I = 800 Amp
V = 32 Volt	V = 32 Volt	V = 32 Volt	V = 32 Volt
Weld quality = Burn through	Weld quality = good	Weld quality = good	Weld quality = good

Welding direction: ←

No gap No gap

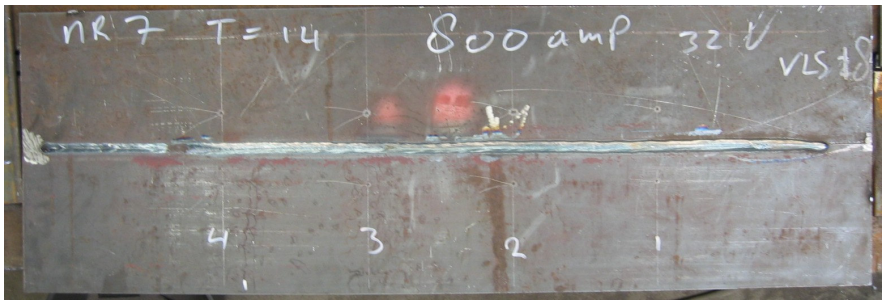

Figure H-11: Topside specimen 7 after welding

H.10. Execution specimen 10

Figure H-12 shows a photograph of the topside of specimen 10 after the SAW-welding process. The weld was made from left to right in the photograph. The travel speed was 600 mm/min (24 inch/min) from start to end. This specimen also had a backing strip.

The properties of the welds were as follows:

Left, 1st quarter:	Left, 2nd quarter:	Right, 3rd quarter:	Right, 4th quarter:
t = 14 mm	t = 14 mm	t = 14 mm	t = 14 mm
v = 600 mm/min	v = 600 mm/min	v = 600 mm/min	v = 600 mm/min
I = 800 Amp	I = 850 Amp	I = 900 Amp	I = 950 Amp
V = 32 Volt	V = 32 Volt	V = 32 Volt	V = 32 Volt
Weld quality = good	Weld quality = good	Weld quality = good	Weld quality = burn through

The location of macros 8 and 9 were marked at the topside of the deck plate after the welding process.

Welding direction: ⟶

No gap Small gap between the plate halves

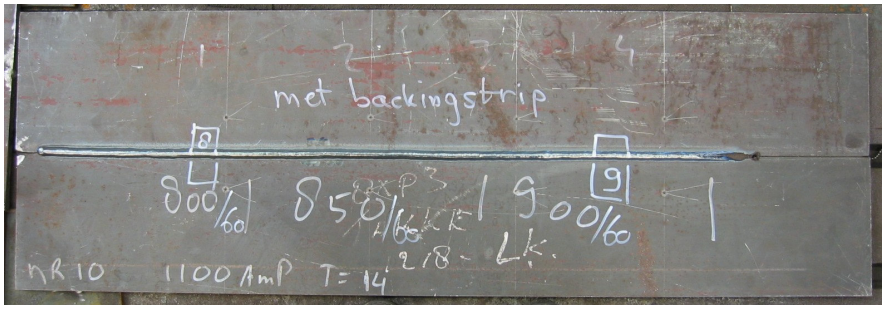

Figure H-12: Topside specimen 10 after welding

H.11. Depth of penetration

Macro 1 From specimen 1 t = 10 mm v = 600 mm/min I = 550 Amp V = 25 Volt Depth of penetration = 5.4 mm	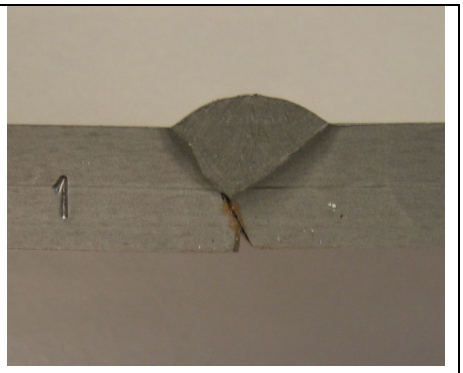
Macro 2 From specimen 2 T = 10 mm v = 600 mm/min I = 650 Amp V = 25 Volt Depth of penetration = 7.5 mm	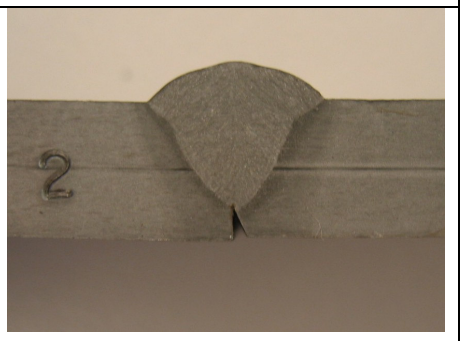
Macro 3 From specimen 3 T = 10 mm v = 600 mm/min I = 650 Amp V = 25 Volt With backing strip Depth of penetration = 6.8 mm	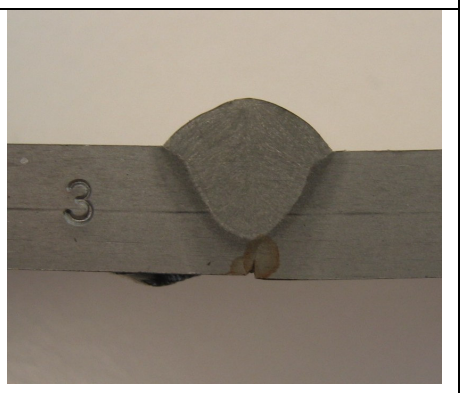

Macro 4 From specimen 4 T = 12 mm v = 450 mm/min I = 650 Amp V = 30 Volt Depth of penetration = 7.9 mm	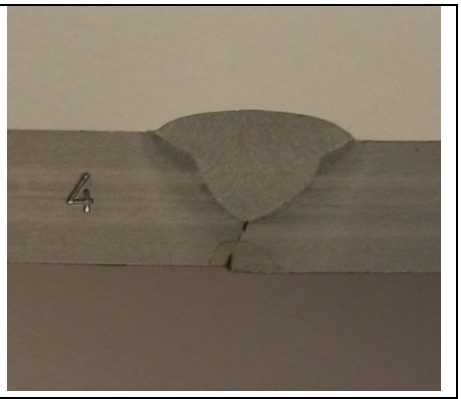
Macro 5 From specimen 4 T = 12 mm v = 600 mm/min I = 650 Amp V = 30 Volt Depth of penetration = 8.3 mm	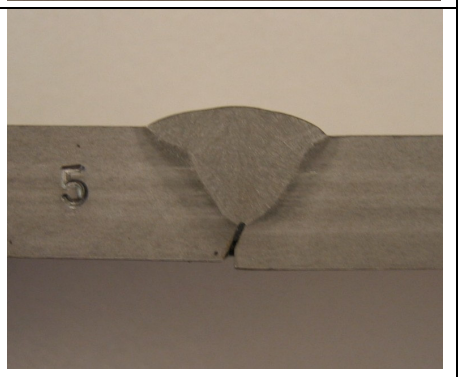
Macro 6 From specimen 6 T = 12 mm v = 600 mm/min I = 720 Amp V = 30 Volt Eccentricity = 4 mm Depth of penetration = 10.4 mm	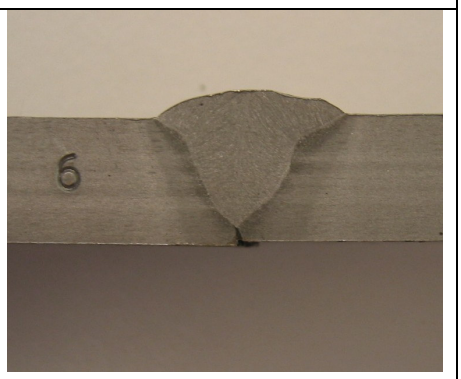
Macro 7 From specimen 5 T = 12 mm v = 600 mm/min I = 730 Amp V = 30 Volt Depth of penetration = 8.25 mm	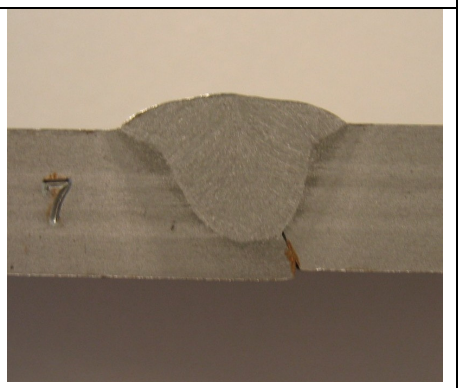

Macro 8 From specimen 10 T = 14 mm v = 600 mm/min I = 800 Amp V = 32 Volt With backing strip Depth of penetration = 9.3 mm	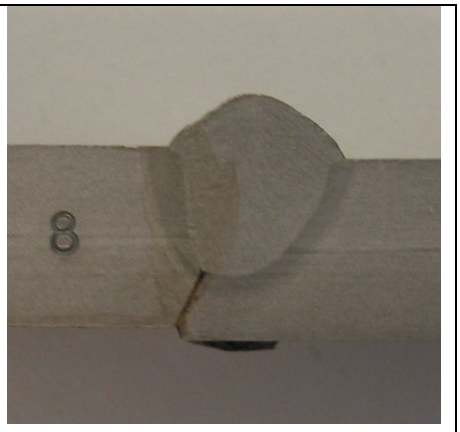
Macro 9 From specimen 10 T = 14 mm v = 600 mm/min I = 900 Amp V = 32 Volt With backing strip Depth of penetration = 10.81 mm	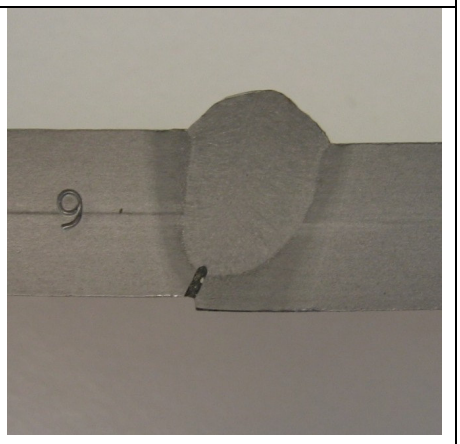
Macro 10 From specimen 8 T = 14 mm v = 600 mm/min I = 800 Amp V = 35 Volt Depth of penetration = 9.32 mm	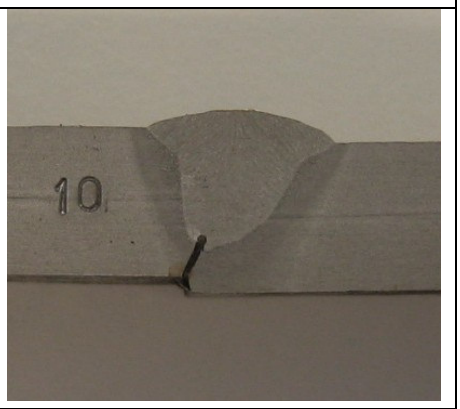

Curriculum vitae

Name: F.B.Peter de Jong
Born: May 30 1975 in Groningen, The Netherlands

Education:

1987-1993	Atheneum, ‘Gomarus College’, Groningen
1993-1999	Doctoral Civil Engineering, Delft University of Technology Faculty of Civil Engineering, Section steel and timber structures
2000-2006	Doctorate (Ph.D.), Delft University of Technology Faculty of Civil Engineering and Geosciences, Steel Structures department

Practical experience:

1999-	Design engineer at the Ministry of Transport, Public Works and Water Management, Civil engineering division, Utrecht